



**Asymmetric Hydrofunctionalisation Reactions
Catalysed by 3d Transition Metal Complexes and
Main Group Element Compounds**

Dissertation

Zur Erlangung des Doktorgrades der Naturwissenschaften

Dr. rer. nat.

an der Fakultät Chemie und Pharmazie der Universität Regensburg

vorgelegt von:

Felix Seeberger

aus Werne

Regensburg, Oktober 2023

Der experimentelle Teil der vorliegenden Arbeit wurde in der Zeit zwischen November 2019 und Juni 2023 unter Anleitung von Prof. Dr. Robert Wolf am Institut für Anorganische Chemie der Universität Regensburg angefertigt.

Die Arbeit wurde angeleitet von:

Prof. Dr. Robert Wolf

Promotionsgesuch eingereicht am:

16.10.2023

Promotionsausschuss:

Vorsitz

Prof. Dr. Patrick Nürnberger

Erstgutachter

Prof. Dr. Robert Wolf

Zweitgutachter

Prof. Dr. Manfred Scheer

Dritter Prüfer

Prof. Dr. Hendrik Zipse

Prologue

This thesis primarily reports on the synthesis and catalytic activity of main group and 3d transition metal-based complexes in hydrofunctionalisation reactions. *Chapter 1* gives an overview of enantioselective (transfer) hydrogenation, hydroboration and hydrosilylation reactions. In *Chapter 2* the catalytic activity of phosphacyclohexadienyl anions is compared with organolithium reagents and alkoxides in hydroboration reactions. *Chapter 3* reports the synthesis of magnesium complexes bearing chiral β -ketiminate ligands and their activity and selectivity in enantioselective hydrofunctionalisation reactions. *Chapter 4* describes the use of chiral bis(aryl)acenaphthenequinonediimines (BIANs) as ligands in the 3d transition metal catalysed enantioselective transfer hydrogenation of olefins. *Chapter 5* covers the synthesis of cobaltate-phosphinine complexes featuring rare or novel coordination modes of the phosphinine. Finally, *Chapter 6* gives a summary of the results described in this thesis and provides a short outlook on asymmetric hydrofunctionalisation reactions.

Prolog

In dieser Arbeit wird in erster Linie über die Synthese sowie die katalytische Aktivität von Komplexen basierend auf Hauptgruppen- und 3d-Übergangsmetallen in Hydrofunktionalisierungsreaktionen berichtet. *Kapitel 1* gibt einen Überblick über enantioselektive (Transfer-)Hydrierungs-, Hydroborierungs- und Hydrosilylierungsreaktionen. *Kapitel 2* vergleicht die katalytische Aktivität von Phosphacyclohexadienyl-Anionen mit Organolithium-Reagenzien und Alkoxiden in Hydroborierungsreaktionen. *Kapitel 3* berichtet über die Synthese von Magnesiumkomplexen mit chiralen β -Ketiminato-Liganden und deren Aktivität sowie Selektivität in enantioselektiven Hydrofunktionalisierungsreaktionen. *Kapitel 4* behandelt die Verwendung von chiralen Bis(aryl)acenaphthenchinondiimininen (BIANs) als Liganden in der enantioselektiven Transferhydrierung von Olefinen katalysiert durch 3d Metalle. *Kapitel 5* behandelt die Synthese von Kobalt-Phosphinin-Komplexen, bei denen das Phosphinin in seltenen oder neuartigen Koordinationsmodi vorliegt. Das letzte Kapitel fasst die Ergebnisse dieser Arbeit zusammen und gibt einen kurzen Ausblick.

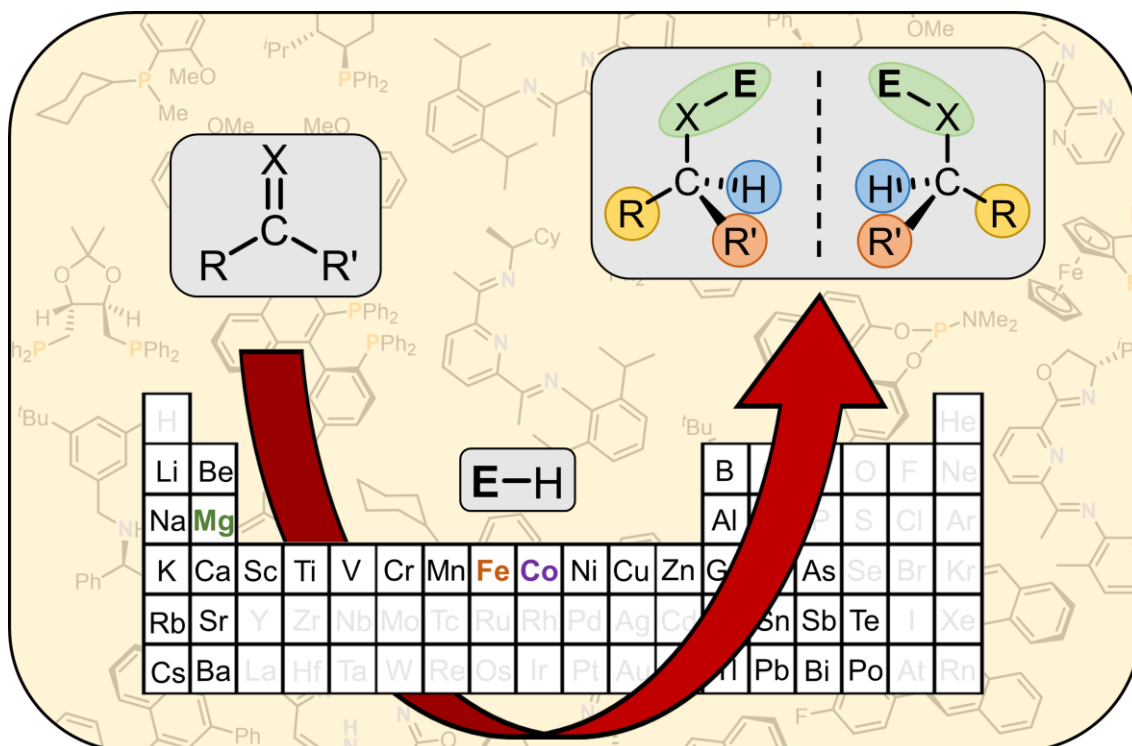
Table of Contents

1	Enantioselective Hydrofunctionalisation Reactions with 3d Transition and Main Group Metals	1
1.1	Discovery of Chirality	3
1.2	Homochirality in Nature	4
1.3	Asymmetric Hydrogenation	5
1.4	Asymmetric Hydroboration of Ketones	16
1.5	Asymmetric Hydrosilylation of Polar Substrates	22
1.6	Conclusion	28
2	Expedient Hydrofunctionalisation of Carbonyls and Imines Initiated by Phosphacyclohexadienyl Anions	33
2.1	Introduction	35
2.2	Results and Discussion	36
2.3	Conclusion	41
2.4	Experimental Details	41
3	Asymmetric Hydrofunctionalisation Reactions Catalysed by Chiral β-Diketiminato Magnesium Complexes	65
3.1	Introduction	67
3.2	Results and Discussion	69
3.3	Conclusion	76
3.4	Experimental Details	77
4	Asymmetric Transfer Hydrogenation Reactions Catalysed by an α-Diimine Stabilised Cobaltate Complex	95
4.1	Introduction	97
4.2	Results and Discussion	99
4.3	Conclusion	95
4.4	Experimental Details	108
5	Synthesis and Characterisation of Low-Valent Phosphinine Cobalt Complexes ..	145
5.1	Introduction	147
5.2	Results and Discussion	149
5.3	Conclusion	158
5.4	Experimental Details	159
6	Summary and Conclusion	203
7	Acknowledgements	211
8	Curriculum Vitae	212
9	List of Publications	213

1 Enantioselective Hydrofunctionalisation Reactions with 3d Transition and Main Group Metals^[a]

Abstract:

Hydroboration, hydrosilylation and hydrogenation reactions are important tools in the synthesis of a multitude of fine and bulk chemicals. Due to the prevalence of stereocenters in natural products, performing such hydrofunctionalisation reactions in an asymmetric manner is a major goal in contemporary research. Typical approaches towards enantioselective hydrofunctionalisation involve the use of catalytically active organometallic complexes bearing chiral ligands. A crucial problem in the field is the prediction of the enantioselectivity of a given system, because small differences in energy (~ 2 kcal/mol) are sufficient for high enantiodiscrimination. Therefore, empirical approaches based on trial and error are, even nowadays, the most common way to find new suitable systems. This introduction reviews enantioselective (transfer) hydrogenation, hydroboration and hydrosilylation reactions with the focus on catalyst systems based on 3d transition elements or main group metals.



^[a] Felix Seeberger wrote the manuscript with input from Robert Wolf.

1.1 Discovery of Chirality

Chirality is the attribute of an item to be distinguishable from its mirror image.^[1,2] This symmetry attribute, which mankind has already observed for thousands of years in our hands and feet, was first detected in crystalline material in the early 19th century, when *Haiiy* observed quartz crystals to be non-superimposable with their mirror image. After *Malus*' discovery of the polarisation of light,^[3] *Arago*,^[4] *Biot*,^[5] and *Herschel*^[6] were independently able to detect the optical activity of these quartz crystals and connect this rotation of the plane-polarised light to the two hemihedral forms. In 1848, *Pasteur* performed the first resolution of enantiomers, confirming that optically inactive, racemic sodium ammonium tartrate contains two chiral molecules, which rotate plane-polarised light in opposite directions (**Figure 1, a**).^[7] Based on these results, *van't Hoff*^[8] and *Le Bel*^[9] proposed that each carbon atom bound to four different substituents is a potential chiral center. This concept was then expanded to inorganic compounds by *Werner* in 1911, when he performed the chiral resolution of racemic $[(\text{NH}_3)(\text{en})_2\text{CoX}]X_2$ (en = ethylenediamine; X = Cl, Br) with bromocamphersulfonic acid, separating the left- (Λ) and right-handed (Δ) enantiomers. (**Figure 1, b**).^[10]

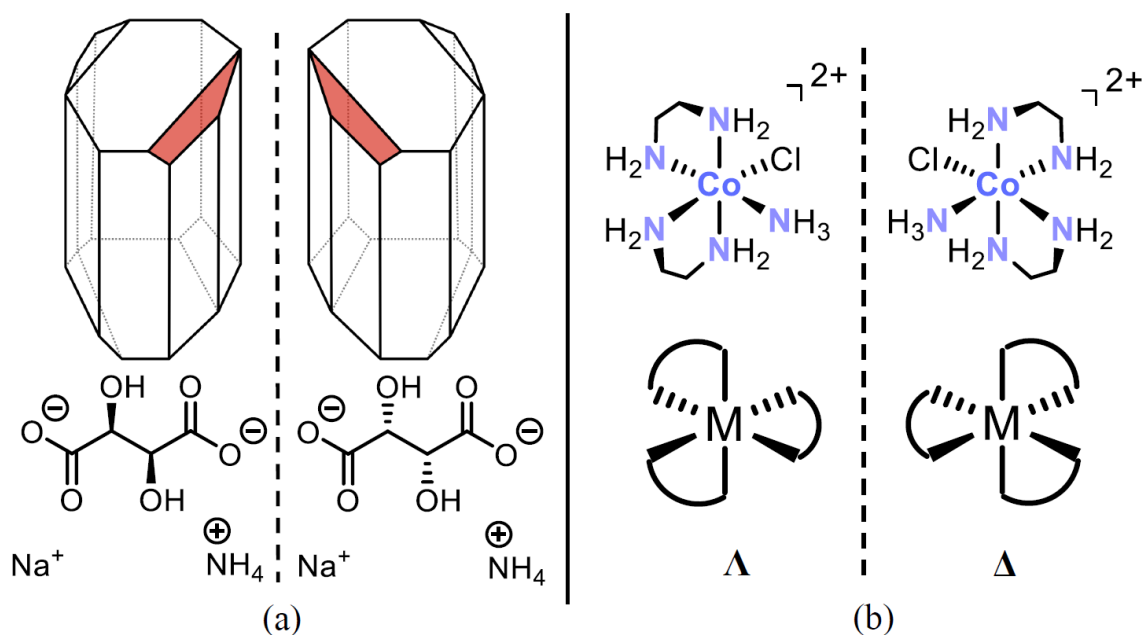


Figure 1. Idealised crystal shapes and the corresponding enantiomer of the sodium ammonium tartrates separated by *Pasteur* (a)^[11] and a chiral cobalt cation resolved by *Werner* (b).

A chiral compound does not possess any symmetry elements of the second kind (a mirror plane, $\sigma = S_1$; a centre of inversion, $i = S_2$; or a rotation-reflexion axis, S_{2n}) and must therefore belong to the point groups C_n , D_n , O , T , or I . Central chirality can be observed in molecules bearing one or more stereocenters. This type of chirality is the most widespread form observed and was described in the 19th century by *van't Hoff* and *Le Bel* (*vide supra*). Examples, such as the tartrates investigated by *Pasteur* (**Figure 1, a**)^[7] amino acids, and sugars, are plentiful in nature as the building blocks for proteins and nucleic acids (**Figure 2, a**).^[12] Enantiomers, however, can also

occur *via* axial chirality, i.e. having a chiral axis, most often along a chemical bond and constrained against rotation by steric effects or torsional stiffness of the bonds. This occurs in sterically hindered biphenyls with the most prominent example being 1,1'-bi-2-naphthol (BINOL, **Figure 2**, b). Planar chirality results from the arrangement of out-of-plane groups with respect to the chiral plane. Planar chirality is found in, for example, (*E*)-cyclooctene as well as asymmetrically substituted ferrocene-derivatives (**Figure 2**, c). Helical chirality is a special case of axial chirality, in which a molecule has a helical, propeller or screw-shaped geometry.^[2] The cobalt complexes resolved by *Werner* (**Figure 1**, b)^[10] and helicenes (**Figure 2**, d) are examples of helical chirality.

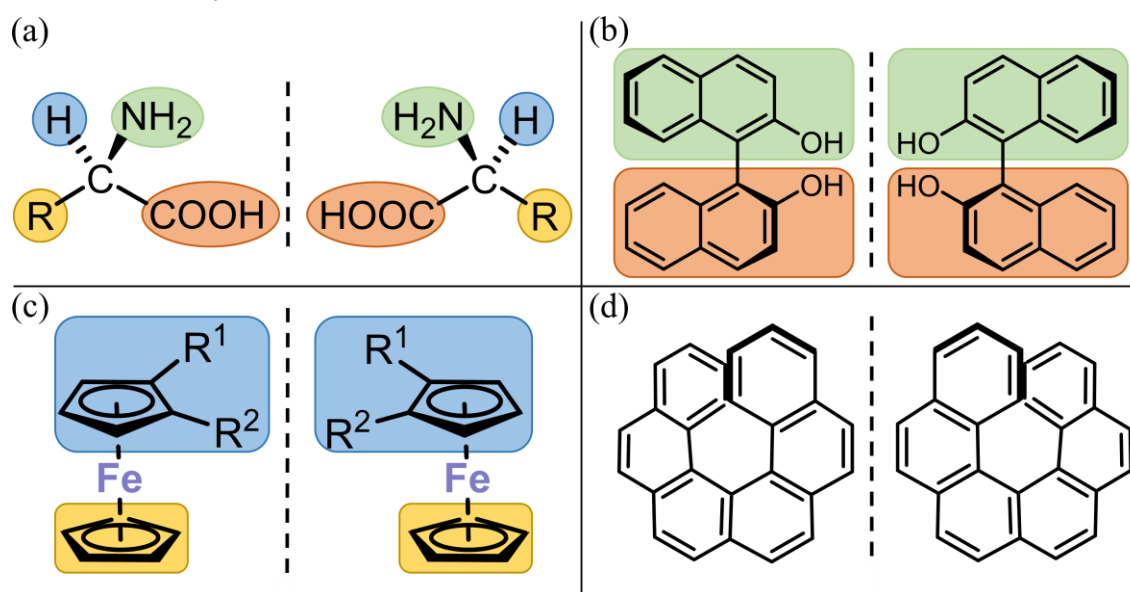


Figure 2. The different types of chirality, including central chirality (a), axial chirality (b), planar chirality (c) and helical chirality (d).

1.2 Homochirality in Nature

Most chiral, naturally occurring sugars and amino acids exist almost exclusively as one enantiomer. Generally, amino acids are *levorotatory*, thus rotating plane-polarised light counterclockwise, whilst most sugars are *dextrorotatory*, rotating the light clockwise. This phenomenon is called homochirality and although there are numerous theories on its origins, no clear answer can be given yet.^[11]

As all known living organisms consist of such chiral amino acids, the effect of homochirality on all of us cannot be understated. Enantiomers can exhibit different reactivity towards other chiral compounds. Therefore discrimination between the stereoisomers can be responsible for differences in taste, odour, as well as further physiological responses to specific enantiomers.^[13] A prominent example is limonene, whose (*R*)-enantiomer possesses the odour of oranges, whilst the (*S*)-enantiomer smells like lemons (**Figure 3**).^[14,15] In a similar fashion, (*R*)-carvone has a spearmint odour, whilst the (*S*)-enantiomer is described to possess a caraway odour.^[14,16] These effects, however, can also include more drastic physiological responses, as found in the use of

thalidomide as a tranquiliser in the 1950s.^[17] Whilst the (*R*)-enantiomer possesses the desired sedative effect, the opposite enantiomer exhibits embryo-toxic and teratogenic effects resulting in children born with birth defects if the drug was taken during pregnancy. In the case of thalidomide, it was later shown that *in vivo* both enantiomers racemise due to the acidic hydrogen at the chiral center.^[18] Therefore, consumption of the enantiopure (*R*)-enantiomer would also lead to the presence of the harmful (*S*)-enantiomer *in vivo*. Nevertheless, this incident demonstrates the importance of chiral molecules in biological systems. Therefore, asymmetric synthesis and catalysis has become a major part of contemporary research. As this very broad topic cannot be sufficiently summarised within the boundaries of this thesis, this chapter gives an overview on asymmetric hydrofunctionalisation reactions with a focus on early transition and main group metal-based catalysts.

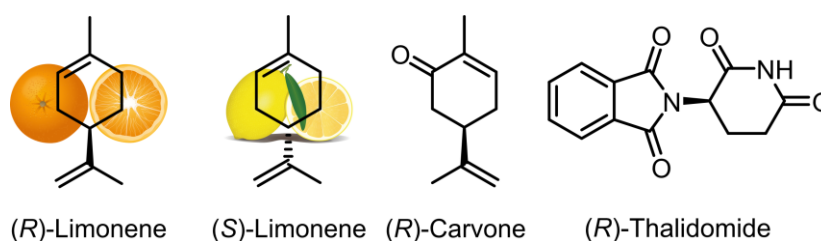


Figure 3. Chiral compounds whose enantiomers induce different physiological responses.

1.3 Asymmetric Hydrogenation

The activation of dihydrogen by transition metal catalysts is one of the most well-known transformations. Since the discovery of the Sabatier reaction,^[19] dihydrogen has been an attractive reducing agent and has been used extensively in the Haber-Bosch^[20] and the Fischer-Tropsch processes.^[21] After *Calvin* reported the catalytic hydrogenation of quinoline by copper(I) acetate,^[22] further homogeneous catalysts followed in the 1960s, when *Dutton* discovered cobalt- and iron carbonyls efficiently catalyse the hydrogenation of unsaturated fats (**Figure 4**, left).^[23] However, in terms of activity, these homogeneous catalysts fell behind contemporary heterogeneous systems. This changed in 1966, when *Wilkinson* reported the synthesis of chlorotris(triphenylphosphine) rhodium(I), which is a highly active homogeneous hydrogenation catalyst, rivalling its heterogeneous counterparts.^[24] This discovery piqued the interest of chemists looking to introduce enantioselectivity into hydrogenation catalysis.

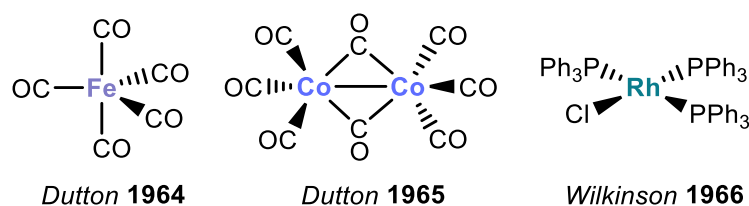


Figure 4. Early examples of homogeneous hydrogenation catalysts.

1.3.1 Initial Developments in Asymmetric Hydrogenation

In the 1960s, *Mislow* and *Horner* reported the synthesis of new optically active phosphines to modify the Wilkinson catalyst.^[25] Utilising either enantioenriched (*R*)- or (*S*)-methylpropylphenylphosphine as a ligand, *Knowles* and *Horner*, respectively, reported the asymmetric hydrogenation of olefins in 1968 (**Figure 5, A1**).^[26] Although the obtained enantiomeric excesses were rather low (1-15 % *ee*) and did not exceed those reported previously for other catalytic systems,^[27] these reports were notable due to the facile combination of such a well-defined catalyst with easily exchangeable chiral ligands. This, combined with the rising need for optically pure *L*-DOPA, which was used in treating Parkinson's disease, led to efforts to find more suitable ligands for asymmetric hydrogenation reactions.^[28]

Morrison and co-workers synthesised (–)-neomenthylidiphenylphosphine (**Figure 5, A2**), based on widely-available (–)-menthol.^[29] Employing this ligand in the rhodium catalysed hydrogenation of β -methylcinnamic acid rewarded them with enantiomeric excesses of up to 61%, the highest enantioinduction for any hydrogenation catalyst observed at that point. Only one year later, *Knowles* reported further chiral phosphines that efficiently induce enantioselectivities in the hydrogenation of α -acylaminoacids with enantiomeric excesses of up to 85% when using the chiral phosphine **A3**.^[30] In the same year, *Kagan* reported the first chelating bis(phosphine), (*R,R*)-DIOP (**A4**), used as a ligand in asymmetric hydrogenation reactions (**Figure 5**).^[31] The ligand was based on tartaric acid and yielded high enantioselectivities in the hydrogenation of α -acylaminoacids (70-80% *ee*).

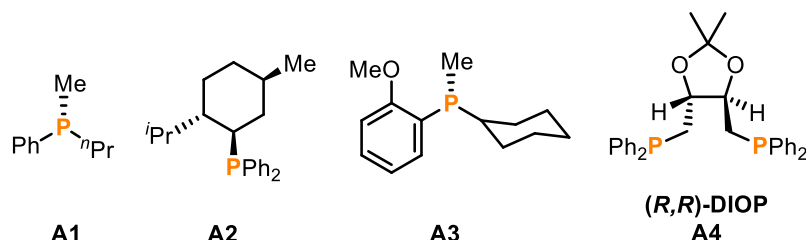
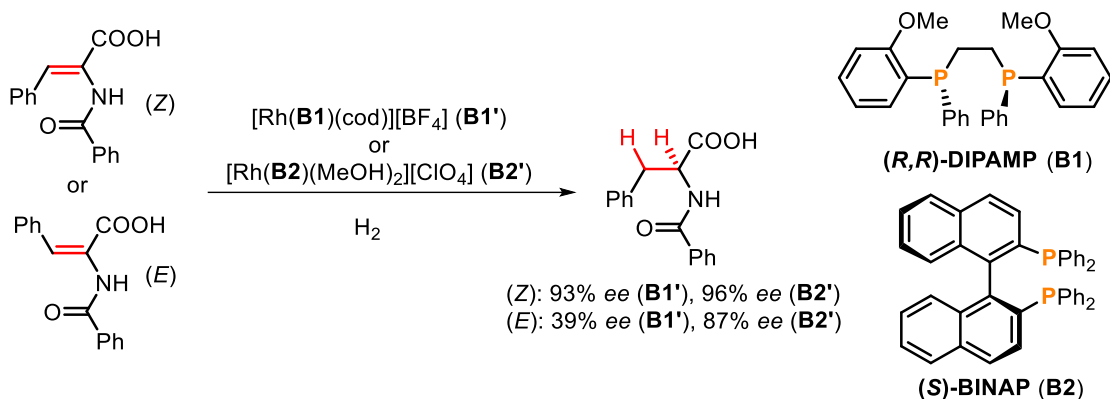


Figure 5. Chiral mono- and bidentate phosphine ligands developed as ligands for rhodium catalysed hydrogenation reactions.

The use of a chelating chiral ligand was then further investigated by *Knowles* and co-workers in 1977, when they synthesised (*R,R*)-DIPAMP (**B1**), a chiral bis(phosphine), by dimerising *o*-anisylmethylphenylphosphine (**Scheme 1**).^[32] High enantiomeric excesses of up to 96% were obtained upon employing **B1** in the hydrogenation of α -acylaminoacids. The enantioinduction, however, was highly dependent on the stereochemistry of the olefin substrate: the *Z*-isomer resulted in the desired selectivity, whilst the *E*-isomer yielded strongly diminished enantioinduction (93% *ee* vs. 39% *ee*). This problem was mitigated when *Noyori* and co-workers synthesised the bidentate phosphine ligand (*S*)-BINAP (**B2**) incorporating chirality into the ligand *via* the axial chirality of the binaphthyl moiety rather than through stereocenters (**Scheme 1**).^[33]



Scheme 1. Rhodium catalysed asymmetric hydrogenation of an α -acylaminoacid with DIPAMP and BINAP.

B2 was quickly observed to be an extraordinarily versatile ligand framework in the hydrogenation of olefins^[34] and ketones.^[35] The electronic and structural properties of **B2** can be tuned by modifying the substituents on the phosphorus atoms or the binaphthyl backbone. This allowed for the synthesis of a plethora of chiral bidentate phosphorus ligands (**Figure 6**). *Takaya* synthesised the partially hydrogenated H₈-BINAP (**Figure 6, B3**) in 1994.^[36] This electron-rich BINAP analogue was superior in the asymmetric hydrogenation of a β -ketoester as a ligand to Ru(OAc)₂ than its predecessor **B2**. *Saito* and co-workers observed that the hydrogenation products were obtained in a higher optical purity, when the BINAP complexes incorporated smaller dihedral angles.^[37] Therefore, they synthesised SegPhos (**Figure 6, B4**), which yielded an increased stereorecognition in the hydrogenation of various ketones when compared to BINAP. **B4** was also shown to selectively yield the desired enantioenriched amines in palladium catalysed imine hydrogenation reactions.^[38]

Since *Kagan's* discovery of an increased enantiomeric induction with chiral bidentate phosphines,^[31] monodentate phosphines were relatively neglected until *Reetz*^[39] and *Feringa*^[40] independently used the binaphthyl moiety to synthesise monodentate phosphines **B5** and **B6** in 2000 (**Figure 6**). These chiral phosphines were highly selective ligands in the rhodium catalysed hydrogenation of olefins.

Zhang and co-workers modified the binaphthyl moiety to synthesise *ortho*-substituted BINAPO ligands (**Figure 6, B7**).^[41] These ligands were observed to be especially effective in the hydrogenation of β -aryl substituted acrylates and β -keto esters.

The DuPhos and bis(phospholano)ethane (BPE) ligands discovered by *Burk* in 1991 are also a noteworthy class of chiral phosphine ligands (**Figure 6, B8 and B9**).^[42] These bidentate ligands exhibited remarkable activity combined with great enantioselectivity (up to 99% *ee*) in the asymmetric hydrogenation of α -acylaminoacids. In 1994, *Togni* and co-workers reported the synthesis of the 'JosiPhos' ligands (**Figure 6, B10**), derived from ferrocene, which bear both central and planar chirality, and were also effective in the asymmetric hydrogenation of olefins or β -ketoesters.^[43]

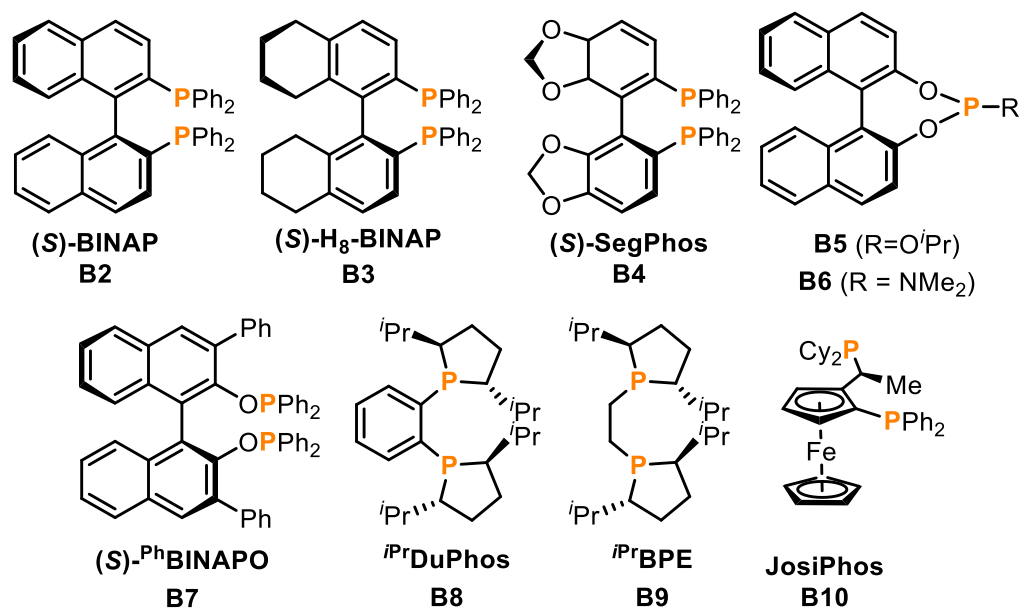
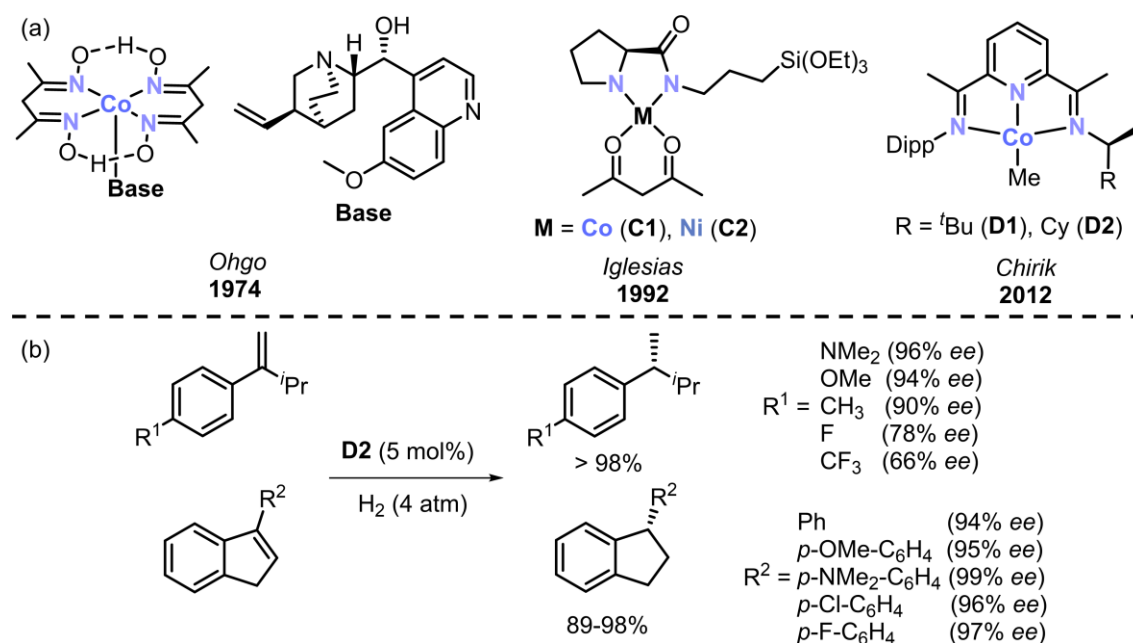


Figure 6. Developments in phosphine-based ligands used in asymmetric hydrogenation reactions.

1.3.2 Asymmetric Hydrogenation Reactions Catalysed by 3d Transition Metal Complexes

Since its discovery, homogeneous asymmetric hydrogenation catalysis has been dominated by 4d and 5d transition metals, such as rhodium, ruthenium and iridium.^[44] With regards to sustainability, however, recent advances have focused on more abundant 3d transition metals, such as iron and cobalt.^[45]



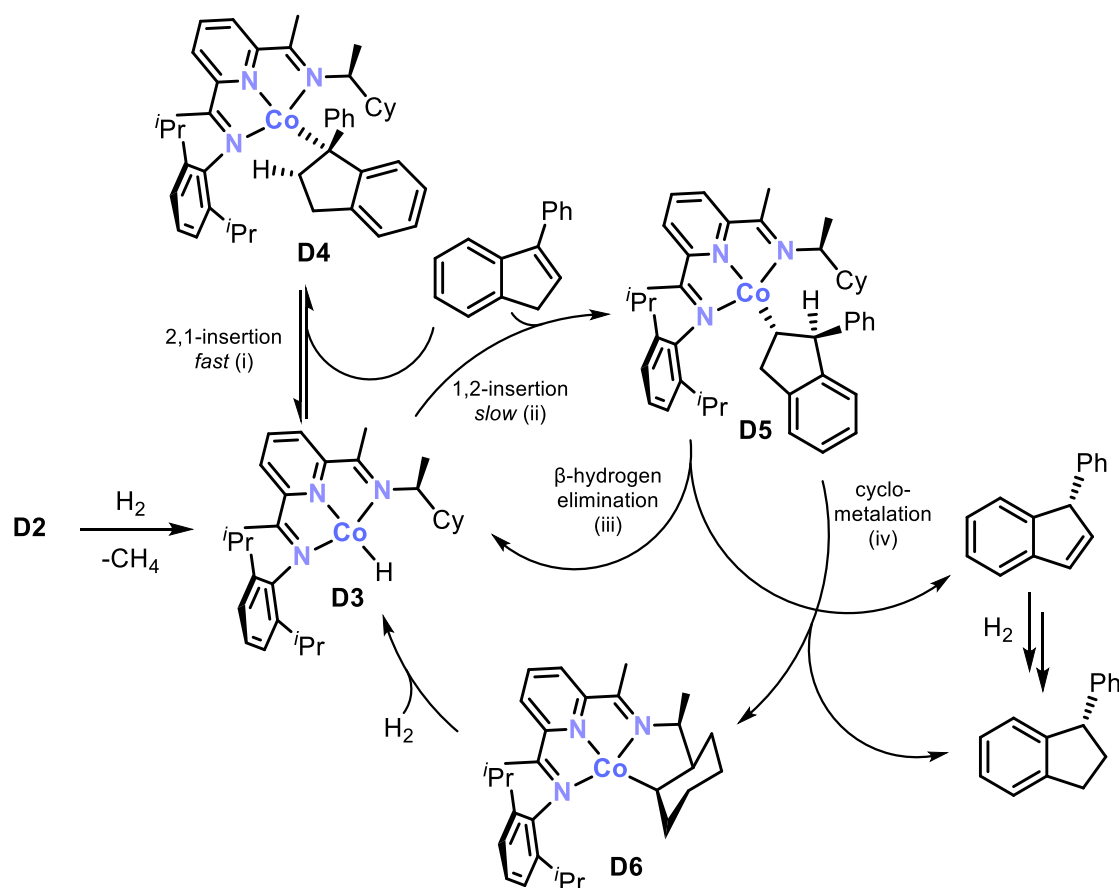
Scheme 2. Cobalt and nickel catalysts for asymmetric hydrogenation reactions (Dipp = 2,6-diisopropylphenyl) (a) and substituent-dependency of the asymmetric hydrogenation utilising D2 (b).

To the best of our knowledge, the first asymmetric hydrogenation reaction catalysed by homogeneous 3d transition metals was reported by Ohgo and co-workers in 1974 (Scheme 2a).^[46] They used an *in situ* generated bis(dimethylglyoximate) cobalt (II) complex together with naturally occurring amines as chiral bases in the asymmetric hydrogenation of ketones, yielding

moderate enantioselectivities for α -diketones (up to 62% *ee*) and α,β -unsaturated esters (up to 49% *ee*). In 1992, *Iglesias* reported cobalt and nickel complexes **C1** and **C2** (**Scheme 2a**) to be active catalysts in the asymmetric hydrogenation of α -acylaminoacids (60% and 69% *ee*, respectively).^[47] However, **C1** and **C2** still fell behind their ruthenium and rhodium analogues (cf. 76% and 92% *ee*, respectively).

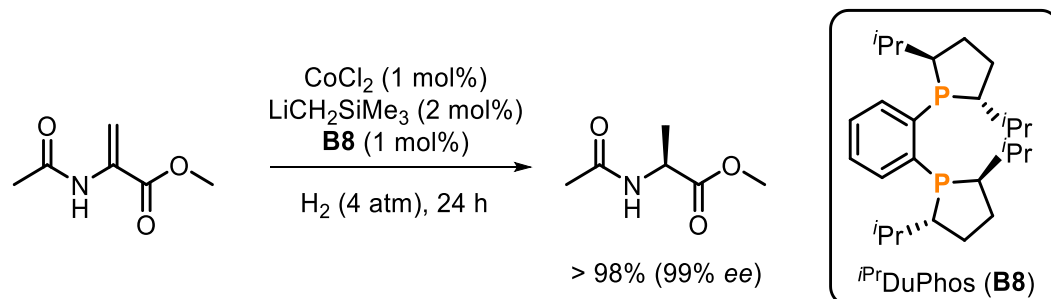
It took two decades until the first highly enantioselective cobalt catalysed asymmetric hydrogenation was developed in a seminal work by *Chirik* and co-workers (**Scheme 2a**).^[48] Using 5 mol% of the C_1 -symmetric bis(imino)pyridine cobalt complexes **D1** and **D2**, the hydrogenation of prochiral geminal disubstituted alkenes bearing one aryl and one alkyl substituent under 4 atm of H_2 was efficiently catalysed within 24 h (**Scheme 3b**). The best results were achieved when electron-donating groups (NMe_2 , OMe) were located at the *para*-position of the aryl substituent, whilst more electron-withdrawing groups (F , CF_3) yielded diminished enantioselectivities. In 2016, *Chirik* expanded the substrate scope of this system to trisubstituted alkenes, including indenenes and dihydronaphthalenes, yielding the reduced products in high enantioselectivities (91-99% *ee*) and generally good to high yields (41-98%) (**Scheme 2b**).^[49] Contrary to the asymmetric hydrogenation of disubstituted olefins with **D2**, both electron-donating and electron-withdrawing substituents were well-tolerated in the asymmetric hydrogenation of indenenes.

A reaction mechanism for the enantioselective hydrogenation of 3-phenyl-1*H*-indene with **D2** was proposed, supported by deuterium labeling experiments^[49] and quantum mechanical studies (**Scheme 3**).^[50] Upon reaction of **D2** with H_2 , the low-spin cobalt(II) hydride complex **D3** is formed, which acts as the resting state in the hydrogenation of hindered alkenes. Reaction of **D3** with the indene proceeds either *via* a fast and reversible 2,1-insertion (step i) to form **D4**, or through a slower 1,2-insertion (step ii) forming **D5**. The lower barrier for product release from **D5** relative to **D4** renders the 1,2-insertion (step ii) the productive pathway and acts as both the rate- and enantio-determining step. Alkyl complex **D5** undergoes a β -hydride elimination (step iii), to regenerate **D3** alongside a chiral olefin, which is then subsequently hydrogenated to yield the desired alkane. Alternatively, cyclometallation (step iv) of **D5** directly generates the chiral alkane together with metallacycle **D6**, which reacts with H_2 to regenerate cobalt hydride **D3**.



Scheme 3. Proposed catalytic mechanism for the asymmetric hydrogenation of 3-phenyl-1H-indene with **D2**.

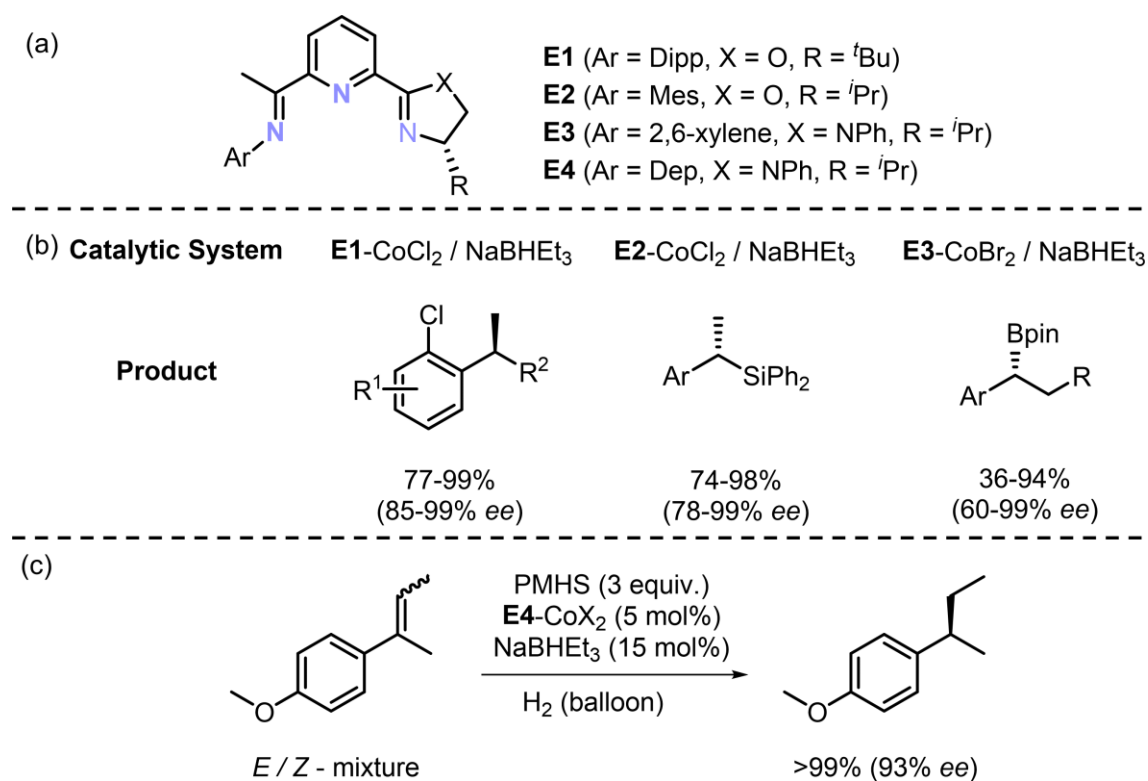
Chirik and co-workers also investigated the use of bidentate phosphines as ligands in cobalt catalysed hydrogenation reactions.^[51] Different combinations of commercially available cobalt(II) sources and chiral bidentate phosphines with various organometallic activators were applied to generate catalysts *in situ*, efficiently inducing high enantioselectivities in the hydrogenation of methyl 2-acetamidoacrylate (MAC). In particular, CoCl_2 activated by two equivalents of $\text{LiCH}_2\text{SiMe}_3$ exhibited a broad applicability with different, chiral phosphines (**Scheme 4**). The best results were obtained using $i^{\text{Pr}}\text{DuPhos}$ (**B8**), originally synthesised by Burk (*vide supra*).^[42] 1 mol% of $i^{\text{Pr}}\text{DuPhos}$ and CoCl_2 combined with 2 mol% of $\text{LiCH}_2\text{SiMe}_3$ allowed for the hydrogenation of MAC in near quantitative conversion and high enantioselectivity.



Scheme 4. Asymmetric hydrogenation of methyl 2-acetamidoacrylate (MAC) with a cobalt catalyst, formed *in situ*.

Similar to *Chirik's* bis(imino)pyridine ligand (see **D1** and **D2**, **Scheme 2a**), *Zhan* developed the chiral oxazoline iminopyridine **E1**, which was an effective ligand in the cobalt catalysed asymmetric hydrogenation of alkenes (**Scheme 5a**).^[52] This system was especially effective for *ortho*-chloro substituted aryl substituents, yielding the alkanes in high yields and enantioselectivities (**Scheme 5b**). Decreased enantioinduction was observed, when the chloride was exchanged with other substituents, such as fluoride (60% *ee*), methoxy (58% *ee*) or alkyl (80-84% *ee*) groups. The modified versions of **E1**, *i.e.* **E2** or **E3** led to efficient reduction of alkynes in cobalt catalysed, sequential hydrosilylation^[53] and hydroboration^[54] followed by asymmetric hydrogenation (**Scheme 6b**), as reported by *Zhan* and co-workers. The desired silane or borane was obtained in high regio- and enantioselectivity from the corresponding alkyne. In both one-pot procedures, the alkyne is initially reduced by the silane or the borane resulting in a vinyl silane or alkenyl boronic ester, respectively. These compounds are then subsequently hydrogenated by the reduced cobalt catalyst, yielding the desired silanes or boranes.

Zhan illustrated the versatility of these ligands by employing **E4** in one of the first enantioconvergent hydrogenations using minimally functionalised *E/Z*-olefin mixtures (**Scheme 5c**).^[55] Addition of silanes (Ph_2SiH_2 or polymethylhydrosiloxane, PMHS) further improved the good yields and enantioselectivities. While detailed mechanistic studies need to be performed, it was proposed that the cobalt alkyl species formed during the reaction can react either with H_2 or the silane. The reaction with silane is presumably more favourable and yields an unidentified cobalt-silane complex, which reacts with H_2 to regenerate both the silane and the initially formed cobalt hydride. The utility of this procedure was then demonstrated by the vast range of different olefins, of both the *E*- and the *Z*-isomers, which were hydrogenated with high enantioselectivities.

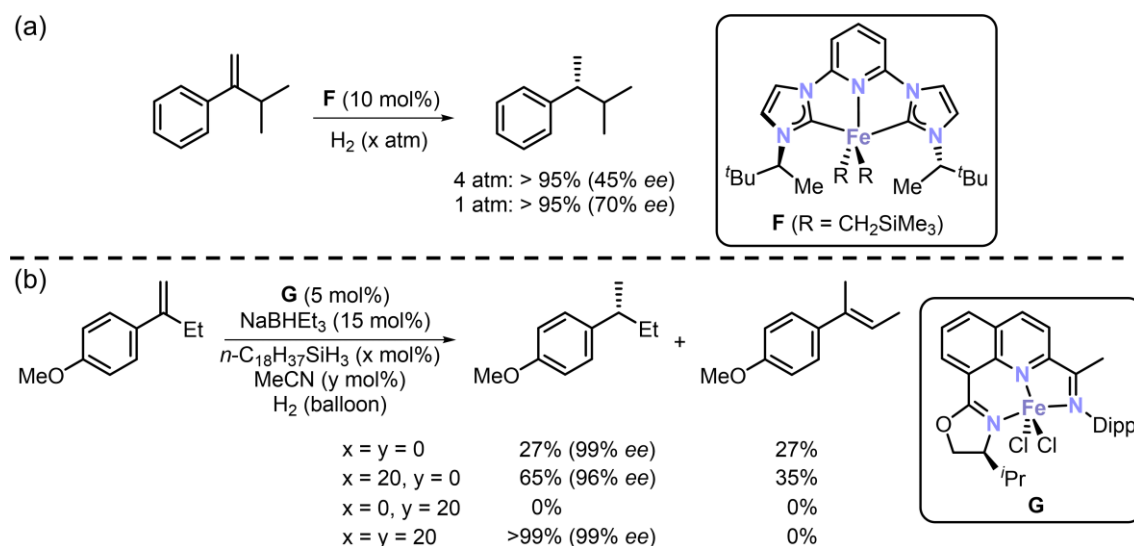


Scheme 5. Bis(imino) pyridine ligands (Mes = 2,4,6-trimethylphenyl, Dep = 2,6-diethylphenyl) (a) employed in cobalt catalysed asymmetric hydrogenation reactions (b, c).

Using iron-based catalysts is also of great interest in contemporary research. With its high abundancy in the Earth's crust (4.3 wt%), iron is cheap and readily available (~ 1800 times more abundant than Co).^[56] Although iron catalysed hydrogenation reactions have been known since the 1960s,^[57] employing iron in asymmetric hydrogenation reactions has remained challenging.^[58]

Contrasting corresponding cobalt-based systems,^[51] the application of chiral bidentate phosphine ligands in iron-based catalysts for asymmetric olefin hydrogenation was largely unsuccessful, attributed to the rapid formation of heterogeneous iron species.^[59] Only with the use of strong field tridentate pincer ligands, whose imine donors were replaced by N-heterocyclic carbenes (NHCs), did iron catalysed asymmetric hydrogenations of olefins first yield products in moderate to good enantioselectivities (**Scheme 7a**).^[60] Employing NHCs as strong σ -donors allowed the synthesis of iron (II) pincer complex **F**, which was an effective catalyst in the hydrogenation of selected minimally functionalised alkenes. Decreasing the H₂ pressure from 4 to 1 atm led to enantioselectivities of up to 70%, whilst high activity retained. However, even with the more stabilised iron complex **F**, decomposition to less enantioselective forms could not be excluded. In the same year, Zhan and co-workers independently reported a tridentate pincer ligand based on quinoline to efficiently promote the first highly asymmetric iron catalysed hydrogenation of olefins (**Scheme 6b**).^[61] Iron(II) complex **G**, reduced *in situ* with NaBHET₃, exhibited low activity (27% yield) but high enantioinduction (99% ee) in the hydrogenation of

2-(4-methoxyphenyl)-butene. The addition of catalytic amounts of octadecylsilane (20 mol%) increased the activity (67% yield), while retaining the high enantioinduction. Unfortunately, the silane also promoted the formation of the isomerisation product (see **Scheme 6b**). Addition of acetonitrile (20 mol%) suppressed the undesired isomerisation, which resulted in a catalytic system with both high activity (>99% yield) and enantioselectivity (99% *ee*). This system was applied to over 30 olefins generally yielding the products in high yields and great enantioselectivities (88-99% *ee*).

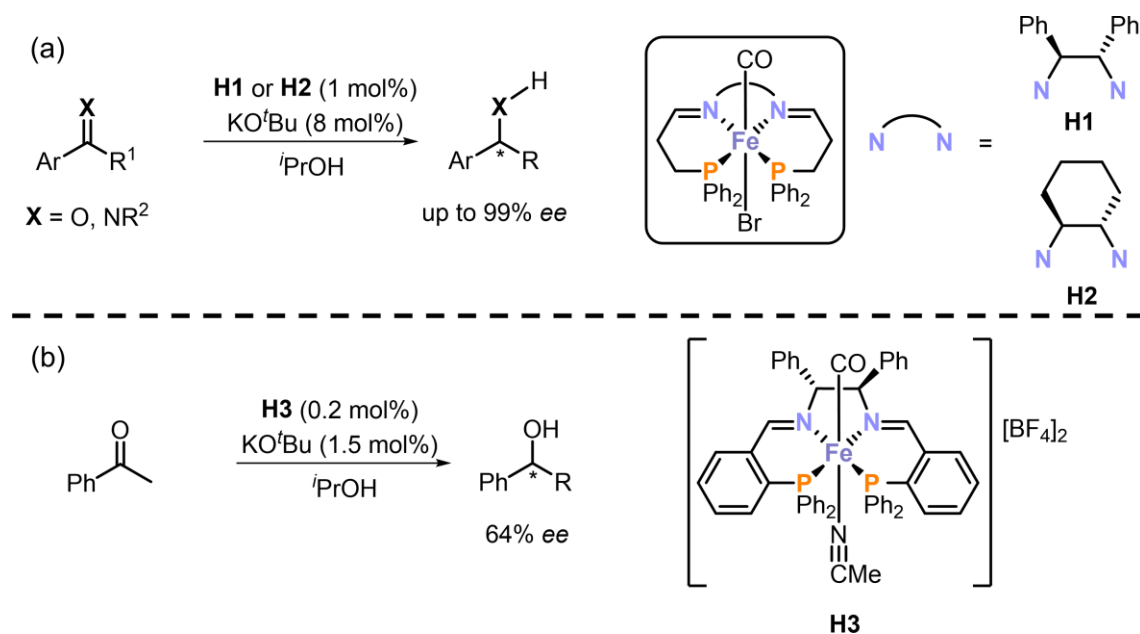


Scheme 6. First reports on good to highly asymmetric iron catalysed hydrogenation reactions of olefins reported by Chirik (a) and Zhan (b).

1.3.3 Enantioselective Transfer Hydrogenation Reactions Catalysed by 3d Transition Metals

Instead of using dihydrogen gas directly, hydrogenation reactions can also be facilitated using transfer reagents, such as *iso*-propanol, Hantzsch ester, or ammonia borane. Similar to “traditional” hydrogenations, 4d and 5d transition metals have received considerable attention as catalysts in transfer hydrogenation reactions.^[62] Nevertheless, recent years have seen an influx of reports in which base transition metals are successfully employed in asymmetric transfer hydrogenations, with the most prominent examples featuring polar substrates, such as ketones and imines.^[63,64] One fairly well-investigated catalytic system for the asymmetric transfer hydrogenation of ketones and imines is based on iron complexes **H1** and **H2** coordinated by chiral tetradentate PNNP ligands (**Scheme 7a**).^[65] The carbonyl ligand was found to be crucial to the activity of the complex, as replacing it with e.g. acetonitrile led to starkly decreased activities in transfer hydrogenation reactions. Introduction of one CO ligand, however, rendered the complexes highly active catalysts in the transfer hydrogenation of imines and ketones. After activation with KO^tBu, and using *iso*-propanol as hydrogen transfer reagent, the complexes successfully catalysed asymmetric transfer hydrogenations with great conversions (up to 99%) and high enantioselectivities (up to 99% *ee*). Morris and co-workers also investigated the catalytic activity of precatalyst **H3**, which after *in situ* reduction with KO^tBu readily catalysed the transfer

hydrogenation of acetophenone (**Scheme 7b**).^[66] Contrary to the homogeneous systems observed for **H1** and **H2**, STEM, SQUID and XPS analysis revealed the catalytically active species formed by the reduction of **H3** to be iron(0) nanoparticles. Interestingly, the desired alcohol was still obtained with moderate enantiodiscrimination (64% *ee*), which was presumed to occur *via* the interaction of the formed iron(0) nanoparticles with free chiral PNNP ligand.



Scheme 7. Asymmetric transfer hydrogenation of ketones and imines catalysed by iron PNNP complexes (a) or by iron(0) nanoparticles formed *in situ* (b).

Compared to their polar counterparts, (non-polar) olefins have received much less attention as unsaturated substrates for transition metal catalysed transfer hydrogenation reactions. Only recently has there been an increase in the number of reports of 3d transition metal complexes applied to catalysing transfer hydrogenation reactions of C=C double bonds (**Figure 7**). In 2013, *Peters* reported a tridentate cobalt(I) dinitrogen complex, which hydrogenated olefins using either H_2 or $\text{NMe}_2\text{H}\cdot\text{BH}_3$.^[67] *Tan* reported a cobalt(II) alkyl complex bearing a PNP pincer ligand that efficiently catalysed the transfer hydrogenation of aromatic and aliphatic alkenes using $i\text{PrOH}$ as the hydrogen transfer reagent.^[68] Two years later, *Renaud* and co-workers achieved the first transfer hydrogenation of α,β -unsaturated ketones using a base transition metal complex.^[69] Together with Cs_2CO_3 , their iron catalyst (see **Figure 7**). selectively hydrogenated olefins using *iso*-propanol. The Wolf group developed a cobalt 1,5-cyclooctadienyl complex bearing a bis(imino)acenaphthene (BIAN) ligand.^[70] Using NH_3BH_3 , this potassium cobaltate complex successfully catalysed the hydrogenation of different olefins and quinolines.

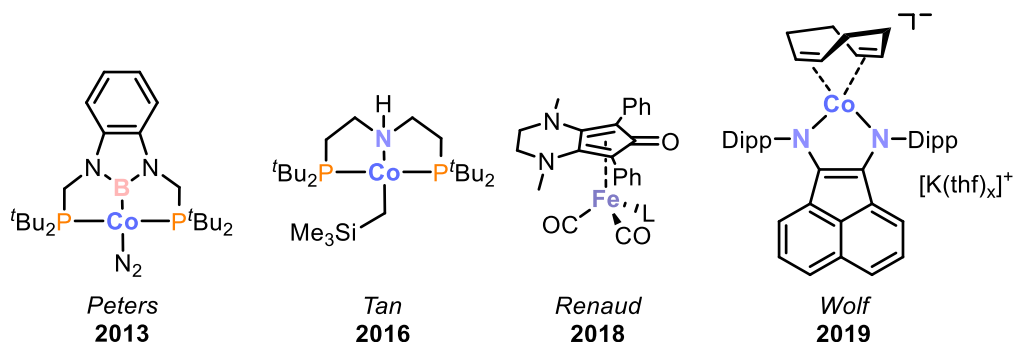
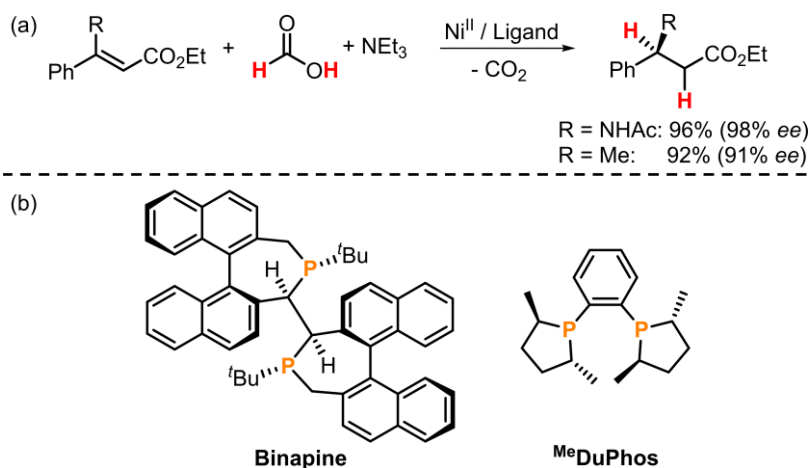


Figure 7. Recently developed 3d transition metal catalysts for the transfer hydrogenation of olefins (L = PPh₃, CO).

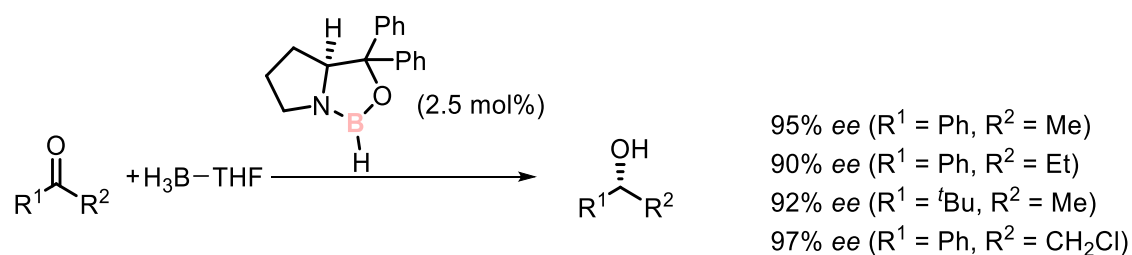
The asymmetric transfer hydrogenation of olefins catalysed by 3d transition metals, however, remained a very challenging task. Only one system reported by *Zhou* and co-workers is able to induce high enantioselectivity in the transfer hydrogenation of olefins (**Scheme 8**).^[71,72] They used the well-established 5:2 mixture of formic acid and triethylamine as a transfer hydrogenation reagent.^[63] Compared to *iso*-propanol, this mixture has the advantage of releasing gaseous carbon dioxide during the transfer hydrogenation, thus leading to an irreversible reaction and promoting the reduction of the unsaturated substrate. Due to the acidity of the mixture, however, decomposition of the catalyst occurred, a factor to be considered when using formic acid/triethylamine as transfer hydrogenation reagent.^[73] Whilst different cobalt, iron and copper precursors were unsuccessful as catalysts when used with the chiral phosphine ligand **Binapine**, high conversions (94-99%) and great enantioinduction (94-99% *ee*) were achieved in the synthesis of amino acids using nickel acetate as the metal precursor.^[71] This system was later expanded to conjugated olefins using NiBr₂(dme) (dme = 1,2-dimethoxyethane) and **MeDuPhos** as the catalytic system.^[72]



Scheme 8. Asymmetric transfer hydrogenation of α,β -unsaturated esters utilising formic acid (a) together with a nickel (II) catalyst and chiral bidentate phosphines (b).

1.4 Asymmetric Hydroboration of Ketones

The asymmetric hydroboration of unsaturated substrates is one of the most important asymmetric transformations providing a wide range of optically pure products.^[74] The formed chiral boranes are used as precursors for different chemical transformations. In the case of the hydroboration of ketones, however, the boranes are usually directly converted into the corresponding alcohols. Initially, enantioselective hydroborations of polar substrates were performed using boranes together with stoichiometric amounts of chiral auxiliaries, such as chiral alcohols or amines.^[75] One of the first examples of catalytic, asymmetric hydroboration of ketones was reported by *Corey, Bakshi and Shibata*.^[76] Using catalytic amounts of a chiral oxazaborole, the Corey-Bakshi-Shibata (CBS) catalyst, and $\text{BH}_3(\text{thf})$, the selective reduction of prochiral ketones to the corresponding alcohols was achieved in quantitative yield and high enantioselectivities (90-97% *ee*, **Scheme 9**). Since then, more catalysts ranging from transition metal complexes to main group-based compounds capable of catalysing the asymmetric hydroboration of polar substrates have surfaced, and some of them will be discussed hereafter.



Scheme 9. Asymmetric reduction of ketones with $\text{BH}_3\cdot(\text{thf})$ and the CBS catalyst.

1.4.1 3d Transition Metal Catalysed Asymmetric Hydroboration

In 1995, *Yamada and Mukaiyama* reported the asymmetric hydroboration of ketones using the chiral salen-based cobalt complex **I1** (**Figure 8**).^[77] Based on these results, they expanded the scope of the catalytic applications using slightly modified cobalt complexes to a plethora of substrates including benzophenones, lactones, diacyl-ferrocenes and imines.^[78] *Frejd* and co-workers reported the titanium catalyst **I2** to efficiently catalyse the hydroboration of ketones (**Figure 8, I2**).^[79] By combining a bicyclo[2.2.2]octane-2,6-diol (BODOL) ligand with $\text{Ti}(\text{O}^i\text{Pr})_4$ as the titanium(IV) precursor, aryl- and alkyl-substituted ketones were catalytically reduced in moderate to high enantioselectivities (20-96% *ee*). *Jeong* and co-workers synthesised a pyrazole-based ligand incorporating *L*-alaninemethyl ester as a chiral moiety.^[80] The zinc dichloride complex **I3**, carrying this ligand, effectively catalysed the hydroboration of acetophenone. However, as the chiral center is located in a remote position from the active metal site, only low enantioinduction was observed (21% *ee*). In 2003, *Cozzi* reported that the zinc complex **I4**, bearing a chiral iminoxazoline ligand, enantioselectively catalysed the hydroboration of aryl methyl ketones (86-93% *ee*).^[81] The sterically demanding trityl group at the imino moiety was proposed to cause the observed enantioinduction by preventing sideways coordination of the

borane, thereby forcing the reducing agent to approach the chiral pocket directly facing the active zinc site.

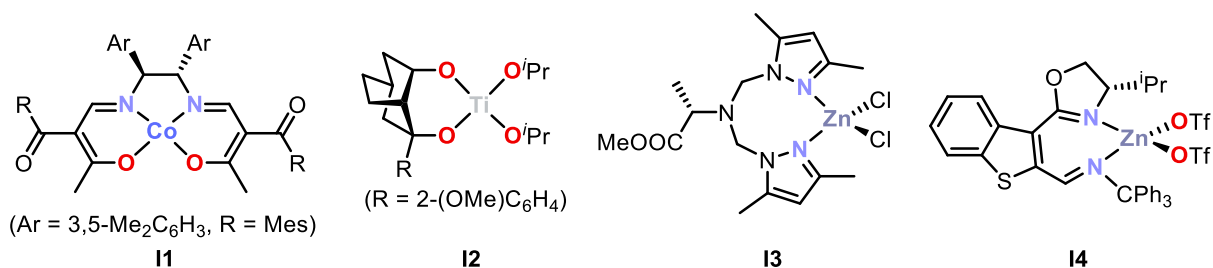
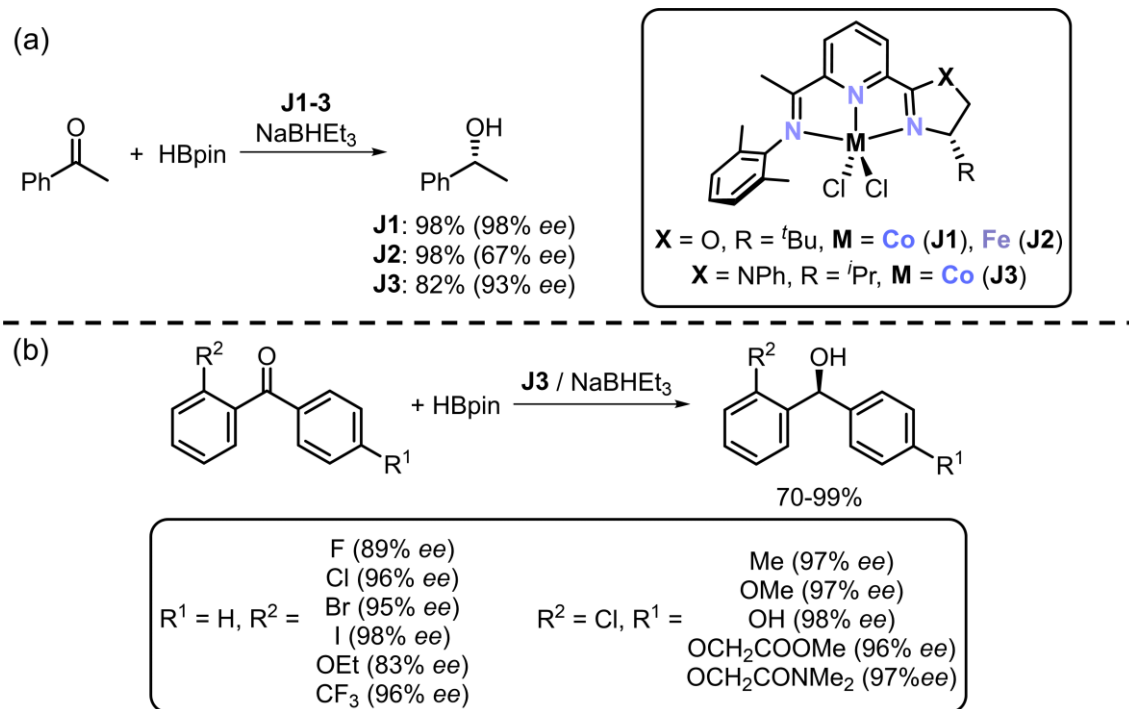


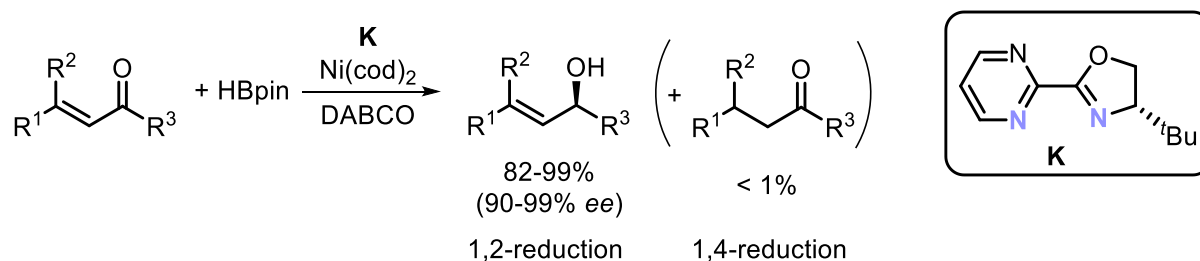
Figure 8. Early examples of first row transition metal complexes used in asymmetric hydroboration reactions.

More recently, *Lu* reported on *in situ* reduced chiral oxazoline iminopyridine based iron and cobalt dichlorides **J1** and **J2** to efficiently catalyse the enantioselective hydroboration of various aryl ketones (**Scheme 10a**).^[82] The corresponding alcohols were obtained either in good (67% *ee*) or high enantioselectivities with the base metal complexes **J2** and **J1**, respectively. Various ketones were successfully reduced using catalytic amounts of **J1** together with NaBHET₃ (2.5 mol%, each), providing the chiral alcohols in high enantioselectivities (91-99% *ee*) under mild conditions. By exchanging the oxazoline moiety with an imidazole ring, *Lu* and co-workers selectively obtained bisaryl substituted alcohols in high optical purities (89-98% *ee*).^[83] Similar to **J1**, the use of the cobalt catalyst **J3** retained high enantiodiscrimination whilst tolerating a wide range of functional groups including halogens, amines and alcohols (**Scheme 10b**).



Scheme 10. Cobalt- and iron catalysed asymmetric hydroboration of ketones (a) and benzophenone derivatives (b), HBpin = pinacolborane.

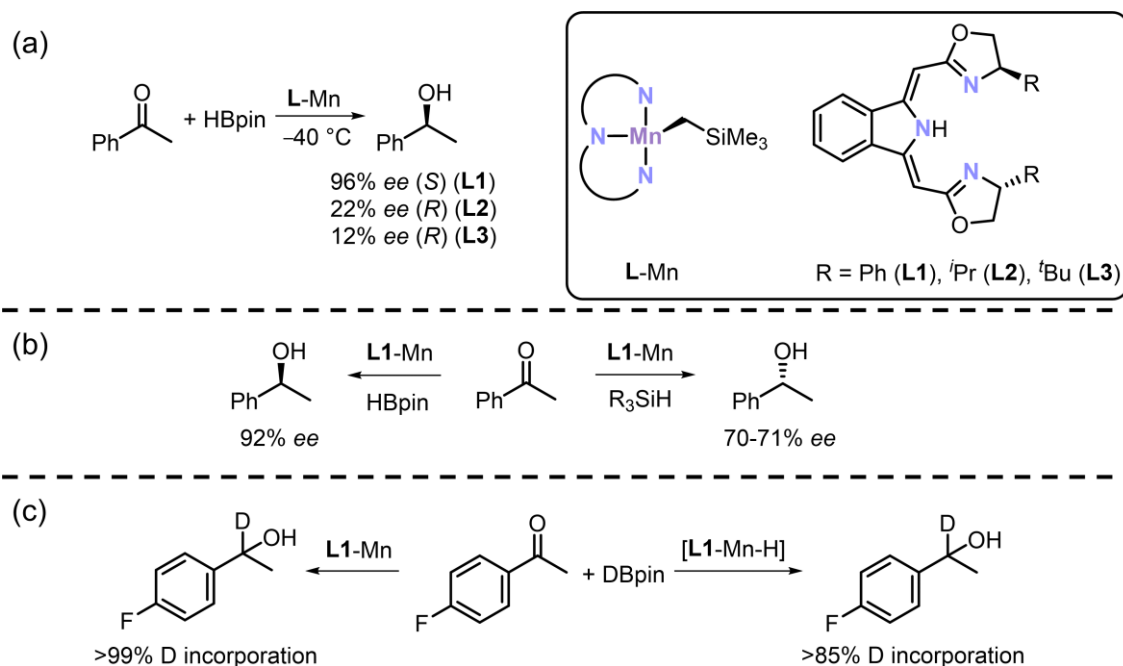
(Chiral) allylic alcohols are a common motif in natural products and pharmaceuticals. The synthesis of compounds containing this structural unit *via* asymmetric reduction of α,β -unsaturated ketones is often challenging due to the competing 1,4-reduction.^[84] Nevertheless, in 2017 *Zhu* and co-workers reported the enantioselective nickel catalysed 1,2-reduction of enones (**Scheme 11**).^[85] This was achieved by using the oxazoline-based ligand **K** with nickel bis(1,5-cyclooctadiene) and pinacolborane (HBpin) as the reducing reagent. This system selectively catalysed the hydroboration of the ketone moiety over the 1,4-reduction. The addition of stoichiometric amounts of DABCO increased both the selectivity for the 1,2-reduction and the enantiodiscrimination. Furthermore, the amine base suppresses the slow, uncatalysed reaction of HBpin with the enone substrate. The catalytic system efficiently yielded the desired allylic alcohols for a wide range of substrates in good yields (82-99%) and high optical purities (90-99% *ee*).



Scheme 11. First asymmetric nickel catalysed 1,2-reduction of α,β -unsaturated ketones.

In 2017, *Gade* reported the asymmetric hydroboration of ketones using alkyl manganese complexes bearing oxazoline based ligands **L1-L3** (**Scheme 12a**).^[86] Using **L1-Mn**, acetophenone was readily reduced to the corresponding alcohol with high enantioselectivity (96% *ee*) at -40°C . The products were obtained in drastically reduced optical purities when the chiral center of the ligand was altered to an *iso*-propyl (**L2**) or *tert*-butyl (**L3**) instead of a phenyl group (**L1**). Furthermore, whilst **L1-Mn** yielded the (*S*)-enantiomer, the opposite enantiomer was obtained when complexes **L2-Mn** and **L3-Mn** were used, hinting at the presence of two enantiodivergent pathways. When the reduction was performed with a hydrosilane instead of a borane, the manganese alkyl catalyst **L1-Mn** also yielded the (*R*)-enantiomer accompanied by a smaller enantioinduction (70% *ee*, **Scheme 12b**). Using HBpin and **L1-Mn**, the addition of stoichiometric (with regards to the substrate) amounts of tetramethylethylenediamine (TMEDA) led to decreased enantioselectivity for the (*S*)-enantiomer, with superstoichiometric amounts of TMEDA (100 equiv.) even switching the enantioselectivity from the (*S*)- to the (*R*)-enantiomer of the desired alcohol. The formation of a catalyst-borane adduct is either impossible or strongly hindered in both of these experiments either due to the absence of borane (when hydrosilanes are used as reducing reagent) or due to the complexation of borane by TMEDA. Therefore, the authors concluded that a catalyst-borane adduct is required in the enantiodivergent pathway leading to the (*S*)-enantiomer. Deuterium labelling experiments further strengthened this theory (**Scheme 12c**).

Full (>99%) deuterium incorporation at the chiral center was observed when the reaction was performed with DBpin, indicating that the borane is the only hydrogen source. As manganese hydrides can act as hydrogen transfer reagents and the reaction of HBpin with **L1-Mn** led to the formation of such a manganese hydride species (**[L1-Mn-H]**), the stoichiometric reaction with the complex **[L1-Mn-H]**, DBpin and ketone was performed. The product was isolated with only >85% D-incorporation, indicating a slow hydride transfer *via* the formed manganese hydride. Therefore, it was concluded that the desired enantiodivergent pathway yielding the (*S*)-enantiomer requires a hydrogen transfer through a borane-manganese adduct, whilst the direct hydride transfer *via* the manganese hydride is proposed to be the main step in the second pathway leading to the opposite enantiomer.

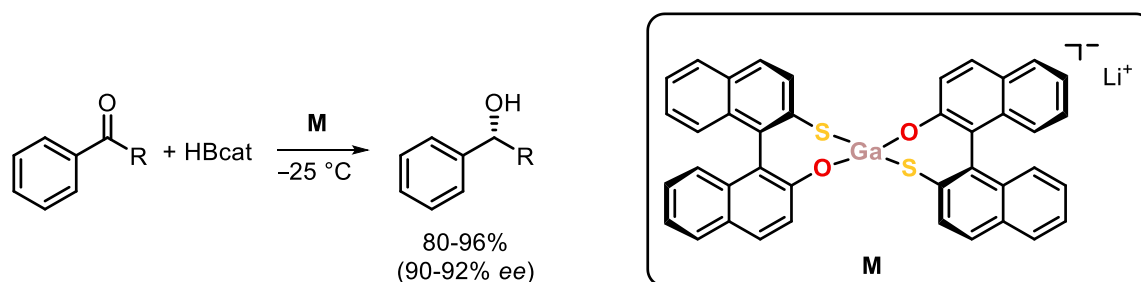


Scheme 12. Enantioselective hydroboration catalysed by manganese alkyl complexes, including ligand screening (a), screening of the hydrogen source (b) and deuterium-labelling experiments (c).

1.4.2 Main Group-Element Catalysed Asymmetric Hydroboration

In recent years an influx in main group metal catalysed hydroboration reactions of aldehydes and ketones has been observed.^[87-91] Enantioselective hydroboration reactions catalysed by main group elements are, however, still in their infancy. In 2000, *Woodward* reported one of the first main group catalysed highly asymmetric hydroboration reactions of ketones (**Scheme 13**).^[92] They investigated the catalytic activities of mixtures containing LiMH_4 ($M = \text{Al}, \text{Ga}$) and either (*R*)-[1,1'-binaphthalene]-2,2'-diol (BINOL) or a thiol-substituted BINOL derivative. The major problem to overcome in this reaction was to promote the selective release of the alkoxide generated from the ketone over the dissociation of the ligand. Whilst generally high yields (70-80%) were observed in all cases, only the anionic gallium(III) complex **M** yielded the desired alcohols in high optical purities (up to 92% *ee*) with catecholborane (HBcat) as the reducing agent.

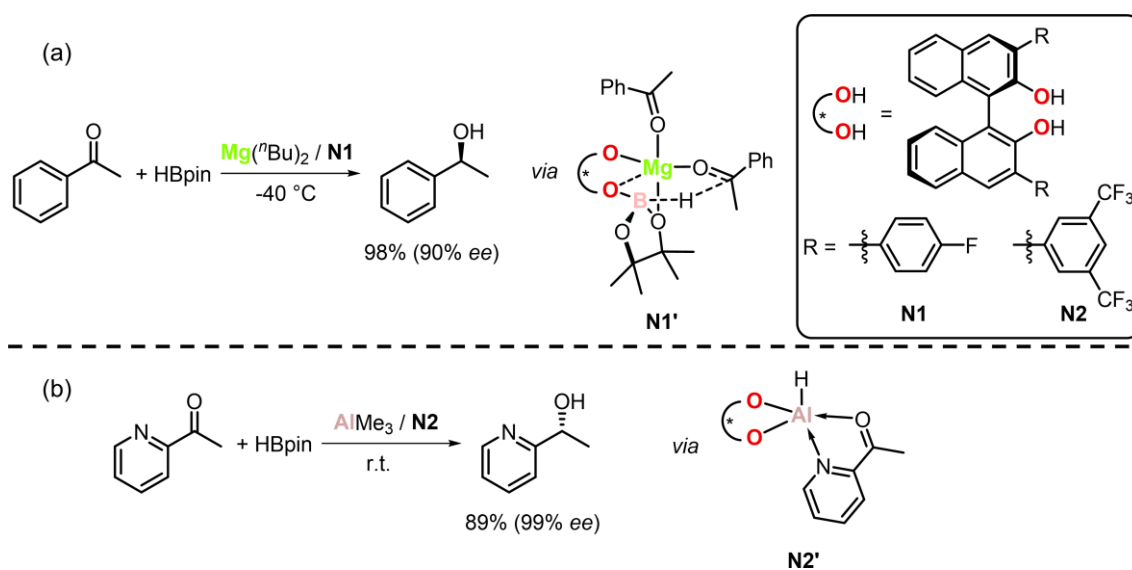
These observations were explained with *Pearson's* “hard/soft acid/base” (HSAB) principle.^[93] Dissociation of the ligand competing with release of the alkoxide product proved a major obstacle, and the combination of either a “hard” metal (aluminium) with a “hard” ligand (BINOL) or a “soft” metal (gallium) with the “softer” thiol-substituted BINOL derivative is preferred to avoid ligand dissociation. The alkoxide product, however, can also be considered “hard”, leading to a slower release of the ketone and increasing the rate of the ligand dissociation for a “hard/hard” metal/ligand system. This explains the poor performance of the aluminium/BINOL system when compared to the systems using gallium and the thiol-substituted BINOL with regard to enantioselectivity (6% vs. 72% *ee*). Using gallium(III) catalyst **M**, mixed aryl-alkyl ketones were reduced in good conversions with high enantioselectivities (up to 92% *ee*). Temperature both higher and lower than $-25\text{ }^{\circ}\text{C}$ led to decreased enantioselectivity. Whilst the decrease in optical purity can easily be explained for higher temperatures, at which thermodynamic over kinetic products are favoured, the decrease of enantioselectivity at lower temperatures was presumed to be due to a competing (non-enantioselective) mechanism. *Woodward* and co-workers suggested that a lithium alkoxide species might promote an achiral catalytic cycle, which was proven correct in 2011, when *Clark* and co-workers found that the related sodium *tert*-butoxide catalysed the hydroboration of acetophenone.^[94,95]



Scheme 13. Asymmetric hydroboration of ketones catalysed by the anionic gallium(III) complex **M**.

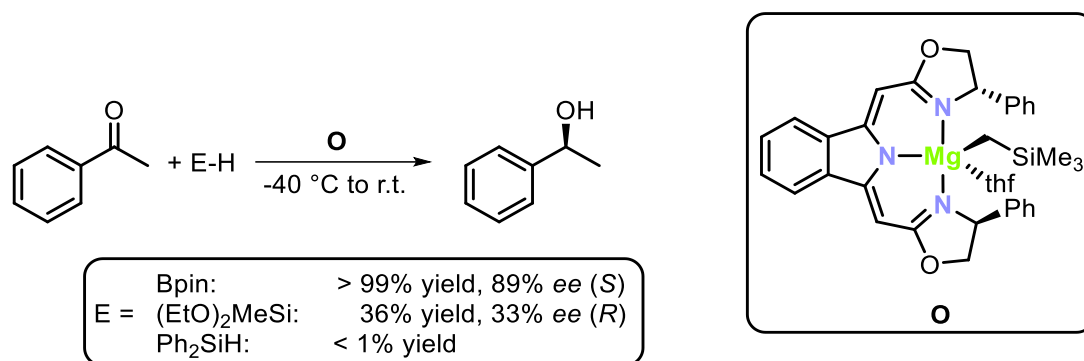
The first magnesium(II) catalysed asymmetric hydroboration was reported in 2019 by *Rueping* and co-workers (**Scheme 14a**).^[96] The *in situ* combination of the BINOL-derivative **N1** with di-*n*-butylmagnesium led to the formation of a catalytically active magnesium species, which efficiently reduced various ketones with HBpin, yielding the corresponding alcohols in high optical purities. This system, however, was limited to aryl-substituted ketones, as almost racemic mixtures of the corresponding alcohols were obtained upon using dialkyl ketones as substrates. Interestingly, the reaction of equimolar amounts of **N1**, Mg^nBu_2 and HBpin did not result in the formation of a magnesium hydride species, but complete consumption of the borane and the formation of a new boron species was observed. DFT calculations suggested that this species exhibits a dual Mg–O and B–O motif (**Scheme 14a**, **N1'**). The catalytic pathway commences with the coordination of **N** to Mg^nBu_2 , eliminating two equivalents of butane. The coordination of two ketone substrates proceeds in successive exergonic steps, after which the borane can approach *via* the aforementioned dual Mg–O and B–O bond coordination motif. The enantio- and rate-

determining step (**Scheme 14a**, **N1'**) is presumed to be the hydride transfer to one of the ketone substrates. The same group also reported the aluminium catalysed hydroboration of heterocyclic ketones using a combination of AlMe_3 and **N2**, a modified BINOL-based ligand (**Scheme 14b**).^[97] The selectivity of this reaction was highly dependent on the presence of the pyridine-moiety, as only low enantioinduction (20% *ee*) was detected upon using acetophenone as the substrate. This behaviour was explained by theoretical calculations, as the coordination of the pyridine-moiety to the aluminium centre is required for the formation of the proposed catalytically active species **N2'**. This system readily reduced various heterocyclic ketones displaying high activity (60-97% yield) and enantiodiscrimination (85-99% *ee*).



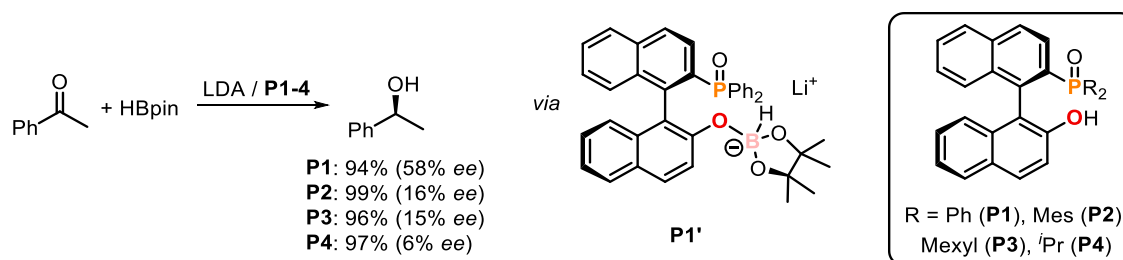
Scheme 14. Magnesium (a) and aluminium (b) catalysed enantioselective hydroboration of ketones.

In 2019, *Gade* reported the magnesium catalysed hydroboration of ketones using the bisoxazoline ligand **L1**, which was previously used in manganese catalysed enantioselective hydroboration reactions (*vide supra*).^[98] Reaction of **L1** and $\text{Mg}(\text{CH}_2\text{SiMe}_3)_2(\text{thf})$ resulted in the magnesium alkyl complex **O**, which catalysed the reduction of acetophenone using different reducing reagents (**Scheme 15**). Whilst the use of silanes generally resulted in reduced yields and low enantiodiscrimination (0% or 33% *ee*), full conversion combined with a high enantioenrichment (89% *ee*) was observed, when pinacolborane was used as the reducing reagent. The catalytic system exhibited a rather high robustness regarding the used solvent, yielding the desired alcohols in high optical purities in a variety of different solvents. The selectivity decreased only in MeCN (70% *ee*) or in the presence of strongly chelating TMEDA (10% *ee*). The system was unable to reduce epoxides, imines or alkenes, but aryl alkyl ketones were quantitatively reduced with generally high optical yields (90-98% *ee*), regardless of electron-donating or -withdrawing groups at the aryl substituent.



Scheme 15. Magnesium catalysed enantioselective hydrofunctionalisation of ketones.

Based on recent findings on alkali metal catalysed hydroboration reactions,^[87–91,94,95] Melen and co-workers investigated systems involving lithium bases together with BINOL derivatives (Scheme 16).^[99] BINOL derivatives with only one hydroxy group were tested in order to obtain a singly deprotonated lithium salt. In addition, the second hydroxy group was substituted by a phosphine oxide unit (P[O]R₂) to increase the stability of the alkali metal catalyst. The use of lithium diisopropylamide (LDA) combined with BINOL derivatives **P1-4** led to the successful hydroboration of acetophenone. However, the products were obtained in only moderate optical purities with **P1** (58% ee). Decreased enantiodiscrimination was observed when the lithium base was exchanged for LiO^tBu or LiH (40% or 36% ee, respectively) and when non-coordinating solvents were used. A range of aryl alkyl ketones were reduced using LDA/**P1** yielding the desired alcohols in good yields and low to moderate enantioselectivities (24–58% ee). The stoichiometric reaction of LDA, **P1** and HBpin led to the formation of two new products, a supposedly inactive borate species and a catalytically active lithiumborohydride (Scheme 16, **P1'**).

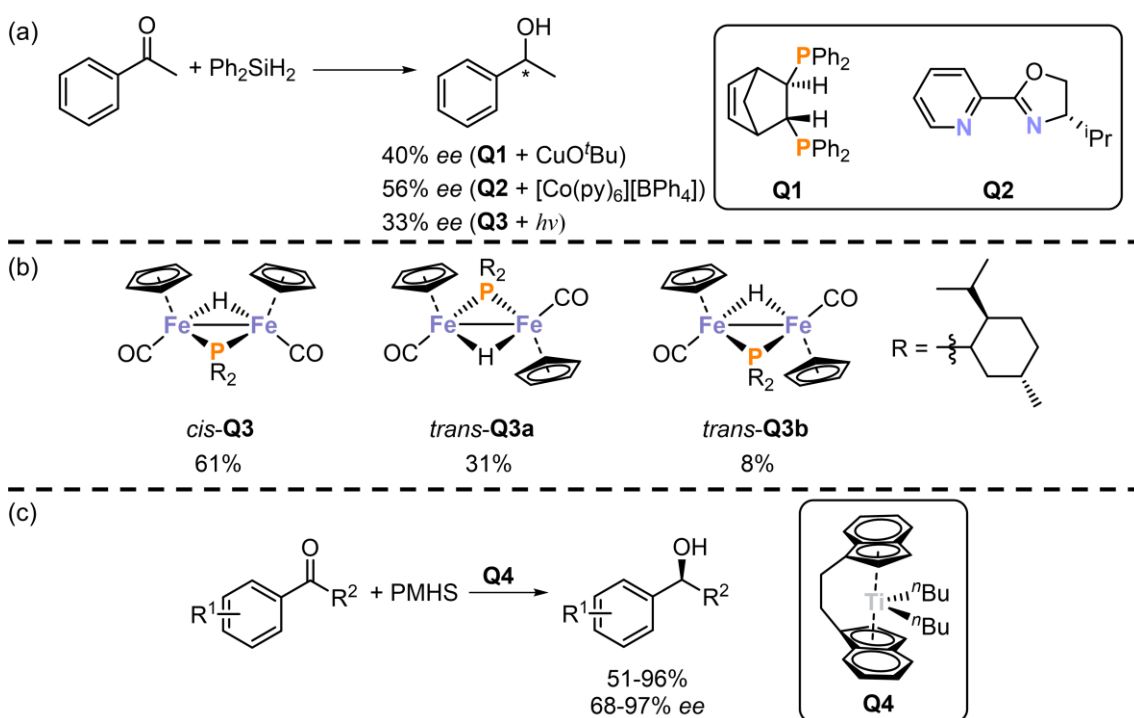
Scheme 16. Asymmetric hydroboration of acetophenone catalysed by LDA and **P1-4** (Mexyl = 3,5-dimethylphenyl).

1.5 Asymmetric Hydrosilylation of Polar Substrates

The addition of Si–H bonds to carbonyls and imines is an important transformation in the chemical industry. The resulting organosilanes find application in various areas, including as adhesives, lubricants or insulations.^[100] Furthermore, similar to boranes, these organosilanes can also be further functionalised by e.g. converting them into the corresponding alcohol or amine. In particular, asymmetric hydrosilylation has become an attractive strategy for the formation of enantiopure compounds.^[100–103]

1.5.1 3d Transition Metal Catalysts

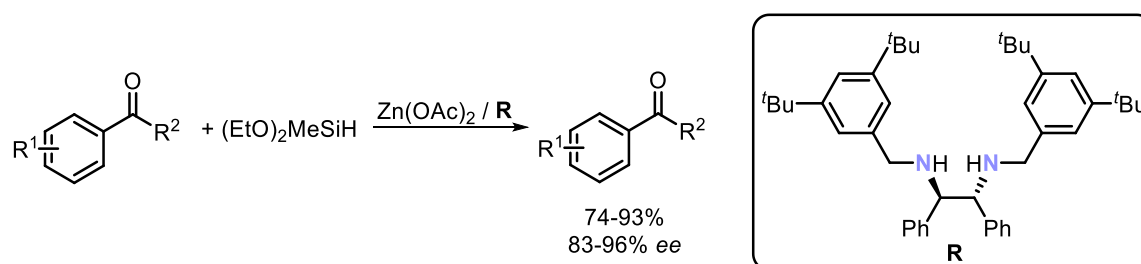
Whilst initial reports on asymmetric reductions of ketones *via* transition metal catalysed hydrosilylation reactions featured rhodium catalysts,^[104] the first 3d transition metal catalysed enantioselective hydrosilylation reactions were discovered shortly thereafter. In 1984, *Brunner* and co-workers studied combinations of copper *tert*-butoxide and chiral bidentate phosphine ligands in 3d transition metal catalysed asymmetric hydrosilylation reactions of ketones (**Scheme 17a**).^[105] However, only low enantiodiscrimination was observed for most systems. The best results were obtained with CuO^{*t*}Bu and ligand **Q1** in the hydrosilylation of acetophenone yielding the respective alcohol in moderate enantioselectivity (40% *ee*). The same group reported the first cobalt^[106] and iron^[107] catalysed asymmetric hydrosilylation reactions, respectively. They used [Co(py)₆][BPh₄] (py = pyridine) with different oxazoline based ligands in the reduction of acetophenone.^[106] It is noteworthy that chiral pyridinyloxazoline **Q2** bearing only one asymmetric carbon atom was observed to be the most effective, surpassing its C₂-symmetric bis(oxazoline) competitors by yielding the desired 1-phenylethanol with moderate enantioenrichment (56% *ee*). The iron complex *cis*-**Q3** was obtained from (+)-dimenthylphosphine and [CpFe(CO)₂]₂ and exhibited only very low activity in the hydrosilylation of acetophenone (**Scheme 17b**).^[107] Upon irradiation of *cis*-**Q3**, two *trans*-isomers were detected in the ¹H NMR spectrum in a ratio of 1 : 0.51 : 0.13 (*cis*-**Q3**:*trans*-**Q3a**:*trans*-**Q3b**). This irradiated mixture was then observed to be catalytically more active and result in slightly enantioenriched 1-phenylethanol (33% *ee*, see **Scheme 17a**).



Scheme 17. First asymmetric 3d transition metal catalysed asymmetric hydrosilylation reactions (a, c) and photo-induced isomerisation of *cis*-**Q3** (b).

The first highly enantioselective 3d transition metal catalysed hydrosilylation was reported in 1994 by *Buchwald* and co-workers (**Scheme 18**, c).^[108] Complex **Q4** is formed upon *in situ* activation of a chiral titanocene diolate with *n*-butyllithium. Reduction of **Q4** by polymethylhydrosiloxane (PMHS) then yields a titanium(III) hydride, postulated as the catalytically active species. Use of this catalyst enabled the efficient hydrosilylation of a wide range of substituted ketones in generally good yields and high enantioselectivities. Notably, high enantiodiscrimination was retained with substrates bearing alkoxy, alkyl or halide substituents (82-97% *ee*). A stark decrease in enantioselectivity was only observed when the strongly electron-withdrawing trifluoromethyl-group was used as a substituent (68% *ee*). Since then, numerous other 3d transition metal catalysts have been reported for asymmetric hydrosilylation reactions.^[100–103]

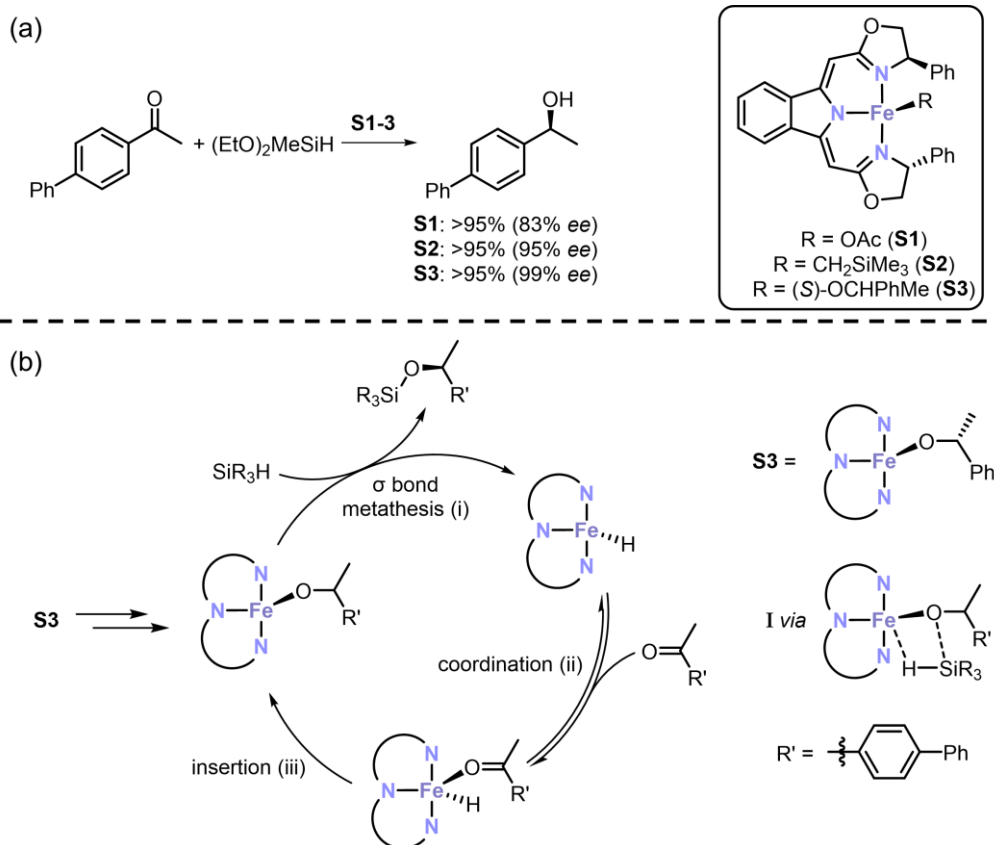
Based on the work of *Mimoun* and co-workers,^[109] *Mlynarski* reported highly enantioselective hydrosilylation reactions of ketones using zinc acetate in combination with a chiral diamine ligand (**Scheme 18**).^[110] Upon screening different amine ligands based on the (*R,R*)-diphenylethylene- or (*R,R*)-cyclohexyldiamine backbone, 3,5-di-*tert*-butylbenzyl substituted diamine **R** was found to be the most effective using (EtO)₂MeSiH as the reducing reagent. The catalytic activity of the system was dependent on the polarity of the solvent. Whilst less polar solvents, such as toluene, THF and DME resulted in full consumption of the ketone, decreased conversion or complete deactivation of the catalytic system was observed when more polar solvents such as CH₂Cl₂ (65%), DMF or MeOH (<1%) were used. Nevertheless, the enantiodiscrimination was independent of the solvent's polarity as can be seen by the highly enantioenriched product even in CH₂Cl₂ (93% *ee*). Whilst various aryl alkyl ketones were efficiently hydrosilylated with high optical purities (76-96% *ee*), the reduction of a dialkyl ketone yielded the corresponding alcohol as a racemate, highlighting the required aryl-substitution of the ketone substrate.



Scheme 18. Zinc catalysed highly enantioselective hydrosilylation of aryl alkyl ketones.

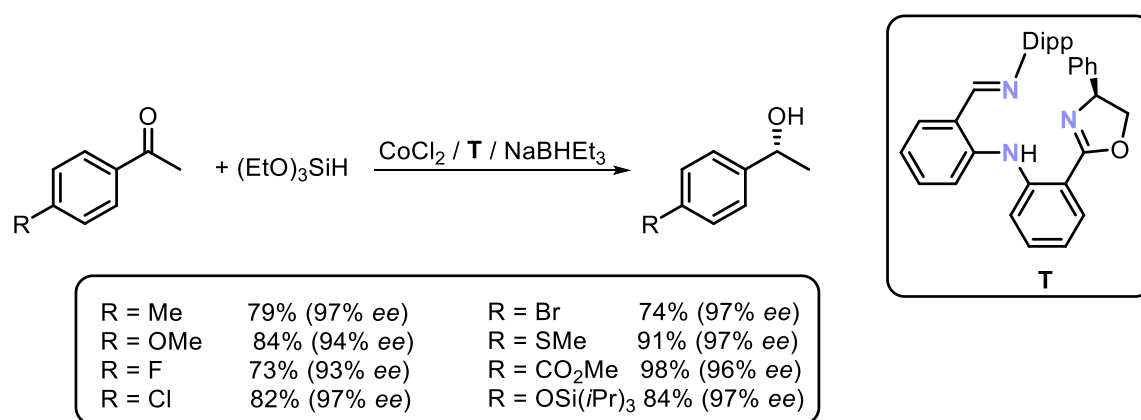
In 2015, *Gade* and co-workers reported the iron catalysed asymmetric hydrosilylation of ketones with both high activity and high enantiodiscrimination, rivalling noble metal catalysts (**Scheme 19a**).^[111] Utilising bis(oxazoline)-based ligand **L1** (*vide supra*), *Gade* investigated the iron complexes **S1-3** in the asymmetric hydrosilylation. The hydrosilylation catalysed by iron acetate complex **S1** required elevated temperatures of 65 °C and prolonged reaction times of 3 days in order to yield the desired alcohol with good enantioselectivity (84% *ee*), which was

common for iron catalysed hydrosilylation reactions. In contrast, the iron trimethylsilylmethyl complex **S2** efficiently catalysed the reaction at $-78\text{ }^{\circ}\text{C}$ within 6 h. This remarkable increase in activity was accompanied by a likewise increase in enantiodiscrimination (95% *ee*). The reaction of **S2** with (*S*)-1-phenylethanol yielded the iron alkoxide complex **S3**, which was presumed to be a key intermediate in the catalytic cycle. Its catalytic activity was investigated in the hydrosilylation of 4-phenylacetophenone and observed to be similar to **S2** with slightly enhanced enantioselectivity (99% *ee*). Whilst trialkyl silanes resulted in strongly reduced conversions and selectivity, using the cheap and readily available PMHS instead of $(\text{EtO})_2\text{MeSiH}$ resulted only in slightly reduced activity, retaining the high enantiodiscrimination (90% conversion, 93% *ee*). Generally, the high enantioselectivity was retained over a range of different solvents of different polarity, such as toluene, *n*-hexane, THF and Et_2O . Only in the strongly coordinating MeCN was a stark decrease in both activity and selectivity observed (7% conversion, 45% *ee*). Various ketones were selectively hydrosilylated using **S3** and $(\text{EtO})_2\text{MeSiH}$ at $-78\text{ }^{\circ}\text{C}$ within 6 h. The proposed catalytic pathway is based on mechanistic and theoretical studies (**Scheme 19b**).^[112] The proposed catalytic cycle includes the enantioselective σ -bond metathesis of the silane and an iron alkoxide complex as the rate-determining step (step i), furnishing the desired silyl ether together with a highly active iron hydride species. The latter is then successively coordinated by the ketone substrate (step ii), which then undergoes an irreversible Fe–H insertion (step iii), regenerating the iron alkoxide intermediate.



Scheme 19. Iron catalysed highly enantioselective hydrosilylation of 4-phenylacetophenone (a) and proposed catalytic pathway (b).

Recently, *Lu* reported very efficient asymmetric hydrosilylation of ketones catalysed by a cobalt complex supported by tridentate imino oxazoline **T** (**Scheme 20**).^[113] A combination of amine **T**, CoCl_2 , and NaBHET_3 efficiently reduced a plethora of aryl-substituted ketones with a wide functional group tolerance, including halide, alkoxide, ester and methyl thiol groups. Different aromatic substituents, such as naphthalene, benzofuran or benzothiophene based ring systems, were also tolerated, yielding the desired alcohol with high enantiodiscrimination (90-99% *ee*). NaBHET_3 was postulated as deprotonating the **T**- CoCl_2 complex, which then reacts with the silane to form a cobalt hydride species. This hydride species was then proposed to react in a similar fashion as the iron hydride complex described previously (**Scheme 19b**). After coordination and subsequent insertion of the ketone into the Co-H bond, a σ -bond metathesis of the generated cobalt alkoxide and the silane regenerates the cobalt hydride and yields the chiral silyl ether.



Scheme 20. Enantioselective cobalt catalysed hydrosilylation of ketones.

1.5.2 Main Group Element-based Catalysts

Main group compounds are a highly sought-after alternative for precious metals as catalysts due to their high abundance and low costs. The first asymmetric hydrosilylation catalysed by a main group compound was reported in 1988 by *Hosomi* and co-workers.^[114] By combining $n\text{BuLi}$ with optically active diols or amino alcohols as chiral auxiliaries, good enantioselectivities were observed in the hydrosilylation of acetophenone (up to 77% *ee*). The selectivity, however, was very dependent on the substrate with only a few ketones leading to moderate optical purities. This concept has been developed further by other groups with varying degrees of success.^[115] The main drawback of this system is that the alkoxides formed by the reduction of the ketones can also act as (less or non-enantioselective) Lewis base catalysts, which eventually limits the enantioselectivity (*vide supra*).

Main group metal catalysed hydrosilylation reactions have been reported with magnesium,^[116] calcium,^[117] tin,^[118] lithium^[119] and potassium^[120] among others.^[121] Nevertheless, main group element catalysed hydrosilylation reactions are still in their infancy with only a limited number of reports on asymmetric variants of this transformation.^[122]

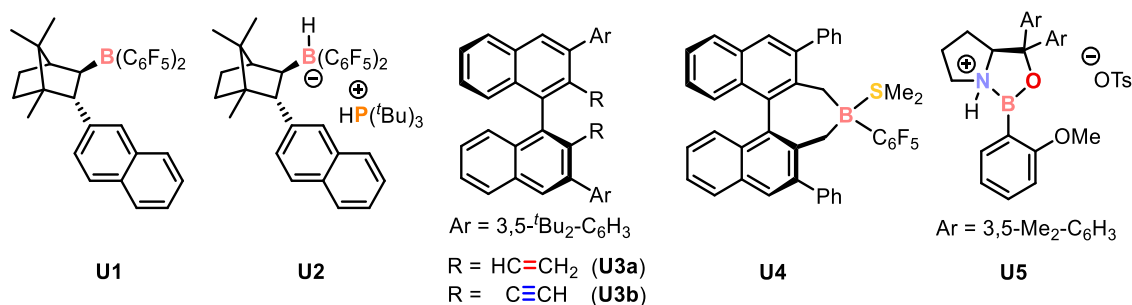


Figure 9. Chiral boron catalysts and dienes/diyne used in enantioselective boron catalysed hydrosilylation reactions.

Based on Piers' borane, $\text{HB}(\text{C}_6\text{F}_5)_2$,^[123] Klankermayer and co-workers reported the synthesis of the chiral camphor-based borane **U1** (Figure 9).^[124] Although **U1** efficiently catalysed the hydrosilylation of prochiral imines at ambient conditions, the corresponding amines were generated as racemic mixtures. The addition of a phosphine (PMes_3 or P^tBu_3) rendered the transformation enantioselective (63% or 79% *ee*, respectively) albeit at the cost of significantly decreased activity. Slightly higher enantioselectivity was observed when the isolated dihydrogen activation product of the borane-phosphine Lewis pair (**U2**) was used as the catalyst (up to 87% *ee*).

In 2014, Du and co-workers used Piers' borane in combination with the chiral diene **U3a** in the asymmetric hydrosilylation of imines.^[125] This system, however, only yielded the products in moderate to good enantioselectivities (44-82% *ee*). Thus, an improved system was developed by the addition of a phosphine base (PCy_3) and exchange of the chiral diene additive with the respective diyne auxiliary (**U3b**).^[126] This strongly increased both the activity and enantioselectivity, enabling the hydrosilylation of various 1,2-diketones and α -keto esters in high yields and great enantioselectivities (86-99% *ee*) at 60 °C.

Oestreich and co-workers synthesised the axially chiral borane **U4**, which catalyses the enantioselective reduction of aryl substituted ketones.^[127] Different silanes were tested as the reducing reagents and whilst sterically hindered di- and trisubstituted silanes were mostly not successful, the use of less hindered silanes led to good activity combined with high enantiodiscrimination (70-99% *ee*). The system tolerated electron-withdrawing groups, however, a stark decrease in enantioselectivity was observed upon introducing electron-donating or sterically demanding substituents at the ketone substrate.

Another Lewis acid, the chiral oxazaborolidinium salt **U5**, was successfully employed in asymmetric hydrosilylation reactions by Ryu and co-workers in 2017.^[128] Using PhMe_2SiH as the reducing reagent, **U5** selectively catalysed the hydrosilylation of acetophenone derivatives with great enantiodiscrimination (85-99% *ee*). **U5** exhibited high robustness against electron-withdrawing substituents and, in contrast to Oestreich's system (*vide supra*), only a slight loss in selectivity was observed for electron rich ketone substrates (88% *ee*). The major

drawback of **U5**, however, is the high catalyst loading of 20 mol% required (in contrast to only 2.4 mol% of **U4** used in *Oestreich's* system).

In summary, this section highlights the need for further research towards main group metal catalysed asymmetric hydrosilylation reactions, which is evident by the absence of any known highly enantioselective (earth) alkali metal catalysts.

1.6 Conclusion

From *Haiiy's* first observation of chiral quartz crystals, through *Pasteur's* chiral resolution and the Le Bel-van't Hoff rule to the still used CIP-convention, various discoveries helped to understand the concept of chirality in chemistry as well as its importance in nature. As all known living organisms contain amino acids and are thus chiral, they can react differently to opposing enantiomers, which renders the targeted synthesis of one enantiomer of great importance. Discovering catalytic systems for hydrofunctionalisation reactions, which are some of the most widely used transformations featuring the addition of an E–H bond (E = B, Si, H) to an unsaturated compound, has therefore been a major goal since the realisation of the importance of chirality in the middle of the 20th century. Starting with *Knowle's* rhodium catalysed hydrogenation of an *L*-DOPA precursor, the last 50 years have seen rapid progress towards highly enantioselective hydrofunctionalisation reactions. Whilst 4d and 5d metals were used almost exclusively in the beginning, contemporary research has shifted towards more sustainable 3d and main group metal based catalytic systems. Over recent years, numerous 3d transition metal and main group complexes have emerged which are able to efficiently catalyse hydrofunctionalisation reactions with high enantiodiscrimination. Nonetheless, catalysts rivalling the established precious metal catalysts in terms of activity and selectivity are still scarce. Therefore, further research towards 3d transition metal and main group metal catalysed hydrofunctionalisation reactions is required to further improve our understanding of this area, which is the topic of *Chapters 2-4*. *Chapter 5* of this thesis has a disparate topic, describing the synthesis of new transition metallate-phosphinine complexes.

References

- [1] V. Gold *The IUPAC Compendium of Chemical Terminology*, International Union of Pure and Applied Chemistry (IUPAC), **2019**.
- [2] G. P. Moss, *Pure Appl. Chem.* **1996**, *68*, 2193–2222.
- [3] E. L. Malus, *Théorie de la double réfraction de la lumière dans les substances cristallisées*, Baudouin, Paris, **1810**.
- [4] M. Arago in *Mémoires de la classe des sciences mathématiques et physiques de l'institut impérial*, Baudouin, Paris, **1811**, 97–134.
- [5] M. Biot in *Mémoires de la classe des sciences mathématiques et physiques de l'institut impérial*, Baudouin, Paris, **1811**, 135–280.
- [6] J. F. W. Herschel, *Trans. Cambridge Philos. Soc.* **1822**, 43–52.
- [7] L. Pasteur, *C. R. Acad. Sci.* **1848**, *26*, 535–538.
- [8] J. H. van't Hoff in *Archives néerlandaises des sciences exactes et naturelles*, Nijhoff, Den Haag, **1874**, 445–454.
- [9] J.-A. Le Bel, *Bull. Soc. chim. Fr.* **1874**, *2*, 337–347.
- [10] A. Werner, *Chem. Ber.* **1911**, *44*, 1887–1898.
- [11] A. Guijarro, M. Yus, *The origin of chirality in the molecules of life. A revision from awareness to the current theories and perspectives of this unsolved problem*, Royal Society of Chemistry, Cambridge, **2009**.
- [12] M. Inaki, J. Liu, K. Matsuno, *Philos. Trans. R. Soc. B* **2016**, 371.
- [13] S. H. Wilen, *Stereochemistry of organic compounds*, Wiley, New York, **1994**.
- [14] L. Friedman, J. G. Miller, *Science* **1971**, *172*, 1044–1046.
- [15] I. Blank, W. Grosch, *J. Food Sci.* **1991**, *56*, 63–67.
- [16] G. F. Russell, J. I. Hills, *Science* **1971**, *172*, 1043–1044.
- [17] W. Sneader, *Drug discovery: A history*, Wiley, Chichester, **2005**.
- [18] T. Eriksson, S. Björkman, B. Roth, A. Fyge, P. Höglund, *Chirality* **1995**, *7*, 44–52.
- [19] S. Rönsch, J. Schneider, S. Matthischke, M. Schlüter, M. Götz, J. Lefebvre, P. Prabhakaran, S. Bajohr, *Fuel* **2016**, *166*, 276–296.
- [20] C. Smith, A. K. Hill, L. Torrente-Murciano, *Energy Environ. Sci.* **2020**, *13*, 331–344.
- [21] F. Fischer, H. Tropsch, *Ber. Dtsch. Chem. Ges.* **1926**, *59*, 830–831.
- [22] M. Calvin, *J. Am. Chem. Soc.* **1939**, *61*, 2230–2234.
- [23] a) E. N. Frankel, E. P. Jones, V. L. Davison, E. Emken, H. J. Dutton, *J. Am. Oil Chem. Soc.* **1965**, *42*, 130–134; b) E. N. Frankel, H. M. Peters, E. P. Jones, H. J. Dutton, *J. Am. Oil Chem. Soc.* **1964**, *41*, 186–191.
- [24] J. A. Osborn, F. H. Jardine, J. F. Young, G. Wilkinson, *J. Chem. Soc. A* **1966**, 1711.
- [25] a) L. Horner, H. Winkler, A. Rapp, A. Mentrup, H. Hoffmann, P. Beck, *Tetrahedron Lett.* **1961**, *2*, 161–166; b) O. Korpiun, R. A. Lewis, J. Chickos, K. Mislow, *J. Am. Chem. Soc.* **1968**, *90*, 4842–4846; c) O. Korpiun, K. Mislow, *J. Am. Chem. Soc.* **1967**, *89*, 4784–4786.
- [26] a) L. Horner, H. Siegel, H. Büthe, *Angew. Chem. Int. Ed.* **1968**, *7*, 942; b) W. S. Knowles, M. J. Sabacky, *Chem. Commun. (London)* **1968**, 1445.
- [27] a) F. Higashi, T. Ninomiya, Y. Izumi, *Bull. Chem. Soc. Jpn.* **1971**, *44*, 1333–1336; b) S. Tatsumi, *Bull. Chem. Soc. Jpn.* **1968**, *41*, 408–418; c) S. Tsuboyama, *Bull. Chem. Soc. Jpn.* **1966**, *39*, 698–702.
- [28] W. S. Knowles, *Angew. Chem. Int. Ed.* **2002**, *41*, 1998.
- [29] J. D. Morrison, R. E. Burnett, A. M. Aguiar, C. J. Morrow, C. Phillips, *J. Am. Chem. Soc.* **1971**, *93*, 1301–1303.
- [30] W. S. Knowles, M. J. Sabacky, B. D. Vineyard, *J. Chem. Soc., Chem. Commun.* **1972**, 10.
- [31] H. B. Kagan, T.-P. Dang, *J. Am. Chem. Soc.* **1972**, *94*, 6429–6433.
- [32] B. D. Vineyard, W. S. Knowles, M. J. Sabacky, G. L. Bachman, D. J. Weinkauff, *J. Am. Chem. Soc.* **1977**, *99*, 5946–5952.
- [33] A. Miyashita, A. Yasuda, H. Takaya, K. Toriumi, T. Ito, T. Souchi, R. Noyori, *J. Am. Chem. Soc.* **1980**, *102*, 7932–7934.
- [34] a) M. Kitamura, Y. Hsiao, R. Noyori, H. Takaya, *Tetrahedron Lett.* **1987**, *28*, 4829–4832; b) W. D. Lubell, M. Kitamura, R. Noyori, *Tetrahedron Asymmetry* **1991**, *2*, 543–554; c) A. Miyashita, H. Takaya, T. Souchi, R. Noyori, *Tetrahedron* **1984**, *40*, 1245–1253; d) R. Noyori, M. Ohta, Y. Hsiao, M. Kitamura, T. Ohta, H. Takaya, *J. Am. Chem. Soc.* **1986**, *108*, 7117–7119; e) H. Takaya, T. Ohta, N. Sayo, H. Kumobayashi, S. Akutagawa, S. Inoue, I. Kasahara, R. Noyori, *J. Am. Chem. Soc.* **1987**, *109*, 1596–1597.
- [35] a) M. Kitamura, T. Ohkuma, S. Inoue, N. Sayo, H. Kumobayashi, S. Akutagawa, T. Ohta, H. Takaya, R. Noyori, *J. Am. Chem. Soc.* **1988**, *110*, 629–631; b) R. Noyori, T. Ohkuma, M. Kitamura, H. Takaya, N. Sayo, H. Kumobayashi, S. Akutagawa, *J. Am. Chem. Soc.* **1987**, *109*, 5856–5858; c) T. Ohkuma, H. Ooka, S. Hashiguchi, T. Ikariya, R. Noyori, *J. Am. Chem. Soc.* **1995**, *117*, 2675–2676.
- [36] X. Zhang, K. Mashima, K. Koyano, N. Sayo, H. Kumobayashi, S. Akutagawa, H. Takaya, *J. Chem. Soc., Perkin Trans. 1* **1994**, *89*, 2309–2322.
- [37] T. Saito, T. Yokozawa, T. Ishizaki, T. Moroi, N. Sayo, T. Miura, H. Kumobayashi, *Adv. Synth. Catal.* **2001**, *343*, 264–267.
- [38] Y.-Q. Wang, S.-M. Lu, Y.-G. Zhou, *J. Org. Chem.* **2007**, *72*, 3729–3734.
- [39] M. T. Reetz, G. Mehler, *Angew. Chem. Int. Ed.* **2000**, *39*, 3889–3890.
- [40] M. van den Berg, A. J. Minnaard, E. P. Schudde, J. van Esch, A. H. M. de Vries, J. G. de Vries, B. L. Feringa, *J. Am. Chem. Soc.* **2000**, *122*, 11539–11540.
- [41] Y.-G. Zhou, W. Tang, W.-B. Wang, W. Li, X. Zhang, *J. Am. Chem. Soc.* **2002**, *124*, 4952–4953.
- [42] M. J. Burk, *J. Am. Chem. Soc.* **1991**, *113*, 8518–8519.

- [43] A. Togni, C. Breutel, A. Schnyder, F. Spindler, H. Landert, A. Tijani, *J. Am. Chem. Soc.* **1994**, *116*, 4062–4066.
- [44] G. Shang, W. Li, X. Zhang in *Catalytic Asymmetric Synthesis*, Wiley, Hoboken, **2010**, 343–436.
- [45] P. Lu, Z. Lu, *Synthesis* **2023**, *55*, 1042–1052.
- [46] a) Y. Ohgo, S. Takeuchi, Y. Natori, J. Yoshimura, *Bull. Chem. Soc. Jpn.* **1981**, *54*, 2124–2135; b) Y. Ohgo, Y. Natori, S. Takeuchi, J. Yoshimura, *Chem. Lett.* **1974**, *3*, 1327–1330.
- [47] A. Corma, M. Iglesias, C. del Pino, F. Sánchez, *J. Organomet. Chem.* **1992**, *431*, 233–246.
- [48] S. Monfette, Z. R. Turner, S. P. Semproni, P. J. Chirik, *J. Am. Chem. Soc.* **2012**, *134*, 4561–4564.
- [49] M. R. Friedfeld, M. Shevlin, G. W. Margulieux, L.-C. Campeau, P. J. Chirik, *J. Am. Chem. Soc.* **2016**, *138*, 3314–3324.
- [50] K. H. Hopmann, *Organometallics* **2013**, *32*, 6388–6399.
- [51] M. R. Friedfeld, M. Shevlin, J. M. Hoyt, S. W. Krska, M. T. Tudge, P. J. Chirik, *Science* **2013**, *342*, 1076–1080.
- [52] J. Chen, C. Chen, C. Ji, Z. Lu, *Org. Lett.* **2016**, *18*, 1594–1597.
- [53] J. Guo, X. Shen, Z. Lu, *Angew. Chem. Int. Ed.* **2017**, *56*, 615–618.
- [54] J. Guo, B. Cheng, X. Shen, Z. Lu, *J. Am. Chem. Soc.* **2017**, *139*, 15316–15319.
- [55] P. Lu, H. Wang, Y. Mao, X. Hong, Z. Lu, *J. Am. Chem. Soc.* **2022**, *144*, 17359–17364.
- [56] K. Hans Wedepohl, *Geochim. Cosmochim. Acta, GCA* **1995**, *59*, 1217–1232.
- [57] a) S. C. Bart, E. Lobkovsky, P. J. Chirik, *J. Am. Chem. Soc.* **2004**, *126*, 13794–13807; b) D. J. Frank, L. Guiet, A. Käslin, E. Murphy, S. P. Thomas, *RSC Adv.* **2013**, *3*, 25698; c) E. N. Frankel, E. A. Emken, H. M. Peters, V. L. Davison, R. O. Butterfield, *J. Org. Chem.* **1964**, *29*, 3292–3297.
- [58] K. Gopalaiah, *Chem. Rev.* **2013**, *113*, 3248–3296.
- [59] J. M. Hoyt, M. Shevlin, G. W. Margulieux, S. W. Krska, M. T. Tudge, P. J. Chirik, *Organometallics* **2014**, *33*, 5781–5790.
- [60] P. Viereck, S. M. Rummelt, N. A. Soja, T. P. Pabst, P. J. Chirik, *Organometallics* **2021**, *40*, 1053–1061.
- [61] P. Lu, X. Ren, H. Xu, D. Lu, Y. Sun, Z. Lu, *J. Am. Chem. Soc.* **2021**, *143*, 12433–12438.
- [62] J.-i. Ito, H. Nishiyama, *Tetrahedron Lett.* **2014**, *55*, 3133–3146.
- [63] M. J. Palmer, M. Wills, *Tetrahedron Asymmetry* **1999**, *10*, 2045–2061.
- [64] a) C. Wang, X. Wu, J. Xiao, *Chem. Asian J.* **2008**, *3*, 1750–1770; b) M. Yoshimura, S. Tanaka, M. Kitamura, *Tetrahedron Lett.* **2014**, *55*, 3635–3640.
- [65] a) A. A. Mikhailine, M. I. Maishan, R. H. Morris, *Org. Lett.* **2012**, *14*, 4638–4641; b) P. E. Sues, K. Z. Demmans, R. H. Morris, *Dalton Trans.* **2014**, *43*, 7650–7667; c) C. Sui-Seng, F. Freutel, A. J. Lough, R. H. Morris, *Angew. Chem. Int. Ed.* **2008**, *47*, 940–943; d) W. Zuo, A. J. Lough, Y. F. Li, R. H. Morris, *Science* **2013**, *342*, 1080–1083.
- [66] J. F. Sonnenberg, N. Coombs, P. A. Dube, R. H. Morris, *J. Am. Chem. Soc.* **2012**, *134*, 5893–5899.
- [67] T.-P. Lin, J. C. Peters, *J. Am. Chem. Soc.* **2013**, *135*, 15310–15313.
- [68] G. Zhang, Z. Yin, J. Tan, *RSC Adv.* **2016**, *6*, 22419–22423.
- [69] A. Lator, S. Gaillard, A. Poater, J.-L. Renaud, *Chemistry* **2018**, *24*, 5770–5774.
- [70] T. M. Maier, S. Sandl, I. G. Shenderovich, A. Jacobi von Wangelin, J. J. Weigand, R. Wolf, *Chemistry* **2019**, *25*, 238–245.
- [71] P. Yang, H. Xu, J. S. Zhou, *Angew. Chem. Int. Ed.* **2014**, *53*, 12210–12213.
- [72] S. Guo, P. Yang, J. S. Zhou, *Chem. Commun.* **2015**, *51*, 12115–12117.
- [73] S. Gladiali, E. Alberico, *Chem. Soc. Rev.* **2006**, *35*, 226–236.
- [74] R. Bigler, L. de Luca, R. Huber, A. Mezzetti in *Non-Noble Metal Catalysis* (Eds.: R. J. M. Klein Gebbink, M.-E. Moret), Wiley-VCH Verlag GmbH & Co. KGaA, Weinheim, Germany, **2019**, 209–240.
- [75] a) J. W. ApSimon, T. Lee Collier, *Tetrahedron* **1986**, *42*, 5157–5254; b) A. Hirao, S. Itsuno, S. Nakahama, N. Yamazaki, *J. Chem. Soc., Chem. Commun.* **1981**, 315; c) S. Itsuno, A. Hirao, S. Nakahama, N. Yamazaki, *J. Chem. Soc., Perkin Trans. 1* **1983**, 1673; d) S. Itsuno, K. Ito, A. Hirao, S. Nakahama, *J. Chem. Soc., Chem. Commun.* **1983**, 469–470.
- [76] a) E. J. Corey, R. K. Bakshi, S. Shibata, *J. Am. Chem. Soc.* **1987**, *109*, 5551–5553; b) E. J. Corey, S. Shibata, R. K. Bakshi, *J. Org. Chem.* **1988**, *53*, 2861–2863.
- [77] T. Nagata, K. Yorozu, T. Yamada, T. Mukaiyama, *Angew. Chem. Int. Ed.* **1995**, *34*, 2145–2147.
- [78] a) T. Yamada, T. Nagata, K. D. Sugi, K. Yorozu, T. Ikeno, Y. Ohtsuka, D. Miyazaki, T. Mukaiyama, *Chemistry* **2003**, *9*, 4485–4509; b) A. Kokura, S. Tanaka, T. Ikeno, T. Yamada, *Org. Lett.* **2006**, *8*, 3025–3027; c) T. Ashizawa, S. Tanaka, T. Yamada, *Org. Lett.* **2008**, *10*, 2521–2524.
- [79] a) F. Almqvist, L. Torstensson, A. Gudmundsson, T. Frejd, *Angew. Chem. Int. Ed.* **1997**, *36*, 376–377; b) I. Sarvary, F. Almqvist, T. Frejd, *Chem. Eur. J.* **2001**, *7*, 2158–2166.
- [80] S.-G. Roh, Y.-C. Park, D.-K. Park, T.-J. Kim, J. H. Jeong, *Polyhedron* **2001**, *20*, 1961–1965.
- [81] M. Locatelli, P. G. Cozzi, *Angew. Chem. Int. Ed.* **2003**, *42*, 4928–4930.
- [82] J. Guo, J. Chen, Z. Lu, *Chem. Commun.* **2015**, *51*, 5725–5727.
- [83] W. Liu, J. Guo, S. Xing, Z. Lu, *Org. Lett.* **2020**, *22*, 2532–2536.
- [84] M. Hudlický, *Reductions in organic chemistry*, E. Horwood, Chichester West Sussex, **1984**.
- [85] F. Chen, Y. Zhang, L. Yu, S. Zhu, *Angew. Chem. Int. Ed.* **2017**, *56*, 2022–2025.
- [86] a) V. Vasilenko, C. K. Blasius, H. Wadepohl, L. H. Gade, *Angew. Chem. Int. Ed.* **2017**, *56*, 8393–8397; b) C. K. Blasius, V. Vasilenko, L. H. Gade, *Angew. Chem. Int. Ed.* **2018**, *57*, 10231–10235.
- [87] M. K. Bisai, T. Das, K. Vanka, S. S. Sen, *Chem. Commun.* **2018**, *54*, 6843–6846.
- [88] K. Kuciński, G. Hreczycho, *Green Chem.* **2019**, *21*, 1912–1915.
- [89] K. Kuciński, G. Hreczycho, *Eur. J. Org. Chem.* **2020**, *2020*, 552–555.
- [90] V. A. Pollard, S. A. Orr, R. McLellan, A. R. Kennedy, E. Hevia, R. E. Mulvey, *Chem. Commun.* **2018**, *54*, 1233–1236.
- [91] Z. Zhu, X. Wu, X. Xu, Z. Wu, M. Xue, Y. Yao, Q. Shen, X. Bao, *J. Org. Chem.* **2018**, *83*, 10677–10683.

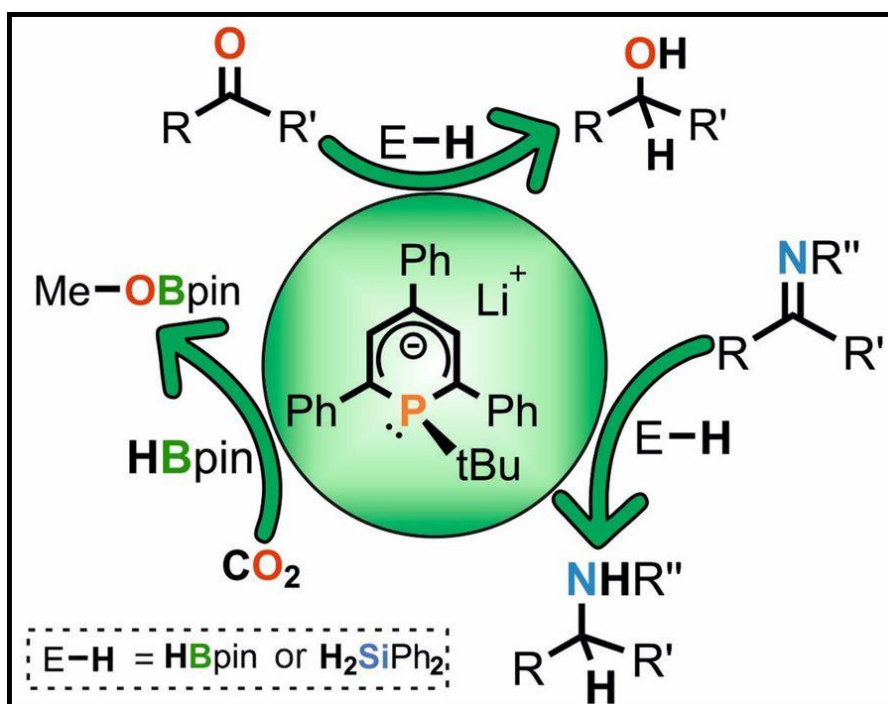
- [92] A. J. Blake, A. Cunningham, A. Ford, S. J. Teat, S. Woodward, *Chem. Eur. J.* **2000**, *6*, 3586–3594.
- [93] R. G. Pearson, *Coord. Chem. Rev.* **1990**, *100*, 403–425.
- [94] I. P. Query, P. A. Squier, E. M. Larson, N. A. Isley, T. B. Clark, *J. Org. Chem.* **2011**, *76*, 6452–6456.
- [95] J. H. Kim, A. K. Jaladi, H. T. Kim, D. K. An, *Bull. Korean Chem. Soc.* **2019**, *40*, 971–975.
- [96] A. Falconnet, M. Magre, B. Maity, L. Cavallo, M. Rueping, *Angew. Chem. Int. Ed.* **2019**, *58*, 17567–17571.
- [97] Y. Lebedev, I. Polishchuk, B. Maity, M. Dinis Veloso Guerreiro, L. Cavallo, M. Rueping, *J. Am. Chem. Soc.* **2019**, *141*, 19415–19423.
- [98] V. Vasilenko, C. K. Blasius, H. Wadepohl, L. H. Gade, *Chem. Commun.* **2020**, *56*, 1203–1206.
- [99] D. Willcox, J. L. Carden, A. J. Ruddy, P. D. Newman, R. L. Melen, *Dalton Trans.* **2020**, *49*, 2417–2420.
- [100] B. Marciniec, *Hydrosilylation. A Comprehensive Review on Recent Advances*, Springer Netherlands, Dordrecht, **2009**.
- [101] C. Arena, *Mini-Rev. Org. Chem.* **2009**, *6*, 159–167.
- [102] H. Nishiyama in *Comprehensive Chirality*, Elsevier, **2012**, 318–333.
- [103] V. M. Uvarov, D. A. de Vekki, *J. Organomet. Chem.* **2020**, *923*, 121415.
- [104] a) W. Dumont, J. C. Poulin, Dang Tuan Phat, H. B. Kagan, *J. Am. Chem. Soc.* **1973**, *95*, 8295–8299; b) T. Hayashi, K. Yamamoto, M. Kumada, *Tetrahedron Lett.* **1974**, *15*, 4405–4408; c) I. Ojima, T. Kogure, M. Kumagai, S. Horiuchi, T. Sato, *J. Organomet. Chem.* **1976**, *122*, 83–97.
- [105] H. Brunner, W. Miehling, *J. Organomet. Chem.* **1984**, *275*, c17–c21.
- [106] H. Brunner, K. Amberger, *J. Organomet. Chem.* **1991**, *417*, C63–C65.
- [107] H. Brunner, M. Rötzer, *J. Organomet. Chem.* **1992**, *425*, 119–124.
- [108] M. B. Carter, B. Schiott, A. Gutierrez, S. L. Buchwald, *J. Am. Chem. Soc.* **1994**, *116*, 11667–11670.
- [109] H. Mimoun, J. Y. de Saint Laumer, L. Giannini, R. Scopelliti, C. Floriani, *J. Am. Chem. Soc.* **1999**, *121*, 6158–6166.
- [110] a) M. Szweczyk, F. Stanek, A. Bezlada, J. Mlynarski, *Adv. Synth. Catal.* **2015**, *357*, 3727–3731; b) M. Szweczyk, A. Bezlada, J. Mlynarski, *ChemCatChem* **2016**, *8*, 3575–3579.
- [111] T. Bleith, H. Wadepohl, L. H. Gade, *J. Am. Chem. Soc.* **2015**, *137*, 2456–2459.
- [112] T. Bleith, L. H. Gade, *J. Am. Chem. Soc.* **2016**, *138*, 4972–4983.
- [113] X. Chen, Z. Lu, *Org. Lett.* **2016**, *18*, 4658–4661.
- [114] S. Kohra, H. Hayashida, Y. Tominaga, A. Hosomi, *Tetrahedron Lett.* **1988**, *29*, 89–92.
- [115] a) F. J. LaRonde, M. A. Brook, *Inorg. Chim. Acta* **1999**, *296*, 208–221; b) R. Schiffers, H. Kagan, *Synlett* **1997**, *1997*, 1175–1178; c) D. Pini, A. Iuliano, P. Salvadori, *Tetrahedron Asymmetry* **1992**, *3*, 693–694.
- [116] a) M. D. Anker, M. S. Hill, J. P. Lowe, M. F. Mahon, *Angew. Chem. Int. Ed.* **2015**, *54*, 10009–10011; b) M. S. Hill, G. Kociok-Köhn, D. J. MacDougall, M. F. Mahon, C. Weetman, *Dalton Trans.* **2011**, *40*, 12500–12509; c) M. Ma, X. Shen, W. Wang, J. Li, W. Yao, L. Zhu, *Eur. J. Inorg. Chem.* **2016**, *2016*, 5057–5062; d) M. Rauch, G. Parkin, *J. Am. Chem. Soc.* **2017**, *139*, 18162–18165.
- [117] a) J. Spielmann, S. Harder, *Eur. J. Inorg. Chem.* **2008**, *2008*, 1480–1486; b) J. Intemann, H. Bauer, J. Pahl, L. Maron, S. Harder, *Chem. Eur. J.* **2015**, *21*, 11452–11461.
- [118] R. M. Lopez, G. C. Fu, *Tetrahedron* **1997**, *53*, 16349–16354.
- [119] M. Hojo, C. Murakami, A. Fujii, A. Hosomi, *Tetrahedron Lett.* **1999**, *40*, 911–914.
- [120] D. Addis, S. Zhou, S. Das, K. Junge, H. Kosslick, J. Harloff, H. Lund, A. Schulz, M. Beller, *Chem. Asian J.* **2010**, *5*, 2341–2345.
- [121] S. Harder in *Early Main Group Metal Catalysis* (Ed.: S. Harder), Wiley, **2020**, 151–173.
- [122] W. Chen, C.-H. Tan, H. Wang, X. Ye, *Eur. J. Org. Chem.* **2021**, *2021*, 3091–3112.
- [123] D. J. Parks, R. E. von H. Spence, W. E. Piers, *Angew. Chem. Int. Ed.* **1995**, *34*, 809–811.
- [124] D. Chen, V. Leich, F. Pan, J. Klankermayer, *Chem. Eur. J.* **2012**, *18*, 5184–5187.
- [125] X. Zhu, H. Du, *Org. Biomol. Chem.* **2015**, *13*, 1013–1016.
- [126] X. Ren, H. Du, *J. Am. Chem. Soc.* **2016**, *138*, 810–813.
- [127] L. Süssé, J. Hermeke, M. Oestreich, *J. Am. Chem. Soc.* **2016**, *138*, 6940–6943.
- [128] B. C. Kang, S. H. Shin, J. Yun, D. H. Ryu, *Org. Lett.* **2017**, *19*, 6316–6319.



2 Expedient Hydrofunctionalisation of Carbonyls and Imines Initiated by Phosphacyclohexadienyl Anions^[a]

Abstract:

The ability of phosphacyclohexadienyl anions [Li(1-R-PC₅Ph₃H₂)] [R = Me (**1a**), *n*Bu (**1b**), *t*Bu (**1c**), Ph (**1d**) and CH₂SiMe₃ (**1e**)] to initiate hydrofunctionalisation reactions was investigated and compared with simple, commercially available compounds, such as LiO^tBu, KO^tBu and ^tBuLi. All compounds are expedient catalysts for the hydroboration of a wide scope of substrates, ranging from aldehydes to imines and esters. In the hydroboration of carbon dioxide, however, only **1a-e** were observed to efficiently produce the desired methanol equivalents.



^[a]Reproduced with permission from M. J. Margeson, F. Seeberger, J. A. Kelly, J. Leitl, P. Coburger, R. Szlosek, C. Müller, R. Wolf, *ChemCatChem* **2021**, *13*, 3761-3764.

M. Margeson synthesised **1a-e**, performed catalytic reactions (see 2.2, Table 4, entry 1 and SI, Tables 1-4), the hydroboration of CO₂ (see 2.2, Table 5, entry 1 and 5) and the kinetic investigation of 2'-methylacetophenone using **1a-e** (SI, Table 5). F. Seeberger synthesised **1c**, **3** and **4**, crystallographically characterised **1c**-[2.2.2]crypt and **4**, performed the kinetic comparison reactions of **1c**, **3**, **4** and the alkoxides/lithium organyls (see 2.2 Tables 2, 3 and Table 4, entries 2-4, see 2.4.3, Table 6), the CO₂ reduction with catalysts other than **1c** (Table 5, entries 2-4), as well as the NMR spectroscopic mechanistic investigation of the reaction of **1c** or **2** with 2'-methylacetophenone and HBpin (Figures 9-23). J. Leitl synthesised adduct **2** and crystallographically characterised **3**-[18]crown-6. P. Coburger performed DFT calculations. M. Margeson and F. Seeberger wrote the manuscript with contributions from all authors. C. Müller and R. Wolf supervised the project.

2.1 Introduction

The past few decades have seen considerable strides in main group chemistry, both from a fundamental and applied point of view. One of the more attractive prospects is the utilisation of main group compounds as precious metal mimics, especially in terms of catalytic applications.^[1] The main goal is the eventual replacement of rare transition metal catalysts with an effective and more abundant main group counterpart.

The hydroelementation of unsaturated organic compounds, in particular hydroboration and hydrosilylation, is a reaction that traditionally was firmly in the remit of precious metal catalysts.^[2] Hydrofunctionalisation processes are highly prevalent in industry; products from these reactions are used extensively in the production of fine chemicals, pharmaceuticals, lubricants, adhesives and insulation.^[3] The past decade has witnessed an influx of main group compounds capable of such transformations and in the case of hydroboration reactions, actually surpassing transition metal catalysts.^[4] Beside these rather sophisticated catalysts, recent years have also seen a plethora of reports with more easily accessible and commercially available compounds, which are able to effectively catalyse hydroelementation reactions. Alkoxides,^[5,6] potassium fluoride or carbonate,^[7] Grignard reagents^[8] as well as *n*-butyl lithium^[9,10] all were able to hydroborate ketones to their respective alkoxyborane. Furthermore, *Leung* and co-workers reported the catalyst-free reduction of ketones with pinacolborane in solvent-free conditions at elevated temperatures.^[11]

Compared to hydroboration, hydrosilylation reactions catalysed by main group compounds are much less common. Noteworthy examples include the highly Lewis acidic borane B(C₆F₅)₃,^[12] and phosphonium cations^[13] as well as commercially available bases, such as KO^tBu,^[14,15] KOH,^[15] and Cs₂CO₃.^[16] Although promising, main groups systems still do not match the efficiency and scope of many transition metal catalysts in terms of the hydrosilylation of carbonyl compounds, thus the demand for more effective main group catalysts remains high.

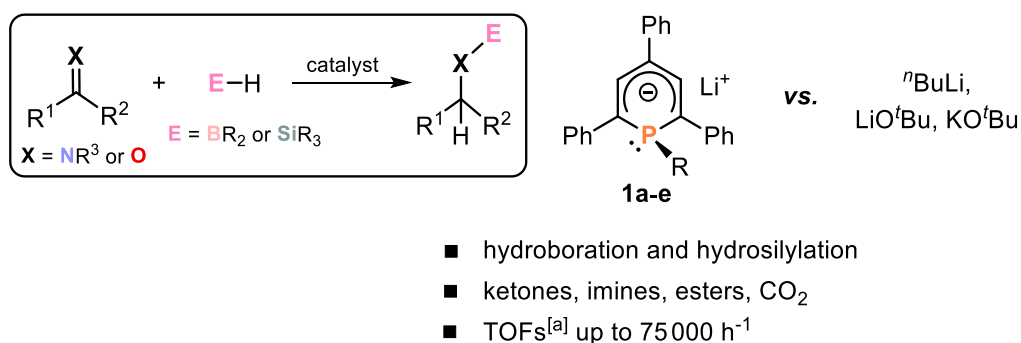


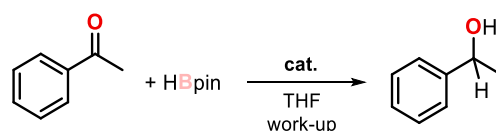
Figure 1. Catalytic hydrofunctionalisation of carbonyl compounds using phosphacyclohexadienyl salts **1a-e** [R = Me (**1a**), ⁿBu (**1b**), ^tBu (**1c**), Ph (**1d**), CH₂SiMe₃ (**1e**)] and [a] Turnover frequency – average value for complete reaction.

Phosphacyclohexadienyl anions **1a-e** (**Figure 1**), which are readily synthesised by treatment of 2,4,6-triphenylphosphinine with alkyl lithium reagents,^[17] were investigated in an effort to devise new main group element based catalysts. These species (typically referred to as λ^4 -phosphinine anions) are best described as anionic tertiary phosphines, although they display distinct chemical properties. It was envisioned that the highly reactive nature of these anions would lend themselves to small molecule activation or catalytic applications. Here it is shown that such anions have excellent properties for the hydrofunctionalisation of ketones, imines and esters. These findings are also compared with commercially available catalysts such as *n*BuLi, LiO*t*Bu and KO*t*Bu.

2.2 Results and Discussion

To test the catalytic potential of anions **1a-e**, a series of hydroboration and hydrosilylation reactions was performed. Acetophenone hydrofunctionalisation was chosen as the benchmark reaction to probe the capability of **1a-e**, and to compare their catalytic activity (**Table 1**). While all compounds displayed high efficiency, the *t*Bu derivative, **1c** performed the best (see **Table 1**, entry 3) and thus was chosen for further optimisation in both hydroboration and hydrosilylation reactions. Using **1c** at a loading of 0.01 mol%, acetophenone was fully converted to 1-phenylethan-1-ol in less than 8 minutes at $T = 23\text{ }^\circ\text{C}$. This equates to a TOF of $\geq 75\ 000\ \text{h}^{-1}$, which is among the most rapid of any reductions employing pinacolborane to date.

Table 1. Acetophenone hydrofunctionalisation catalysed by phosphacyclohexadienyl anions in comparison to literature-known alkoxides and *n*BuLi.^[a]



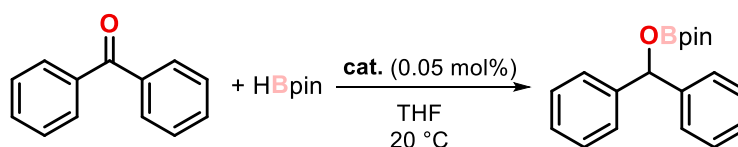
Entry	cat. (mol%)	Reducing Reagent (equiv.)	Temperature [$^\circ\text{C}$]	Time [h] ^[b]	TOF [$10^3\ \text{h}^{-1}$] ^[c]
1	1a (0.01)	HBpin (1.0)	23	0.40	25
2	1b (0.01)	HBpin (1.0)	23	0.25	40
3	1c (0.01)	HBpin (1.0)	23	<0.13	≥ 75
4	1d (0.01)	HBpin (1.0)	23	0.17	60
5	1e (0.01)	HBpin (1.0)	23	0.17	60
6 ^[d]	LiO <i>t</i> Bu (1.0)	HBpin (1.3)	rt	0.5	0.2
7 ^[e]	NaO <i>t</i> Bu (5.0)	HBpin (1.1)	22	3	< 0.007
8 ^[f]	<i>n</i> BuLi (0.1)	HBpin (1.1)	rt	0.17	5.8

^[a]Reducing reagent = 0.20 mmol, substrate = 0.20 mmol, 0.1 mL solvent. ^[b]Time for complete substrate conversion, detected by GC-FID using *n*-pentadecane as an internal standard. ^[c]Turnover frequency - average value for complete reaction. ^[d]See ref. 6. ^[e]See ref. 5. Reaction performed in toluene. ^[f]See ref. 9. Reaction performed without solvent.

The catalyst was able to readily hydroborate a wide array of substrates, including aldehydes, ketones, esters, aldimines and ketimines as well as benzoic acid (see SI for details). Besides its good functional group tolerance, **1c** also showed exceptional chemoselectivity in the presence of other reducible moieties such as nitro, nitrile, pyridyl, and alkenyl groups. In hydrosilylation reactions, **1c** showcased a similar substrate scope, excluding only esters, benzoic acid and ketimines (see SI, Tables 1-4).

It is known that simple inorganic bases such as alkali metal *tert*-butoxides and *n*-butyllithium can also catalyse the hydroboration of acetophenone, but with comparatively higher catalyst loadings and longer reaction times.^[5,6,9,10] Considering these results, it was intriguing to compare **1c** to such commercially available catalysts. With previously reported results in mind, it was anticipated to see **1c** to be faster than these compounds. Surprisingly, initial tests using 2'-methylacetophenone resulted in a similar activity for all catalysts (see 2.4.3, Table 6). In order to better compare the catalytic activities, ReactIR measurements were conducted, revealing high activities that surpassed expectations for these commercial compounds, especially for *n*-butyl lithium. Benzophenone was used as a sterically more demanding substrate to give a more manageable reaction timeframe. Both alkoxides achieved a conversion of at least 50% within 105 seconds, while **1c** and *n*-butyl lithium only required 60 and 30 seconds, respectively. These short reaction times translate into an approximate turnover frequency (TOF) of 64 800 h⁻¹, 35 000 h⁻¹, 34 300 h⁻¹ and 153 500 h⁻¹ for **1c**, LiO^tBu, KO^tBu and ⁿBuLi, respectively. To our knowledge, the best known main group based catalyst for hydroboration reactions is Okuda's lithium triphenylborohydride complex containing tris[2-(dimethylamino)ethyl]amine, which was reported to achieve a TOF of at least 66 666 h⁻¹.^[18] This TOF, however, was calculated after the reaction was completed, meaning the actual TOF could be much higher. Taken together, it is clear that ⁿBuLi possesses great catalytic activity, rivalling even the most active main group hydroboration catalysts.

Table 2. ReactIR monitored catalyst comparison in the hydroboration of benzophenone.^[a]

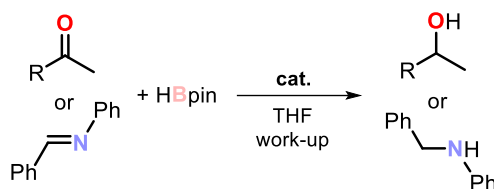


Entry	cat.	Time [s] ^[b]	Conversion [%]	Time _{50%} [s] ^[c]	TOF [h ⁻¹] ^[d]
1	1c	480	>99	60 (54%)	64 800
2	LiO ^t Bu	1155	>99	105 (51%)	34 971
3	KO ^t Bu	2895	91	105 (50%)	34 286
4	ⁿ BuLi	105	>99	30 (64%)	153 600

^[a]Reducing reagent = 0.51 mmol, benzophenone = 0.50 mmol. ^[b]Time until the given conversion was observed. ^[c]Time until a conversion of at least 50% was reached. ^[d]Turnover frequency – calculated at the first point when the conversion was greater than 50%.

A similar trend was also observed for the hydroboration of octan-2-one, N-benzylidenaniline and ethyl acetate with pinacolborane (**Table 3**). Low catalyst loadings are sufficient to achieve high conversions within 5 – 30 min. While in most cases KO^tBu was observed to be slightly slower, especially in the hydroboration of the ethyl acetate, there was no major difference between **1c**, ⁿBuLi and LiO^tBu.

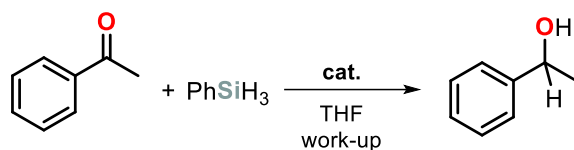
Table 3. Comparison of **1c**, LiO^tBu, KO^tBu and ⁿBuLi in the reduction of different substrates using pinacolborane.



Entry	Substrate	cat. (mol%)	Solvent (mL)	Time [min.]	Conversion [%] ^[b]
1		1c (0.05)	THF (0.5)	5	82
2		LiO ^t Bu (0.05)	THF (0.5)	5	87
3		KO ^t Bu (0.05)	THF (0.5)	5	73
4		ⁿ BuLi (0.05)	THF (0.5)	5	83
5		1c (0.05)	THF (0.5)	5	70
6		LiO ^t Bu (0.05)	THF (0.5)	5	59
7		KO ^t Bu (0.05)	THF (0.5)	5	52
8		ⁿ BuLi (0.05)	THF (0.5)	5	77
9		1c (0.5)	THF (0.2)	15	49
10		LiO ^t Bu (0.5)	THF (0.2)	15	63
11		KO ^t Bu (0.5)	THF (0.2)	15	55
12		ⁿ BuLi (0.5)	THF (0.2)	15	64
13 ^[c]		1c (3.0)	THF (0.1)	30	49 ^[d]
14 ^[c]		LiO ^t Bu (3.0)	THF (0.1)	30	44 ^[d]
15 ^[c]		KO ^t Bu (3.0)	THF (0.1)	30	15 ^[d]
16 ^[c]		ⁿ BuLi (3.0)	THF (0.1)	30	45 ^[d]

^[a]HBpin = 0.26 mmol, substrate = 0.25 mmol. ^[b]Conversion detected *via* GC-FID using *n*-pentadecane as internal standard. ^[c]HBpin = 0.66 mmol, ethyl acetate = 0.30 mmol. ^[d]Conversion detected *via* ¹H NMR integration using mesitylene as internal standard.

As potassium *tert*-butoxide has been reported as an efficient hydrosilylation catalyst, we went on to also test **1c**, LiO^tBu, and *n*-butyl lithium in the hydrosilylation of acetophenone. In these reactions, however, none of the lithium salts was able to compete with potassium *tert*-butoxide hinting at a more pronounced cation effect on the activity in hydrosilylation reactions (see **Table 4**).

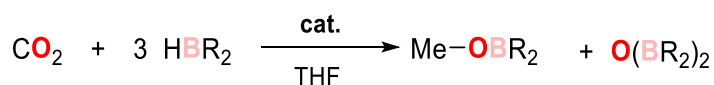
Table 4. Acetophenone hydrofunctionalisation catalysed by phosphacyclohexadienyl anions.^[a]

Entry	cat. (mol%)	Temperature [°C]	Time [h] ^[b]	TOF [h ⁻¹] ^[c]
1 ^[d]	1c (0.5)	23 (40)	3 (1)	67 (200)
2	LiO ^t Bu (0.5)	23	1	200
3	KO ^t Bu (0.1)	23	<0.17	6000
4	ⁿ BuLi (0.5)	23	1	200

^[a]PhSiH₃ = 0.20 mmol, substrate = 0.20 mmol, 0.1 mL solvent. ^[b]Time for complete substrate conversion, detected by GC-FID using *n*-pentadecane as an internal standard. ^[c]Turnover frequency - average value for complete reaction.

^[d]Solvent free.

As all tested catalysts displayed the ability to reduce very demanding substrates, their ability to catalyse the hydroboration of CO₂ was investigated next. With LiO^tBu and KO^tBu, no conversion was observed even at elevated temperatures. **1c** and ⁿBuLi both were able to catalyse the full consumption of pinacolborane, as observed in the ¹H and ¹¹B NMR spectra. However, in the case of ⁿBuLi a mixture of products was observed. The hydroboration of CO₂ worked significantly better with **1c**, leading to the clean formation of methanol equivalent (MeOBpin). The hydrofunctionalisation of CO₂ could be further optimised by using catechol borane (HBcat), giving TOFs of 13 h⁻¹. Throughout the reaction with pinacolborane, the formate equivalent HCO₂Bpin and acetal equivalent H₂C(OBpin)₂ were identified by ¹H and ¹¹B NMR spectroscopy. These species have been previously proposed as intermediates in certain reductions mediated by main group catalytic systems.^[19]

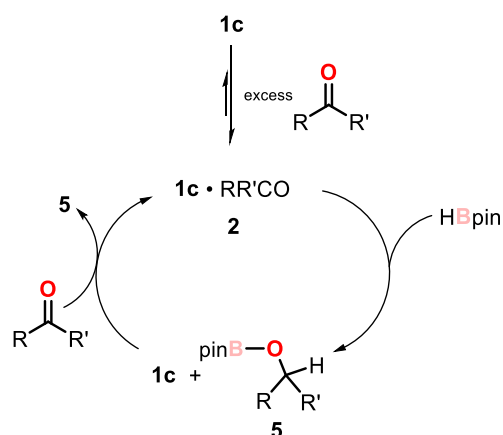
Table 5. Borane reduction of CO₂ catalysed by **1c** compared to alkali metal alkoxides and ⁿBuLi.^[a]

Entry	cat. (mol%)	BR ₂	Time [h] ^[b]	TOF [h ⁻¹] ^[c]
1	1c (2)	Bpin	16	3.1
2	LiO ^t Bu (5)	Bpin	72 ^[d]	-
3	KO ^t Bu (5)	Bpin	72 ^[d]	-
4	ⁿ BuLi (5)	Bpin	16	<0.2 ^[e]
5	1c (0.5)	Bcat	16	13

^[a]HBR₂ = 0.20 mmol, ~1 bar CO₂, 0.2 mL THF-*d*₈, T = 25 °C. ^[b]Time for complete substrate conversion, followed by ¹H and ¹¹B NMR spectroscopy. ^[c]Turnover frequency - average value for complete reaction. ^[d]Reaction performed at 60 °C. ^[e]Yield < 15%.

Studies of 2'-methylacetophenone hydroboration in THF and benzene using $[K(1\text{-}t\text{Bu-PC}_5\text{Ph}_3\text{H}_2)]$ (**3**) and $[N(^n\text{Bu})_4][1\text{-}t\text{Bu-PC}_5\text{Ph}_3\text{H}_2]$ (**4**) revealed similar catalytic activities as observed for **1c** (see **2.4.3, Table 6**). This was also observed for the alkoxides **MOMe** and **MO^tBu** (**M** = Li, Na, K). Therefore, it can be inferred that the cation only has a minor influence on the reactivity in hydroboration reactions. Similar conversions in the range of 73-89% were observed for all alkoxides with the exception of NaOMe, which gave a conversion of only 30% (see **2.4.3, Table 6**).

In order to shed light onto the mechanism, further ReactIR kinetic measurements were conducted. The reaction order was determined using the method of initial rates and the time normalisation approach (see SI for details).^[20] The results clearly suggest a zero-order dependence on ketone concentration and a first order dependence on **1c** and HBpin. Furthermore, a stoichiometric reaction between **1c**, ketone and HBpin was performed. The full consumption of HBpin was observed by ¹¹B NMR spectroscopy. Upon comparing the integrals of the methyl signals of the ketone ($\delta = 2.26$ ppm) with the signals of the product ($\delta = 2.30$ ppm) the yield of the desired borolane can be estimated to be >95%. The ¹¹B{¹H} NMR spectrum displays major signal ($\delta = 22.2$ ppm) that can be assigned to the borolane (**5**) with two minor signals (<10%) at $\delta = 6.3$ and 5.8 ppm that could not be identified. The ³¹P{¹H} NMR spectrum shows **1c** to be the main component (86%) with the formation of a new signal at $\delta = -24.3$ ppm (11%). The signal at $\delta = -24.3$ ppm was also observed, when reacting **1c** with the ketone in the absence of borane. Therefore, we propose this to be an adduct of the ketone with **1c**. The presumed adduct (**2**) was isolated but could not yet be crystallographically characterised. Upon testing **2** in the hydroboration of 2'-methylacetophenone, only a slight decrease in catalytic activity was observed when compared to **1c** (see **2.4.3, Table 6**). When stoichiometric amounts of HBpin were added to **2**, the desired product **5** as well as the released catalyst **1c** could be observed as the main products. Altogether, these experiments suggest the mechanism starts with the formation of an adduct between the ketone and **1c**, which then reacts with the reducing reagent. The catalytic cycle is subsequently closed by the release of **5** and the reformation of **1c**.



Scheme 1. Proposed mechanism of the hydroboration of ketones initiated by **1c**.

2.3 Conclusion

When comparing the effectiveness of phosphacyclohexadienyl anions in hydroboration and hydrosilylation catalysis of polar substrates with those for commercially available bases LiO^tBu, KO^tBu and ⁿBuLi, we have found that these catalysts also show a remarkable efficiency, rivalling the most active catalysts available to date. All of these catalysts can reduce very challenging substrates, such as imines and esters. However, LiO^tBu, KO^tBu and ⁿBuLi were ineffective in the hydroboration of CO₂. This is in contrast to compounds **1a-e** which were able to efficiently reduce CO₂ to the corresponding methanol equivalent under ambient conditions with HBpin and HBcat. On-going work in our group concerns the utilisation of this methodology and the development of asymmetric hydrofunctionalization reactions.

2.4 Experimental Details

General Synthetic Methods

Unless otherwise stated, all manipulations were performed in flame-dried glassware under an atmosphere of dry argon using standard Schlenk techniques or in an MBraun UniLab glovebox. Diethyl ether (HPLC grade, Fisher), ethyl acetate (HPLC grade, >99.8%, Fisher), methanol (HPLC grade, > 99.9%, Fisher), ethanol (ACS reagent grade, >99.8%, Sigma Aldrich), *n*-hexane (HPLC grade, >99%, Sigma Aldrich), and tetrahydrofuran (HPLC grade, Fisher) were used without further drying. Tetrahydrofuran was dried over sodium and distilled under argon atmosphere. Diethyl ether, *n*-hexane, benzene and toluene were dried and degassed with an MBraun SPS800 solvent purification system. C₆D₆ (99.6%, Sigma Aldrich), d₈-THF (99.5, Fluorochem) and d₃-MeCN (99.8%, Sigma Aldrich) were used as received. All dry solvents were stored under argon over activated 3 Å molecular sieves or potassium mirror in gas-tight ampules. All substances used in this work were commercially available, with the exception of P(SiMe₃)₃,^[21] (*E*)-*N*-(4-methoxybenzylidene)aniline^[22] and (*E*)-*N*-(4-(trifluoromethyl)benzylidene)aniline,^[22] which were synthesised by literature procedures. **1d** and **1e** were previously synthesized in our lab according to literature procedures. All liquid substrates were distilled, degassed and stored over molecular sieves (3 Å) prior to catalytic testing. ¹³CO₂ (99 atom% ¹³C) was purchased from Sigma Aldrich and used as received.

General Analytical Techniques

NMR spectra were recorded on Bruker Avance 300 or 400 spectrometers at 300 K and internally referenced to residual solvent resonances (¹H NMR: d₈-THF: 1.72 ppm, CDCl₃: 7.26 ppm, C₆D₆: 7.16 ppm, d₃-MeCN: 1.94 ppm). Chemical shifts δ are given in ppm referring to external standards of tetramethylsilane (¹H, ¹³C{¹H}), or 85% phosphoric acid (³¹P and ³¹P{¹H} spectra). IR spectra were recorded with a Bruker ALPHA spectrometer equipped with a diamond ATR unit. In-situ IR spectra were recorded on a Mettler-Toledo ReactIR 15 with silicon crystal ATR probe in absorbance mode and processed using iC IR. Scans were recorded between 650–4000 cm⁻¹, and integration of the carbonyl peak at 1690 cm⁻¹ was used for substrate

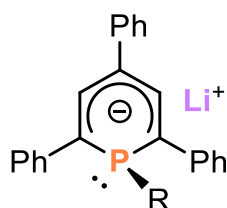
concentration determination. Gas chromatography with FID (GC FID): Shimadzu GC2010plus. Carrier gas: H₂. Colum: Restek Rxi®, (30 m x 0.25 mm x 0.25 μm) Carrier gas: H₂. Standard heating procedure: 50 °C (2 min), 25 °C/min. → 280 °C (5 min). HP6890 GC-System with injector 7683B and Agilent 7820A System. Column: HP-5, 19091J-413 (30 m x 0.32 mm x 0.25 μm), carrier gas: H₂. Column: RT-bDEXsmTM (30 m x 0.25 mm x 0.25 μm), carrier gas: H₂. Standard heating procedure: 50 °C (0.5 min), 25 °C/min. → 230 °C (6 min). Calibration of substrates and products with internal standard *n*-pentadecane and analytically pure samples. Gas chromatography with mass selective detector (GC MS): Agilent 7820A GC system, mass detector 5977B. Carrier gas: H₂. Column: HP-5MS (30 m x 0.25 mm x 0.25 μm). Standard heating procedure: 50 °C → 300 °C. Agilent 6890N Network GC-System, mass detector 5975 MS. Column: HP-5MS (30 m x 0.25 mm x 0.25 μm), 5% phenylmethylsiloxane, carrier gas: H₂. Standard heating procedure: 50 °C (2 min), 25 °C/min. → 300 °C (5 min). Mass spectra were performed with Jeol AccuTOF GCX EI-MS (LR/HR) by the analytical Department of Regensburg University.

Single-crystal X-ray diffraction data were recorded on an Agilent Technologies SuperNova diffractometer with Cu-K_α radiation (λ = 1.54184 Å). Either semi-empirical multi-scan absorption corrections^[23] or analytical ones^[24] were applied to the data. The structures were solved with SHELXT^[25] and least-square refinements on *F*² were carried out with SHELXL.^[26] The hydrogen atoms were located in idealized positions and refined isotropically with a riding model. 1978560 (for **1c**-[2.2.2]crypt) 1978559 (for **3**-[18]crown-6) and 1988454 (for **4**) contain the supplementary crystallographic data for this paper. The data can be obtained free of charge from the Cambridge Crystallographic Data Centre.

2.4.1 Synthesis of Compounds

[Li(1-R-PC₃Ph₃H₂)] [R = Me (**1a**), ⁿBu (**1b**), ^tBu (**1c**), Ph (**1d**) and CH₂SiMe₃ (**1e**)]:^[27]

General procedure for phosphacyclohexadienyl lithium salts according to a procedure by Märkl: TPP (1 equiv.) was dissolved in dry diethyl ether (200 mL), cooled to -80 °C and RLi (1 equiv.; R = Me, ^tBu, ⁿBu, Ph, Me₃SiCH₂) was added dropwise *via* syringe. The resulting dark purple solution was slowly warmed to room temperature over 16 hours. The solvent was removed *in vacuo* to yield **1a-1e** as pure pink solids. Crystals of **1c**-[2.2.2]crypt were obtained upon layering a 1:1:1 reaction mixture of **1c**, benzophenone and [2.2.2]cryptand dissolved in THF with *n*-hexane.



For **1a** (R = Me): TPP (300 mg, 0.989 mmol); MeLi in diethyl ether (0.581 mL, 0.989 mmol, 1.7 M).

Molecular formula: C₂₄H₂₀PLi (346.33 g·mol⁻¹)

Yield: 0.318 g (90%).

¹H NMR (400.13 MHz, 300K, C₆D₆): δ = 0.78 (br d, 3H, ³J_{HP} = 3.83 Hz, *Me*), 6.92 (t, 2H, ³J_{HH} = 7.24 Hz), 7.06 (t, 1H, ³J_{HH} = 7.24 Hz), 7.15 (t, 4H, ³J_{HH} = 7.60 Hz), 7.27 (t, 2H, ³J_{HH} = 7.60 Hz), 7.45 (d, 2H, ³J_{HH} = 7.85 Hz), 7.55 (d, 2H, ³J_{HP} = 5.63 Hz), 7.61 (br d, 4H, ³J_{HH} = 7.24 Hz).

³¹P{¹H} NMR (161.98 MHz, 300 K, C₆D₆): δ = -72.5 (s).

³¹P NMR (161.98 MHz, 300 K, C₆D₆): δ = -72.5 (s).

For **1b** (R = *n*Bu): TPP (300 mg, 0.989 mmol); *n*BuLi in *n*-hexane (0.581 mL, 0.989 mmol, 1.7 M).

Molecular formula: C₂₇H₂₆PLi (388.42 g·mol⁻¹)

Yield: 0.313 g (87%).

¹H NMR (400.13 MHz, 300K, C₆D₆): δ = 0.69 (t, 3H, ³J_{HH} = 7.26 Hz), 1.20 (m, 2H), 1.36 (m, 2H), 1.45 (m, 2H), 6.98 (t, 2H, ³J_{HH} = 7.15 Hz), 7.12 (t, 1H, ³J_{HH} = 7.25 Hz), 7.22 (t, 4H, ³J_{HH} = 7.67 Hz), 7.32 (t, 2H, ²J_{HH} = 7.68 Hz), 7.51 (d, 2H, ³J_{HH} = 7.68 Hz), 7.64 (br d, 2H, ³J_{HP} = 5.19 Hz).

³¹P{¹H} NMR (161.98 MHz, 300 K, C₆D₆): δ = -64.3 (s).

³¹P NMR (161.98 MHz, 300 K, C₆D₆): δ = -64.3 (s).

For **1c** (R = *t*Bu): TPP (300 mg, 0.989 mmol); *n*BuLi in *n*-hexane (0.581 mL, 0.989 mmol, 1.7 M).

Molecular formula: C₂₇H₂₆PLi (388.42 g·mol⁻¹)

Yield: 0.359 g (92%).

¹H NMR (400.13 MHz, 300K, C₆D₆): δ = 0.78 (d, 3H, ³J_{HP} = 11.8 Hz), 6.99 (t, 2H, ³J_{HH} = 7.28 Hz), 7.10 (t, 1H, ³J_{HH} = 7.23 Hz), 7.25 (t, 6H, ³J_{HH} = 7.66 Hz), 7.31 (m, 2H), 7.45 (d, 2H, ³J_{HH} = 7.66), 7.44 (br d, 2H, ³J_{HH} = 7.60 Hz), 7.82 (br d, 2H, ³J_{HP} = 3.87 Hz), 8.00 (br s, 4H).

³¹P{¹H} NMR (161.98 MHz, 300 K, C₆D₆): δ = -41.2 (s).

³¹P NMR (161.98 MHz, 300 K, C₆D₆): δ = -41.2 (s).

Elemental analysis calc. for C₂₇H₂₆LiP(Et₂O)_{2.0}: C, 78.33; H, 8.64; found: C, 78.14; H, 8.59.

For **1d** (R = Ph): TPP (500 mg, 0.15 mmol); PhLi in dibutyl ether (0.81 mL, 0.15 mmol, 1.9 M).

Molecular formula: C₂₉H₂₂PLi (408.41 g·mol⁻¹)

Yield: 626 mg (76%).

¹H NMR (400.13 MHz, 300K, C₆D₆): δ = 6.89–7.03 (m, 7H), 7.08 (s, 2H), 7.12–7.17 (overlapped m, 3H), 7.25 (d, 2H, ³J_{HH} = 7.58 Hz), 7.38 (t, 2H, ³J_{HH} = 6.68 Hz), 7.60 (d, 2H, ³J_{HH} = 6.01 Hz), 7.70 (br d, 4H, ³J_{HH} = 6.88 Hz).

³¹P{¹H} NMR (161.98 MHz, 300 K, C₆D₆): δ = -59.1 (s).

³¹P NMR (161.98 MHz, 300 K, C₆D₆): δ = -59.1 (s).

For **1e** (R = CH₂SiMe₃): TPP (334 mg, 0.10 mmol); Me₃SiCH₂Li in *n*-pentane (1 mL, 0.10 mmol, 1 M).

Molecular formula: C₂₇H₂₈PLiSi (418.52 g·mol⁻¹)

Yield: 266 mg (53%).

¹H NMR (400.13 MHz, 300K, C₆D₆): δ = 0.00 (s, 9H), 6.95 (m, 2H), 7.24 (m, 4H), 7.34 (m, 2H), 7.60 (m, 4H), 7.87 (m, 3H).

³¹P{¹H} NMR (161.98 MHz, 300 K, C₆D₆): δ = -60.3 (s).

Preparation of adduct **2 from **1c** and 2'-methylacetophenone:**

2'-Methylacetophenone (13 μL, 0.10 mmol) was added to a solution of **1c** (50 mg, 0.10 mmol) in *n*-hexane (1 mL) at room temperature. An immediate color change from deep pink to neon orange was observed. After stirring the mixture for 30 minutes at room temperature, the solvent was completely removed *in vacuo* in order to obtain a solid. **2** was isolated as a light orange powder.

Yield: 30 mg, 58%.

¹H NMR (400.13 MHz, 300 K, C₆D₆): δ = 0.70 (d, 9H, ³J_{PH} = 11 Hz, *t*Bu), 2.08 (s, 1H), 2.49 (s, 1H), 4.07 (t, 1H, 4 Hz), 6.45 (d, 1H, 4 Hz), 6.88–7.14 (m, 6H), 7.18–7.31 (m, 10 Hz), 7.45–7.48 (m, 4H), 7.66–7.68 (m, 1H), 7.85–7.87 (m, 2 H).

¹³C{¹H} NMR (100.61 MHz, 300 K, C₆D₆): δ = 21.8 (s), 29.3 (d, 12 Hz), 35.1 (d, 27 Hz), 42.5 (d, 22 Hz), 124.7 (d, 3 Hz), 125.7 (s), 126.3 (d, 3 Hz), 127.5 (s), 128.8 (m), 128.9 (s), 129.2 (s), 129.4 (s), 138.8 (s), 139.9 (s), 140.2 (s), 140.9 (d, 4 Hz), 142.4 (s), 144.5 (s), 144.7 (s), 172.2 (s), 172.7 (s).

³¹P{¹H} NMR (161.98 MHz, 300 K, C₆D₆): δ = -25.1 (s).

³¹P NMR (161.98 MHz, 300 K, C₆D₆): δ = -25.1 (m).

⁷Li NMR (155.58 MHz, 300 K, C₆D₆): δ = 1.1 (m).

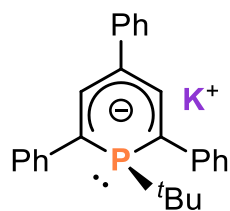
Elemental analysis calc. for C₃₆H₃₆PLiO: C 82.74, H 6.94; found C 82.05, H 7.04.

UV-Vis (*n*-hexane, λ_{max} / nm, ε_{max} / L·mol⁻¹·cm⁻¹): 314 (6565).

ATR-IR (THF, ν_{max} / cm⁻¹): 2116, 1687, 1589, 1549, 1461, 1457, 1446, 1377, 1351, 1289, 1251.

[K(1'-Bu- PC₅Ph₃H₂)] (3**):**

The potassium salt of **1c** was synthesized by reaction of KO^tBu (28.5 mg, 0.25 mmol) with **1c** (130 mg, 0.25 mmol) in *n*-hexane (2 mL). The resulting suspension was allowed to stir for 18 h. Afterwards, the precipitate was filtered off and washed with *n*-hexane (3 x 1.5 mL). The solid was dried *in vacuo* to yield **3** as a green powder. Crystals suitable for X-ray diffractometry were obtained by slow diffusion of *n*-hexane into a solution of **3** and [18]crown-6 in THF.



Molecular formula: C₂₇H₂₆PK (420.58 g·mol⁻¹)

Yield: 75.0 mg (54%).

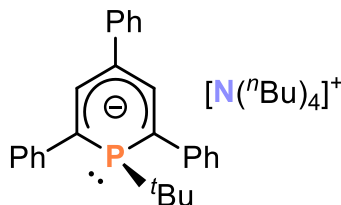
¹H NMR (400.13 MHz, 300K, C₆D₆) δ = 1.20 (d, 9H, ³J_{HP} = 11.6 Hz, PC(CH₃)₃), 7.02 (t, 2H, ³J_{HH} = 7.2 Hz, 2,6-*p*-H_{aryl}), 7.07 (t, 1H, ³J_{HH} = 7.3 Hz, 4-*p*-H_{aryl}), 7.32 (t, 4H, ³J_{HH} = 7.8 Hz, 2,6-*m*-H_{aryl}), 7.36 (t, 2H, ³J_{HH} = 7.5 Hz, 4-*m*-H_{aryl}) 7.52 (br d, 2H, ³J_{HH} = 7.9 Hz, 4-*o*-H_{aryl}), 7.69 (br d, 2H, ³J_{HP} = 5.6 Hz, 3-5-H_{aryl}), 8.04 (m, 4H, 2,6-*o*-H_{aryl}).

³¹P{¹H} NMR (161.98 MHz, 300 K, C₆D₆): δ = -39.2 (s).

³¹P NMR (161.98 MHz, 300 K, C₆D₆): δ = -39.2 (s).

[(N(ⁿBu)₄)(1-^tBu-PC₅Ph₃H₂)] (4):

1c (50 mg, 0.097 mmol) was dissolved in toluene and cooled to -30 °C. The cooled solution was slowly added to a pre-cooled suspension of tetrabutylammonium bromide (31.3 mg, 0.097 mmol) in toluene. The resulting green solution was warmed to room temperature overnight. The solvents were removed after filtration to yield **4** as a green oil. Crystals suitable for X-ray diffraction were obtained by dissolving **4** in THF and layering the solution with *n*-hexane. The amount of residual toluene was determined by ¹H NMR spectroscopy to be 33 mol%.



Molecular formula: C₄₃H₆₂PN (623.95 g·mol⁻¹)

Yield: 34.2 mg, 54%.

¹H NMR (400.13 MHz, 300K, C₆D₆): δ = 0.60 (m, 8H, N(CH₂CH₂Et)₄), 0.66 (t, 12H, ³J_{HH} = 7.3 Hz, N((CH₂)₃CH₃)₄), 0.92 (m, 8H, N((CH₂)₂CH₂Me)₄), 1.36 (d, 9H, ³J_{HP} = 11.2 Hz, PC(CH₃)₃), 2.10 (m, 8H, N(CH₂Pr)₄), 6.90 (t, 2H, ³J_{HH} = 7.1 Hz, 2,6-*p*-H_{aryl}), 7.02 (t, 1H, ³J_{HH} = 7.2 Hz, 4-*p*-H_{aryl}), 7.29 (t, 4H, ³J_{HH} = 7.7 Hz, 2,6-*m*-H_{aryl}), 7.37 (t, 2H, ³J_{HH} = 7.7 Hz, 4-*m*-H_{aryl}), 7.76 (d, 2H, ³J_{HH} = 7.7 Hz, 4-*o*-H_{aryl}), 8.18 (d, 2H, ³J_{HP} = 6.2 Hz, 3,5-H_{aryl}), 8.32 (m, 4H, 2,6-*o*-H_{aryl}).

³¹P{¹H} NMR (161.98 MHz, 300 K, C₆D₆): δ = -38.7 (s).

³¹P NMR (161.98 MHz, 300 K, C₆D₆): δ = -38.7 (s).

2.4.2 Catalytic Studies

General hydroboration procedure

To a screw-cap vial equipped with a stir-bar was added the required amount of catalyst **1c** either as a crystalline solid or as a stock solution. The desired volume of solvent (generally 1 mL if not stated otherwise) was then added. To the resultant solution was added neat substrate for liquids or as a THF solution for solid substrates (1.00 equiv.), and neat HBpin or HBcat (1.03 equiv.) using a Hamilton syringe. For acetophenone hydroboration, *n*-pentadecane was added as an internal standard (20 μ L). After the reaction was completed, aqueous NaOH was added (0.5 mL, 3M) followed by H₂O₂ (0.5 mL, 30%) and ethyl acetate (ca. 0.5 mL), and the resulting mixture was allowed to stir for 1 hour. The organic layer was then separated, dried over Na₂SO₄, filtered, and the solvent removed to give the raw product, which was purified by column chromatography using silica gel (*n*-hexane/ethyl acetate; 5:1). The solvent was then removed *in vacuo* for yield determination and NMR characterization.

Hydroboration of CO₂

The desired amount of catalyst was dissolved in THF-*d*₈ (0.5 mL) and added to a J. Young NMR tube along with HBpin (32 mg, 0.2 mmol, 36 μ L). The tube was degassed and exposed to an atmosphere of CO₂ (~1 bar), after which was monitored by ¹H and ¹¹B NMR spectroscopy to follow the reaction until completion.

General hydrosilylation procedure

To a screw-cap vial equipped with a stir-bar was added the required amount of catalyst **1c** either as a crystalline solid or as a stock solution. The desired volume of solvent (generally 1 mL if not stated otherwise) was then added. To the resultant solution was added neat substrate for liquids or as a THF solution for solid substrates (1.00 equiv.), and neat silane (1.03 equiv.) using a Hamilton syringe. For acetophenone hydrosilylation, *n*-pentadecane was added as an internal standard (20 μ L). After the reaction was completed, tetrabutylammonium fluoride (TBAF) was added dropwise, and the resulting mixture was allowed to stir for 2 hours. The mixture was then washed with H₂O, separated and dried over Na₂SO₄. Following filtration and removal of the solvent, the crude reaction mixture was purified by column chromatography using silica gel (*n*-hexane/ethyl acetate; 5:1). Aliquots were directly taken for GC-MS analysis. The solvent was then removed *in vacuo* for yield determination and NMR characterization.

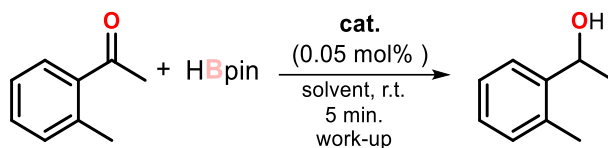
2.4.3 Kinetic Studies

General procedure for kinetic studies.

The substrate was weighed in or added *via* a microliter syringe to a GC vial equipped with a stir-bar. Internal Standard (*n*-pentadecane or mesitylene) and the required amount of a stock solution of the catalyst were added, as well as the desired volume of THF. The timer was started upon

addition of the HBpin and stopped with the addition of either water or CDCl_3 . Conversion was determined either by NMR spectroscopy or after extraction with ethyl acetate by GC-FID.

Table 6. Catalyst comparison during the hydroboration of 2'-methylacetophenone.^[a]



Entry	cat.	Solvent [mL]	Conversion [%] ^[b]
1	1c	THF (0.5)	82
2	2	THF (0.5)	64
3	3	THF (0.5)	40
4	5	THF (0.5)	66
5	1c	C_6H_6 (0.5)	17
6	2	C_6H_6 (0.5)	15
7	3	C_6H_6 (0.5)	17
8	5	C_6H_6 (0.5)	17
4	MeLi	THF (0.5)	86
5	ⁿ BuLi	THF (0.5)	83
6	^t BuLi	THF (0.5)	86
7	PhLi	THF (0.5)	86
8	$(\text{SiMe}_3)\text{CH}_2\text{Li}$	THF (0.5)	88
9	LiOMe	THF (0.5)	89
10	NaOMe	THF (0.5)	30
11	KOMe	THF (0.5)	78
12	LiO ^t Bu	THF (0.5)	87
13	NaO ^t Bu	THF (0.5)	76
14	KO ^t Bu	THF (0.5)	73
15	-	THF (0.5)	20 ^[c]

^[a]HBpin = 0.26 mmol, 2'-methylacetophenone = 0.25 mmol ^[b]Determined by GC-FID using *n*-pentadecane as an internal standard. ^[c]22% conversion after 18h.

General procedure for the kinetic studies with the ReactIR.

The strong vibrational frequency of the C=O bond stretch provides an easy method to study the kinetics of the hydroboration reaction. The consumption of the ketone is proportional to the decrease in intensity of the carbonyl peak at 1663 cm^{-1} .

The catalyst was added to a fitted Schlenk finger equipped with a stir-bar from a stock solution, followed by the desired amount of a stock solution of benzophenone. THF was added to reach the required volume, the *in situ* IR probe was then inserted into the reaction mixture and placed into a 20°C water bath. Once the temperature was steady, the experiment was started and a stock solution of HBpin was added *via* syringe. IR spectra were collected every 15 seconds over the course of the reaction.

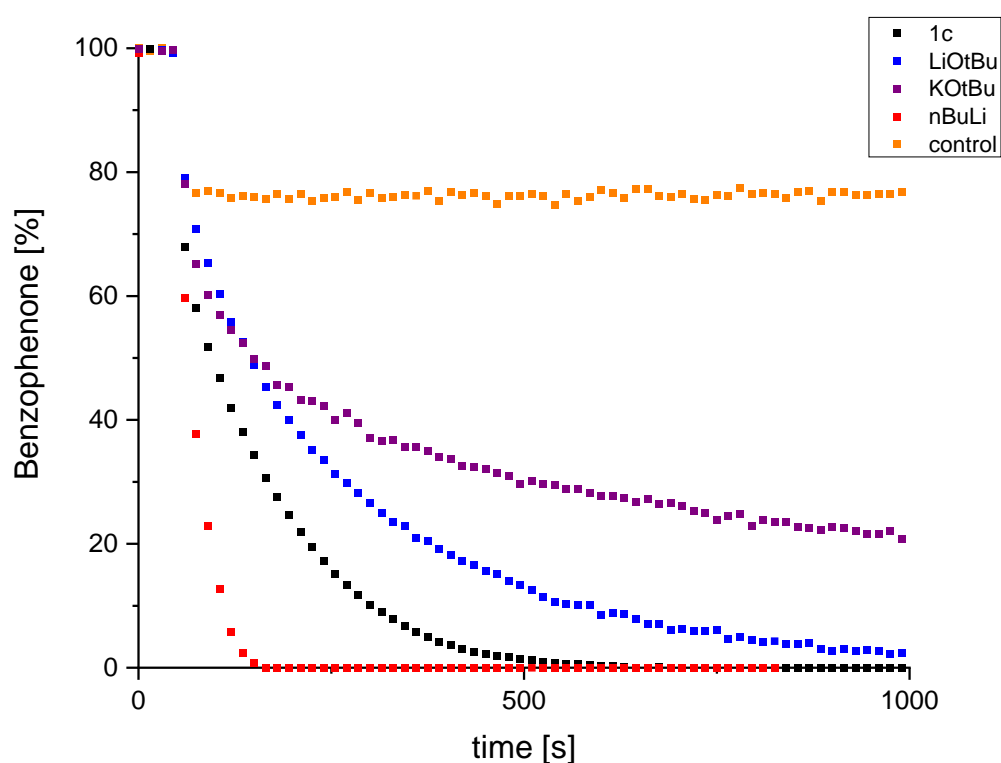


Figure 2. Hydroboration of benzophenone catalysed by different catalysts.

Mechanistic Studies

General Procedure: **1c** (20 mg, 0.039 mmol) was dissolved in 0.4 mL THF-*d*₈ in a Youngs-NMR tube. To this solution was added the desired amount of HBpin (1 or 15 equiv.) and/or the desired amount of 2'-methylacetophenone (1 or 25 equiv.). The reaction mixture was then analysed *via* NMR spectroscopy.

The reactions between **1c** and HBpin result in similar spectra for 1 and 15 equivalents of HBpin, in which most of **1c** (~ 90%)^[a] did not react. The ³¹P spectra also reveal a new broad signal at 10.6 ppm (~ 8-10%)^[a] as well as a minor signal at -24.4 ppm (< 2%)^[a]. The ¹¹B spectra show the unreacted HBpin (28.1 ppm) as the major species, together with minor signals at 22.2 and 21.3ppm (likely O(Bpin)₂ and B₂pin₃, respectively) as well as an unknown signal at 8.4 ppm. The ¹¹B spectra also reveal the formation of small amounts of LiBH₄ (-41.8 ppm). Therefore, whilst **1c** showcases some reactivity with HBpin in the absence of ketone, the low conversions even with an excess of HBpin suggest this to not be part of the (main) catalytic cycle.

The reaction between **1c** and 2'-methylacetophenone requires an excess of ketone in order to fully convert **1c** into the supposed adduct. Since a large excess of ketone (typically 1 000 – 10 000 -fold) is used in the catalysis this observation still fits with the measured 0th order dependance of the ketone concentration.

^[a]Amounts estimated by ³¹P{¹H} integration.

2.4.4 NMR Spectra

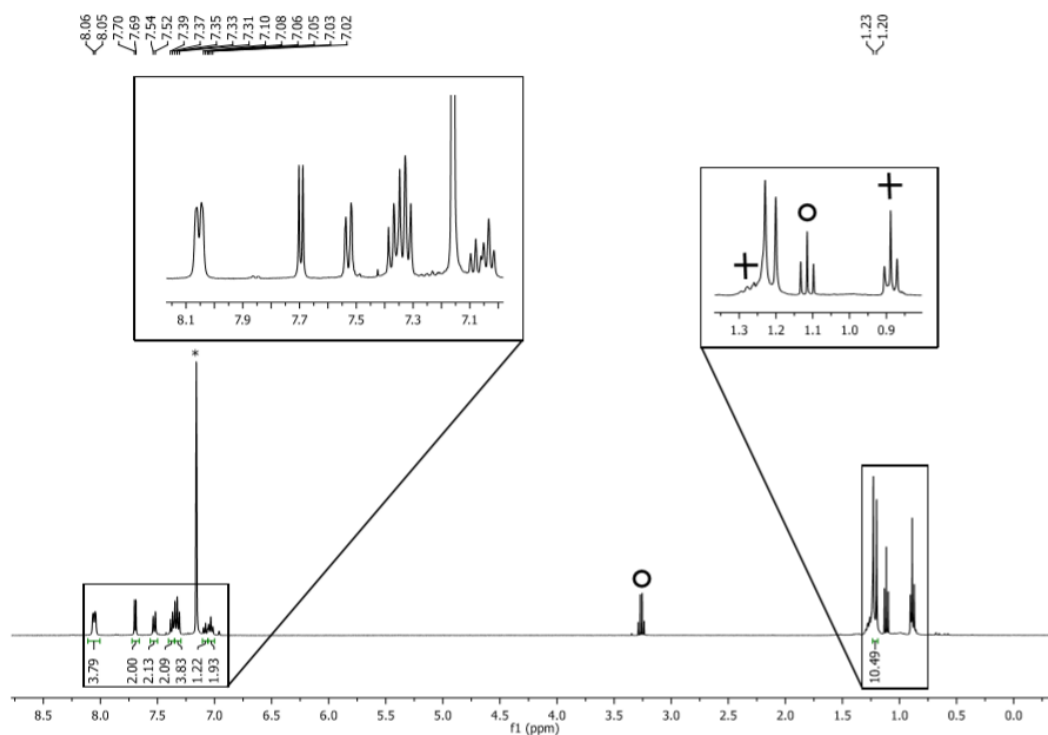


Figure 3. ^1H NMR spectrum (400.13 MHz, 300 K, C_6D_6) of **3**. * residual solvent, o Et_2O , + *n*-hexane.

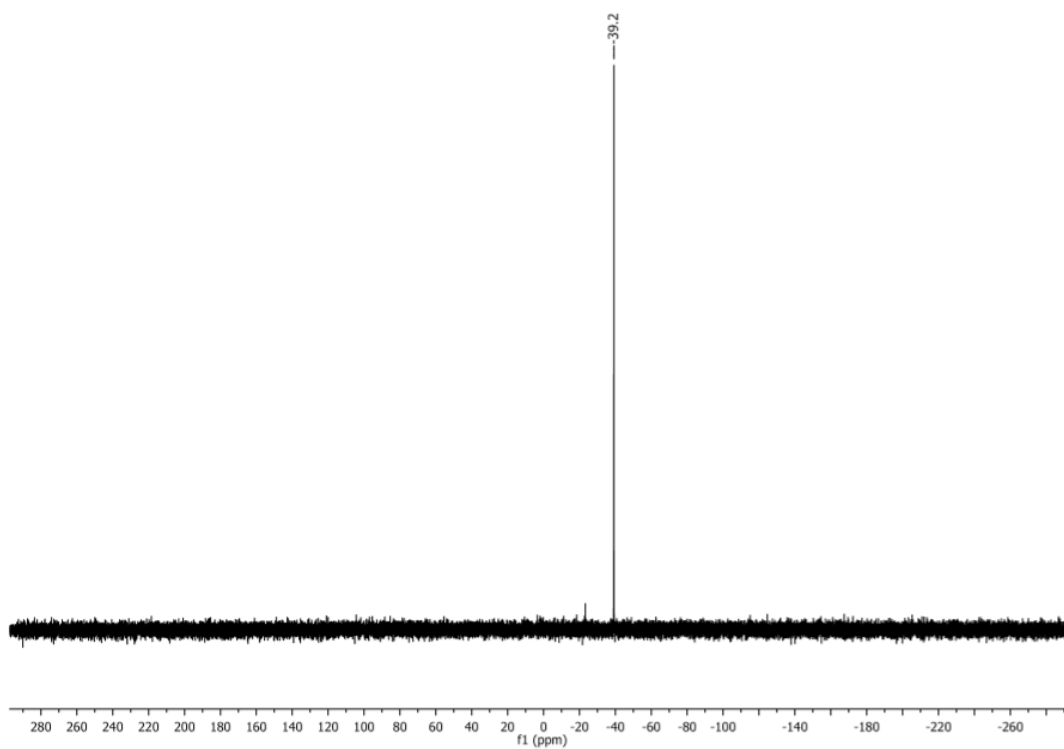


Figure 4. $^{31}\text{P}\{^1\text{H}\}$ NMR spectrum (161.98 MHz, 300 K, C_6D_6) of **3**.

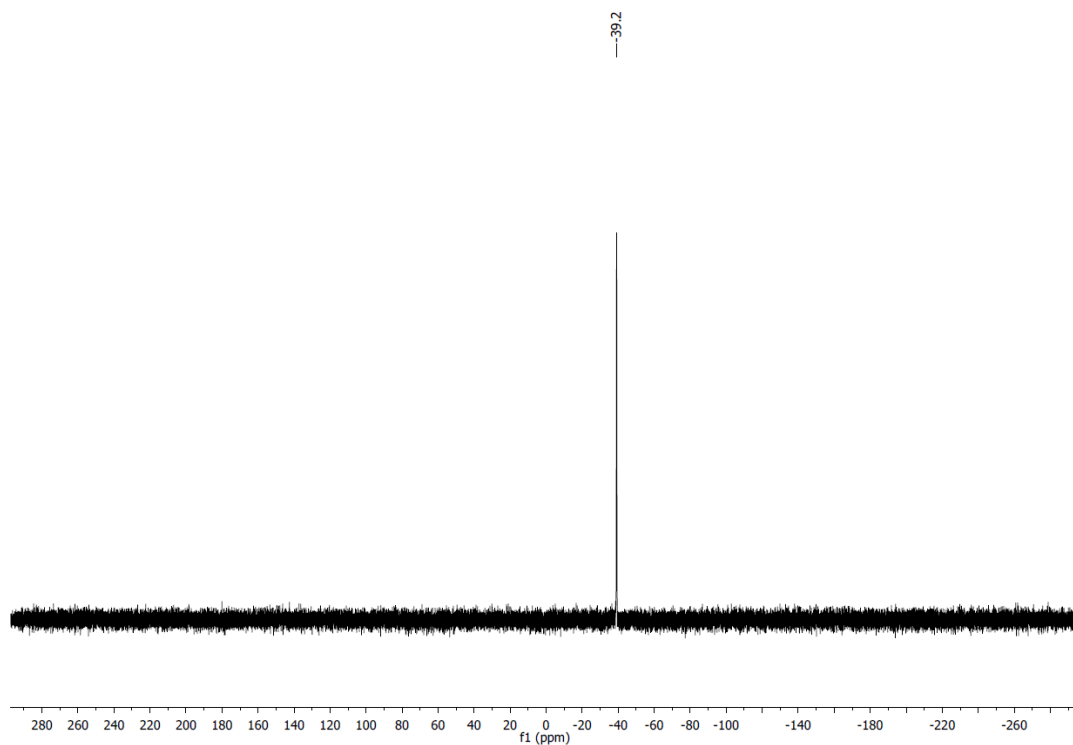


Figure 5. ^{31}P NMR spectrum (161.98 MHz, 300 K, C_6D_6) of **3**.

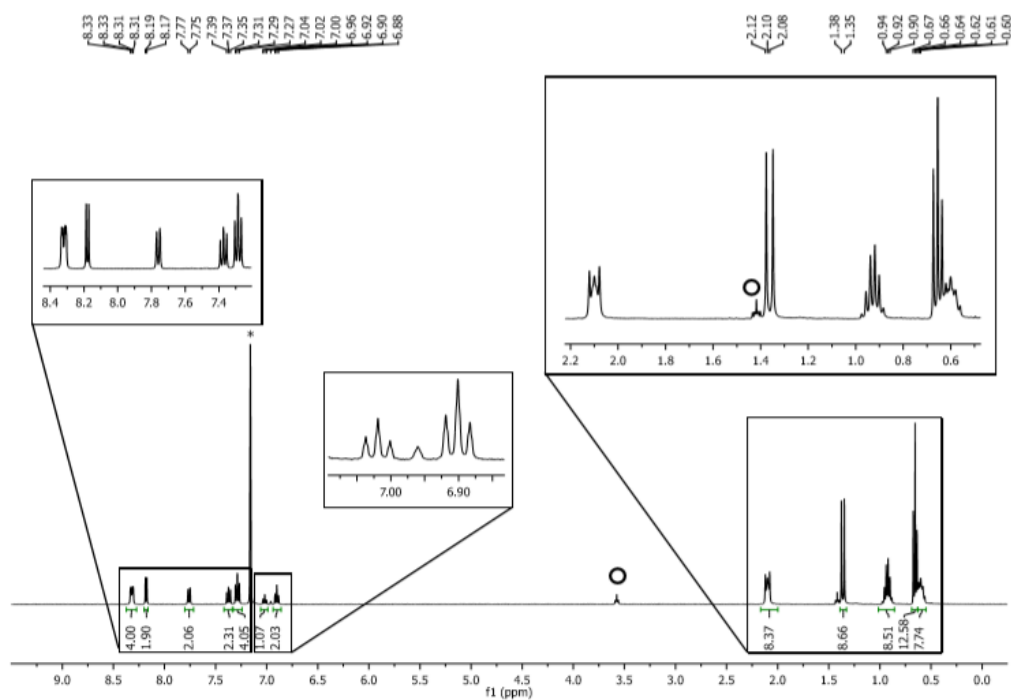


Figure 6. ^1H NMR spectrum (400.13 MHz, 300 K, C_6D_6) of **4**. * residual solvent, \circ THF

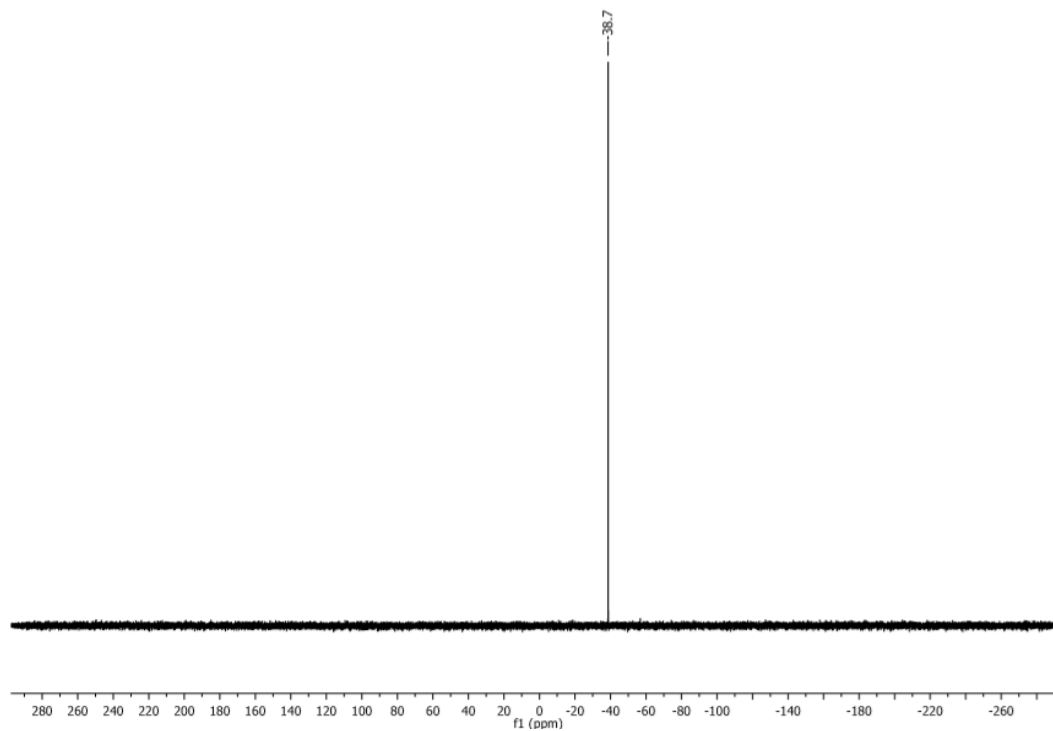


Figure 7. $^{31}\text{P}\{^1\text{H}\}$ NMR spectrum (161.98 MHz, 300 K, C_6D_6) of **4**.

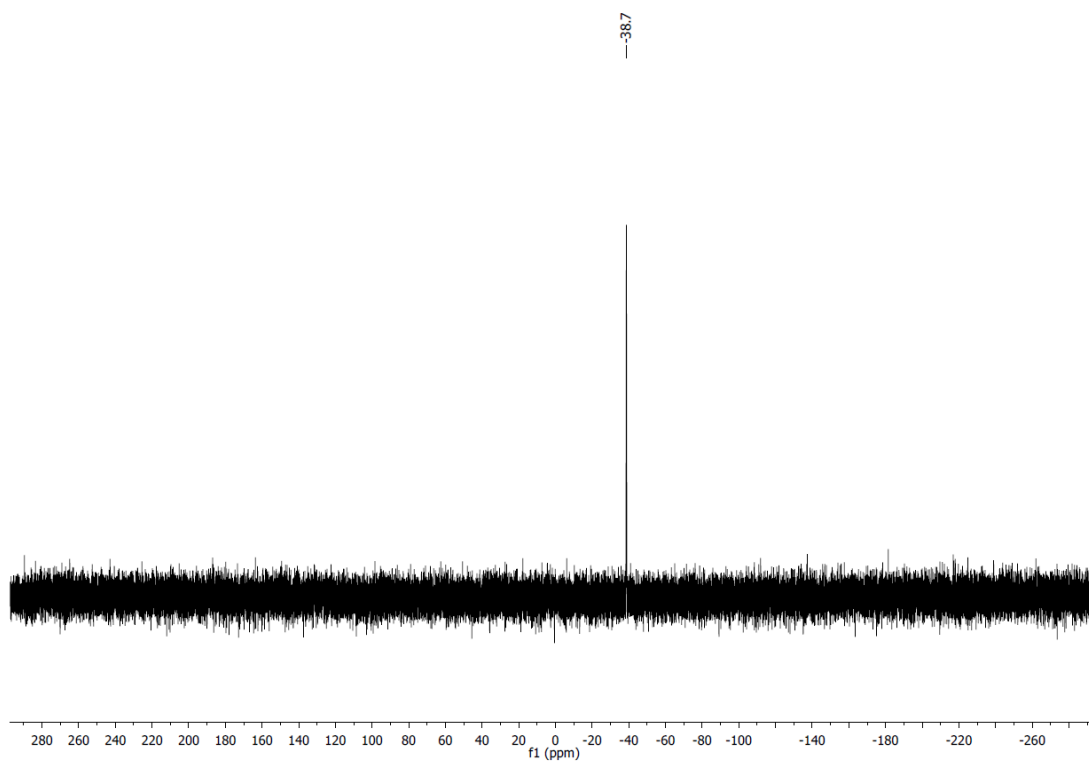


Figure 8. ^{31}P NMR spectrum (161.98 MHz, 300 K, C_6D_6) of **4**.

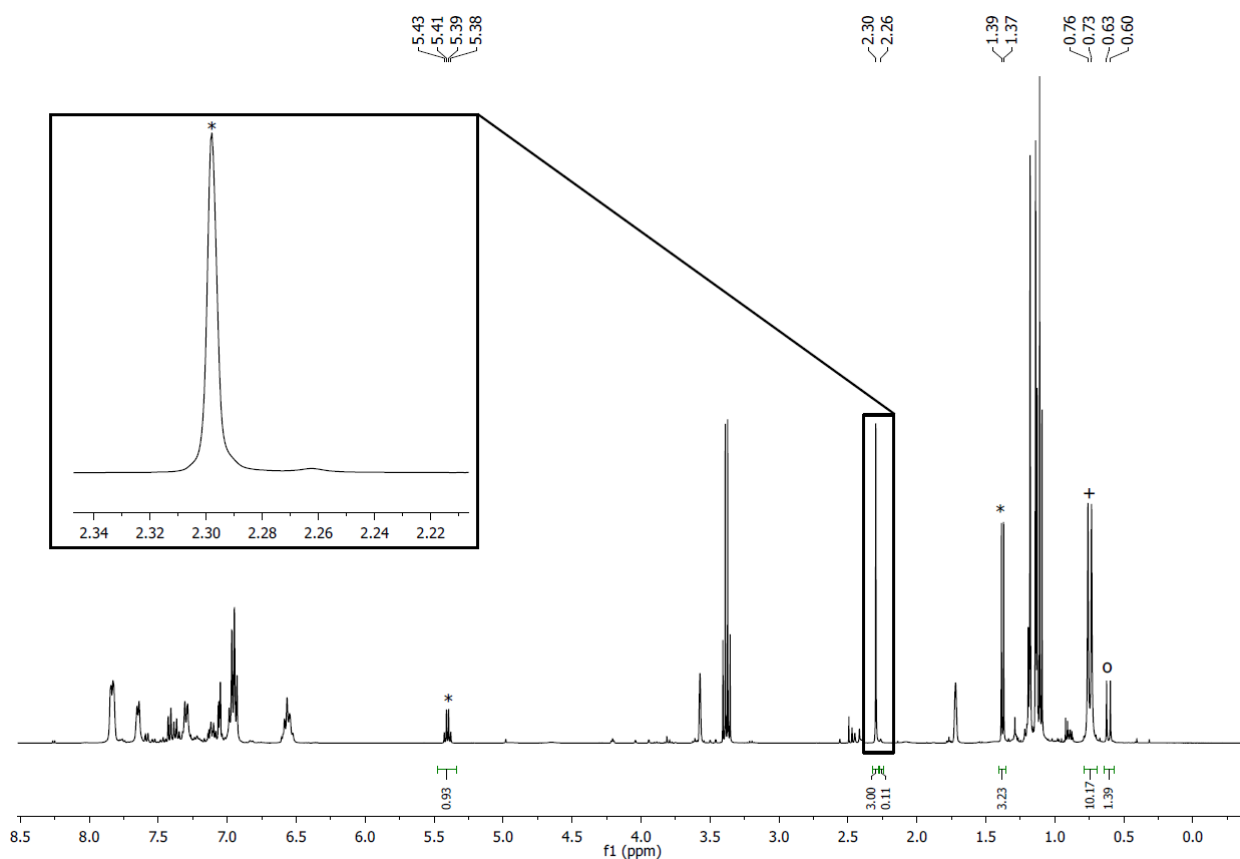


Figure 9. ^1H NMR spectrum (400.13 MHz, 300 K, $\text{THF-}d_8$) of the stoichiometric reaction of **1c**, HBpin and 2'-methylacetophenone. The marked signals belong to: *borolane, + **1c**, O adduct (**2**).

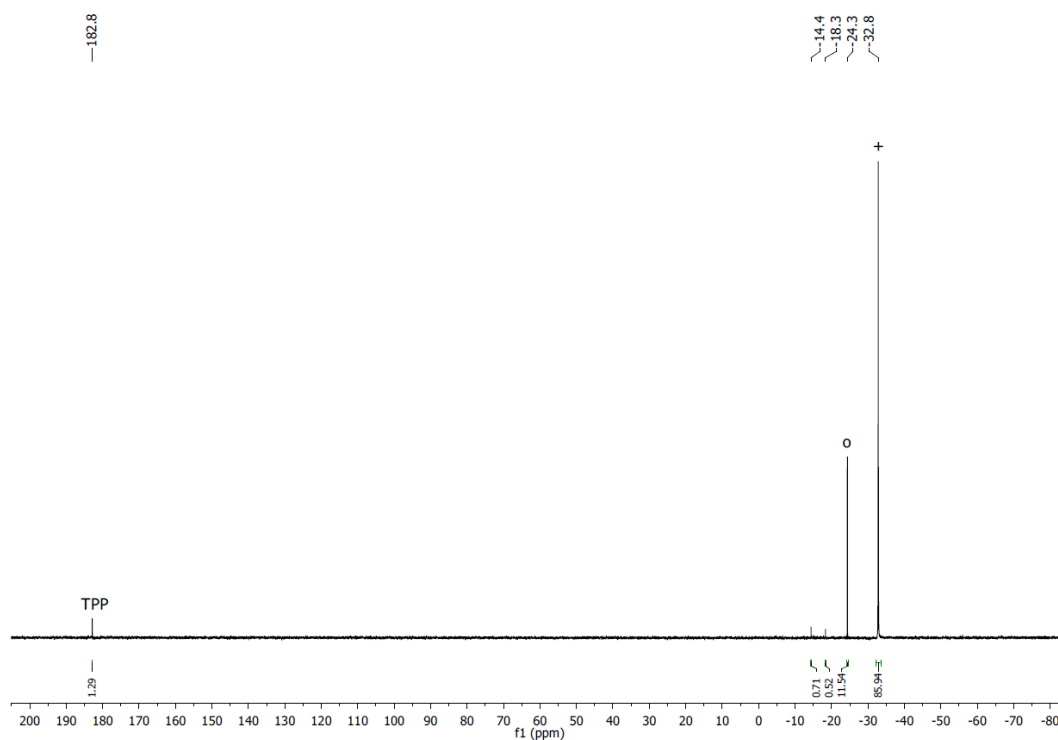


Figure 10. $^{31}\text{P}\{^1\text{H}\}$ NMR spectrum (161.98 MHz, 300 K, $\text{THF-}d_8$) of the stoichiometric reaction of **1c**, HBpin and 2'-methylacetophenone. + **1c**, O adduct (**2**).

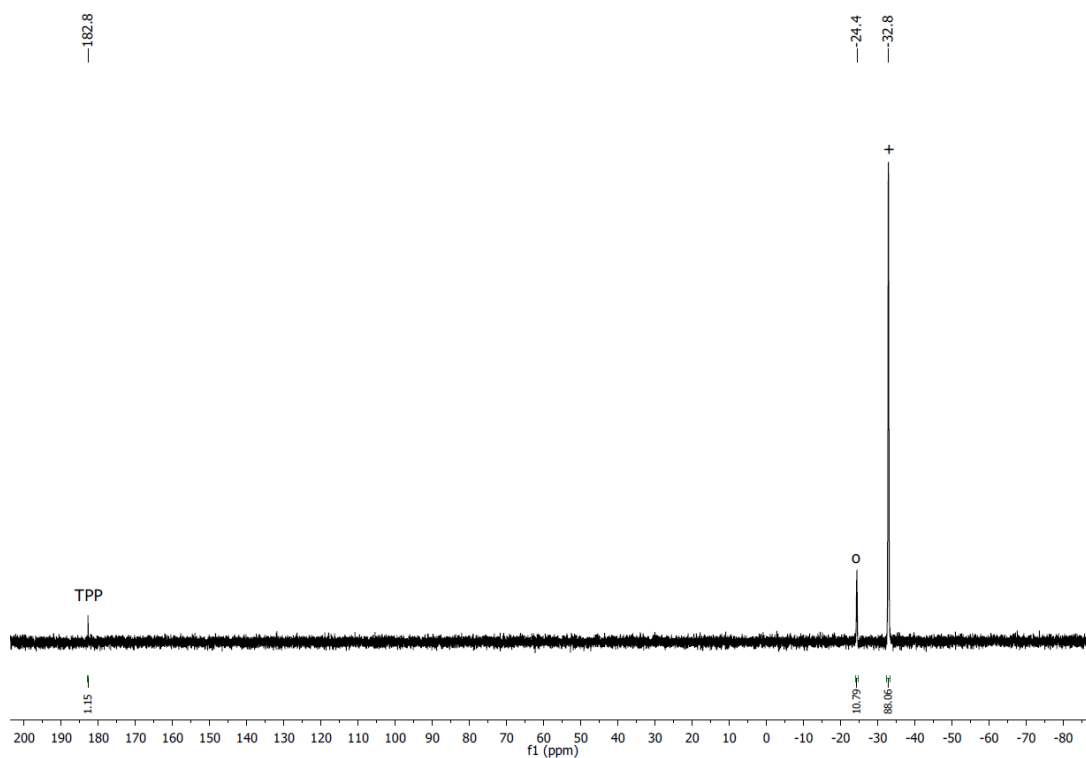


Figure 11. ^{31}P NMR spectrum (161.98 MHz, 300 K, $\text{THF-}d_8$) of the stoichiometric reaction of **1c**, HBpin and 2'-methylacetophenone. + **1c**, O adduct (**2**).

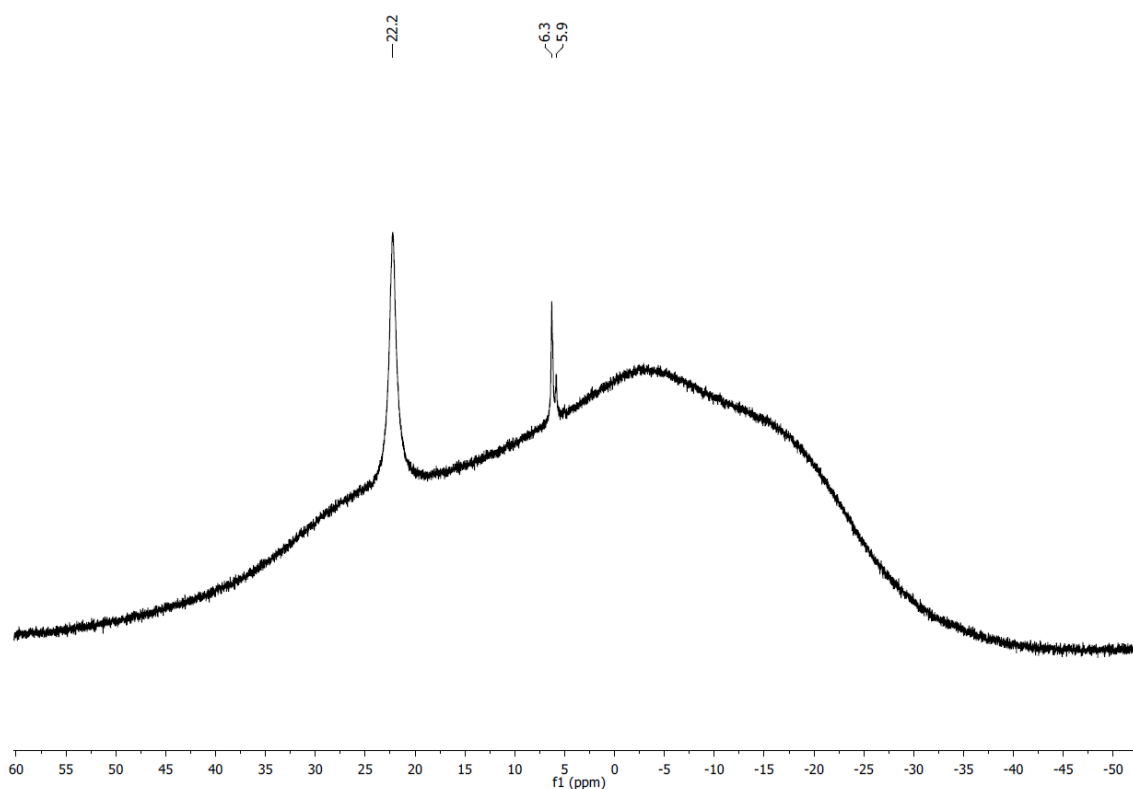


Figure 12. $^{11}\text{B}\{^1\text{H}\}$ NMR spectrum (128.43 MHz, 300 K, $\text{THF-}d_8$) of the stoichiometric reaction of **1c**, HBpin and 2'-methylacetophenone.

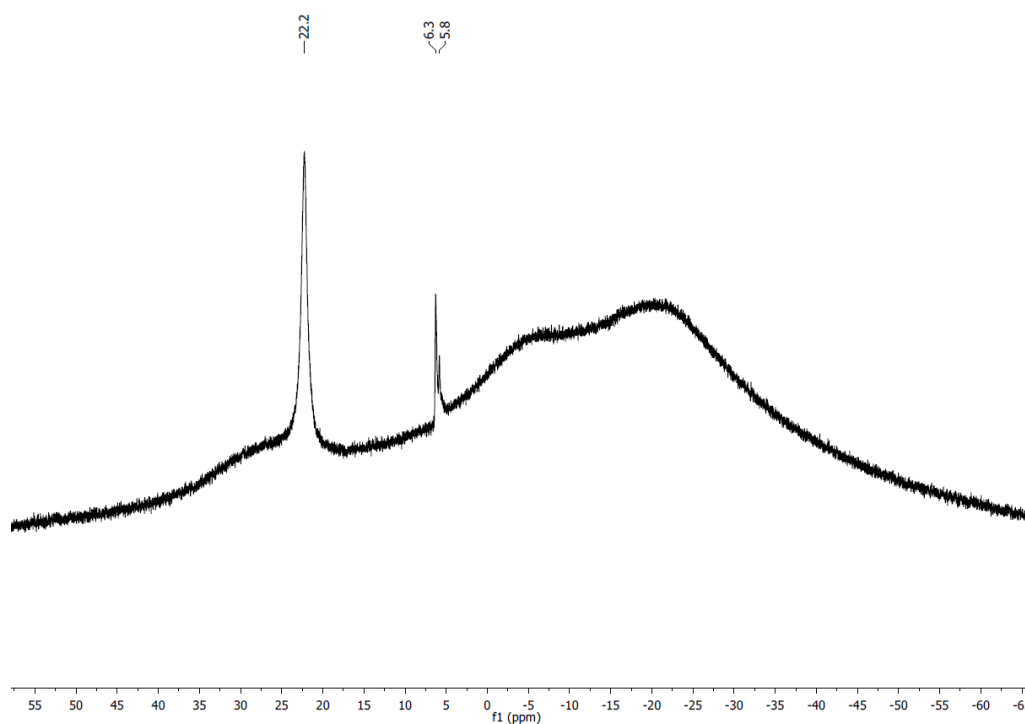


Figure 13. ^{11}B NMR spectrum (128.43 MHz, 300 K, THF-d_8) of the stoichiometric reaction of **1c**, HBpin and 2'-methylacetophenone.

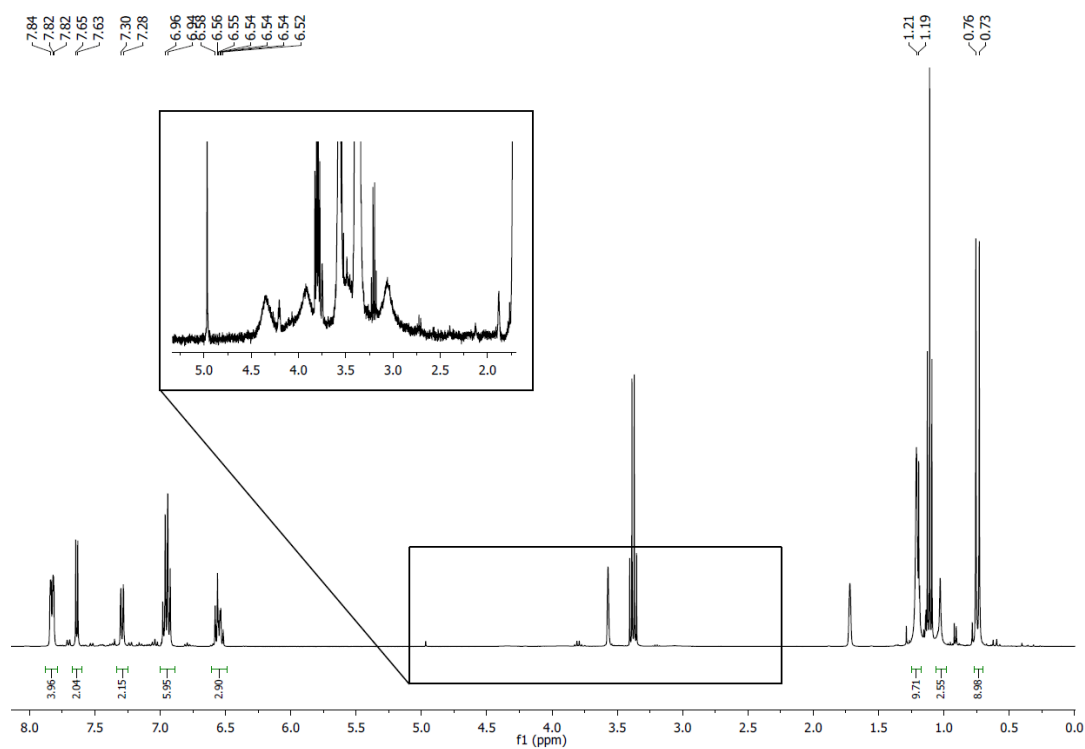


Figure 14. ^1H NMR spectrum (400.13 MHz, 300 K, THF-d_8) of the reaction of **1c** with HBpin (1:1).

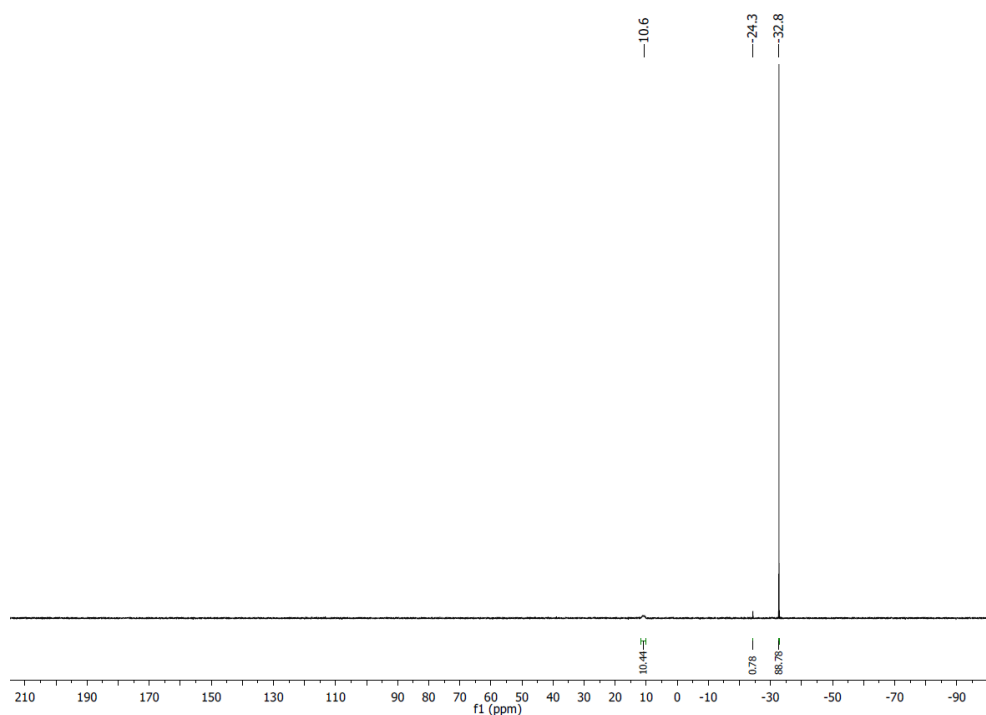


Figure 15. $^{31}\text{P}\{^1\text{H}\}$ NMR spectrum (161.98 MHz, 300 K, THF-*d*₈) of the reaction of **1c** with HBpin (1:1).

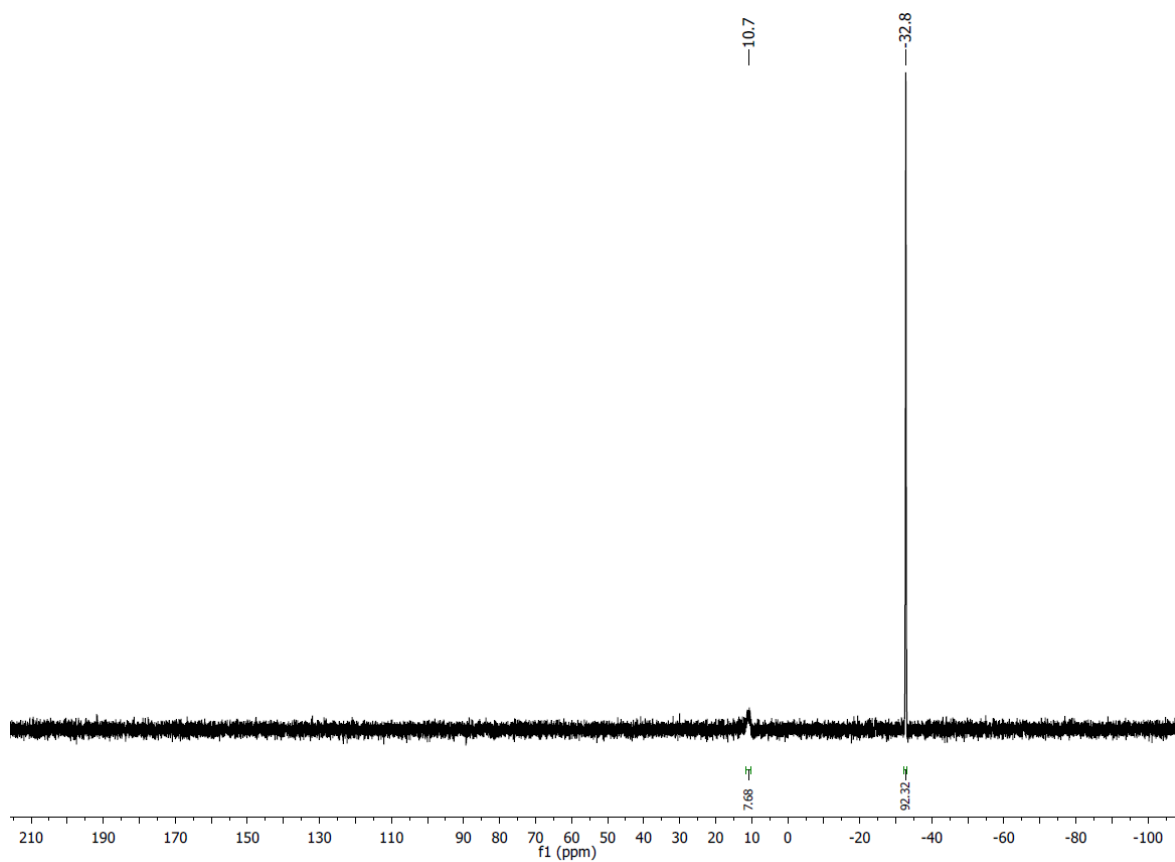


Figure 16. ^{31}P NMR spectrum (161.98 MHz, 300 K, THF-*d*₈) of the reaction of **1c** with HBpin (1:1).

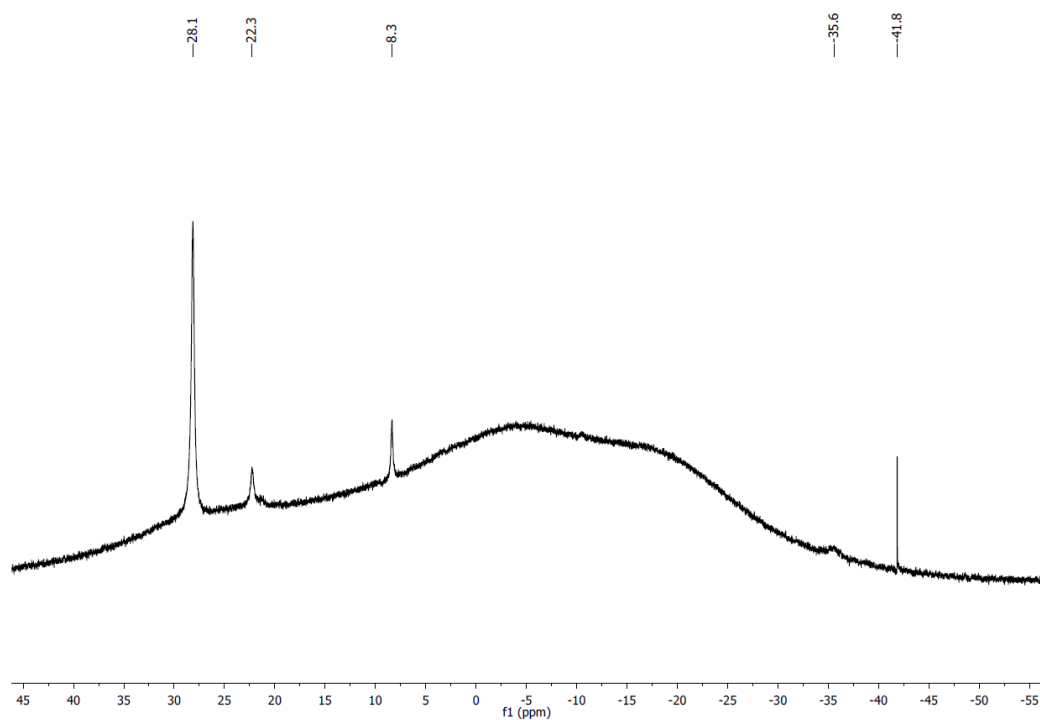


Figure 17. $^{11}\text{B}\{^1\text{H}\}$ NMR spectrum (128.43 MHz, 300 K, THF-*d*₈) of the reaction of **1c** with HBpin (1:1).

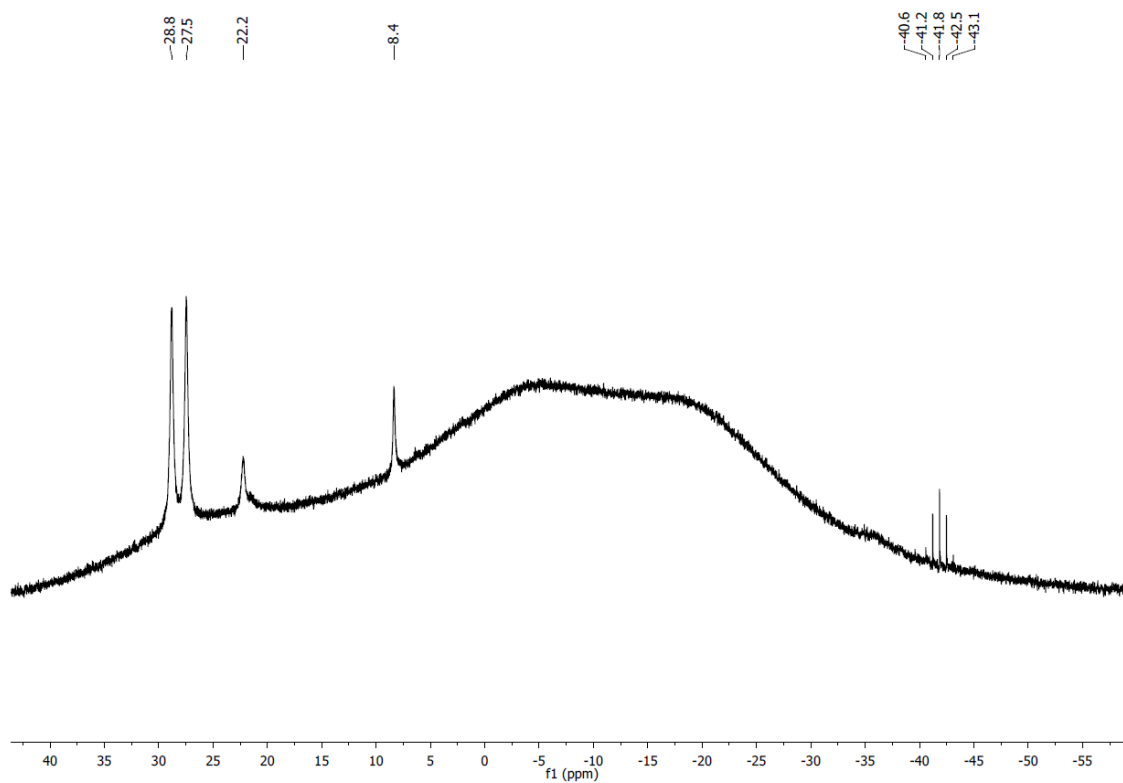


Figure 18. ^{11}B NMR spectrum (128.43 MHz, 300 K, THF-*d*₈) of the reaction of **1c** with HBpin (1:1).

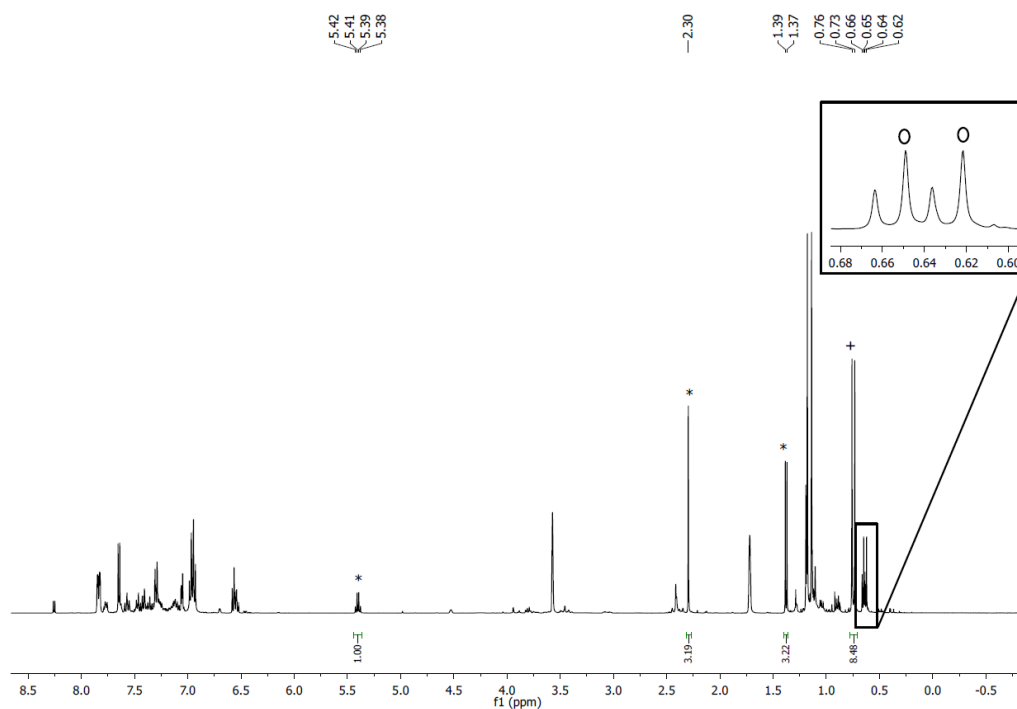


Figure 19. ^1H NMR spectrum (400.13 MHz, 300 K, $\text{THF-}d_8$) of the reaction of adduct **2** with HBpin. The marked signals belong to: *borolane, + **1c**, O adduct (**2**).

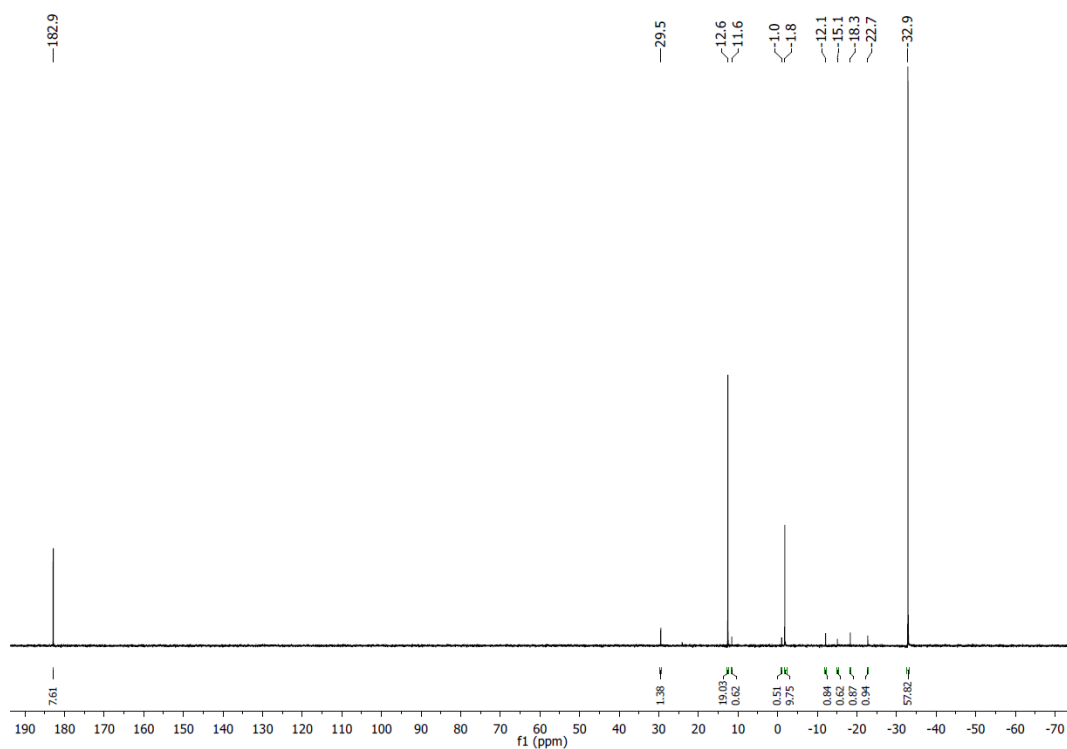


Figure 20. $^{31}\text{P}\{^1\text{H}\}$ NMR spectrum (161.98 MHz, 300 K, $\text{THF-}d_8$) of the reaction of adduct **2** with HBpin.

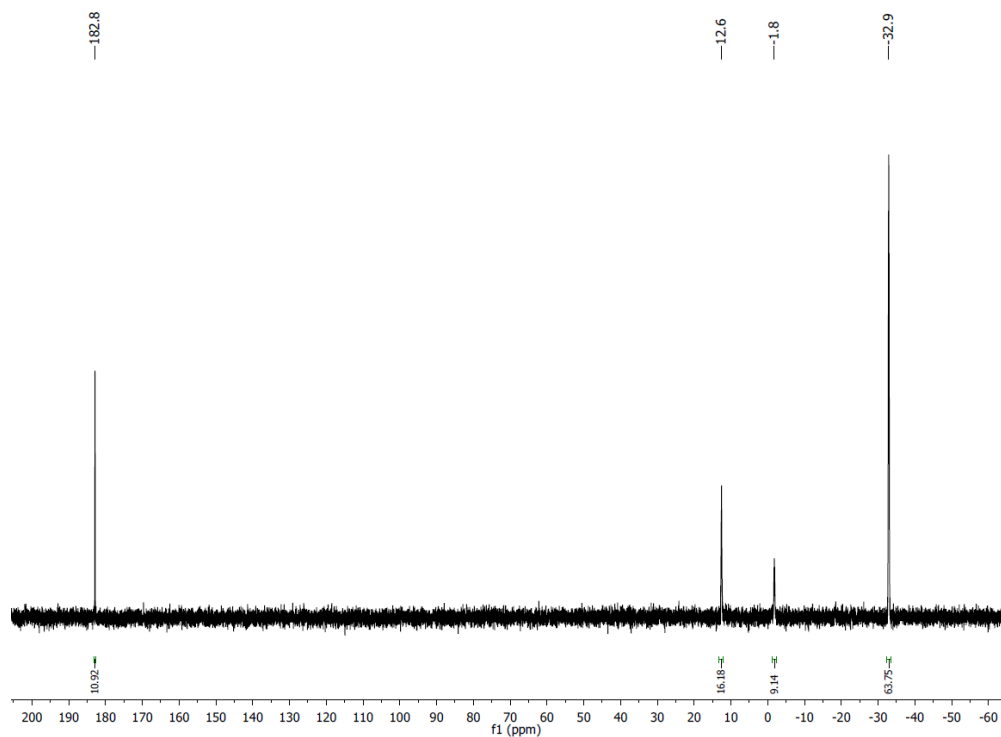


Figure 21. ^{31}P NMR spectrum (161.98 MHz, 300 K, $\text{THF-}d_8$) of the reaction of adduct **2** with HBpin.

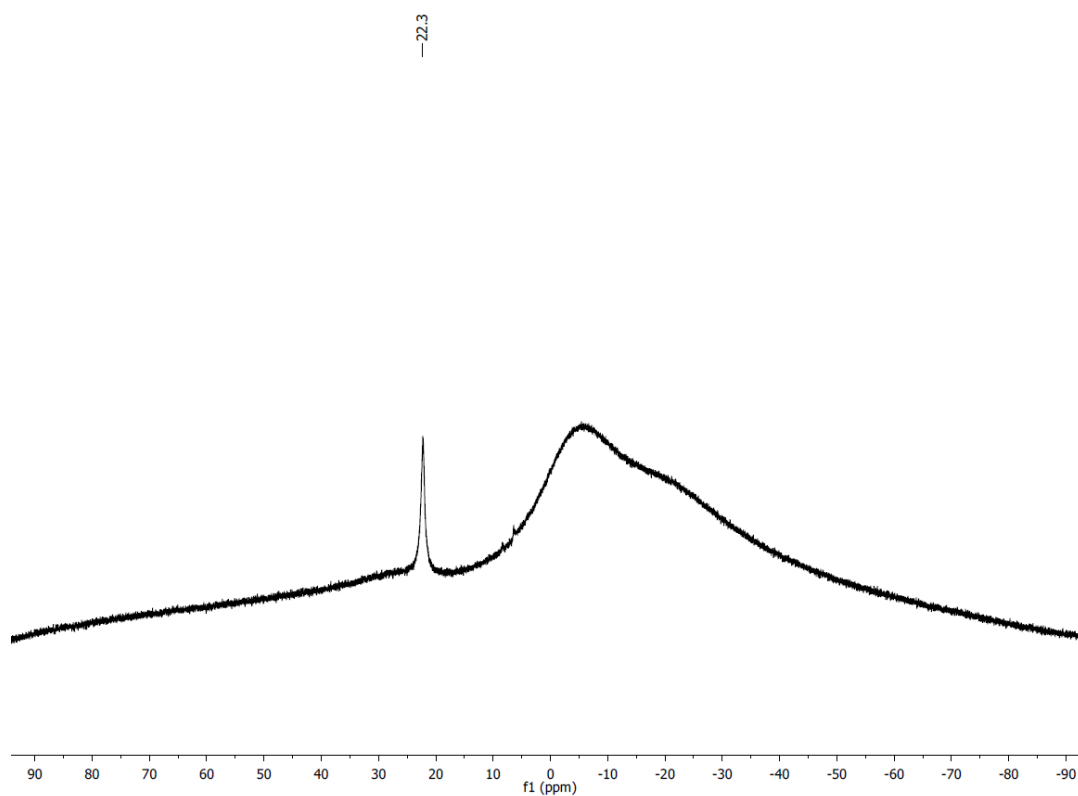


Figure 22. $^{11}\text{B}\{^1\text{H}\}$ NMR spectrum (128.43 MHz, 300 K, $\text{THF-}d_8$) of the reaction of adduct **2** with HBpin.

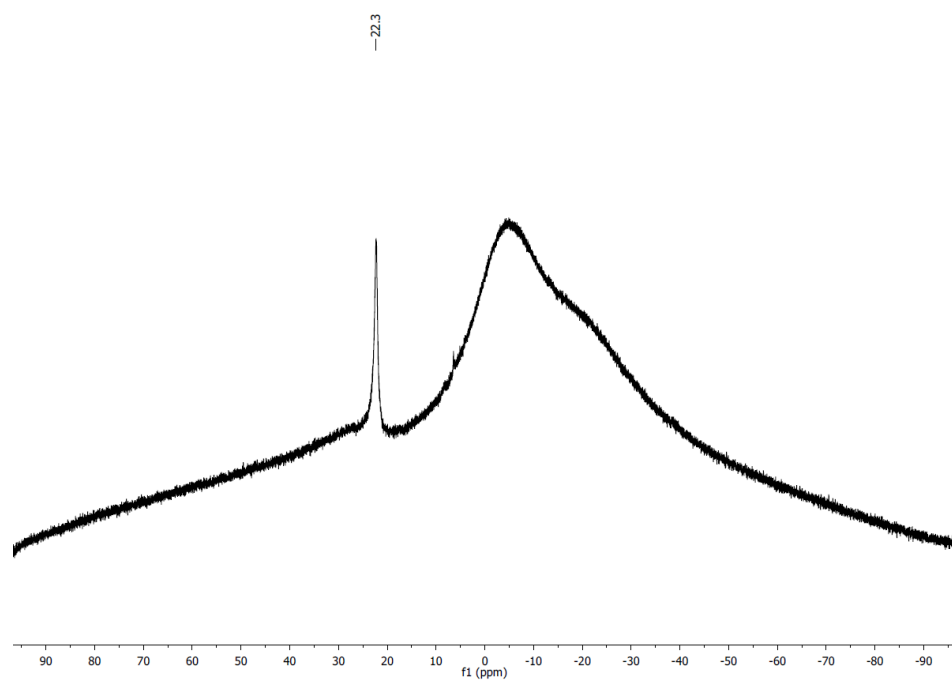


Figure 23. ^{11}B NMR spectrum (128.43 MHz, 300 K, $\text{THF-}d_8$) of the reaction of adduct **2** with HBpin.

2.4.5 Crystallographic Data

Table 7. X-ray Crystallographic Data for Compounds **1c**-[2.2.2]crypt, **3**-[18]crown-6, and **4**.

	1c -[2.2.2]crypt	3 -[18]crown-6	4
Empirical formula	C ₄₅ H ₆₂ LiN ₂ O ₆ P	C ₄₃ H ₅₈ KO ₈ P	C ₄₃ H ₆₂ NP
Formula weight / g·mol ⁻¹	764.87	772.96	623.90
Temperature / K	293(2)	123.01(10)	123.0(1)
Crystal system	monoclinic	triclinic	orthorhombic
Space group	P2 ₁ /n	P-1	Pbca
<i>a</i> / Å	11.6845(2)	19.4554(4)	15.9629(3)
<i>b</i> / Å	14.3840(3)	21.1335(5)	20.2379(3)
<i>c</i> / Å	25.0072(5)	34.8627(5)	23.9175(4)
α / °	90	74.367(2)	90
β / °	102.155(2)	89.608(2)	90
γ / °	90	64.045(2)	90
<i>V</i> / Å ³	4108.73(15)	12309.0(5)	7726.7(2)
<i>Z</i>	4	12	8
ρ_{calc} / g cm ⁻³	1.236	1.251	1.073
μ / mm ⁻¹	0.987	1.912	0.824
<i>F</i> (000)	1648.0	4968.0	2736.0
Crystal size / mm ³	0.260 × 0.218 × 0.055	0.478 × 0.293 × 0.226	0.235 × 0.1 × 0.053
Radiation / Å	Cu K α (λ = 1.54184)	Cu K α (λ = 1.54184)	Cu K α (λ = 1.54184)
2 θ range for data collection / °	7.13 – 147.452	6.872 – 148.38	7.964 – 151.998
Diffractometer	Supernova	Supernova	Supernova
Index ranges	-13 ≤ <i>h</i> ≤ 14, -13 ≤ <i>k</i> ≤ 17, -31 ≤ <i>l</i> ≤ 30	-19 ≤ <i>h</i> ≤ 24, -17 ≤ <i>k</i> ≤ 26, -41 ≤ <i>l</i> ≤ 43	-19 ≤ <i>h</i> ≤ 19, -25 ≤ <i>k</i> ≤ 17, -25 ≤ <i>l</i> ≤ 29
Reflections collected	16850	100433	20326
Independent reflections	8070 [R _{int} = 0.0182, R _{sigma} = 0.0233]	48493 [R _{int} = 0.0302, R _{sigma} = 0.0361]	7882 [R _{int} = 0.0249, R _{sigma} = 0.0270]
Data/restraints/parameters	8070/0/499	48493/812/3046	7882/0/413
Goodness-of-fit on F ²	1.010	1.128	1.014
Final R indexes [I ≥ 2 σ (I)]	R ₁ = 0.0331, wR ₂ = 0.0832	R ₁ = 0.0761, wR ₂ = 0.2002	R ₁ = 0.0387, wR ₂ = 0.0971
Final R indexes [all data]	R ₁ = 0.0391, wR ₂ = 0.0875	R ₁ = 0.0839, wR ₂ = 0.2040	R ₁ = 0.0500, wR ₂ = 0.1047
Largest diff. peak/hole/e Å ⁻³	0.30/-0.28	1.25/-0.61	0.30/-0.27

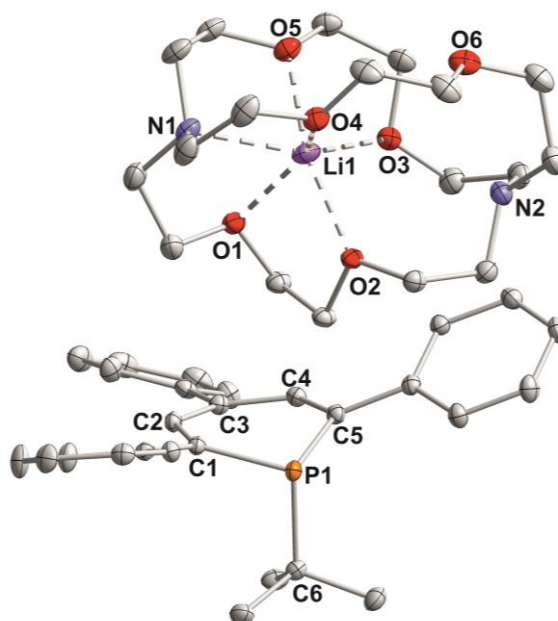


Figure 24. Solid state molecular structure of **1c**-[2.2.2]crypt; ellipsoids are drawn at the 40% probability level; H atoms are omitted for clarity; selected bond lengths [Å] and bond angles [°]: P1–C1 1.8229(11), C1–C2 1.3787(16), C2–C3 1.4205(16), C3–C4 1.4105(16), C4–C5 1.3858(16), C5–P1 1.8127(12), P1–C6 1.8991(12), C1–P1–C5 98.83(5), fold angle C1–P1–C5 25.7567(3).

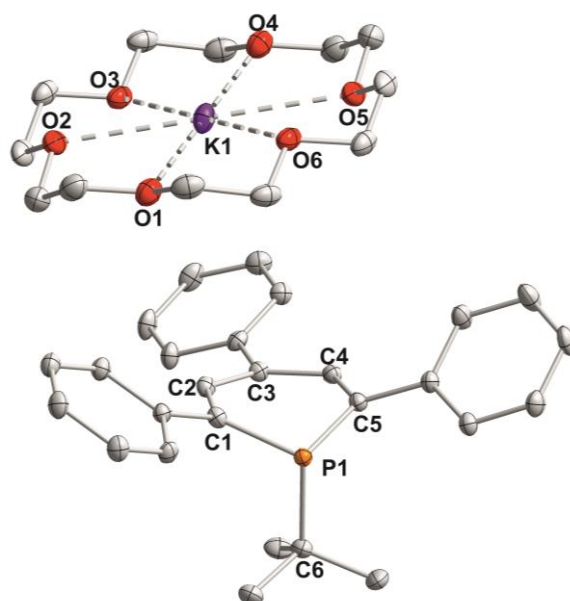


Figure 25. Solid state molecular structure of **3**-[18]crown-6; ellipsoids are drawn at the 40% probability level; H atoms are omitted for clarity; the asymmetric unit contains six molecules of **3**-[18]-crown-6, only one molecule is shown for clarity; three [K([18]crown-6)] units are coordinated by two dioxane molecules, the other three units are solvent free.

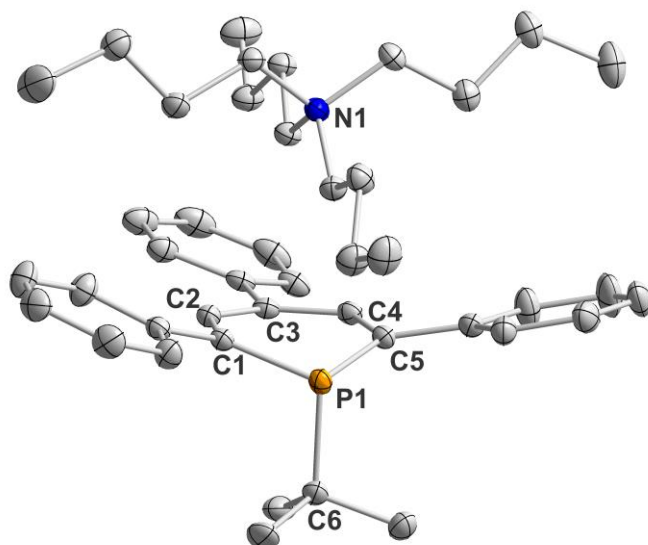


Figure 26. Solid state molecular structure of **4**; ellipsoids are drawn at the 40% probability level; H atoms are omitted for clarity; selected bond lengths [Å] and bond angles [°]: P1–C1: 1.8251(12), C1–C2: 1.3809(18), C2–C3: 1.4182(17), C3–C4: 1.4107(17), C4–C5: 1.3790(17), C5–P1: 1.8238(12), P1–C6: 1.9003(14), C1–P1–C5: 99.22(6), fold angle C1–P1–C5: 22.3(1).

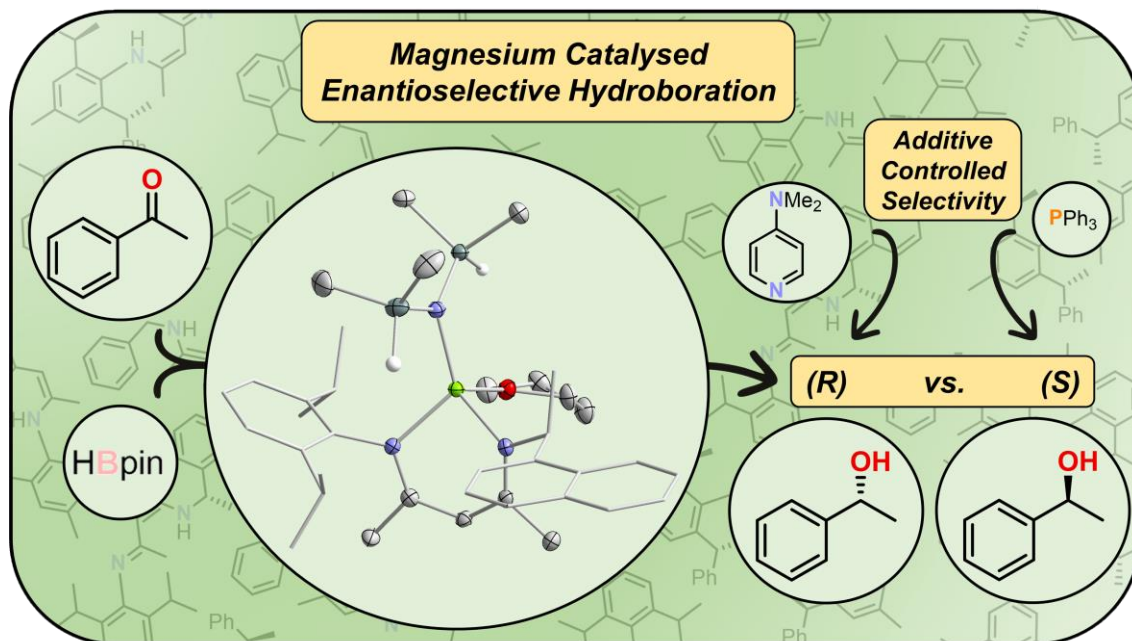
References

- [1] P. P. Power, *Nature* **2010**, *463*, 171–177.
- [2] a) J.-F. Carpentier, V. Bette, *Curr. Org. Chem.* **2002**, *6*, 913–936; b) C. C. Chong, R. Kinjo, *ACS Catal.* **2015**, *5*, 3238–3259; c) S. Díez-González, S. P. Nolan, *Org. Prep. Proced. Int.* **2007**, *39*, 523–559; d) K. Kuciński, G. Hreczycho, *Green Chem.* **2020**, *22*, 5210–5224.
- [3] a) E. P. Beaumier, A. J. Pearce, X. Y. See, I. A. Tonks, *Nature reviews. Chemistry* **2019**, *3*, 15–34; b) J. Magano, J. R. Dunetz, *Org. Process Res. Dev.* **2012**, *16*, 1156–1184; c) Z. Rappoport, Y. Apeloig (Eds.) *The Chemistry of Organic Silicon Compounds*, John Wiley & Sons, Chichester, UK, **1998**.
- [4] a) M. R. Adams, C.-H. Tien, B. S. N. Huchenski, M. J. Ferguson, A. W. H. Speed, *Angew. Chem. Int. Ed.* **2017**, *56*, 6268–6271; b) M. Arrowsmith, M. S. Hill, G. Kociok-Köhn, *Chemistry* **2013**, *19*, 2776–2783; c) M. S. Hill, D. J. Liptrot, C. Weetman, *Chem. Soc. Rev.* **2016**, *45*, 972–988; d) M. Oestreich, J. Hermeke, J. Mohr, *Chem. Soc. Rev.* **2015**, *44*, 2202–2220; e) M. L. Shegavi, S. K. Bose, *Catal. Sci. Technol.* **2019**, *9*, 3307–3336; f) C. Weetman, S. Inoue, *ChemCatChem* **2018**, *10*, 4213–4228; g) Q. Yin, Y. Soltani, R. L. Melen, M. Oestreich, *Organometallics* **2017**, *36*, 2381–2384.
- [5] J. H. Kim, A. K. Jaladi, H. T. Kim, D. K. An, *Bull. Korean Chem. Soc.* **2019**, *40*, 971–975.
- [6] I. P. Query, P. A. Squier, E. M. Larson, N. A. Isley, T. B. Clark, *J. Org. Chem.* **2011**, *76*, 6452–6456.
- [7] D. H. Ma, A. K. Jaladi, J. H. Lee, T. S. Kim, W. K. Shin, H. Hwang, D. K. An, *ACS omega* **2019**, *4*, 15893–15903.
- [8] W. Wang, K. Lu, Y. Qin, W. Yao, D. Yuan, S. A. Pullarkat, L. Xu, M. Ma, *Tetrahedron* **2020**, *76*, 131145.
- [9] S. J. Yang, A. K. Jaladi, J. H. Kim, S. Gundeti, D. K. An, *Bull. Korean Chem. Soc.* **2018**.
- [10] Z. Zhu, X. Wu, X. Xu, Z. Wu, M. Xue, Y. Yao, Q. Shen, X. Bao, *J. Org. Chem.* **2018**, *83*, 10677–10683.
- [11] W. Wang, M. Luo, W. Yao, M. Ma, S. A. Pullarkat, L. Xu, P.-H. Leung, *New J. Chem.* **2019**, *43*, 10744–10749.
- [12] J. M. Blackwell, E. R. Sonmor, T. Scoccitti, W. E. Piers, *Org. Lett.* **2000**, *2*, 3921–3923.
- [13] a) T. Lundrigan, E. N. Welsh, T. Hynes, C.-H. Tien, M. R. Adams, K. R. Roy, K. N. Robertson, A. W. H. Speed, *J. Am. Chem. Soc.* **2019**, *141*, 14083–14088; b) J. Zhang, J.-D. Yang, J.-P. Cheng, *Nat. Commun.* **2021**, *12*, 2835.
- [14] D. Addis, S. Zhou, S. Das, K. Junge, H. Kosslick, J. Harloff, H. Lund, A. Schulz, M. Beller, *Chem. Asian J.* **2010**, *5*, 2341–2345.
- [15] K. Revunova, G. I. Nikonov, *Chemistry* **2014**, *20*, 839–845.
- [16] M. Zhao, W. Xie, C. Cui, *Chemistry* **2014**, *20*, 9259–9262.
- [17] a) A. J. Ashe, T. W. Smith, *Tetrahedron Lett.* **1977**, *18*, 407–410; b) M. Bruce, G. Meissner, M. Weber, J. Wiecko, C. Müller, *Eur. J. Inorg. Chem.* **2014**, *2014*, 1719–1726; c) G. Märkl, F. Lieb, A. Merz, *Angew. Chem. Int. Ed.* **1967**, *6*, 87–88; d) G. Märkl, C. Martin, *Angew. Chem. Int. Ed.* **1974**, *13*, 408–409; e) G. Märkl, A. Merz, *Tetrahedron Lett.* **1968**, *9*, 3611–3614.
- [18] D. Mukherjee, H. Osseili, T. P. Spaniol, J. Okuda, *J. Am. Chem. Soc.* **2016**, *138*, 10790–10793.
- [19] T. J. Hadlington, C. E. Kefalidis, L. Maron, C. Jones, *ACS Catal.* **2017**, *7*, 1853–1859.
- [20] a) J. Burés, *Angew. Chem. Int. Ed.* **2016**, *55*, 16084–16087; b) C. D.-T. Nielsen, J. Burés, *Chem. Sci.* **2019**, *10*, 348–353.
- [21] G. Becker, W. Hölderich, *Chem. Ber.* **1975**, *108*, 2484–2485.
- [22] S. Perrone, A. Salomone, A. Caroli, A. Falcicchio, C. Citti, G. Cannazza, L. Troisi, *Eur. J. Org. Chem.* **2014**, *2014*, 5932–5938.
- [23] a) SCALE3ABS, CrysAlisPro, Agilent Technologies Inc., Oxford, GB, **2012**; b) G. M. Sheldrick, SADABS, Bruker AXS, Madison, USA, **2007**.
- [24] R. C. Clark, J. S. Reid, *Acta Cryst.* **1995**, *51*, 887–897.
- [25] G. M. Sheldrick, *Acta Cryst.* **2015**, *71*, 3–8.
- [26] G. M. Sheldrick, *Acta Cryst.* **2008**, *64*, 112–122.
- [27] G. Märkl, C. Martin, W. Weber, *Tetrahedron Letters* **1981**, *22*, 1207–1210.

3 Asymmetric Hydrofunctionalisation Reactions Catalysed by Chiral β -Diketiminato Magnesium Complexes^[a]

Abstract:

The synthesis of a magnesium hydridoborate complex bearing a chiral β -diketiminato (NacNac) ligand has been attempted. To this end, magnesium butyl and amide complexes containing chiral NacNac ligands were synthesised and their suitability to act as catalysts in the asymmetric hydrofunctionalisation of acetophenone was investigated. Pinacolborane (HBpin) and silanes ($\text{Ph}_x\text{SiH}_{3-x}$, PMHS) have been shown to act as reducing reagents. Whilst the reduction with silanes yielded racemates, enantiomeric excesses of up to 36% were observed when HBpin was used. Furthermore, it was shown that addition of different Lewis bases can allow the reversal of the enantioselectivity.



^[a] Felix Seeberger performed the reactions and the characterisation of all compounds. Robert Wolf supervised and directed the project.

3.1 Introduction

Traditionally, transition metal complexes are the mostly employed type of homogeneous catalysts. Variable oxidation states, the availability of d orbitals, as well as vacant coordination sites, all factor into the prevalent use of transition metal catalysts.^[1] The usage of the mainly utilised noble metals, however, brings forth issues such as their toxicity, low relative abundance, and high associated costs. These problems are particularly acute in asymmetric reactions, where scarce metals including ruthenium, iridium, palladium and platinum predominate. Therefore, different approaches such as organo- and, recently, main group-catalysis have attracted ever more attention over the years. However, whilst asymmetric organocatalysis can already be considered an established field,^[2] asymmetric main group catalysis is far less developed. Magnesium, as one of the most abundant metals in the earth's crust,^[3] has received increasing interest in asymmetric catalysis, due to its capability to catalyse a plethora of fundamental chemical transformations.^[4] In 1992, Corey and Ishihara reported the first enantioselective Diels-Alder addition catalysed by a magnesium complex.^[5] In order to introduce chirality, they used an asymmetric bis(oxazoline) ligand (BOX; see **Figure 1**) together with magnesium iodide. Following this seminal work, further multiple *in situ* generated BOX/Mg(II) systems were developed and used as catalysts in Diels-Alder reactions, yielding the desired products with excellent selectivity.^[6] Furthermore, in recent years, BOX-type ligands have been further established in magnesium-catalysed asymmetric cycloaddition,^[7] Friedel-Crafts,^[8] or hydroboration reactions.^[9] Besides BOX ligands, chiral phosphates have also been employed as ligands as shown in a series of reports by the Antilla group.^[10–12] These BINOL-based phosphates (**Figure 1**) were shown to selectively promote Aza-Darzens,^[10] phosphination,^[11] or addition reactions.^[12] Other phosphates and BINOL-derivatives have also been used to support magnesium(II)-based chiral catalysts in Friedel-Crafts,^[13] hydride transfer-cyclisation,^[14] Baeyer-Villiger oxidation,^[15] Diels-Alder,^[16] Mannich-type,^[17] and hydroboration reactions.^[18] In recent years, the Feng group showcased the wide applicability of *N,N*-dioxides (**Figure 1**) as ligands in magnesium-catalysed transformations. Together with a magnesium(II) source, the ligand facilitated enantioselective catalytic α -hydroxylation, Diels-Alder,^[19] ketone-ene^[20] as well as ring opening reactions.^[21] This field was further expanded by Yamamoto, who reported an *N,N*-dioxide/Mg(II) system to be effective in the asymmetric hydroxyamination of β -ketoesters.^[22]

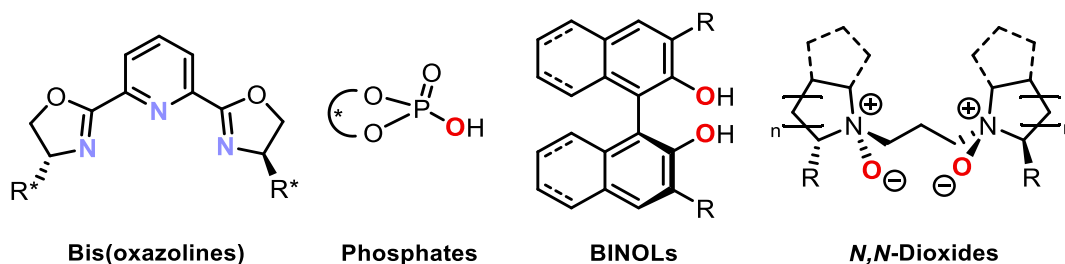


Figure 1. Recently used ligands in magnesium(II) catalysed asymmetric reactions.

Altogether, there are numerous ligands which have been demonstrated to effect asymmetric magnesium catalysis. However, whilst there have been extensive reports using BOX-type ligands, further Schiff base ligands have been, besides some (mono)oxazoline-^[23] and salen-based ligands,^[24] mostly unnoticed. Since β -diketiminato (NacNac) complexes have steadily gained attention as catalysts for a wide range of chemical reactions,^[25] it is unsurprising that NacNac-supported magnesium complexes have been reported as precatalysts in the hydroboration of pyridine,^[26] carbonyls,^[27] and isonitriles.^[28,29] In asymmetric catalysis, however, chiral β -diketiminato magnesium complexes have, to the best of my knowledge, only been investigated in ring-opening polymerisation reactions, where they showcased moderate to high heteroselectivity.^[30] Therefore, we were interested in investigating the potential of chiral β -diketiminates as ligands to facilitate enantioselectivity in Mg(II)-catalysed hydrofunctionalisation reactions.

In 2016, *Okuda* reported the magnesium hydridoborate **A** (**Figure 2**) to be an active catalyst in the hydroboration of a wide range of substrates, including ketones, pyridines and carbon dioxide.^[31] Showcasing turnover frequencies of over 60,000 h⁻¹, this hydridoborate is one of the most active hydroboration catalysts to date. A year later, *Hill* reported a similar complex **B** based on B(C₆F₅)₃ (**Figure 2**).^[32] Contrary to **A**, however, the magnesium cation in complex **B** is not coordinated purely by solvent molecules, but instead bears a NacNac-ligand. This leads to a direct coordination of the hydridoborate to the formal M⁺¹ analogue *via* the hydride. Similar to **A**, complex **B** catalyses the hydroboration of carbon dioxide and carbodiimides. The scandium hydridoborate **C** (**Figure 2**), reported by *Piers* and co-workers, is able to catalyse the hydrosilylation of carbon dioxide.^[33] A combination of experimental mechanistic and computational studies suggest that CO₂ is activated to accept the hydride of the borate anion by [Cp*₂Sc]⁺ acting as a Lewis Acid in a mechanism not unlike a “frustrated Lewis-pair”.^[34] Based on this, we envisioned a magnesium hydridoborate bearing a chiral NacNac-ligand to be both highly active and great for inducing enantioselectivity in hydrofunctionalisation reactions.

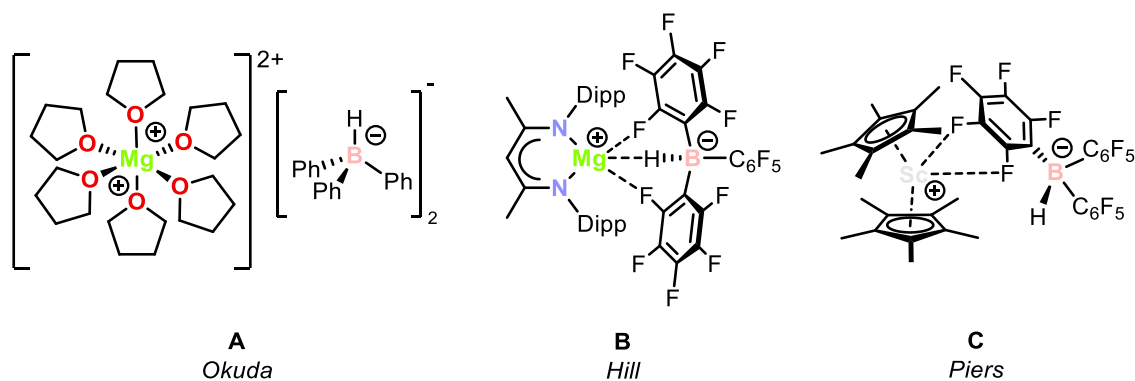
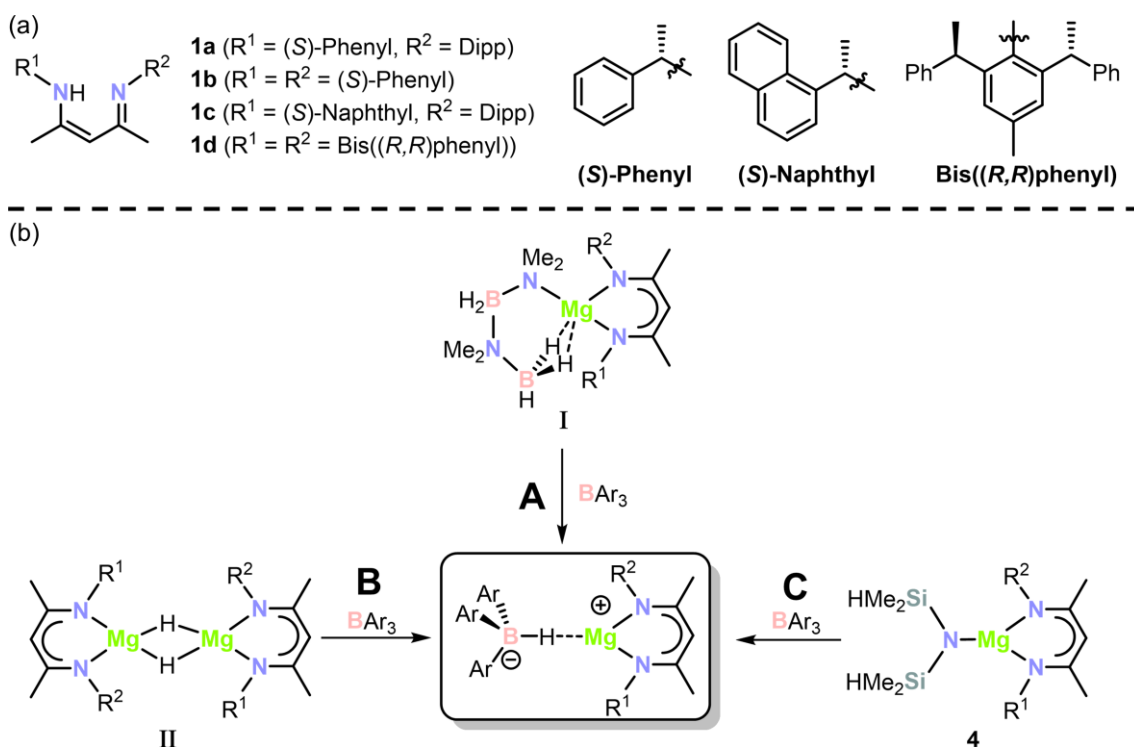


Figure 2. Hydridoborates with magnesium and scandium-based cations.

3.2 Results and Discussion

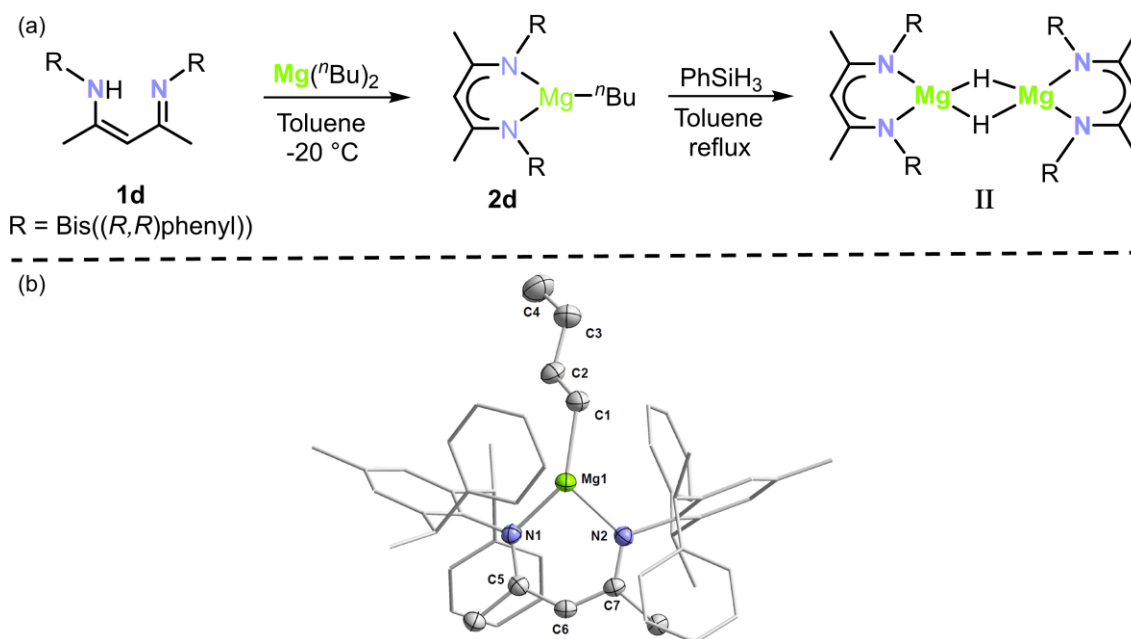
3.2.1 Attempted Synthesis of a Chiral NacNac Magnesium Hydridoborate Complex

The targeted NacNac magnesium hydridoborate can theoretically be synthesised by three different routes (**Scheme 1a**). The triarylborane BAr_3 is reacted either with a NacNac-supported magnesium compound bearing an amidoborane derivate (**route A**),^[35] to a magnesium hydride (**route B**),^[35] or to the respective tetramethyldisilazide (**route C**).^[36]



Scheme 1. Chiral NacNacH compounds (a) used in different synthetic strategies towards the desired magnesium hydridoborate (b).

The synthesis of the required amidoborane **I** for **route A** was conducted as a one-pot reaction. After **1a** was deprotonated with $\text{Mg}({}^n\text{Bu})_2$ in hexane at $-30\text{ }^\circ\text{C}$, the solvent was removed, NMe_2HBH_3 was added, and the mixture was dissolved in toluene. Although the ^{11}B NMR spectra revealed the formation of two promising signals at $\delta = 2.6$ and -17.0 ppm,^[37] the desired product could not be isolated cleanly, even after multiple crystallisation attempts. Therefore, the synthesis of a magnesium hydride **II** (**route B**) was attempted next. Since ligand **1d** (**Scheme 1a**) was suspected to offer the greatest stabilisation to the hydride due to its steric bulk, the synthesis of its magnesium alkyl complex was targeted first. The target compound **2d** was isolated as a clean white powder after recrystallisation from *n*-pentane at $-30\text{ }^\circ\text{C}$ after deprotonation of **2d** with $\text{Mg}({}^n\text{Bu})_2$ in toluene at $-20\text{ }^\circ\text{C}$. The complex was characterised by X-ray crystallography, multinuclear NMR spectroscopy, and elemental analysis.



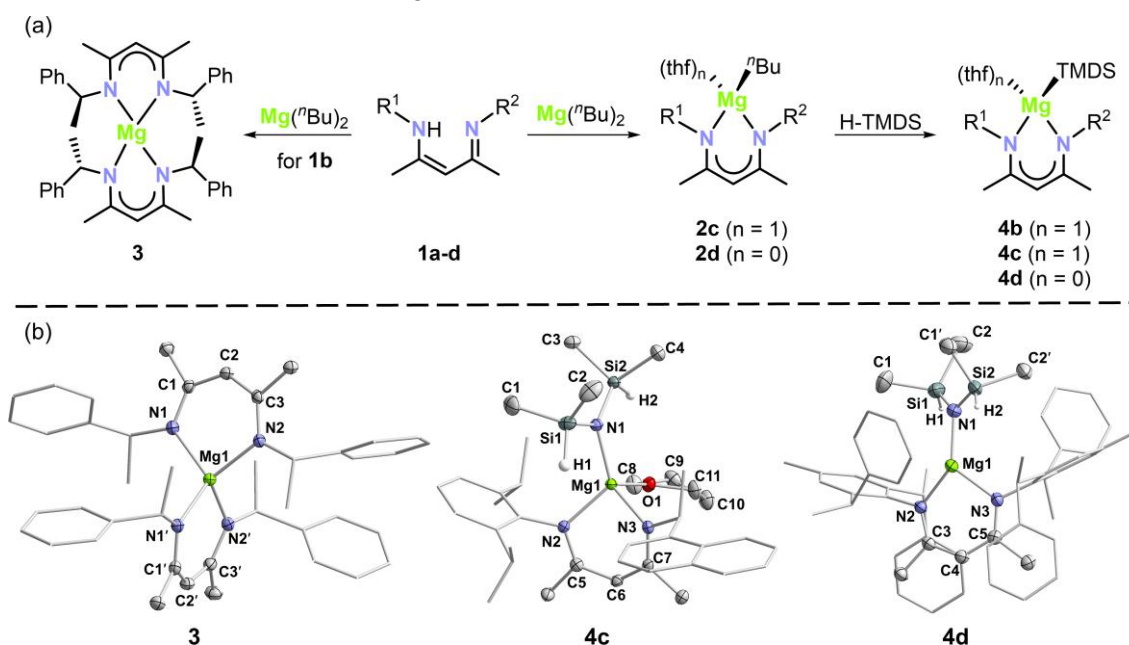
Scheme 2. Synthesis of **2d** and follow up ligand exchange to form **II** (a) as well as the solid-state molecular structure of **2d** (b). Thermal ellipsoids are set at the 50% probability level. Hydrogen atoms are omitted for clarity. Selected bond lengths [Å] and angles [°]: Mg1-N1 2.046(3), Mg1-N2 2.031(3), Mg1-C1 2.116(4), N1-C5 1.340(4), N2-C7 1.342(5), C1-C2 1.532(6), C2-C3 1.516(6), C3-C4 1.522(7), C5-C6 1.397(5), C6-C7 1.413(5), N1-Mg1-N2 93.2(1), N1-Mg1-C1 124.3(1), N2-Mg1-C1 136.9(1).

Contrary to most NacNac magnesium complexes, which feature tetra-coordinated magnesium centers, the magnesium atom in **2d** is three-coordinate, distorted trigonal planar environment (**Scheme 2b**). This can be attributed to the steric bulk of **1d**, as *Hill* reported a magnesium butyl compound bearing a sterically very demanding NacNac ligand to also bear a three-coordinated magnesium center.^[38] The average Mg–N distance (2.04 Å), the average C–C and C–N bond lengths within the NacNac backbone (1.41 Å and 1.31 Å, respectively) as well as the Mg1–C1 distance (2.116(4) Å) of **2d** are all comparable to that of *Hill*'s magnesium alkyl complex. Further similarities include the average C–C distance of the butyl group (1.52 Å) as well as the rather sharp N1–Mg1–N2 bite angle (93.21(12)°).

To substitute the *n*Bu ligand by a hydrido ligand, **2d** was refluxed with PhSiH₃ in toluene for three days, according to a procedure adapted from *Jones* and co-workers (see **Scheme 2a**).^[39] The formation of the desired magnesium hydrido dimer **II** could be confirmed by single-crystal X-ray diffraction analysis (see SI, **Figure 19**). However, the ¹H NMR spectrum of the isolated solid revealed some unidentified side products. Despite extensive efforts to purify **II** by recrystallisation, the contaminants persisted.

As the desired magnesium hydride **II** could be isolated neither in analytically pure form nor in good yields, the synthesis of the magnesium borohydride *via* the disilazide complex (**Scheme 1, route C**) was investigated. To this end, **1a-d** were deprotonated with Mg(*n*Bu)₂ according to a modified procedure reported by *Ren*^[30] followed by addition of 1,1,3,3-tetramethyldisilazane (H-TMDS), either *in situ* (for **2b** and **c**) or after isolation of the magnesium butyl intermediate

(**2d**; see **Scheme 3a**). For **1a**, signals corresponding to the desired magnesium alkyl complex **2a** were not detected in the ^1H NMR spectrum, therefore the subsequent reaction with H-TMDS was not attempted. In the case of **1b**, the reaction presumably led to the formation of the heteroleptic complex **2b**, which however, immediately reacted with a second equivalent of ligand **1b** to form the homoleptic complex $[(^{S}\text{-Phenyl})\text{NacNac}]_2\text{Mg}$ (**3**). Therefore, the reaction was repeated with only 10 min of stirring after the addition of $\text{Mg}(^n\text{Bu})_2$, whereupon 1.1 equivalents of THF as a coordinating solvent and 1.1 equivalents of H-TMDS were added, yielding a brown oil. Upon storing a solution of the oil in *n*-hexane at $-80\text{ }^\circ\text{C}$, a white powder precipitated, which was isolated by filtration at $-80\text{ }^\circ\text{C}$. The product **4b** is an oil at ambient temperatures, which still contains substantial impurities according to ^1H NMR analysis. All attempts to crystallise **4b** were unsuccessful. Derivative **4c** was synthesised using a similar protocol as for **4b**. Addition 1.2 equivalents of THF after the deprotonation of **1c** greatly improved the crystallisation of the final product **4c**. In contrast to **4b** and **4c**, THF was not required to isolate **4d**, which was presumably due to the high steric bulk of the bis(*R,R*)phenyl ligand (*vide supra*), which suppresses the coordination of THF to the magnesium cation (**Scheme 3**).^[38]



Scheme 3. Synthesis of the $[\text{NacNacMg}(\text{TMDS})(\text{thf})_n]$ complexes **4b-d** (a) and solid-state molecular structures of **3**, **4c** and **4d** (b). Selected bond lengths [\AA] and angles [$^\circ$] for **3**: Mg1-N1 2.077(2), Mg1-N2 2.0836(19), Mg1-N1' 2.079(2), Mg1-N2' 2.086(2), N1-Mg1-N2 95.85(8), N1'-Mg1-N2' 96.91(8), N1-Mg1-N2 to N1'-Mg1-N2' plane twist angle 87.37(7), N1-Mg1-N2 to N1'-Mg1-N2' plane fold angle 175.73(9). **4c**: Mg1-N1 2.000(2), Mg1-N2 2.058(2), Mg1-N3 2.059(2), Mg1-O1 2.073(2), N1-Si1 1.695(2), N1-Si2 1.691(2), N1-Mg1-N2 93.41(7). **4d**: Mg1-N1 2.031(2), Mg1-N2 2.028(2), Mg1-N3 1.964(2), N3-Si1 1.693(3), N3-Si2 1.692(3), N1-Mg1-N2 95.25(8).

The molecular structures of the crystallised compounds **3**, **4c**, and **4d** feature sharp NacNac-magnesium bite angles (95.85(8), 93.41(7) and 95.25(8) $^\circ$, respectively). Whilst **3** and **4c** both are four-coordinate magnesium complexes, **4d** features a tri-coordinate magnesium

cation. Both the Mg–N and N–Si bond lengths of **4c** and **4d** were similar to the observed distances for comparable magnesium amide complexes.^[40]

As the synthesis of **4c** was the most convenient, even upon scale-up of the reaction (2.91 mmol scale, 88% yield), it was used as the precursor for the attempted synthesis of the targeted asymmetric magnesium hydridoborate. According to a modified version of *Okuda*'s procedure,^[36] **4c** and BPh₃ were dissolved in THF-*d*₈ and the reaction was monitored by ¹H and ¹¹B{¹H} NMR spectroscopy. Since only the starting materials were observed after 18 h, the reaction was heated to 60 °C overnight. The ¹H NMR spectrum showed the formation of small amounts of new unidentified products. Besides unreacted BPh₃, the ¹¹B{¹H} NMR spectrum revealed the formation of a new boron species resonating at $\delta = -9.6$ ppm in a small quantity. Isolation of these minor products, however, was not successful. No change in the ¹H NMR spectra was observed upon repeating the reaction in C₆D₆. Therefore, the reaction was repeated with B(C₆F₅)₃ (BCF), as it was hoped that the stronger electrophilic character would promote the β -SiH elimination and thus yield the desired magnesium hydridoborate. After 18 h following addition of BCF to **4c** in THF-*d*₈, the ¹¹B{¹H} NMR spectrum showed full conversion of BCF. Of the two new boron signals observed at $\delta = -5.6$ and -25.3 ppm, the latter was found to resolve into a doublet in the coupled spectrum, hinting at the formation of a hydridoborate. Whilst the ¹⁹F{¹H} NMR spectrum showed the expected three signals almost exclusively, the formation of multiple sideproducts could be detected in the ¹H NMR spectrum. Attempted crystallisation from the reaction mixture yielded poorly diffracting crystals, whose cell parameters matched the ones reported for the undesired NaCNac-free [Mg(thf)₆][HB(C₆F₅)₃]₂.^[41]

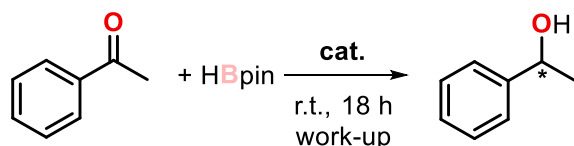
In order to avoid the generation of this fully solvated magnesium species, the reaction was repeated in toluene. Contrary to the reaction in THF, only one signal was observed in the ¹¹B{¹H} NMR spectrum at $\delta = -24.6$ ppm. Similar to the reaction in THF, the ¹⁹F{¹H} spectrum showed only the expected signals, whilst the ¹H NMR spectrum revealed the formation of multiple species, which could not be isolated even after multiple crystallisation attempts. Thus, all tested synthetic routes to the magnesium hydridoborate were without success. Nonetheless, as magnesium alkyl complexes have already been reported as (pre)catalysts in hydroboration and -silylation reactions (*vide supra*),^[26–29] the potential enantioinduction of the synthesised magnesium alkyl and amide complexes in the hydrofunctionalisation of acetophenone was investigated.

3.2.2 Magnesium-Catalysed Asymmetric Hydrofunctionalisation of Acetophenone

The prochiral ketone acetophenone can be reduced with hydroboranes or -silanes, which after work-up yields 1-phenylethanol. The product was analysed by chiral GC-FID using *n*-pentadecane as an internal standard. For initial hydrofunctionalisation tests, performed in *n*-hexane, the magnesium butyl complexes were either generated *in situ* (for **1a**, **1b** and **1c**) or the isolated complexes were used directly as precatalysts (**2c**, **2d** and **3**). For the mixtures of chiral

NacNac **1a-1c** and $Mg(nBu)_2$, no enantioselectivity was invariably observed with either HBpin or $PhSiH_3$ (see **3.4.2**, **Table 4**). When using the isolated magnesium alkyl complexes **2c** and **2d**, however, slight enantioinduction was observed (**Table 1**, entries 1-6). The enantioselectivity was solvent-dependent, as for both **2c** and **2d**, a decrease in solvent polarity led to diminished enantiomeric excesses. The same trend of solvent influence as detected for the butyl complexes was observed for the magnesium amide complexes **4b-4d**. However, contrary to **4b** and **4c**, which required THF to induce enantioselectivity (**Table 1**, entries 7-11), a small enantiomeric excess of 9% was already detected in *n*-hexane when utilising **4d** as the catalyst. This selectivity was increased to 19% or 16% in toluene or THF, respectively (**Table 1**, entries 12-14). Further testing of different solvents yielded no improvement in the enantioselectivity of the hydroboration catalysed by **4c** (see **3.4.2**, **Table 5**). It should be noted that while the enantiomeric excess usually favoured the (*S*)-enantiomer, the (*R*)-enantiomer was observed in the hydroboration reactions catalysed by magnesium complexes employing **1d** as the proligand (**2d** and **4d**).

Table 1. Influence of the solvent on the catalytic asymmetric hydroboration of acetophenone.^[a]



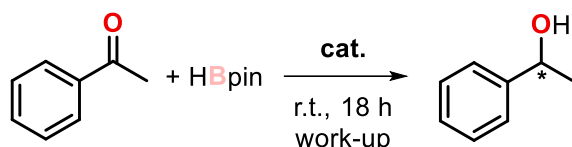
Entry	cat. (mol%)	Solvent (mL)	Yield (Conversion) [%] ^[b]	ee [%] ^[b]
1	2c (5.0)	<i>n</i> -Hexane (0.5)	93 (98)	< 5
2	2c (5.0)	Toluene (0.5)	99 (98)	5 (<i>S</i>)
3	2c (5.0)	THF (0.5)	98 (98)	10 (<i>S</i>)
4	2d (2.5)	<i>n</i> -Hexane (0.5)	89 (> 99)	< 5
5	2d (2.5)	Toluene (0.5)	99 (> 99)	5 (<i>R</i>)
6	2d (2.5)	THF (0.5)	96 (99)	12 (<i>R</i>)
7	4b (5.1)	<i>n</i> -Hexane (0.5)	7 (5)	< 5
8	4b (5.1)	THF (0.5)	94 (95)	11 (<i>S</i>)
9	4c (5.0)	<i>n</i> -Hexane (0.5)	90 (> 99)	< 5
10	4c (5.0)	Toluene (0.5)	97 (98)	< 5
11	4c (5.0)	THF (0.5)	97 (98)	15 (<i>S</i>)
12	4d (2.5)	<i>n</i> -Hexane (0.5)	99 (99)	9 (<i>R</i>)
13	4d (2.5)	Toluene (0.5)	99 (99)	19 (<i>R</i>)
14	4d (2.5)	THF (0.5)	89 (98)	16 (<i>R</i>)

^[a]Acetophenone (0.257 mmol), HBpin (0.262 mmol), *n*-pentadecane (0.072 mmol). ^[b]Determined by chiral GC-FID.

Due to the previously mentioned efficient synthesis, further optimisation was performed using **4c** as the catalyst. Experiments employing different catalyst loadings were performed for **4c**. Increasing the catalyst loading from 2 to 20 mol% led to an inversion of the observed product

from the (*S*)- to the (*R*)-enantiomer (**Table 2**, entries 1-4). Furthermore, it was observed that whilst the conversion of acetophenone remained high, yields of the corresponding alcohol dropped upon increasing the catalyst loading (**Table 2**, entries 3 and 4). The formation of insoluble magnesium alkoxides could be a potential reason for these decreased yields. Similar results were obtained when the reactions were performed without any solvent (**Table 2**, entries 5-10). However, contrary to the reaction in THF, the neat reactions did not yield the (*S*)-, but rather the (*R*)-enantiomer.

Table 2. Influence of the catalyst loading of **4c** on the hydroboration of acetophenone.^[a]



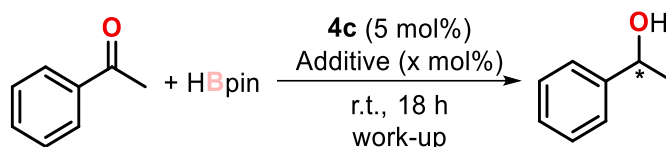
Entry	cat. (mol%)	Solvent (mL)	Yield (Conversion) [%] ^[b]	ee [%] ^[b]
1	4c (2.0)	THF (0.5)	99 (99)	8 (<i>S</i>)
2	4c (5.0)	THF (0.5)	97 (98)	15 (<i>S</i>)
3	4c (10.0)	THF (0.5)	88 (97)	11 (<i>S</i>)
4	4c (20.0)	THF (0.5)	68 (98)	8 (<i>R</i>)
5	4c (2.0)	-	99 (> 99)	8 (<i>R</i>)
6	4c (5.0)	-	98 (98)	< 5
7	4c (10.0)	-	88 (98)	11 (<i>R</i>)
8	4c (20.0)	-	67 (98)	14 (<i>R</i>)
9	4c (50.0)	-	58 (97)	11 (<i>R</i>)
10	4c (100.0)	-	50 (99)	9 (<i>R</i>)

^[a]Acetophenone (0.257 mmol), HBpin (0.262 mmol), *n*-pentadecane (0.080 mmol). ^[b]Determined by chiral GC-FID.

Since the isolated precatalyst **4c** already contains one molecule of THF, even in neat conditions, the observed change in enantioselectivity was rather surprising. In order to further investigate this observation, the effect of the addition of different coordinating amine bases, such as DMAP, DABCO, DBU and 2,6-lutidine, as well as phosphines and a carbene was investigated. No increase in enantioselectivity was observed when DABCO, 2,6-lutidine or tetramethylcarbene (TMC, 1,3,4,5-tetramethyl-1*H*-imidazol-3-ium-2-ide) were used as additives (see **3.4.2, Table 6**). Improved enantioinduction was detected with DMAP, DBU, PPh₃, and PMe₃. Contrary to **4c** bearing only one THF ligand, the **4c**/additive mixtures showcased enantioselectivity not only in THF, but also in the less polar solvents toluene and *n*-hexane. Addition of PPh₃ or, to a lesser extent, PMe₃ showed a similar trend to **4c** without additives, yielding increased enantiomeric excesses with THF as a more polar solvent (**Table 3**, entries 9-11 and see **3.4.2, Table 6**). Similar to the reaction without any additives, the (*S*)-enantiomer was detected as the major product for both phosphines. DMAP and DBU addition, on the other hand, resulted in an improved selectivity

towards the (*R*)-enantiomer (**Table 3**, entries 3-8). Furthermore, the lowest enantiomeric excesses were observed, when DMAP or DBU addition was performed in THF. This was unsurprising, as THF is proposed to promote the formation of the (*S*)-enantiomer, while the (*R*)-enantiomer was favoured for DMAP and DBU. A slight increase in enantioinduction up to 20% *ee* was detected using DBU as an additive in toluene. This effect was even more pronounced when DMAP was used instead of DBU, resulting in enantiomeric excesses of up to 33% in toluene or *n*-hexane (**Table 3**, entries 3-5). Whilst lower amounts of DMAP did not greatly change the enantioselectivity, two equivalents with respect to **4c** lead to the complete loss of the enantioinduction (**Table 3**, entries 12 and 13). DMAP addition also improved the observed enantiomeric excess when using **4d**. The increase, however, was lower than for **4c** (**Table 3**, entries 14-16). The high steric bulk of the $\text{Bis}((R,R)\text{phenyl})\text{NacNac}$ ligand might be responsible for this dampened effect of DMAP as an additive.

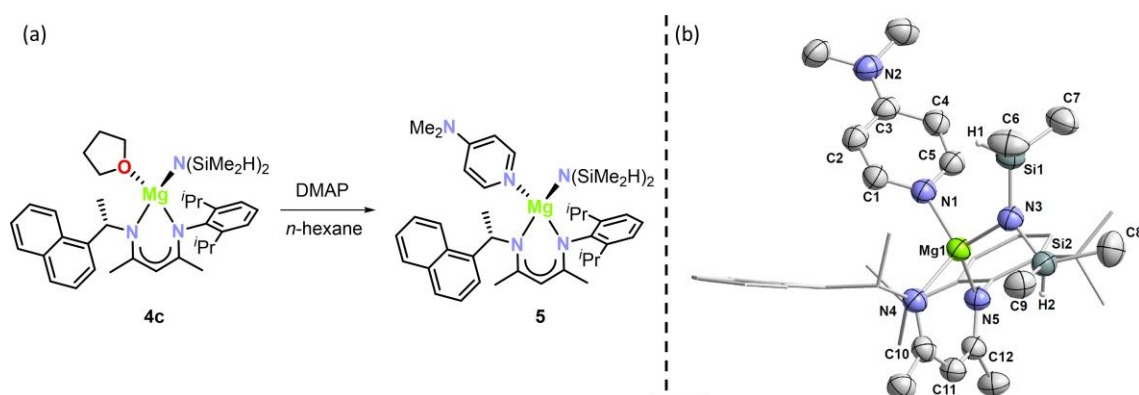
Table 3. Acetophenone hydroboration catalysed by magnesium amides and the influence of additives.^[a]



Entry	Additive (mol%)	Solvent	Yield (Conversion) [%] ^[b]	<i>ee</i> [%] ^[b]
1	-	<i>n</i> -Hexane	90 (> 99)	< 5
2	-	THF	97 (98)	15 (<i>S</i>)
3	DMAP (5.1)	<i>n</i> -Hexane	99 (99)	33 (<i>R</i>)
4	DMAP (5.1)	Toluene	99 (99)	33 (<i>R</i>)
5	DMAP (5.1)	THF	99 (99)	22 (<i>R</i>)
6	DBU (5.2)	<i>n</i> -Hexane	83 (99)	12 (<i>R</i>)
7	DBU (5.2)	Toluene	88 (99)	20 (<i>R</i>)
8	DBU (5.2)	THF	99 (99)	5 (<i>R</i>)
9	PPh ₃ (4.9)	<i>n</i> -Hexane	98 (98)	8 (<i>S</i>)
10	PPh ₃ (4.9)	Toluene	99 (97)	14 (<i>S</i>)
11	PPh ₃ (4.9)	THF	99 (97)	33 (<i>S</i>)
12	DMAP (2.5)	<i>n</i> -Hexane	94 (98)	36 (<i>R</i>)
13	DMAP (9.9)	<i>n</i> -Hexane	99 (97)	< 5
14 ^[c]	DMAP (2.5)	<i>n</i> -Hexane	87 (98)	6 (<i>R</i>)
15 ^[c]	DMAP (2.5)	Toluene	92 (99)	22 (<i>R</i>)
16 ^[c]	DMAP (2.5)	THF	99 (99)	16 (<i>R</i>)

^[a]Acetophenone (0.257 mmol), HBpin (0.262 mmol), *n*-pentadecane (0.072 mmol), solvent (0.5 mL). ^[b]Determined by chiral GC-FID. ^[c]**4d** (2.5 mol%) was used instead of **4c**.

The molecular structure of the proposed precatalyst generated by the addition of DMAP to **4c** was determined by single crystal X-ray diffraction. The adduct $[(S)\text{-Naph,Dipp}]\text{NacNacMg}(\text{TMDs})(\text{DMAP})$ (**5**) exhibits a Mg–N bond length of 2.127(3) Å between the Mg center and DMAP, which is in agreement with similar magnesium-DMAP complexes.^[42,43] Based on the negligible elongation of the magnesium amide bond by less than 0.03 Å, it was deduced that the Lewis base addition did not lead to any significant reduction in the magnesium amide bond strength. The same trend was also observed in the literature for the Mg–C bond length of a NacNac magnesium butyl complex.^[43,44] Furthermore, the solid state structure of **5** shows a decreased fold angle between the N4–C11–N5 and the N3–Mg1–N4 plane (41.2(1)° for **4c**, 24.1(2)° for **5**). The remaining structural parameters of **5** are essentially identical with **4c**.



Scheme 4. Formation (a) and solid-state molecular structure of **5** (b). Thermal ellipsoids are set at the 50% probability level. Hydrogen atoms except for H1 and H2 are omitted for clarity. Selected bond lengths [Å] and angles [°]: Mg1–N2 2.127(3), Mg1–N1 2.050(3), Mg1–N2 2.076(3), Mg1–N3 2.023(3), Mg1–N4 2.127(3), N3–Si1 1.686(3), N3–Si2 1.689(3), Si1–C4 1.890(4), Si1–C5 1.852(4), Si2–C6 1.885(4), Si2–C7 1.849(4), N1–C1 1.336(4), N2–C3 1.331(4), C1–C2 1.410(5), C2–C3 1.401(5), N1–Mg1–N2 93.5(1), N3–Mg1–N4 108.5(1), Si1–N3–Si2 126.3(2), plane-to-plane twist angle of the planes between N1–Mg1–N2 and N3–Mg1–N4 79.0(1).

3.3 Conclusion

The synthesis of a chiral magnesium hydridoborate was attempted by three different synthetic routes. While the targeted complex was not obtained in a spectroscopically pure form despite extensive purification efforts, the intermediate NacNac magnesium complexes **2d**, **3**, **4c** and **4d** have been isolated and characterised. The potential enantioinduction of these complexes, as well as the homoleptic NacNac magnesium complex **3**, in mediating the catalytic hydrofunctionalisation of acetophenone was investigated. No enantioselectivity was observed in hydrosilylation reactions. In hydroboration reactions with HBpin, however, small enantiomeric excesses were observed with the tested magnesium alkyl and amide complexes $[(\text{NacNac})\text{Mg}(\text{R})(\text{L})]$ (**2c**, **2d**, **4b**, **4c** and **4d**). The enantioselectivity, however, was highly dependent on both the coordinating base, **L**, and the substitution of the NacNac ligand. Magnesium complexes bearing ligands **1b** or **1c** generally yielded the (*S*)-enantiomer, whilst the opposite enantiomer was observed for complexes supported by **1d**. The addition of different

Lewis bases usually resulted in the (*R*)-enantiomer being the preferred stereoisomer, with the exception of $\mathbf{L} = \text{PR}_3$, which favoured the (*S*)-enantiomer. Altogether, it has been demonstrated that chiral NacNac ligands are capable of inducing enantioselectivity in magnesium catalysed hydroboration reactions.

3.4 Experimental Details

General Synthetic Methods

All reactions and product manipulations were carried out in flame-dried glassware under an inert atmosphere of nitrogen using standard Schlenk line or glovebox techniques (maintained at <0.1 ppm H₂O and <0.1 ppm O₂). **1a**, **1b**, **1c** and **2c** were prepared according to literature procedures.^[30] All other chemicals were purchased from commercial suppliers and used without further purification.

Solvents were dried and degassed with an MBraun SPS800 solvent purification system. All dry solvents except *n*-hexane and *n*-pentane were stored under argon over activated 3 Å molecular sieves in gas-tight ampules. *n*-Hexane and *n*-pentane were stored over potassium mirrors.

General Analytical Techniques

NMR spectra were recorded on Bruker Avance 300 or 400 spectrometers at 300 K unless otherwise noted and internally referenced to residual solvent resonances (¹H NMR: THF-d₈: 1.72 ppm, C₆D₆: 7.16 ppm; ¹³C{¹H} NMR: THF-d₈: 25.31 ppm, C₆D₆: 128.06 ppm). Chemical shifts δ are given in ppm referring to external standards of tetramethylsilane (¹H, ¹³C{¹H}).

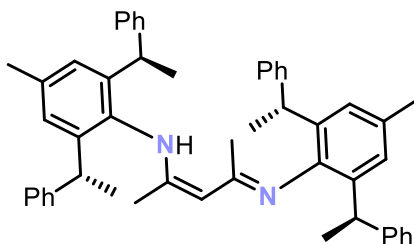
Elemental analysis was performed by the Central Analytical Services department of the University of Regensburg.

Single-crystal X-ray diffraction data were recorded on a Rigaku Oxford Diffraction SuperNova Atlas or a XtaLAB Synergy R (DW system, Hypix-Arc 150) device with Cu- K_{α} radiation ($\lambda = 1.54184$ Å). Crystals were selected under mineral oil, mounted on micromount loops and quench-cooled using an Oxford Cryosystems open flow N₂ cooling device. Either semi-empirical multi-scan absorption corrections^[21] or analytical ones^[22] were applied to the data. The structures were solved with SHELXT^[23] solution program using dual methods and by using Olex2 as the graphical interface.^[24] The models were refined with ShelXL^[25] using full matrix least squares minimisation on F².^[26] The hydrogen atoms were located in idealised positions and refined isotropically with a riding model.

3.4.1 Synthesis of Compounds

$\text{H}^{\text{Bis}((R,R)\text{phenyl})}\text{NacNac}$ (**1d**):

Toluene (30 mL) was added to a mixture of 4-methyl-2,6-bis((*R*)-1-phenylethyl)aniline (900 mg, 2.85 mmol, 2.1 equiv.), acetylacetone (0.14 mL, 1.37 mmol, 1.0 equiv.) and *p*-toluenesulfonic acid (550 mg, 2.89 mmol, 2.11 equiv.). The reaction mixture was refluxed in a Dean-Stark apparatus at 140 °C for 2 days. An aqueous NaOH solution (10 mL, 3M) was added, and the product was subsequently extracted with CH_2Cl_2 (3 x 50 mL). The solvent was evaporated under vacuum and the crude product was then recrystallised from EtOH at -30 °C and dried *in vacuo*.



Molecular formula: $\text{C}_{51}\text{H}_{54}\text{N}_2$ (695.01 $\text{g}\cdot\text{mol}^{-1}$)

Yield: 3.10 g (4.46 mmol, 72%)

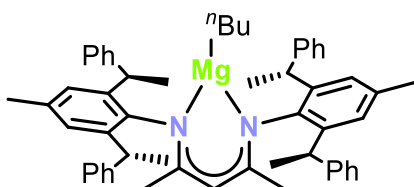
^1H NMR (300.13 MHz, 300 K, C_6D_6): δ [ppm] = 1.13 (s, 6H, $\text{NC}(\text{CH}_3)$), 1.30 (d, 6H, $^3J_{\text{HH}} = 7.2$ Hz, CHCH_3), 1.66 (d, 6H, $^3J_{\text{HH}} = 7.2$ Hz, CHCH_3), 2.13 (s, 6H, Ar- CH_3), 4.42 (q, 2H, $^3J_{\text{HH}} = 7.1$ Hz, CHCH_3), 4.66 (s, 1H, $\text{NC}(\text{CH}_3)\text{CH}$), 4.79 (q, 2H, $^3J_{\text{HH}} = 7.2$ Hz, CHCH_3), 6.89-6.97 (m, 2H), 6.99 (m, 3H), 7.01 (m, 2H), 7.04 (m, 2H), 7.06-7.13 (m, 5H), 7.18-7.25 (m, 6H), 7.33 (d, $^3J_{\text{HH}} = 7.3$ Hz, 4H), 12.30 (s, 1H, NH).

$^{13}\text{C}\{^1\text{H}\}$ NMR (75.47 MHz, 300 K, C_6D_6): δ [ppm] = 20.6, 21.1, 21.5, 23.6, 38.2, 41.2, 95.0, 125.9, 126.0, 127.3, 127.9, 128.5, 128.5, 128.7, 134.7, 140.4, 140.6, 141.2, 146.7, 147.1, 163.1.

Elemental analysis calc. for $\text{C}_{51}\text{H}_{54}\text{N}_2$: C 88.14, H 7.83, N 4.03 found C 88.02 H 7.94 N 3.86.

$[(\text{Bis}((R,R)\text{phenyl})\text{NacNac})\text{Mg}(\textit{n}\text{Bu})]$ (**2d**):

1d (435 mg, 0.63 mmol, 1.0 equiv.) was dissolved in toluene (10 mL) and cooled to -20 °C. $\text{Mg}(\textit{n}\text{Bu})_2$ (0.65 mL, 1.0 M in heptane, 1.0 equiv.) was slowly added *via* a syringe and the resulting slightly yellow solution was allowed to warm to room temperature. The reaction mixture was stirred for 5 days during which additional dibutylmagnesium (1.0 M in heptane, 0.75 mL, 1.2 equiv.) was added. The solvent was removed *in vacuo* and the product was recrystallised from *n*-hexane at -30 °C. The orange precipitate was then washed with cold *n*-hexane until only colourless material remained. Upon drying *in vacuo*, the desired product was obtained as a white powder.



Molecular formula: C₆₂H₆₆MgN₂ (863.53 g·mol⁻¹)

Yield: 230 mg (0.30 mmol, 47%)

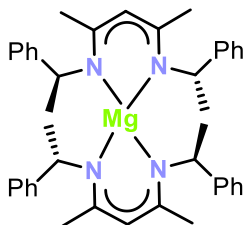
¹H NMR (400.13 MHz, 300 K, C₆D₆): δ [ppm] = - (0.99-0.83) (m, 2H, Mg-CH₂), 0.73-0.78 (m, 3H, Mg-(CH₂)₃CH₃), 0.83-0.96 (m, 2H, CH₂), 1.00 (s, 6H, NC(CH₃)), 1.05-1.17 (m, 2H, CH₂), 1.36 (d, 6H, ³J_{HH} = 7.2 Hz, CHCH₃), 1.42 (d, 6H, ³J_{HH} = 7.2 Hz, CHCH₃), 2.07 (s, 6H, Ar-CH₃), 3.99 (q, 2H, ³J_{HH} = 7.2 Hz, CHCH₃), 4.21 (q, 2H, ³J_{HH} = 7.1 Hz, CHCH₃), 4.57 (s, 1H, NC(CH₃)CH), 6.86-6.98 (m, 6H), 6.99-7.04 (m, 6H), 7.09-7.17 (m, 8H), 7.20-7.25 (m, 4H).

¹³C{¹H} NMR (100.61 MHz, 300 K, C₆D₆): δ [ppm] = 5.1, 14.5, 21.6, 22.1, 23.3, 23.8, 31.6, 31.6, 39.3, 41.4, 95.6, 126.1, 126.3, 126.8, 126.9, 127.6, 128.6, 129.6, 134.3, 139.4, 139.7, 144.0, 146.6, 146.9, 169.9.

Elemental analysis calc. for C₆₂H₆₆MgN₂: C 85.19, H 8.06, N 3.61 found C 85.50, H 7.64, N 3.51.

[(^S-PhNacNac)₂Mg] (3):

1b (253 mg, 0.83 mmol, 1.00 equiv.) was dissolved in *n*-hexane (12 mL) and cooled to -30 °C. After dropwise addition of Mg(^tBu)₂ (0.85 mL, 1 M, 1.03 equiv.), the solution was allowed to warm to room temperature and stirred for 18 h. The mixture was concentrated, filtered, and stored at -30 °C for 4 days to yield a white powder, which was isolated by filtration and recrystallised from *n*-hexane.



Molecular formula: C₄₂H₅₀MgN₄ (635.191 g·mol⁻¹)

Yield: 87 mg (0.14 mmol, 32%)

¹H NMR (400.13 MHz, 300 K, C₆D₆): δ [ppm] = 1.71 (s, 12H, NC(CH₃)), 1.82 (d, 12H, ³J_{HH} = 7.0 Hz, CHCH₃), 4.53 (s, 2H, NC(CH₃)CH), 4.82 (q, 4H, ³J_{HH} = 6.9 Hz, CHCH₃), 6.94-7.02 (m, 4H, Ar-H), 7.02-7.09 (m, 8H, Ar-H), 7.24 (d, 8H, ³J_{HH} = 7.4 Hz, Ar-H).

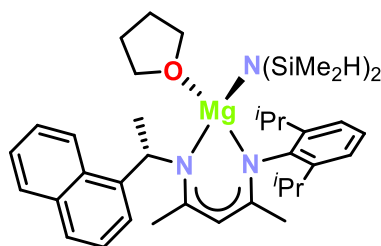
¹³C{¹H} NMR (100.61 MHz, 300 K, C₆D₆): δ [ppm] = 25.0, 25.6, 58.6, 96.1, 126.0, 126.7, 128.5, 147.9, 169.6.

Elemental analysis calc. for C₄₂H₅₀MgN₄: C 79.42, H 7.93, N 8.82, found C 79.71 H 7.79 N 8.53.

[(^S-Naph,DippNacNac)Mg(N(SiMe₂H)₂)(thf)] (4c):

1c (1200 mg, 2.91 mmol, 1.00 equiv.) was dissolved in *n*-hexane (30 mL) and cooled to -30 °C. After dropwise addition of Mg(^tBu)₂ (3 mL, 1 M, 1.03 equiv.), the solution was allowed to warm to room temperature and stirred for 1.5 h. Upon addition of THF (270 μ L, 3.33 mmol, 1.15 equiv.) the solution turned orange. After stirring for another 18 h, HN(SiMe₂H)₂ (550 μ L, 3.10 mmol,

1.07 equiv.) was added. The solution was concentrated *in vacuo* and stored at $-30\text{ }^{\circ}\text{C}$ to yield **4c** as a white powder. Single crystals suitable for X-ray crystallography were obtained upon recrystallisation from *n*-hexane.



Molecular formula: $\text{C}_{37}\text{H}_{57}\text{MgN}_3\text{OSi}_2$ ($640.36\text{ g}\cdot\text{mol}^{-1}$)

Yield: 1.46 g (2.57 mmol, 88%)

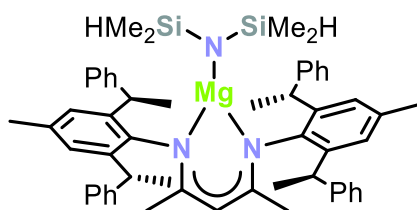
^1H NMR (400.13 MHz, 300 K, C_6D_6): δ [ppm] = 0.34 (br s, 6H, SiCH_3), 0.44 (br d, 6H, $^3J_{\text{HH}} = 2.8\text{ Hz}$, SiCH_3), 1.06-1.21 (m, 4H, OCH_2CH_2), 1.26 (d, 3H, $^3J_{\text{HH}} = 6.8\text{ Hz}$, CHCH_3), 1.30 (d, 3H, $^3J_{\text{HH}} = 6.8\text{ Hz}$, CHCH_3), 1.36 (d, 3H, $^3J_{\text{HH}} = 6.5\text{ Hz}$, CHCH_3), 1.53 (d, 3H, $^3J_{\text{HH}} = 6.8\text{ Hz}$, CHCH_3), 1.70 (s, 3H, $\text{NC}(\text{CH}_3)$), 1.73 (s, 3H, $\text{NC}(\text{CH}_3)$), 1.94 (d, 3H, $^3J_{\text{HH}} = 6.8\text{ Hz}$, $\text{NCH}(\text{CH}_3)$), 3.28 (br s, 2H), 3.47 (sept, 1H, $^3J_{\text{HH}} = 6.8\text{ Hz}$, $\text{CH}(\text{CH}_3)_2$), 3.56-3.76 (br m, 3H, OCH_2), 4.77 (s, 1H, $\text{NC}(\text{CH}_3)\text{CH}$), 4.91 (sept, 2H, $^3J_{\text{HH}} = 2.9\text{ Hz}$, SiH), 5.54 (q, 1H, $^3J_{\text{HH}} = 6.7\text{ Hz}$, $\text{NCH}(\text{CH}_3)$), 7.14-7.16 (overlapped m, 2H, Ar-H), 7.17-7.22 (m, 1H, Ar-H), 7.29-7.36 (m, 1H, Ar-H), 7.36-7.42 (m, 1H, Ar-H), 7.47 (t, 1H, $^3J_{\text{HH}} = 6.7\text{ Hz}$, Ar-H), 7.62 (d, 1H, $^3J_{\text{HH}} = 8.1\text{ Hz}$, Ar-H), 7.73 (d, 1H, $^3J_{\text{HH}} = 7.3\text{ Hz}$, Ar-H), 7.81 (d, 1H, $^3J_{\text{HH}} = 7.1\text{ Hz}$, Ar-H), 7.99 (d, 1H, $^3J_{\text{HH}} = 8.4\text{ Hz}$, Ar-H).

$^{13}\text{C}\{^1\text{H}\}$ NMR (100.06 MHz, 300 K, C_6D_6): δ [ppm] = 4.5, 4.8, 23.9, 24.5, 24.7, 24.8, 24.8, 25.1, 25.2, 25.9, 28.2, 28.3, 54.6, 70.3, 96.7, 123.0, 123.1, 124.0, 124.1, 125.1, 125.8, 126.2, 126.4, 127.4, 129.5, 131.3, 134.6, 142.9, 143.2, 144.6, 146.9, 168.4, 169.6.

Elemental analysis: calc. for $\text{C}_{37}\text{H}_{57}\text{MgN}_3\text{OSi}_2 \cdot (\text{C}_6\text{H}_{14})_{0.4}$: C 70.13, H 9.35, N 6.23 found C 70.58 H 9.38 N 6.41.

$[(\text{Bis}((R,R)\text{phenyl}))\text{NacNac}]\text{Mg}(\text{N}(\text{SiMe}_2\text{H})_2)$ (4d**):**

H-TMDS (49 μL , 0.28 mmol, 1.07 equiv.) was added to a solution of **2d** (200 mg, 0.26 mmol, 1.00 equiv.) in toluene (3 mL). After stirring for 18 h, the solvent was removed *in vacuo*. The crude product was recrystallized from *n*-pentane at $-30\text{ }^{\circ}\text{C}$ to yield the desired product as a white powder.



Molecular formula: $\text{C}_{55}\text{H}_{67}\text{MgN}_3\text{Si}_2$ ($850.63\text{ g}\cdot\text{mol}^{-1}$)

Yield: 51 mg (0.06 mmol, 23%)

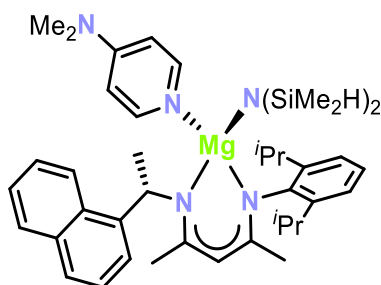
^1H NMR (400.13 MHz, 300 K, C_6D_6): δ [ppm] = -0.52 (d, 6H, $^3J_{\text{HH}} = 2.9$ Hz, SiCH_3), 0.15 (d, 6H, $^3J_{\text{HH}} = 2.9$ Hz, SiCH_3), 0.90 (s, 6H, $\text{NC}(\text{CH}_3)$), 1.53 (d, 6H, $^3J_{\text{HH}} = 7.2$ Hz, CHCH_3), 1.64 (d, 6H, $^3J_{\text{HH}} = 7.1$ Hz, CHCH_3), 2.27 (s, 6H, $\text{C}_{\text{aryl}}\text{CH}_3$), 4.17 (quint, 2H, $^3J_{\text{HH}} = 2.9$ Hz, SiH), 4.33 - 4.42 (overlapping q, 4H, CHCH_3), 4.61 (s, 1H, $\text{NC}(\text{CH}_3)\text{CH}$), 6.95 - 7.02 (m, 2H, Ar-H), 7.11 (t, 6H, $^3J_{\text{HH}} = 7.7$ Hz, Ar-H), 7.15 - 7.17 (m overlapped by residual solvent signal, 2H, Ar-H), 7.29 - 7.36 (m, 6H, Ar-H), 7.42 (t, 4H, $^3J_{\text{HH}} = 7.7$ Hz, Ar-H), 7.57 (d, 4H, $^3J_{\text{HH}} = 7.1$ Hz, Ar-H).

$^{13}\text{C}\{^1\text{H}\}$ NMR (100.61 MHz, 300 K, C_6D_6): δ [ppm] = 4.2 , 21.7 , 22.9 , 23.3 , 24.6 , 40.4 , 42.3 , 95.5 , 126.1 , 126.5 , 127.0 , 127.4 , 127.9 , 128.6 , 128.7 , 129.9 , 134.6 , 139.6 , 140.0 , 144.1 , 146.3 , 147.2 , 171.6 .

Elemental analysis calc. for $\text{C}_{55}\text{H}_{67}\text{MgN}_3\text{Si}_2 \cdot (\text{C}_6\text{H}_{14})_{0.1}$: C 77.72, H 8.12, N 4.89 found C 78.19 H 8.36 N 4.72.

$[(^{\text{S}}\text{-Naph,DippNacNac})\text{Mg}(\text{N}(\text{SiMe}_2\text{H})_2)(\text{NC}_5\text{H}_4(\text{NMe}_2))]$ (5):

4c (50 mg, 0.08 mmol, 1.00 equiv.) and DMAP (10 mg, 0.08 mmol, 1.05 equiv.) were dissolved in *n*-hexane (3 mL) and stirred for 18 h. The reaction mixture was then concentrated *in vacuo* and stored at -30 °C for 5 days to yield the desired product as a white powder.



Molecular formula: $\text{C}_{40}\text{H}_{59}\text{MgN}_5\text{Si}_2$ (690.42 $\text{g}\cdot\text{mol}^{-1}$)

Yield: 23 mg (0.03 mmol, 41%)

^1H NMR (400.13 MHz, 300 K, C_6D_6): δ [ppm] = 0.54 (d, 12H, $^3J_{\text{HH}} = 2.9$ Hz, SiCH_3), 0.80 (d, 3H, $^3J_{\text{HH}} = 6.9$ Hz, $\text{CH}(\text{CH}_3)_2$), 1.21 (d, 3H, $^3J_{\text{HH}} = 6.8$ Hz, $\text{CH}(\text{CH}_3)_2$), 1.47 (d, 3H, $^3J_{\text{HH}} = 6.8$ Hz, $\text{CH}(\text{CH}_3)_2$), 1.74 (s, 6H, $\text{NC}(\text{CH}_3)_2$), 1.79 (d, 3H, $^3J_{\text{HH}} = 6.8$ Hz, $\text{CH}(\text{CH}_3)_2$), 1.84 (s, 3H, NCH_3), 1.88 (s, 3H, NCH_3), 2.23 (d, 3H, $^3J_{\text{HH}} = 6.8$ Hz, CHCH_3), 3.41 (sept, 1H, $^3J_{\text{HH}} = 6.9$ Hz, $\text{CH}(\text{CH}_3)_2$), 4.23 (sept, 1H, $^3J_{\text{HH}} = 6.8$ Hz, $\text{CH}(\text{CH}_3)_2$), 4.98 (s, 1H, $\text{NC}(\text{CH}_3)\text{CH}$), 5.02 (sept, 2H, $^3J_{\text{HH}} = 3.0$ Hz, SiH), 5.81 (q, 1H, $^3J_{\text{HH}} = 6.8$ Hz, CHCH_3), 6.94 - 6.97 (m, 1H, Ar-H), 7.15 - 7.18 (overlapped m, 2H, Ar-H), 7.25 - 7.42 (m, 4H, Ar-H), 7.51 (t, 1H, $^3J_{\text{HH}} = 7.7$ Hz, Ar-H), 7.64 - 7.71 (m, 3H, Ar-H), 7.73 - 7.79 (m, 1H, Ar-H), 7.99 - 8.07 (m, 2H, Ar-H).

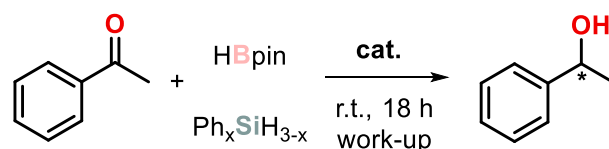
$^{13}\text{C}\{^1\text{H}\}$ NMR (100.61 MHz, 300 K, C_6D_6): δ [ppm] = 4.7 , 23.9 , 23.9 , 24.7 , 25.0 , 25.3 , 25.8 , 28.1 , 28.3 , 37.8 , 54.9 , 64.3 , 97.2 , 106.1 , 122.9 , 123.6 , 123.8 , 124.1 , 124.7 , 126.0 , 126.6 , 127.4 , 128.6 , 129.3 , 131.6 , 134.8 , 142.8 , 143.9 , 145.1 , 147.7 , 148.8 , 154.4 , 167.9 , 169.2 .

3.4.2 Catalytic Studies

General hydrofunctionalisation procedure.

To a screw-cap vial equipped with a stir-bar was added the required amount of the desired precatalyst. The desired volume of solvent (generally 0.5 mL if not stated otherwise) was then added. If required, additives were then added, and the mixture was stirred for 30 min at ambient temperature. To the resultant solution was added acetophenone, followed by the desired reducing reagent (HBpin, PhSiH₃, Ph₂SiH₂ or PMHS) and *n*-pentadecane as an internal standard. After the reaction was completed, hydroboration reactions were worked up by adding aqueous NaOH (0.5 mL, 3M) followed by H₂O₂ (0.5 mL, 30%) and ethyl acetate (ca. 0.5 mL), and the resulting mixture was allowed to stir for 1 hour at room temperature. Work-up of hydrosilylation reactions commenced with the addition of [N(^{*n*}Bu)₄]F (1.1 equiv., 1M in THF). The resulting solution was allowed to stir for 2 h at ambient temperature, before water (ca. 0.5 mL) was added. All hydrofunctionalisation reactions were then extracted with ethyl acetate (3 x 0.5 mL), filtered and analysed by chiral GC-FID.

Table 4. Hydrofunctionalisation of acetophenone.^[a]

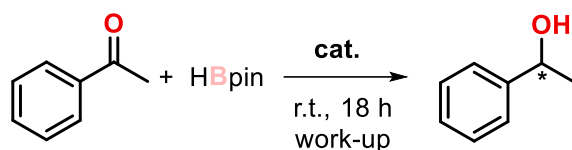


Entry	cat.	Reducing reagent (equiv.)	Yield (Conversion) [%] ^[b]	<i>ee</i> [%] ^[b]
1 ^[c]	1a /Mg(^{<i>n</i>} Bu) ₂	HBpin (1.4)	87 (> 99)	< 5
2 ^[c]	1a /Mg(^{<i>n</i>} Bu) ₂	PhSiH ₃ (1.0)	77 (98)	< 5
3 ^[c]	1b /Mg(^{<i>n</i>} Bu) ₂	HBpin (1.4)	87 (> 99)	< 5
4 ^[c]	1b /Mg(^{<i>n</i>} Bu) ₂	PhSiH ₃ (1.0)	82 (98)	< 5
5 ^[c]	1c /Mg(^{<i>n</i>} Bu) ₂	HBpin (1.4)	87 (> 99)	< 5
6 ^[c]	1c /Mg(^{<i>n</i>} Bu) ₂	PhSiH ₃ (1.0)	86 (99)	< 5
7 ^[d]	2c	HBpin (1.0)	99 (> 99)	< 5
8 ^[d]	2c	Ph ₂ SiH ₂ (1.1)	37 (64)	< 5
9	2d	HBpin (1.0)	89 (> 99)	< 5
10	2d	Ph ₂ SiH ₂ (1.1)	60 (81)	< 5
11 ^[e]	3	HBpin (1.1)	92 (98)	< 5
12 ^[e]	3	PhSiH ₃ (1.1)	52 (> 99)	< 5

^[a]Acetophenone (0.197 mmol), cat. (5 mol%), *n*-pentadecane (0.072 mmol), *n*-hexane (0.5 mL). ^[b]Determined by chiral GC-FID. ^[c]HNacNac (5 mol%), Mg(^{*n*}Bu)₂ (4.5 mol%). ^[d]Reaction performed in C₆H₆ (0.5 mL) instead of *n*-hexane.

^[e]Acetophenone (0.249 mmol), reaction time 3 days instead of 18 h.

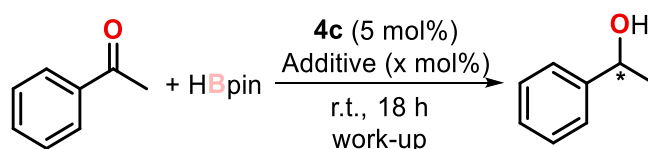
Table 5. Solvent influence on the hydroboration of acetophenone.^[a]



Entry	cat. (mol%)	Solvent (mL)	Yield (Conversion) [%] ^[b]	ee [%] ^[b]
1	4c (5.0)	THF	97 (98)	15 (<i>S</i>)
2	4c (5.0)	Et ₂ O (1.5)	94 (97)	10 (<i>S</i>)
3	4c (5.0)	DME (0.5)	96 (99)	< 5
4	4c (5.0)	Dimethoxymethane (0.5)	95 (98)	< 5
5	4c (5.0)	-	98 (98)	< 5

^aAcetophenone (0.257 mmol), HBpin (0.262 mmol), *n*-pentadecane (0.072 mmol). ^[b]Determined by chiral GC-FID.

Table 6. Acetophenone hydroboration catalysed by magnesium amides and the influence of additives.^[a]

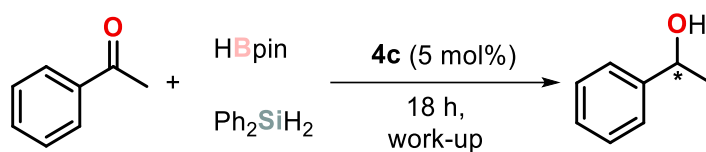


Entry	Additive (mol%)	Solvent (mL)	Yield (Conversion) [%] ^[b]	ee [%] ^[b]
1	DABCO (5.2)	<i>n</i> -Hexane	97 (97)	< 5
2	DABCO (5.2)	Toluene	19 (37)	< 5
3	DABCO (5.2)	THF	99 (98)	< 5
4	TMC (5.0)	<i>n</i> -Hexane	94 (97)	5 (<i>R</i>)
5	TMC (5.0)	Toluene	92 (98)	10 (<i>R</i>)
6	TMC (5.0)	THF	92 (99)	< 5
7	2,6-Lutidine (5.0)	<i>n</i> -Hexane	96 (98)	11 (<i>S</i>)
8	2,6-Lutidine (5.0)	Toluene	91 (97)	7 (<i>S</i>)
9	2,6-Lutidine (5.0)	THF	92 (99)	9 (<i>S</i>)
10	PMe ₃ (5.3)	<i>n</i> -Hexane	93 (98)	7 (<i>S</i>)
11	PMe ₃ (5.3)	Toluene	90 (98)	< 5
12	PMe ₃ (5.3)	THF	96 (98)	15 (<i>S</i>)
13 ^[c]	DMAP (2.5)	<i>n</i> -Hexane	87 (98)	< 5
14 ^[c]	DMAP (5.1)	<i>n</i> -Hexane	99 (98)	27 (<i>R</i>)
15 ^[c]	DMAP (9.9)	<i>n</i> -Hexane	95 (97)	< 5

^aAcetophenone (0.257 mmol), HBpin (0.262 mmol), *n*-pentadecane (0.072 mmol). ^[b]Determined by chiral GC-FID.

^[c]Internal standard, substrate and HBpin were added directly after DMAP addition without stirring for 30 min.

Table 7. Influence of the temperature on the hydrofunctionalisation of acetophenone.^[a]



Entry	Reducing Reagent (equiv.)	Solvent (mL)	T [°C]	Yield (Conversion) [%] ^[b]	<i>ee</i> [%] ^[b]
1 ^[c]	HBpin (1.0)	THF (0.5)	-30	84 (80)	< 5
2	HBpin (1.0)	THF (0.5)	60	34 (77)	< 5
3	Ph ₂ SiH ₂ (1.1)	THF (0.5)	60	< 5 (< 5)	<i>n.d.</i>
4 ^[d]	HBpin (1.0)	<i>n</i> -Hexane (0.5)	-30	44 (55)	< 5
5 ^[d,e]	HBpin (1.0)	<i>n</i> -Hexane (0.5)	-30	67 (66)	< 5

^[a]Acetophenone (0.257 mmol), *n*-pentadecane (0.072 mmol). ^[b]Determined by chiral GC-FID. ^[c]Reaction stopped after 5 h. ^[d]Reaction stopped after 2 h. ^[e]DMAP (5.0 mol%) was added, and the solution stirred for 1 h, before the reaction was cooled and acetophenone and HBpin were added.

3.4.3 NMR Spectra

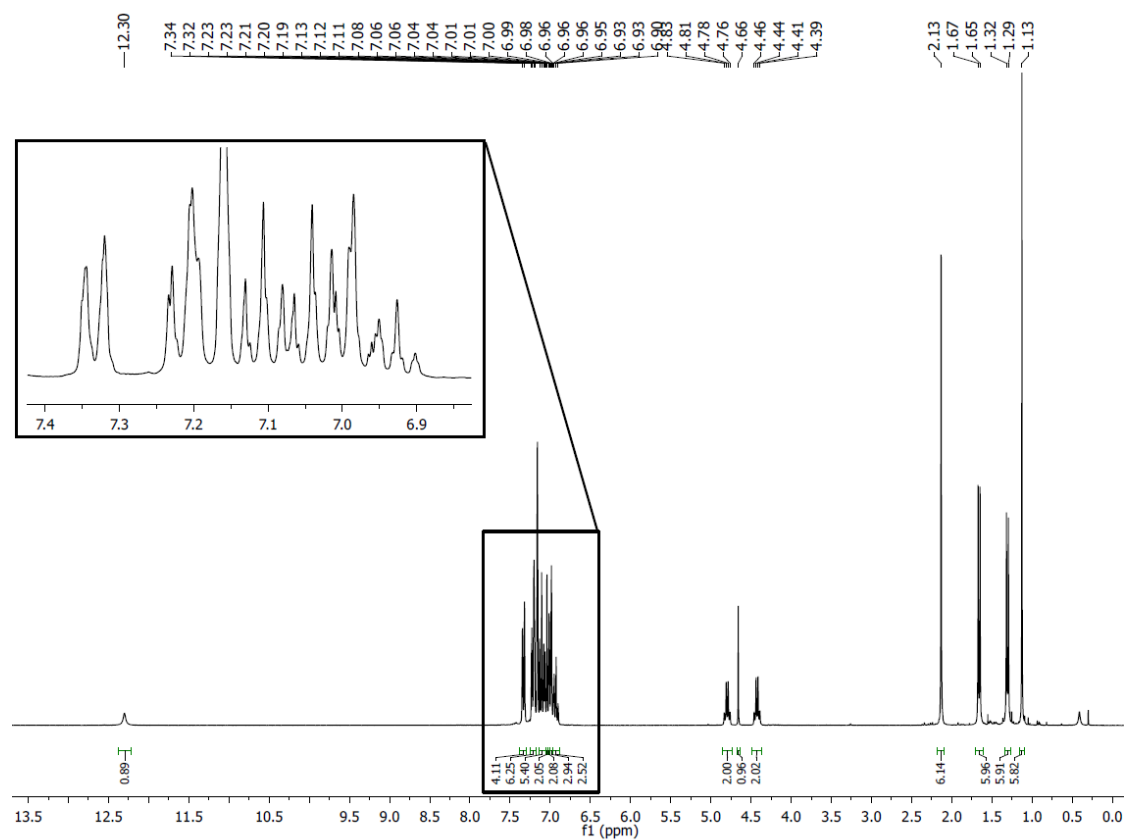


Figure 3. ¹H NMR spectrum (300.13 MHz, 300 K, C₆D₆) of **1d**.

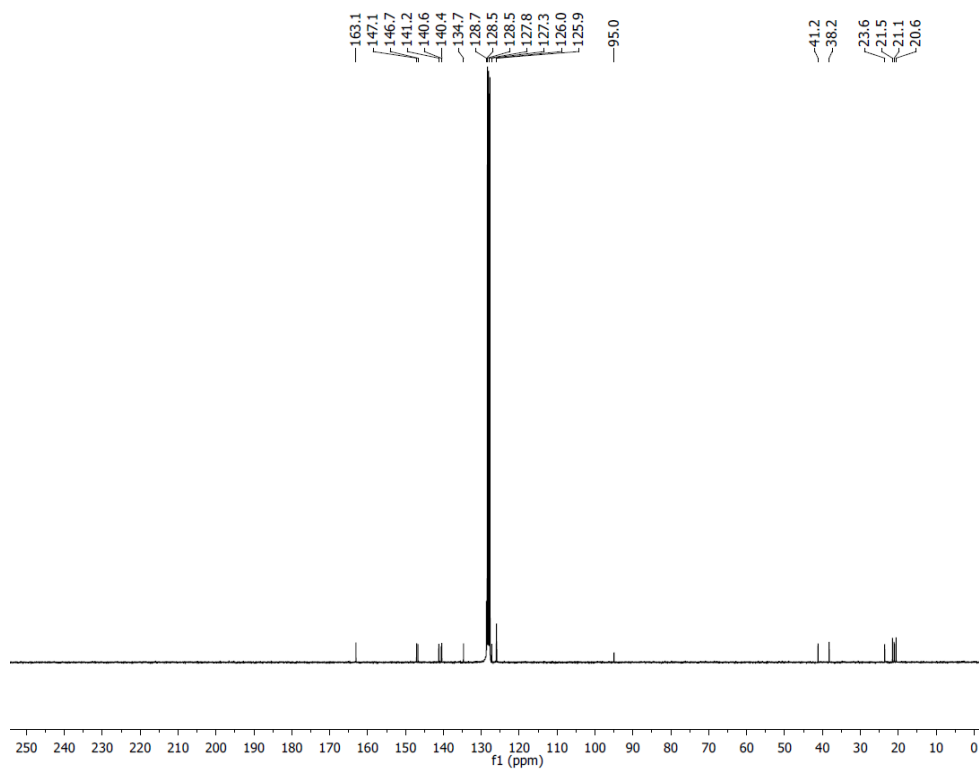


Figure 4. $^{13}\text{C}\{^1\text{H}\}$ NMR spectrum (75.47 MHz, 300 K, C_6D_6) of **1d**.

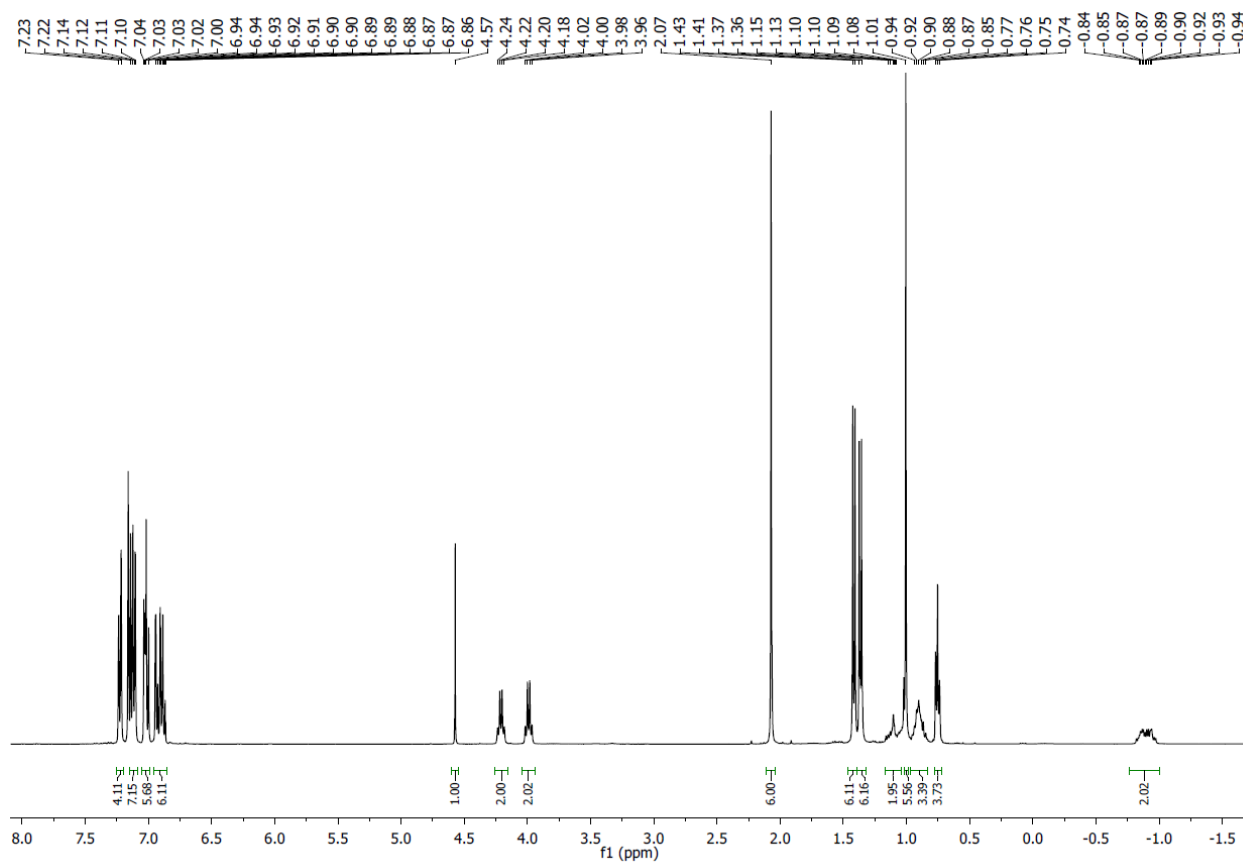


Figure 5. ^1H NMR spectrum (400.13 MHz, 300 K, C_6D_6) of **2d**.

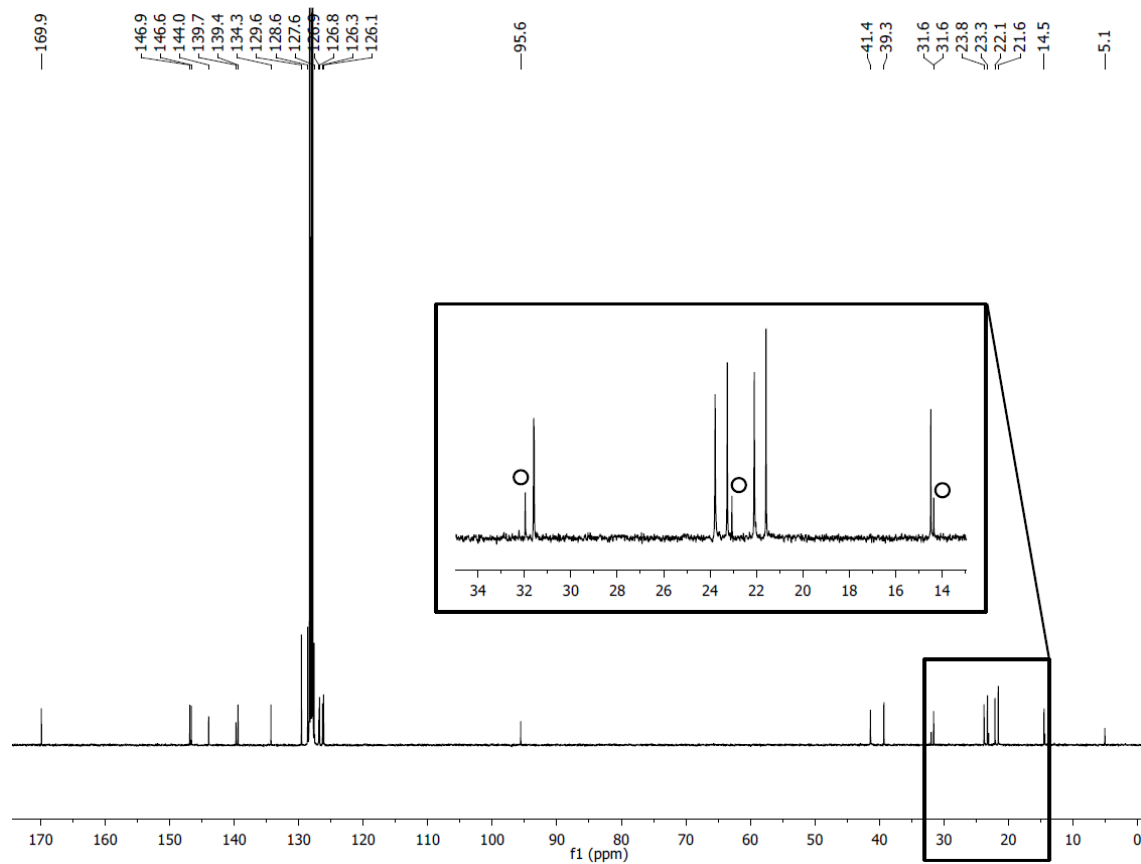


Figure 6. $^{13}\text{C}\{^1\text{H}\}$ NMR spectrum (100.61 MHz, 300 K, C_6D_6) of **2d**, \odot *n*-hexane.

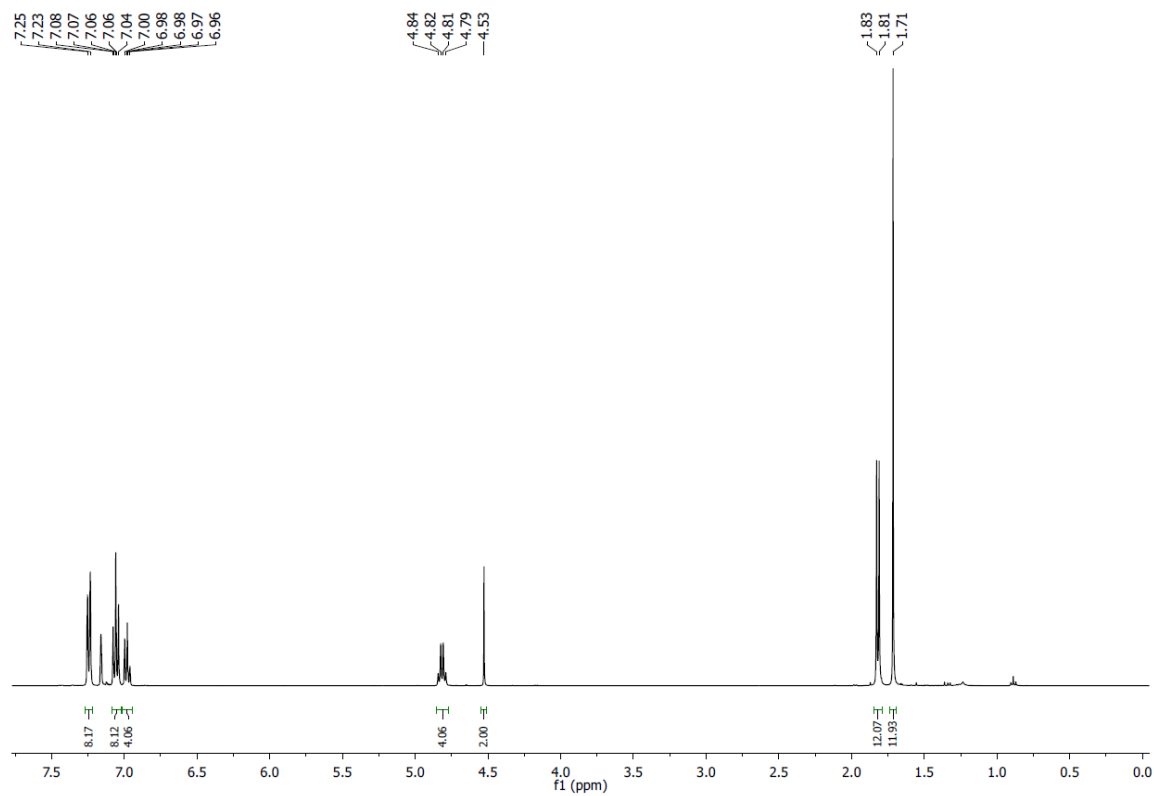


Figure 7. ^1H NMR spectrum (400.13 MHz, 300 K, C_6D_6) of **3**.

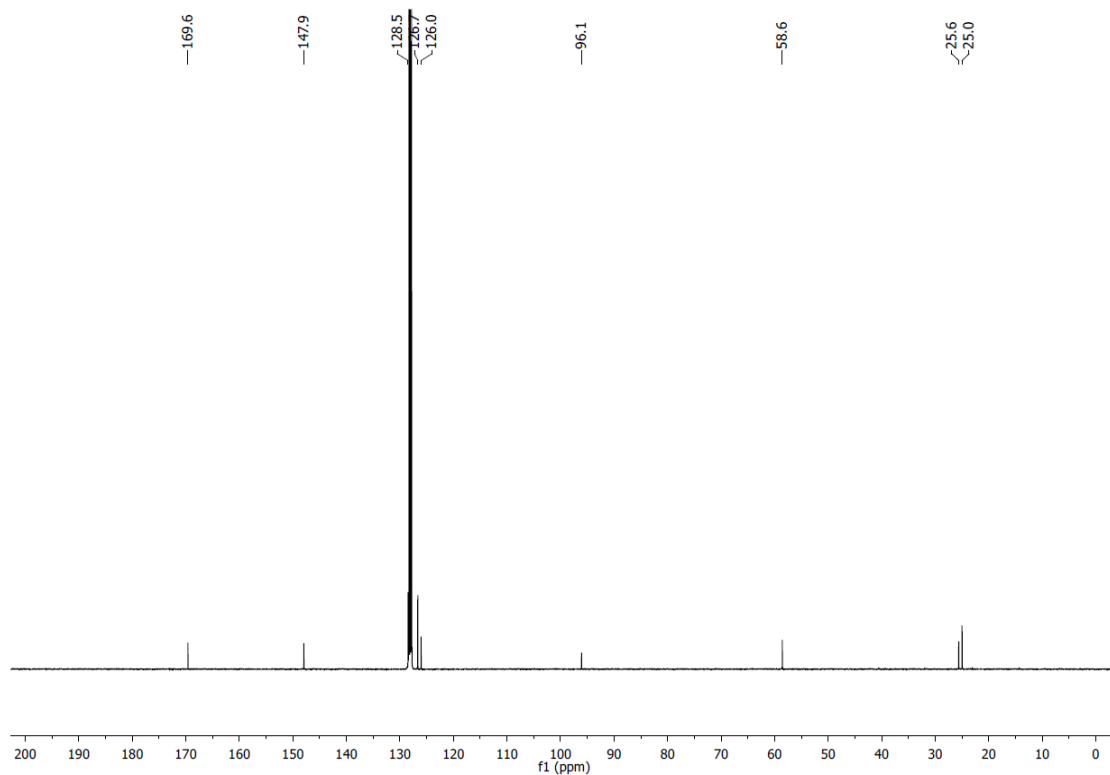


Figure 8. $^{13}\text{C}\{^1\text{H}\}$ NMR spectrum (100.61 MHz, 300 K, C_6D_6) of **3**.

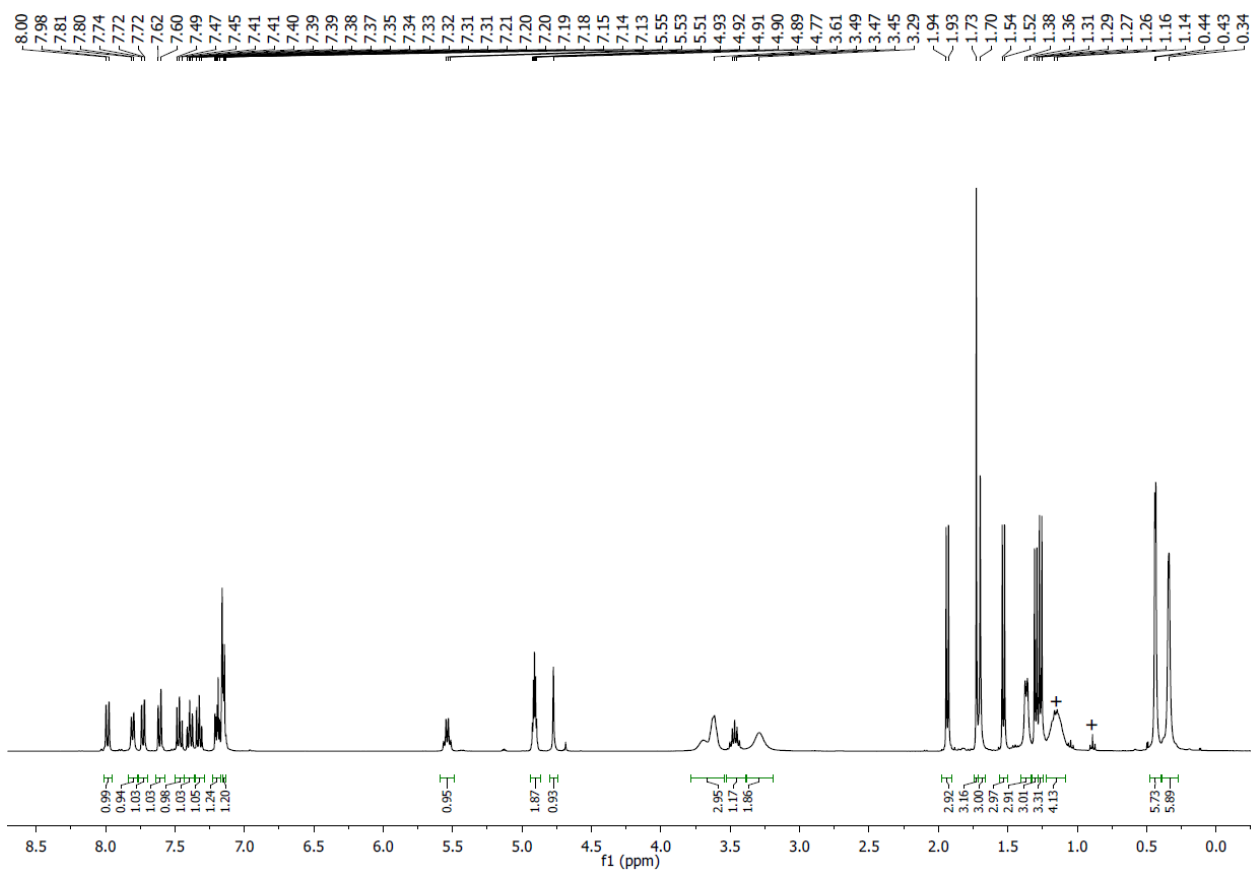


Figure 9. ^1H NMR spectrum (400.13 MHz, 300 K, C_6D_6) of **4c**, + *n*-hexane.

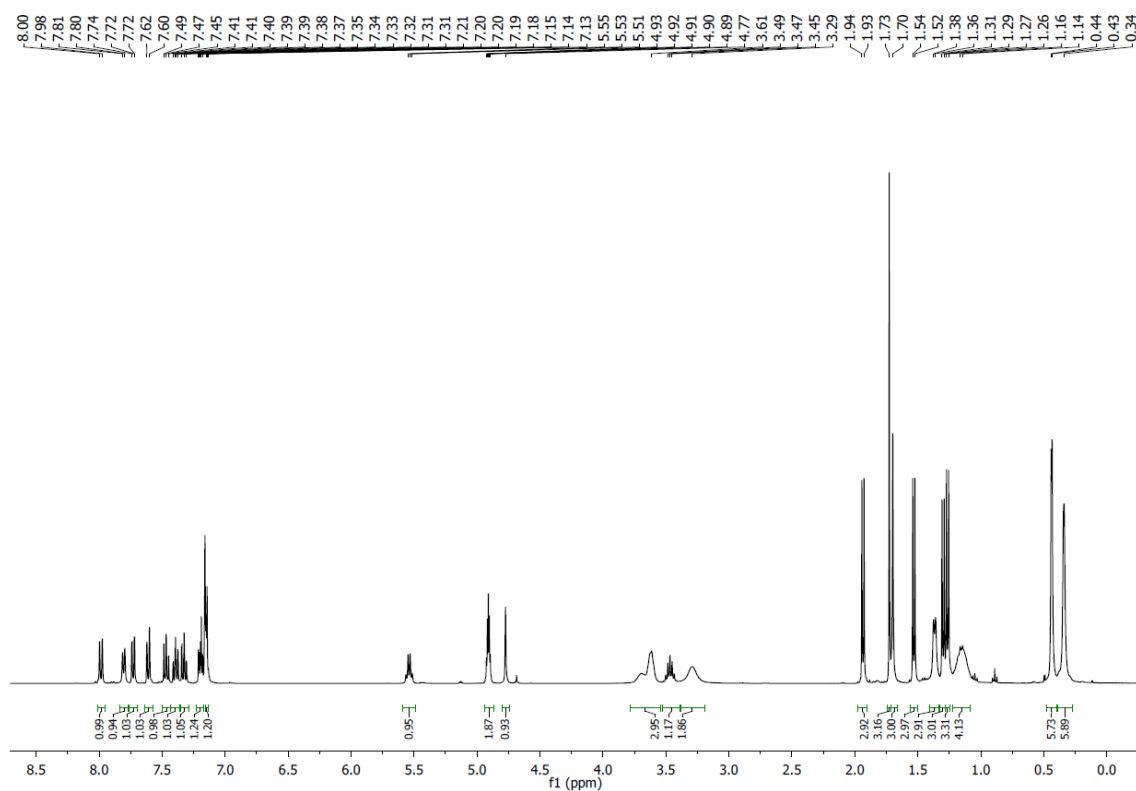


Figure 10. $^{13}\text{C}\{^1\text{H}\}$ NMR spectrum (100.06 MHz, 300 K, C_6D_6) of **4c**.

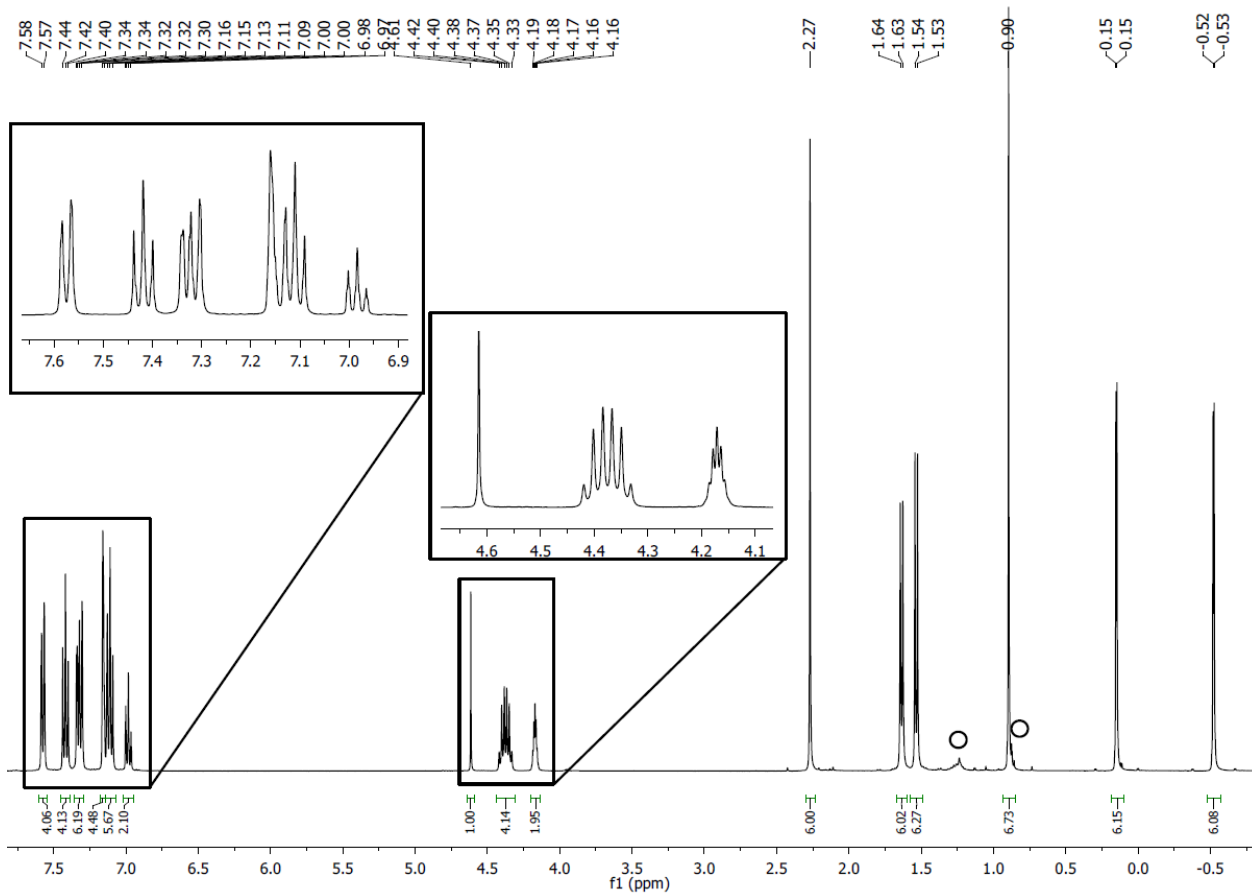


Figure 11. ^1H NMR spectrum (400.13 MHz, 300 K, C_6D_6) of **4d**, \circ *n*-hexane.

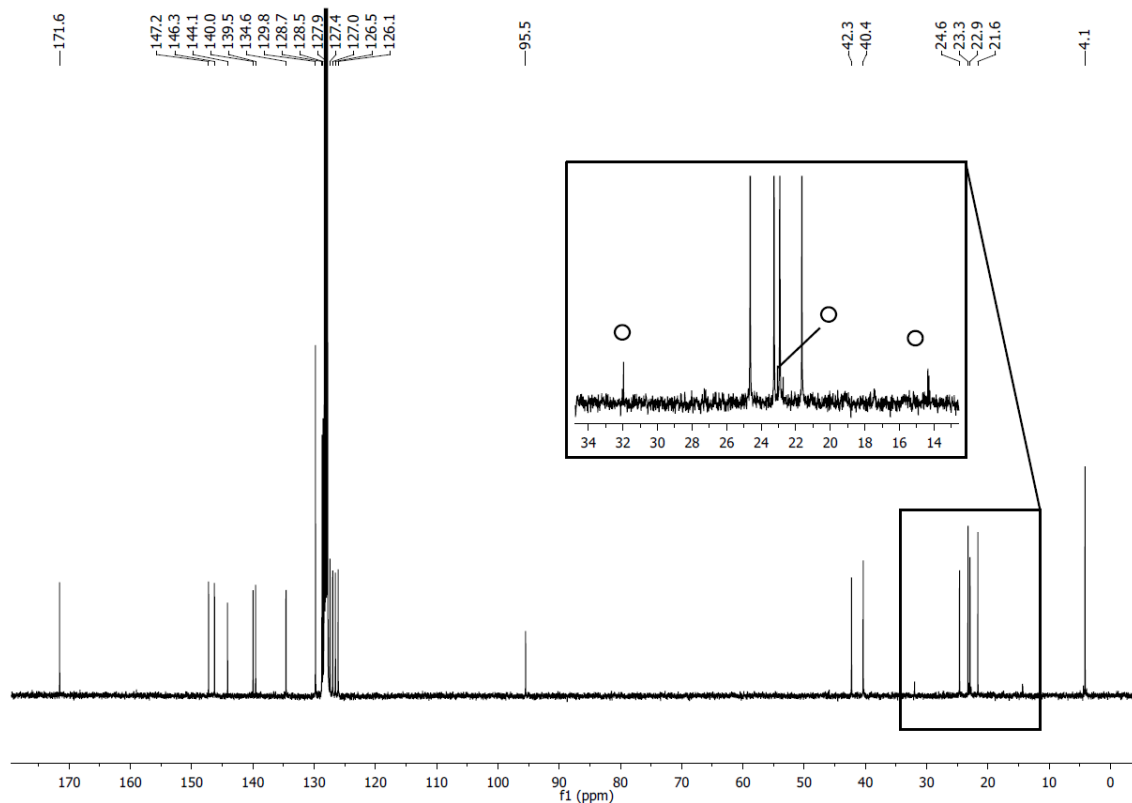


Figure 12. $^{13}\text{C}\{^1\text{H}\}$ NMR spectrum (100.61 MHz, 300 K, C_6D_6) of **4d**, \circ *n*-hexane.

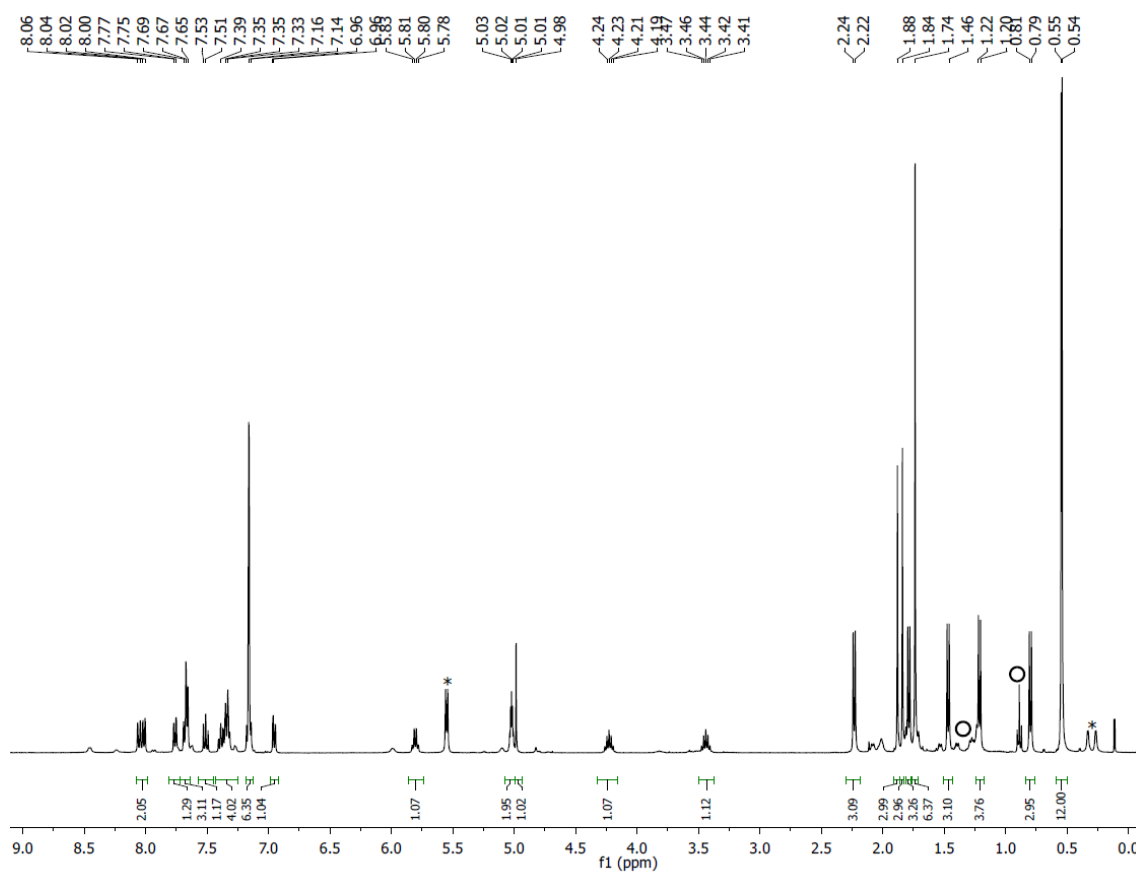


Figure 13. ^1H NMR spectrum (400.13 MHz, 300 K, C_6D_6) of **5**, *unidentified side-product, \circ *n*-hexane.

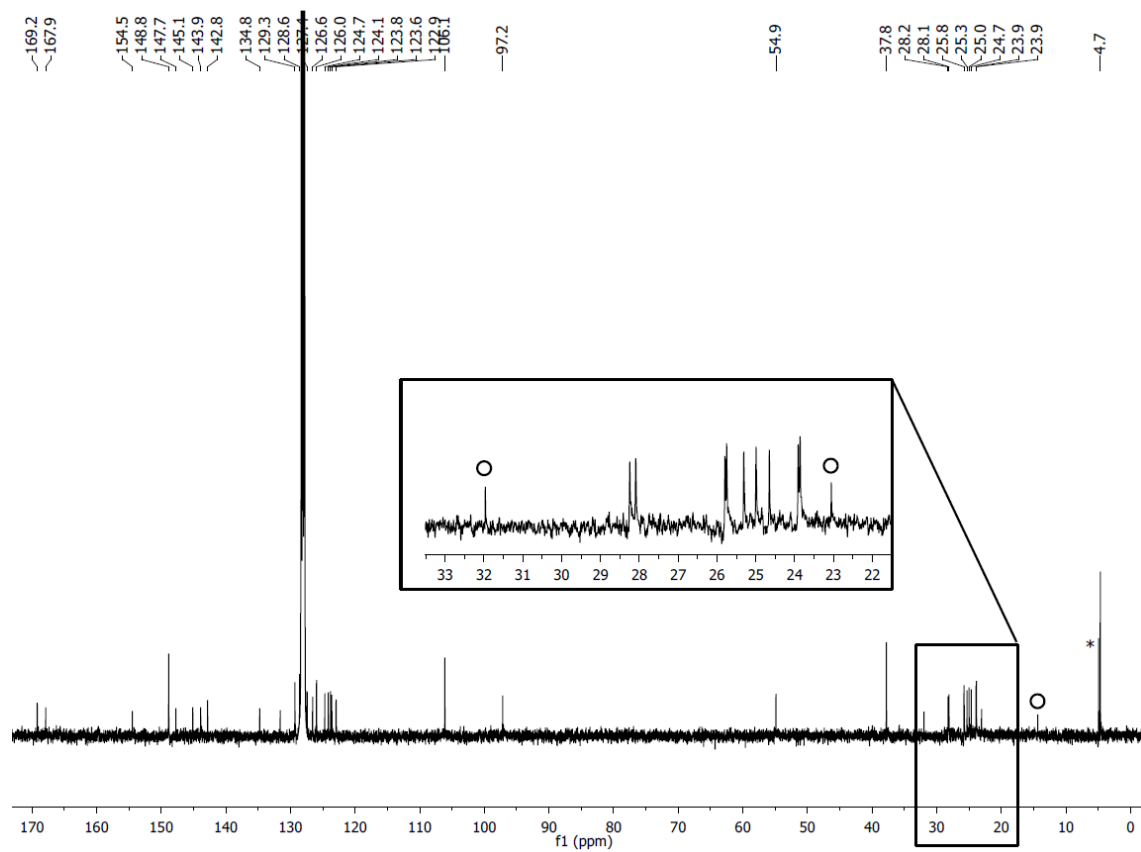


Figure 14. $^{13}\text{C}\{^1\text{H}\}$ NMR spectrum (100.61 MHz, 300 K, C_6D_6) of **5**, *unidentified side-product, \circ *n*-hexane.

3.4.4 Crystallographic Data

Table 8. X-ray Crystallographic Data for Compounds **1d**, **2d**, and **3**.

	1d	2d	3
Empirical formula	C ₅₁ H ₅₄ N ₂	C ₅₅ H ₆₂ MgN ₂	C ₄₂ H ₅₀ MgN ₄
Formula weight / g·mol ⁻¹	694.96	775.37	635.17
Temperature / K	123.00(10)	123.01(10)	100.01(10)
Crystal system	monoclinic	monoclinic	monoclinic
Space group	P2 ₁	P2 ₁	P2 ₁
<i>a</i> / Å	11.4367(1)	10.7210(2)	11.8736(2)
<i>b</i> / Å	16.1443(1)	10.0524(2)	10.9811(2)
<i>c</i> / Å	12.2507(1)	21.4986(4)	14.4558(2)
α / °	90	90	90
β / °	116.210(1)	100.148(2)	107.884(2)
γ / °	90	90	90
<i>V</i> / Å ³	2029.37(3)	2280.70(8)	1793.75(5)
<i>Z</i>	2	2	2
ρ_{calc} / g cm ⁻³	1.137	1.129	1.176
μ / mm ⁻¹	0.489	0.609	0.681
F(000)	748.0	836.0	684.0
Crystal size / mm ³	0.274 × 0.189 × 0.068	0.278 × 0.195 × 0.167	0.12 × 0.039 × 0.036
Radiation / Å	Cu K α (λ = 1.54184)	Cu K α (λ = 1.54184)	Cu K α (λ = 1.54184)
2 θ range for data collection / °	8.044 to 150.678	8.356 to 133.364	6.424 to 147.772
Diffractometer	Synergy DW	Synergy DW	Supernova
Index ranges	-14 ≤ <i>h</i> ≤ 14, -19 ≤ <i>k</i> ≤ 17, -14 ≤ <i>l</i> ≤ 15	-12 ≤ <i>h</i> ≤ 12, -11 ≤ <i>k</i> ≤ 11, -25 ≤ <i>l</i> ≤ 21	-14 ≤ <i>h</i> ≤ 14, -13 ≤ <i>k</i> ≤ 13, -17 ≤ <i>l</i> ≤ 16
Reflections collected	61362	35374	24152
Independent reflections	8097 [R _{int} = 0.0384, R _{sigma} = 0.0265]	8012 [R _{int} = 0.0584, R _{sigma} = 0.0384]	6900 [R _{int} = 0.0340, R _{sigma} = 0.0355]
Data/restraints/parameters	8097/1/475	8012/1/532	6900/1/432
Goodness-of-fit on F ²	1.048	1.087	1.035
Final R indexes [<i>I</i> > 2 σ (<i>I</i>)]	R ₁ = 0.0409, wR ₂ = 0.1019	R ₁ = 0.0515, wR ₂ = 0.1412	R ₁ = 0.0329, wR ₂ = 0.0776
Final R indexes [all data]	R ₁ = 0.0453, wR ₂ = 0.1048	R ₁ = 0.0533, wR ₂ = 0.1433	R ₁ = 0.0369, wR ₂ = 0.0791
Largest diff. peak/hole/e Å ⁻³	0.40/-0.32	0.32/-0.22	0.16/-0.17
Flack parameter	-0.1(2)	0.07(3)	0.02(2)

Table 9. X-ray Crystallographic Data for Compounds **4c**, **4d**, and **5**.

	4c	4d	5
Empirical formula	C ₃₇ H ₅₇ MgN ₃ OSi ₂	C ₅₅ H ₆₇ N ₃ MgSi ₂	C ₄₀ H ₅₉ MgN ₅ Si ₂
Formula weight / g·mol ⁻¹	640.34	850.60	690.41
Temperature / K	100.01(10)	123.00(10)	123.01(10)
Crystal system	orthorhombic	monoclinic	orthorhombic
Space group	P2 ₁ 2 ₁ 2 ₁	P2 ₁	P2 ₁ 2 ₁ 2 ₁
<i>a</i> / Å	12.8437(1)	11.2547(1)	12.5845(2)
<i>b</i> / Å	15.7049(1)	21.2395(1)	17.4715(5)
<i>c</i> / Å	18.8687(1)	11.7502(1)	20.5529(5)
α / °	90	90	90
β / °	90	115.232(1)	90
γ / °	90	90	90
<i>V</i> / Å ³	3805.99(4)	2540.82(4)	4518.97(18)
<i>Z</i>	4	2	4
ρ_{calc} / g cm ⁻³	1.118	1.112	1.015
μ / mm ⁻¹	1.233	1.028	1.067
F(000)	1392.0	916.0	1496.0
Crystal size / mm ³	0.14 × 0.118 × 0.07	0.229 × 0.080 × 0.040	0.317 × 0.064 × 0.031
Radiation / Å	Cu K α (λ = 1.54184)	Cu K α (λ = 1.54184)	Cu K α (λ = 1.54184)
2 θ range for data collection / °	7.324 to 133.636	8.318 to 148.974	6.64 to 150.946
Diffractometer	Supernova	Synergy DW	Synergy DW
Index ranges	-15 ≤ <i>h</i> ≤ 13, -18 ≤ <i>k</i> ≤ 18, -22 ≤ <i>l</i> ≤ 20	-13 ≤ <i>h</i> ≤ 14, -26 ≤ <i>k</i> ≤ 26, -14 ≤ <i>l</i> ≤ 14	-12 ≤ <i>h</i> ≤ 15, -21 ≤ <i>k</i> ≤ 21, -25 ≤ <i>l</i> ≤ 24
Reflections collected	30404	55599	53577
Independent reflections	6720 [R _{int} = 0.0319, R _{sigma} = 0.0237]	10145 [R _{int} = 0.0256, R _{sigma} = 0.0176]	9227 [R _{int} = 0.0344, R _{sigma} = 0.0290]
Data/restraints/parameters	6720/0/420	10145/1/562	9227/0/447
Goodness-of-fit on F ²	1.022	1.085	1.018
Final R indexes [I >= 2 σ (I)]	R ₁ = 0.0260, wR ₂ = 0.0674	R ₁ = 0.0360, wR ₂ = 0.0987	R ₁ = 0.0463, wR ₂ = 0.1217
Final R indexes [all data]	R ₁ = 0.0275, wR ₂ = 0.0687	R ₁ = 0.0370, wR ₂ = 0.0993	R ₁ = 0.0600, wR ₂ = 0.1303
Largest diff. peak/hole/e Å ⁻³	0.18/-0.18	0.25/-0.41	0.24/-0.40
Flack parameter	-0.004(9)	-0.013(6)	0.001(7)

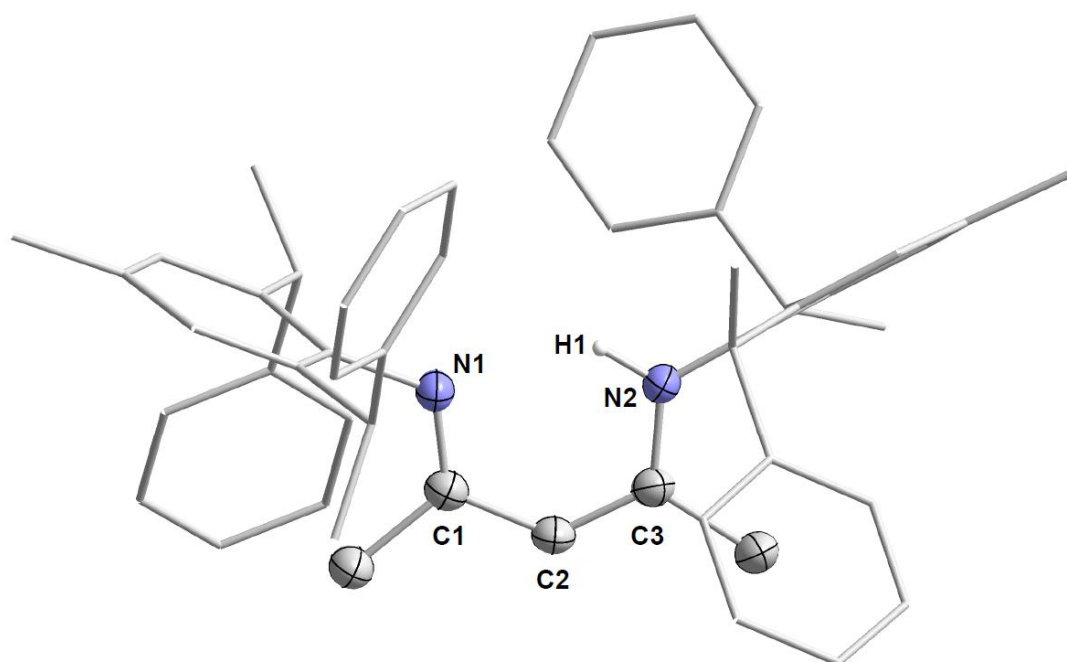


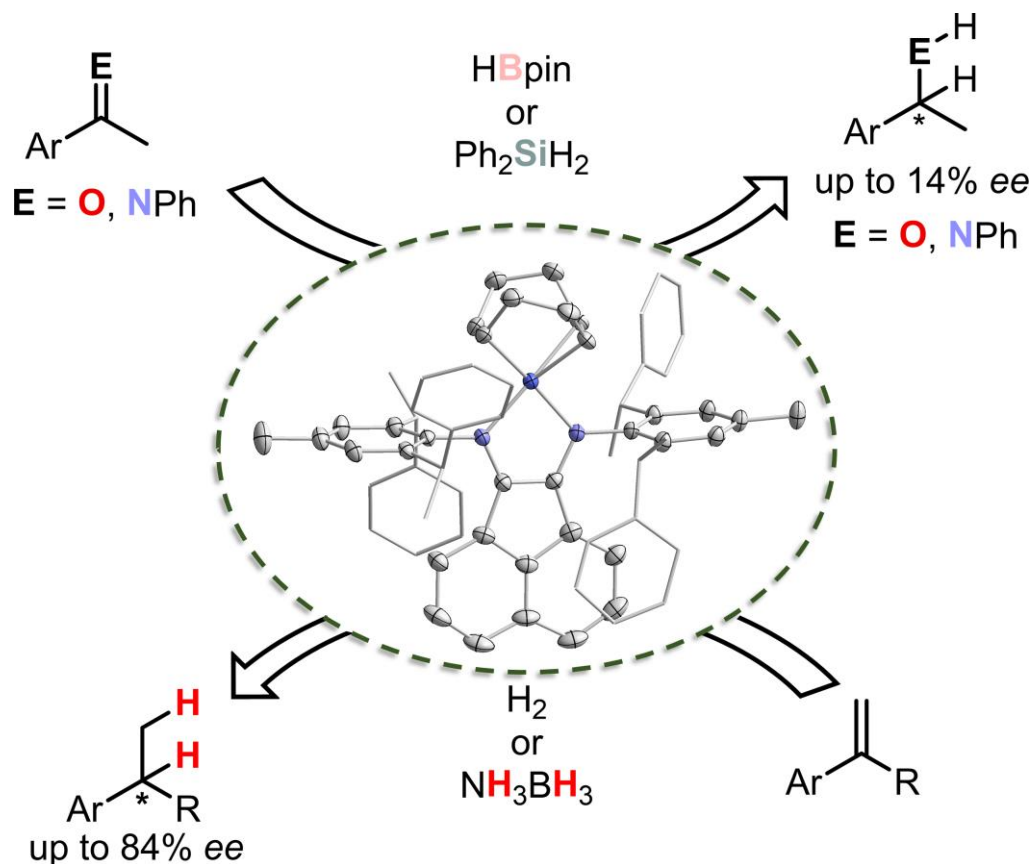
Figure 15. Solid-state molecular structure of **1d**. Thermal ellipsoids are set at the 50% probability level. Hydrogen atoms except for H1 are omitted for clarity. Selected bond lengths [Å] and angles [°] for **1d**: N1-C1 1.361(3), N2-C3 1.309(3), C1-C2 1.368(3), C2-C3 1.435(3). The NacNac backbone is planar with the plane-to-plane twist angle of the planes between N1-C1-C2 and C2-C3-N2 being 0.0(2).

References

- [1] a) R. Giri, B.-F. Shi, K. M. Engle, N. Mangel, J.-Q. Yu, *Chem. Soc. Rev.* **2009**, *38*, 3242–3272; b) K. C. Hultzsich, *Adv. Synth. Catal.* **2005**, *347*, 367–391; c) B. M. Trost, D. L. van Vranken, *Chem. Rev.* **1996**, *96*, 395–422.
- [2] a) D. Křištofiková, V. Modrocká, M. Mečiarová, R. Šebesta, *ChemSusChem* **2020**, *13*, 2828–2858; b) H. Pellissier, *Tetrahedron* **2007**, *63*, 9267–9331; c) J. Seayad, B. List, *Org. Biomol. Chem.* **2005**, *3*, 719–724.
- [3] W. M. Haynes *CRC handbook of chemistry and physics. A ready-reference book of chemical and physical data*, CRC Press, Boca Raton, **2016**.
- [4] D. Yang, L. Wang, D. Li, R. Wang, *Chem* **2019**, *5*, 1108–1166.
- [5] E. J. Corey, K. Ishihara, *Tetrahedron Lett.* **1992**, *33*, 6807–6810.
- [6] a) G. Desimoni, G. Faita, A. Gamba Invernizzi, P. Righetti, *Tetrahedron* **1997**, *53*, 7671–7688; b) Y. Honda, T. Date, H. Hiramatsu, M. Yamauchi, *Chem. Commun.* **1997**, 1411–1412; c) S. Kanemasa, Y. Oderaotoshi, S.-i. Sakaguchi, H. Yamamoto, J. Tanaka, E. Wada, D. P. Curran, *J. Am. Chem. Soc.* **1998**, *120*, 3074–3088.
- [7] D.-C. Wang, M.-S. Xie, H.-M. Guo, G.-R. Qu, M.-C. Zhang, S.-L. You, *Angew. Chem. Int. Ed.* **2016**, *55*, 14111–14115.
- [8] S. M. Wales, M. M. Walker, J. S. Johnson, *Org. Lett.* **2013**, *15*, 2558–2561.
- [9] V. Vasilenko, C. K. Blasius, H. Wadeppohl, L. H. Gade, *Chem. Commun.* **2020**, *56*, 1203–1206.
- [10] S. E. Larson, G. Li, G. B. Rowland, D. Junge, R. Huang, H. L. Woodcock, J. C. Antilla, *Org. Lett.* **2011**, *13*, 2188–2191.
- [11] G. K. Ingle, Y. Liang, M. G. Mormino, G. Li, F. R. Fronczek, J. C. Antilla, *Org. Lett.* **2011**, *13*, 2054–2057.
- [12] S. K. Nimmagadda, Z. Zhang, J. C. Antilla, *Org. Lett.* **2014**, *16*, 4098–4101.
- [13] J. Lv, X. Li, L. Zhong, S. Luo, J.-P. Cheng, *Org. Lett.* **2010**, *12*, 1096–1099.
- [14] Z. Mao, F. Mo, X. Lin, *Synlett* **2016**, *27*, 546–550.
- [15] C. Bolm, O. Beckmann, A. Cosp, C. Palazzi, *Synlett* **2001**, *2001*, 1461–1463.
- [16] H. Du, X. Zhang, Z. Wang, H. Bao, T. You, K. Ding, *Eur. J. Org. Chem.* **2008**, *2008*, 2248–2254.
- [17] M. Hatano, T. Horibe, K. Yamashita, K. Ishihara, *Asian J. Org. Chem.* **2013**, *2*, 952–956.
- [18] A. Falconnet, M. Magre, B. Maity, L. Cavallo, M. Rueping, *Angew. Chem. Int. Ed.* **2019**, *58*, 17567–17571.
- [19] a) J. Zheng, L. Lin, K. Fu, Y. Zhang, X. Liu, X. Feng, *Chem. Eur. J.* **2014**, *20*, 14493–14498; b) J. Zheng, L. Lin, Y. Kuang, J. Zhao, X. Liu, X. Feng, *Chem. Commun.* **2014**, *50*, 994–996.
- [20] K. Zheng, Y. Yang, J. Zhao, C. Yin, L. Lin, X. Liu, X. Feng, *Chem. Eur. J.* **2010**, *16*, 9969–9972.
- [21] J. Li, Y. Liao, Y. Zhang, X. Liu, L. Lin, X. Feng, *Chem. Commun.* **2014**, *50*, 6672–6674.
- [22] B. Maji, M. Baidya, H. Yamamoto, *Chem. Sci.* **2014**, *5*, 3941–3945.
- [23] a) L. Wang, D. Yang, D. Li, P. Wang, K. Wang, J. Wang, X. Jiang, R. Wang, *Chem. Eur. J.* **2016**, *22*, 8483–8487; b) D. Yang, L. Wang, M. Kai, D. Li, X. Yao, R. Wang, *Angew. Chem. Int. Ed.* **2015**, *54*, 9523–9527.
- [24] a) G. Lu, T. Yoshino, H. Morimoto, S. Matsunaga, M. Shibasaki, *Angew. Chem. Int. Ed.* **2011**, *50*, 4382–4385; b) D. Yang, L. Wang, F. Han, D. Zhao, B. Zhang, R. Wang, *Angew. Chem. Int. Ed.* **2013**, *52*, 6739–6742; c) T. Yoshino, H. Morimoto, G. Lu, S. Matsunaga, M. Shibasaki, *J. Am. Chem. Soc.* **2009**, *131*, 17082–17083.
- [25] R. L. Webster, *Dalton Trans.* **2017**, *46*, 4483–4498.
- [26] M. Arrowsmith, M. S. Hill, T. Hadlington, G. Kociok-Köhn, C. Weetman, *Organometallics* **2011**, *30*, 5556–5559.
- [27] M. Arrowsmith, T. J. Hadlington, M. S. Hill, G. Kociok-Köhn, *Chem. Commun.* **2012**, *48*, 4567–4569.
- [28] C. Weetman, M. D. Anker, M. Arrowsmith, M. S. Hill, G. Kociok-Köhn, D. J. Liptrot, M. F. Mahon, *Chem. Sci.* **2016**, *7*, 628–641.
- [29] C. Weetman, M. S. Hill, M. F. Mahon, *Chem. Commun.* **2015**, *51*, 14477–14480.
- [30] Z. Xu, S. Zhang, W. Ren, *Inorg. Chim. Acta* **2019**, *495*, 118970.
- [31] D. Mukherjee, H. Osseili, T. P. Spaniol, J. Okuda, *J. Am. Chem. Soc.* **2016**, *138*, 10790–10793.
- [32] M. D. Anker, M. Arrowsmith, R. L. Arrowsmith, M. S. Hill, M. F. Mahon, *Inorg. Chem.* **2017**, *56*, 5976–5983.
- [33] A. Berkefeld, W. E. Piers, M. Parvez, L. Castro, L. Maron, O. Eisenstein, *Chem. Sci.* **2013**, *4*, 2152.
- [34] a) D. W. Stephan, *Acc. Chem. Res.* **2015**, *48*, 306–316; b) D. W. Stephan, *Science* **2016**, *354*.
- [35] M. D. Anker, M. Arrowsmith, P. Bellham, M. S. Hill, G. Kociok-Köhn, D. J. Liptrot, M. F. Mahon, C. Weetman, *Chem. Sci.* **2014**, *5*, 2826–2830.
- [36] D. Mukherjee, S. Shirase, T. P. Spaniol, K. Mashima, J. Okuda, *Chem. Commun.* **2016**, *52*, 13155–13158.
- [37] D. J. Liptrot, M. S. Hill, M. F. Mahon, D. J. MacDougall, *Chem. Eur. J.* **2010**, *16*, 8508–8515.
- [38] M. Arrowsmith, B. Maitland, G. Kociok-Köhn, A. Stasch, C. Jones, M. S. Hill, *Inorg. Chem.* **2014**, *53*, 10543–10552.
- [39] S. P. Green, C. Jones, A. Stasch, *Angew. Chem. Int. Ed.* **2008**, *47*, 9079–9083.
- [40] a) T. Deschner, M. Klimpel, M. Tafipolsky, W. Scherer, K. W. Törnroos, R. Anwender, *Dalton Trans.* **2012**, *41*, 7319–7326; b) G. Ballmann, B. Rösch, S. Harder, *Chem. Ber.* **2019**, *2019*, 3683–3689; c) C. Bakewell, *Dalton Trans.* **2020**, *49*, 11354–11360.
- [41] L. R. Doyle, A. J. Wooles, S. T. Liddle, *Angew. Chem. Int. Ed.* **2019**, *58*, 6674–6677.
- [42] a) V. Balasanthiran, M. H. Chisholm, K. Choojun, C. B. Durr, *Dalton Trans.* **2014**, *43*, 2781–2788; b) S. J. Bonyhady, C. Jones, S. Nembenna, A. Stasch, A. J. Edwards, G. J. McIntyre, *Chem. Eur. J.* **2010**, *16*, 938–955; c) C. Jones, L. McDyre, D. M. Murphy, A. Stasch, *Chem. Commun.* **2010**, *46*, 1511–1513; d) A.-F. Pécharman, A. L. Colebatch, M. S. Hill, C. L. McMullin, M. F. Mahon, C. Weetman, *Nat. Commun.* **2017**, *8*, 15022.
- [43] V. Balasanthiran, M. H. Chisholm, K. Choojun, C. B. Durr, P. M. Wambua, *Polyhedron* **2016**, *103*, 235–240.
- [44] C. N. Ayala, M. H. Chisholm, J. C. Gallucci, C. Krempner, *Dalton Trans.* **2009**, 9237–9245.

4 Asymmetric Transfer Hydrogenation Reactions Catalysed by an α -Diimine Stabilised Cobaltate Complex^[a]

Abstract: Chiral cobalt and iron complexes $[(\mathbf{L1})\text{CoBr}_2]$ (**1**) and $[(\mathbf{L1})\text{FeBr}_2]$ (**2**) were synthesised from bis(4-methyl-2,6-bis((*R*)-1-phenylethyl)phenyl)acenaphthylene-1,2-diimine (**L1**) and iron or cobalt dibromide. Complexes **1** and **2** were then evaluated as precatalysts in asymmetric hydrofunctionalisation reactions. Catalysts generated by addition of LiBEt_3H to **1** or **2** efficiently promoted hydroboration, hydrosilylation and hydrogenation reactions. However, only low, if any, enantiomeric excesses (up to 14% *ee*) were observed for all reactions. Ligand exchange of 1,5-cyclooctadiene (cod) in $[\text{K}(\text{thf})_x][\text{Co}(\text{cod})_2]$ (**3**) with **L1** gave $[\text{K}(\text{thf})_x][(\mathbf{L}^1)\text{Co}(\text{cod})]$ (**4**). This complex catalysed asymmetric transfer hydrogenation reactions of olefins with ammonia borane (NH_3BH_3) as a sacrificial hydrogen donor. Whilst low conversions were mostly observed, good enantiomeric excesses of up to 84% were obtained when 5 mol% of **L1** and **3** were used together with 5 equivalents of NH_3BH_3 . Modification of the ligand scaffold did not result in improved reaction yields or enantioselectivities. Poisoning experiments with mercury, $\text{P}(\text{OMe})_3$ and dibenzo[*a,e*]cyclooctatetraene (DCT) were conducted, which strongly suggested the catalytically active species to be homogeneous in nature.



^[a] Felix Seeberger performed the reactions and the characterisation of all compounds. Robert Wolf supervised and directed the project.

4.1 Introduction

Hydrogenation is one of the most fundamental transformations in chemistry. Among other applications, hydrogenation reactions are employed in the synthesis of fine chemicals used in pharmaceutical, agricultural and food industries.^[1] Besides the direct addition of dihydrogen (H_2), transfer hydrogenations (THs) also serve to convey hydrogen to an unsaturated substrate. THs have the advantage of avoiding hazardous, pressurised H_2 gas and can offer increased control over the degree of reduction.^[2] Nowadays, a plethora of reagents which can act as hydrogen sources in THs, is known, including secondary alcohols,^[3] Hantzsch esters,^[4] ammonium formate^[5] or cyclohexadienes (Figure 1).^[6] Recently, ammonia borane (NH_3BH_3) (and its amine borane derivatives $[NR_2H \cdot BH_3]$) has attracted increasing attention due to its bench stability, low molecular weight ($30.97 \text{ g} \cdot \text{mol}^{-1}$) and high hydrogen content (19.6 wt%).^[2,7] While there are some reports on 4d and 5d transition-metal-catalysed THs with ammonia borane,^[8] contemporary research focuses on the use of organocatalysts^[2,9] and 3d transition metal catalysts.

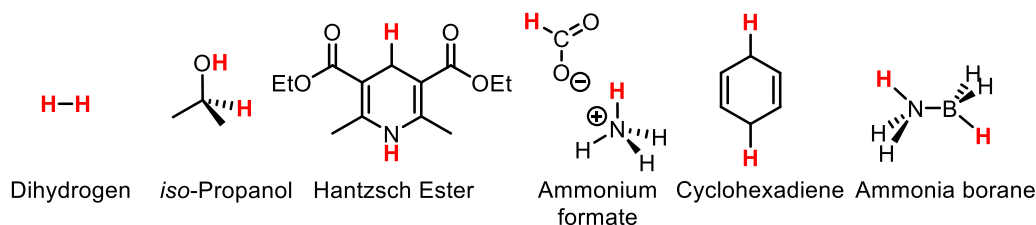
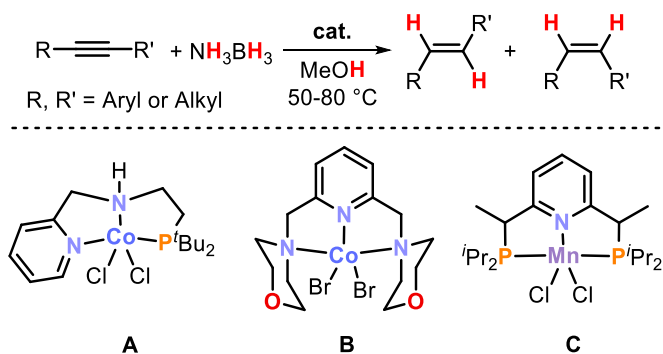


Figure 1. Dihydrogen and examples of TH reagents.

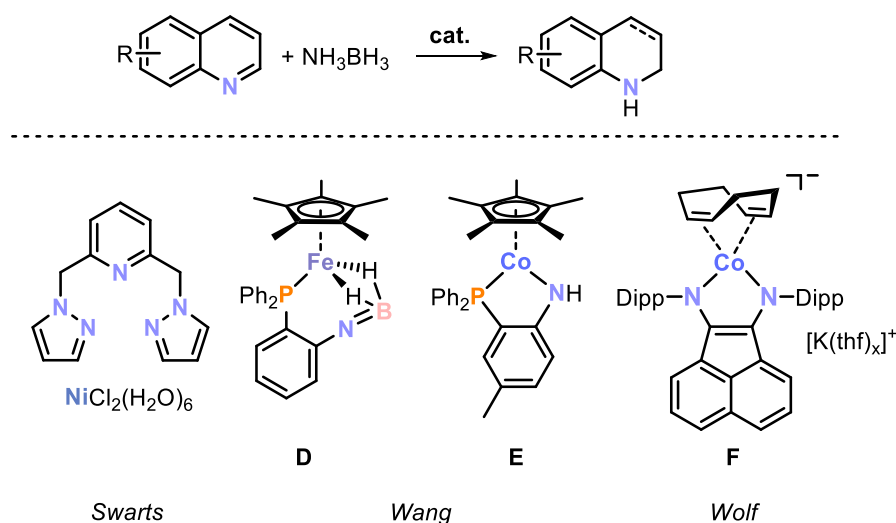
Molecular complexes of manganese, cobalt, nickel, and copper have been shown to catalyse transfer hydrogenations of alkenes and alkynes using ammonia borane.^[10-11] However, the scope is generally limited to easily hydrogenated alkynes and activated alkenes. For example, alkyne transfer hydrogenations catalysed by cobalt and manganese complexes **A-C** required increased temperatures and stopped at the corresponding alkene (Scheme 1). Whilst Liu's cobalt catalyst **A** selectively yielded the E-alkene,^[12] **B** and **C** synthesised by Balaraman^[13] and El-Sepelgy,^[10] respectively, afford the Z-alkene. Furthermore, for all three cases the solvent, methanol, played a major role in the catalysis by acting as a proton donor to yield the desired alkene.



Scheme 1. Transfer semihydrogenation using ammonia borane catalysed by 3d-metal complexes.

In 2015, *Waterman* and co-workers reported on the catalytic activity of $[\text{CpCo}(\text{CO})\text{I}_2]$ and $[\text{Cp}^*\text{Co}(\text{CO})\text{I}_2]$ in transfer hydrogenation reactions using ammonia borane.^[14] This Co(III)-based system, which is stabilised *via* the Cp or Cp* ligand, was able to smoothly reduce alkenes, even in the presence of air.

Recent years have seen an increasing number of reports on the transfer hydrogenation of quinolines. *Swarts* and co-workers reported that an in-situ generated Ni(II) hydride catalysed the transfer hydrogenation of a wide range of quinolines (**Scheme 2**).^[15] The pentamethylcyclopentadienyliron and -cobalt complexes **D** and **E** synthesised by *Wang* and co-workers also catalysed the transfer hydrogenation of quinolines (**Scheme 2**).^[16] While **D** selectively reduced quinolines to the corresponding 1,2-dihydroquinoline, the cobalt catalyst **E** promoted either partial or full quinoline hydrogenation depending on the amount of ammonia borane. Therefore, the 1,2-dihydroquinoline or the 1,2,3,4-tetrahydroquinoline could be obtained simply by using either one or two equivalents of ammonia borane, respectively. *Wolf* and co-workers reported on the transfer hydrogenation of alkenes and quinolines catalysed by an α -diimine-cobaltate salt (**Scheme 2, F**).^[17] The high efficiency of this catalytic system was demonstrated by one equivalent of ammonia borane proving sufficient to fully reduce quinolines to the corresponding 1,2,3,4-tetrahydroquinolines, through the uptake of up to two equivalents of H_2 per ammonia borane.

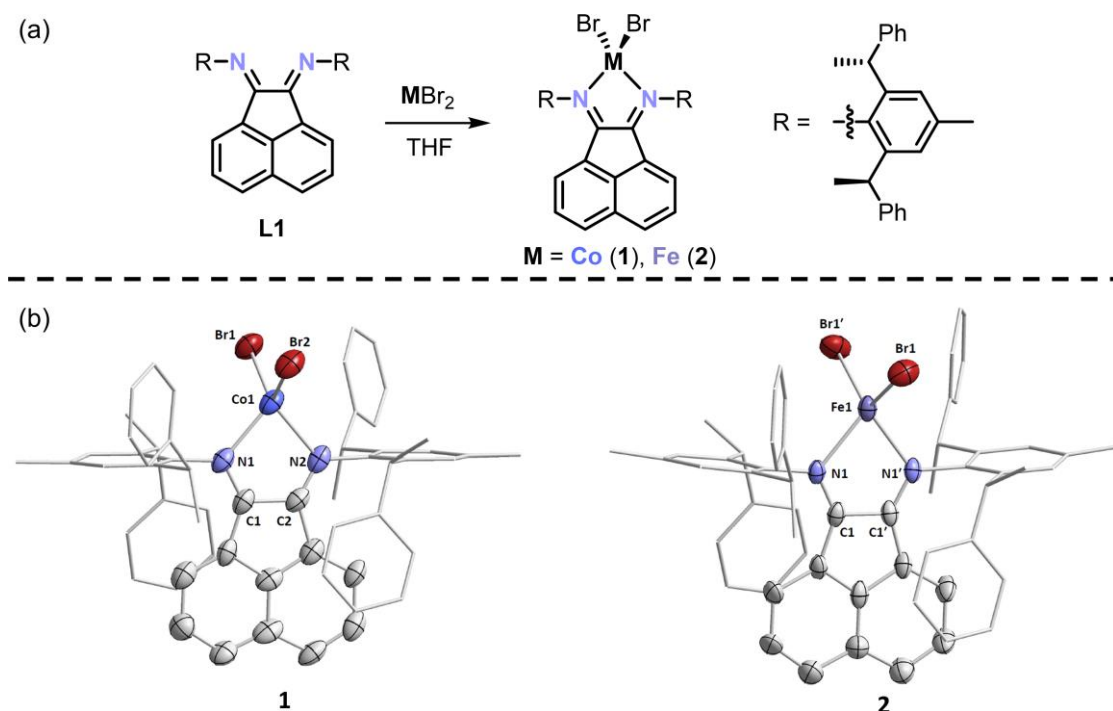


Scheme 2. (Partial) Transfer hydrogenation of quinolines using ammonia borane catalysed by 3d transition metal complexes.

All of these examples showcase the capabilities of 3d transition metal complexes in THs using ammonia borane. Reports of asymmetric THs, however, are limited. Whilst enantioselective THs with organocatalysts and frustrated Lewis pairs are known,^[18] to the best of our knowledge, base metal catalysed routes have yet to be reported. Therefore, we were interested in developing a metal catalysed TH by modifying our aforementioned cobaltate precatalyst with chiral α -diimine ligands.

4.2 Results and Discussion

The chiral bis(aryl)acenaphthenequinonediimine (BIAN) ligand **L1** (see **Scheme 3a**) was synthesised according to a procedure by *Cramer* and co-workers.^[19] Initially the BIAN cobalt (**1**) and iron (**2**) dibromides were synthesised (**Scheme 3**), as *in situ* reduced BIAN cobalt halides have been reported to form catalytically active species for hydrogenations.^[20] Furthermore, these complexes offer the advantage of a much higher stability towards air and moisture when compared to isolated highly reduced metal species.

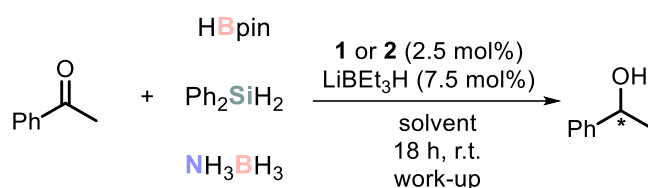


Scheme 3. Synthesis of cobalt (**1**) and iron (**2**) dibromide complexes supported by chiral BIAN ligand **L1** and (a) their solid-state molecular structures (b). Thermal ellipsoids are set at the 50% probability level. Residual solvent molecules as well as hydrogen atoms are omitted for clarity. Selected bond lengths [Å] and angles [°] for **1**: Co1-Br1 2.341(1), Co1-Br2 2.360(1), Co1-N1 2.072(6), Co1-N2 2.110(5), N1-C1 1.304(9), N2-C2 1.25(1), C1-C2 1.55(1), N1-Co1-N2 82.6(2), Br1-Co1-Br2 112.91(6), N1-Co1-N2 to Br1-Co1-Br2 plane twist angle 91.2(2). Selected bond lengths [Å] and angles [°] for **2**: Fe1-Br1 2.3567(8), Fe1-N1 2.148(4), N1-C1 1.276(6), C1-C1' 1.473(7), N1-Fe1-N1' 77.1(2), Br1-Fe1-Br1' 112.86(5) N1-Fe1-N1' to Br1-Fe1-Br1' plane twist angle 81.0(2).

The α -diimine backbones of both complexes feature C–N bond lengths in the range of C=N double bonds (1.304(9) and 1.25(1) Å for **1**, 1.276(6) Å for **2**) as well as C1–C2 or C1–C1' bond lengths in the range of, or close to, a carbon–carbon single bond (1.54(1) or 1.473(7) Å for **1** and **2**, respectively). These observations strongly suggest the expected neutral form of the BIAN ligand for both complexes. **1** and **2** are also isostructural to their previously reported ^{Dipp}BIAN analogues.^[21] With these complexes in hand, their catalytic potential in asymmetric hydroboration, hydrosilylation and (transfer) hydrogenation reactions was investigated.

Based on our previous results,^[20] initial screening experiments were performed using precatalyst **1** and **2**, reduced *in situ* by addition of three equivalents of LiBEt₃H (see **4.4.2, Table 1**). Pinacolborane (HBpin), Ph₂SiH₂ and NH₃BH₃ were investigated as reducing reagents in the

asymmetric hydrofunctionalisation of acetophenone, which yielded 1-phenylethanol upon work-up (**Scheme 4**). Enantiomeric excesses were determined *via* chiral GC-FID analysis. The hydrofunctionalisation with HBpin or Ph₂SiH₂ yielded the desired alcohol in high conversions (> 95%), but no enantioselectivity was observed (**Table 1**, entries 1-4). When these reactions were performed without additional LiBEt₃H, the desired product was not detected in the hydroboration reaction of acetophenone. In the hydrosilylation reaction on the other hand, a high conversion (> 95%) of the ketone was observed together with slightly enantioenriched alcohol formation (17% *ee*, **Table 1**, entries 5-6). Transfer hydrogenation reactions of acetophenone catalysed by **1** or **2** reduced *in situ* by LiBEt₃H, with NH₃BH₃ as the sacrificial H₂ donor resulted in almost full conversion of the ketone. However, the desired alcohol was observed in only low to moderate yields (28-48%) and no, or low, enantioenrichment (up to 9% *ee*) (**Table 1**, entries 7-10). Moderate to good conversions were detected, when the hydrofunctionalisation was performed with the ketimine 1-diphenylethan-1-imine as the substrate (**Table 1**, entries 11-13). However, none of the investigated reducing reagents (HBpin, Ph₂SiH₂ or NH₃BH₃) led to the enantioenriched formation of the desired amine (< 5% *ee*).



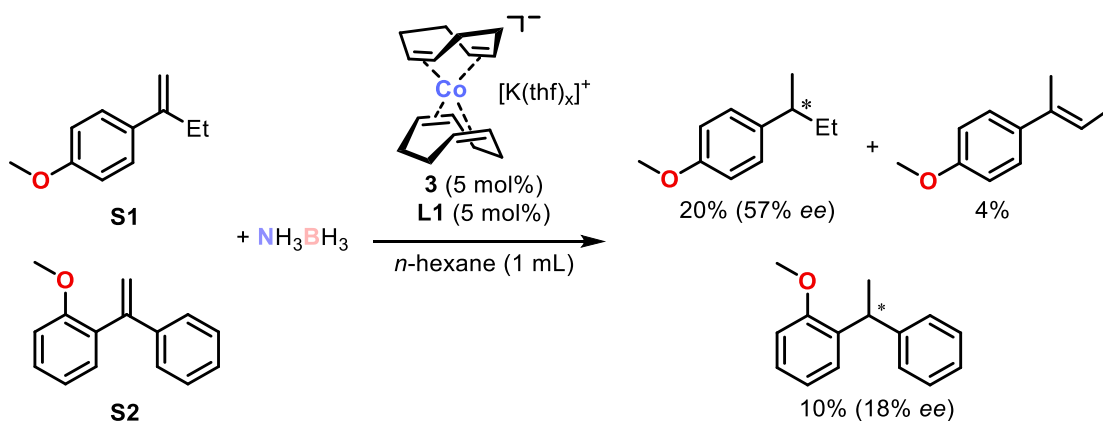
Scheme 4. Hydrofunctionalisation of acetophenone catalysed by **1** or **2** reducing *in situ* with LiBEt₃H.

Next, the hydroboration and -silylation of acetophenone with precatalyst **2** was screened with varying amounts of LiBEt₃H (0.5, 1.0 and 1.5 equiv. with respect to **2**) (see 4.4.2, **Table 2**). Generally, incomplete conversions were observed when less than 1.0 equivalents of LiBEt₃H was added (**Table 2**, entries 1-3 and 9-12). 1.0 to 1.5 equivalents of LiBEt₃H were required for high to full conversion of acetophenone in the hydrofunctionalisation reactions (**Table 2**, entries 4-8 and 12-17). While no solvent dependency was observed for the hydroboration of acetophenone catalysed by **2**/LiBEt₃H, the hydrosilylation reaction resulted in the increased conversion of the ketone when the reactions were performed in more polar solvents (**Table 2**, entries 12-17). Interestingly, diminished conversions were observed in the less polar solvents toluene and *n*-hexane upon increasing the loading of LiBEt₃H in the hydrosilylation reaction from 1.0 to 1.5 equivalents. Unfortunately, low, if any, enantioselectivity (up to 5% *ee*) was detected for all reactions.

The hydrogenation of *trans*- α -methylstilbene, but-1-en-2-ylbenzene and acetophenone in different solvents was investigated, next (see 4.4.2, **Table 3**). C=C double bonds were generally converted fully to the desired alkane (**Table 3**, entries 1-6), while the hydrogenation of acetophenone was much less efficient (up to 22% conversion, **Table 3**, entries 7-8). No

enantioinduction was observed for the ketone, whilst low enantiomeric excesses of up to 14% were detected for the olefins.

In an attempt to improve the enantiomeric excess, catalytic reactions were conducted using the reduced potassium bis(1,5-cyclooctadiene)cobaltate salt (**3**) as the precatalyst. Initially, different transfer hydrogenation reagents, HBpin, and Ph_2SiH_2 were tested in the asymmetric transfer hydrogenation of 1-(but-1-en-2-yl)-4-methoxybenzene (**S1**, see **Scheme 5**) with precatalyst **3** in combination with α -diimine **L1**. The reaction products were analysed by chiral GC-FID or HPLC. Potassium cobaltate **3** was stirred with **L1** for 30 min in THF, before the olefin was added together with the hydrofunctionalisation reagent (see **4.4.2**, **Table 4**). No conversion was observed with ammonium formate, cyclohexa-1,3-diene, cyclohexa-1,4-diene, Hantzsch ester or Ph_2SiH_2 (**Table 4**, entries 3-7). With NH_3BH_3 and HBpin, yields of 43% and 30% were obtained, however, no enantioinduction was detected for either reaction (**Table 4**, entries 1-2). Notably, isomerisation of the starting material to the more stable 1-(but-2-en-2-yl)-4-methoxybenzene was observed as a major side reaction. Using NH_3BH_3 , the best performing reducing agent, and switching the solvent from THF to the less polar toluene or *n*-hexane drastically lowered the observed isomerisation whilst also increasing the enantiomeric excess up to 57% (see **4.4.2**, **Table 5**). However, the increased enantioselectivity was accompanied by diminished yields. To circumvent isomerisation as a side reaction, the non-isomerisable olefin 1-methoxy-2-(1-phenylvinyl)benzene (**S2**, see **Scheme 5**) was tested as a prochiral substrate (see **4.4.2**, **Table 6**). Contrary to expectations, however, lower enantiomeric excesses (up to 18% *ee*) were observed than with **S1**. The conditions that provided the highest enantiomeric excesses using the precatalyst **3** with ligand **L1** are depicted in **Scheme 5**.



Scheme 5. Asymmetric transfer hydrogenation of prochiral olefins with NH_3BH_3 catalysed by a mixture of **3** and **L1**.

As precatalyst **3** exhibited greater enantioselectivity than **1** or **2**, focus was given to optimizing this system by modification of the ligand. α -Diimines **L2** and **L3** (**Figure 2**) were synthesised according to a procedure by *Cramer* and co-workers.^[19] Further α -diimines **L4-L9** were graciously provided by the *Cramer* group (**Figure 2**). Ligands **L2-L9** were then compared to **L1** in the transfer hydrogenation of **S1** or **S2** with precatalyst **3** in THF, toluene and *n*-hexane (see

4.4.2, Table 7 and 8 for **S1** and **S2**, respectively). Similar to **L1**, the TH with **L2** and **L3** showcased a strong solvent dependency with decreasing conversion and isomerisation from THF to the non-polar *n*-hexane (Table 7, entries 1-6; Table 8 entries 1-5). The yields, conversions and enantioselectivities, however, were lower than with **L1** (up to 22% *ee* for substrate **S1**). Interestingly, the opposing trend was observed when the TH of **S1** was performed with **L5**, **L6** or **L9** (Table 7, entries 7-15). An increase in conversion and isomerisation was detected when the solvent polarity was decreased from THF to *n*-hexane (up to 47% yield). When **L4-L8** were used in the TH of **S2** moderate to high conversions (up to 90%) were detected (Table 8, entries 6-20). **L6** and **L7** yielded the highest conversions in polar solvents, whilst lower conversions were observed in *n*-hexane, thereby illustrating the same trend as **L1** (Table 8, entries 12-17). Conversely, **L4** and **L5** yielded the highest conversions when the reaction was conducted in *n*-hexane (Table 8, entries 6-12). Unlike for any of the other ligands, the highest conversions with **L8** were obtained in toluene (Table 8, entries 18-20). Nonetheless, none of the ligands **L4-L9** yielded the desired alkanes in high optical purity (only up to 11% *ee*). Therefore, of ligands **L1-L9**, the BIAN-based **L1** remained the best-performing in the TH of **S1** and **S2** with precatalyst **3**.

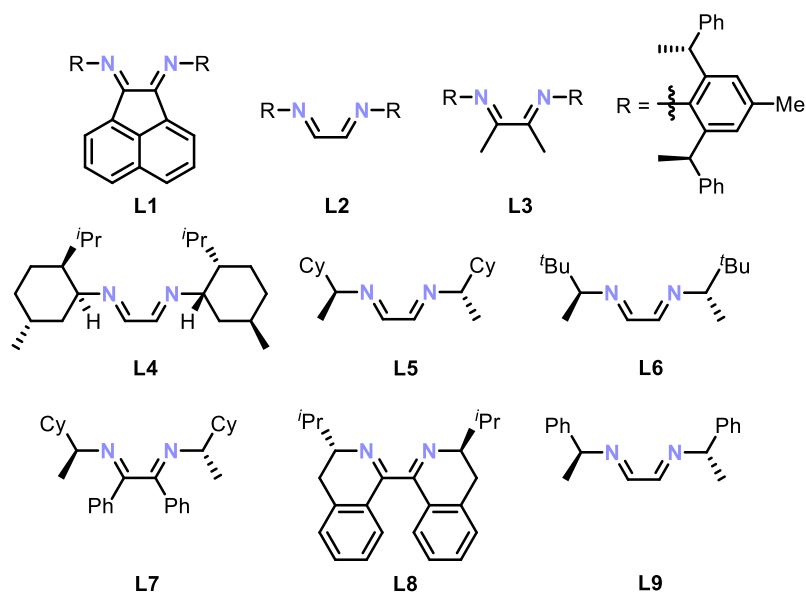


Figure 2. Investigated chiral α -diimines **L1-L9**.

Building on this, further ligand optimisation was undertaken by varying the aryl substituent at the *N*-atom, while maintaining the BIAN backbone from **L1**. BIAN ligands **L10-L17** were synthesised and their influence on the TH of olefins **S1** and **S2** was investigated (Figure 3 and see 4.4.2, Tables 9 and 10 for **S1** and **S2**, respectively). The screened ligands generally exhibited a similar solvent dependency to **L1** with decreasing catalytic activity in less polar solvents, and low enantioenrichment in THF contrasting with moderate enantioselectivity in toluene and *n*-hexane. Substitution at the *para*-position of the flanking aniline of the ligand (Figure 3, **L10-L13**) generally led to decreased yields of the desired alkane (Table 9, entries 1-11) in each

solvent. An increased enantiomeric excess (63% *ee*) was only observed upon substituting the methyl group with a strongly electron-drawing CF_3 group (**L13**, **Table 9**, entry 11). Substitution of the aryl group adjacent to the chiral centers (**Figure 3**, **L14-L17**) was found to have a significant effect on the enantioinduction. The observed enantioselectivity steadily increased with the electron-withdrawing strength of the aryl substituent from **L14** to **L17** (**Table 9**, entries 12-21). Increased enantiomeric excesses of up to 74% were observed with **L16** and **L17** (**Table 9**, entries 18, 20 and 21) whilst **L14** and **L15** yielded the desired alkane in slightly decreased optical purities (44 and 52% *ee*, **Table 9**, entries 14 and 16). Thus, for both sets of ligand modifications electron-donating substituents decreased the enantioselectivity, whilst electron-withdrawing substituents increased the enantioinduction. **L1** (57% *ee*) is consistent with this trend as the electron-withdrawing strength of the phenyl substituent lies between the 3,5-dimethylphenyl- and the 4-fluorophenyl-substitution of **L15** (52% *ee*) and **L16** (66% *ee*). Despite increased enantiomeric excesses in some cases (**L13**, **L16** and **L17**) modification of ligand **L1** led to decreased yields. Furthermore, increased isomerisation to the internal olefin was generally observed. This was especially pronounced for the CF_3 -substituted BIAN (**L13**), where a starkly increased isomerisation (9% yield vs. 22% isomerisation, **Table 9**, entry 11). Therefore, whilst the highest enantioinduction was observed with **L17**, **L1** remained the preferred ligand, as it facilitated higher product yields and lower, undesired isomerisation.

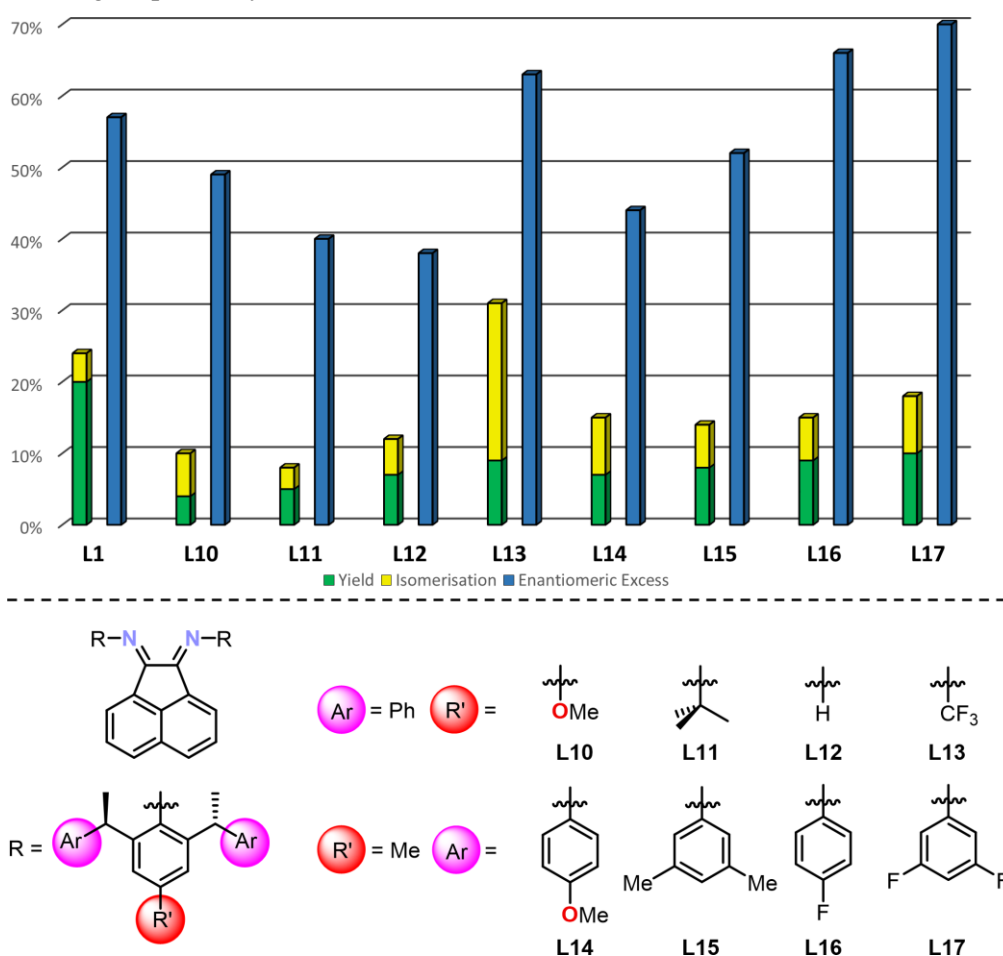
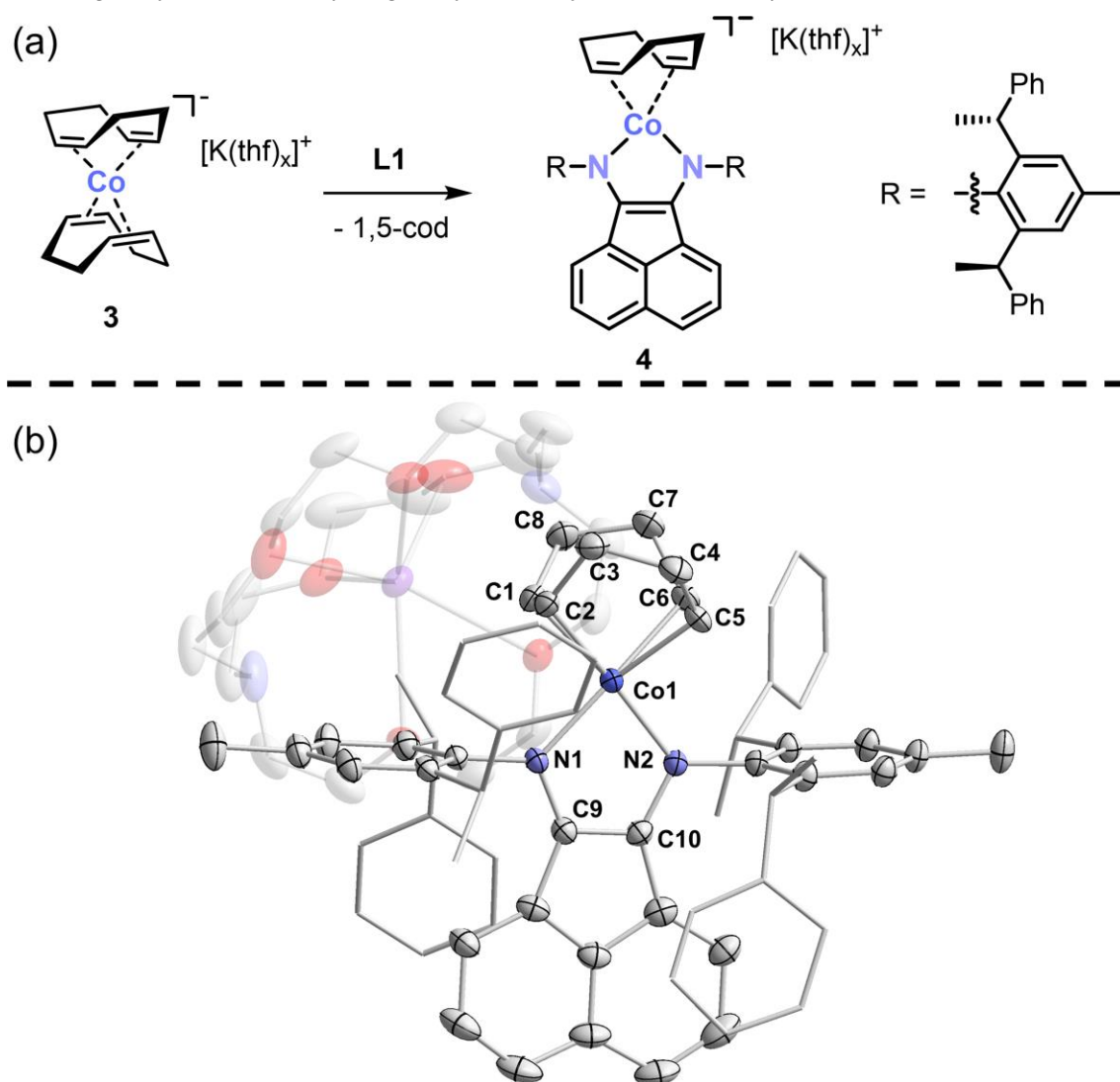


Figure 3. Activity and enantioselectivity of ligands **L10-L17** in the transfer hydrogenation with precatalyst **3**.

To confirm the formation of the cobaltate salt $[\text{K}(\text{thf})][\text{L1Co}(\text{cod})]$ (**4**), this compound was independently synthesised (**Scheme 6**). Upon combining THF solutions of **L1** and **3** at ambient temperature, the solution turned dark green and was stirred for 18 h. After isolation and recrystallisation of the product, the ^1H NMR spectrum revealed broad signals indicating the formation of a paramagnetic side product. In order to improve the recrystallisation of cobaltate **4**, one equivalent of [2.2.2]cryptand or [18]crown-6 was added. However, minute amounts of paramagnetic impurities remained despite repeated recrystallisations from THF/*n*-hexane (see 4.4.3, **Figure 11**). Nonetheless, the solid-state molecular structure of **4**-[2.2.2]cryptand was unambiguously determined by single-crystal X-ray diffraction analysis.

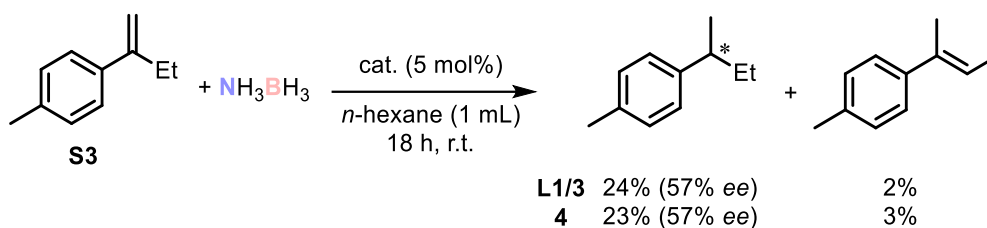


Scheme 6. Synthesis of cobaltate **4** and (a) solid-state molecular structure of **4**-[2.2.2]cryptand (b). Thermal ellipsoids are set at the 50% probability level. $[\text{K}([2.2.2]\text{cryptand})]^+$ is transparent and hydrogen atoms are omitted for clarity. Selected bond lengths [\AA] and angles [$^\circ$]: Co1-C1 2.082(4), Co1-C2 2.044(4), Co1-C5 2.010(4), Co1-C6 2.031(4), Co1-N1 1.930(3), Co1-N2 1.938(3), N1-C9 1.366(4), N2-C10 1.376(4), C9-C10 1.382(5), N1-Co1-N2 83.2(1).

4-[2.2.2]cryptand crystallises in the monoclinic space group $P2_1$ with two formula units per asymmetric unit. The α -diimine backbone of **4**-[2.2.2]cryptand features C–N (1.366(4) and 1.376(4) \AA) and C–C (1.382(5) \AA) bond lengths commensurate with a dianionic BIAN $^{2-}$ ligand,

L1²⁻. Additionally, the Co–C bond lengths (2.01–2.08 Å) render **4** isostructural with its previously reported analogue [K(thf)₂][(Dipp)BIAN)Co(cod)].^[22]

The isolated cobaltate **4** was compared to catalyst generated *in situ* from **L1** and **3** in the TH of 1-(but-1-en-2-yl)-4-methylbenzene (**S3**) with NH₃BH₃ (**Scheme 7**, see 4.4.2, Table 11). Complex **4** provided essentially identical activity and selectivity to the mixture of **L1** and **3** stirred for 30 min, thus providing strong evidence that complex **4** is generated *in situ* to engage in the hydrogenation.



Scheme 7. Comparison of the *in situ* formed precatalyst **L1/3** with the isolated cobaltate salt **4** as catalysts in the asymmetric TH of **S3**.

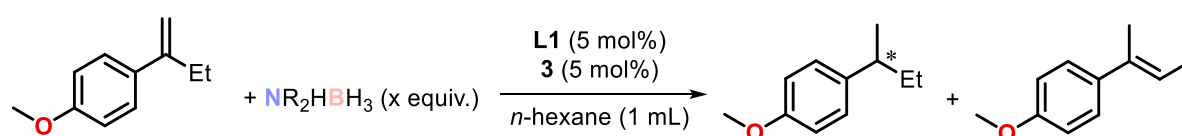
In order to expand the substrate scope from olefins to ketones (acetophenone), imines (N-1-diphenylethan-1-imine) and quinolines (3-methylquinoline), THs were performed with precatalyst **4** and the desired substrate in THF, toluene and *n*-hexane (see 4.4.2, Table 12). High conversions (> 95%) were observed for acetophenone and 3-methylquinoline in all screened solvents (Table 12, entries 4–6 and 10–12). In the imine reduction, non-polar solvents were observed to drastically impede the reaction (75% to 14% THF vs. *n*-hexane, Table 12, entries 7–9). Moreover, low, if any, enantiomeric excess was observed for all substrates with the highest optical purity (10% ee) found for the transfer hydrogenation of acetophenone in THF (Table 12, entry 4). Altogether, cobaltate **4** struggled to selectively catalyse the asymmetric hydrofunctionalisation of olefins, ketones, imines and quinolines.

Improving the catalytic activity of precatalyst **4** was targeted next. It has been reported that the use of ammonia borane in the presence of an H₂ atmosphere can drastically increase the obtained yields, allowing the (transfer) hydrogenation of more demanding substrates such as substituted olefins or quinolines.^[17] Therefore, the (transfer) hydrogenation of these previously mentioned substrates with 5 mol% of precatalyst **4** was also performed with NH₃BH₃ in an H₂ atmosphere of 10 bar (see 4.4.2, Table 13). Whilst the addition of H₂ resulted in increased product formation of up to 80% for olefin substrates (but-1-en-2-ylbenzene and *trans*- α -methylstilbene) enantioinduction was severely inhibited in all solvents (Table 13, entries 1–4 and 17–20). Surprisingly, the opposite trend was observed for ketones, imines and quinolines, resulting in generally lower yield, when compared to the H₂-free reactions, but slightly increased enantioselectivities (e.g. 20% conversion, 38% ee in the reduction of acetophenone, Table 13, entry 6). Furthermore, almost no conversion was observed, when NH₃BH₃ was used in catalytic amounts (see SI, Table 1). This indicates that the ammonia borane is not only required in the

activation step (e.g. precatalyst \rightarrow active catalyst), but also as a transfer hydrogenation reagent, even in the presence of H_2 .

As the H_2 atmosphere was shown to drastically increase the yield, it was investigated whether different additives could similarly promote the activity, while retaining a high enantioinduction (see 4.4.2, Table 14). While the addition of a stoichiometric amount of i PrOH greatly increased the conversion (71% yield), it also decreased the enantioselectivity (9% *ee*, Table 14, entry 2). A slightly increased yield was also observed, when only a catalytic amount of i PrOH was added (24% yield, Table 14, entry 3). However, even with only 5 mol% of i PrOH, the products were obtained in a lesser degree of optical purity (46% *ee*). Stoichiometric amounts of a chiral alcohol, (+) or (-)-menthol, also resulted in decreased enantioenrichment (Table 14, entries 4-5). The importance of the ammonia borane was emphasised again, as no catalytic activity was observed when stoichiometric amounts of i PrOH or (-)-menthol were used in its absence (Table 14, entries 6-7). As the addition of bases has been reported to be required for some transfer hydrogenation reactions,^[23] K_2CO_3 was tested as an additive (Table 14, entry 8). Stoichiometric amounts of K_2CO_3 , however, resulted in decreased enantioselectivity combined with slightly increased isomer formation (11% isomerisation, 39% *ee*). In order to investigate the influence of the cation, crown ethers [18]crown-6 and [12]crown-4 were tested as additives (Table 14, entries 9-10). A stark decrease in the observed product yield was detected upon adding catalytic amounts of [18]crown-6 or [12]crown-4 (5 or 9% yield, respectively). Moreover, both additives resulted in decreased enantioenrichment, which was especially pronounced during the addition of [12]crown-4 (10% *ee*). This together with the previously observed solvent dependency (*vide supra*) suggests a significant role is played by the potassium cation.

In order to investigate the influence of NH_3BH_3 as the transfer hydrogenation reagent, different amine boranes (NR_2HBH_3) as well as varying stoichiometries of NH_3BH_3 were tested in the TH of **S1** with 5 mol% **3** and **L1** (Scheme 8, see 4.4.2, Table 15). Substitution of NH_3BH_3 with different amine boranes NR_2HBH_3 showed that the increased steric bulk on the amine moiety drastically influences the transfer hydrogenation rate as well as the enantioselectivity. Upon using NMe_2HBH_3 , a reduced yield of 8% without any enantioenrichment was observed, whilst no product was detected when the more sterically congested $N^iPr_2HBH_3$ was used (Table 15, entries 2-3). Use of two equivalents of NH_3BH_3 did not significantly affect the yield or the enantiomeric excess. However, upon adding five equivalents of NH_3BH_3 , a slightly increased yield as well as high enantiomeric excess was observed (28% yield, 84% *ee*).



Scheme 8. Investigation of the influence of the amine borane.

Poisoning experiments were performed in order to evaluate if the catalytic mechanism is homogeneous, heterogeneous or a mixture of both (see **4.4.2, Table 16**).^[24,25] Metal particles can form catalytically inactive amalgams upon addition of mercury.^[26] Whilst this poisoning is not as effective for all metals, cobalt has been shown to effectively form stable mercury cobalt amalgams.^[27] The addition of an excess of mercury regarding the catalyst did not significantly change the yield or the enantioinduction (**Table 16**, entry 2), hinting at a molecular catalyst species. In order to validate these results, further poisoning studies using P(OMe)₃ and dibenzo[*a,e*]cyclooctatetraene (DCT) were conducted.^[28] The quantitative poison P(OMe)₃ can bind both heterogeneous and homogeneous catalysts,^[25,29] whilst DCT strongly binds to molecular metal complexes, but is unable to bind to (heterogeneous) surfaces due to its steric bulk.^[30] A significant change was observed in neither the yield nor the optical purity of the products upon addition of one equivalent of P(OMe)₃ with respect to the catalyst (**Table 16**, entry 3). One equivalent of P(OMe)₃ would be sufficient to fully poison a heterogeneous cobalt catalyst, further corroborating the hypothesis of a molecular catalyst species. Moreover, a drastically lowered yield (6%) combined with a consistently good optical purity was observed upon addition of two equivalents of DCT, which is again indicative of a homogeneous reaction pathway. Therefore, the performed poisoning studies suggest the active cobalt species to be molecular in nature.

4.3 Conclusion

The performance of cobalt and iron complexes **1**, **2** and **4** in asymmetric hydroboration, hydrosilylation and transfer hydrogenation reactions was investigated. Whilst the catalysts obtained from *in situ* reduction of **1** or **2** by LiBEt₃H did not give good enantioselectivities, the cobaltate **4**, formed *in situ* from **3** and **L1**, showed promising results, yielding enantiomeric excesses of up to 57% in the transfer hydrogenation of olefins using ammonia borane. An increase in the observed enantioinduction was achieved by modification of the BIAN ligand (up to 74% *ee*). This was at the cost of the catalytic activity, however. Additives such as H₂, *i*PrOH or [18]crown-6, did not improve the catalytic properties significantly. Increasing the amount of NH₃BH₃ from one to five equivalents resulted in slightly increased yields with good enantioselectivity (28% yield, 84% *ee*). Poisoning experiments with Hg, P(OMe)₃ and DCT suggest the catalytically active species to be a molecular compound. Whilst this catalytic system gave good enantioselectivities, its low yields are to be improved upon. Nonetheless, this is a first step into the underexplored area of metal catalysed asymmetric transfer hydrogenation reactions with ammonia borane, highlighting the possibilities of such systems.

4.4 Experimental Details

General Synthetic Methods

All reactions and product manipulations were carried out in flame-dried glassware under an inert atmosphere of nitrogen using standard Schlenk-line or glovebox techniques (maintained at <0.1 ppm H₂O and <0.1 ppm O₂). **L1-L3**,^[19] **3** (see SI),^[31] and prochiral olefins (see SI)^[32] were prepared according to procedures previously reported in the literature. **L4-L9** were graciously provided by the *Cramer* group. All other chemicals were purchased from commercial suppliers and used without further purification.

Solvents were dried and degassed with a MBraun SPS800 solvent purification system. All dry solvents except *n*-hexane and *n*-pentane were stored under argon over activated 3 Å molecular sieves in gas-tight ampules. *n*-Hexane and *n*-pentane were stored over potassium mirrors.

General Analytical Techniques

NMR spectra were recorded on Bruker Avance 300 or 400 spectrometers at 300 K unless otherwise noted and internally referenced to residual solvent resonances (¹H NMR THF-d₈: 1.72 ppm, C₆D₆: 7.16 ppm; ¹³C{¹H} NMR THF-d₈: 25.31 ppm, C₆D₆: 128.06 ppm). Chemical shifts δ are given in ppm referring to external standards of tetramethylsilane (¹H, ¹³C{¹H}).

Elemental analysis was performed by the Central Analytical Services department of the University of Regensburg.

Gas chromatography with flame ionisation detector (GC FID): Shimadzu GC2010plus. Column: RT-bDEXsmTM (30 m \times 0.25 mm \times 0.25 μ m), carrier gas: H₂. Standard heating procedure: 50 °C (20 min), 1 °C/min \rightarrow 130 °C, 25 °C/min \rightarrow 230 °C. Calibration of substrates and products with internal standard *n*-pentadecane and analytically pure samples. Gas chromatography with mass selective detector (GC MS): Agilent 7820A GC system, mass detector 5977B. Column: HP-5M (30 m \times 0.25 mm \times 0.25 μ m), 5% phenylmethylsiloxane. Carrier gas: H₂. Standard heating procedure: 50 °C (2 min), 25 °C/min \rightarrow 300 °C (5 min). Mass spectra were performed with Jeol AccuTOF GCX EI-MS (LR/HR) by the analytical Department of Regensburg University.

High-pressure liquid chromatography (HPLC): Normal-phase HPLC using a chiral stationary column: Chiralpack IG. *n*-Hexane containing 0.5% *i*PrOH was used as the eluent with a flow rate of 0.5 mL/min. The enantiomers of 1-(*sec*-butyl)-4-methoxybenzene were detected at 254 nm with retention times of 9.5 and 9.9 minutes.

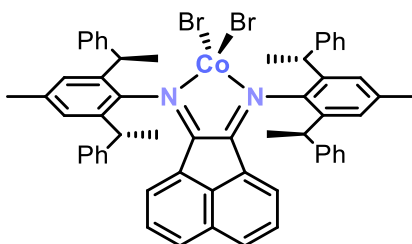
Single-crystal X-ray diffraction data were recorded on a XtaLAB Synergy R (DW system, Hypix-Arc 150) device with Cu-K α radiation ($\lambda = 1.54184$ Å). Crystals were selected under mineral oil, mounted on micromount loops and quench-cooled using an Oxford Cryosystems open flow N₂ cooling device. Either semi-empirical multi-scan absorption corrections^[33] or analytical ones^[34] were applied to the data. The structures were solved with SHELXT^[35] solution program using dual methods and by using Olex2 as the graphical interface.^[36] The models were refined with

ShelXL^[37] using full matrix least squares minimisation on F².^[38] The hydrogen atoms were located in idealised positions and refined isotropically with a riding model.

4.4.1 Synthesis of Compounds

[(L1)CoBr₂] (1):

A solution of **L1** (100 mg, 0.13 mmol, 1.00 equiv.) in THF (5 mL) was added to a suspension of CoBr₂ (28.1 mg, 0.13 mmol, 1.00 equiv.) in THF (3 mL). The mixture was stirred for three days, before the solvent was removed *in vacuo*. The crude product was washed with *n*-hexane (3 x 2 mL) and recrystallised by layering a THF solution with *n*-hexane at ambient conditions. Even after multiple recrystallisation attempts, the product still contained minor amounts of free **L1** (0.05 equiv.).



Molecular Formula: C₅₈H₅₂Br₂CoN₂ (995.81 g·mol⁻¹)

Yield: 81 mg (0.08 mmol, 63%)

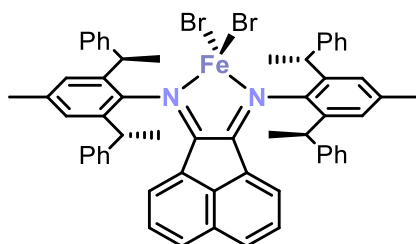
¹H NMR (400.13 MHz, 300 K, THF-*d*₈): δ [ppm] = -5.5 (s, 4H), -2.3 (s, 2H), 0.0 (s, 2H), 1.4-1.5 (m, 2H), 2.2-2.3 (m, 2H), 2.4 (s, 1H), 2.6 (s, 5H), 4.3 (m, 1H), 5.3 (s, 3H), 6.1 (m, 2H), 6.3-6.6 (m, 2H), 6.8-6.9 (m, 2H), 7.1-7.2 (m, 2H), 7.7-7.8 (m, 2H), 8.0 (t, ³J_{HH} = 6.9 Hz, 2H), 9.6 (d, ³J_{HH} = 5.9 Hz, 4H), 10.2 (s, 5H), 15.6 (s, 5H), 20.5 (s, 3H), 59.0 (s, 1H).

¹³C{¹H} NMR (100.06 MHz, 300 K, THF-*d*₈): δ [ppm] = 5.9, 6.9, 17.4, 20.7, 21.5, 22.4, 26.4, 30.8, 35.8, 38.8, 41.6, 73.7, 79.7, 85.7, 107.6, 111.7, 125.6, 126.3, 126.6, 126.9, 127.9, 128.1, 128.2, 128.5, 128.8, 129.1, 131.3, 133.7, 135.6, 168.3, 180.1, 225.7, 227.0, 245.4, 250.0.

Elemental analysis calculated for C₅₈H₅₂Br₂CoN₂·(C₄H₈O)_{1.5}·(C₆H₁₄)_{0.5}·(C₅₈H₅₂N₂)_{0.05}: C 70.80, H 6.26, N 2.48 found C 71.08 H 6.43 N 2.29.

[(L1)FeBr₂] (2):

A solution of **L1** (400 mg, 0.51 mmol, 1.01 equiv.) in THF (5 mL) was added to a suspension of FeBr₂ (110 mg, 0.51 mmol, 1.00 equiv.) in THF (2 mL). The mixture was stirred for three days, before the solvent was removed *in vacuo*. The crude product was washed with *n*-hexane (3 x 2 mL) and dried *in vacuo*. Crystals suitable for X-ray diffraction analysis were obtained upon layering a THF solution of **1** with *n*-hexane at ambient conditions.



Molecular formula: $C_{58}H_{52}Br_2FeN_2$ ($992.72 \text{ g}\cdot\text{mol}^{-1}$)

Yield: 454 mg (0.46 mmol, 90%)

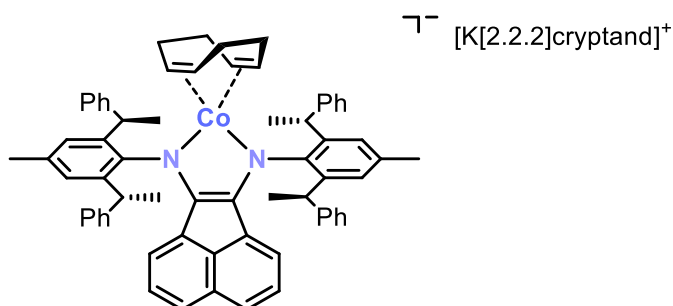
$^1\text{H NMR}$ (400.13 MHz, 300K, THF- d_8): δ [ppm] = -6.5 (s, br, 4H), -1.7 (s, br, 2H), -0.6 (s, 2H), 1.5 (d, $^3J_{\text{HH}} = 19.2$ Hz, 3H), 2.4 (br s, 7H), 4.3 (s, 4H), 4.4 (s, 1H), 4.8 (s, 2H), 6.2 - 6.6 (m, 2H), 6.8 - 7.7 (m, 5H), 8.5 (s, 2H), 8.8 (s, 2H), 9.4 (s, 4H), 12.4 (s, br, 4H), 13.4 (s, 2H), 15.8 (s, 6H).

$^{13}\text{C}\{^1\text{H}\}$ NMR (100.61 MHz, 300K, CDCl_3): δ [ppm] = -16.7 , 31.5 , 34.3 , 71.8 , 73.3 , 88.6 , 110.4 , 125.2 , 125.8 , 128.0 , 128.5 , 130.7 , 132.1 , 133.6 , 146.7 , 149.7 , 168.2 , 176.5 , 214.5 , 217.5 , 218.8 , 232.7 , 242.0 , 253.4 .

Elemental analysis calculated for $C_{58}H_{52}Br_2FeN_2\cdot(C_4H_8O)_{1.8}\cdot(C_6H_{14})_{0.2}$: C 69.97, H 6.12, N 2.46; found C 70.48, H 5.97, N 2.55.

[K(thf)][(L1)Co(cod)] (4):

A solution of **L1** (60 mg, 0.08 mmol, 1.00 equiv.) in THF (5 mL) was added to a solution of $[\text{K}(\text{thf})_{1.2}][\text{Co}(\text{cod})_2]$ (26 mg, 0.08 mmol, 1.02 equiv.) in THF (2 mL). The mixture was stirred for 18 h, before the solvent was removed *in vacuo*. The crude product was washed with *n*-hexane (3 x 2 mL) and dried *in vacuo*. Crystals suitable for single crystal X-ray diffraction were obtained after the addition of solid [2.2.2]cryptand (30 mg, 0.08 mmol, 1.03 equiv.) followed by crystallisation from THF/*n*-hexane. Minor paramagnetic sideproducts can still be observed in the $^1\text{H NMR}$, even after multiple recrystallisations of the isolated compound (see **Figure 11**). These impurities were also detrimental in obtaining a suitable elemental analysis.



Molecular formula: $C_{84}H_{100}CoKO_6N_4$ ($1359.77 \text{ g}\cdot\text{mol}^{-1}$)

Yield: 64 mg (0.05 mmol, 61%)

$^1\text{H NMR}$ (400.13 MHz, 300K, THF- d_8): δ [ppm] = 0.60 - 0.70 (m, cod-*H*, 2H), 0.93 - 1.06 (m, cod-*H* 2H), 1.35 (d, $^3J_{\text{HH}} = 7.2$ Hz, CHCH_3 , 6H), 1.79 (d, $^3J_{\text{HH}} = 7.3$ Hz, CHCH_3 , 6H), 1.82 - 1.90 (m, cod-*H*, 2H), 2.25 - 2.49 (s overlapped by m, $C_{\text{aryl}}\text{CH}_3$, cod-*H*, NCH_2 , 6+2+12 H), 2.69 - 2.77 (m, cod-*H*, 2H), 2.84 - 2.91 (m, cod-*H*, 2H), 3.16 - 3.46 (m, OCH_2 , 24 H), 4.42 (d, $^3J_{\text{HH}} = 6.9$ Hz, $C_{\text{aryl}}\text{H}$,

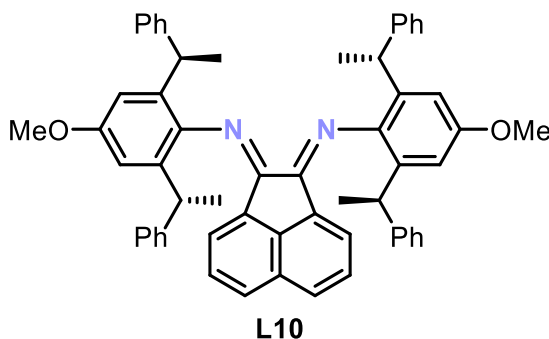
2H), 5.79 (q, $^3J_{\text{HH}} = 7.1$ Hz, CHCH_3 , 2H), 5.85 (dd, $^3J_{\text{HH}} = 8.0, 7.1$ Hz, $\text{C}_{\text{aryl}}\text{H}$, 2H), 6.05 (q, $^3J_{\text{HH}} = 7.3$ Hz, CHCH_3 , 2H), 6.11 (d, $^3J_{\text{HH}} = 8.1$ Hz, $\text{C}_{\text{aryl}}\text{H}$, 2H), 6.34-6.39 (m, $\text{C}_{\text{aryl}}\text{H}$, 2H), 6.44 (t, $^3J_{\text{HH}} = 7.3$ Hz, $\text{C}_{\text{aryl}}\text{H}$, 4H), 6.88 (d, $J_{\text{HH}} = 1.5$ Hz, $\text{C}_{\text{aryl}}\text{HC}(\text{CH}_3)$, 2H), 7.04 (t, $^3J_{\text{HH}} = 7.3$ Hz, $\text{C}_{\text{aryl}}\text{H}$, 2H), 7.21 (t, $^3J_{\text{HH}} = 7.7$ Hz, $\text{C}_{\text{aryl}}\text{H}$, 4H), 7.25 (d, $J_{\text{HH}} = 1.6$ Hz, $\text{C}_{\text{aryl}}\text{HC}(\text{CH}_3)$, 2H), 7.29 (d, $^3J_{\text{HH}} = 7.1$ Hz, $\text{C}_{\text{aryl}}\text{H}$, 4H), 7.73 (d, $^3J_{\text{HH}} = 7.7$ Hz, $\text{C}_{\text{aryl}}\text{H}$, 4H).

$^{13}\text{C}\{^1\text{H}\}$ NMR (100.61 MHz, 300K, CDCl_3): δ [ppm] = 22.1, 24.4, 26.4, 31.5, 33.0, 39.5, 40.0, 54.7, 64.8, 66.5, 68.4, 71.2, 114.5, 118.6, 124.6, 125.2, 125.3, 126.4, 126.7, 127.1, 127.2, 128.1, 129.4, 129.6, 130.9, 134.2, 136.7, 137.6, 141.4, 142.6, 143.0, 144.0, 145.1, 148.0, 148.2, 150.4, 151.9, 152.6.

Elemental analysis calculated for $\text{C}_{84}\text{H}_{100}\text{N}_4\text{O}_6\text{CoK} \cdot \{\text{C}_4\text{H}_8\text{O}\}_{0.5} \cdot \{\text{C}_6\text{H}_{14}\}_{0.2}$: C 74.12, H 7.62, N 3.97; found C 71.93, H 7.61, N 3.95.

General Procedure for the Synthesis of BIAN Ligands L10-17:

Acenaphthenequinone (1.00 equiv.), *para*-toluenesulfonic acid (1.05 equiv.) and the corresponding aniline (2.10 equiv.) were dissolved in toluene (0.03 M) and refluxed for 2-3 days. The reaction was shaken with NaOH (1M) and extracted with DCM (3 x 10 mL). The combined organic phases were dried over Na_2SO_4 , filtered and concentrated. The crude product was then purified by silica-flash column chromatography and dried *in vacuo*. **L11**, **L12** and **L16** were subsequently recrystallised from acetonitrile.



Silica-column chromatography: ethyl acetate:*n*-pentane = 1:15 \rightarrow 1:3, 0.1 vol% NEt_3 .

Molecular formula: $\text{C}_{58}\text{H}_{52}\text{N}_2\text{O}_2$ (809.07 $\text{g} \cdot \text{mol}^{-1}$)

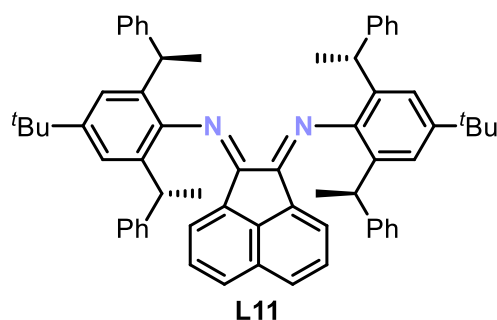
Yield: 182 mg (0.22 mmol, 58%)

^1H NMR (400.13 MHz, 300K, CDCl_3): δ [ppm] = 1.38 (d, $^3J_{\text{HH}} = 7.2$ Hz, 6H, CH_3), 1.54 (d, $^3J_{\text{HH}} = 7.1$ Hz, 6H, CH_3), 3.84 (s, 6H, OCH_3), 4.30 (q, $^3J_{\text{HH}} = 7.1$ Hz, 2H, CH), 4.44 (q, $^3J_{\text{HH}} = 7.1$ Hz, 2H, CH), 6.30 (d, $^3J_{\text{HH}} = 7.2$ Hz, 2H), 6.37 (t, $^3J_{\text{HH}} = 7.4$ Hz, 2H), 6.51 (t, $^3J_{\text{HH}} = 7.6$ Hz, 4H), 6.72 (d, $^3J_{\text{HH}} = 2.7$ Hz, 2H), 6.91 (d, $^3J_{\text{HH}} = 7.1$ Hz, 4H), 7.00 (d, $^3J_{\text{HH}} = 2.6$ Hz, 2H), 7.05-7.10 (m, 3H), 7.13 (t, $^3J_{\text{HH}} = 7.3$ Hz, 3H), 7.23-7.27 (m, 2H), 7.40 (d, $^3J_{\text{HH}} = 7.7$ Hz, 4H), 7.62 (d, $^3J_{\text{HH}} = 8.1$ Hz, 2H).

$^{13}\text{C}\{^1\text{H}\}$ NMR (100.61 MHz, 300K, CDCl_3): δ [ppm] = 21.2, 22.5, 38.5, 41.1, 55.5, 111.3, 111.4, 123.6, 125.2, 126.1, 127.0, 127.7, 127.8, 127.9, 128.4, 128.4, 129.0, 130.0, 135.0, 135.0, 140.2, 142.1, 145.6, 145.8, 156.5, 163.9.

Elemental analysis calculated for $\text{C}_{58}\text{H}_{52}\text{N}_2\text{O}_2$: C 86.10, H 6.48, N 3.40; found C 85.53, H 6.57, N 3.09.

HR-MS: m/z = 809.4115, $[(\text{C}_{58}\text{H}_{52}\text{N}_2\text{O}_2)+\text{H}]^+$; 831.3932, $[(\text{C}_{58}\text{H}_{52}\text{N}_2\text{O}_2)+\text{Na}]^+$.



Silica-column chromatography: ethyl acetate:*n*-pentane = 1:15, 0.1 vol% NEt_3 .

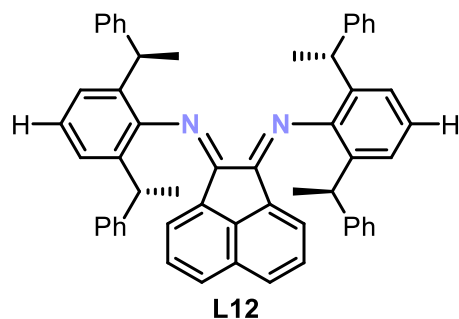
Recrystallisation: MeCN (60 °C \rightarrow 0 °C).

Molecular Formula: $\text{C}_{64}\text{H}_{64}\text{N}_2$ (861.23 $\text{g}\cdot\text{mol}^{-1}$)

Yield: 253 mg (0.29 mmol, 27%)

^1H NMR (300.13 MHz, 300 K, CDCl_3): δ [ppm] = 1.37 (s, 18H), 1.43 (d, $^3J_{\text{HH}} = 7.3$ Hz, 6H), 1.56 (d, $^3J_{\text{HH}} = 7.0$ Hz, 6H), 4.33 (q, $^3J_{\text{HH}} = 7.0$ Hz, 2H), 4.45 (q, $^3J_{\text{HH}} = 7.1$ Hz, 2H), 6.14 (d, $^3J_{\text{HH}} = 7.2$ Hz, 2H), 6.31 (t, $^3J_{\text{HH}} = 7.3$ Hz, 2H), 6.48 (t, $^3J_{\text{HH}} = 7.6$ Hz, 4H), 6.88 (d, $^3J_{\text{HH}} = 7.2$ Hz, 4H), 6.99-7.18 (m, 6H), 7.19-7.25 (m, 6H), 7.41 (s, 2H), 7.42-7.47 (m, 4H), 7.59 (d, $^3J_{\text{HH}} = 8.2$ Hz, 2H).

$^{13}\text{C}\{^1\text{H}\}$ NMR (75.47 MHz, 300 K, CDCl_3): δ [ppm] = 21.4, 22.7, 31.8, 34.8, 38.5, 41.3, 122.0, 123.1, 123.7, 125.0, 125.9, 127.0, 127.5, 127.6, 127.8, 127.9, 128.3, 128.5, 128.7, 129.8, 132.9, 133.0, 140.4, 145.1, 146.0, 146.4, 147.2, 163.2.



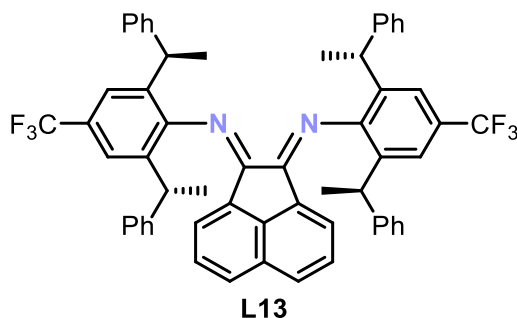
Silica-column chromatography: ethyl acetate:*n*-pentane = 1:15 \rightarrow 1:3, 0.1 vol% NEt_3 .

Recrystallisation: MeCN (45 °C \rightarrow 0 °C).

Molecular Formula: $\text{C}_{56}\text{H}_{48}\text{N}_2$ (749.01 $\text{g}\cdot\text{mol}^{-1}$)

Yield: 14 mg (0.02 mmol, 9%)

^1H NMR (400.13 MHz, 300 K, CDCl_3): δ [ppm] = 1.41 (d, $^3J_{\text{HH}} = 7.2$ Hz, CHCH_3 , 6H), 1.57 (d, $^3J_{\text{HH}} = 7.1$ Hz, CHCH_3 , 6H), 4.31 (q, $^3J_{\text{HH}} = 7.0$ Hz, CHCH_3 , 2H), 4.48 (q, $^3J_{\text{HH}} = 7.1$ Hz, CHCH_3 , 2H), 6.21 (d, $^3J_{\text{HH}} = 7.2$ Hz, 2H), 6.36 (d, $^3J_{\text{HH}} = 7.3$ Hz, 2H), 6.51 (t, $^3J_{\text{HH}} = 7.6$ Hz, 2H), 6.91 (d, $^3J_{\text{HH}} = 7.4$ Hz, 4H), 7.05 (t, $^3J_{\text{HH}} = 7.7$ Hz, 2H), 7.10-7.20 (m, 4H), 7.21-7.27 (m overlapped by CDCl_3 , 6H), 7.42 (m, 6H), 7.61 (d, $^3J_{\text{HH}} = 8.2$ Hz, 2H).



Silica-column chromatography: ethyl acetate:*n*-pentane = 1:10.

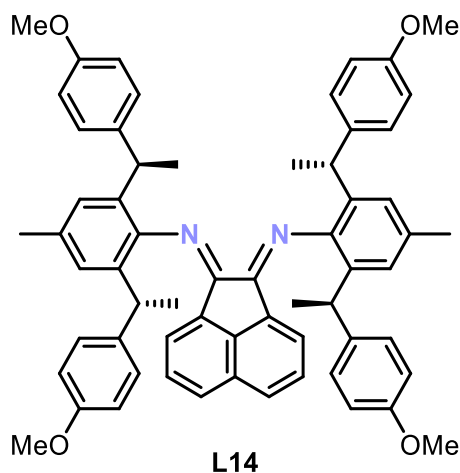
Molecular Formula: $\text{C}_{58}\text{H}_{46}\text{F}_6\text{N}_2$ (885.01 $\text{g}\cdot\text{mol}^{-1}$)

Yield: 15 mg (0.01 mmol, 51%)

^1H NMR (600.13 MHz, 300 K, CDCl_3): δ [ppm] = 1.46 (d, $^3J_{\text{HH}} = 7.2$ Hz, CHCH_3 , 6H), 1.56 (d overlapped by H_2O , 6H), 4.29 (q, $^3J_{\text{HH}} = 6.9$ Hz, CHCH_3 , 2H), 4.48 (q, $^3J_{\text{HH}} = 6.9$ Hz, CHCH_3 , 2H), 6.22 (d, $^3J_{\text{HH}} = 7.1$ Hz, 2H), 6.34 (t, $^3J_{\text{HH}} = 7.2$ Hz, 2H), 6.48 (t, $^3J_{\text{HH}} = 7.4$ Hz, 2H), 7.12 (t, $^3J_{\text{HH}} = 7.6$ Hz, 2H), 7.17 (t, $^3J_{\text{HH}} = 7.3$ Hz, 2H), 7.25-7.29 (m overlapped by CDCl_3 , 4H), 7.38 (d, $^3J_{\text{HH}} = 7.7$ Hz, 2H), 7.47 (s, 2H), 7.64-7.71 (m, 4H).

$^{13}\text{C}\{^1\text{H}\}$ NMR (150.61 MHz, 300 K, CDCl_3): δ [ppm] = 21.1, 22.5, 29.9, 38.3, 41.3, 122.1, 123.6, 125.5, 126.5, 127.3, 127.7, 127.9, 128.4, 128.6, 129.1, 130.0, 134.0, 134.4, 134.5, 134.5, 139.8, 140.3, 141.9, 144.7, 145.0, 145.1, 150.9, 151.0, 160.1, 162.7.

^{19}F NMR (376.66 MHz, 300 K, CDCl_3): δ [ppm] = -61.4.



Silica-column chromatography: ethyl acetate:*n*-pentane = 1:5.

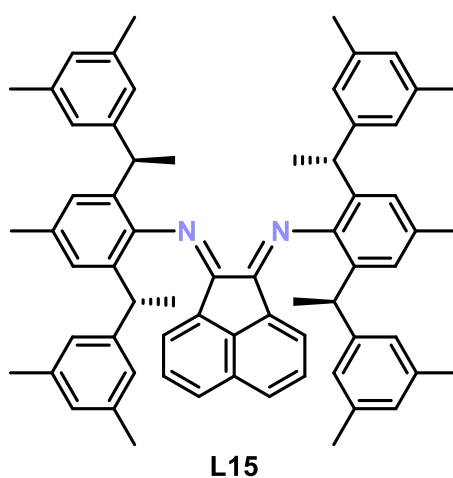
Molecular Formula: $\text{C}_{62}\text{H}_{60}\text{N}_2\text{O}_4$ (897.17 $\text{g}\cdot\text{mol}^{-1}$)

Yield: 31 mg (0.04 mmol, 25%)

^1H NMR (400.13 MHz, 300 K, CDCl_3): δ [ppm] = 1.42 (d, $^3J_{\text{HH}} = 7.2$ Hz, CHCH_3 , 6H), 1.53 (d, $^3J_{\text{HH}} = 7.2$ Hz, CHCH_3 , 6H), 2.42 (s, CH_3 , 6H), 3.20 (s, OCH_3 , 6H), 3.72 (s, OCH_3 , 6H), 4.21 (q, $^3J_{\text{HH}} = 7.1$ Hz, CHCH_3 , 2H), 4.39 (q, $^3J_{\text{HH}} = 7.1$ Hz, CHCH_3 , 2H), 5.98 (d, $^3J_{\text{HH}} = 8.6$ Hz, 4H), 6.23 (d, $^3J_{\text{HH}} = 7.2$ Hz, 2H), 6.78 (t, $^3J_{\text{HH}} = 8.2$ Hz, 8H), 6.96 (s, 2H), 7.08 (t, $^3J_{\text{HH}} = 7.8$ Hz, 2H), 7.19 (s, 2H), 7.31 (d, $^3J_{\text{HH}} = 8.6$ Hz, 4H), 7.62 (d, $^3J_{\text{HH}} = 8.2$ Hz, 2H).

$^{13}\text{C}\{^1\text{H}\}$ NMR (100.61 MHz, 300 K, CDCl_3): δ [ppm] = 21.4, 21.7, 22.6, 37.7, 40.1, 54.8, 55.3, 113.1, 113.7, 113.7, 123.7, 125.7, 126.8, 126.9, 128.0, 128.8, 129.0, 129.9, 133.3, 133.3, 133.8, 138.2, 138.5, 140.0, 145.9, 156.7, 157.7, 163.2, 166.9.

HR-MS: $m/z = 897.4626$ $[(\text{C}_{62}\text{H}_{60}\text{N}_2\text{O}_4)+\text{H}]^+$, 919.4453 $[(\text{C}_{62}\text{H}_{60}\text{N}_2\text{O}_4)+\text{Na}]^+$.

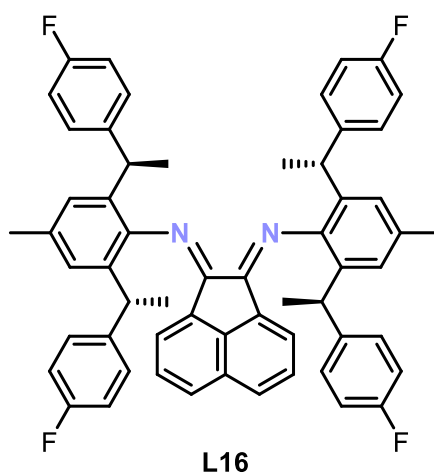


Silica-column chromatography: ethyl acetate:*n*-pentane = 1:20 \rightarrow 1:10.

Molecular Formula: $\text{C}_{66}\text{H}_{68}\text{N}_2$ ($889.28 \text{ g}\cdot\text{mol}^{-1}$)

Yield: 15 mg (0.02 mmol, 19%)

^1H NMR (400.13 MHz, 300 K, CDCl_3): δ [ppm] = 1.46 (d, $^3J_{\text{HH}} = 7.2$ Hz, 6H), 1.50 (d, $^3J_{\text{HH}} = 7.2$ Hz, 6H), 1.54 (s, 12H), 2.25 (s, 12H), 2.47 (s, 6H), 4.16 (q, $^3J_{\text{HH}} = 7.1$ Hz, 2H), 4.40 (q, $^3J_{\text{HH}} = 7.2$ Hz, 2H), 5.93 (s, 2H), 6.32 (d, $^3J_{\text{HH}} = 7.1$ Hz, 2H), 6.45 (s, 4H), 6.77 (s, 2H), 7.03 (t, $^3J_{\text{HH}} = 7.7$ Hz, 2H), 7.10 (s, 6H), 7.26 (s, overlapped by CDCl_3 , 2H), 7.61 (d, $^3J_{\text{HH}} = 8.2$ Hz, 2H).



Silica-column chromatography: ethyl acetate:*n*-pentane = 1:15.

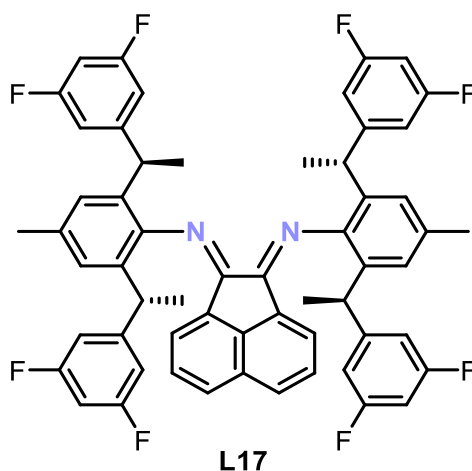
Recrystallisation: MeCN (45 °C → 0 °C)

Molecular Formula: C₅₈H₄₈F₄N₂ (849.03 g·mol⁻¹)

Yield: 9 mg (0.01 mmol, 13%)

¹H NMR (400.13 MHz, 300 K, CDCl₃): δ [ppm] = 1.38 (d, ³*J*_{HH} = 7.2 Hz, 6), 1.52 (d, ³*J*_{HH} = 7.2 Hz, 6H), 2.42 (s, 6H), 4.23 (q, ³*J*_{HH} = 7.1 Hz, 2H), 4.33 (q, ³*J*_{HH} = 7.2 Hz, 2H), 6.16 (t, ³*J*_{HH} = 8.7 Hz, 4H), 6.25 (d, ³*J*_{HH} = 7.2 Hz, 2H), 6.78-6.84 (m, 4H), 6.89-6.96 (m, 6H), 7.11 (two overlapping d, ³*J*_{HH} = 7.2 Hz, 2H), 7.20 (s, 2H), 7.30-7.36 (m, 4H), 7.70 (d, ³*J*_{HH} = 8.2 Hz, 2H).

¹⁹F NMR (376.66 MHz, 300 K, CDCl₃): δ [ppm] = -118.5 to -118.4 (m), -117.72 to -117.6 (m).



Silica-column chromatography: Ethyl acetate:*n*-Pentane = 1:10 → 1:3.

Molecular Formula: C₅₈H₄₄F₈N₂ (920.99 g·mol⁻¹)

Yield: 392 mg (0.426 mmol, 86%)

¹H NMR (400.13 MHz, 300 K, CDCl₃): δ [ppm] = 1.40 (d, ³*J*_{HH} = 7.1 Hz, CHCH₃, 6H), 1.52 (d, ³*J*_{HH} = 7.2 Hz, CHCH₃, 6H), 2.48 (s, CH₃, 6H), 4.18 (q, ³*J*_{HH} = 6.9 Hz, CHCH₃, 2H), 4.27 (q, ³*J*_{HH} = 6.9 Hz, CHCH₃, 2H), 5.74 (t, *J* = 8.9 Hz, 2H), 6.32-6.40 (m, 6H), 6.57 (t, *J* = 8.8 Hz, 2H), 6.89 (d, *J* = 7.1 Hz, 2H), 7.19 (t, *J* = 7.7 Hz, 2H), 7.25 (s, 2H), 7.73 (d, *J* = 8.2 Hz, 2H).

$^{13}\text{C}\{^1\text{H}\}$ NMR (100.61 MHz, 300 K, CDCl_3): δ [ppm] = 20.7, 21.7, 22.2, 37.8, 41.0, 100.4 (pseudo t, $^2J_{\text{CF}} = 25.6$ Hz), 101.5 (pseudo t, $^2J_{\text{CF}} = 25.4$ Hz), 110.3-110.9 (m), 123.3, 126.2, 127.1, 127.2, 128.6, 129.1, 130.1, 131.9, 132.1, 134.1, 140.0, 145.7, 149.9 (pseudo t, $^3J_{\text{CF}} = 8.4$ Hz), 150.6 (pseudo t, $^2J_{\text{CF}} = 8.1$ Hz), 162.5 (dd, $^1J_{\text{CF}} = 248.2$ Hz, $^3J_{\text{CF}} = 12.9$ Hz), 162.9, 163.1 (dd, $^1J_{\text{CF}} = 247.5$ Hz, $^3J_{\text{CF}} = 12.9$ Hz).

^{19}F NMR (376.66 MHz, 300 K, CDCl_3): δ [ppm] = -110.5 (t, $^3J_{\text{HF}} = 8.1$ Hz), -110.3 (t, $^3J_{\text{HF}} = 8.5$ Hz).

HR-MS: $m/z = 921.3463$, $[(\text{C}_{58}\text{H}_{44}\text{F}_8\text{N}_2)+\text{H}]^+$; 943.3282 , $[(\text{C}_{58}\text{H}_{44}\text{F}_8\text{N}_2)+\text{Na}]^+$.

4.4.2 Catalytic Studies

General hydrofunctionalisation procedure using precatalysts 1 or 2.

To a screw-cap vial equipped with a stir-bar was added the required amount of the desired precatalyst. The desired volume of solvent (0.5 mL if not stated otherwise), followed by LiBEt_3H (1 M, THF) was added, and the mixture was stirred for 30 min at ambient temperature. If required, the desired additive was added. To the resultant solution was added the substrate, followed by the reducing reagent and, in the case of acetophenone, *n*-pentadecane as an internal standard (20 μL). After the reaction was completed, hydroboration reactions were worked up by adding aqueous NaOH (0.5 mL, 3M) followed by H_2O_2 (0.5 mL, 30%) and ethyl acetate (ca. 0.5 mL), and the resulting mixture was allowed to stir for 1 hour at room temperature. Work-up of hydrosilylation reactions commenced with the addition of $[\text{N}(\textit{n}\text{Bu})_4]\text{F}$ (1.1 equiv., 1 M in THF). The resulting solution was allowed to stir for 2 h, before water (ca. 0.5 mL) was added. (Transfer) Hydrogenation reactions were quenched with water (ca. 0.5 mL). All hydrofunctionalisation reactions were then extracted with ethyl acetate (3 x 0.5 mL), filtered and analysed by chiral GC-FID.

General hydrofunctionalisation procedure using 3/L1 or 4 analysed by chiral GC-FID.

To a screw-cap vial equipped with a stir-bar was added the required amount of the desired precatalyst. If required, **L1** was added as a solid. The desired volume of solvent (0.5 mL if not stated otherwise) was added, and the mixture was stirred for 30 min at ambient temperature, before the desired additive was added. To the resultant solution was added the substrate, followed by the desired reducing reagent, and if required, *n*-pentadecane as an internal standard (20 μL). After the reaction was completed, hydroboration reactions were worked up by adding aqueous NaOH (0.5 mL, 3M) followed by H_2O_2 (0.5 mL, 30%) and ethyl acetate (ca. 0.5 mL), and the resulting mixture was allowed to stir for 1 hour at ambient temperature. Work-up of hydrosilylation reactions commenced with the addition of $[\text{N}(\textit{n}\text{Bu})_4]\text{F}$ (1.1 equiv., 1M in THF). The resulting solution was allowed to stir for 2 h at room temperature, before water (ca. 0.5 mL) was added. (Transfer) Hydrogenation reactions were quenched with water (ca. 0.5 mL). All

hydrofunctionalisation reactions were then extracted with ethyl acetate (3 x 0.5 mL), filtered and analysed by chiral GC-FID.

General hydrofunctionalisation procedure using 3/LX analysed by chiral HPLC.

To a screw-cap vial equipped with a stir-bar was added the required amount of the desired precatalyst **3** and the desired ligand was added as a solid. The desired volume of solvent (generally 0.5 mL if not stated otherwise) was then added, and the mixture was stirred for 30 min at ambient temperature, before the desired additive was added. To the resultant solution was added the substrate, followed by the desired reducing reagent. (Transfer) Hydrogenation reactions were quenched with water (ca. 0.5 mL) and the solvent was removed in vacuum (40 °C, > 100 mbar). Mesitylene was added as an internal standard and the solids dissolved in CDCl₃ in order to measure a ¹H NMR spectrum. When using 1-(but-1-en-2-yl)-4-methoxybenzene (**S1**) as the substrate, the solvent was removed *in vacuo* and redissolved in CH₂Cl₂. *m*CPBA was added and the mixture stirred for 1 h at ambient temperature. This step was taken in order to epoxidise the isomerisation product ((E)-1-(but-2-en-2-yl)-4-methoxybenzene), as its retention time with the used HPLC method was close to one of the enantiomers and thus overlap with the enantiomers signal. After the epoxidation was finished, the solution was extracted with ethyl acetate (3 x 0.5 mL) and filtered over silica. The solvents were removed *in vacuo* and the obtained mixture analysed by chiral HPLC.

Table 1. Hydrofunctionalisation using *in-situ* reduced cobalt and iron dibromides.^[a]

$$\text{Ph}-\text{C}(=\text{E})-\text{R} + \text{Ph}_2\text{SiH}_2 + \text{NH}_3\text{BH}_3 \xrightarrow[\text{solvent, 18 h, r.t., work-up}]{\text{HBpin, cat. 1 or 2 (2.5 mol\%), LiBEt}_3\text{H (7.5 mol\%)}} \text{Ph}-\text{C}(\text{E})-\text{R}^*$$

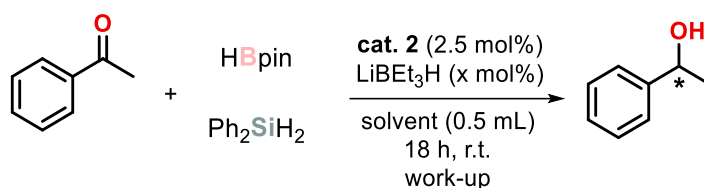
E = O, NPh

Entry	Substrate	Reducing Reagent	cat. (mol%)	Solvent (mL)	Conversion [%] ^[b]	<i>ee</i> [%] ^[b]
1		HBpin	1 (2.5)	THF (1.0 mL)	> 95	< 5
2		HBpin	2 (1.3)	THF (1.0 mL)	> 95	< 5
3		Ph ₂ SiH ₂	1 (2.5)	THF (1.0 mL)	> 95	< 5
4		Ph ₂ SiH ₂	2 (2.5)	THF (1.0 mL)	> 95	< 5
5 ^[c]		HBpin	2 (2.5)	THF (0.5 mL)	< 5	<i>n.d.</i>
6 ^[c]		Ph ₂ SiH ₂	2 (2.5)	THF (0.5 mL)	> 95	17 (<i>S</i>)
7 ^[d]		NH ₃ BH ₃	1 (4.9)	<i>n</i> -Hexane (0.5 mL)	>99 (36) ^[e]	9 (<i>S</i>)
8 ^[d]		NH ₃ BH ₃	2 (4.9)	THF (0.6 mL)	99 (28) ^[e]	< 5
9 ^[d]		NH ₃ BH ₃	2 (4.9)	Toluene (0.6 mL)	99 (47) ^[e]	< 5
10 ^[d]		NH ₃ BH ₃	2 (4.9)	<i>n</i> -Hexane (0.6 mL)	99 (48) ^[e]	< 5
11		HBpin	2 (4.9)	THF (0.5 mL)	> 95	< 5
12		Ph ₂ SiH ₂	2 (4.9)	THF (0.5 mL)	> 95	< 5
13 ^[d]		NH ₃ BH ₃	2 (4.9)	<i>n</i> -Hexane (0.6 mL)	64	< 5

^[a]Substrate (0.20 mmol), HBpin (0.21 mmol), Ph₂SiH₂ (0.22 mmol). ^[b]Determined by comparison of the areas of the starting material and the product *via* chiral GC-FID. ^[c]The reaction was performed without LiBEt₃H and stirred for 3 d.

^[d]Substrate (0.12 mmol), LiBEt₃H (15 mol%). ^[e]*n*-Pentadecane (0.04 mmol) was added, yield given in parentheses.

Table 2. LiBEt₃H loading screening.^[a]



Entry	Reducing Reagent	LiBEt ₃ H [mol%]	Solvent	Yield (Conversion) [%] ^[b]	ee[%] ^[b]
1	HBpin	1.25	THF	47 (52)	< 5
2	HBpin	1.25	Toluene	50 (56)	< 5
3	HBpin	1.25	<i>n</i> -Hexane	75 (86)	< 5
4	HBpin	2.5	THF	92 (> 99)	< 5
5	HBpin	2.5	Toluene	99 (98)	< 5
6	HBpin	2.5	<i>n</i> -Hexane	90 (98)	< 5
7	HBpin	3.75	Toluene	95 (> 99)	< 5
8	HBpin	3.75	<i>n</i> -Hexane	98 (98)	< 5
9	Ph ₂ SiH ₂	1.25	THF	57 (58)	< 5
10	Ph ₂ SiH ₂	1.25	Toluene	37 (41)	< 5
11	Ph ₂ SiH ₂	1.25	<i>n</i> -Hexane	49 (51)	< 5
12	Ph ₂ SiH ₂	2.5	THF	87 (> 99)	< 5
13	Ph ₂ SiH ₂	2.5	Toluene	88 (99)	< 5
14	Ph ₂ SiH ₂	2.5	<i>n</i> -Hexane	48 (64)	< 5
15	Ph ₂ SiH ₂	3.75	THF	97 (> 99)	5 (<i>S</i>)
16	Ph ₂ SiH ₂	3.75	Toluene	56 (63)	< 5
17	Ph ₂ SiH ₂	3.75	<i>n</i> -Hexane	39 (45)	< 5

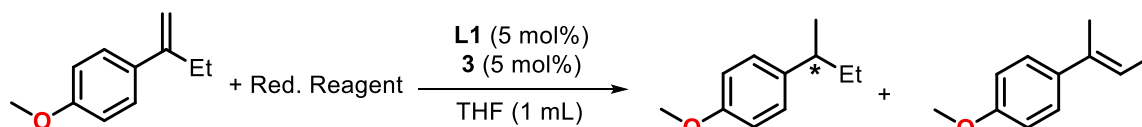
^[a]Substrate (0.20 mmol), HBpin (0.21 mmol) or Ph₂SiH₂ (0.22 mmol), *n*-pentadecane (0.07 mmol). ^[b]Determined by chiral GC-FID.

Table 3. Hydrogenation of unsaturated compounds using **1**/LiBEt₃H.^[a]

Entry	Substrate	Solvent (mL)	Conversion [%] ^[b]	ee [%] ^[b]
1		THF (2 mL)	> 95	6
2		Toluene (2 mL)	> 95	7
3		<i>n</i> -Hexane (2 mL)	> 95	8
4		THF (2 mL)	> 95	13
5		Toluene (2 mL)	> 95	14
6		<i>n</i> -Hexane (2 mL)	> 95	8 ^[c]
7		THF (2 mL)	9	< 5
8		Toluene (2 mL)	22	< 5

^[a]Substrate (0.20 mmol). ^[b]Determined by chiral GC-FID. ^[c]The opposite enantiomer was observed (compared to entry 4 and 5).

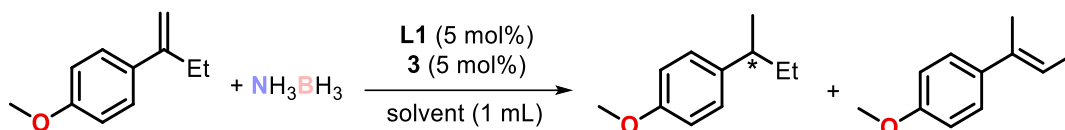
Table 4. Reducing reagent screening in the hydrofunctionalisation of **S1**.^[a]



Entry	Reducing Reagent	Yield (Conversion) [%] ^[b]	Isomerisation [%] ^[b]	ee [%] ^[c]
1	NH ₃ BH ₃	43 (97)	43	< 5
2	HBpin	30 (51)	20	< 5
3	Ph ₂ SiH ₂	< 5 (< 5)	< 1	<i>n.d.</i>
4	[NH ₄][HCO ₂]	< 5 (< 5)	< 1	<i>n.d.</i>
5	Cyclohexa-1,3-dien	< 5 (< 5)	< 1	<i>n.d.</i>
6	Cyclohexa-1,4-dien	< 5 (< 5)	< 1	<i>n.d.</i>
7	Hantzsch ester	< 5 (< 5)	< 1	<i>n.d.</i>

^[a]Substrate (0.12 mmol), red. reagent (0.13 or 0.14 mmol), mesitylene (0.04 mmol). ^[b]Determined by ¹H NMR spectroscopy. ^[c]Determined by chiral HPLC.

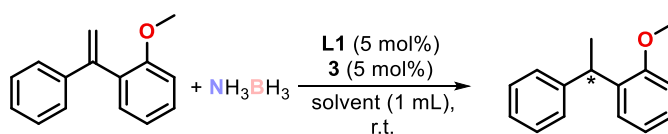
Table 5. Ligand and solvent screening of the transfer-hydrogenation of **S1**.^[a]



Entry	Solvent	Yield (Conversion) [%] ^[b]	Isomerisation [%] ^[b]	ee [%] ^[b]
1	THF	43 (97)	54	< 5
2	Toluene	10 (15)	4	42
3	<i>n</i> -Hexane	20 (24)	4	57

^[a]Substrate (0.20 mmol), NH_3BH_3 (0.22 mmol). ^[b]Determined by chiral GC-FID.

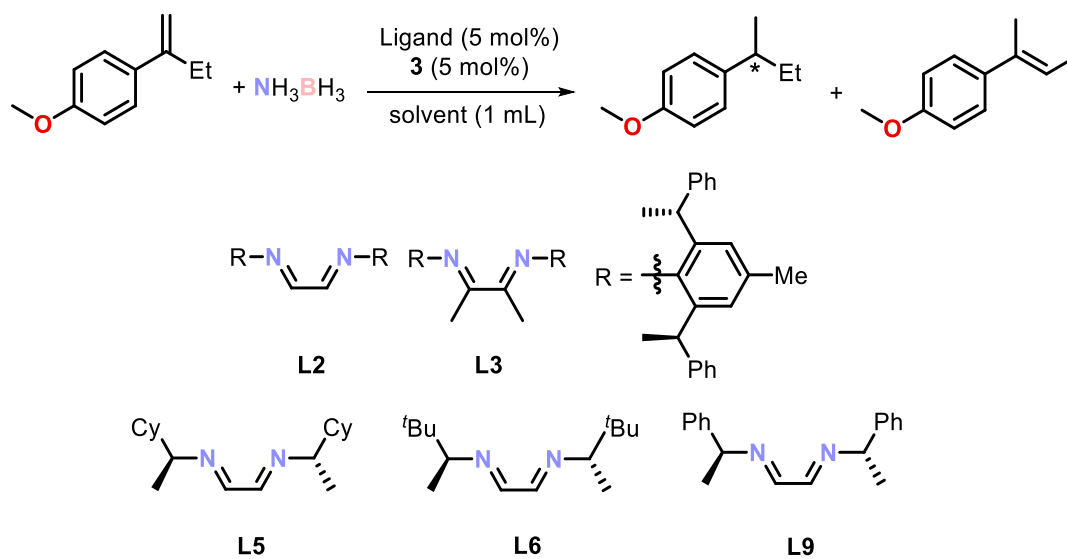
Table 6. Solvent screening of the TH of **S2**.^[a]



Entry	Solvent	Conversion [%] ^[b]	ee [%] ^[c]
1	THF	40	< 5
2	Toluene	29	< 5
3	<i>n</i> -Hexane	10	18

^[a]1-Methoxy-2-(1-phenylvinyl)benzene (0.10 mmol), NH_3BH_3 (0.11 mmol). ^[b]Conversion determined by ^1H spectroscopy, by comparing the integral of the methoxy group at $\delta = 3.64$ and 3.79 ppm for the substrate and the product, respectively. ^[c]Determined by chiral HPLC.

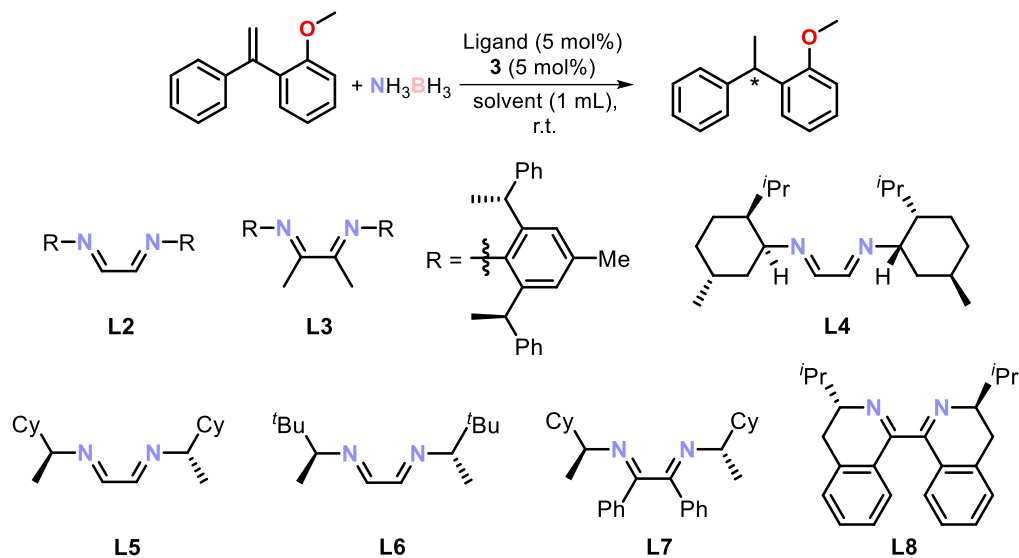
Table 7. Ligand and solvent screening of the TH of **S1**.^[a]



Entry	Ligand	Solvent	Yield (Conversion) [%] ^[b]	Isomerisation [%] ^[b]	<i>ee</i> [%] ^[c]
1	L2	THF	37 (87)	51	< 5
2	L2	Toluene	19 (32)	13	11
3	L2	<i>n</i> -Hexane	4 (10)	6	22
4	L3	THF	8 (40)	32	7
5	L3	Toluene	15 (28)	14	< 5
6	L3	<i>n</i> -Hexane	8 (27)	18	8
7 ^[d]	L5	THF	12 (28)	16	5
8 ^[d]	L5	Toluene	14 (21)	8	< 5
9 ^[d]	L5	<i>n</i> -Hexane	25 (85)	51	6
10 ^[d]	L6	THF	10 (22)	12	< 5
11 ^[d]	L6	Toluene	31 (56)	25	< 5
12 ^[d]	L6	<i>n</i> -Hexane	47 (91)	44	< 5
13 ^[d]	L9	THF	9 (23)	15	5
14 ^[d]	L9	Toluene	16 (31)	15	< 5
15 ^[d]	L9	<i>n</i> -Hexane	37 (88)	52	< 5

^[a]Substrate (0.20 mmol), NH₃BH₃ (0.22 mmol). ^[b]Determined by ¹H NMR spectroscopy. ^[c]Determined by chiral HPLC. ^[d]Substrate (0.12 mmol), NH₃BH₃ (0.13 mmol), solvent (0.6 mL).

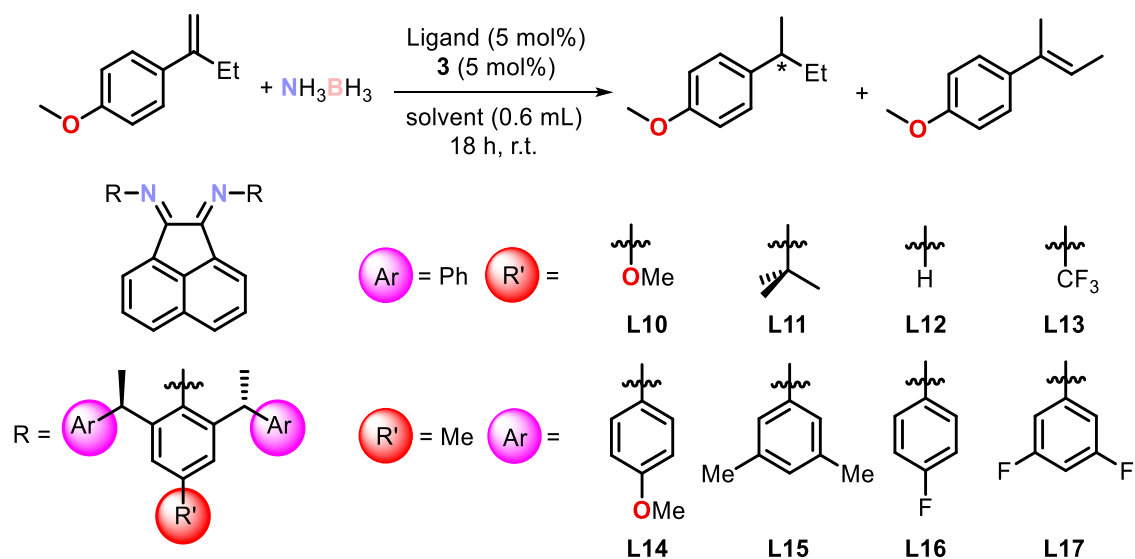
Table 8. Ligand screening of the TH of **S2**.^[a]



Entry	Ligand	Solvent	Conversion [%] ^[b]	<i>ee</i> [%] ^[c]
1	L2	THF	13	9
2	L2	<i>n</i> -Hexane	9	6
3	L3	THF	20	< 5
4	L3	Toluene	10	< 5
5	L3	<i>n</i> -Hexane	5	< 5
6 ^[d]	L4	THF	18	7
7 ^[d]	L4	Toluene	29	8
8 ^[d]	L4	<i>n</i> -Hexane	24	5
9 ^[d]	L5	THF	50	7
10 ^[d]	L5	Toluene	60	8
11 ^[d]	L5	<i>n</i> -Hexane	90	7
12 ^[d]	L6	THF	81	< 5
13 ^[d]	L6	Toluene	61	< 5
14 ^[d]	L6	<i>n</i> -Hexane	40	8
15 ^[d]	L7	THF	63	5
16 ^[d]	L7	Toluene	66	< 5
17 ^[d]	L7	<i>n</i> -Hexane	34	< 5
18 ^[d]	L8	THF	25	11
19 ^[d]	L8	Toluene	60	6
20 ^[d]	L8	<i>n</i> -Hexane	23	11

^[a]Substrate (0.10 mmol), NH_3BH_3 (0.11 mmol). ^[b]Conversion determined by ^1H NMR spectroscopy, by comparing the integral of the methoxy group at $\delta = 3.64$ and 3.79 ppm for the substrate and the product, respectively. ^[c]Determined by chiral HPLC. ^[d]Substrate (0.12 mmol), NH_3BH_3 (0.13 mmol), ligand (10 mol%), **3** (10 mol%), solvent (0.6 mL).

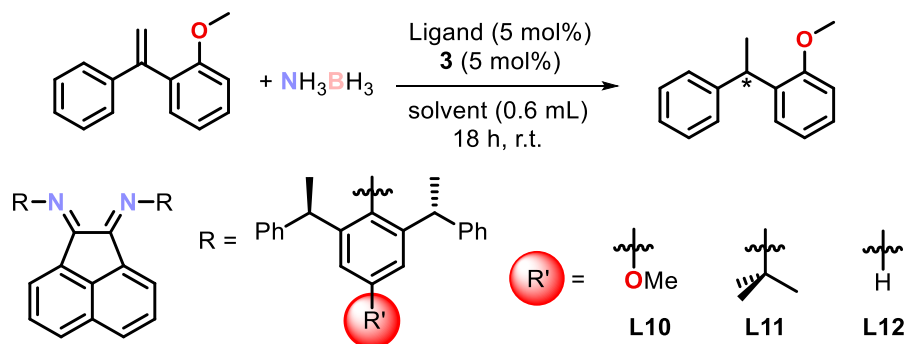
Table 9. Ligand screening of the TH of **S1** with BIAN ligands **L10-L17**.^[a]



Entry	Ligand	Solvent	Yield (Conversion) [%] ^[b]	Isomerisation [%] ^[b]	ee [%] ^[c]
1	L10	THF	40 (90)	49	< 5
2	L10	Toluene	17 (29)	11	32
3	L10	<i>n</i> -Hexane	4 (11)	6	49
4	L11	THF	33 (83)	50	< 5
5	L11	Toluene	9 (15)	6	36
6	L11	<i>n</i> -Hexane	5 (8)	3	40
7	L12	THF	54 (94)	40	< 5
8	L12	Toluene	10 (15)	5	43
9	L12	<i>n</i> -Hexane	7 (13)	5	38
10	L13	THF	17 (37)	20	8
11	L13	<i>n</i> -Hexane	9 (32)	22	63
12	L14	THF	52 (93)	41	6
13	L14	Toluene	8 (11)	4	59
14	L14	<i>n</i> -Hexane	7 (15)	8	44
15	L15	THF	11 (30)	18	< 5
16	L15	<i>n</i> -Hexane	8 (14)	6	52
17	L16	THF	22 (54)	32	< 5
18	L16	<i>n</i> -Hexane	9 (15)	6	66
19	L17	THF	5 (13)	8	41
20	L17	Toluene	11 (16)	5	74
21	L17	<i>n</i> -Hexane	10 (19)	8	70

^[a]Substrate (0.12 mmol), NH₃BH₃ (0.13 mmol). ^[b]Determined by ¹H NMR. ^[c]Determined by chiral HPLC.

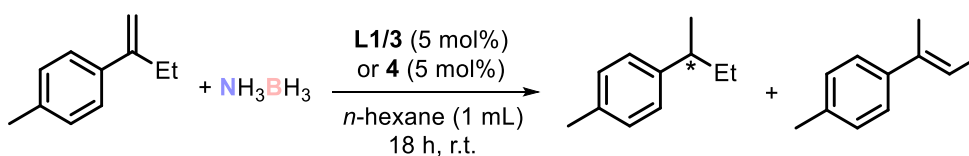
Table 10. Ligand screening of the TH of **S2** with **L10-L12**.^[a]



Entry	Ligand	Solvent	Conversion [%] ^[b]	ee [%] ^[c]
1	L10	THF	37	< 5
2	L10	Toluene	14	< 5
3	L10	<i>n</i> -Hexane	6	63
4	L11	THF	48	< 5
5	L11	Toluene	11	7
6	L11	<i>n</i> -Hexane	3	58
7	L12	THF	32	< 5
8	L12	Toluene	14	< 5
9	L12	<i>n</i> -Hexane	5	26

^[a]Substrate (0.12 mmol), NH_3BH_3 (0.13 mmol). ^[b]Determined by ^1H NMR spectroscopy. ^[c]Determined by chiral HPLC.

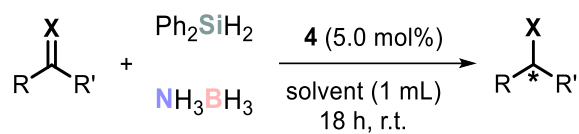
Table 11. Comparison of **4** with the catalyst generated *in situ* from **3** and **L1**.^[a]

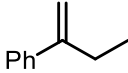
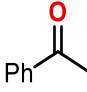
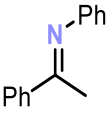
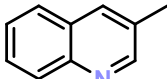


Entry	Cat.	Yield (Conversion) [%] ^[b]	Isomerisation [%] ^[b]	ee [%] ^[b]
1	L1/3	24 (26)	2	57
2	4	23 (26)	3	57

^[a]Substrate (0.20 mmol), NH_3BH_3 (0.20 mmol), **L1** and **3** were suspended in *n*-hexane for 30 min before reducing reagent and the substrate were added. ^[b]Determined by chiral GC-FID.

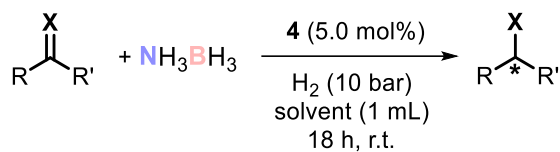
Table 12. Hydrosilylation and transfer hydrogenation of unsaturated substrates with **4**.^[a]

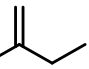
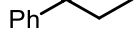
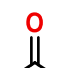
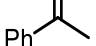
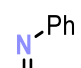
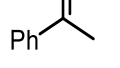
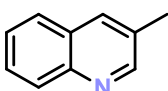
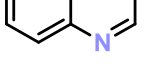
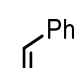
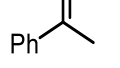


Entry	Substrate	Reducing Reagent	Solvent	Conversion [%] ^[b]	<i>ee</i> [%] ^[c]
1		NH ₃ BH ₃	THF	39	< 5
2		NH ₃ BH ₃	Toluene	16	50
3		NH ₃ BH ₃	<i>n</i> -Hexane	14	67
4		NH ₃ BH ₃	THF	> 95	10
5		NH ₃ BH ₃	Toluene	> 95	9
6		NH ₃ BH ₃	<i>n</i> -Hexane	> 95	9
7		NH ₃ BH ₃	THF	75	< 5
8		NH ₃ BH ₃	Toluene	19	8
9		NH ₃ BH ₃	<i>n</i> -Hexane	14	< 5
10		NH ₃ BH ₃	THF	> 95	< 5
11		NH ₃ BH ₃	Toluene	> 95	< 5
12		NH ₃ BH ₃	<i>n</i> -Hexane	> 95	< 5

^[a]Substrate (0.20 mmol), NH₃BH₃ (0.21 mmol). ^[b]Determined by GC-FID upon comparison of the areas for the substrate and the products. ^[c]Determined by chiral GC-FID.

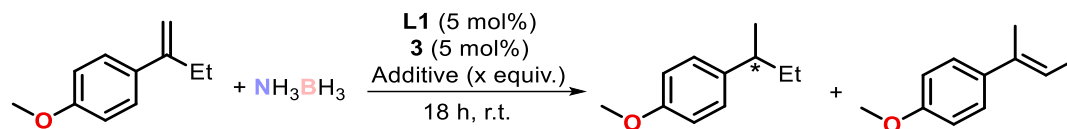
Table 13. (Transfer)Hydrogenation of unsaturated substrates using **4**.^[a]



Entry	Substrate	Solvent	Conversion [%] ^[b]	ee [%] ^[c]
1		THF	> 95	< 5
2		Toluene	72	< 5
3		<i>n</i> -Hexane	80	12
4 ^[d]		THF	< 5	<i>n.d.</i>
5		THF	> 95	< 5
6		Toluene	20	38
7		<i>n</i> -Hexane	51	< 5
8 ^[d]		THF	< 5	<i>n.d.</i>
9		THF	> 95	10
10		Toluene	17	8
11		<i>n</i> -Hexane	28	8
12 ^[d]		THF	< 5	<i>n.d.</i>
13		THF	> 95	< 5
14		Toluene	11	22
15		<i>n</i> -Hexane	35	< 5
16 ^[d]		THF	< 5	<i>n.d.</i>
17		THF	65	< 5
18		Toluene	26	10
19		<i>n</i> -Hexane	36	8.
20 ^[d]		THF	< 5	<i>n.d.</i>

^[a]Substrate (0.20 mmol), NH₃BH₃ (0.06 mmol). ^[b]Determined by GC-FID upon comparison of the areas for the substrate and the products. ^[c]Determined by chiral GC-FID. ^[d]The reaction was performed without NH₃BH₃.

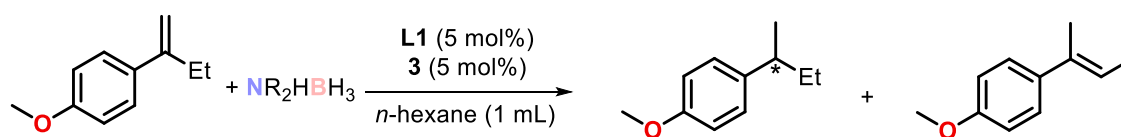
Table 14. Influence of additives on the transfer hydrogenation of **S1**.^[a]



Entry	Additive (equiv.)	Yield (Conversion) [%] ^[b]	Isomerisation [%] ^[b]	<i>ee</i> [%] ^[b]
1	-	20 (24)	4	57
2	<i>i</i> PrOH (1.09)	71 (94)	23	9
3	<i>i</i> PrOH (0.06)	24 (32)	7	46
4	(-)-Menthol (1.08)	72 (98)	26	10
5	(+)-Menthol (1.08)	87 (99)	12	< 5
6 ^[c]	<i>i</i> PrOH (1.09)	< 1 (< 1)	< 1	<i>n.d.</i>
7 ^[c]	(-)-Menthol (1.08)	< 1 (< 1)	< 1	<i>n.d.</i>
8	K ₂ CO ₃ (1.05)	18 (28)	11	39
9	[18]crown-6 (0.06)	5 (10)	4	42
10	[12]crown-4 (0.11)	9 (14)	5	10

^[a]Substrate (0.12 mmol), NH₃BH₃ (0.13 mmol), *n*-hexane (0.6 mL). ^[b]Determined by chiral GC-FID or HPLC. ^[c]The reaction was performed without NH₃BH₃.

Table 15. Influence of different amine boranes and ammonia borane stoichiometry on the TH of **S1**.^[a]



Entry	NR ₂ HBH ₃ (equiv.)	Yield (Conversion) [%] ^[b]	Isomerisation [%] ^[b]	<i>ee</i> [%] ^[b]
1	NH ₃ BH ₃ (1.0)	19 (21)	2	57
2	NMe ₂ HBH ₃ (1.0)	8 (17)	9	< 5
3	N ^{<i>i</i>} Pr ₂ HBH ₃ (1.0)	<1 (9)	9	<i>n.d.</i>
4	NH ₃ BH ₃ (2.0)	14 (15)	1	58
5	NH ₃ BH ₃ (5.0)	28 (33)	5	84

^[a]Substrate (0.20 mmol). ^[b]Determined by chiral GC-FID.

Table 16. Poisoning experiments.^[a]

Entry	Additive (equiv.) ^[b]	Yield (Conversion) [%]	Isomerisation [%]	ee [%]
1	-	20 (24)	4	57
2	Hg (16.33)	20 (22)	3	63
3	P(OMe) ₃ (0.05)	19 (28)	9	50
4	DCT (0.10)	6 (8)	2	63

^[a]Substrate (0.12 mmol), NH₃BH₃ (0.13 mmol), *n*-hexane (0.6 mL). ^[b]The mixture was stirred for 30 min after the additive addition and before **S1** or ammonia borane was added.

4.4.3 NMR Spectra

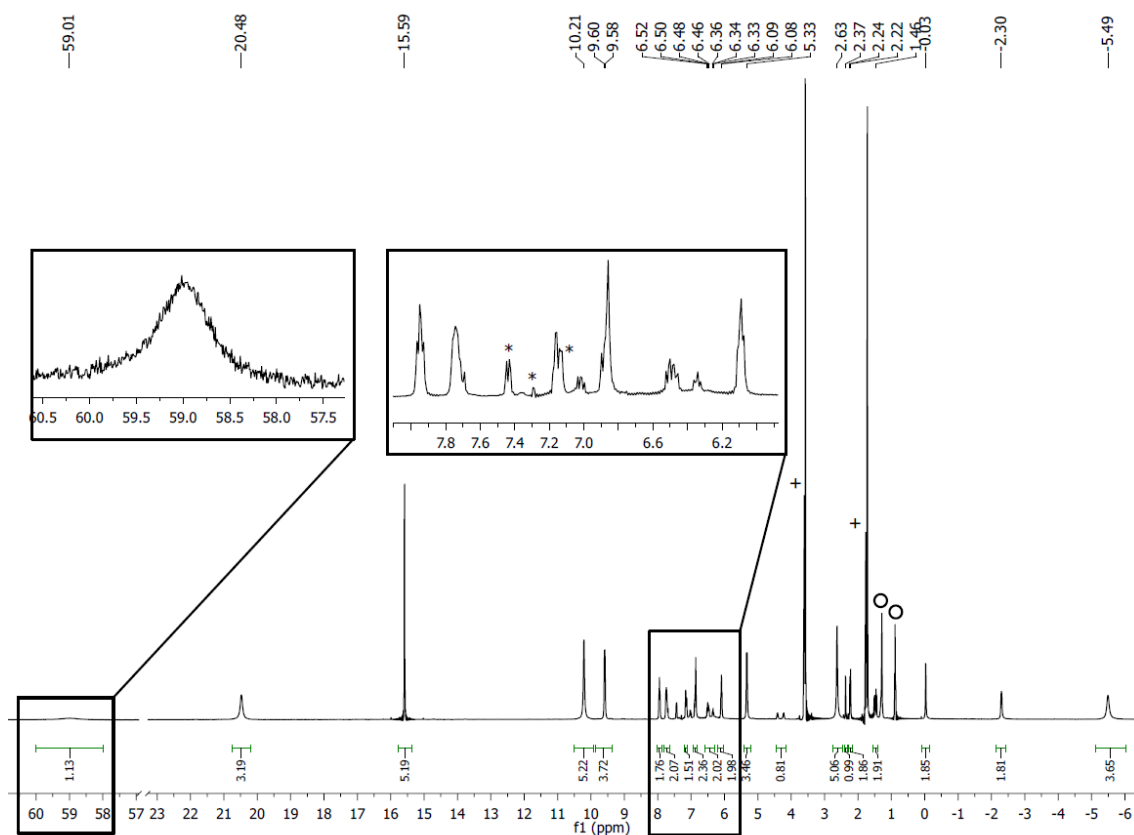


Figure 5. ¹H NMR spectrum (400.13 MHz, 300 K, THF-*d*₈) of **1**, + THF, ○ *n*-hexane, * residual **L1**.

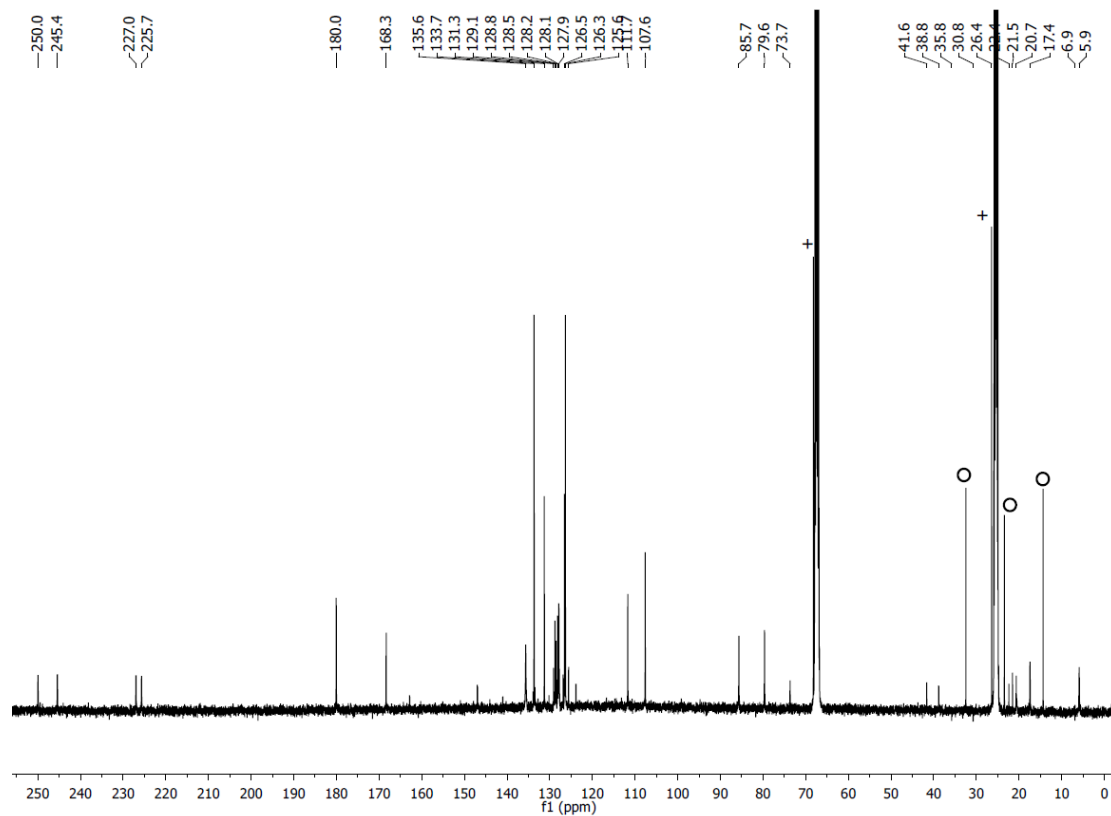


Figure 6. $^{13}\text{C}\{^1\text{H}\}$ NMR spectrum (100.06 MHz, 300 K, $\text{THF-}d_8$) of **1**, + THF, \circ *n*-hexane

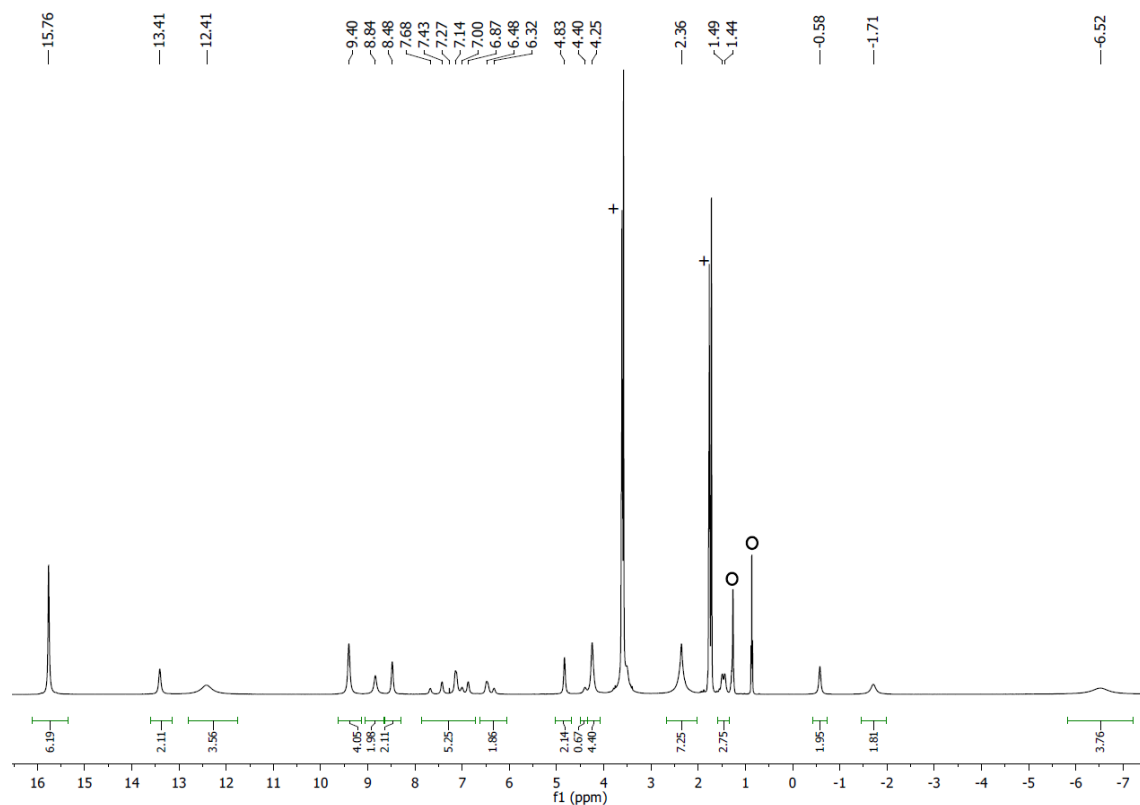


Figure 7. ^1H NMR spectrum (400.13 MHz, 300 K, $\text{THF-}d_8$) of **2**, + THF, \circ *n*-hexane.

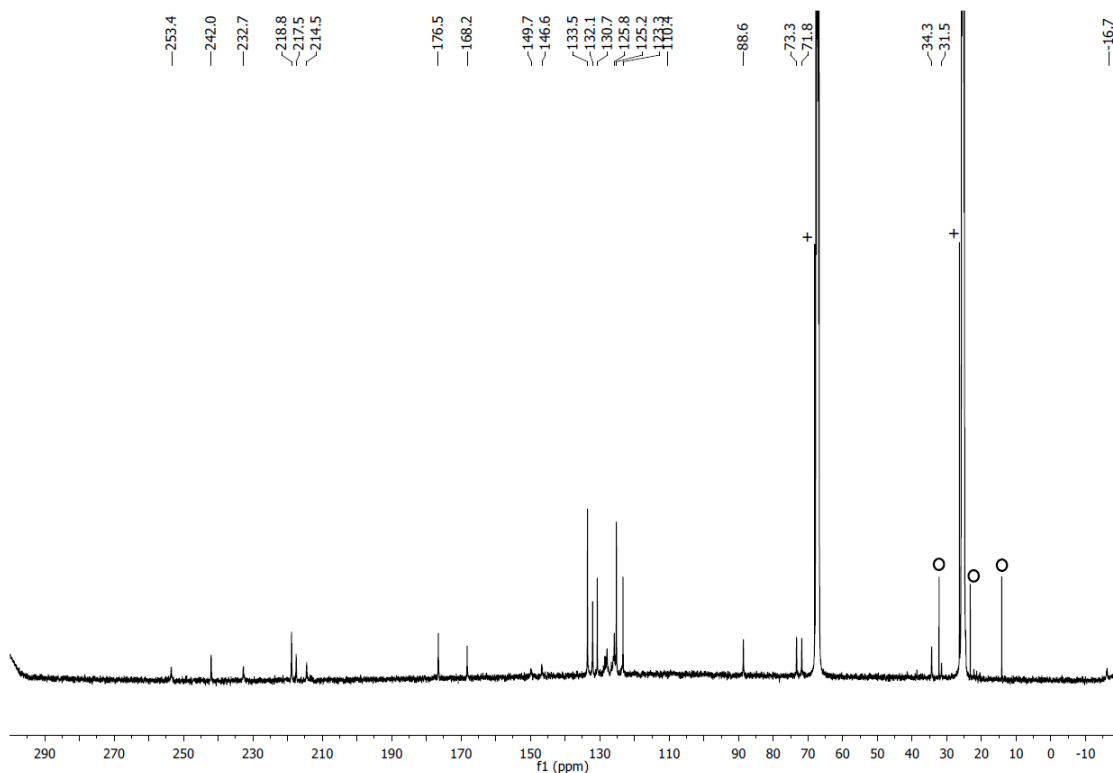


Figure 8. $^{13}\text{C}\{^1\text{H}\}$ NMR spectrum (100.06 MHz, 300 K, $\text{THF-}d_8$) of **2**, + THF, \circ *n*-hexane.

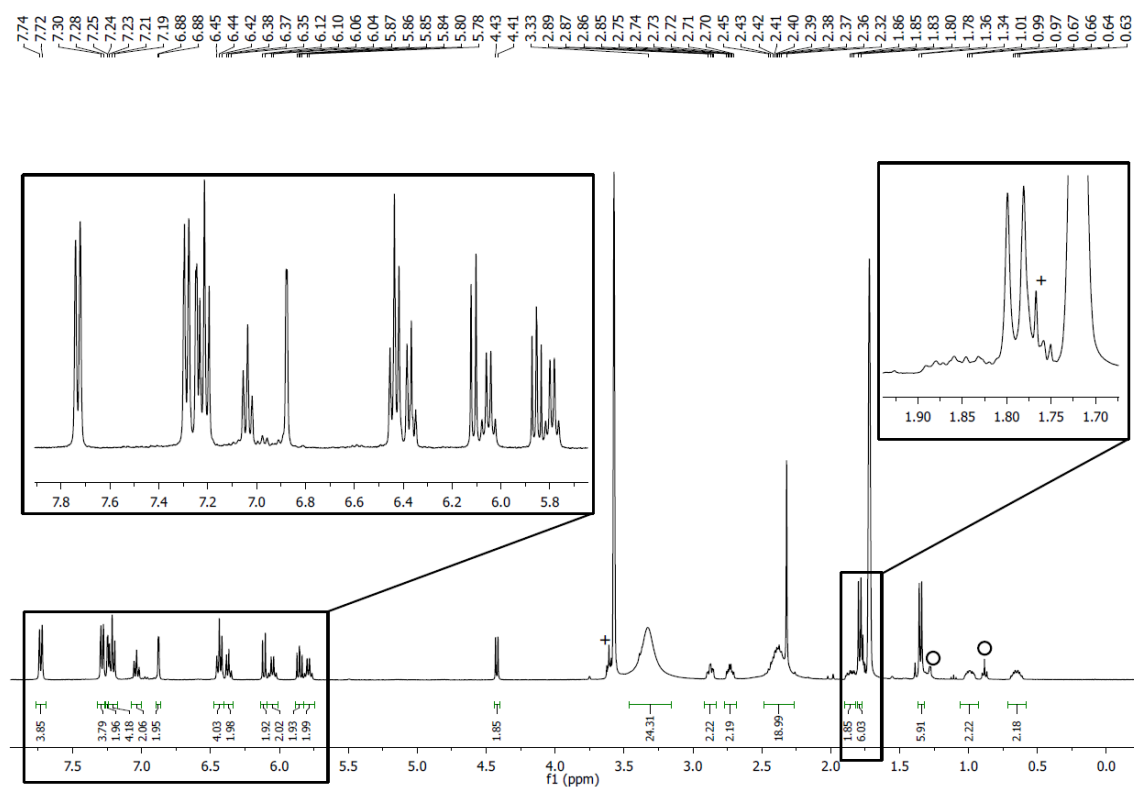


Figure 9. ^1H NMR spectrum (400.13 MHz, 300 K, $\text{THF-}d_8$) of **4**, + THF, \circ *n*-hexane.

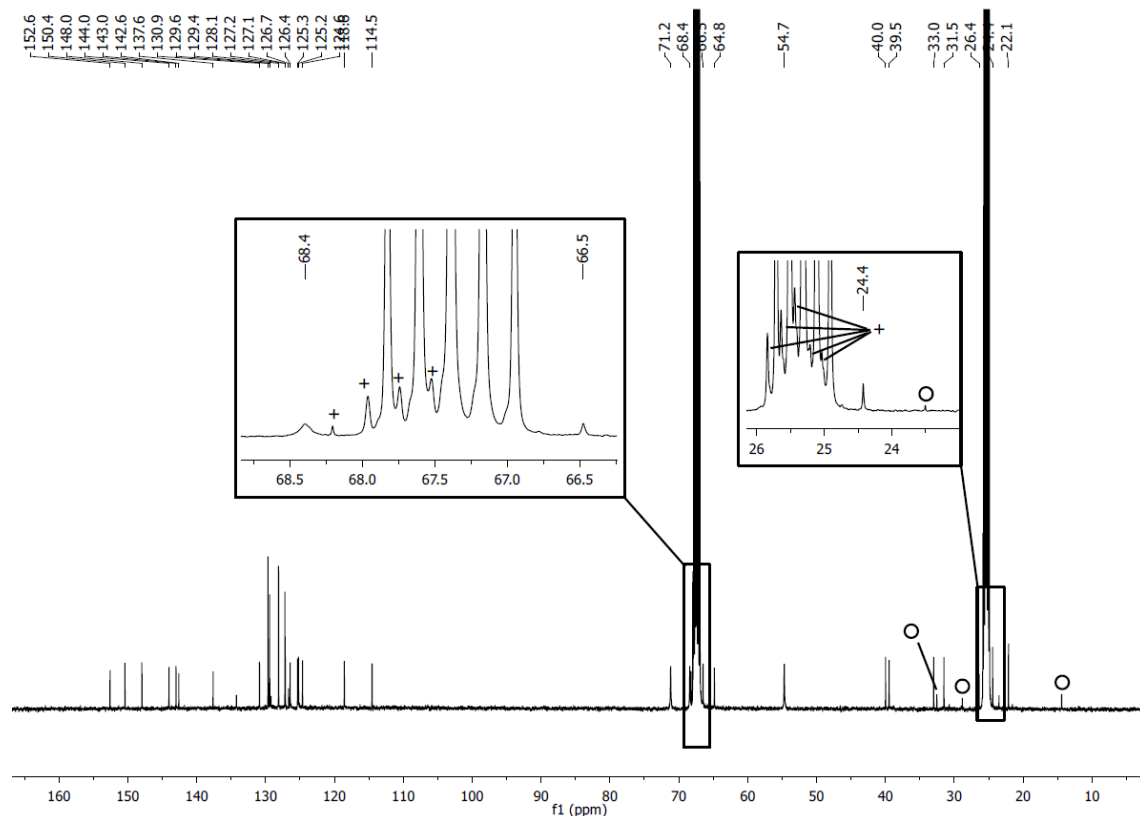


Figure 10. $^{13}\text{C}\{^1\text{H}\}$ NMR spectrum (100.06 MHz, 300 K, $\text{THF-}d_8$) of **4**, + THF, \circ *n*-hexane.

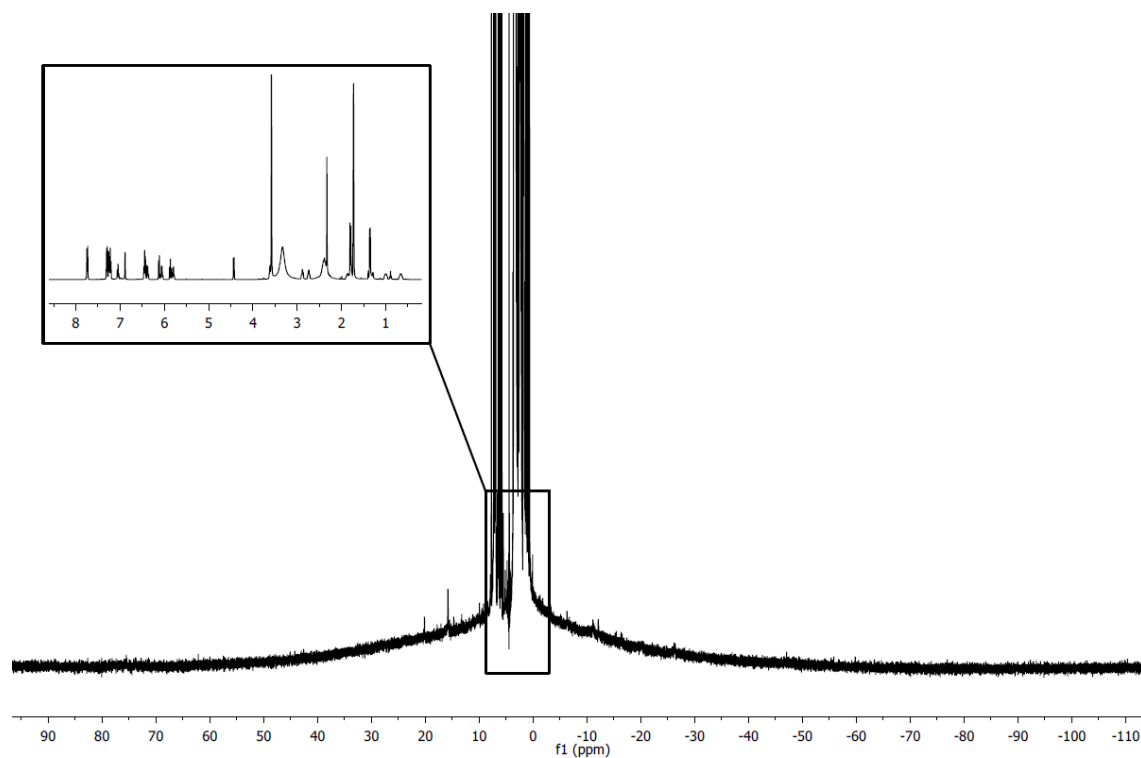


Figure 11. ^1H NMR spectrum (400.13 MHz, 300K, $\text{THF-}d_8$) of **4** showing the paramagnetic impurities.

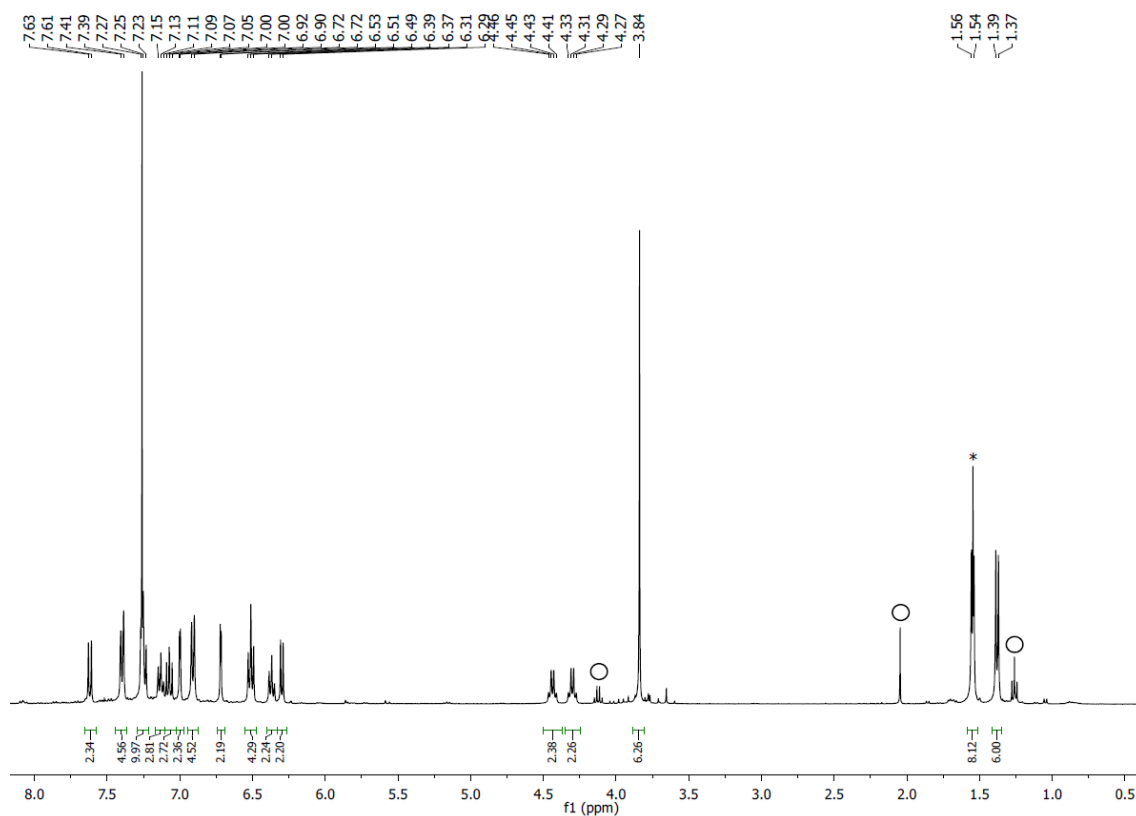


Figure 12. ^1H NMR spectrum (400.13 MHz, 300 K, CDCl_3) of **L10**, \circ ethyl acetate, $*$ water.

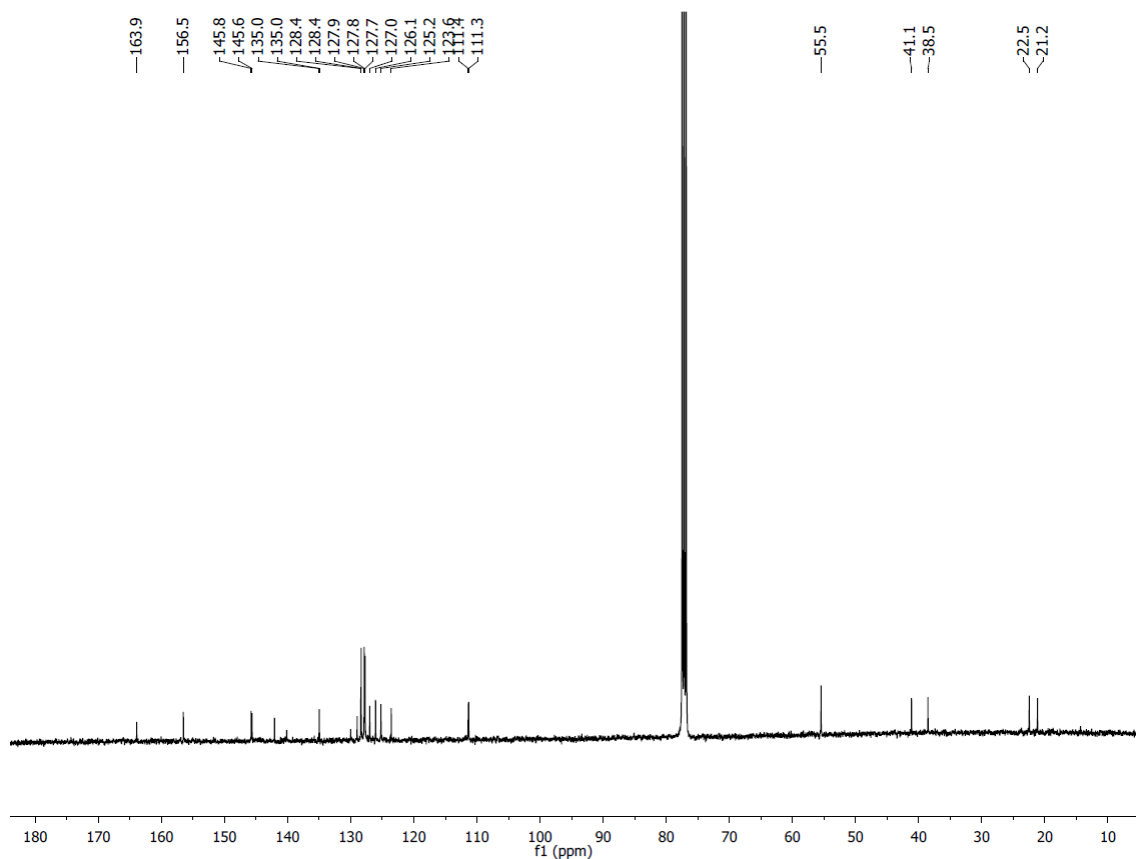


Figure 13. $^{13}\text{C}\{^1\text{H}\}$ NMR spectrum (100.06 MHz, 300 K, CDCl_3) of **L10**.

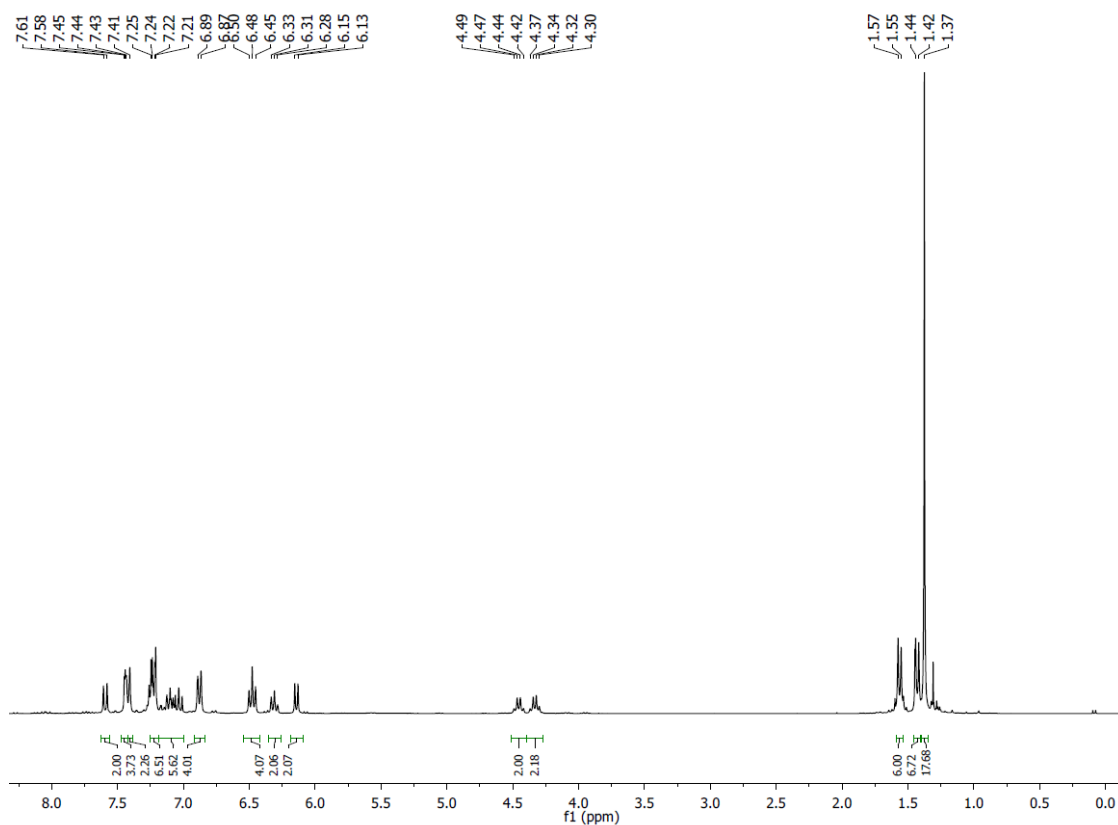


Figure 14. ^1H NMR spectrum (300.13 MHz, 300 K, CDCl_3) of **L11**.

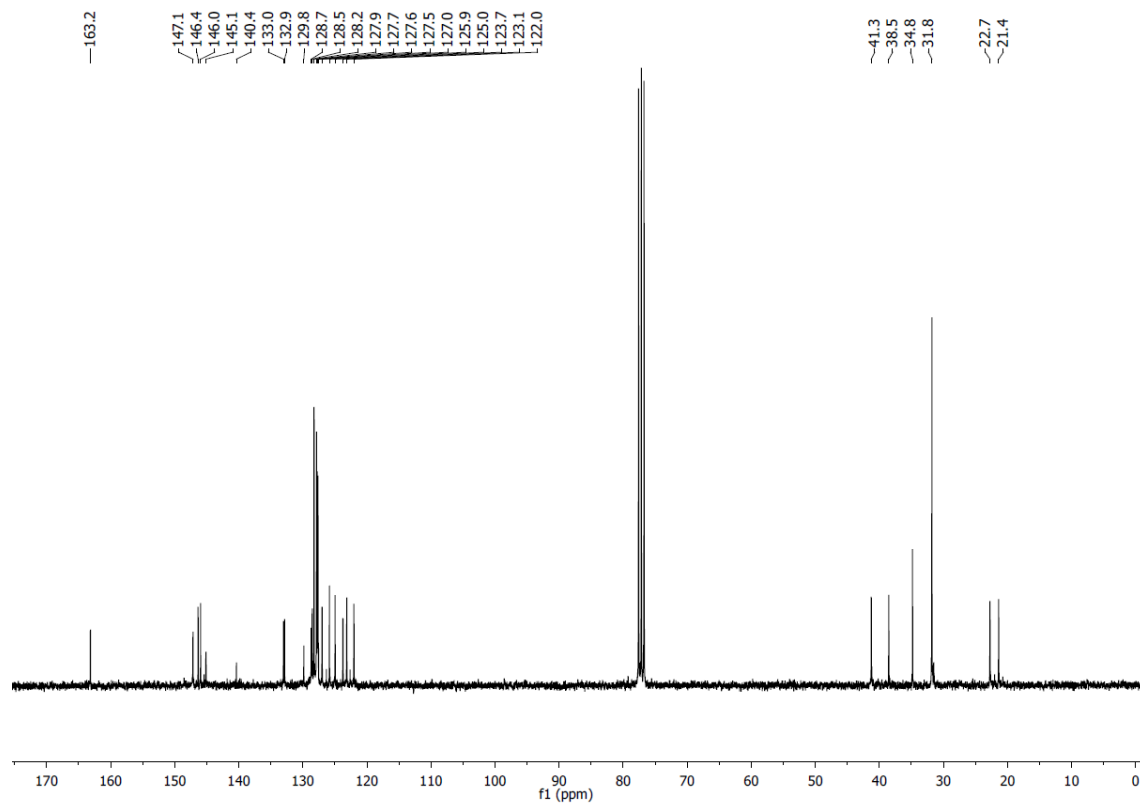


Figure 15. $^{13}\text{C}\{^1\text{H}\}$ NMR spectrum (75.47 MHz, 300 K, CDCl_3) of **L11**.

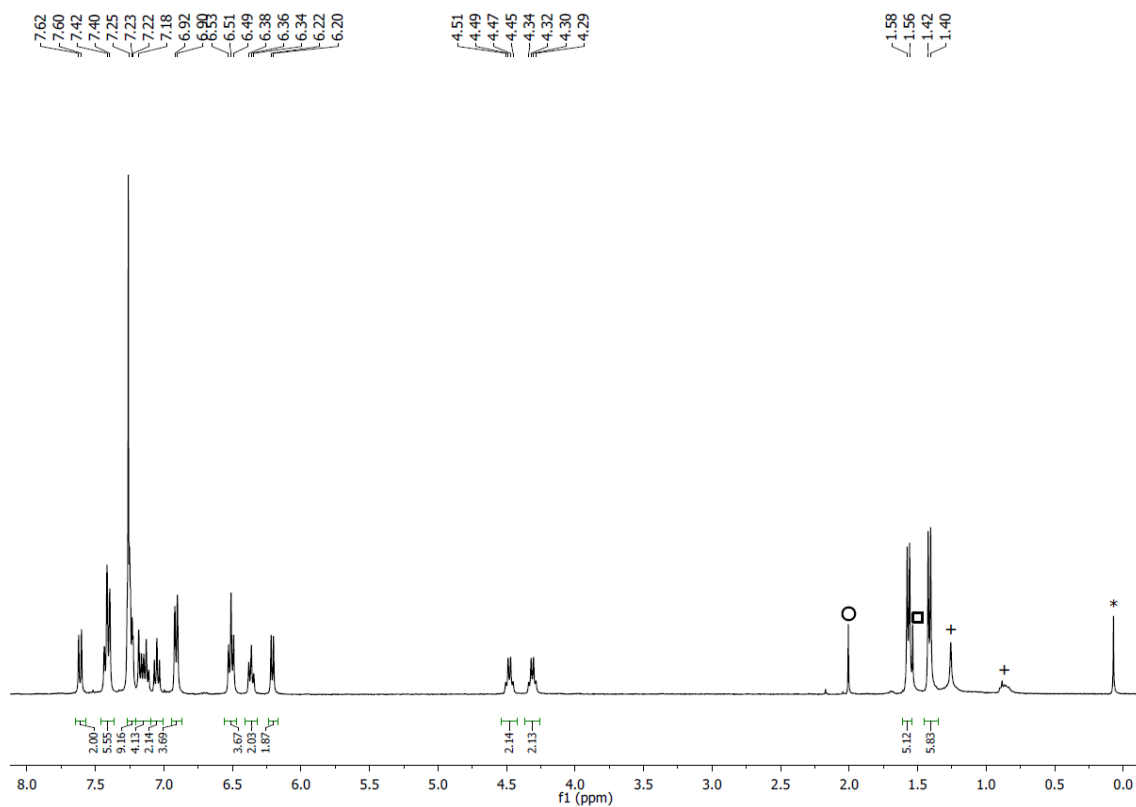


Figure 16. ^1H NMR spectrum (400.13 MHz, 300 K, CDCl_3) of **L12**, \circ MeCN, \square water, $+$ *n*-pentane, $*$ silicone grease.

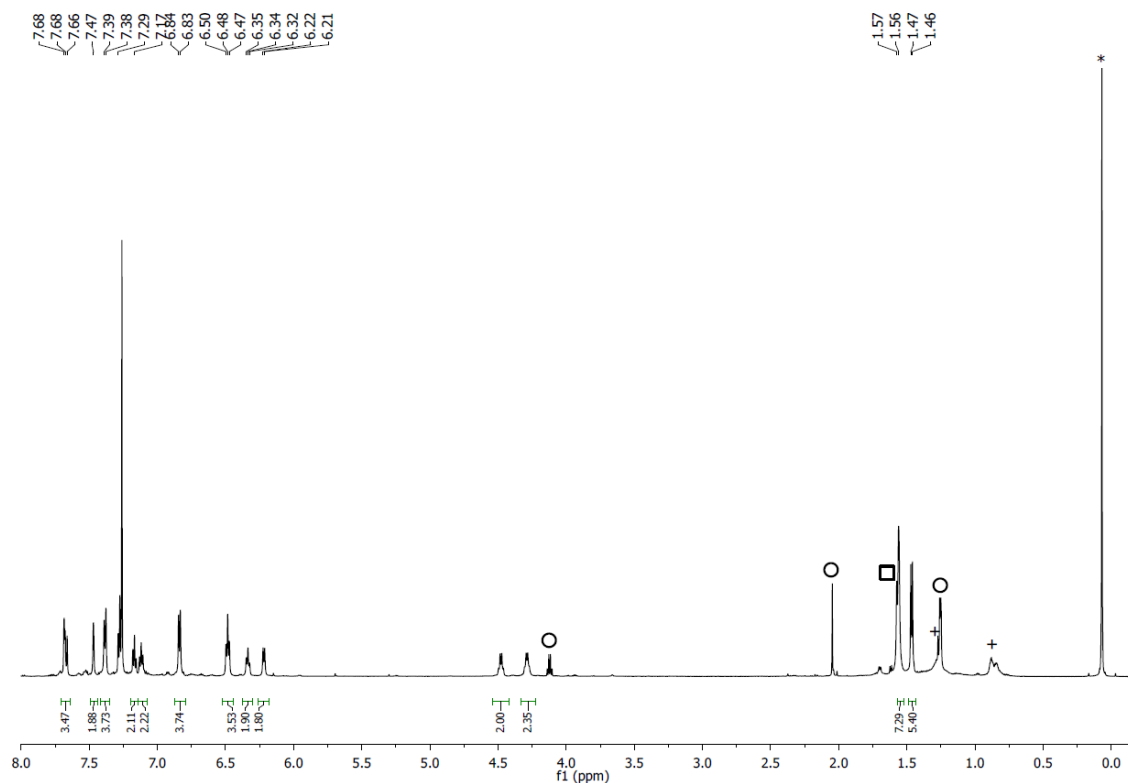


Figure 17. ^1H NMR spectrum (400.13 MHz, 300 K, CDCl_3) of **L13**, \circ ethyl acetate, \square water, $+$ *n*-pentane, $*$ silicone grease.

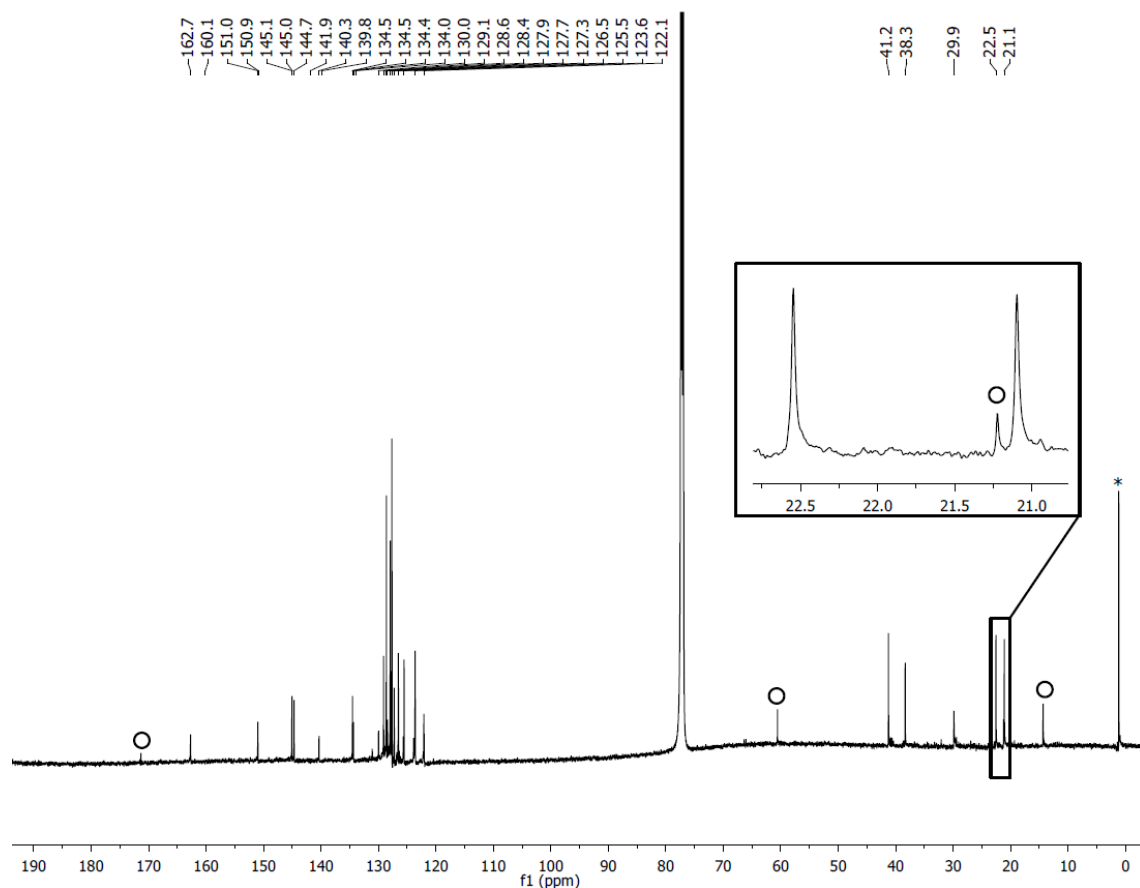


Figure 18. $^{13}\text{C}\{^1\text{H}\}$ NMR spectrum (100.06 MHz, 300 K, CDCl_3) of L13, \circ ethyl acetate, * silicone grease.

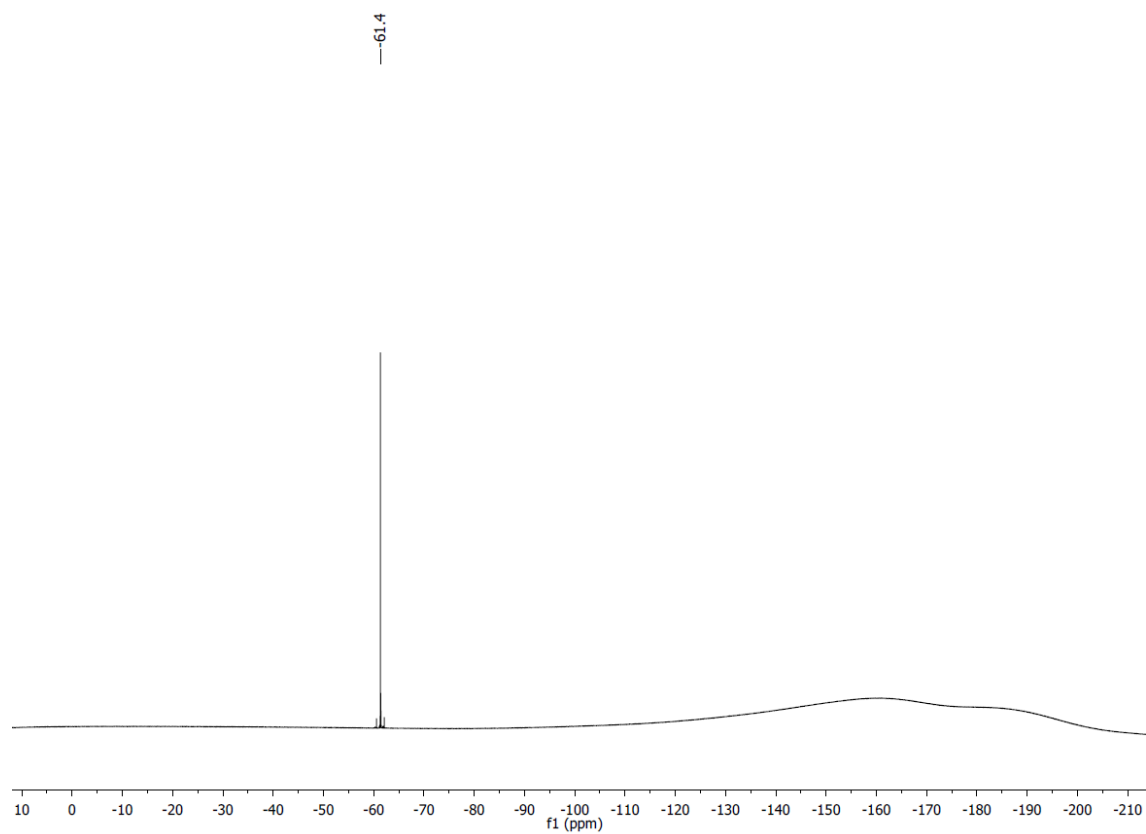


Figure 19. ^{19}F NMR spectrum (376.66 MHz, 300 K, CDCl_3) of L13.

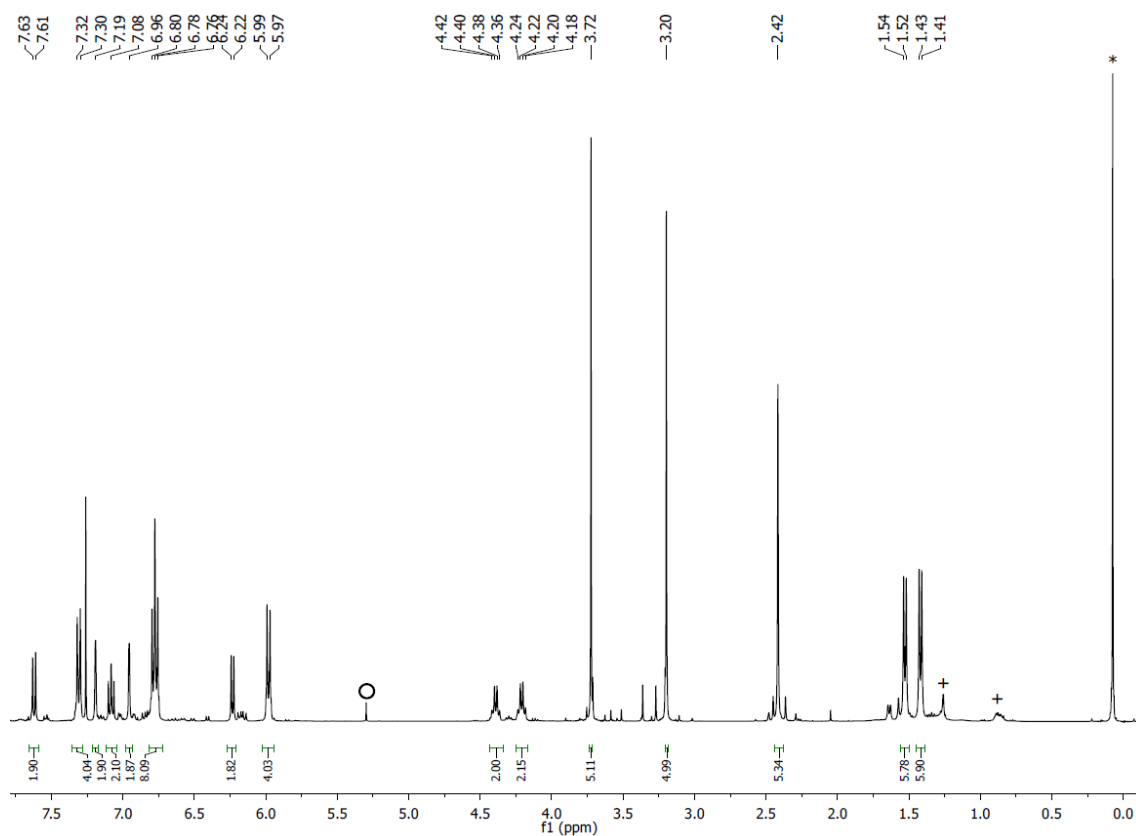


Figure 20. ^1H NMR spectrum (400.13 MHz, 300 K, CDCl_3) of **L14**, o DCM, +, *n*-pentane, * silicone grease.

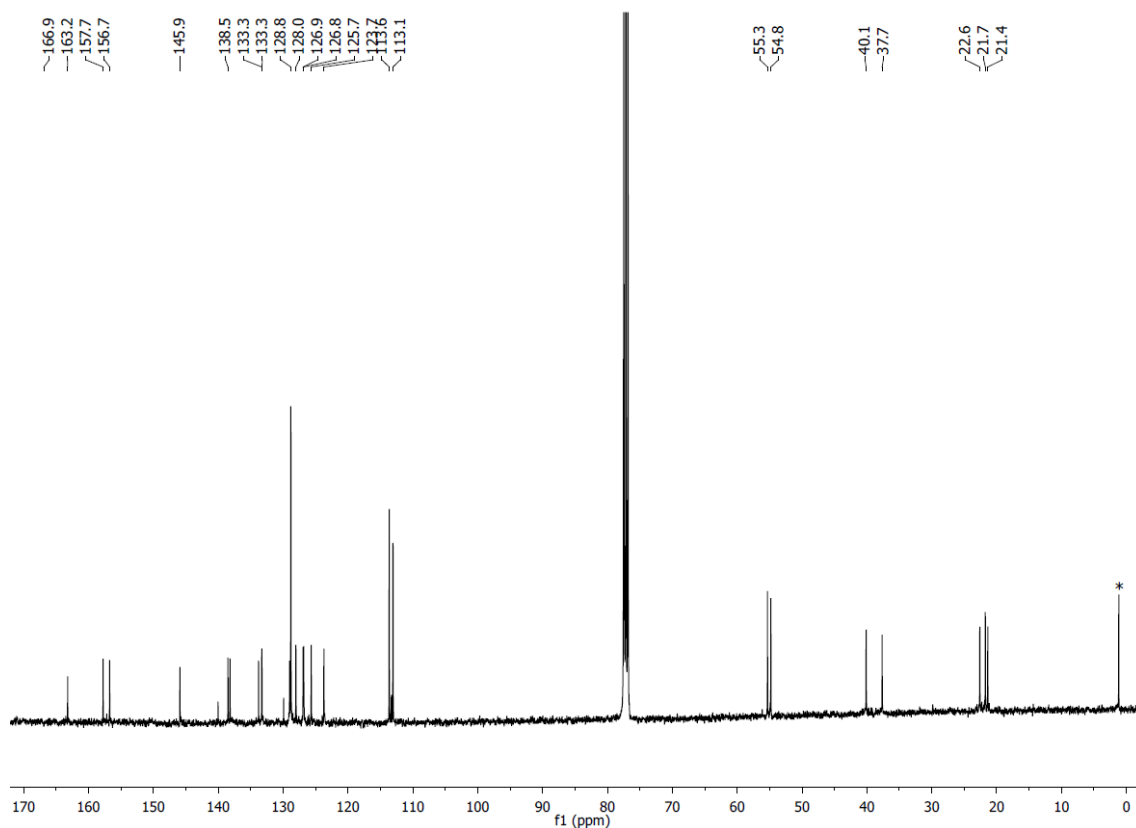


Figure 21. $^{13}\text{C}\{^1\text{H}\}$ NMR spectrum (100.06 MHz, 300 K, CDCl_3) of **L14**, * silicone grease.

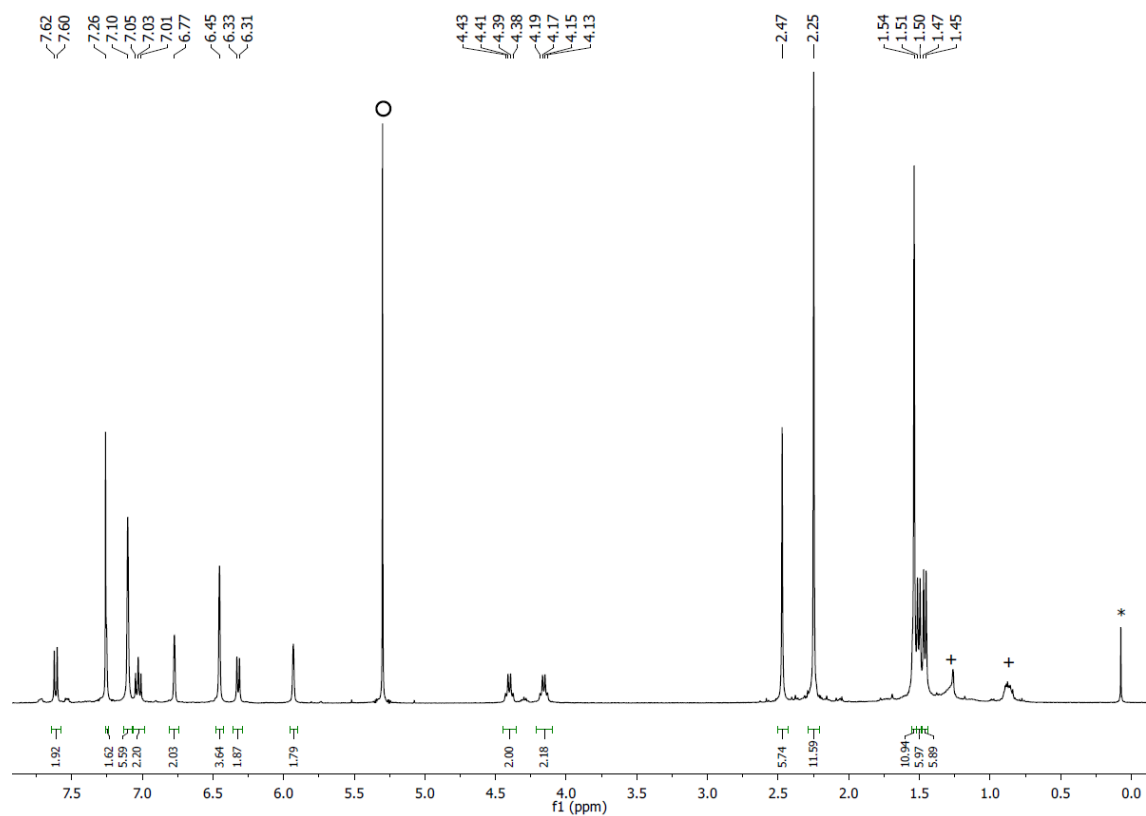


Figure 22. ^1H NMR spectrum (400.13 MHz, 300 K, CDCl_3) of **L15**, \circ DCM, + *n*-pentane, * silicone grease.

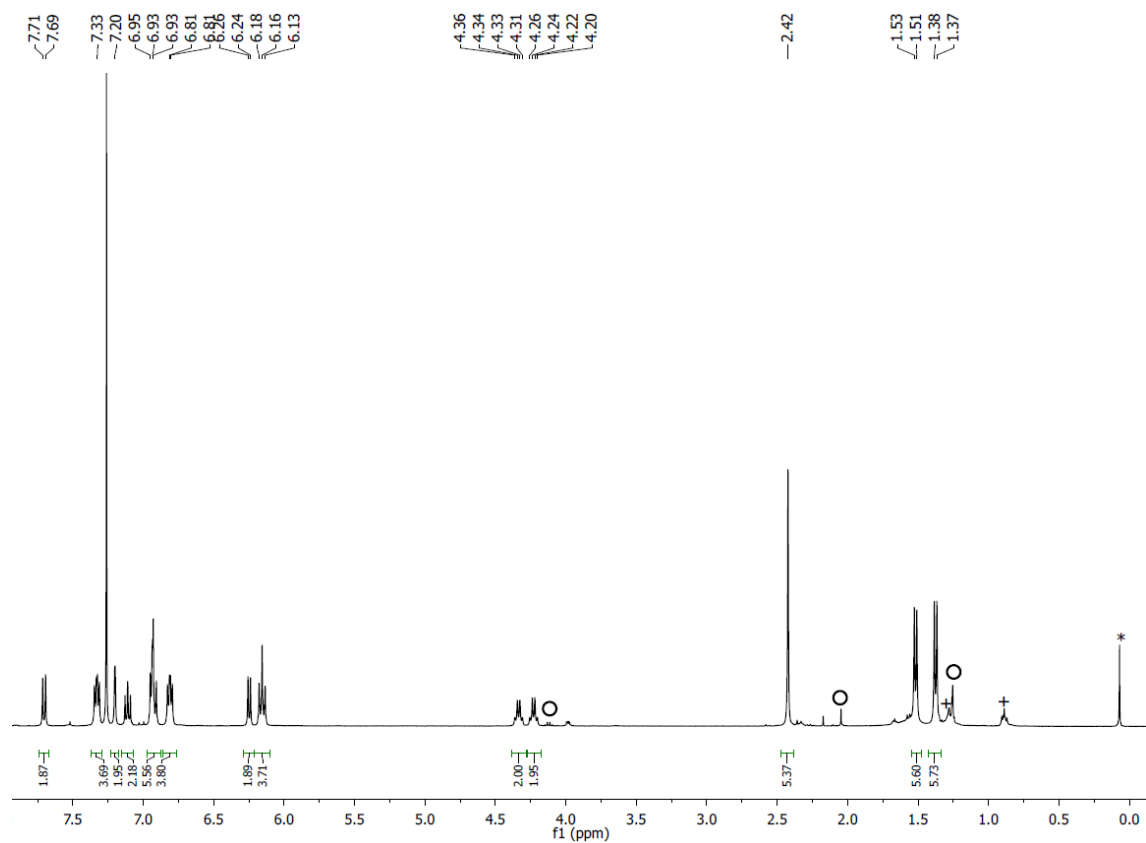


Figure 23. ^1H NMR spectrum (400.13 MHz, 300 K, CDCl_3) of **L16**, \circ ethyl acetate, + *n*-pentane, * silicone grease.

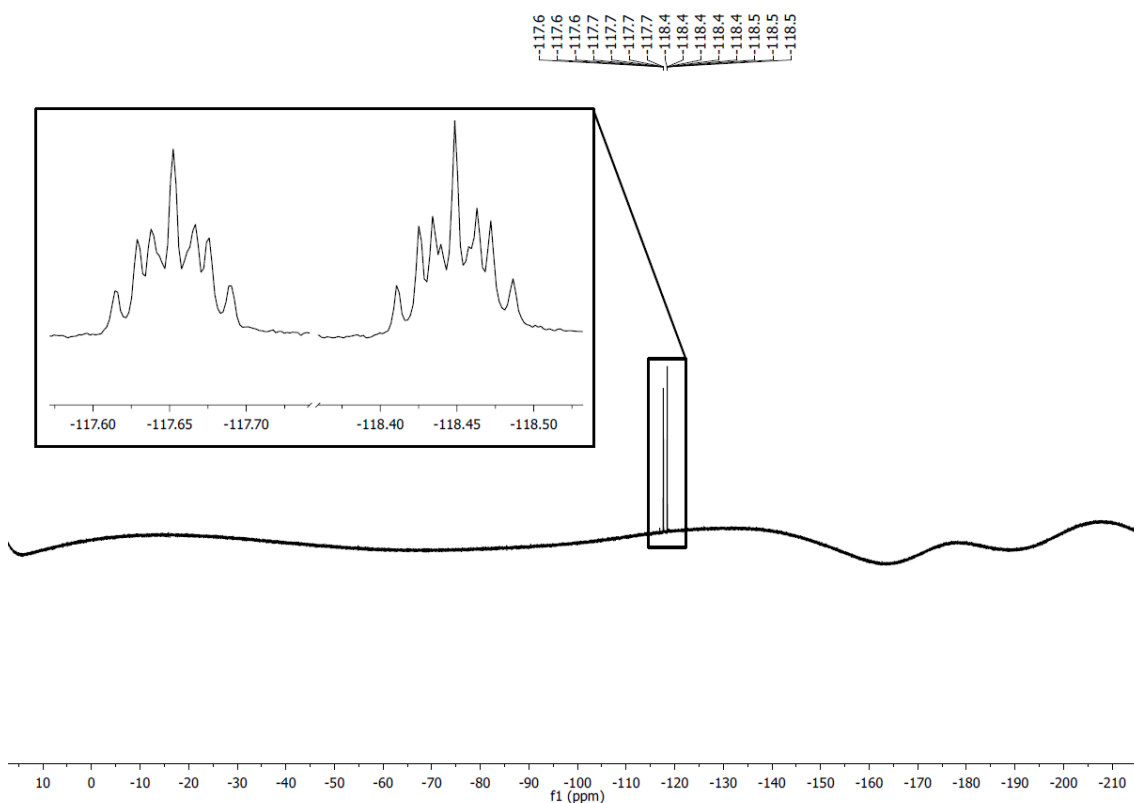


Figure 24. ^{19}F NMR spectrum (376.66 MHz, 300 K, CDCl_3) of L16.

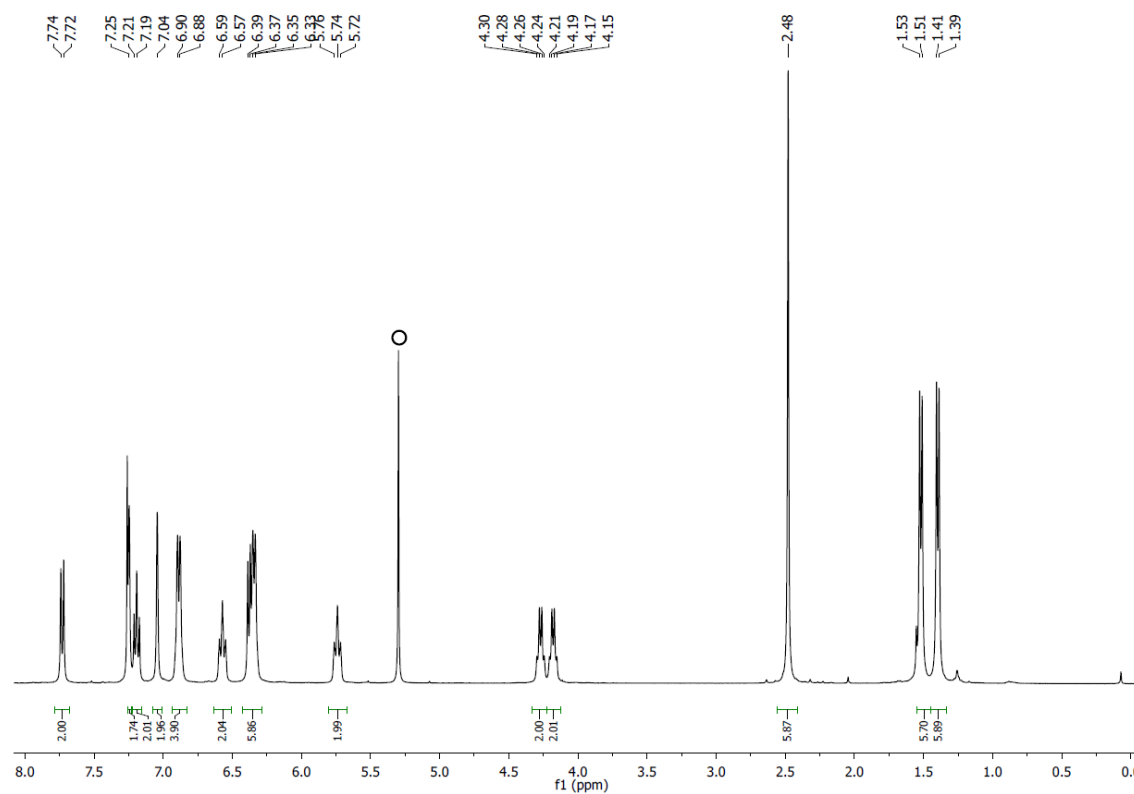


Figure 25. ^1H NMR spectrum (400.13 MHz, 300 K, CDCl_3) of L17, o DCM.

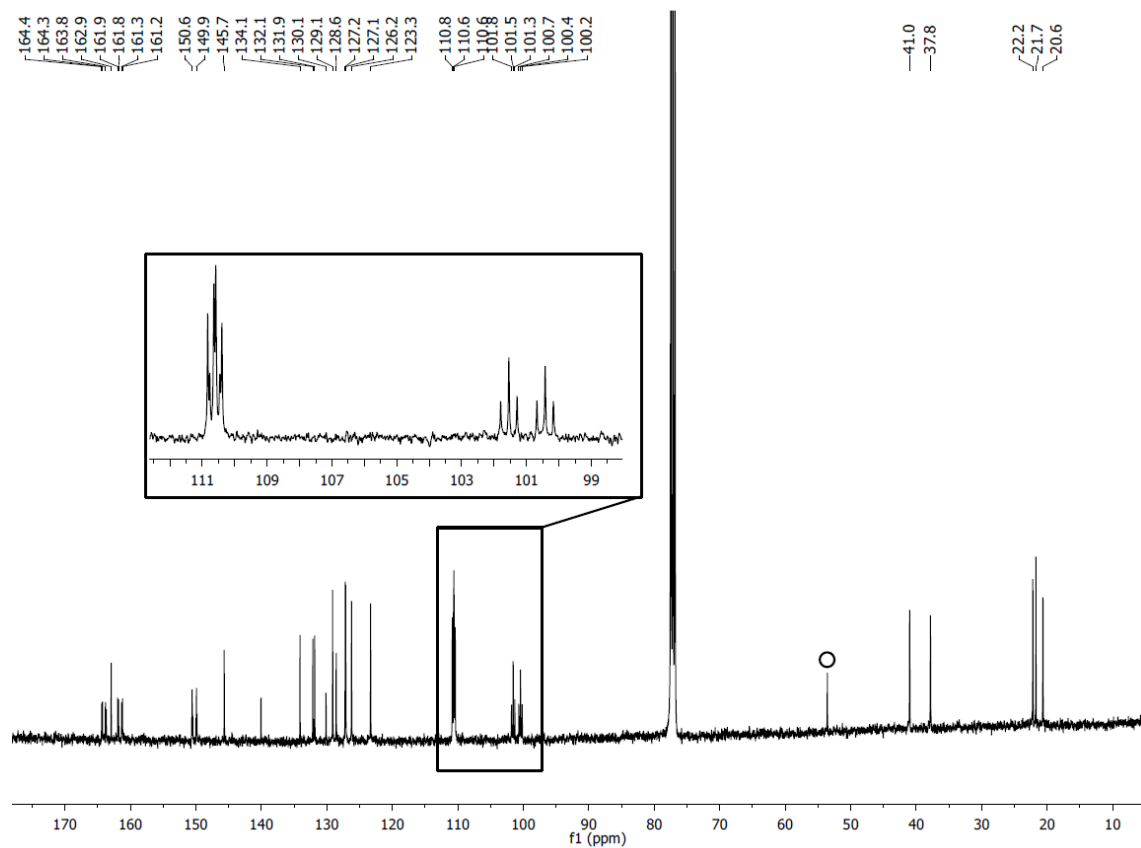


Figure 26. $^{13}\text{C}\{^1\text{H}\}$ NMR spectrum (100.06 MHz, 300 K, CDCl_3) of L17.

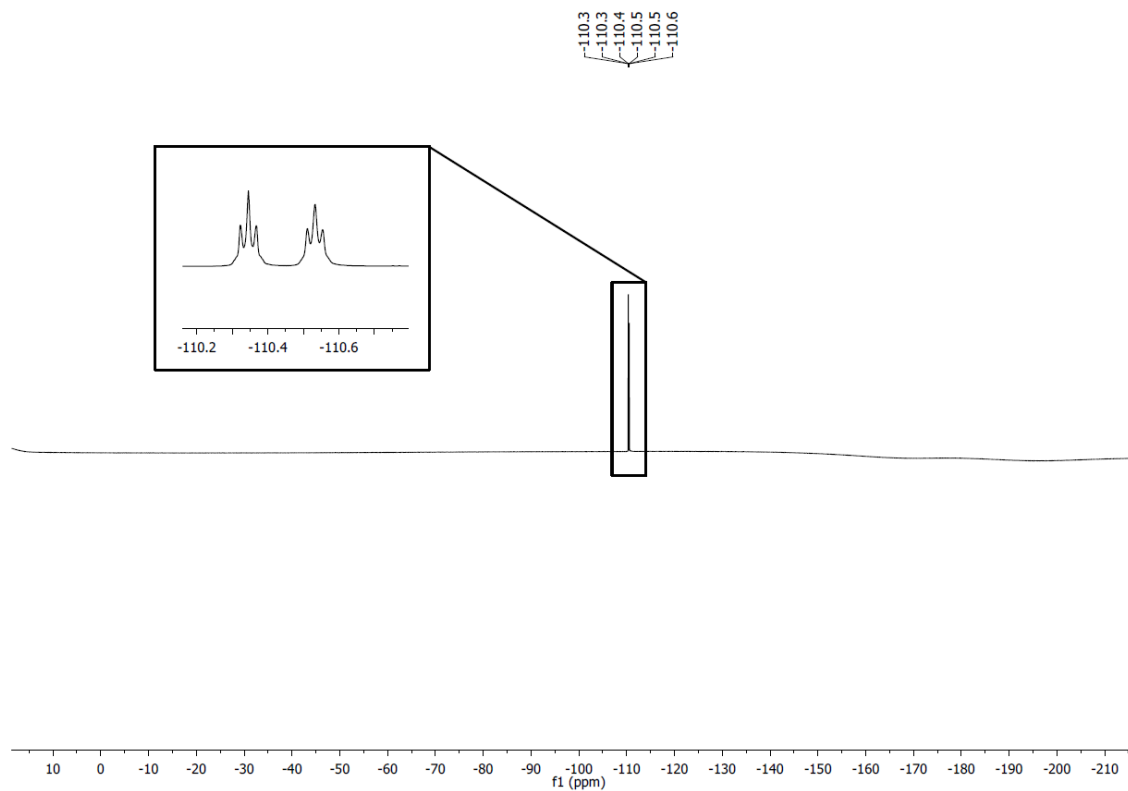


Figure 27. ^{19}F NMR spectrum (376.66 MHz, 300 K, CDCl_3) of L17.

3.4.4 Crystallographic Data

Table 17. X-ray Crystallographic Data for Compounds **1**, **2**, and **4**-[2.2.2]cryptand.

	1	2	4 -[2.2.2]cryptand
Empirical formula	C ₇₂ H ₈₀ Br ₂ CoN ₂ O _{3.5}	C ₂₉ H ₂₆ BrFe _{0.5} N	C ₁₆₈ H ₂₀₀ Co ₂ K ₂ N ₈ O ₁₂
Formula weight / g·mol ⁻¹	1248.189	496.34	2719.41
Temperature / K	100.02(10)	123(1)	123(1)
Crystal system	orthorhombic	trigonal	monoclinic
Space group	P2 ₁ 2 ₁ 2 ₁	P3 ₂ 2 ₁	P2 ₁
<i>a</i> / Å	13.2113(6)	21.88940(10)	14.57096(8)
<i>b</i> / Å	16.8972(4)	21.88940(10)	26.68796(14)
<i>c</i> / Å	28.7152(8)	11.90900(10)	20.68785(11)
α / °	90	90	90
β / °	90	90	101.4868(5)
γ / °	90	120	90
<i>V</i> / Å ³	6410.2(4)	4941.67(6)	7883.74(7)
<i>Z</i>	4	6	2
ρ_{calc} / g cm ⁻³	1.293	1.001	1.146
μ / mm ⁻¹	3.927	3.472	2.584
F(000)	2596.7	1530.0	2904.0
Crystal size / mm ³	0.28 × 0.124 × 0.065	0.145 × 0.073 × 0.067	0.183 × 0.091 × 0.074
Radiation / Å	Cu K α (λ = 1.54184)	Cu K α (λ = 1.54184)	Cu K α (λ = 1.54184)
2 θ range for data collection / °	6.06 to 134.16	4.662 to 147.446	4.358 to 147.548
Diffractometer	Synergy DW	Synergy DW	Synergy DW
Index ranges	-15 ≤ <i>h</i> ≤ 15, -20 ≤ <i>k</i> ≤ 19, -22 ≤ <i>l</i> ≤ 33	-27 ≤ <i>h</i> ≤ 25, -26 ≤ <i>k</i> ≤ 26, -13 ≤ <i>l</i> ≤ 11	-16 ≤ <i>h</i> ≤ 17, -29 ≤ <i>k</i> ≤ 32, -25 ≤ <i>l</i> ≤ 25
Reflections collected	30204	98587	129045
Independent reflections	10872 [R _{int} = 0.0475, R _{sigma} = 0.0496]	6405 [R _{int} = 0.0342, R _{sigma} = 0.0138]	29553 [R _{int} = 0.0280, R _{sigma} = 0.0269]
Data/restraints/parameters	10872/3/570	6405/0/289	29553/168/1808
Goodness-of-fit on F ²	0.985	1.035	1.029
Final R indexes [I >= 2 σ (I)]	R ₁ = 0.0845, wR ₂ = 0.2211	R ₁ = 0.0475, wR ₂ = 0.1260	R ₁ = 0.0432, wR ₂ = 0.1066
Final R indexes [all data]	R ₁ = 0.0956, wR ₂ = 0.2321	R ₁ = 0.0501, wR ₂ = 0.1281	R ₁ = 0.0480, wR ₂ = 0.1095
Largest diff. peak/hole/e Å ⁻³	1.85/-1.23	1.02/-0.76	0.28/-0.33
Flack parameter	0.013(2)	0.003(4)	-0.0219(13)

References

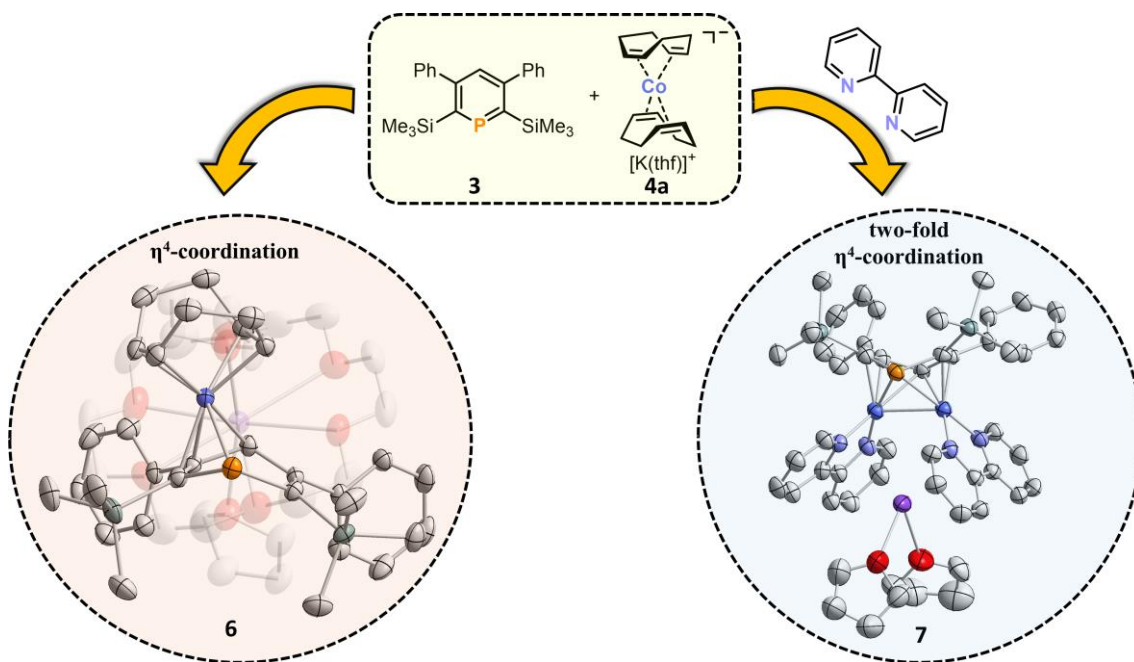
- [1] a) J. G. d. Vries, C. J. Elsevier *The handbook of homogeneous hydrogenation*, Wiley-VCH, Weinheim, **2007**; b) C. Pettinari, F. Marchetti, D. Martini in *Comprehensive Coordination Chemistry II*, Elsevier, **2003**, 75–139.; c) P. A. Chase, G. C. Welch, T. Jurca, D. W. Stephan, *Angew. Chem. Int. Ed.* **2007**, *46*, 8050–8053.
- [2] S. Lau, D. Gasperini, R. L. Webster, *Angew. Chem. Int. Ed.* **2021**, *60*, 14272–14294.
- [3] a) H. Meerwein, R. Schmidt, *Justus Liebigs Ann. Chem.* **1925**, *444*, 221–238; b) A. Verley, *Bull. Soc. Chim. Fr.* **1925**, 537–542; c) W. Ponndorf, *Angew. Chem.* **1926**, *39*, 138–143; d) C. F. de Graauw, J. A. Peters, H. van Bekkum, J. Huskens, *Synthesis* **1994**, *1994*, 1007–1017.
- [4] a) N. J. A. Martin, L. Ozores, B. List, *J. Am. Chem. Soc.* **2007**, *129*, 8976–8977; b) Q. Wang, J. Chen, X. Feng, H. Du, *Org. Biomol. Chem.* **2018**, *16*, 1448–1451; c) J. W. Yang, M. T. Hechavarria Fonseca, B. List, *Angew. Chem. Int. Ed.* **2004**, *43*, 6660–6662.
- [5] a) X. Chen, X.-Y. Zhou, H. Wu, Y.-Z. Lei, J.-H. Li, *Synth. Commun.* **2018**, *48*, 2475–2484; b) G. K. Jnaneshwara, A. Sudalai, V. H. Deshpande, *J. Chem. Res.* **1998**, 160–161; c) P. P. Pande, G. C. Joshi, C. S. Mathela, *Synth. Commun.* **1998**, *28*, 4193–4200.
- [6] a) H. Bauer, K. Thum, M. Alonso, C. Fischer, S. Harder, *Angew. Chem. Int. Ed.* **2019**, *58*, 4248–4253; b) I. Chatterjee, M. Oestreich, *Angew. Chem. Int. Ed.* **2015**, *54*, 1965–1968; c) J. F. Quinn, D. A. Razzano, K. C. Golden, B. T. Gregg, *Tetrahedron Lett.* **2008**, *49*, 6137–6140.
- [7] N. C. Smythe, J. C. Gordon, *Eur. J. Inorg. Chem.* **2010**, *2010*, 509–521.
- [8] a) M. Couturier, J. L. Tucker, B. M. Andresen, P. Dubé, J. T. Negri, *Org. Lett.* **2001**, *3*, 465–467; b) H. Dong, H. Berke, *J. Organomet. Chem.* **2011**, *696*, 1803–1808; c) C. Gelis, A. Heusler, Z. Nairoukh, F. Glorius, *Chem. Eur. J.* **2020**, *26*, 14090–14094; d) Y. Jiang, H. Berke, *Chem. Commun.* **2007**, 3571–3573; e) Y. Jiang, O. Blacque, T. Fox, C. M. Frech, H. Berke, *Organometallics* **2009**, *28*, 5493–5504.
- [9] a) C. C. Chong, H. Hirao, R. Kinjo, *Angew. Chem. Int. Ed.* **2014**, *53*, 3342–3346; b) F. Ding, Y. Zhang, R. Zhao, Y. Jiang, R. L.-Y. Bao, K. Lin, L. Shi, *Chem. Commun.* **2017**, *53*, 9262–9264.
- [10] A. Brzozowska, L. M. Azofra, V. Zubar, I. Atodiresei, L. Cavallo, M. Rueping, O. El-Sepelgy, *ACS Catal.* **2018**, *8*, 4103–4109.
- [11] E. Korytiaková, N. O. Thiel, F. Pape, J. F. Teichert, *Chem. Commun.* **2017**, *53*, 732–735.
- [12] S. Fu, N.-Y. Chen, X. Liu, Z. Shao, S.-P. Luo, Q. Liu, *J. Am. Chem. Soc.* **2016**, *138*, 8588–8594.
- [13] V. G. Landge, J. Pitchaimani, S. P. Midya, M. Subaramanian, V. Madhu, E. Balaraman, *Catal. Sci. Technol.* **2018**, *8*, 428–433.
- [14] J. K. Pagano, J. P. W. Stelmach, R. Waterman, *Dalton Trans.* **2015**, *44*, 12074–12077.
- [15] V. Vermaak, H. C. M. Vosloo, A. J. Swarts, *Adv. Synth. Catal.* **2020**, *362*, 5788–5793.
- [16] a) M. Pang, J.-Y. Chen, S. Zhang, R.-Z. Liao, C.-H. Tung, W. Wang, *Nat. Commun.* **2020**, *11*, 1249; b) X. Zhai, M. Pang, L. Feng, J. Jia, C.-H. Tung, W. Wang, *Chem. Sci.* **2021**, *12*, 2885–2889.
- [17] T. M. Maier, S. Sandl, I. G. Shenderovich, A. Jacobi von Wangelin, J. J. Weigand, R. Wolf, *Chem. Eur. J.* **2019**, *25*, 238–245.
- [18] a) S. Li, G. Li, W. Meng, H. Du, *J. Am. Chem. Soc.* **2016**, *138*, 12956–12962; b) S. Li, W. Meng, H. Du, *Org. Lett.* **2017**, *19*, 2604–2606; c) W. Meng, X. Feng, H. Du, *Acc. Chem. Res.* **2018**, *51*, 191–201; d) W. Zhao, X. Feng, J. Yang, H. Du, *Tetrahedron Lett.* **2019**, *60*, 1193–1196; e) W. Zhao, Z. Zhang, X. Feng, J. Yang, H. Du, *Org. Lett.* **2020**, *22*, 5850–5854; f) Q. Zhou, W. Meng, J. Yang, H. Du, *Angew. Chem. Int. Ed.* **2018**, *57*, 12111–12115.
- [19] J. Diesel, A. M. Finogenova, N. Cramer, *J. Am. Chem. Soc.* **2018**, *140*, 4489–4493.
- [20] S. Sandl, T. M. Maier, N. P. van Leest, S. Kröncke, U. Chakraborty, S. Demeshko, K. Koszinowski, B. de Bruin, F. Meyer, M. Bodensteiner et al., *ACS Catal.* **2019**, *9*, 7596–7606.
- [21] a) M. N. Alnajrani, S. A. Alshimri, O. A. Alsager, *RSC Adv.* **2016**, *6*, 113803–113814; b) M. J. Supej, A. Volkov, L. Darko, R. A. West, J. M. Darmon, C. E. Schulz, K. A. Wheeler, H. M. Hoyt, *Polyhedron* **2016**, *114*, 403–414.
- [22] S. Pelties, T. Maier, D. Herrmann, B. de Bruin, C. Rebreyend, S. Gärtner, I. G. Shenderovich, R. Wolf, *Chem. Eur. J.* **2017**, *23*, 6094–6102.
- [23] a) S. Enthaler, B. Hagemann, G. Erre, K. Junge, M. Beller, *Chem. Asian J.* **2006**, *1*, 598–604; b) C. Sui-Seng, F. Freutel, A. J. Lough, R. H. Morris, *Angew. Chem. Int. Ed.* **2008**, *47*, 940–943; c) R. ter Halle, A. Bréhéret, E. Schulz, C. Pinel, M. Lemaire, *Tetrahedron Asymmetry* **1997**, *8*, 2101–2108.
- [24] a) D. Gärtner, S. Sandl, A. Jacobi von Wangelin, *Catal. Sci. Technol.* **2020**, *10*, 3502–3514; b) R. H. Crabtree, *Chem. Rev.* **2012**, *112*, 1536–1554.
- [25] J. A. Widegren, R. G. Finke, *J. Mol. Catal. A: Chem.* **2003**, *198*, 317–341.
- [26] J. K. Dunleavy, *Platin. Met. Rev.* **2006**, *50*, 156.
- [27] F. Lihl, *Int. J. Mat. Res.* **1953**, *44*, 160–166.
- [28] V. M. Chernyshev, A. V. Astakhov, I. E. Chikunov, R. V. Tyurin, D. B. Eremin, G. S. Ranny, V. N. Khrustalev, V. P. Ananikov, *ACS Catal.* **2019**, *9*, 2984–2995.
- [29] J. F. Sonnenberg, R. H. Morris, *Catal. Sci. Technol.* **2014**, *4*, 3426–3438.
- [30] D. R. Anton, R. H. Crabtree, *Organometallics* **1983**, *2*, 855–859.
- [31] K. Jonas, US patent 4169845, **1977**.
- [32] S. McIntyre, E. Hörmann, F. Menges, S. P. Smidt, A. Pfaltz, *Adv. Synth. Catal.* **2005**, *347*, 282–288.
- [33] a) SCALE3ABS, CrysAlisPro, Agilent Technologies Inc., Oxford, GB, **2012**; b) G. M. Sheldrick, SADABS, Bruker AXS, Madison, USA, **2007**.
- [34] R. C. Clark, J. S. Reid, *Acta Cryst. A* **1995**, *51*, 887–897.
- [35] G. M. Sheldrick, *Acta Cryst. A* **2015**, *71*, 3–8.

- [36] O. V. Dolomanov, L. J. Bourhis, R. J. Gildea, J. A. K. Howard, H. Puschmann, *J. Appl. Crystallogr.* **2009**, *42*, 339–341.
- [37] G. M. Sheldrick, *Acta Cryst. A* **2008**, *64*, 112–122.
- [38] G. M. Sheldrick, *Acta Cryst. C* **2015**, *71*, 3–8.

5 Synthesis and Characterisation of Low-Valent Phosphine Cobalt Complexes^[a]

Abstract:

The synthesis of highly reduced iron and cobalt complexes of phosphinines was investigated. To this end, the substitution of cyclooctadiene and polyarenes in a variety of metalates was investigated. It is shown that the reaction of 2,6-bis(trimethylsilyl)-3,5-diphenylphosphinine (**3**) with potassium bis(1,5-cyclooctadiene)cobaltate (**4a**) slowly forms $[\text{K}([\text{18}] \text{crown-6})][(\text{3,5-Ph}_2\text{-2,6-(SiMe}_3)_2\text{-PC}_5\text{H)Co(cod)}]$ (**6**), which is the first cobalt phosphinine complex featuring a phosphinine in an η^4 -coordination mode. Upon investigating the reactivity of **6**, unselective reactions were observed with P_4 , $t\text{BuCP}$, CO_2 or CO . However, the addition of 2,2'-bipyridine (bpy) converts **6** to the dinuclear complex $[\text{K}(\text{thf})_2\text{Co}_2(\text{bpy})_2(\mu, \eta^4: \eta^4\text{-}(3,5\text{-Ph}_2\text{-2,6-(SiMe}_3)_2\text{-PC}_5\text{H}))]$ (**7**), featuring the phosphinine **3** as a $\mu, \eta^4: \eta^4$ coordinating ligand. The electronic properties of **7** were investigated by determination of the magnetic susceptibility (Evans NMR method), EPR spectroscopy, and DFT calculations. In combination, these indicate that **7** features a quartet spin ground state ($S = 3/2$) with both bpy moieties being best described as radical anions ($\text{bpy}^{\cdot-}$).



^[a] Felix Seeberger performed the reactions and the characterisation of all compounds. Gábor Balázs helped with the EPR measurements. Robert Wolf supervised and directed the project.

5.1 Introduction

Phosphinines (phosphabenzenes), initially reported by Märkl in 1966,^[1] are the heavy homologues of pyridines and this compound class feature a low-valent and formally sp^2 -hybridised phosphorus atom. Aromaticities of 80-97% with respect to benzene were calculated depending on the utilised aromaticity index.^[2] The electronic structure of this class of compounds enables versatile coordination, as the phosphinine can coordinate *via* the aromatic π -system (high lying π and low lying π^* orbitals) and the lone pair of the phosphorus atom.^[3] The most common mode, η^1 , features σ -coordination of the phosphorus atom to a metal center and is most often observed for transition metals in low oxidation states.^[4] This coordination mode was observed in numerous complexes, including phosphinine metal carbonyl complexes **A1-3**^[5] as well as various phosphinine metal halides.^[6] This η^1 -coordination mode was also realised with base metals, as demonstrated by *Elschenbroich* and co-workers in the early 1990s, when they synthesised homoleptic $[M(\eta^1-C_5H_5P)_x]$ complexes of nickel,^[7] iron,^[8] and chromium^[9] ($x = 4, 5$ and 6, respectively). Coordination *via* the π -system is another rather common coordination motif of phosphinine ligands. This η^6 -coordination mode is most often observed for early transition metal complexes, such as $[V(\eta^6-C_5H_5P)_2]$ ^[10] and $[Ti\{\eta^6-(2,4,6-tBu_3C_5H_2P)\}_2]$,^[11] however, late transition metal complexes bearing η^6 -coordinated phosphinines have also been isolated (**Figure 1, B**).^[12,13]

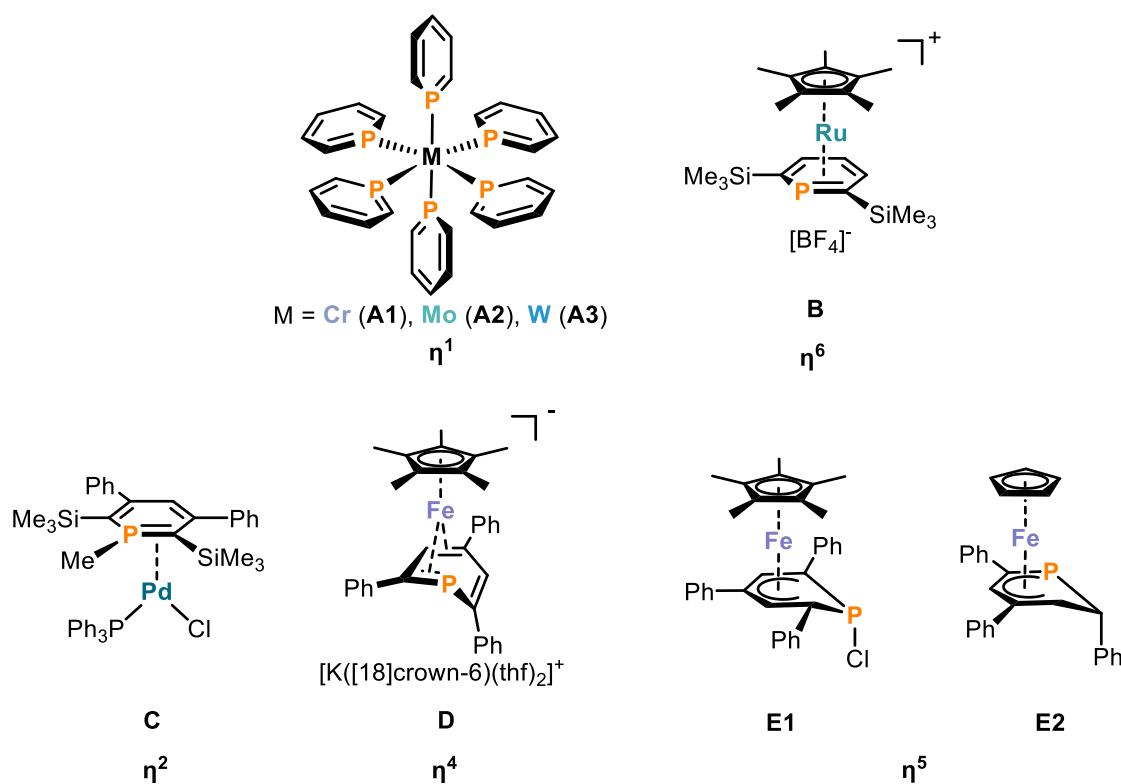


Figure 1. Selected examples of the more common coordination modes of transition metal phosphinine complexes.

Contrary to the previously mentioned coordination modes, the η^2 -coordination *via* the P=C double bond is rather rare and has only been observed for a λ^4 -phosphinine in palladium and platinum (II) complexes.^[14] Similarly, there are only few reports on both η^4 - and η^5 -coordination modes of the phosphinine.^[15–18] One example for the η^4 coordination is the ferrate **D**, in which the η^4 coordination of the phosphinine ligand *via* a PC₃ moiety has been calculated to be energetically favoured compared to the η^4 coordination *via* a C₄ unit.^[15] The opposite trend is usually observed for η^5 -coordinating phosphinines, which is most often observed for λ^4 -phosphinines. In this type of complex the phosphorus atom bears an additional substituent and is bent out of the C₅ plane of the ligand (e.g. **E1**, **Figure 1**).^[16,17] Contrary to this trend, however, *Nief* and *Fischer* reported the iron complex [CpFe{ η^5 -(2,4,6-Ph₃C₅H₃P)}] (**E2**), which incorporates the phosphorus atom in the η^5 -coordination *via* a PC₄ moiety.^[18]

Besides these coordination modes, phosphinines are also capable of coordinating to more than one metal center (**Figure 2**). This can occur by coordination *via* the π -system combined with σ -coordination *via* the phosphorus lone pair, resulting in a $\mu, \eta^6: \eta^1$ -coordination. The first examples for this type of coordination were complexes **F1-3**, which were obtained upon heating group 6 carbonyls together with 4-cyclohexylphosphinine.^[19] The very rare $\mu, \eta^1: \eta^1$ -coordination of a phosphinine *via* the phosphorus atom was observed in complex **G**, which was synthesised by the reaction of the bidentate **NIPHOS** with [Ir₂Cl₂(cod)₂] or [RhCl₂(nbd)₂] (nbd = norbornadiene), followed by an anion exchange reaction with Na[SbF₆].^[20] Interestingly, for the iridium dimer **G**, the pyridine moieties face each other, which is presumed to result in an increased stabilisation of the dimer through π - π stacking. This might explain the preferred formation of the dimeric dication **G** over a neutral monomer, such as [IrCl(**NIPHOS**)(cod)]. Recently, *Mansel* reported the molybdenum complex **H** with a $\mu, \eta^6\text{-}\kappa^2\text{-}\eta^1: \eta^6$ -coordination mode. This unique motif was obtained upon heating the initially formed dinuclear molybdenum carbonyl phosphinine, which featured an η^6 -coordination of each molybdenum metal to one phosphinine moiety, with [PdCl₂(cod)].^[21] Nevertheless, reports on di- or multinuclear phosphinine complexes still remain scarce.

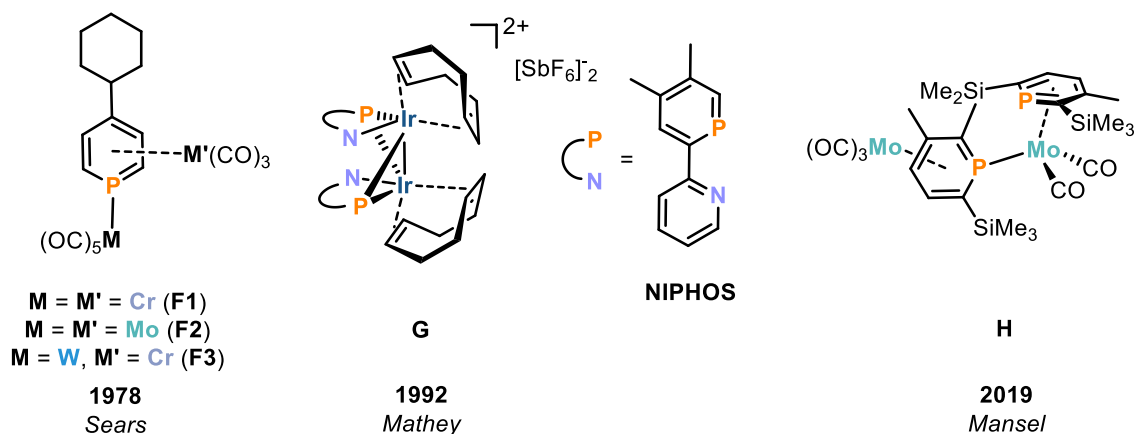
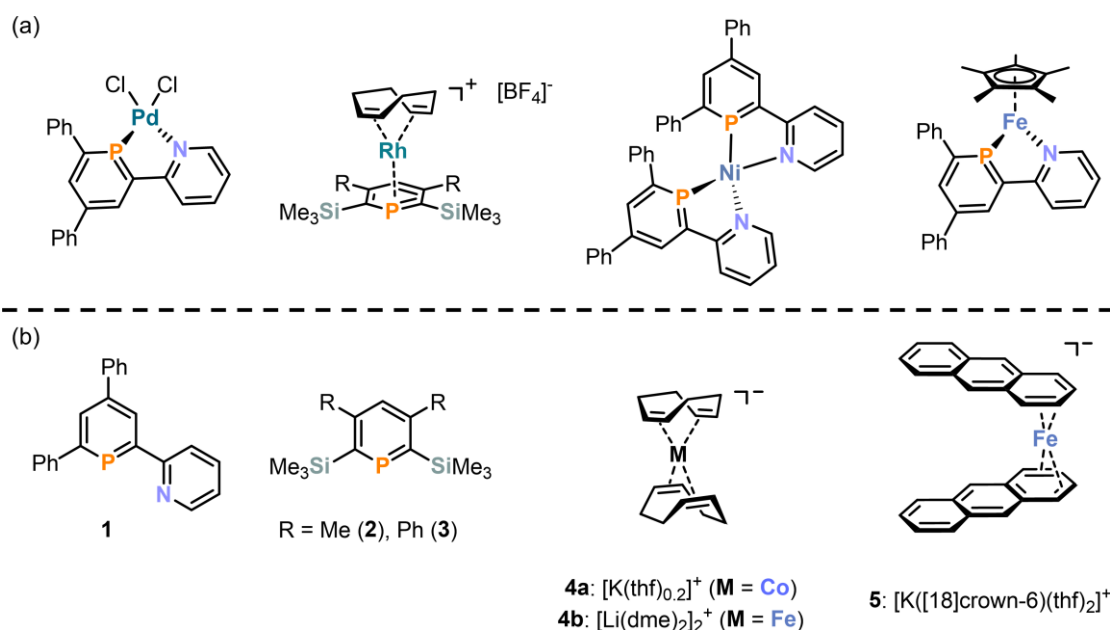


Figure 2. Selected dinuclear phosphinine transition metal complexes.

Phosphinines **1-3** have been used as ligands for transition metal complexes (**Scheme 1**).^[12-14,22] However, whilst most reports have focused on 4d and 5d transition metals, our group recently found that complexes based on 3d transition metals such as nickel^[23] and iron^[24] also possess interesting capabilities in the activation of carbon halogen bonds and carbon dioxide, respectively. Based on these results, the reactivity of different metallates towards phosphinines **1-3** was investigated, with the expectation that the resulting complexes might exhibit interesting properties in the activation of small molecules.



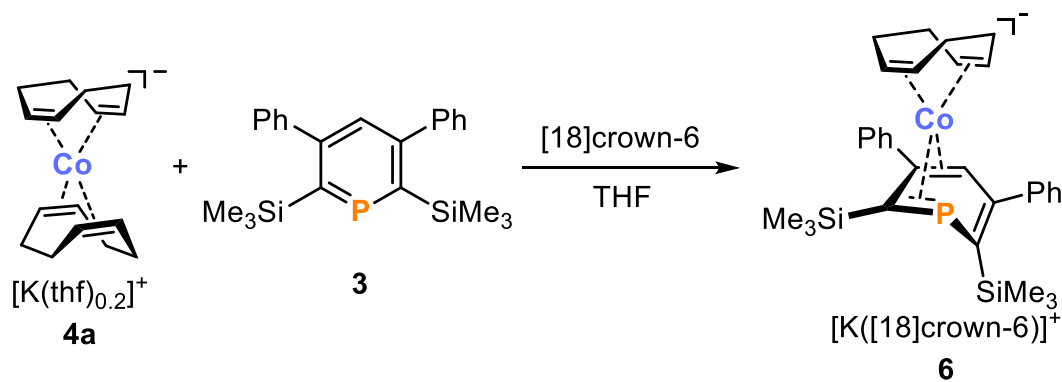
Scheme 1. Previously reported transition metal phosphinine complexes (a) and the phosphinines and metallates investigated in this work (b).

5.2 Results and Discussion

Initially, the reactivity of the metallates **4a** and **4b** towards P,N-phosphinine **1** was investigated. The ³¹P NMR spectra revealed the formation of several new phosphorus species upon adding a solution of potassium cobaltate **4a** to a three-fold excess of **1** at -30 °C. Besides remaining free phosphinine, the most prominent signal (~ 40% P-content according to the integration of the ³¹P{¹H} NMR spectrum) appears as a broad singlet at 137 ppm. When the reaction was repeated with two equivalents of **1**, full consumption of the free phosphinine was observed in the ³¹P{¹H} NMR spectrum. However, no product signals were detected. Interestingly, the previously observed main signal at 137 ppm (1:3 stoichiometry) was not detected in this spectrum. The silent ³¹P{¹H} NMR spectrum indicates the formation of either a paramagnetic complex or a complex involved in dynamic processes in solution. When the reaction was performed with ferrate **4b** instead of **4a**, no signal was observed in the ³¹P NMR spectra besides small amounts of unreacted phosphinine **1**, hinting at the formation of a paramagnetic species. Similar results were obtained when bis(anthracene)ferrate **5** was used. For the latter case, the starting material **1** was completely consumed. This was accompanied by the formation of signals at -0.8, 56.5 and 57 ppm in the ³¹P{¹H} NMR spectrum, which are presumed to belong to side products. Due to the very broad

^1H NMR spectrum, the main product of this reaction is presumed to be paramagnetic and thus likely not observed in the $^{31}\text{P}\{^1\text{H}\}$ NMR spectrum. Unfortunately, the structures of the formed products remain ambiguous as various crystallisation attempts have failed in isolating the formed species due to their high tendency to form oils.

The reaction of bis(trimethylsilyl)-substituted phosphinines **2** and **3** with **4a** was investigated next. When the phosphinines **2** or **3** were combined with **4a** in an equimolar ratio, incomplete and slow conversion of the free phosphinine was observed in the $^{31}\text{P}\{^1\text{H}\}$ NMR spectra for both cases. Unfortunately, the reaction of the dimethyl-substituted phosphinine **2** with **4a** was rather unselective, resulting in the formation of several new resonances in the $^{31}\text{P}\{^1\text{H}\}$ NMR spectrum. No significant change in the phosphorus spectra was observed after further 0.5 equivalents of **4a** were added in order to promote the full consumption of the phosphinine. Contrary to this, a rather slow, yet selective conversion to a single phosphorus species was detected in the $^{31}\text{P}\{^1\text{H}\}$ NMR spectrum (singlet at -4.7 ppm), when the reaction was performed with the diphenyl-substituted phosphinine **3**. Although 50-60% of the starting material is converted within the first 24 h (according to the integration of the ^{31}P NMR spectra), the reaction slows down drastically afterwards. As **3** is not fully consumed, even after several weeks, another 0.5 equivalents of **4a** were added, which resulted in the full consumption of the free phosphinine within the span of three weeks. The formed heteroleptic cobaltate **6** was isolated in a moderate yield (15 mg, 38%, **Scheme 2**).



Scheme 2. Synthesis of phosphinine cobaltate **6** bearing the phosphinine in the rare η^4 -coordination mode.

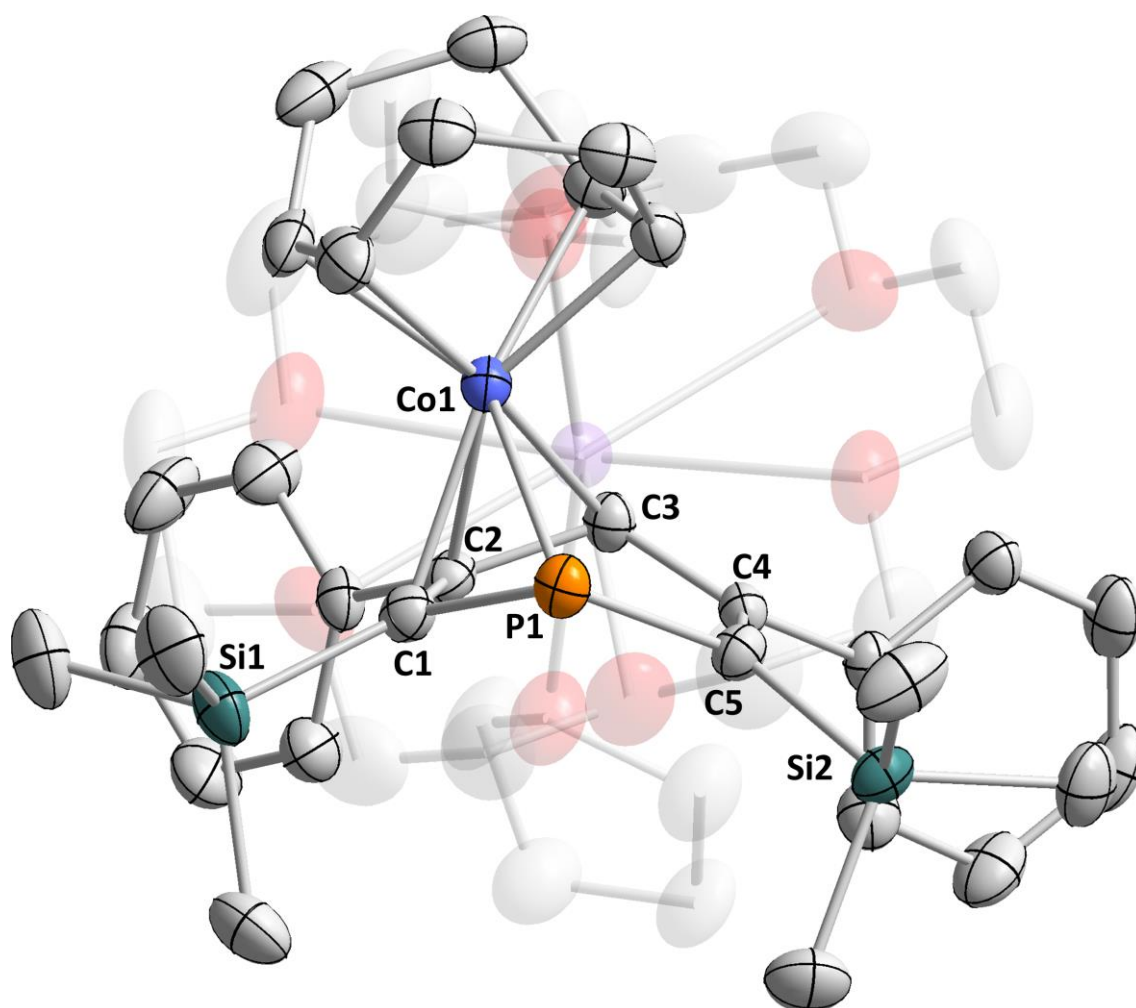


Figure 3. Solid-state molecular structure of **6**. Thermal ellipsoids are set at the 50% probability level. $[K([18]crown-6)(thf)_2]^+$ is transparent and hydrogen atoms are omitted for clarity. Selected bond lengths [Å] and angles [°]: Co1–P1 2.320(1), Co1–C1 2.056(3), Co1–C2 2.022(3), Co1–C3 2.081(3), P1–C1 1.826(3), C1–C2 1.417(5), C2–C3 1.449(4), C3–C4 1.480(4), C4–C5 1.352(4), P1–C5 1.836(3), C1–P1–C5 101.8(2).

Crystals suitable for single-crystal X-ray diffractometry were obtained after storing a THF solution of the extracted product, layered with *n*-hexane for 6 months (**Figure 3**, b). The solid-state molecular structure of **6** displays η^4 -coordination for both the 1,5-cyclooctadiene and the phosphinane. Whilst this η^4 -coordination is the typical bonding mode for cod, it is rather rare for phosphinanes and has previously only been observed in 2,4,6-triphenylphosphinine iron complexes.^[15,25] The only other reported phosphinine cobalt complex was reported by *Le Floch* and involved an η^1 -coordination of a cobalt to two biphosphinine ligands.^[26] The Co1–C(cod) bond lengths of **6** (2.000(3)–2.055(3) Å) are similar to **4a**-[2.2.2]-cryptand (2.047(2)–2.057(2) Å).^[27] The Co1–C1/C2/C3 bonds (2.022(3)–2.080(3) Å), whilst the Co1–P1 bond lengths of the phosphinine are comparable (2.319(1) Å). The phosphinine is folded along the P1–C3 axis (fold angle: 45.1(2)°), displaying a slightly smaller fold angle than the

phosphinine ligand in the previously reported potassium ferrate [K([18]crown-6)(thf)₂][Cp*Fe(η^4 -2,4,6-triphenylphosphinine)] (average fold angle: 48.7°)¹.^[15] Upscaling of the reaction has so far been unsuccessful due to the very long reaction times. Only the starting material was observed when the reaction mixture was heated to 60 °C for 2 h. However, various new ³¹P resonances were detected when the mixture was heated to 60 °C for 18 h. Another attempt to increase the reaction rate was to use irradiation. Potassium cobaltate **4a**, however, is not stable towards irradiation ($\lambda=365$ nm, 10 W), and decomposes by the formation of insoluble black precipitate, presumably metallic cobalt. Furthermore, an increasingly strong signal-broadening was detected in the ¹H NMR spectrum indicating the presence of metallic, paramagnetic cobalt in the sample. Upon irradiating **4a** in the presence of **3**, neither the formation of the grey solid, nor signal-broadening in the ¹H NMR spectrum was observed. The reaction solution of **3** and **4a** was monitored by ¹H and ³¹P{¹H} NMR spectroscopy after 2, 4 and 21 h of irradiation. Unfortunately, whilst **6** was cleanly formed without any observable side products, the reaction rate did not increase significantly. Based on the signal intensity in ³¹P{¹H} NMR spectrum, the conversion was determined to be 27%, 36% and 62% after 2, 4 and 21 h of irradiation, respectively, which is only slightly higher, when compared to the non-irradiated reaction (vide supra).

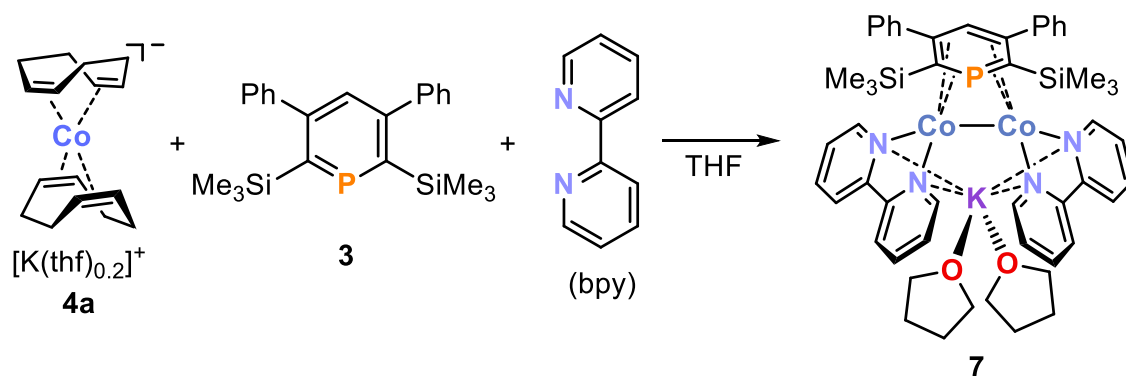
Since **6** possesses a rather labile cod ligand, often allowing access to ligand exchange reactions, the reactivity of **6** towards small molecules such as P₄ was investigated. The reaction of **6** with one equivalent of P₄ in THF resulted in the immediate formation of an insoluble black precipitate. The ³¹P{¹H} NMR spectrum of the supernatant solution reveals the complete consumption of P₄ accompanied by the reformation of free phosphinine **3**. Other signals, besides that of **3** were not observed. Therefore, it was assumed, that the formed precipitate contains cobalt-phosphide particles.^[28] Unfortunately, isolation or crystallisation of the formed precipitate was not possible. The reaction of **6** with *tert*-butyl phosphalkyne was investigated next. The ³¹P{¹H} NMR spectrum of the reaction solution shows the full consumption of the phosphalkyne together with the formation of multiple phosphorus containing species. Besides the main product (ca. 45% P content) detected as a singlet at 3.6 ppm, the ³¹P{¹H} NMR spectrum also reveals the release of free phosphinine **3** (ca. 14%). Similar to the reaction of **6** with P₄, isolation or crystallisation of the formed phosphorus-containing species was not successful.

Upon exposing a THF solution of **6** to a CO₂ atmosphere (1 bar), complex **6** was completely consumed within 6 h accompanied by the appearance of a new signal at 74.8 ppm and the characteristic signal of the free phosphinine ligand **3** in a ratio of roughly 1:1 as observed in the

¹ The unit cell contains two disordered ferrate molecules. Thus, the given value is the average calculated based on the fold angles of these molecules.

$^{31}\text{P}\{^1\text{H}\}$ NMR spectrum. The ^1H NMR spectrum of the reaction solution also reveals broadened signals hinting at the formation of a paramagnetic cobalt species, most likely metallic cobalt particles, due to decomposition of **6**. The $^{31}\text{P}\{^1\text{H}\}$ NMR spectrum of the reaction solution after one day at room temperature displays various new signals corresponding to unidentified species, while the intensity of the signal of the presumed product at 74.8 ppm is strongly diminished, indicating its low stability.

Due to the previously mentioned difficulties in the synthesis and isolation of **6**, attempts have been made to develop a one pot procedure to further investigate the reactivity of **6** (Scheme 3). When **3** was reacted with **4a** and 2,2'-bipyridine (bpy) in a 1:2:4 stoichiometry in THF at $-30\text{ }^\circ\text{C}$, the $^{31}\text{P}\{^1\text{H}\}$ NMR spectrum of this reaction solution revealed the formation of a new species apparent as a singlet at -47 ppm accompanied by the formation of the intermediate **6**. Similar to the reaction of **3** with **4a**, leading to **6**, this reaction was also rather slow. A deep purple powder was isolated after stirring the reaction solution for 6 weeks, followed by slow precipitation from THF/*n*-hexane. The $^{31}\text{P}\{^1\text{H}\}$ NMR spectrum of this purple solid showed only a singlet of very low intensity at 47 ppm, which very probably belongs to an unidentified impurity. Repeated recrystallisation attempts of this powder yielded small amounts of purple crystals suitable for X-ray diffraction measurements (Figure 4).



Scheme 3. Synthesis of the dinuclear phosphinine cobaltate complex **7**.

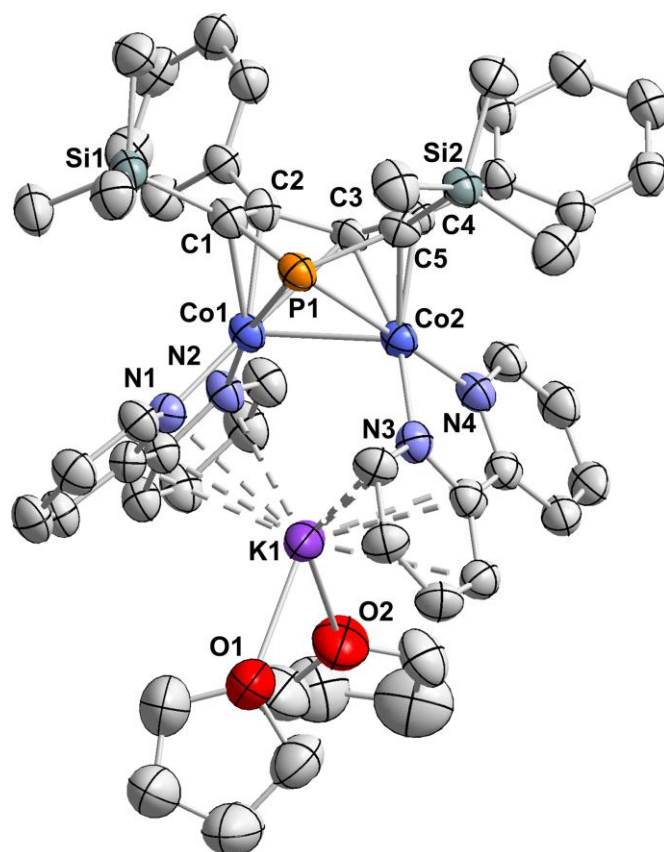


Figure 4. Solid-state molecular structure of **7**. Thermal ellipsoids are set at the 50% probability level. Disorder and hydrogen atoms are omitted for clarity. Selected bond lengths [\AA] and angles [$^\circ$]: Co1–Co2 2.516(1), Co1–P1 2.416(2), Co2–P1 2.421(2), Co1–C1 2.062(5), Co1–C2 2.018(5), Co1–C3 2.338(5), Co1–N1 1.924(4), Co1–N2 1.942(4), Co2–C3 2.229(5), Co2–C4 2.002(5), Co2–C5 2.083(5), Co2–N3 1.914(4), Co2–N4 1.914(4), Co1–P1–Co2 62.71(4), C1–P1–C5 105.2(2).

A single crystal X-ray diffraction experiment confirmed the molecular structure of $[\text{K}(\text{thf})_2\text{Co}_2(\text{bpy})_2(\mu, \eta^4: \eta^4\text{-}(3,5\text{-Ph}_2\text{-}2,6\text{-}(\text{SiMe}_3)_2\text{-PC}_5\text{H}))]$ (**7**).² The structure contains two cobalt atoms connected by a Co–Co bond and the phosphinine bearing a $\mu, \eta^4: \eta^4$ -coordination mode. A similar coordination mode was previously observed for arene derivatives in a few dinuclear complexes.^[30] The cobalt atoms are additionally coordinated by one bpy ligand each, between which the potassium counterion is located in the solid state molecular structure. The Co–Co distance (2.516(1) \AA) of **7** is well within the range of typical Co–Co single bonds.^[31] The Co1–C1/C2 and Co2–C4/C5 bond lengths (2.002(5)–2.083(5) \AA) in **7** are similar to the corresponding

² An analogous structure was also obtained during the reaction of **6** with CO in the presence of 2 equivalents of bpy. The reaction mixture yielded two differently coloured crystals, colourless and purple. A preliminary WhatIsThis X-ray diffraction measurement suggested the colourless crystals to consist of $[\text{K}([18]\text{crown-}6)][\text{Co}(\text{CO})_4]$, which was already observed by *Ellis* as $[\text{K}([2.2.2]\text{cryptand})][\text{Co}(\text{CO})_4]$.^[29] For the purple crystals, the WhatIsThis X-ray diffraction measurement suggested the formation of $[\text{K}([18]\text{crown-}6)][\text{Co}_2(\text{bpy})_2(\mu, \eta^4: \eta^4\text{-}(3,5\text{-Ph}_2\text{-}2,6\text{-}(\text{SiMe}_3)_2\text{-PC}_5\text{H}))]$, an analogous complex to **7**.

bond lengths in **6**, whilst the P1–Co1/Co2 (2.416(2) and 2.421(2) Å, respectively) are slightly longer. The Co1/Co2–C3 bond lengths are considerably longer (2.338(5) and 2.229(5) Å, respectively) than observed in **6**. The phosphinine ligand in **7** is folded along the P1–C3 axis. The fold angle (43.16(4) °) is similar to that in **6** (45.1(2)°). The Co–N bond lengths are within the usual range of bpy ligands coordinating to cobalt atoms (1.91–1.94 Å).^[32] The K⁺ cation is coordinated by two THF molecules and lies between the two bpy ligands (K–N distance: 3.044 Å, K–C distance: 3.19 Å)³. The C–C and C–N bond-distances within the bpy ligands fit well with [K([2.2.2]cryptand)][Co(cod)(bpy)] reported by Ellis^[27] (1.35–1.42 and 1.37–1.40 Å, respectively), which hints at the presence of a coordinated bpy radical anion (bpy^{•−}, see **5.4.4, Table 2**).^[33,34]

Complex **7** contains at least one unpaired electron rendering the complex paramagnetic. In accordance with this, the ¹H NMR spectrum showed broad signals and the ³¹P and ¹³C{¹H} NMR spectra were silent. The magnetic moment of **7** was determined by the Evans method (THF-*d*₈, μ_{eff} = 3.42 μ_B) lies between the spin-only values for two and three unpaired electrons (2.83 and 3.87 μ_B, respectively).^[35] This may suggest that **7** possesses a quartet spin state.⁴ Complex **7** was also investigated by EPR spectroscopy in a frozen THF solution at 77 K. Multiple samples were measured, all of which revealed the presence of two signals in the EPR spectrum. The relative intensity of these two signals was not consistent, indicating that one of them could be due to an unidentified impurity. Although no EPR spectrum of a pure sample was obtained, repeated recrystallisation of **7** allowed for the measurement of a comparably clean EPR spectrum (**Figure 5**, c.f. section **5.4.3, Figure 50** for a comparison), which shows a broad rhombic signal that was tentatively simulated with the principal components $g_{11} = 2.42$, $g_{22} = 1.95$, and $g_{33} = 1.97$ in the quartet state. Similar results are obtained, when the spectrum is simulated in the doublet ground-state (see **5.4.3, Figure 51**). Thus, the measured spectra do not give precise information regarding the spin state of **7**. Unfortunately, due to the broad signals in the EPR spectra, no hyperfine couplings can be observed.

³ Average values for the bond distances marked in **Figure 4**.

⁴ Due to the odd number of electrons, compound **7** cannot possess a triplet spin state.

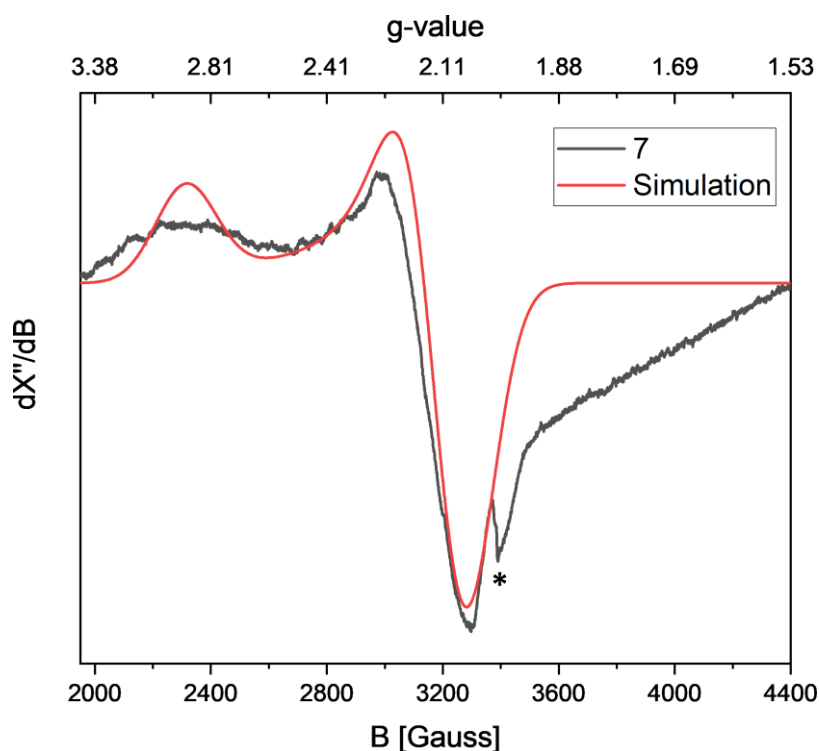


Figure 5. Experimental (black) and simulated (red) X-band EPR spectra of **7** recorded in THF at 77 K. Experimental parameters: microwave frequency, 9.448213 GHz; modulation amplitude, 3.000 G (red), 3.000 G (black). The experimental spectrum of **7** was fitted with the following parameters for a $S = 3/2$ system. $g_{11} = 2.42$, $g_{22} = 1.95$, $g_{33} = 1.97$, * unidentified impurity.

DFT calculations utilising r^2 SCAN-3c, a method constructed by *Grimme* and co-workers,^[36] were performed in order to further unravel the electronic situation present in the dinuclear complex **7**. The geometry was optimised with the conductor-like polarizable continuum model (CPCM) for three different ground-state multiplicities ($S = 1/2, 3/2, 5/2$; for details, see 5.4.5). The optimised geometries were in good agreement with the structure determined by single-crystal X-ray crystallography. Analysis of the total energy of the different multiplicities suggest that the doublet and the quartet state are very similar in energy ($\Delta E = 0.3 \text{ kcal}\cdot\text{mol}^{-1}$ in favour of the quartet). The sextet state was calculated to be much higher in energy ($\Delta E = 9.9 \text{ kcal}\cdot\text{mol}^{-1}$). Single point calculations on the r^2 SCAN-3c optimised geometries for the three multiplicities were also performed at the PBE0^[37]/def2-TZVPP^[38] level of theory. The sextet state remains the energetically least favourable ($\Delta E = 19.6 \text{ kcal}\cdot\text{mol}^{-1}$) state, but the quartet state increases in energy ($\Delta E = 8.1 \text{ kcal}\cdot\text{mol}^{-1}$) resulting in the doublet state being the energetically lowest state, i.e. ground-state.

The spin-density according to a Mulliken population analysis is mainly localised on the cobalt nuclei for both the doublet and the quartet state. Analysis of the SOMOs of **7** with $S = 1/2$ and $3/2$ reveals that for the doublet-state of **7**, the SOMO shows strong ligand character, further hinting at the presence of a bpy radical anion (**Figure 6, a**). A similar trend is observed in the case of the quartet state of **7**, where only one of the three SOMOs exhibits a high d-orbital character, whilst the other two SOMOs feature strong contributions from bpy and the phosphinine (**Figure 6, b**).

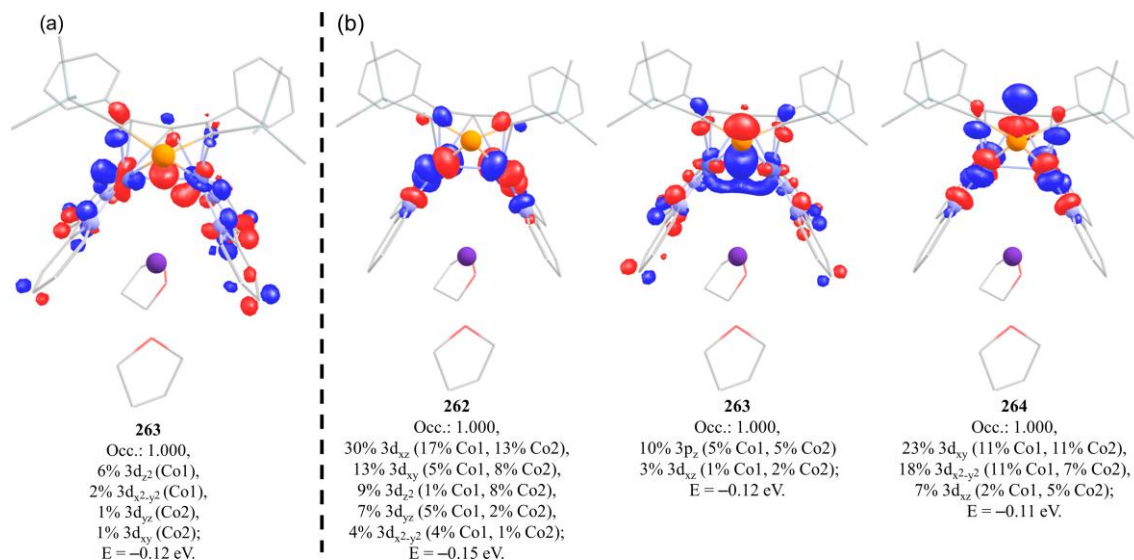


Figure 6. Single occupied molecular orbitals of **7** in the spin states $S = 1/2$ (a) and $S = 3/2$ (b) obtained from calculations using the r^2 SCAN-3c method. The contour plots are displayed with an isosurface value of 0.05 a.u..

5.3 Conclusion

The reactivity of phosphinines **1-3** towards metallates **4a-b** and **5** was investigated. The slow, yet selective formation of cobaltate **6** was observed upon addition of **4a** to the bis(trimethylsilyl)-substituted phosphinine **3**. Complex **6** is the second example of a phosphinine cobalt complex and the first cobalt complex to employ a phosphinine ligand in the rare η^4 -coordination mode. While the complex clearly is highly reactive, investigations of the follow-up chemistry of **6** with P_4 , $t\text{-BuCP}$ and CO_2 failed to give tractable reaction products. However, the addition of bpy gives the highly unusual complex $[\text{K}(\text{thf})_2\text{Co}_2(\text{bpy})_2(\mu, \eta^4:\eta^4\text{-(3,5-Ph}_2\text{-2,6-(SiMe}_3\text{)}_2\text{-PC}_5\text{H)})]$ (**7**), which features the phosphinine as a bridging doubly η^4 -coordinated ligand. A similar coordination mode was previously only observed for arenes. The dinuclear complex **7** contains an uneven number of electrons and is thus paramagnetic. The electronic properties were further investigated by Evans NMR, EPR, as well as quantum chemical calculations. Based on all of the available data, the ground state of **7** is presumed to be the quartet state ($S = 3/2$). Furthermore, both the single crystal X-ray analysis and theoretical calculations indicate the presence of bpy radical anions ($\text{bpy}^{\cdot-}$). Based on the EPR spectra, however, clean isolation of **7** has so far not been accomplished, yet. Due to the intriguing structure of this dinuclear complex and its unexplored reactivity, the clean isolation and investigation of its reactivity will be of great interest.

5.4 Experimental Details

General Synthetic Methods

All reactions and product manipulations were carried out in flame-dried glassware under an inert atmosphere of nitrogen using standard Schlenk-line or glovebox techniques (maintained at <0.1 ppm H₂O and <0.1 ppm O₂). **4a** was synthesised according to a procedure by *Jonas*.^[39] Phosphinines **1-3** and metallates **4b** and **5** were graciously provided by the *Müller* and the *Wolf* group, respectively.

All other chemicals were purchased from commercial suppliers and used without further purification.

Solvents were dried and degassed with a MBraun SPS800 solvent purification system. All dry solvents except *n*-hexane and *n*-pentane were stored under argon over activated 3 Å molecular sieves in gas-tight ampules. *n*-Hexane and *n*-pentane were stored over potassium mirrors.

General Analytical Techniques

NMR spectra were recorded on Bruker Avance 300 or 400 spectrometers at 300 K unless otherwise noted and internally referenced to residual solvent resonances (¹H NMR: THF-d₈: 1.72 ppm, C₆D₆: 7.16 ppm; ¹³C{¹H} NMR: THF-d₈: 25.31 ppm, C₆D₆: 128.06 ppm). Chemical shifts δ are given in ppm referring to external standards of tetramethylsilane (¹H, ¹³C{¹H}) or 85% phosphoric acid (³¹P and ³¹P{¹H} spectra).

Elemental analysis was performed by the Central Analytical Services department of the University of Regensburg.

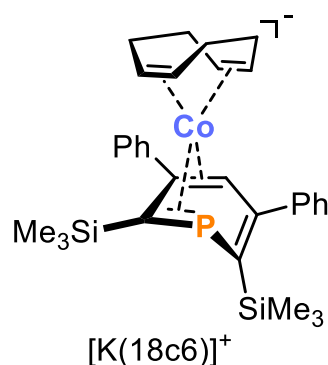
Mass spectra were performed with Jeol AccuTOF GCX EI-MS (LR/HR) by the analytical Department of Regensburg University.

The X-Band EPR measurements were carried out with a MiniScope MS400 device with a frequency of 9.5 GHz and rectangular resonator TE102 of the company Magnettech GmbH. Computer simulations of the EPR spectra were carried out with EasySpin toolbox in MATLAB. Single-crystal X-ray diffraction data were recorded on a Rigaku Oxford Diffraction SuperNova Atlas or a XtaLAB Synergy R (DW system, Hypix-Arc 150) device with Cu-K_α radiation (λ = 1.54184 Å). Crystals were selected under mineral oil, mounted on micromount loops and quench-cooled using an Oxford Cryosystems open flow N₂ cooling device. Either semi-empirical multi-scan absorption corrections^[40] or analytical ones^[41] were applied to the data. The structures were solved with SHELXT^[42] solution program using dual methods and by using Olex2 as the graphical interface.^[43] The models were refined with ShelXL^[44] using full matrix least squares minimisation on F².^[45] The hydrogen atoms were located in idealised positions and refined.

5.4.1 Synthesis of Compounds

[K([18]crown-6)][(3,5-Ph₂-2,6-(SiMe₃)₂-PC₅H)Co(cod)] (6):

3,5-Diphenyl-2,6-bis(trimethylsilyl)phosphinine (**3**) (20.0 mg, 0.05 mmol, 1.00 equiv.) and [K(thf)][Co(cod)₂] (**4a**) (16.7 mg, 0.05 mmol, 1.00 equiv.) were separately dissolved in THF (2 mL each) and cooled to -30 °C. The solution of **3** was then slowly added to the solution of **4a** resulting in a slow colour change to dark brown/black. After 10 min. [18]crown-6 (13.5 mg, 0.05 mmol, 1.00 equiv.) was added as a solid. The mixture was stirred for three days, before **4a** (8.6 mg, 0.03 mmol, 0.51 equiv.) together with [18]crown-6 (6.8 mg, 0.03 mmol, 0.051 equiv.) was added as a THF solution (1 mL) in order to further promote the reaction towards the desired complex **6**. The solution was then stirred until the phosphinine was completely consumed (3 weeks) as observed *via* the ³¹P{¹H} NMR spectrum. The solvent was removed *in vacuo*, washed with *n*-hexane (3 x 2 mL), the product extracted with toluene, and dried *in vacuo*. Crystals suitable for single crystal X-ray diffraction analysis were obtained upon storing a THF solution of the product, layered with *n*-hexane for 6 months. The elemental analysis (*vide infra*) of these crystals revealed the presence of minor impurities, presumably cobalt particles.



Molecular formula: C₄₃H₆₅CoKO₆PSi₂ (863.16 g·mol⁻¹)

Yield: 15 mg (0.02 mmol, 35%)

¹H NMR (400.13 MHz, 300 K, THF-*d*₈): δ [ppm] = -0.24 (s, Si(CH₃)₃, 9H), -0.09 (s, Si(CH₃)₃, 9H), 0.00-0.24 (m, cod-*H*, 2H), 1.24-1.35 (m, cod-*H*, 2H), 1.80-1.91 (m, cod-*H*, 2H), 2.10-2.34 (m, cod-*H*, 2H), 3.22 (d, ³*J* = 4.8 Hz, 1H), 3.58-3.64 (m, [18]crown-6 + cod-*H*, 28 H), 6.69 (d, ³*J*_{HH} = 7.1 Hz, C_{aryl}H, 2H), 6.75-6.91 (m, C_{aryl}H, 3H), 7.00-7.07 (m, C_{aryl}H, 1H), 7.19 (t, ³*J*_{HH} = 7.3 Hz, C_{aryl}H, 2H), 8.06 (d, ³*J*_{HH} = 7.3 Hz, C_{aryl}H, 2H).

¹³C{¹H} NMR (100.06 MHz, 300 K, THF-*d*₈): δ [ppm] = 2.2 (d, ³*J*_{CP} = 6.6 Hz), 3.2 (d, ³*J*_{CP} = 8.6 Hz), 15.7, 22.0, 24.0, 26.3, 28.9, 30.6, 35.1, 35.8, 36.6, 71.2, 85.8, 110.7, 124.2, 124.8, 126.8, 127.1, 128.9, 131.2, 131.7, 135.2, 150.3, 152.0, 167.1, 167.5.

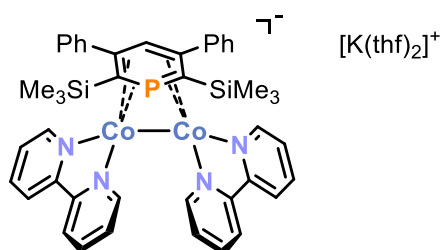
³¹P{¹H} NMR (161.98 MHz, 300 K, THF-*d*₈): δ [ppm] = -4.7.

³¹P NMR (161.98 MHz, 300 K, THF-*d*₈): δ [ppm] = -4.7.

Elemental analysis calculated for C₄₃H₆₅CoKO₆PSi₂: C 59.84, H 7.59; found C 58.37, H 7.44.

[K(thf)₂Co₂(bpy)₂(μ,η⁴:η⁴-(3,5-Ph₂-2,6-(SiMe₃)₂-PC₅H)] (7):

3,5-Diphenyl-2,6-bis(trimethylsilyl)phosphinine (**3**) (30.0 mg, 0.08 mmol, 1.00 equiv.) and [K(thf)][Co(cod)₂] (**4a**) (90.0 mg, 0.16 mmol, 2.04 equiv.) were separately dissolved in THF (2 mL each) and cooled to -30 °C. The solution of **3** was then slowly added to the **4a** solution resulting in a colour change to dark brown/black. After 10 min. a cooled solution of 2,2'-bipyridine (50.0 mg, 0.32 mmol, 4.19 equiv.) in THF (1 mL) was added. The solution was stirred until full consumption of the free phosphinine, which was monitored by ³¹P{¹H} NMR spectroscopy. The solvent was removed *in vacuo* and the crude product washed with *n*-hexane (3 x 1 mL) and extracted in toluene. After removal of the solvent, the product was recrystallised from THF/*n*-hexane to obtain crystals suitable for single crystal X-ray diffraction analysis. As observed *via* EPR (*vide supra*) these crystals contained minor amounts of an unidentified impurity, which was also detrimental in obtaining a suitable elemental analysis.



Molecular formula: C₅₁H₆₁Co₂KN₄O₂PSi₂ (1006.18 g·mol⁻¹)

Yield: 11 mg (0.01 mmol, 13%)

¹H NMR (400.13 MHz, 300 K, THF-*d*₈): δ [ppm] = -0.05 (br s, SiCH₃, 9H), 0.90 (br s, SiCH₃, 9H), 1.74 (br s, OCH₂CH₂, 8H), 3.59 (br s, OCH₂, 8H), 7.23 (br s, C_{aryl}H, 16H), 8.65 (br s, C_{aryl}H, 10H), 13.31 (s, PC(SiMe₃)C(Ph)CH, 1H).

¹³C{¹H} NMR (100.06 MHz, 300 K, THF-*d*₈): silent

³¹P{¹H} NMR (161.98 MHz, 300 K, THF-*d*₈): silent

³¹P NMR (161.98 MHz, 300 K, THF-*d*₈): silent

Magnetic moment (Evans method, THF-*d*₈, 300 K): μ_{eff} = 3.4(3) μ_B

Elemental analysis calculated for C₅₁H₆₁N₄O₂Co₂PKSi₂: C 60.88, H 6.11, N 5.57; found C 61.66, H 5.53, N 6.52.

General Procedure for the Reaction of Phosphinines 1-3 with metallates 4-5:

The desired amounts of phosphinine and metallate were separately dissolved in THF (0.02-0.05 M) and cooled to -30 °C. The phosphinine solution was then slowly added to the metallate solution. The reaction mixture was stirred and the reaction progress monitored by ³¹P{¹H} NMR spectroscopy. The reaction work-up initially involved the removal of the solvent *in vacuo*, followed by washing with *n*-hexane. Extraction with toluene or THF yielded complex reaction mixtures.

Reaction of **6** with **P₄**

A solution of **P₄** (2.5 mg, 0.02 mmol, 1.01 equiv.) in C_6H_6 (197 μ L) was added to a solution of **6** (20 mg, 0.02 mmol, 1.00 equiv.) in THF (0.4 mL). Immediate formation of a black precipitate was observed. The $^{31}P\{^1H\}$ NMR spectrum revealed the formation of free phosphinine **3**.

$^{31}P\{^1H\}$ NMR (161.98 MHz, 300 K, C_6D_6): δ [ppm] = -7.1 (s, complex **6**), 271.0 (s, free phosphinine **3**).

Reaction of **6** with **^tBuCP**

A solution of **^tBuCP** (5.7 μ L, 0.02 mmol, 1.00 equiv.) in toluene was added to a solution of **6** (20 mg, 0.02 mmol, 1.00 equiv.) in C_6D_6 (0.4 mL). The $^{31}P\{^1H\}$ NMR spectrum revealed the formation of free phosphinine **3**.

$^{31}P\{^1H\}$ NMR (161.98 MHz, 300 K, C_6D_6): δ [ppm] = -18.0 (s), -4.1 (s), 3.6 (s), 5.9 (s), 10.0 (s), 271.8 (s, free phosphinine **3**), 331.2 (s).

Reaction of **6** with **CO₂**

A solution of **6** (10 mg, 0.01 mmol, 1.00 equiv.) in THF-*d*₈ (0.4 mL) in a J. Young NMR tube was exposed to an atmosphere of **CO₂** (1 bar) *via* freeze-pump-thaw. 1H and $^{31}P\{^1H\}$ NMR spectra were measured after 6 h and one day.

$^{31}P\{^1H\}$ NMR (161.98 MHz, 300 K, C_6D_6): δ [ppm] = -97.9 (s), 62.4 (s), 74.9 (s), 233.6 (s), 270.7 (s, free phosphinine **3**).

Reaction of **6** with **bpy** and **CO**

Bpy (4.7 mg, 0.03 mmol, 1.01 equiv.) was added to a solution of **6** (30 mg, 0.03 mmol, 1.00 equiv.) in THF (0.5 mL). The mixture was transferred to a J. Young NMR tube, which was exposed to an atmosphere of **CO** (1 bar) *via* freeze-pump-thaw. $^{31}P\{^1H\}$ NMR spectra were measured before and one day after the addition of carbon monoxide.

$^{31}P\{^1H\}$ NMR (161.98 MHz, 300 K, C_6D_6): δ [ppm] = 270.4 (s, free phosphinine **3**).

Attempted Synthesis of **6** Promoted by Irradiation:

3,5-Diphenyl-2,6-bis(trimethylsilyl)phosphinine (**3**) (12.5 mg, 0.03 mmol, 1.00 equiv.) and $[K(thf)][Co(cod)_2]$ (**4a**) (10.5 mg, 0.03 mmol, 1.00 equiv.) were separately dissolved in cooled (-30 °C) THF-*d*₈ (0.4 and 0.2 mL, respectively). The solution of **3** was then slowly added to the **4a** solution and transferred into an J. Young NMR tube. 1H and $^{31}P\{^1H\}$ NMR spectra were recorded before irradiation and after irradiating the solution ($\lambda=353$ nm, 10 W) for 2 h, 4 h and 21 h.

A solution of **4a** (10.5 mg, 0.03 mmol, 1.00 equiv.) in THF-*d*₈ (0.6 mL) was prepared and 1H NMR spectra of the sample were recorded analogously (see SI).

5.4.2 NMR Spectra

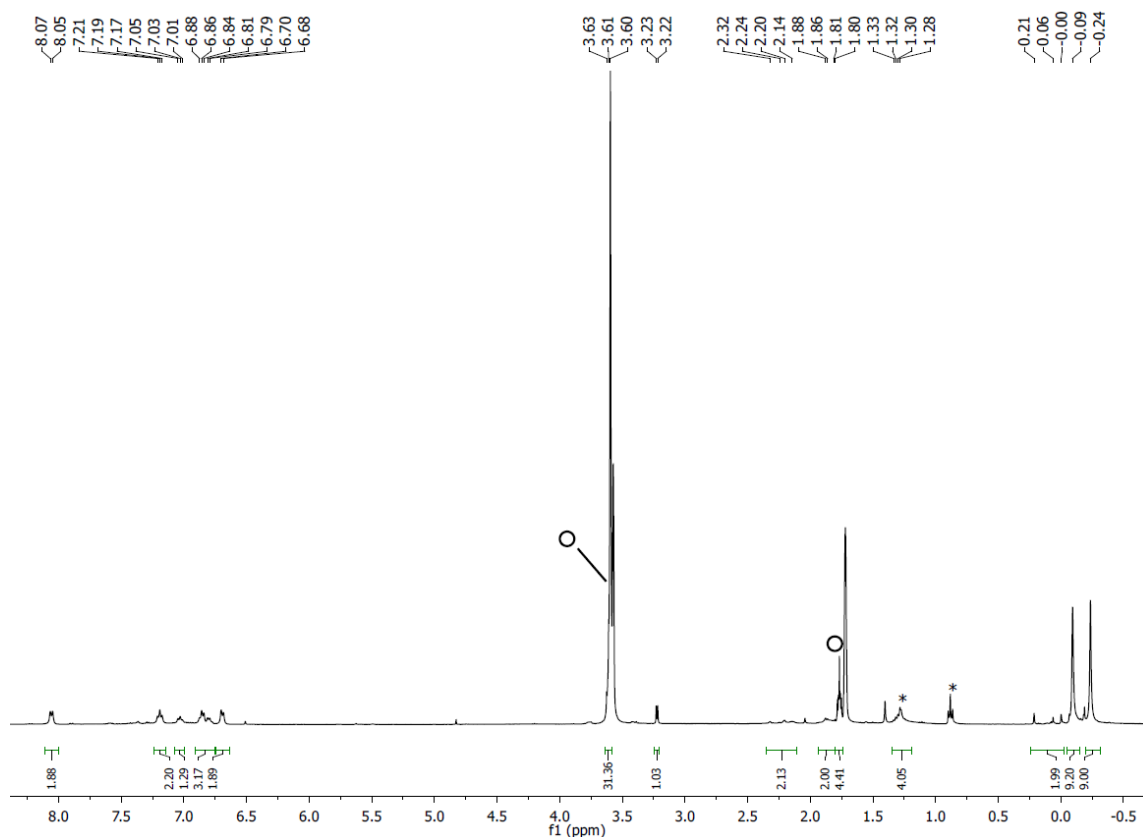


Figure 7. ^1H NMR spectrum (400.13 MHz, 300 K, $\text{THF-}d_8$) of **6**, O THF, * *n*-hexane.

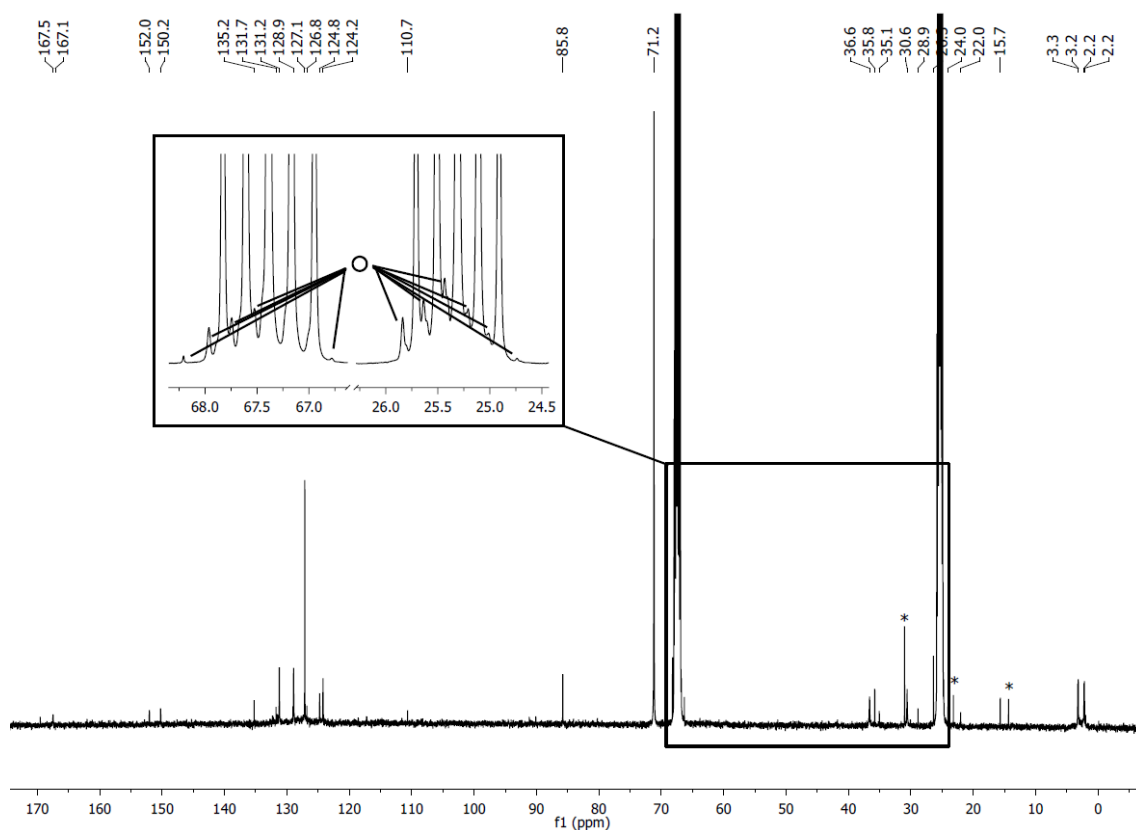


Figure 8. $^{13}\text{C}\{^1\text{H}\}$ NMR (100.06 MHz, 300 K, $\text{THF-}d_8$) of **6**, O THF, * *n*-hexane.

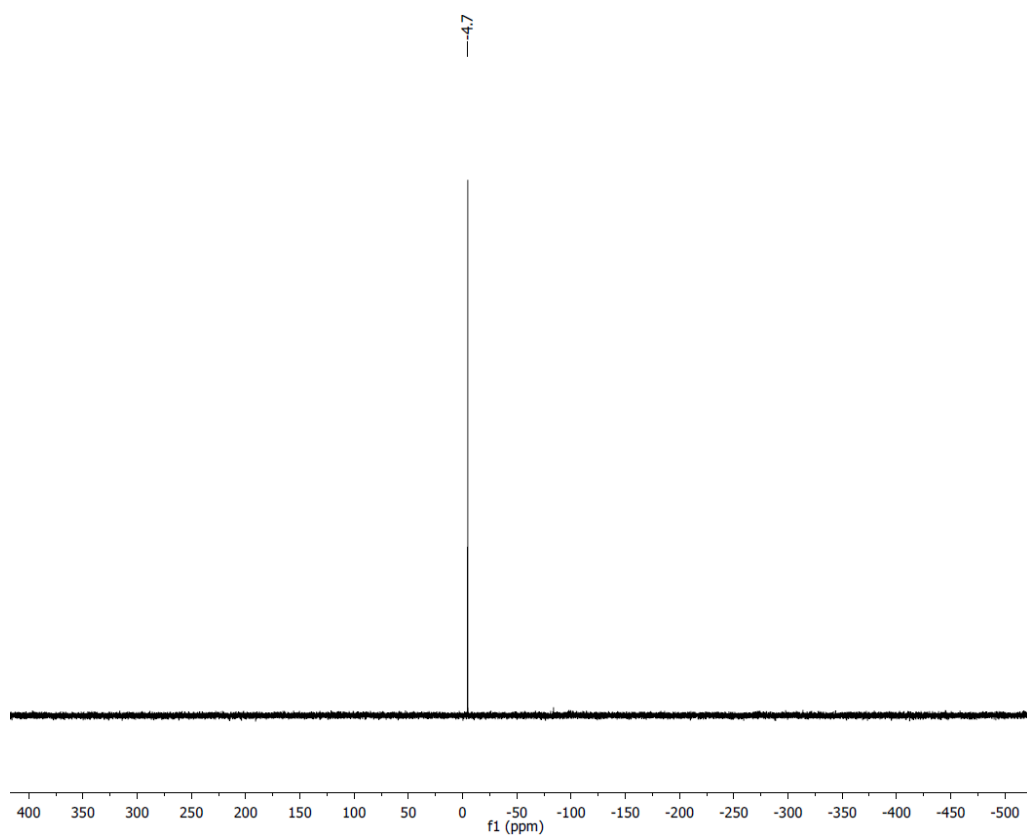


Figure 9. $^{31}\text{P}\{^1\text{H}\}$ NMR (161.98 MHz, 300 K, $\text{THF-}d_8$) of **6**.

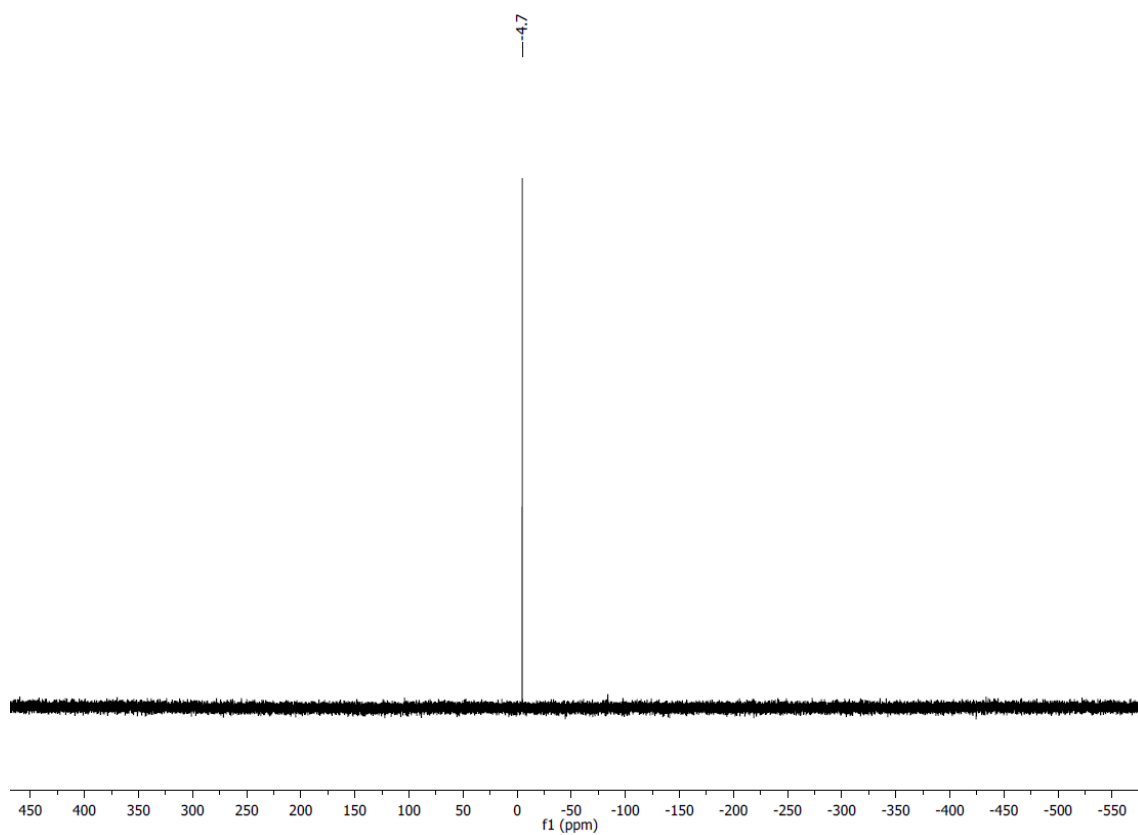


Figure 10. ^{31}P NMR (161.98 MHz, 300 K, $\text{THF-}d_8$) of **6**.

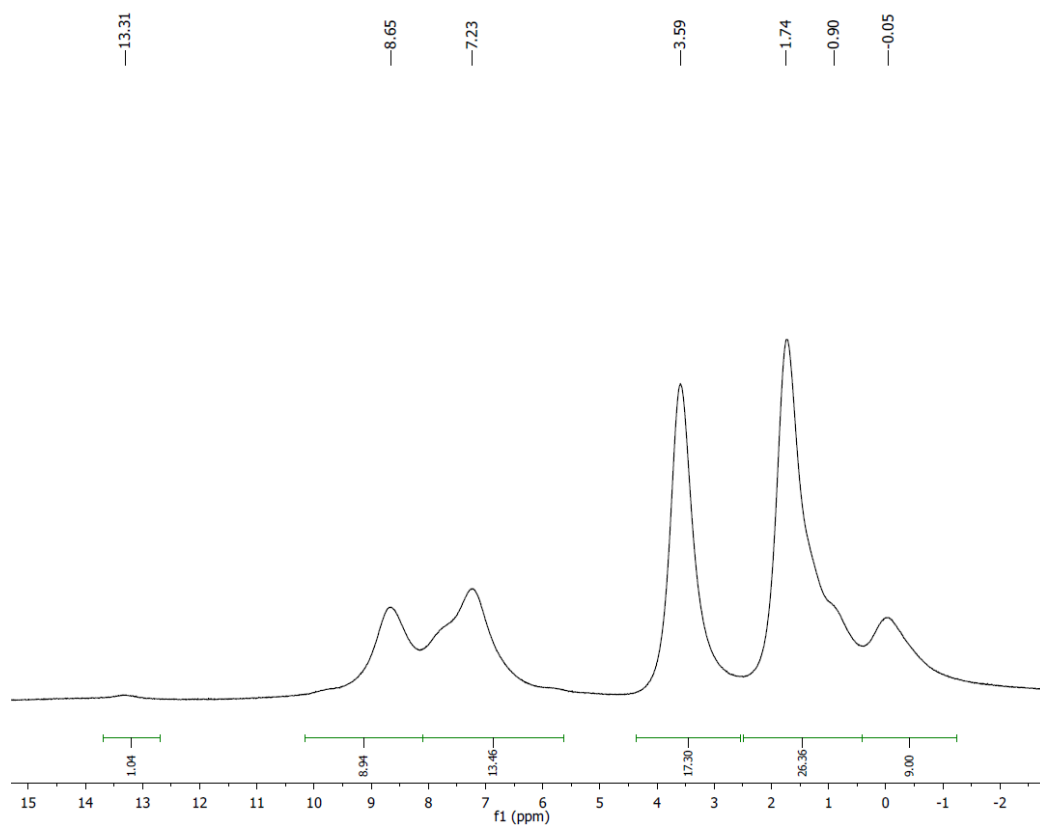


Figure 11. ^1H NMR spectrum (400.13 MHz, 300 K, $\text{THF-}d_8$) of **7**.

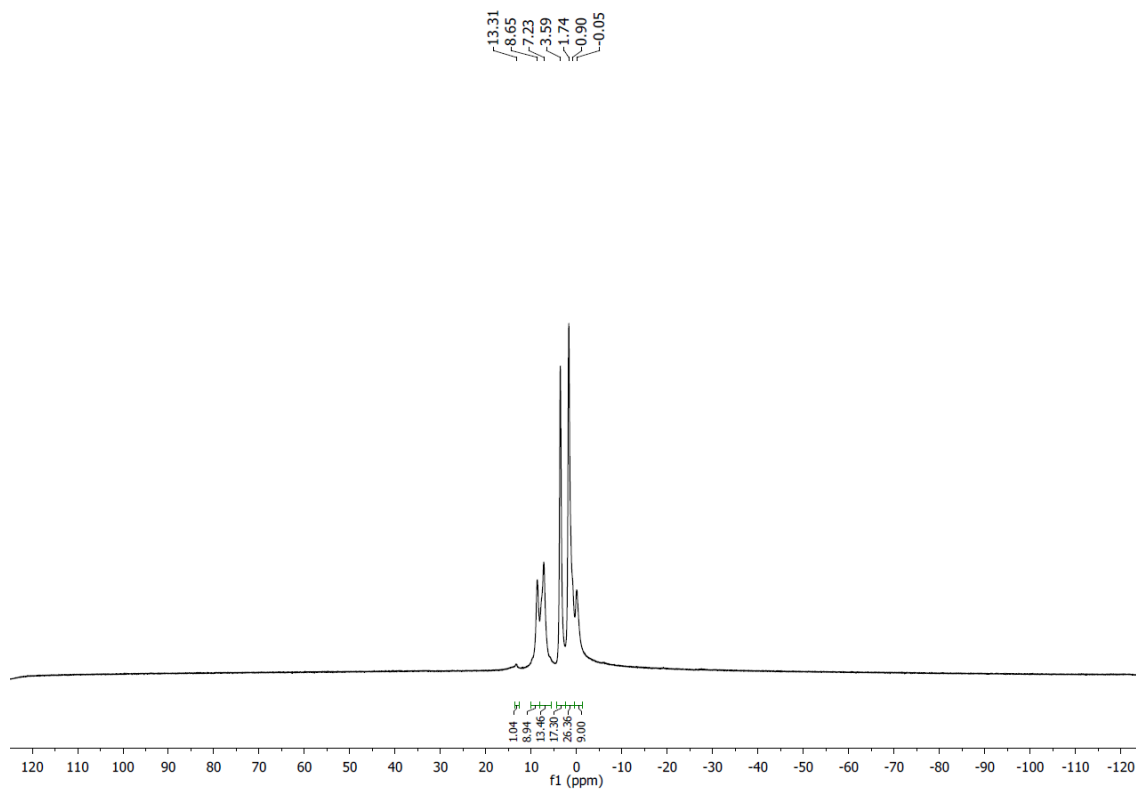


Figure 12. ^1H NMR spectrum (400.13 MHz, 300 K, $\text{THF-}d_8$) of **7**.

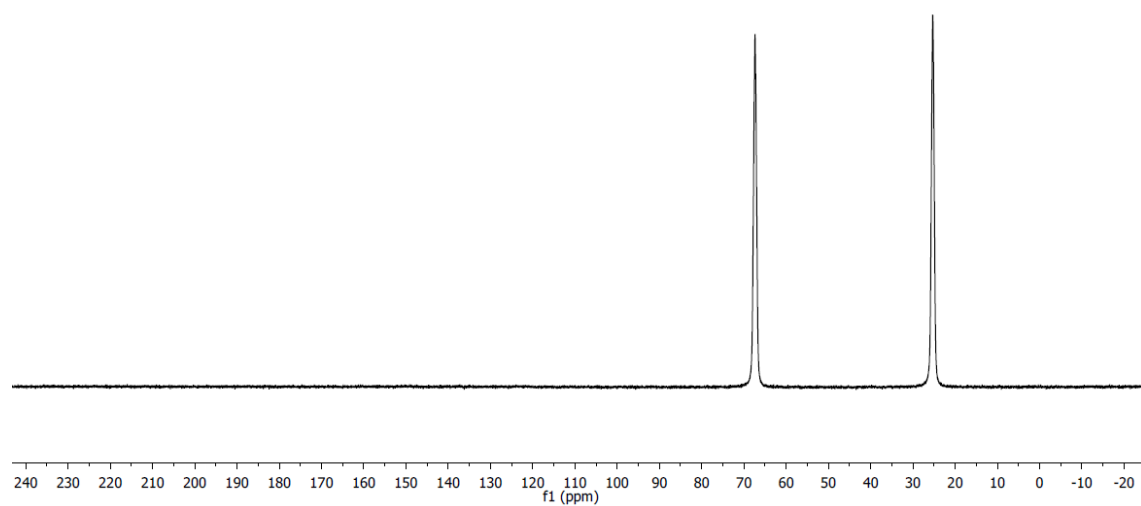


Figure 13. $^{13}\text{C}\{^1\text{H}\}$ NMR (100.06 MHz, 300 K, THF-*d*₈) of **7**.

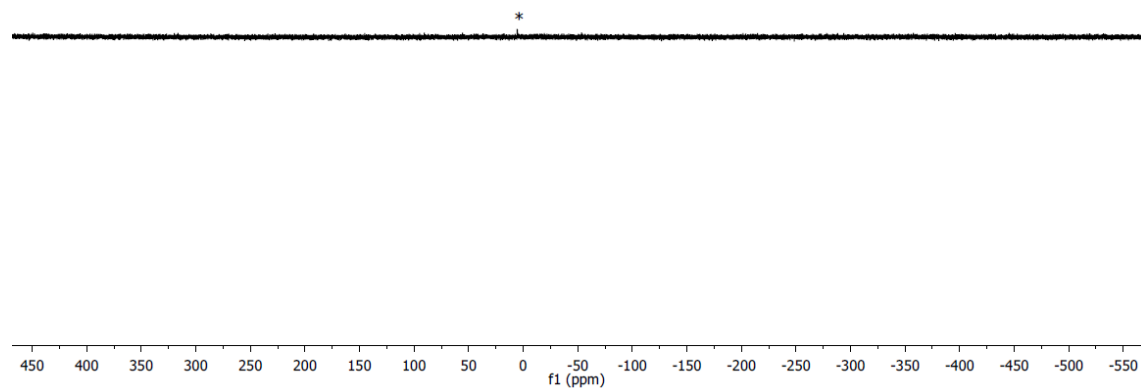


Figure 14. $^{31}\text{P}\{^1\text{H}\}$ NMR (161.98 MHz, 300 K, THF-*d*₈) of **7**, * residual **6**.

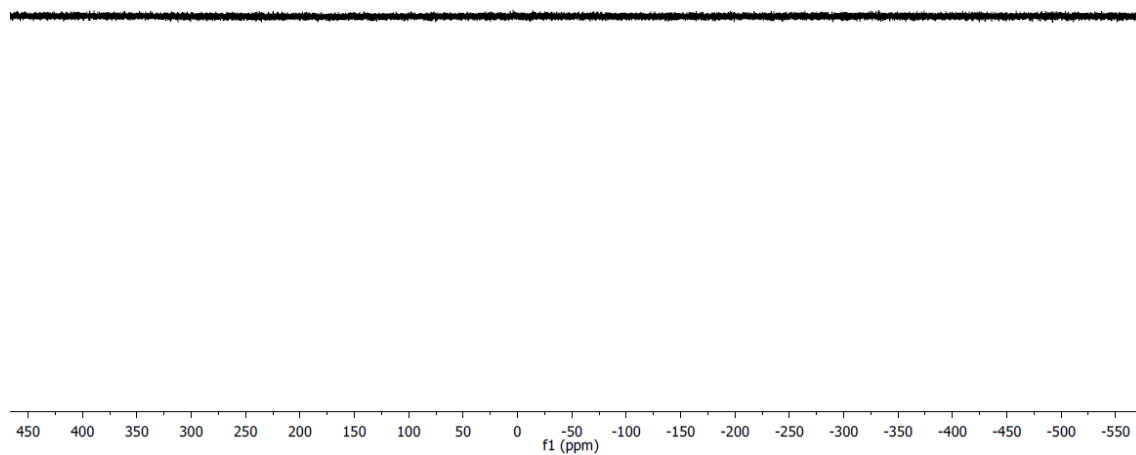


Figure 15. ^{31}P NMR (161.98 MHz, 300 K, $\text{THF-}d_8$) of **7**.

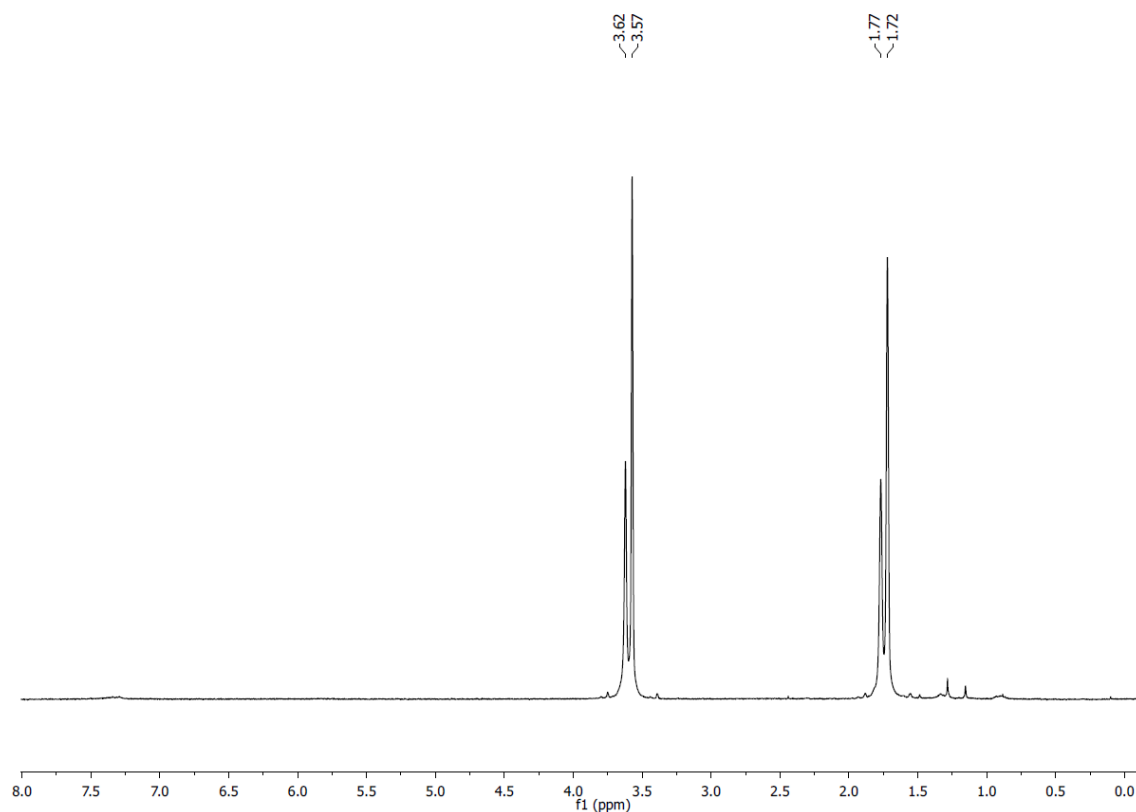


Figure 16. ^1H NMR spectrum (400.13 MHz, 300 K, $\text{THF-}d_8$) of **7-[18]crown-6** according to Evans method.

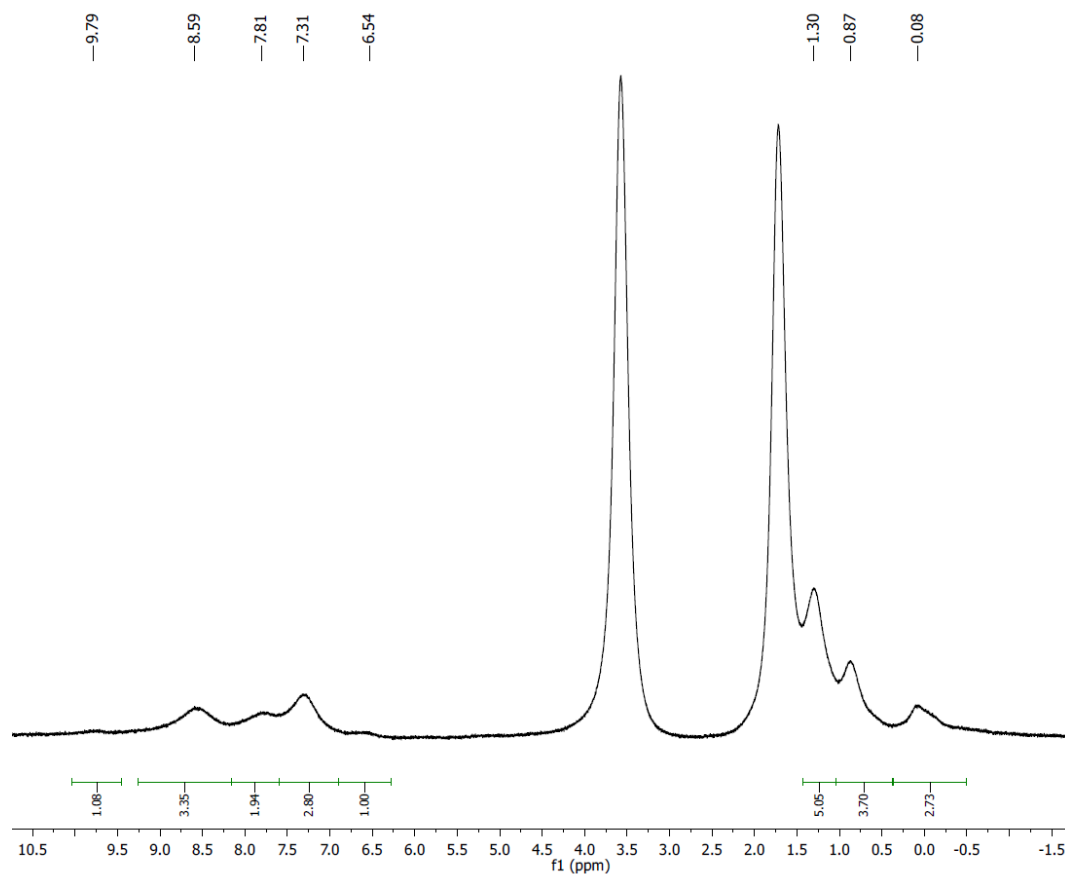


Figure 17. ^1H NMR spectrum (400.13 MHz, 300 K, $\text{THF-}d_8$) of **7** containing a higher amount of impurity according to the EPR spectra.

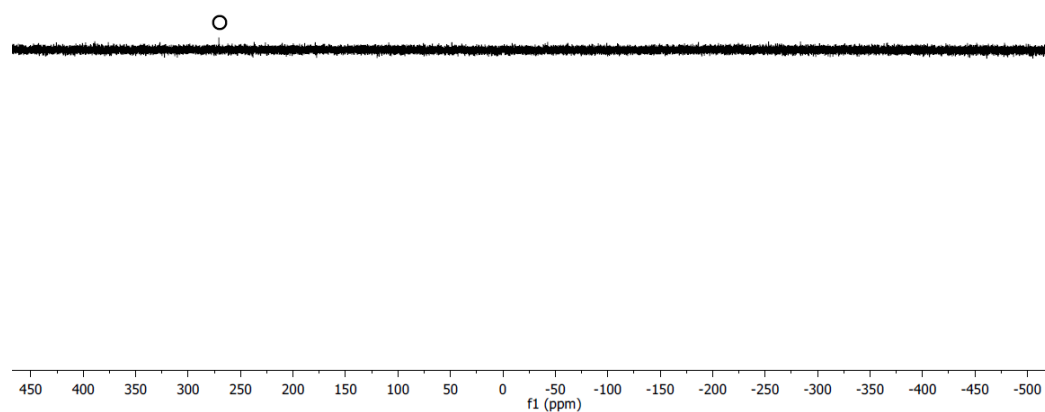


Figure 18. $^{31}\text{P}\{^1\text{H}\}$ NMR spectrum (161.98 MHz, 300 K, $\text{THF-}d_8$) of **7** containing a higher amount of impurity according to the EPR spectra, **O** free **3**.

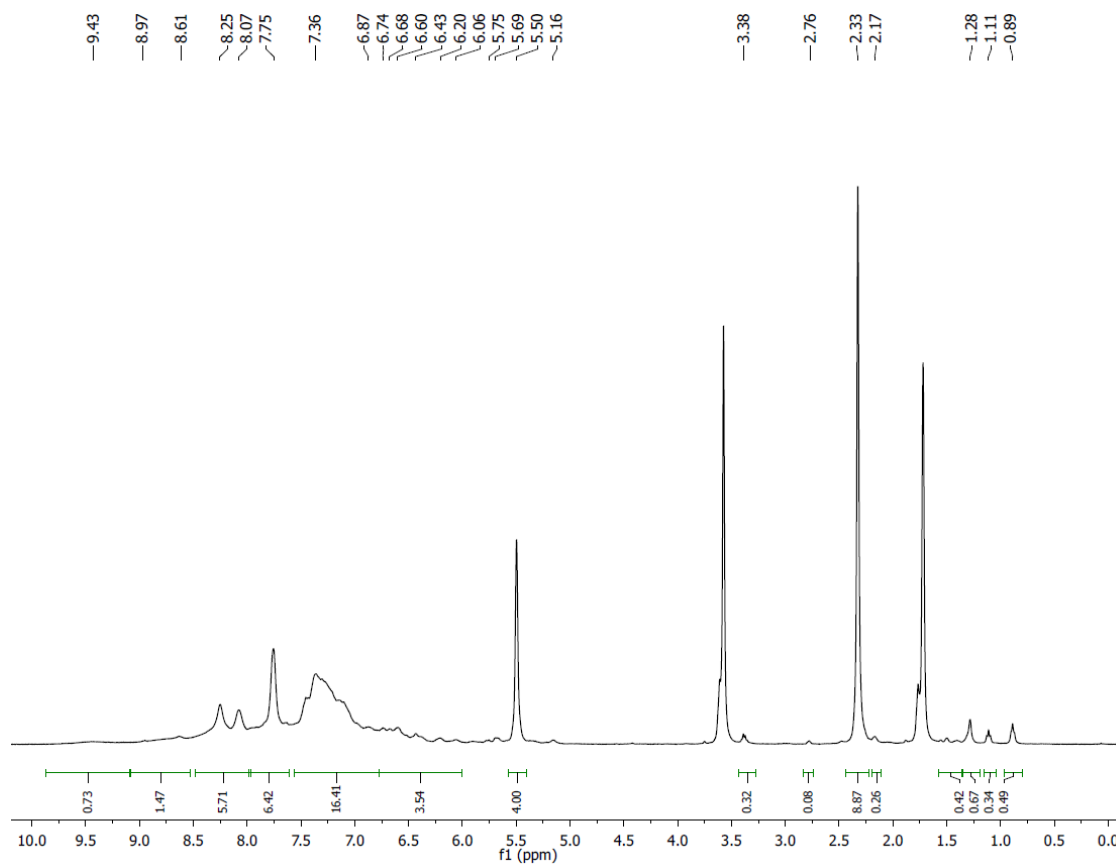


Figure 19. ^1H NMR spectrum (400.13 MHz, 300 K, $\text{THF-}d_8$) of the reaction of **1** with **4a** (3:1).

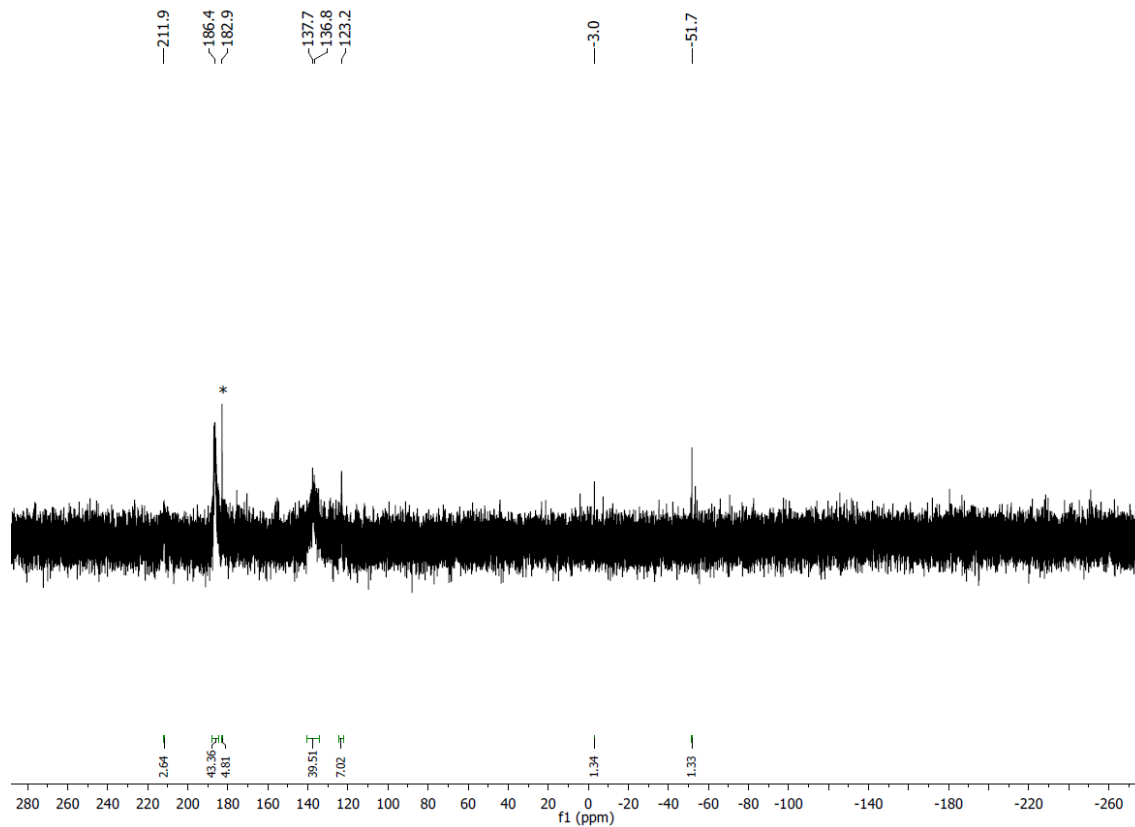


Figure 20. $^{31}\text{P}\{^1\text{H}\}$ NMR spectrum (161.98 MHz, 300 K, $\text{THF-}d_8$) of the reaction of **1** with **4a** (3:1), * free **1**.

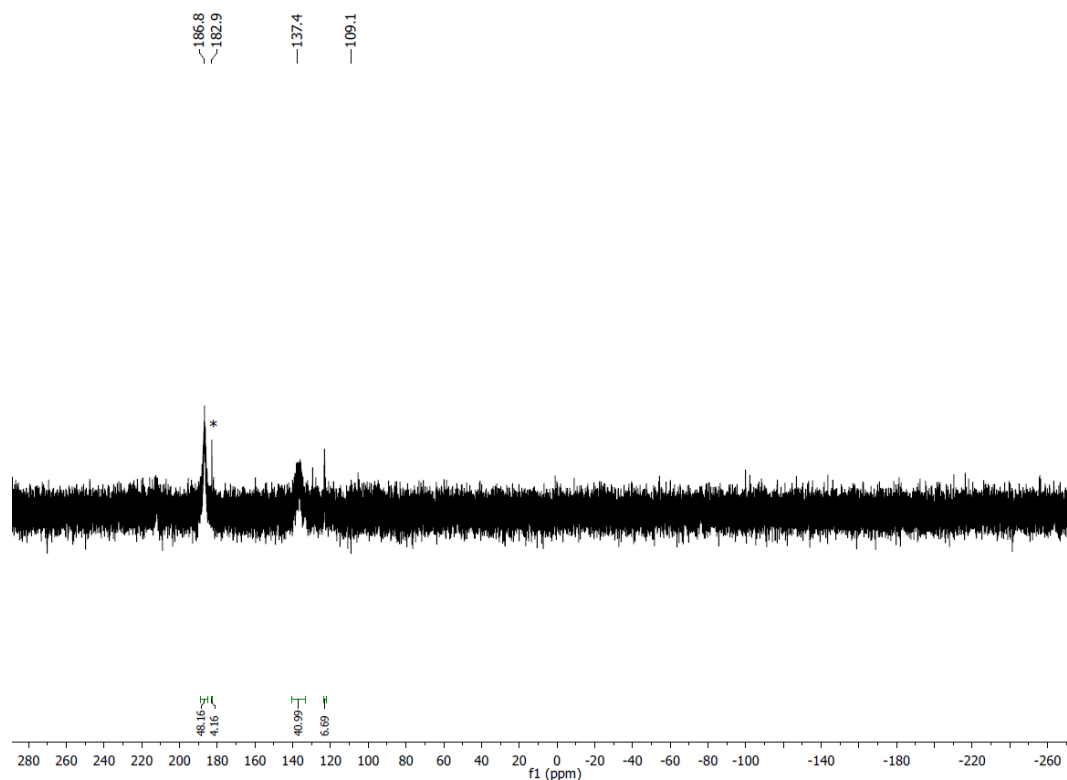


Figure 21. ^{31}P NMR spectrum (161.98 MHz, 300 K, $\text{THF-}d_8$) of the reaction of **1** with **4a** (3:1), * free **1**.

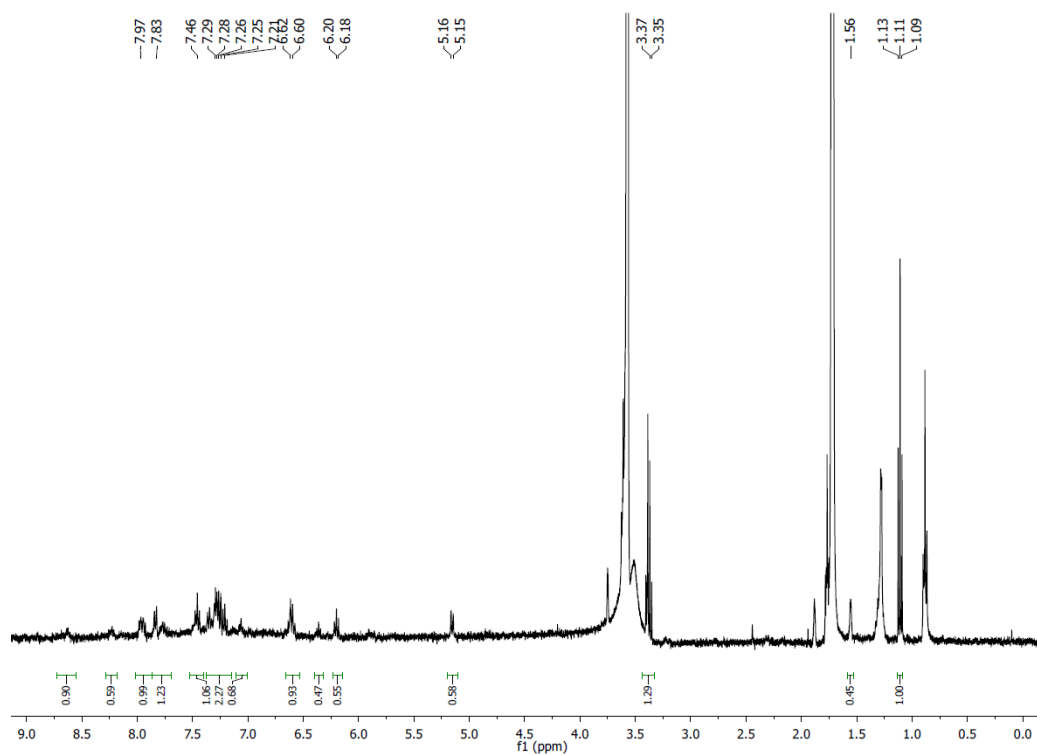


Figure 22. ^1H NMR spectrum (400.13 MHz, 300 K, $\text{THF-}d_8$) of the reaction of **1** with **4a** (2:1).

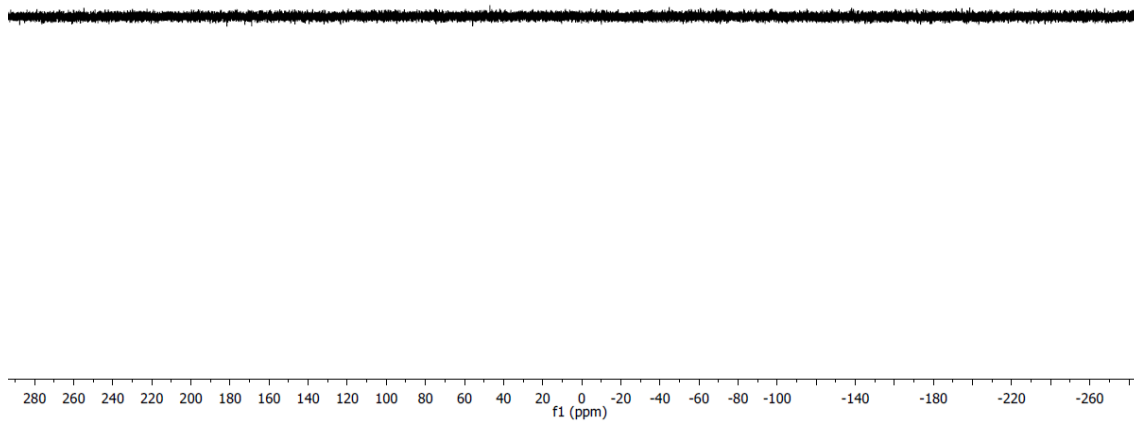


Figure 23. $^{31}\text{P}\{^1\text{H}\}$ NMR spectrum (161.98 MHz, 300 K, THF-*d*₈) of the reaction of **1** with **4a** (2:1).

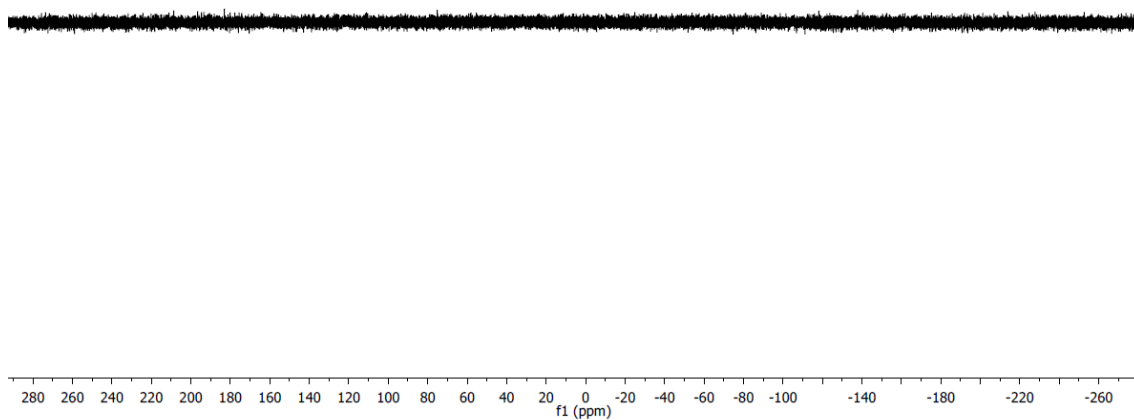


Figure 24. $^{31}\text{P}\{^1\text{H}\}$ NMR spectrum (161.98 MHz, 300 K, THF-*d*₈) of the reaction of **1** with **4a** (2:1).

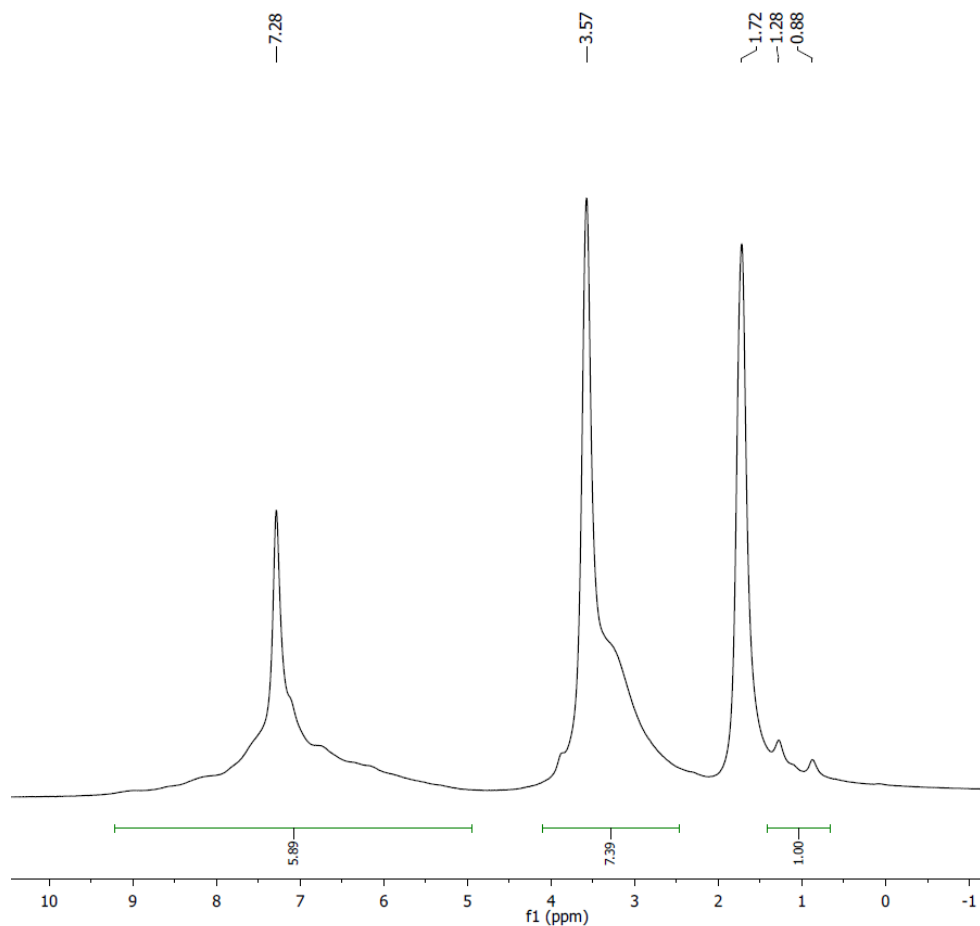


Figure 25. ^1H NMR spectrum (400.13 MHz, 300 K, $\text{THF-}d_8$) of the reaction of **1** with **5** (2:1).

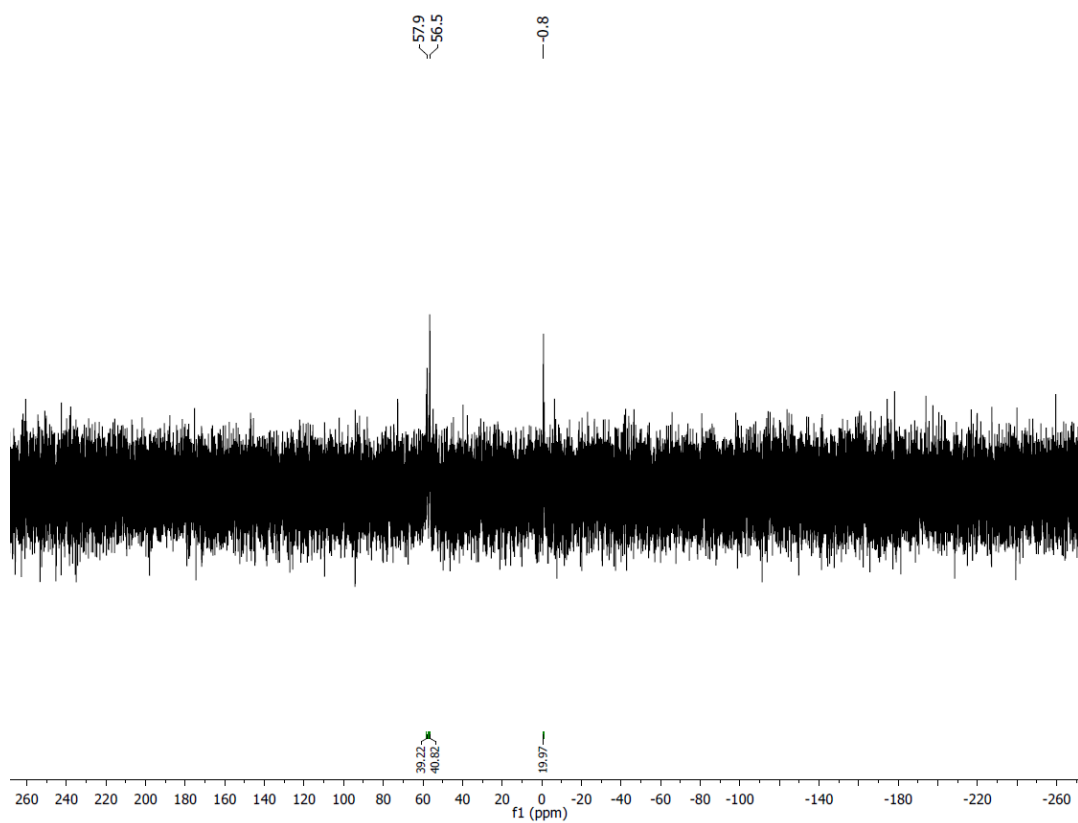


Figure 26. $^{31}\text{P}\{^1\text{H}\}$ NMR spectrum (161.98 MHz, 300 K, $\text{THF-}d_8$) of the reaction of **1** with **5** (2:1).

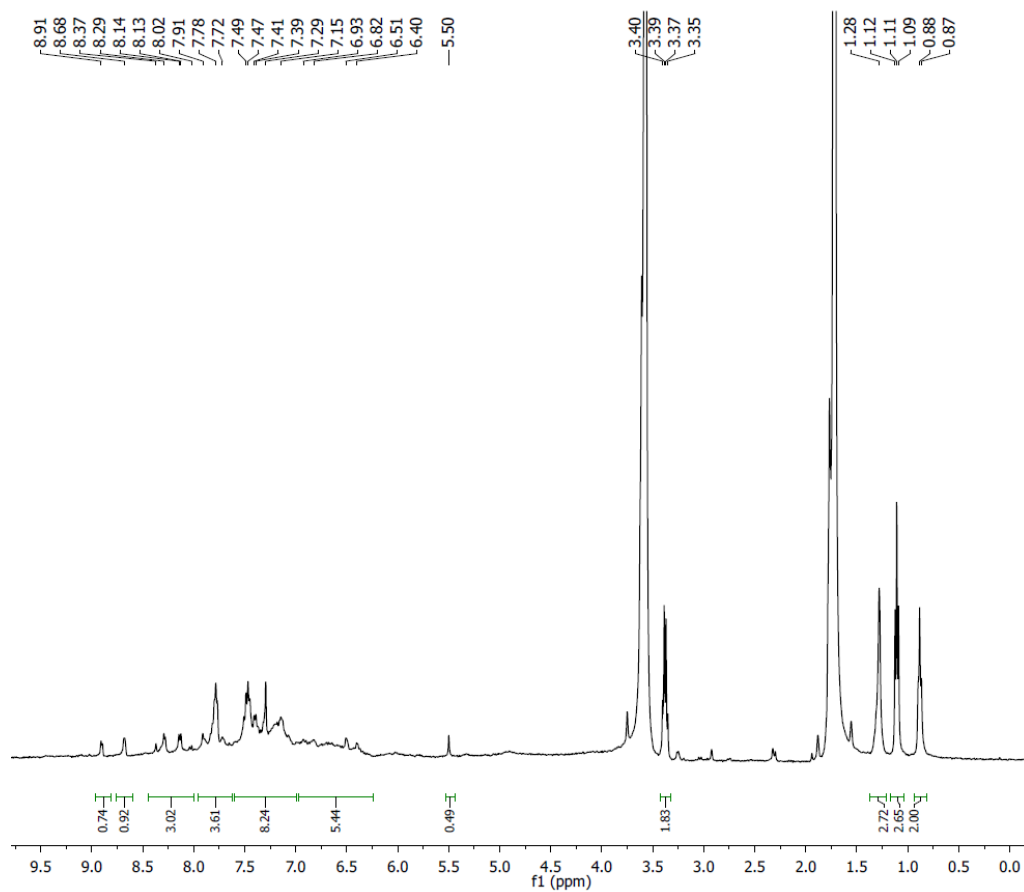


Figure 27. ¹H NMR spectrum (400.13 MHz, 300 K, THF-*d*₈) of the reaction of **1** with **4b** (2:1).

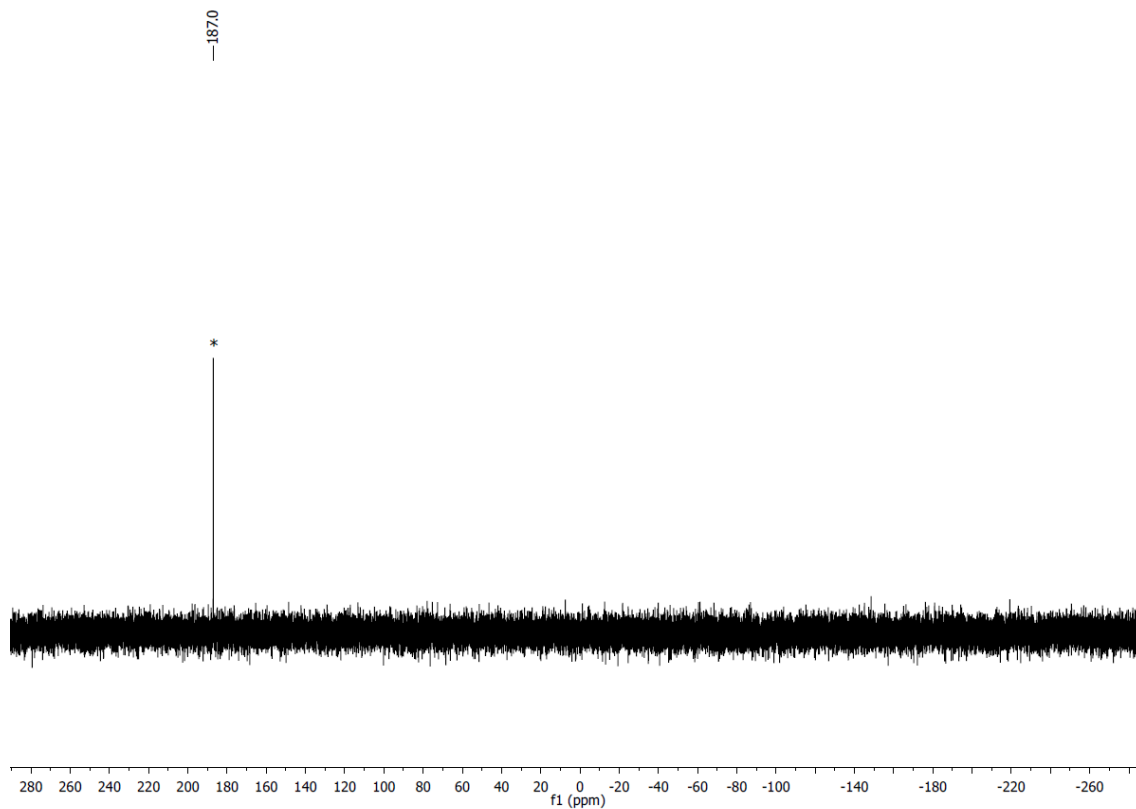


Figure 28. ³¹P{¹H} NMR spectrum (161.98 MHz, 300 K, THF-*d*₈) of the reaction of **1** with **4b** (2:1), * free **1**.

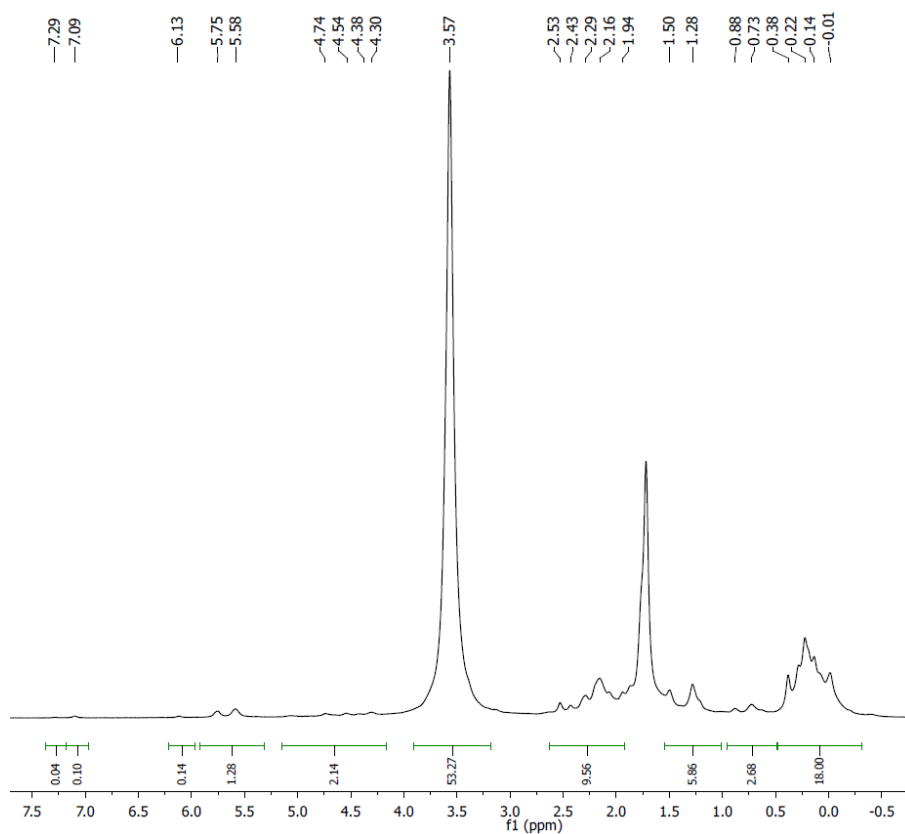


Figure 29. ^1H NMR spectrum (400.13 MHz, 300 K, $\text{THF-}d_8$) of the reaction of **2** with **4a** (1:1).

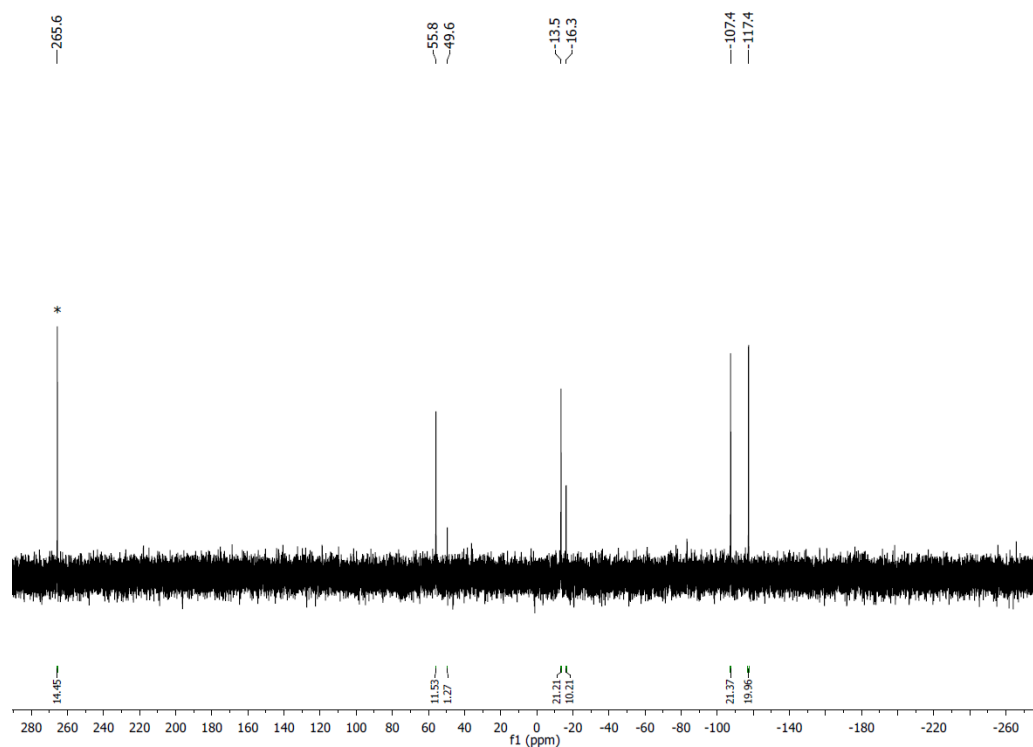


Figure 30. $^{31}\text{P}\{^1\text{H}\}$ NMR spectrum (161.98 MHz, 300 K, $\text{THF-}d_8$) of the reaction of **2** with **4a** (1:1), * residual **2**.

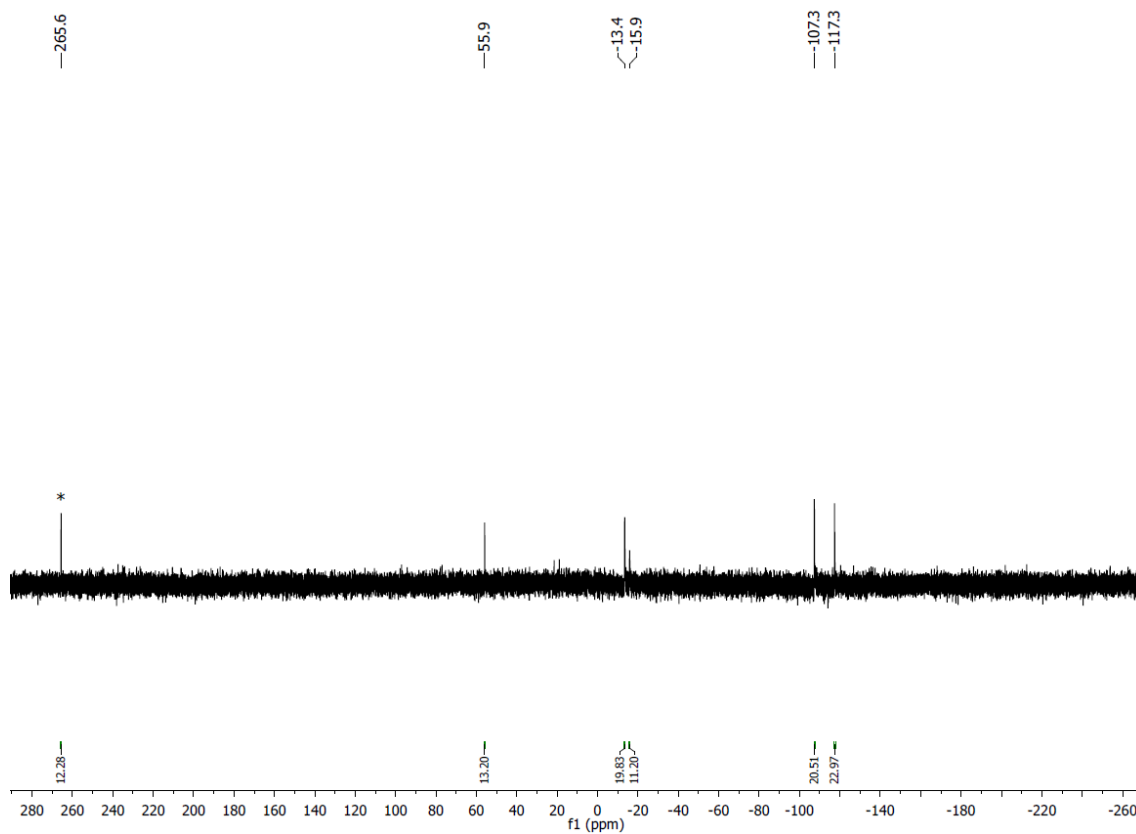


Figure 31. $^{31}\text{P}\{^1\text{H}\}$ NMR spectrum (161.98 MHz, 300 K, C_6D_6) of the reaction of **2** with **4a** (1:1.5), * residual **2**.

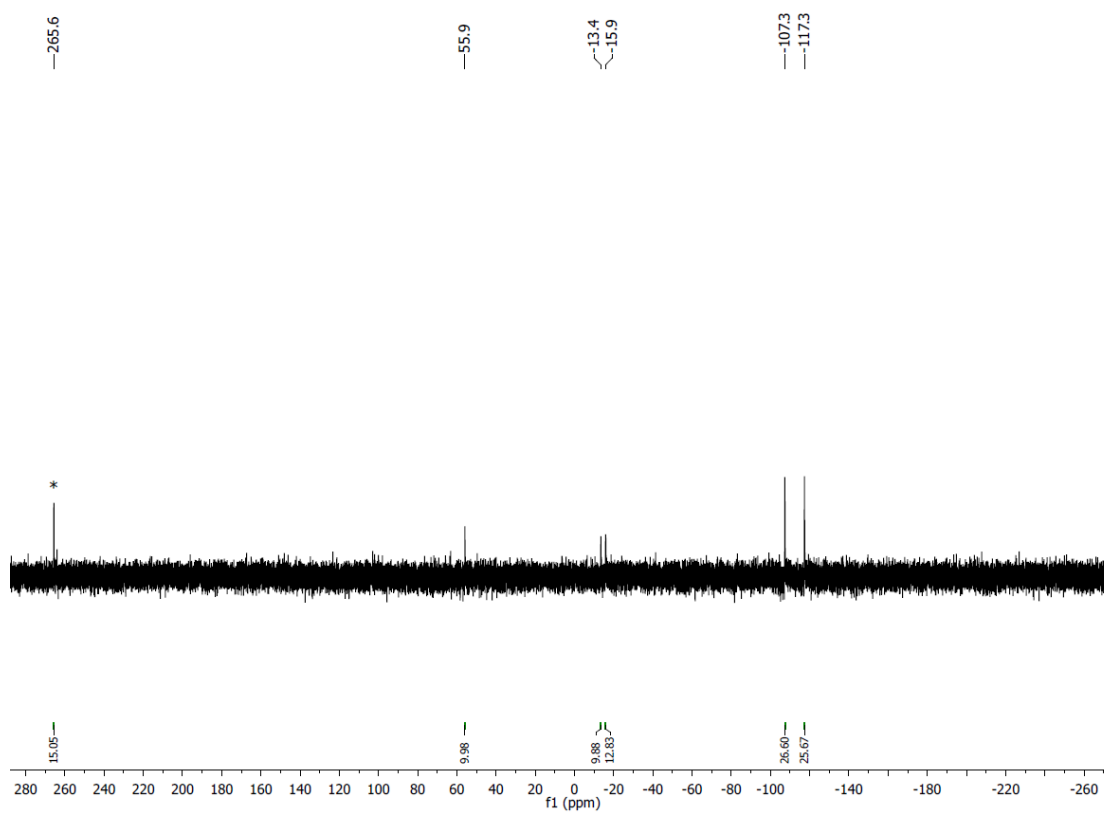


Figure 32. ^{31}P NMR spectrum (161.98 MHz, 300 K, C_6D_6) of the reaction of **2** with **4a** (1:1.5), * residual **2**.

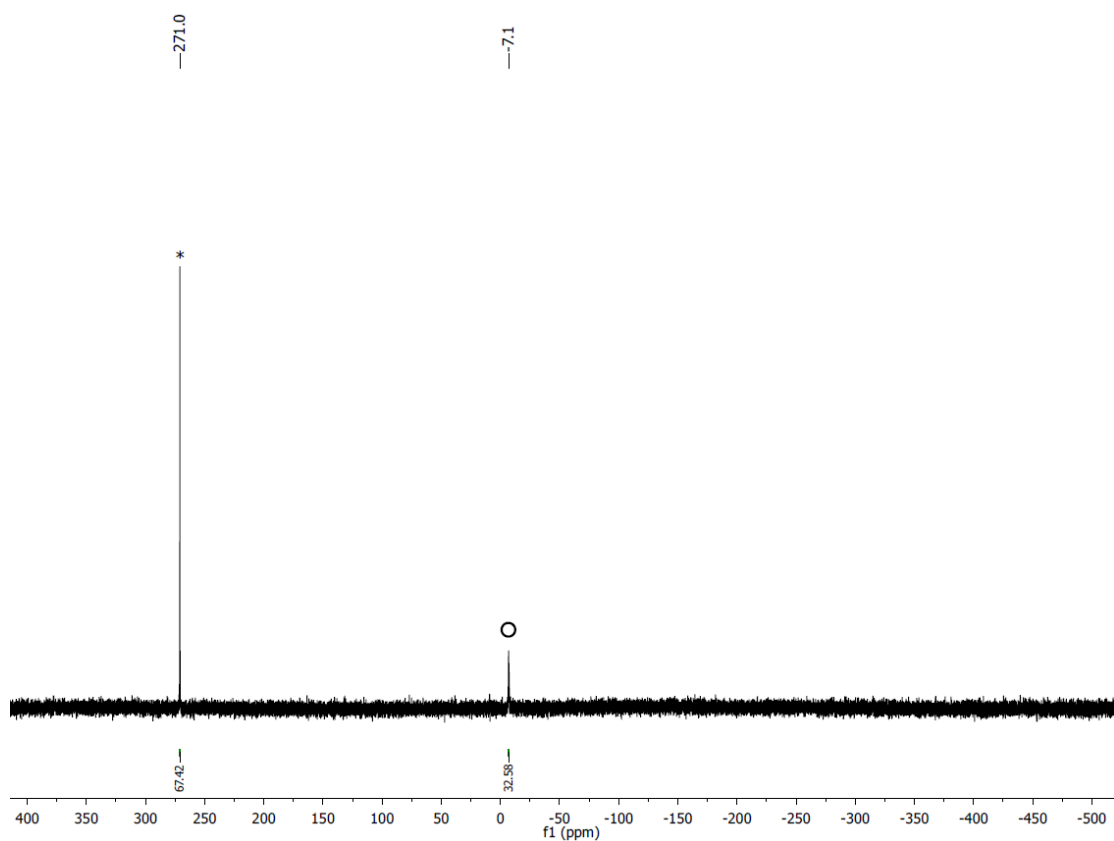


Figure 33. $^{31}\text{P}\{^1\text{H}\}$ NMR spectrum (161.98 MHz, 300 K, C_6D_6) of the reaction of **6** with P_4 (1:1), * free **3**, o **6**.

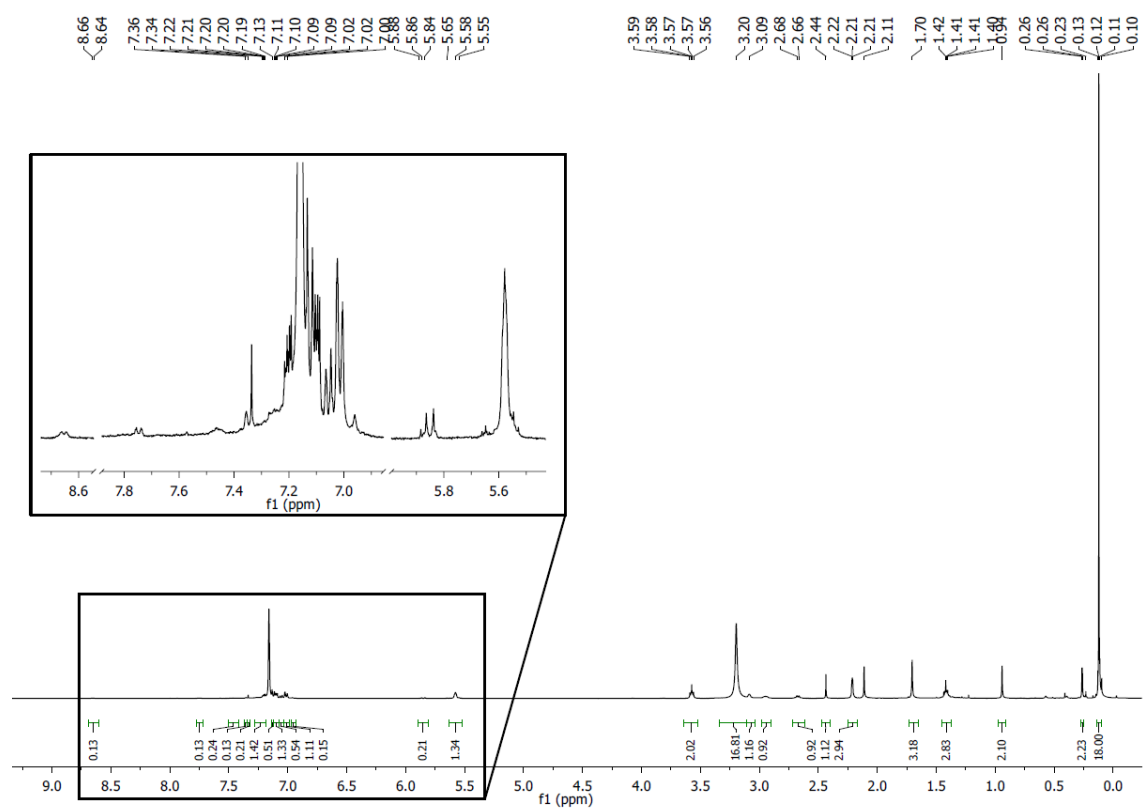


Figure 34. ^1H NMR spectrum (400.13 MHz, 300 K, C_6D_6) of the reaction of **6** with $^t\text{BuCP}$ (1:1).

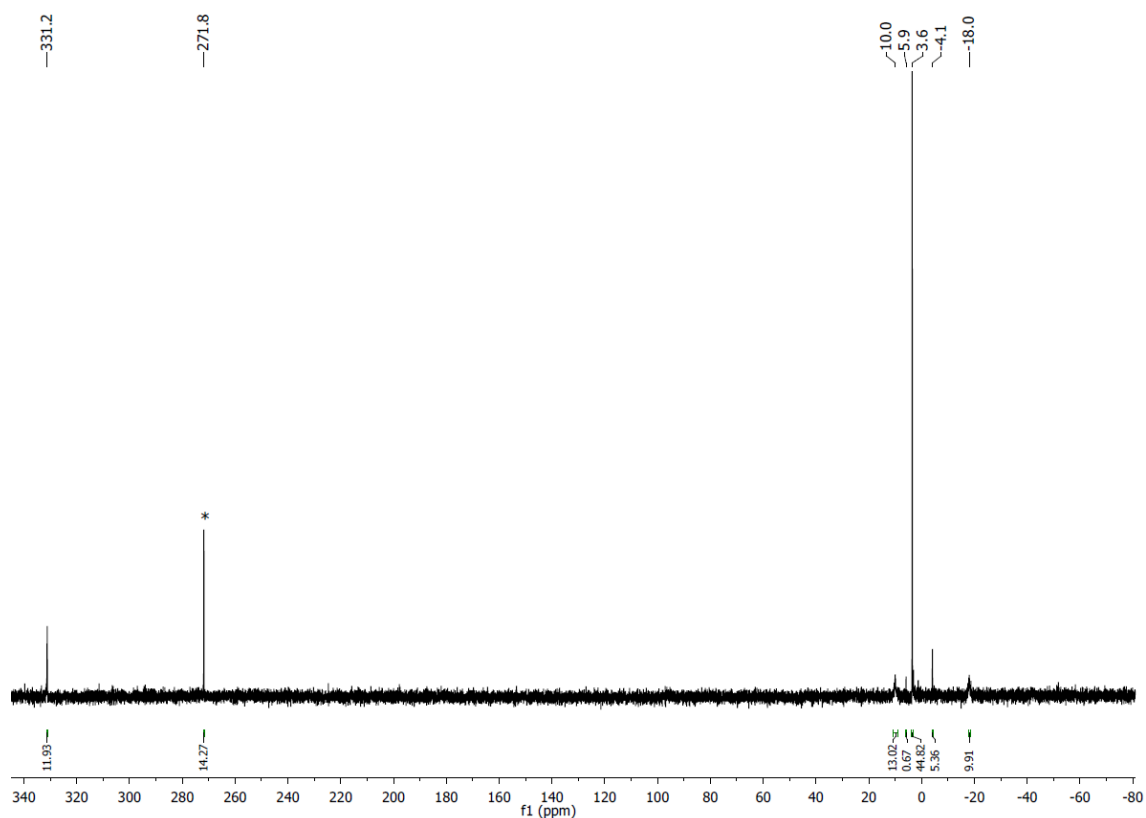


Figure 35. $^{31}\text{P}\{^1\text{H}\}$ NMR spectrum (161.98 MHz, 300 K, C_6D_6) of the reaction of **6** with $t\text{BuCP}$ (1:1).

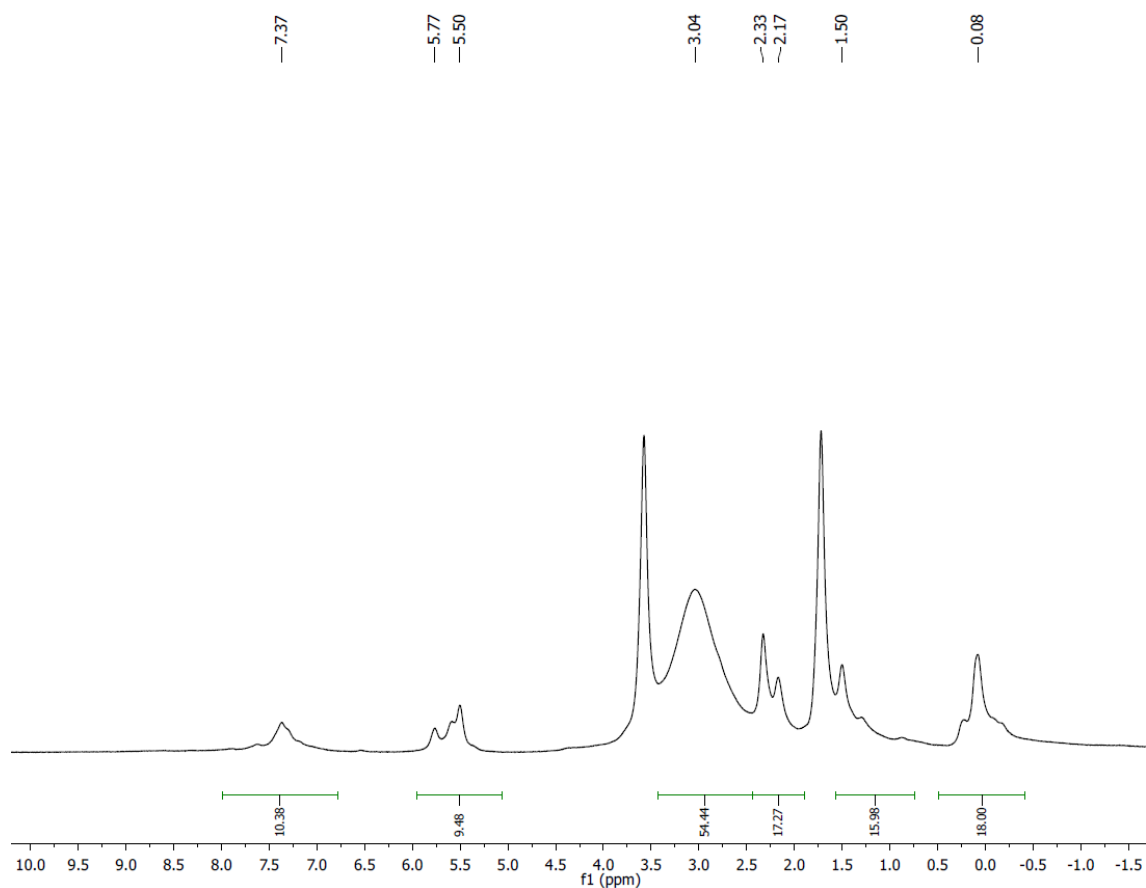


Figure 36. ^1H NMR spectrum (400.13 MHz, 300 K, $\text{THF-}d_8$) of the reaction of **6** with CO_2 (1 bar) after 6 h.

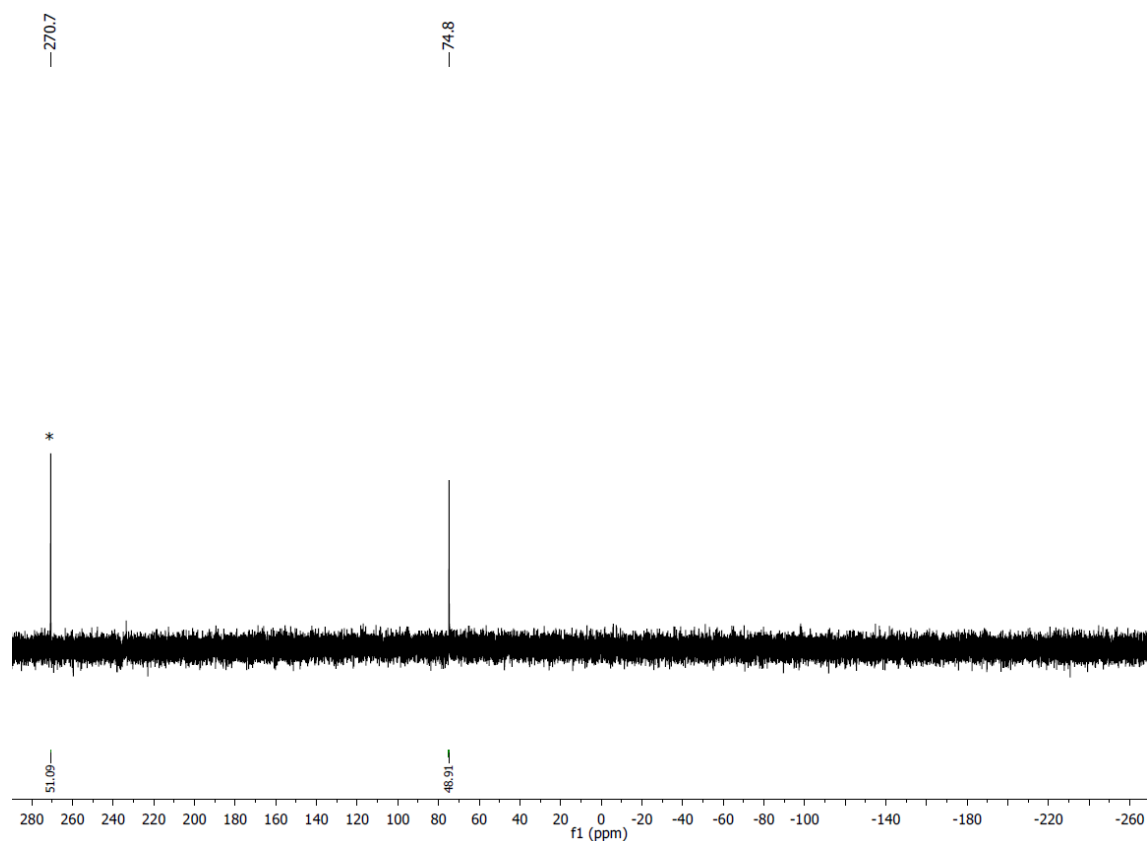


Figure 37. $^{31}\text{P}\{^1\text{H}\}$ NMR spectrum (161.98 MHz, 300 K, $\text{THF-}d_8$) of the reaction of **6** with CO_2 (1 bar) after 6 h, * free **3**.

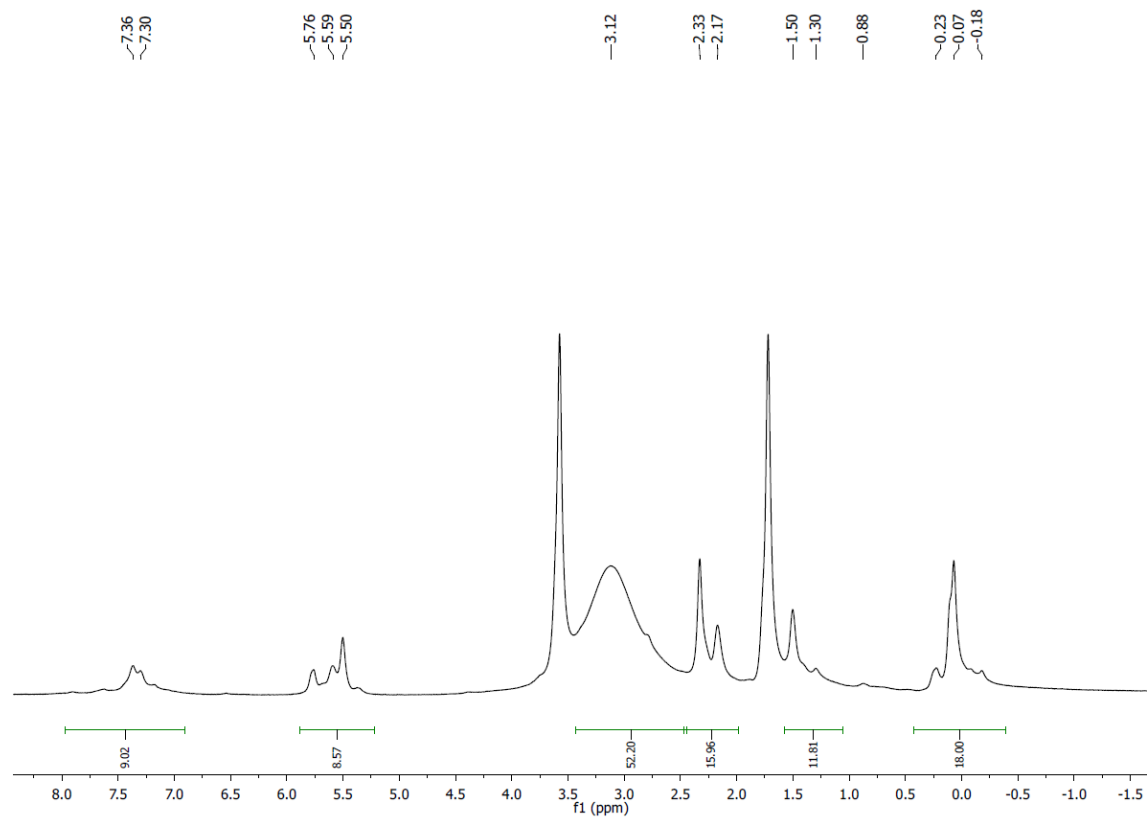


Figure 38. ^1H NMR spectrum (400.13 MHz, 300 K, $\text{THF-}d_8$) of the reaction of **6** with CO_2 (1 bar) after one day.

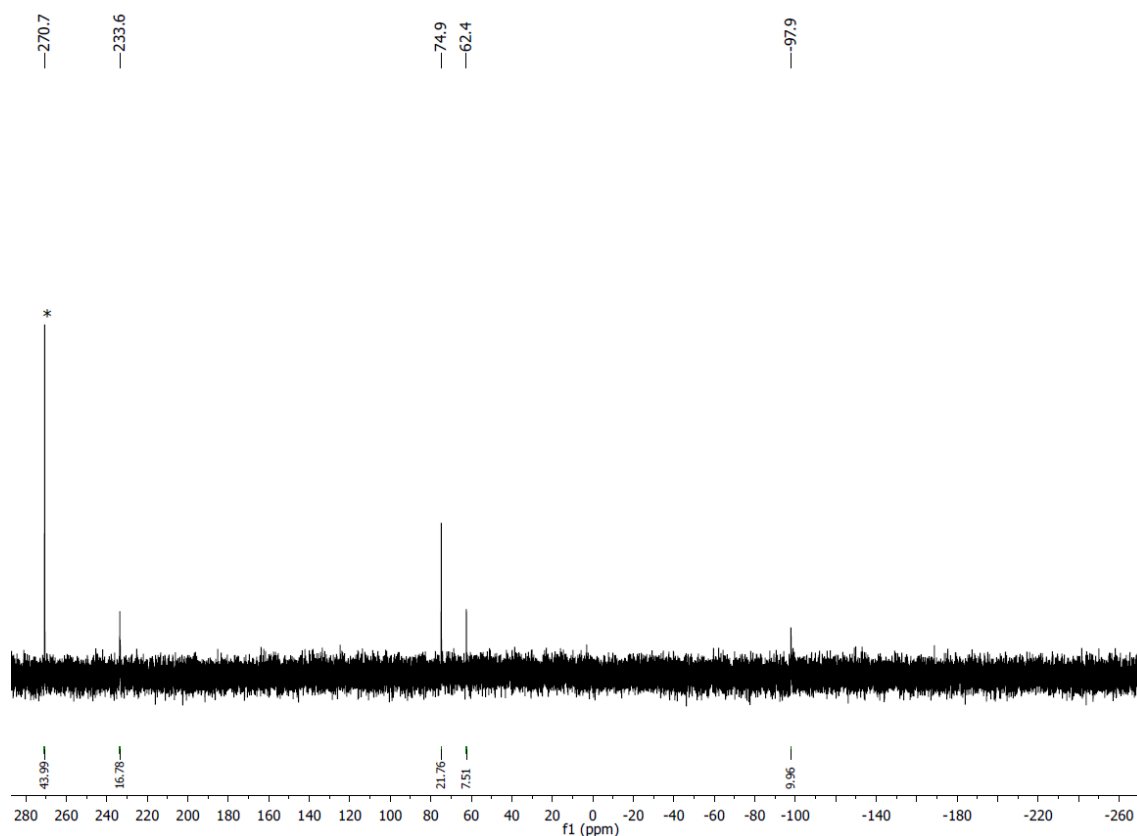


Figure 39. $^{31}\text{P}\{^1\text{H}\}$ NMR spectrum (161.98 MHz, 300 K, $\text{THF-}d_8$) of the reaction of **6** with CO_2 (1 bar) after one day, * free **3**.

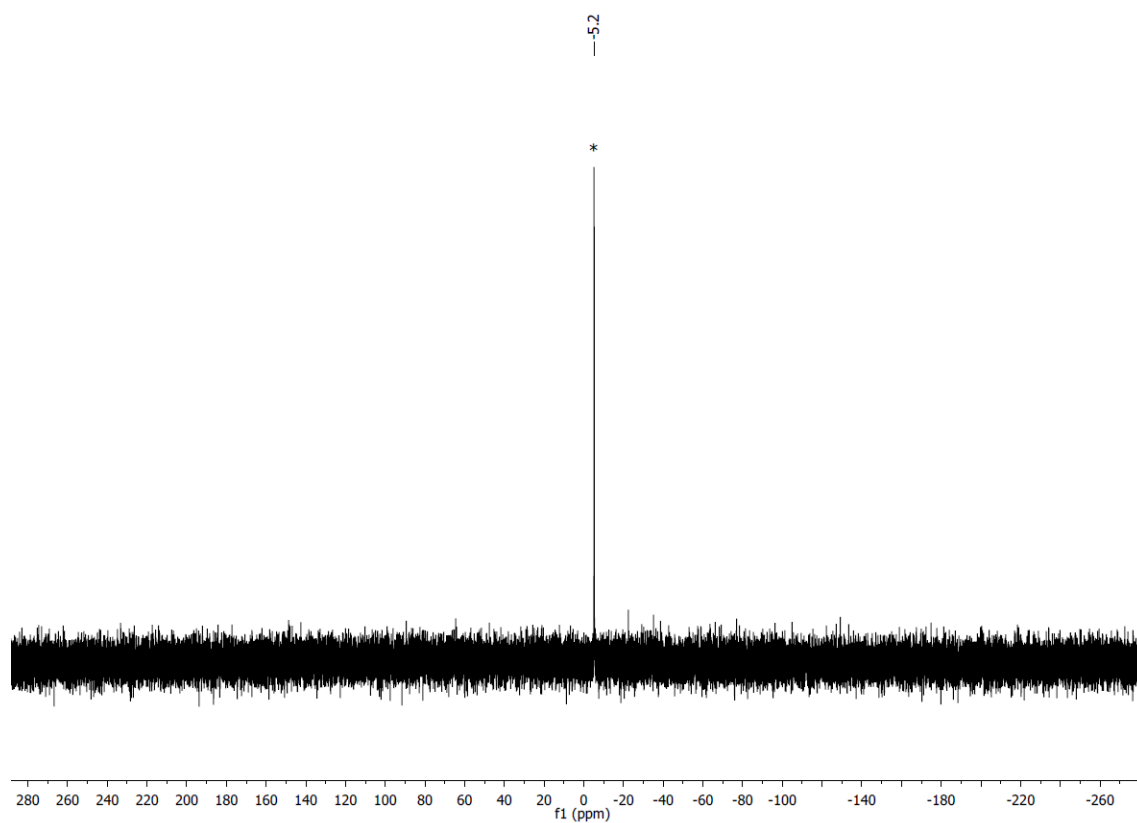


Figure 40. $^{31}\text{P}\{^1\text{H}\}$ NMR spectrum (161.98 MHz, 300 K, C_6D_6) of the reaction of **6** with bpy (1:1), * **6**.

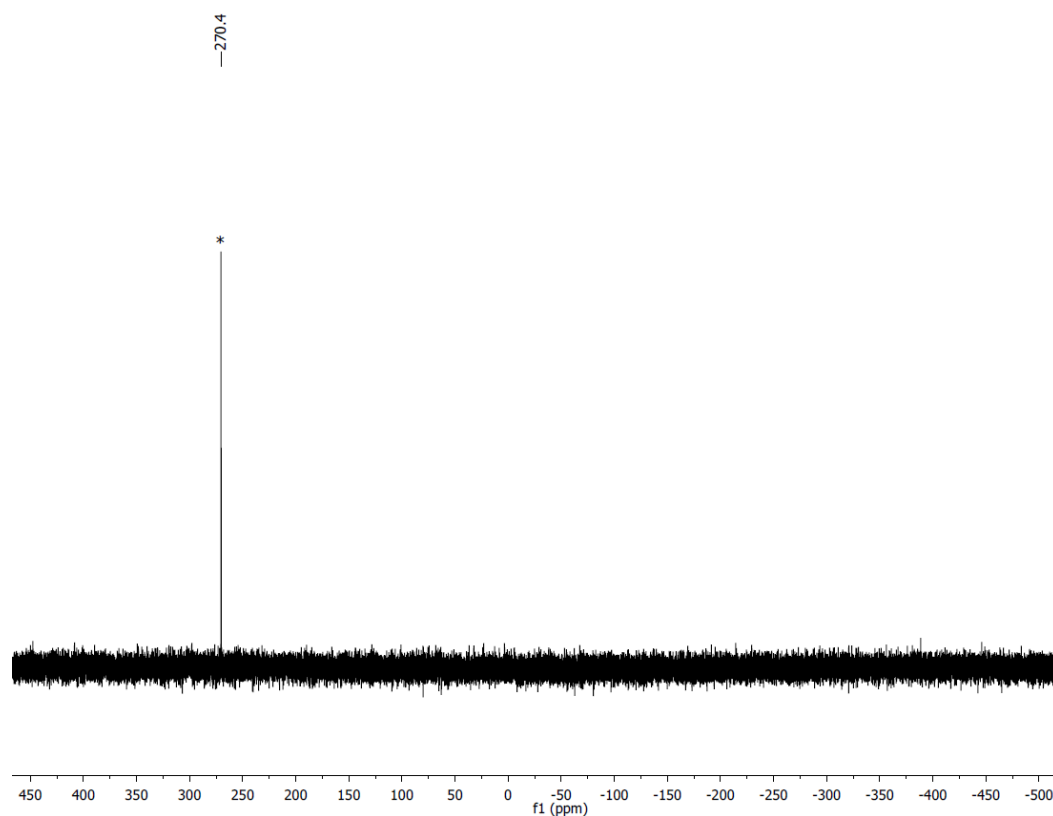


Figure 41. $^{31}\text{P}\{^1\text{H}\}$ NMR spectrum (161.98 MHz, 300 K, C_6D_6) of the reaction of **6** with bpy (1:1) and CO (1 bar), * free **3**.

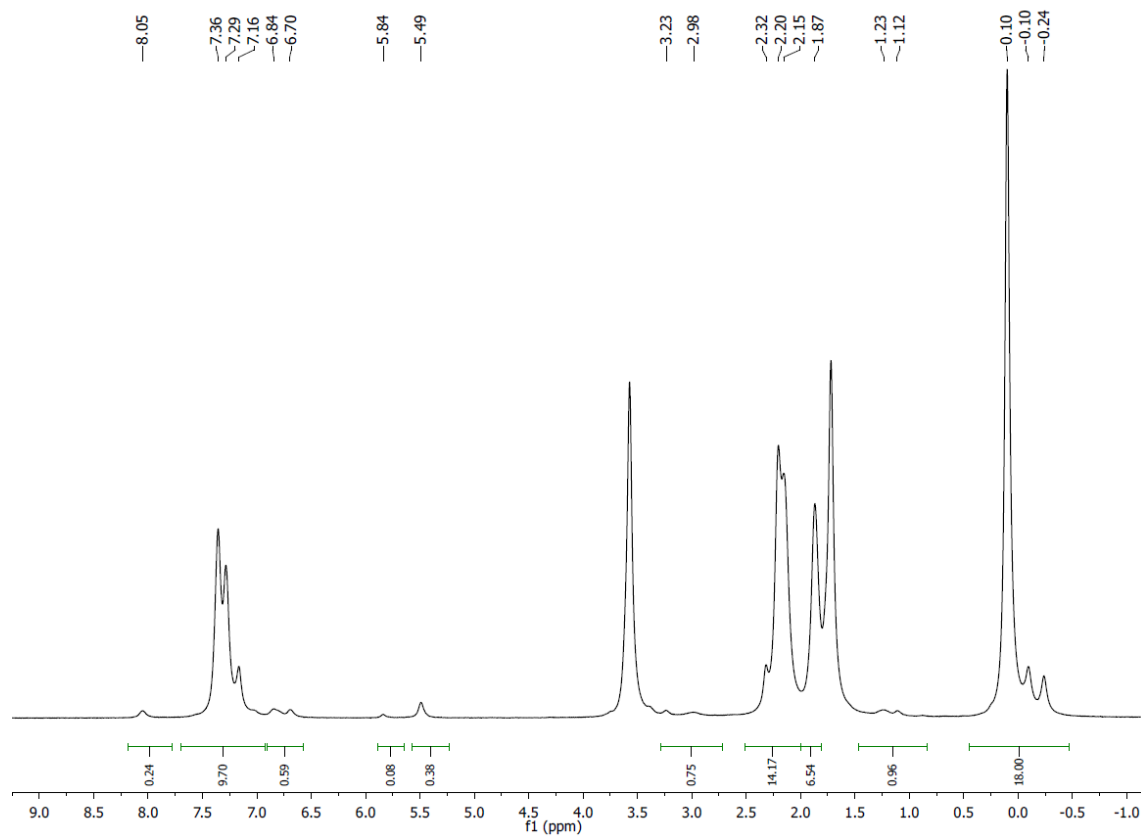


Figure 42. ^1H NMR spectrum (400.13 MHz, 300 K, $\text{THF}-d_8$) of the reaction of **3** with **4a** (1:1) before irradiation.

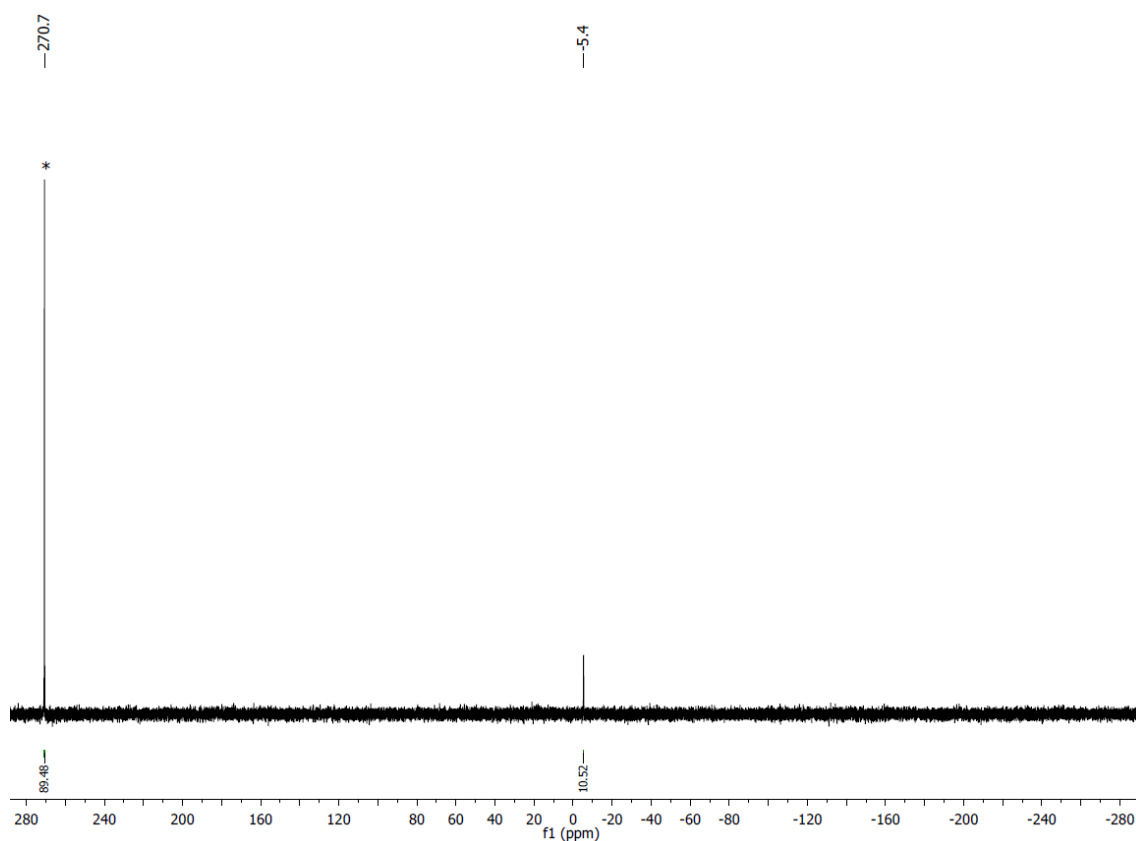


Figure 43. $^{31}\text{P}\{^1\text{H}\}$ NMR spectrum (161.98 MHz, 300 K, $\text{THF-}d_8$) of the reaction of **3** with **4a** (1:1) before irradiation, * free **3**.

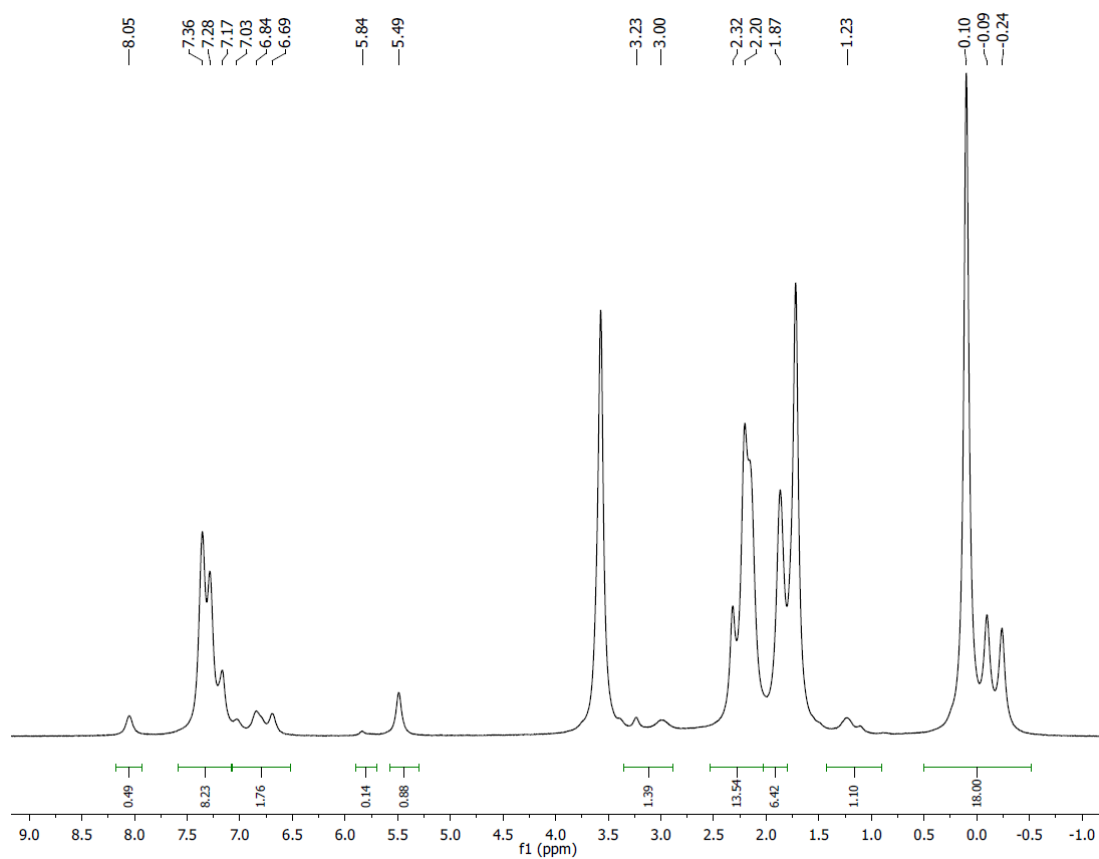


Figure 44. ^1H NMR spectrum (400.13 MHz, 300 K, $\text{THF-}d_8$) of the reaction of **3** with **4a** (1:1) after 2 h of irradiation.

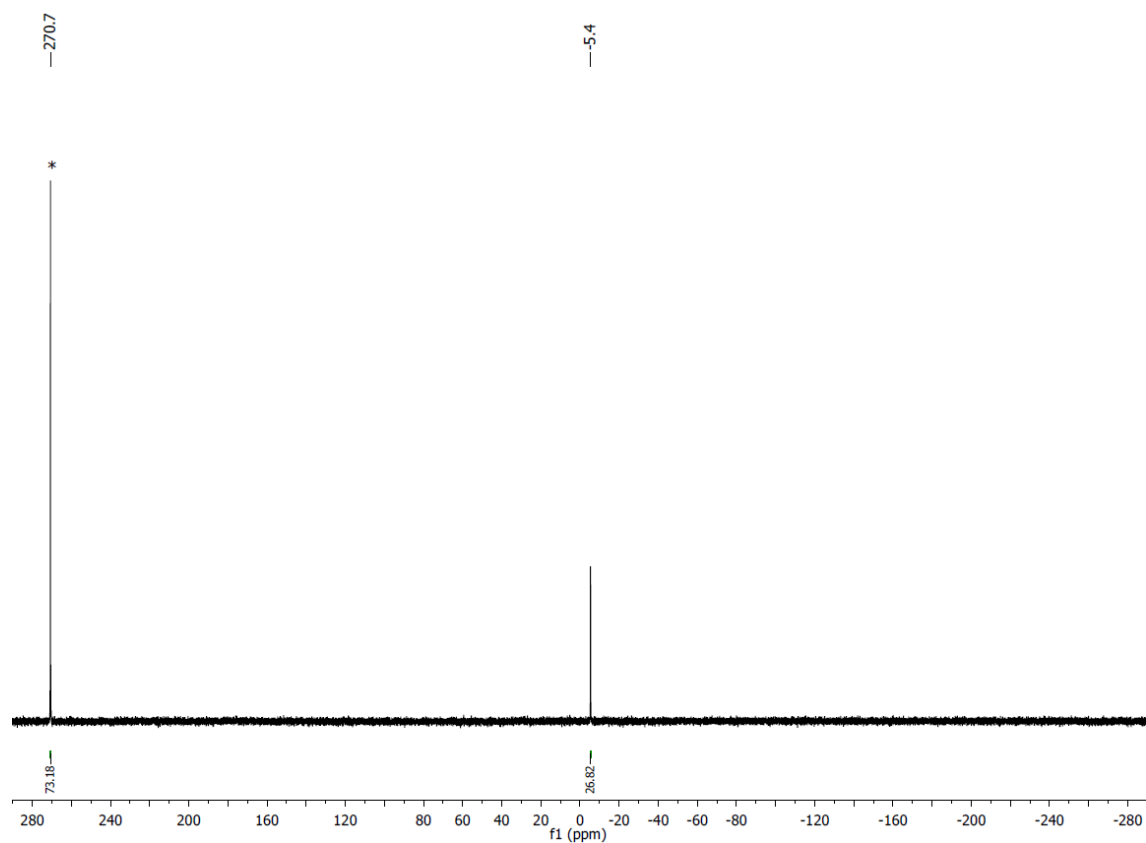


Figure 45. $^{31}\text{P}\{^1\text{H}\}$ NMR spectrum (161.98 MHz, 300 K, $\text{THF-}d_8$) of the reaction of **3** with **4a** (1:1) after 2 h of irradiation, * free **3**.

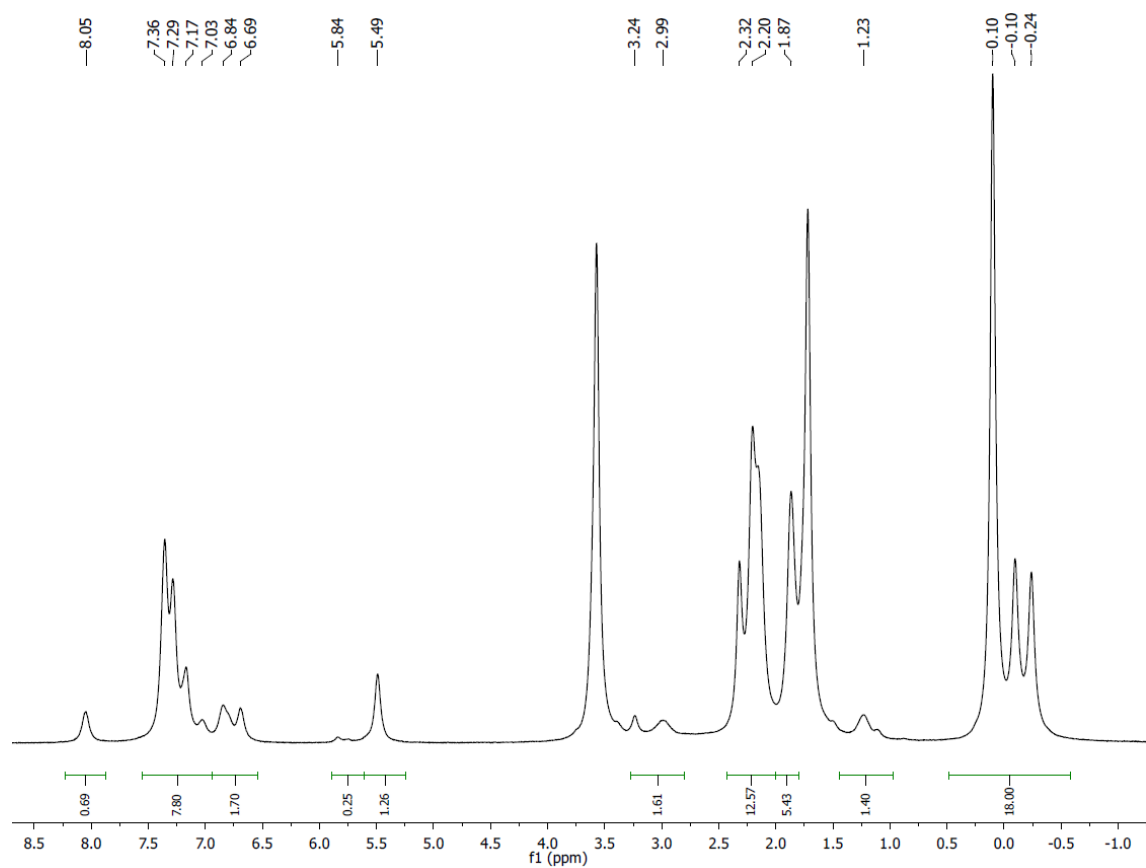


Figure 46. ^1H NMR spectrum (400.13 MHz, 300 K, $\text{THF-}d_8$) of the reaction of **3** with **4a** (1:1) after 4 h of irradiation.

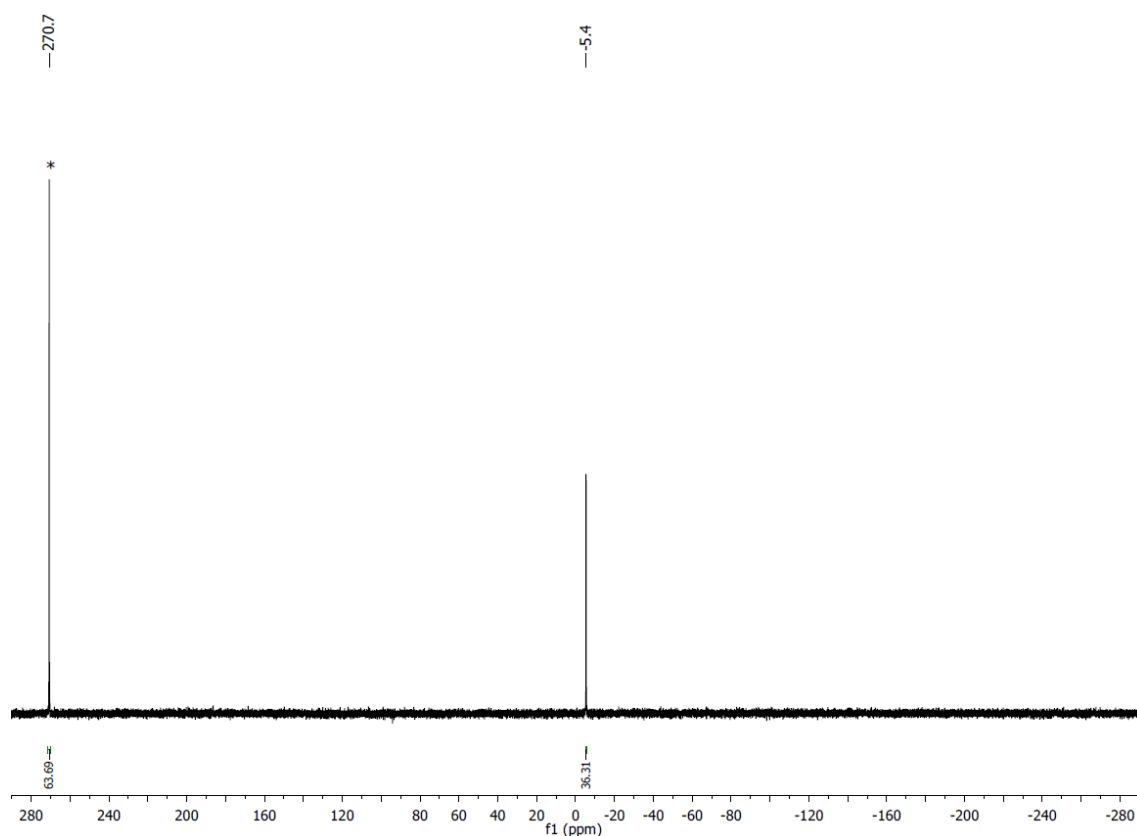


Figure 47. $^{31}\text{P}\{^1\text{H}\}$ NMR spectrum (161.98 MHz, 300 K, $\text{THF-}d_8$) of the reaction of **3** with **4a** (1:1) after 4 h of irradiation, * free **3**.

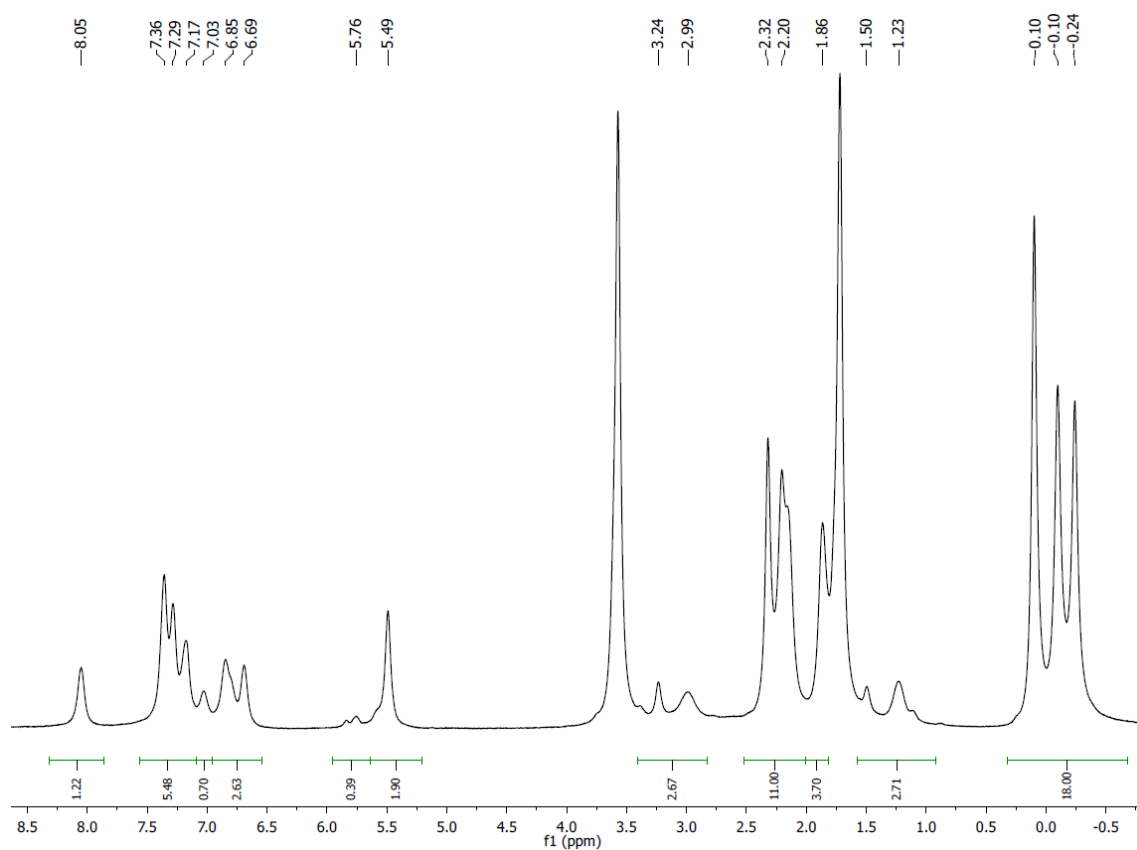


Figure 48. ^1H NMR spectrum (400.13 MHz, 300 K, $\text{THF-}d_8$) of the reaction of **3** with **4a** (1:1) after 21 h of irradiation.

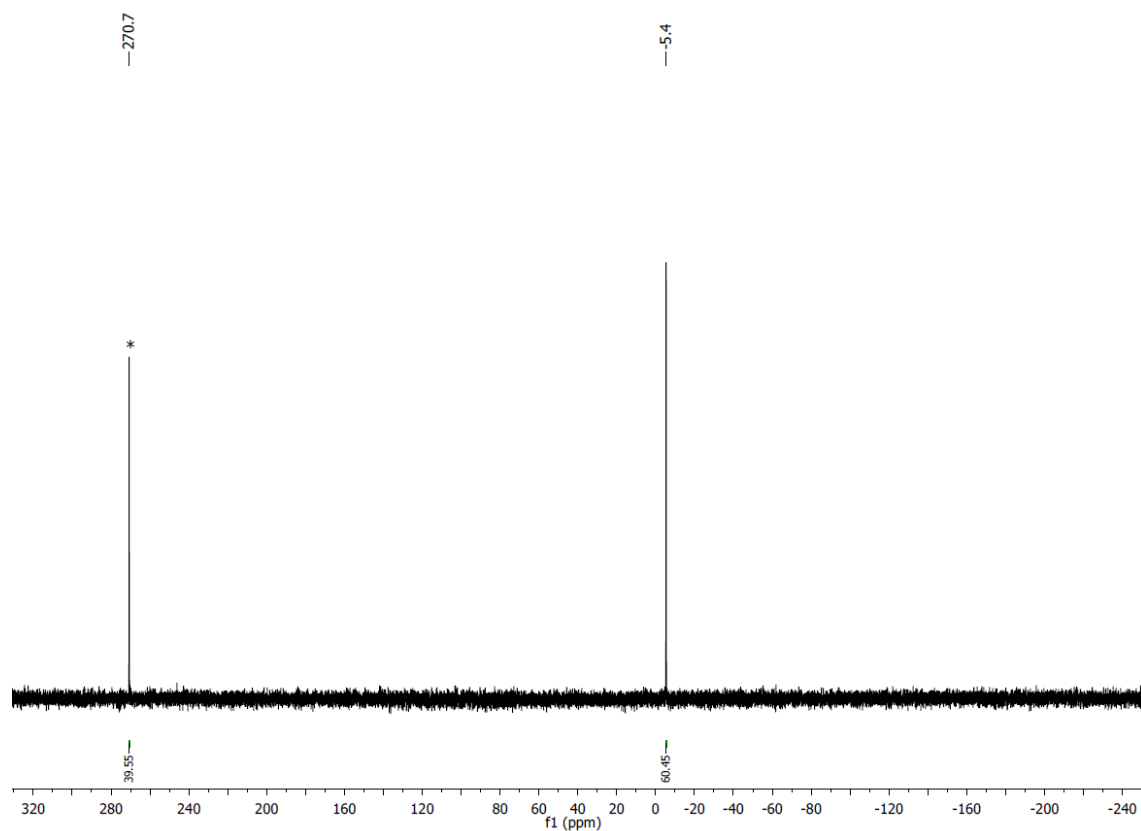


Figure 49. $^{31}\text{P}\{^1\text{H}\}$ NMR spectrum (161.98 MHz, 300 K, $\text{THF-}d_8$) of the reaction of **3** with **4a** (1:1) after 21 h of irradiation.

5.4.3 EPR Spectra

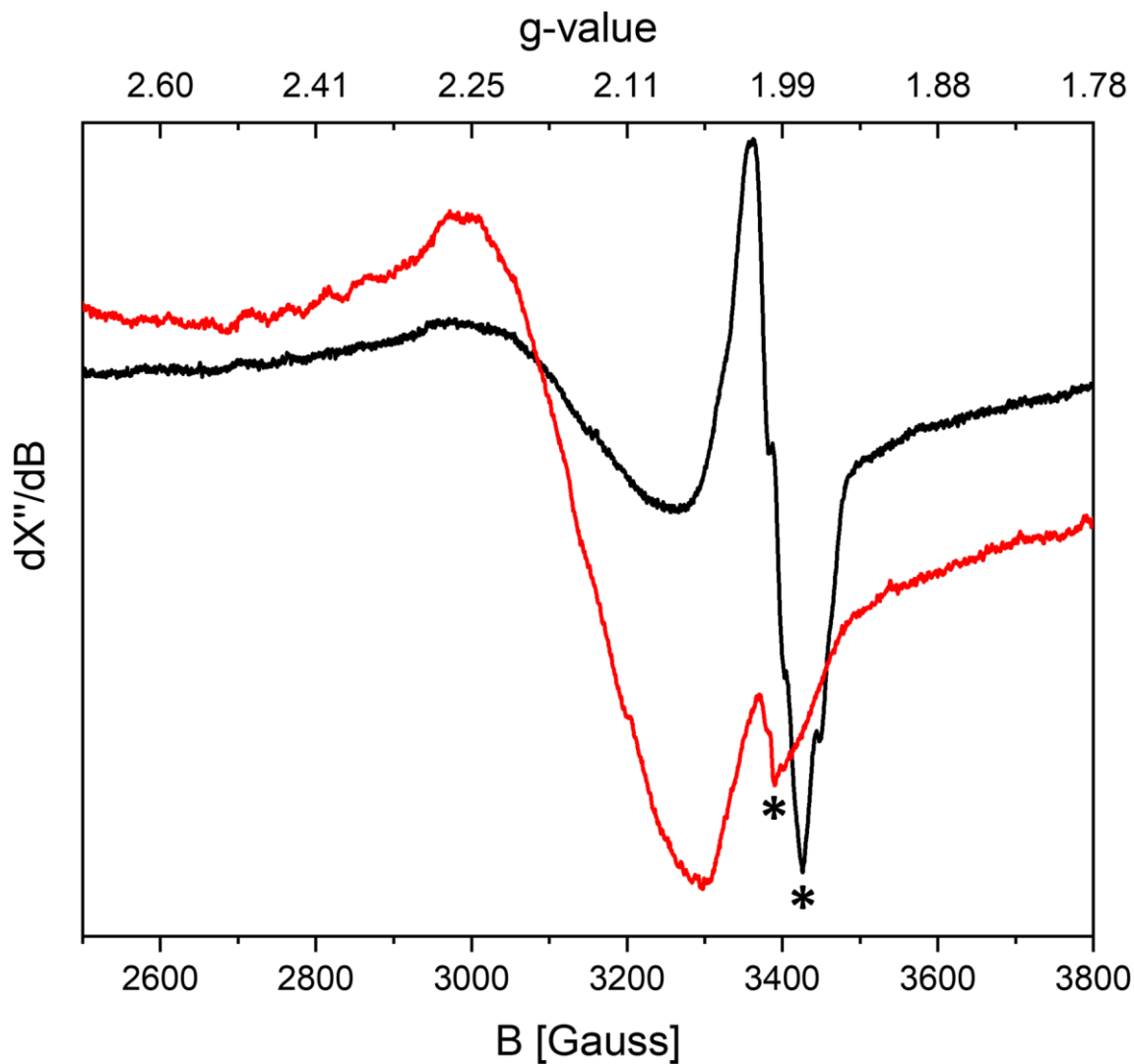


Figure 50. Experimental X-band EPR spectra of **7** containing different amounts (less – red or more – black) of an unidentified impurity (marked with *) recorded in THF at 77 K. Experimental parameters: microwave frequency, 9.448213 GHz (red) and 9.448445 GHz (black); modulation amplitude, 5.000 G (red), 3.000 G (black).

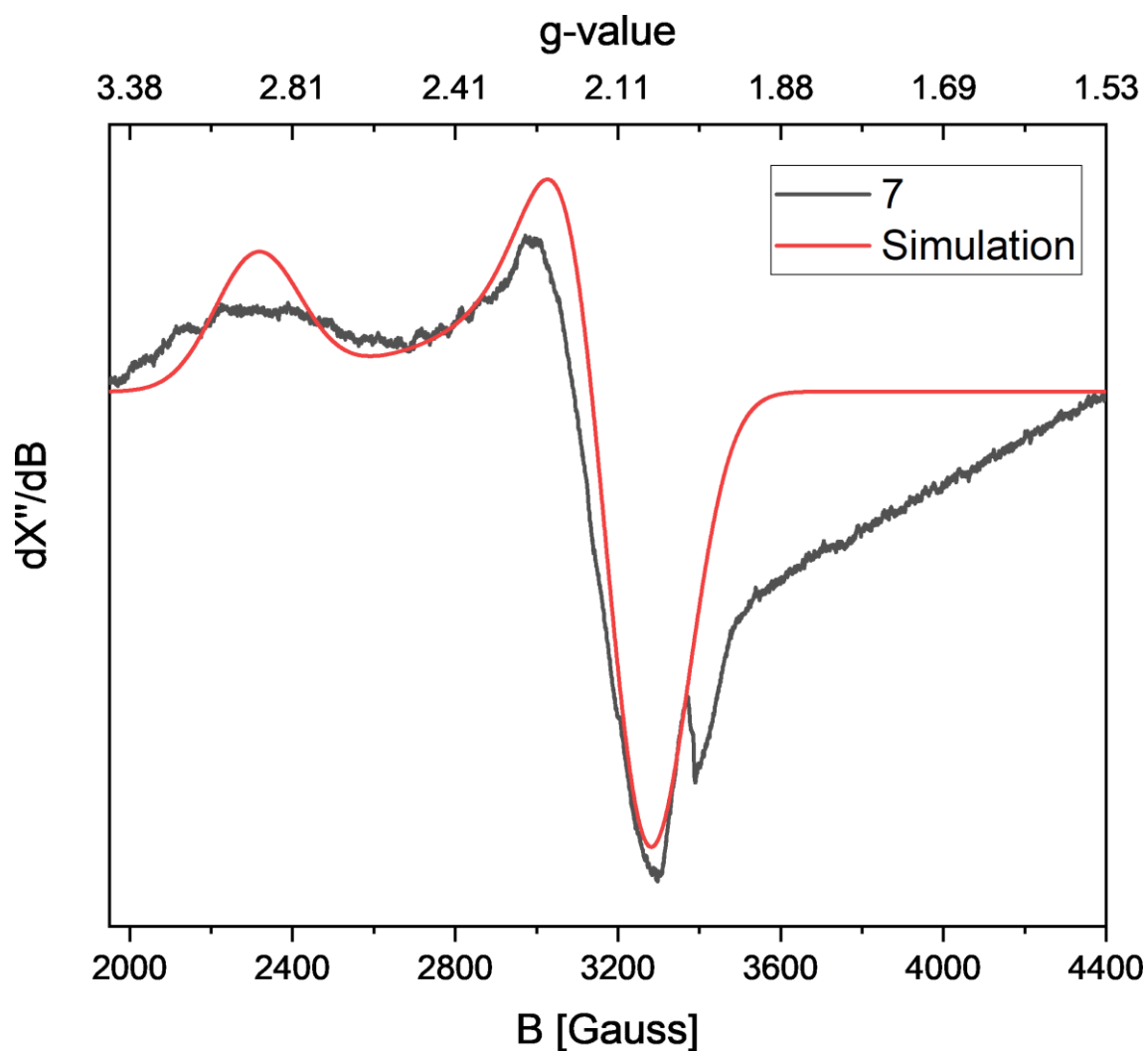


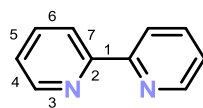
Figure 51. Experimental (black) and simulated (red) X-band EPR spectra of **7** recorded in THF at 77 K. Experimental parameters: microwave frequency, 9.448213 GHz; modulation amplitude, 3.000 G (red), 3.000 G (black). The experimental spectrum of **7** was fitted with the following parameters for a $S = 1/2$ system. $g_{11} = 2.42$, $g_{22} = 1.95$, $g_{33} = 1.97$, * unidentified impurity.

5.4.4 Crystallographic Data

Table 1. X-ray Crystallographic Data for Compounds **6** and **7**.

	6	7
Empirical formula	C ₅₁ H ₈₁ CoKO ₈ PSi ₂	C ₅₁ H ₆₁ Co ₂ KN ₄ O ₂ PSi ₂
Formula weight / g·mol ⁻¹	1007.34	1006.14
Temperature / K	100.01(10)	123.01(10)
Crystal system	monoclinic	triclinic
Space group	I2/a	P-1
<i>a</i> / Å	33.8832(5)	9.8552(3)
<i>b</i> / Å	9.9150(2)	13.8414(6)
<i>c</i> / Å	32.2908(4)	19.1336(7)
α / °	90.00	87.408(3)
β / °	93.1770(10)	79.008(3)
γ / °	90.00	74.311(3)
<i>V</i> / Å ³	10831.5(3)	2466.62(16)
<i>Z</i>	8	2
ρ_{calc} / g cm ⁻³	1.235	1.355
μ / mm ⁻¹	4.261	7.131
F(000)	4320.0	1054.0
Crystal size / mm ³	0.353 × 0.263 × 0.11	0.17 × 0.13 × 0.064
Radiation / Å	Cu K α (λ = 1.54184)	Cu K α (λ = 1.54184)
2 θ range for data collection / °	7.36 to 133.36	4.704 to 147.81
Diffractometer	Supernova	Synergy DW
Index ranges	-40 ≤ <i>h</i> ≤ 38, -11 ≤ <i>k</i> ≤ 11, -25 ≤ <i>l</i> ≤ 38	-12 ≤ <i>h</i> ≤ 12, -17 ≤ <i>k</i> ≤ 17, -23 ≤ <i>l</i> ≤ 23
Reflections collected	43998	17422
Independent reflections	9477 [R _{int} = 0.0640, R _{sigma} = 0.0337]	17422 [R _{int} = 0.2128, R _{sigma} = 0.0242]
Data/restraints/parameters	9477/122/699	17422/126/619
Goodness-of-fit on F ²	1.024	1.062
Final R indexes [I >= 2 σ (I)]	R ₁ = 0.0575, wR ₂ = 0.1324	R ₁ = 0.0786, wR ₂ = 0.2145
Final R indexes [all data]	R ₁ = 0.0725, wR ₂ = 0.1447	R ₁ = 0.0938, wR ₂ = 0.2333
Largest diff. peak/hole/e Å ⁻³	0.80/-0.36	0.69/-0.99

Several crystals of [(K(thf)₂)Co₂(bpy)₂(μ , η^4 : η^4 -(3,5-Ph₂-2,6-(SiMe₃)₂PC₅H)] (**7**) were screened and all of them turned out to be non-merohedrally twinned. The twinning was identified with the Crystals Pro Software (Version 41.93). Two components with 66.7 and 33.0% were identified which were refined with the hklf5 command of SHELXL.

Table 2. Bond lengths [Å] of the bpy moieties in 2,2'-bipyridine,^[46] a 2,2'-bipyridyl radical^[33] and dinuclear complex **7**.

Bond ^[a]	Bpy	Bpy ^{•-} ^[b]	7 ^[c]
1	1.490(3)	1.430(av)	1.418(av)
2	1.346(2)	1.389(av)	1.391(av)
3	1.341(2)	1.337(av)	1.379(av)
4	1.341(2)	1.337(av)	1.359(av)
5	1.383(3)	1.404(av)	1.416(av)
6	1.385(2)	1.364(av)	1.365(av)
7	1.394(2)	1.428(av)	1.412(av)

^[a]C–X (X = C, N) bond numbered as depicted above. ^[b]Average values of the four crystallographically unique bpy radicals present in the asymmetric unit.^[33] ^[c]Average values of the two coordinating bpy moieties. The values of bpy or bpy^{•-}, which are closer to the measured values for **7** are coloured.

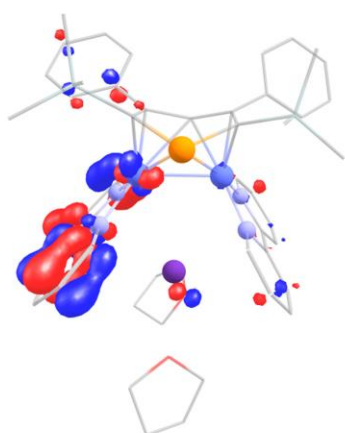
5.4.5 Computational Details

Initial calculations on $[\text{K}(\text{thf})_2][\text{Co}_2(\text{bpy})_2(\mu, \eta^4: \eta^4\text{-}(3,5\text{-Ph}_2\text{-}2,6\text{-(SiMe}_3)_2\text{PC}_5\text{H)})]$ (**7**) were performed with neglect of the cation (see SI for details). As the optimised geometries, however, did not agree with the structure determined by single-crystal X-ray crystallography, the calculations were repeated including the cation.

All calculations were performed using the r²SCAN-3c^[36] method with a conductor-like polarizable continuum model (CPCM). Population analysis was conducted using Löwdin reduced orbital populations. The orbitals for **7** with $S = 1/2$ are depicted in **Figure 52**, and the orbitals for **7** with $S = 3/2$ are displayed in **Figure 53**. The spin density is mainly located on the cobalt nuclei with a spin population for the cobalt atoms of 0.38 and 1.19 (for $S = 1/2$) or 1.73 and 1.72 (for $S = 3/2$) according to natural population analysis.

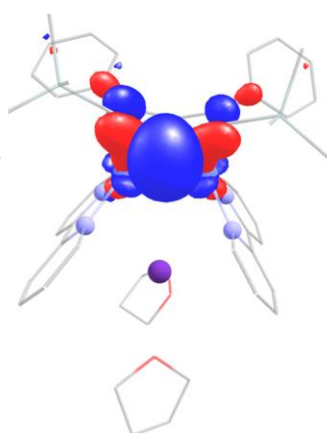
a) $S = 1/2$:

Analysis of the natural orbitals reveals the doubly occupied orbitals with the highest energies (**255-262**) to exhibit high d-orbital character. Contrary, the SOMO (**263**) displays only low d-orbital character (11%), but high contribution from the bpy moieties. With the exception of **266**, which still displays high d-orbital character (54%), the unoccupied orbitals **264-267** also exhibit high contribution from the bpy ligands.



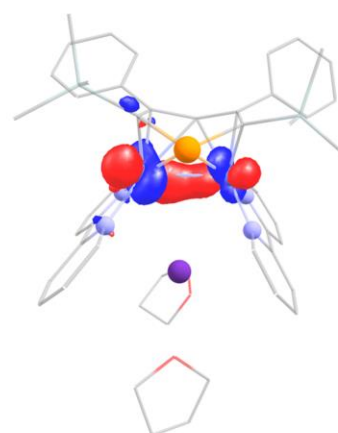
253

Occ.: 1.999,
3% $3d_{z^2}$ (3% Co1, 1% Co2),
2% $3d_{yz}$ (Co1),
1% $3d_{xz}$ (Co1),
1% $3d_{x^2-y^2}$ (Co1);
E = -0.22 eV.



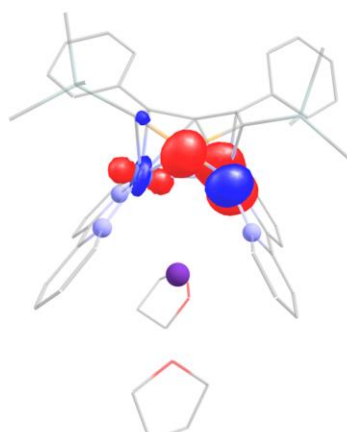
254

Occ.: 1.999,
16% $3d_{x^2-y^2}$ (7% Co1, 8% Co2),
4% $3d_{yz}$ (1% Co1, 3% Co2),
2% $3d_{xy}$ (Co1),
1% $3d_{z^2}$ (Co1);
E = -0.21 eV.



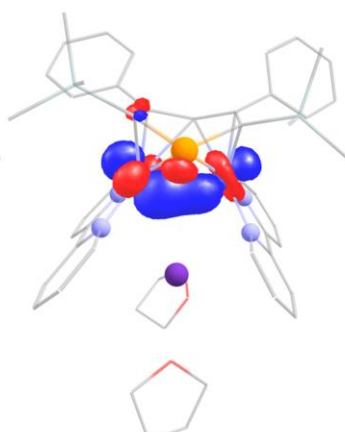
255

Occ.: 1.999,
34% $3d_{yz}$ (18% Co1, 16% Co2),
26% $3d_{xz}$ (25% Co1, 1% Co2),
9% $3d_{xy}$ (8% Co1, 1% Co2),
6% $3d_{z^2}$ (1% Co1, 4% Co2),
3% $3d_{x^2-y^2}$ (Co1);
E = -0.19 eV.



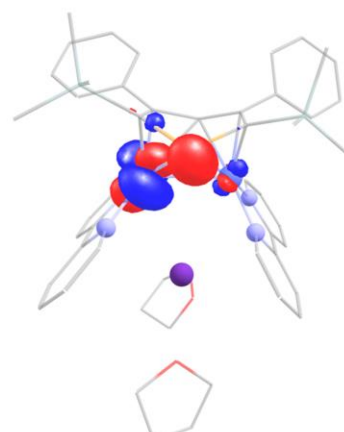
256

Occ.: 1.999,
31% $3d_{x^2-y^2}$ (Co2),
23% $3d_{xy}$ (Co2),
14% $3d_{yz}$ (2% Co1, 11% Co2),
10% $3d_{z^2}$ (5% Co1, 6% Co2),
4% $3d_{xz}$ (1% Co1, 3% Co2);
E = -0.18 eV.



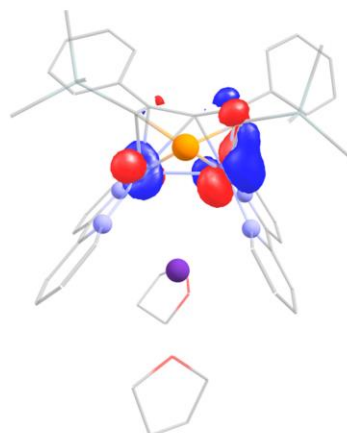
257

Occ.: 1.999,
21% $3d_{xz}$ (8% Co1, 14% Co2),
17% $3d_{z^2}$ (16% Co1, 1% Co2),
17% $3d_{xy}$ (15% Co1, 3% Co2),
13% $3d_{yz}$ (6% Co1, 7% Co2),
8% $3d_{x^2-y^2}$ (5% Co1, 3% Co2);
E = -0.18 eV.



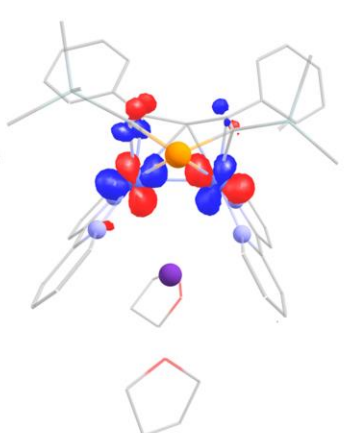
258

Occ.: 1.999,
30% $3d_{x^2-y^2}$ (27% Co1, 2% Co2),
19% $3d_{xy}$ (Co1),
17% $3d_{xz}$ (Co1),
12% $3d_{yz}$ (11% Co1, 1% Co2);
E = -0.17 eV.



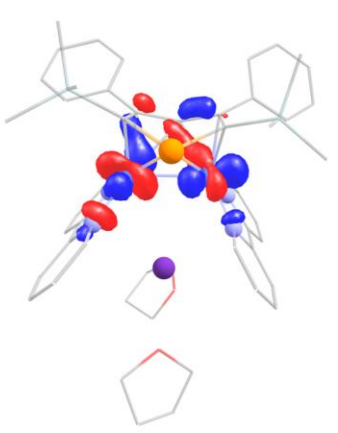
259

Occ.: 1.994,
19% $3d_{xz}$ (4% Co1, 15% Co2),
17% $3d_{x^2-y^2}$ (1% Co1, 16% Co2),
16% $3d_{xy}$ (11% Co1, 5% Co2),
13% $3d_{z^2}$ (1% Co1, 12% Co2),
11% $3d_{yz}$ (2% Co1, 9% Co2);
E = -0.17 eV.



260

Occ.: 1.988,
29% $3d_{z^2}$ (11% Co1, 19% Co2),
22% $3d_{yz}$ (12% Co1, 10% Co2),
6% $3d_{xz}$ (Co1),
4% $3d_{x^2-y^2}$ (3% Co1, 1% Co2),
2% $3d_{xy}$ (Co2);
E = -0.15 eV.



261

Occ.: 1.979,
36% $3d_{xz}$ (9% Co1, 27% Co2),
17% $3d_{z^2}$ (12% Co1, 5% Co2),
12% $3d_{x^2-y^2}$ (Co1),
2% $3d_{xy}$ (Co1),
1% $3d_{yz}$ (Co1);
E = -0.17 eV.

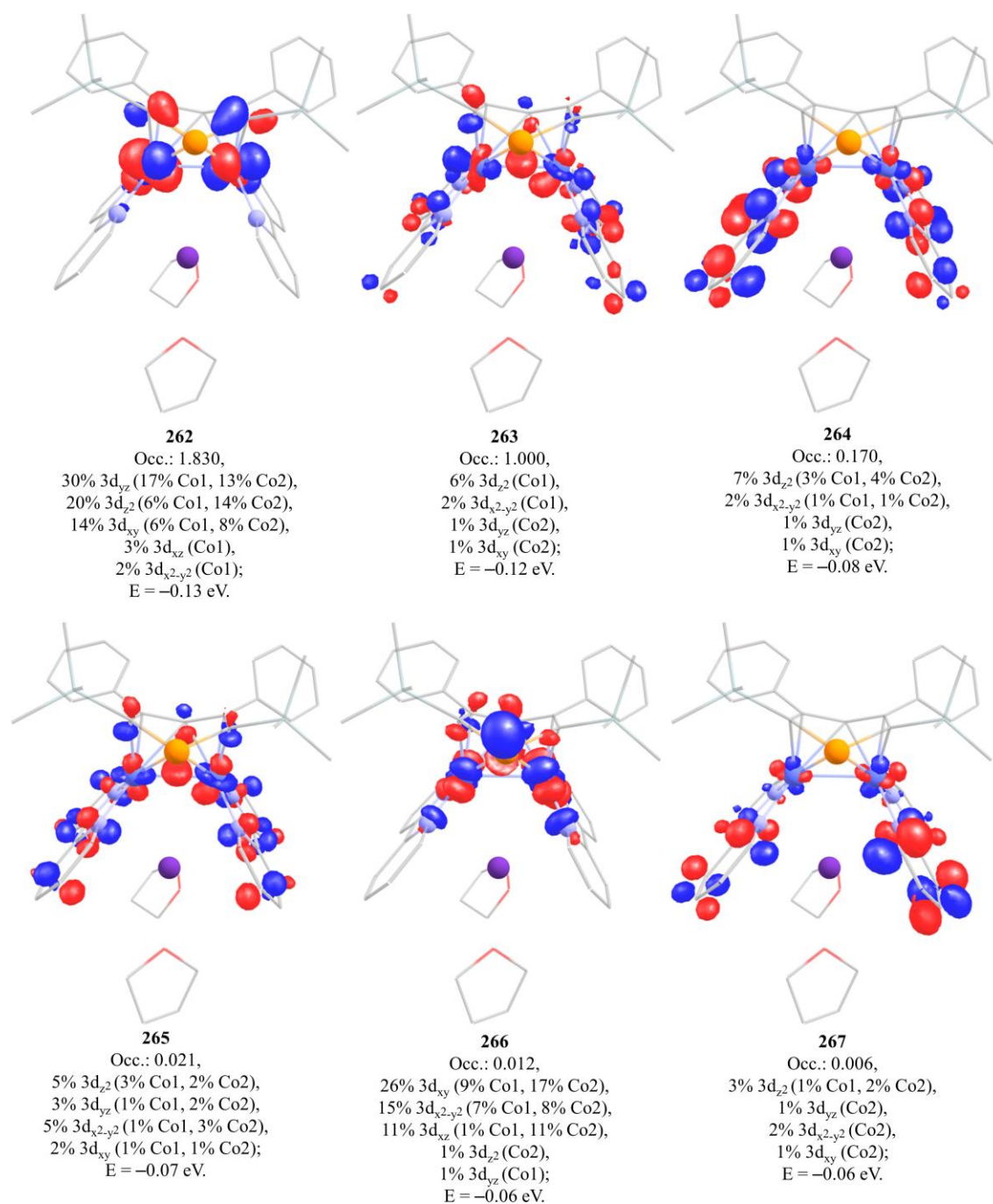
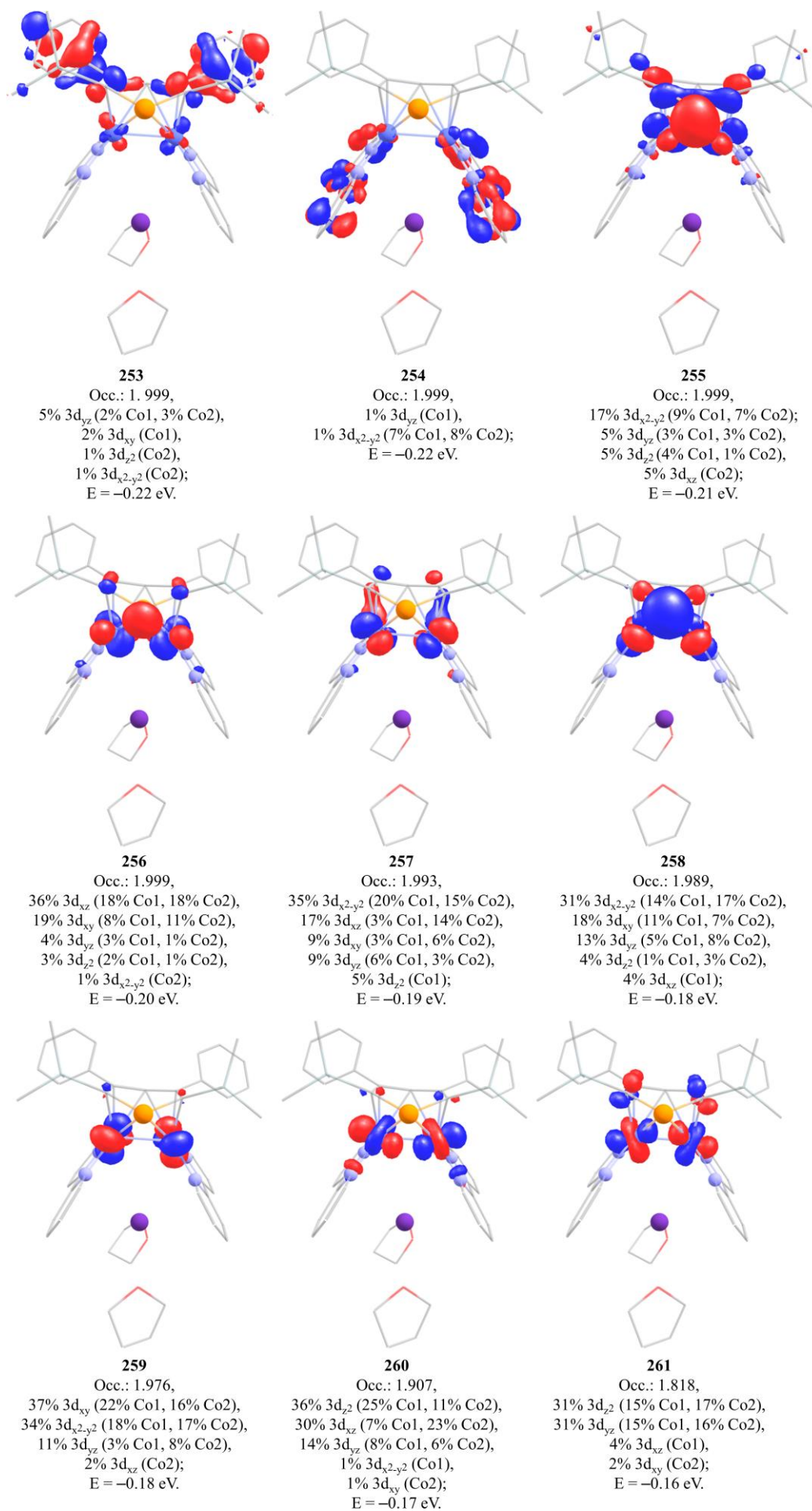


Figure 52. Selected molecular orbitals of **7** ($S = 1/2$) obtained from calculations using the r^2 SCAN-3c method. The contour plots are displayed with an isosurface value of 0.05 a.u..

b) $S = 3/2$:

Analysis of the natural orbitals reveals the doubly occupied orbitals with the highest energies (**256-261**) to exhibit high d-orbital character. Of the three SOMOs (**262-264**) only the energetically lowest SOMO (**262**) displays a high d-orbital character (63%). The other two SOMOs (**263-264**) exhibit high contribution from the bpy ligands and the phosphinine. Similarly, the unoccupied orbitals **265** and **266** also display high contribution from the bpy ligands.



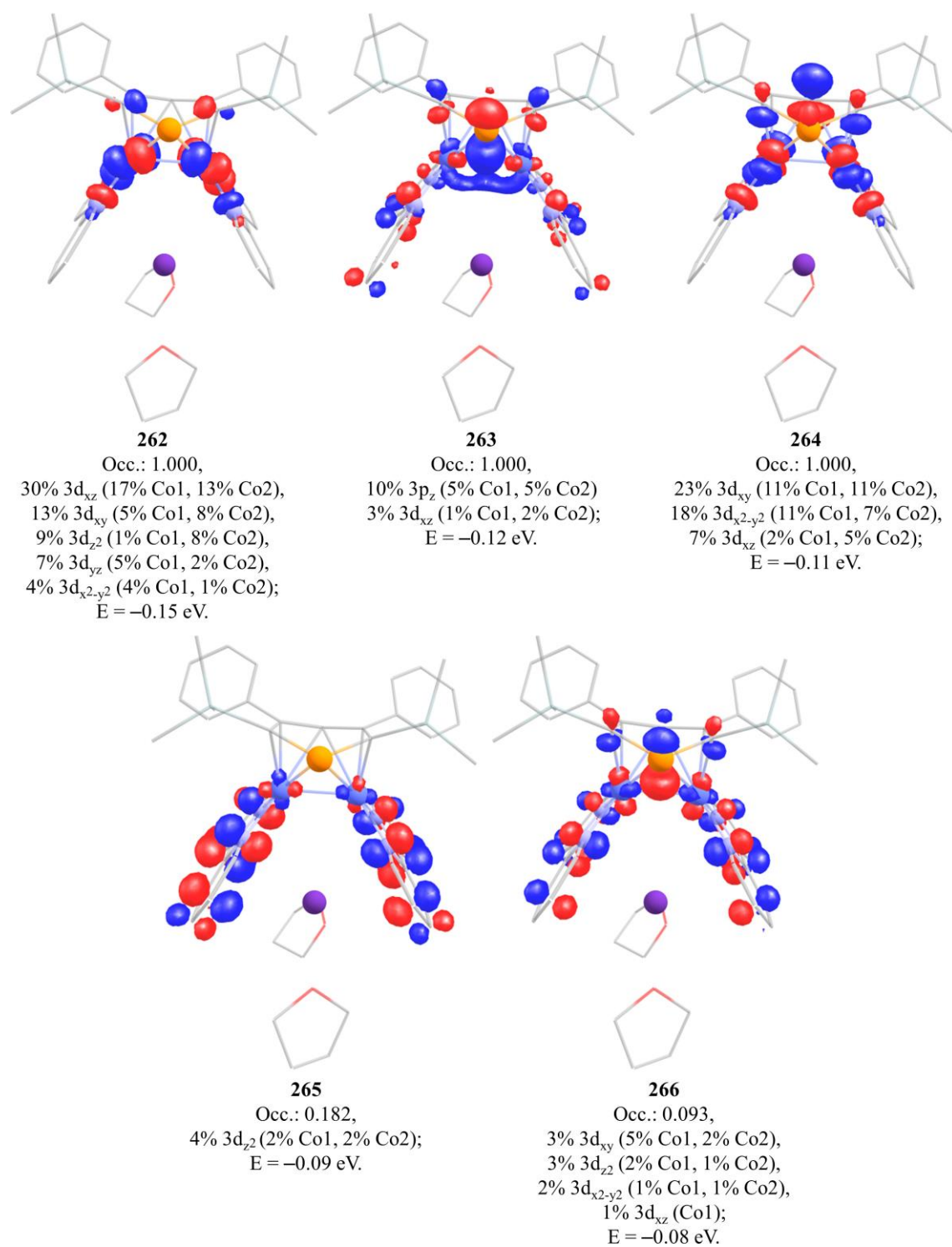


Figure 53. Molecular orbitals of **7** ($S = 3/2$) obtained from calculations using the r^2 SCAN-3c method. The contour plots are displayed with an isosurface value of 0.05 a.u..

Cartesian Coordinates of the Optimised Geometries

a) S = 1/2

Co	10.19116930829715	8.81254626344624	15.29388338964638
Co	9.63458230728228	8.73594371296203	12.81747075318512
P	8.92935028754949	10.57779804729445	14.28967141439127
K	8.46052724484433	5.93827181325528	4.26038970172044
Si	9.75451644466899	11.79499613548292	17.14529890742780
Si	9.08111035047891	11.91416298254643	11.40458288140841
N	10.29956168914626	7.17348338397555	11.89460062361952
N	8.80237465767686	8.06810524407440	16.36867184180385
N	7.92752742889388	8.04725963287693	12.17619186454863
N	11.13143622055566	7.26123524466447	15.86683518331660
C	11.49222828218406	10.32533034329564	15.25547806920644
C	7.53952942431402	8.55525783014772	16.55664746887680
H	7.29476868847110	9.44650354822973	15.98469416391161
C	9.14955765717450	6.92189423665593	17.08515246657570
C	12.66217682629539	10.42013613890753	16.16941794058425
C	11.97563369604531	10.12487180103241	11.50634632900663
C	11.65018304354918	9.67426257945157	13.97446550523125
C	10.46577877180548	6.46650308075075	16.80218193130283
C	8.01822976361174	6.93515167740930	11.33790929187519
C	11.07901670565933	10.10662570602780	12.68956314572548
O	6.12186052086438	4.67278277168721	14.68588074426976
C	9.79467003818860	10.74183624539567	12.68738919170148
C	12.40822689779617	6.88978916863517	15.55179350581614
H	12.92201899672505	7.51610590634210	14.83306238285512
C	6.68311156350123	8.54800888077502	12.42210196846863
H	6.65691843636743	9.41303411353509	13.08251627128756
C	13.78112613450917	9.91970343891687	18.26215700486196
H	13.78313917363538	9.41529543696189	19.22512344873545
C	12.68573450202016	9.78395699902472	17.41426955653449
H	11.83993156251554	9.16565847173209	17.70017685408950
C	9.35073106522129	6.44843366027725	11.17640713915069
C	9.73177565598294	5.33877353452583	10.39634133281907
C	11.59674520644468	6.76715365132521	11.81257987012580
C	8.22954899973956	6.29765754874442	17.95226152831201
H	8.52841395161701	5.40204492351051	18.48802592373389
C	13.77635232037636	11.17563949366960	15.78285308168176
H	13.76667847568985	11.67795798116449	14.81863732044305
O	9.51990810636645	3.45931204729647	14.44771554750363
C	13.31116412567128	10.53593091550439	11.62108639938845
H	13.69388605289048	10.84020511754833	12.59147664343198
C	11.07969456673639	5.33621914466088	17.37498287761703
H	10.52833946021709	4.73948479844183	18.09491191320389
C	10.20043534550415	10.82546175815942	15.59398165465219
C	14.87747846346688	10.68830591296456	17.87499573507515
H	15.73368408719410	10.79279215944993	18.53582172347977
C	5.62230814534803	6.90196666613754	11.02650085670754
H	4.72946080777418	6.46768270332666	10.58780408485759
C	6.61853771783210	7.97949894872594	17.39288546617778
H	5.63489221075155	8.42824748506849	17.48715915627814
C	13.04581600740917	5.80566661961159	16.09673199949081
H	14.06564315774303	5.58652839790782	15.79646754206723
C	6.96698594035650	6.81410815327524	18.11640647477038
H	6.25484803838572	6.33839524689709	18.78301404407933

C	12.01013857642800	5.68998442942325	11.06987995684773
H	13.06216244938718	5.42381767740583	11.04989922506997
C	11.51521927584236	9.73570098756394	10.24068356525787
H	10.49946971388453	9.36249904202058	10.15211185454083
C	10.41944632075246	13.08504226555940	10.76981125922941
H	10.93448684110768	13.56829279699759	11.60856250759966
H	9.97213642000475	13.87020513591393	10.14768213606737
H	11.17002319469763	12.55855916711562	10.17153794667151
C	6.86189980741351	6.36803647346018	10.76387032193182
H	6.95661200496934	5.50348461180994	10.11378326089668
C	13.66399807137254	10.21862498648042	9.25143980904513
H	14.31446221217358	10.25556159962188	8.38188599867705
C	14.14459405493289	10.58647085688752	10.50599932351376
H	15.17372177165252	10.91825677189190	10.61839411436430
C	5.53368912753374	8.02379583904037	11.88805808644322
H	4.57645713105693	8.47669288826705	12.12593926345148
C	14.87257068815146	11.31393190574515	16.62923512573492
H	15.72369801956262	11.91363075995349	16.31727675910259
C	11.05096813097323	4.95195118551379	10.33556216451797
H	11.34877157948516	4.09866090812473	9.73423353118415
C	11.01816589911795	13.17129228018963	17.41304446964982
H	12.00586897059305	12.76538989703807	17.65651915460669
H	10.70046557055202	13.81967279765397	18.23906929121179
H	11.11888306481267	13.79081839463481	16.51415769157504
C	12.34231082920328	9.78871013060680	9.12619197276759
H	11.96013881731567	9.47875436647724	8.15671118215118
C	12.36776300110596	4.99693447892451	17.03758559317300
H	12.84969494359127	4.13081683264805	17.47960931168624
C	8.22774797222377	11.08681833823848	9.93455665146440
H	8.93284073160914	10.63194088281726	9.23215442508730
H	7.64648299319182	11.83884731022235	9.38579806477108
H	7.53493989729406	10.30742955031379	10.27351344439866
C	7.75522194897725	12.97089953839223	12.23522476668323
H	6.91201729308054	12.36177719389409	12.58028531179889
H	7.37122951067855	13.70982322698726	11.52058283452353
H	8.15363572974111	13.50805451722921	13.10359040070775
C	9.63315837443500	10.76986615174774	18.72857353245614
H	9.09051328734586	9.83370792284256	18.55619593083645
H	9.08798675403510	11.34369518284885	19.48868901233166
H	10.61846559954667	10.52405495469080	19.13587066699203
C	8.06810456124658	12.60092639533178	16.89699976707823
H	8.04996632805093	13.23433521860674	16.00313685314739
H	7.83398359219087	13.22691406763668	17.76727464591820
H	7.27182397297721	11.85506299358463	16.79422172618603
C	6.04775112849029	3.80059320027587	15.84279462148901
H	5.66442151891083	4.37646735955052	16.69712391986957
H	7.06167610466239	3.45336089664555	16.07644729053844
C	10.91260592789154	3.44885123749871	14.02553520579932
H	11.54921033792144	3.30732917167619	14.90588370250513
H	11.14371938729063	4.43111044748636	13.58784739296862
C	8.82266004663049	2.37660807957859	13.79309037532835
H	8.81634083166658	1.48968656663345	14.44599818093731
H	7.78957564996871	2.70105977963075	13.62530732102397
C	5.04884721157913	4.34615518276529	13.76556333401723
H	5.47894473812063	3.84392996141581	12.88613533753018
H	4.57758723574500	5.28033092298103	13.44200734508703

C	5.09181869324462	2.68067016953838	15.45330051076133
H	5.62363612019427	1.89819174206736	14.89879913959986
H	4.60842484918690	2.22687422488663	16.32273339865049
C	11.04903756208793	2.31975168030162	13.00003006078346
H	11.41553158530389	1.40705251593778	13.48277852140973
H	11.73691231712328	2.58519412941705	12.19231907737463
C	4.11443938025674	3.41723937237025	14.53128096795741
H	3.55914495176322	2.74940550259921	13.86709744164637
H	3.39766801473764	3.99792976299506	15.12356734290866
C	9.60843162279964	2.11904320775840	12.51733626966088
H	9.35160079486347	2.86896081044186	11.76003527998854
H	9.42822347406840	1.12225803572770	12.10483258987250
H	12.59058141375946	9.13824321928274	13.86213416783320
H	8.97815807792700	4.79273048077631	9.83690004507818
H	12.30859145615784	7.36435172371793	12.37564613099406

b) $S = 3/2$

Co	10.22889935220539	8.73176292290211	15.25047950855955
Co	9.88638400700251	8.77551837823427	12.90696074871118
P	9.02039971817844	10.63919385672164	14.27285896290000
K	7.83455978947513	6.09196603066165	14.38253355151850
Si	9.89299806006072	11.73900323271043	17.11879743264736
Si	9.01678859516786	11.82050722706077	11.32620378850389
N	10.67929756977652	7.23867201696590	11.98522691935763
N	8.86108531709151	7.93723745439997	16.46796547131877
N	8.22469818609979	7.98721196738493	12.13723307537118
N	11.24586769970767	7.17706421197083	15.87879062957965
C	11.62565705610353	10.32035432188185	15.17953751893935
C	7.58755972786699	8.36839742642092	16.68083746631937
H	7.32224149414789	9.29280410015674	16.16960753091329
C	9.25820667674063	6.76403977014285	17.09761908947346
C	12.76515634025396	10.35194723345401	16.13863626364069
C	12.05917231354456	10.46151143710603	11.38941195159191
C	11.93923751205323	9.96904690627318	13.82409125026667
C	10.60073456053175	6.36155196104657	16.79405828606934
C	8.42092356830758	6.81059596074528	11.42022689580959
C	11.24376346016540	10.36894476676244	12.63353290697022
O	5.55765162220528	4.70818400239378	14.78254703445718
C	9.88654655916607	10.81971358699723	12.66665880304616
C	12.52709315355154	6.86564797252401	15.55429511521282
H	13.00236525008421	7.53597212482570	14.84274083457752
C	6.94219244805409	8.40715796659083	12.32056834908234
H	6.83768764490285	9.33871569086088	12.87466491176314
C	13.75616868679960	9.79901040615649	18.28546113307652
H	13.68001744497456	9.30335124527083	19.24998498235106
C	12.69459486188703	9.72852990060758	17.38969173891706
H	11.80238587876607	9.16422471756089	17.64274809161310
C	9.79386655892358	6.42297035330682	11.29724416176657
C	10.25603228001381	5.31980428391116	10.55365381510142
C	12.00081443029980	6.93293586695292	11.91309611179772
C	8.35626127550110	6.03552727064500	17.89873423629311
H	8.67658397422984	5.10740980330223	18.36195227661426
C	13.94736872468756	11.02482201116528	15.79948695873748
H	14.01819125713468	11.51530505924736	14.83191043564083
O	9.09226304652615	3.71687810064503	14.52954851386737

C	13.26274417974590	11.18038802106626	11.39808457469840
H	13.58769363661857	11.65635829794326	12.31990462069930
C	11.25039627017065	5.24552025683393	17.35335581822977
H	10.72608952140046	4.61949169342482	18.06843118006972
C	10.32142116382431	10.76930656128410	15.55919914159532
C	14.91976363194827	10.48641570934030	17.94335562487285
H	15.75091198480482	10.53896542503602	18.64129103323307
C	6.03481135963229	6.49702836296525	11.17684756980013
H	5.18638385472685	5.91908562154508	10.82495813060854
C	6.67569079297090	7.69535567360666	17.45763242936151
H	5.67401977484870	8.09458003832763	17.58140281398234
C	13.20671826712311	5.79269288346844	16.07776630438922
H	14.23395548408084	5.60921847668373	15.77906703407533
C	7.06871367437315	6.48840087818837	18.08474047008913
H	6.36930289470537	5.92736328615025	18.69606656592279
C	12.49919215486139	5.86595802741617	11.20647384965242
H	13.56939115434236	5.68622967488870	11.18710301054612
C	11.65813406064488	9.85705611525358	10.19287750969360
H	10.75249121057383	9.25830703930169	10.18708960635697
C	10.13393288328346	13.22397543418391	10.73279635437186
H	10.48057121653918	13.83301137253455	11.57597089371304
H	9.58278531582976	13.87787625696949	10.04533382565046
H	11.01536296954230	12.84150746616069	10.20698908753915
C	7.32175080818829	6.06030898446105	10.95304549217184
H	7.49250306163525	5.12744173404188	10.42393306091101
C	13.60104751031215	10.72503260116228	9.05085085598261
H	14.19489734012441	10.82838055831165	8.14678797574025
C	14.02378450053193	11.31513921823070	10.24072405235562
H	14.94741303822396	11.88759049961693	10.26666779989687
C	5.84187670070446	7.71519240124393	11.87551141505959
H	4.84697651261922	8.10750096320598	12.06084624251028
C	15.01190048047108	11.09572503352264	16.69340357150756
H	15.91488638046772	11.63268713791312	16.41451403710931
C	11.60093090359638	5.03216241041325	10.50182075129872
H	11.96355559490957	4.18828657782150	9.92316994648940
C	11.16004626737584	13.11372928848750	17.38759012683255
H	12.15058318849444	12.70633600151852	17.61670387429140
H	10.85165533081382	13.75430292417129	18.22335287214123
H	11.25077548827614	13.74186305329760	16.49357283529284
C	12.41589158094068	9.99166594237080	9.03403492000187
H	12.08592906369141	9.51039204626899	8.11681789501658
C	12.55029734052589	4.95336017097243	17.00549046945242
H	13.05918601643232	4.09730380568960	17.43750231431219
C	8.43971878532754	10.84438389352884	9.81234817717876
H	9.25571896429379	10.64742802328826	9.11082483683071
H	7.67434818303506	11.42662159695624	9.28359271019642
H	7.99715592839154	9.88424785441642	10.10026341197796
C	7.46098710629829	12.60750193075678	12.04910170259927
H	6.72853508639426	11.85458088797612	12.36107817497732
H	6.99243269971036	13.23645782498047	11.28129368071005
H	7.68431658377476	13.23403028034527	12.91921642329808
C	9.76132977674310	10.72972362710465	18.71431391318497
H	9.26383080779936	9.76946030228636	18.53846992415536
H	9.16595308587587	11.29300863213201	19.44390704100835
H	10.73991274856329	10.53083564604555	19.16104321127183
C	8.20664641115875	12.55639859942675	16.89667489259091

H	8.17875274208953	13.20804947250186	16.01684365561929
H	7.98652929494274	13.16318838055830	17.78433583258639
H	7.40714940017301	11.81477401357273	16.78786374424488
C	5.49892216490606	3.81126051938559	15.92114570214382
H	5.06435653537814	4.34985158647404	16.77521617485435
H	6.52272160791899	3.51202160789016	16.17634680633725
C	10.46511700792603	3.73762441747351	14.04129810987494
H	11.14289281640001	3.68579282688327	14.89961092184196
H	10.63127344363216	4.69110610921437	13.51880270889500
C	8.37409567033342	2.64078741195022	13.88138016875419
H	8.34601936356951	1.76450293781331	14.54714876471430
H	7.34676350463127	2.98020976862564	13.70284426499958
C	4.52232902365680	4.34904193237523	13.83127584921733
H	4.99670825116114	3.89078348323367	12.95090548914499
H	4.00959821206014	5.26517055386887	13.51873886091703
C	4.61230210059169	2.65226009827725	15.48566366400937
H	5.19757585912292	1.91053851783398	14.92896152650616
H	4.13305502835513	2.15543895221175	16.33358777599392
C	10.59839265955022	2.54824541052898	13.09212246828587
H	10.94421721579724	1.66060036213156	13.63417350213064
H	11.29660036848853	2.75621908757689	12.27688551740060
C	3.61974912143772	3.35713183540993	14.55524791593058
H	3.11482342644402	2.67613856142587	13.86471234596647
H	2.86066386931588	3.88772619892435	15.14165534286974
C	9.15810262005183	2.34621722899016	12.61219319997263
H	8.90811874457145	3.08001018034821	11.83640641466862
H	8.96769477186757	1.34194342376108	12.22320162754424
H	12.93710367166024	9.56489191321612	13.66546253334883
H	9.54831161594108	4.70593484324301	10.00530430736418
H	12.66189305353653	7.60297379378899	12.45676199396852

c) $S = 5/2$

Co	10.16089664612342	8.76751928755027	15.40594666274260
Co	9.74074172434896	8.72322350505185	13.09235555767762
P	8.96117712703494	10.66977573481734	14.39019338420249
K	8.44316077199738	5.93832748767075	14.42990756469089
Si	9.95755576805795	11.86464373123167	17.16632145928984
Si	8.91075170335394	11.75078966868431	11.39892874771054
N	10.42739287511803	7.04535907730313	12.17773047428943
N	8.76770174709272	8.00242437307645	16.61749833940866
N	7.95856805596257	7.96262160863761	12.37189873069716
N	11.15121527181766	7.21220424129211	16.08072539592175
C	11.58347815459394	10.31219990458365	15.23383942242437
C	7.49070463378705	8.43981556959899	16.78929523906161
H	7.24506480814845	9.36164797047926	16.26447911464358
C	9.13681777716423	6.82940736271746	17.26517026993184
C	12.76181768001975	10.36451773692942	16.14257944275167
C	11.90060245653085	10.26622534755794	11.43027183061224
C	11.82428817822083	9.86029960790034	13.88454899811407
C	10.47951798455000	6.41026573804864	16.99411619823427
C	8.16365262920948	6.98207669864710	11.40518184422338
C	11.12571789758351	10.28630153713687	12.70236183390948
O	6.05913193070498	4.69042355096033	14.46946260190780
C	9.79577940836290	10.79006747534675	12.75792560244518
C	12.44062542702911	6.88830042030121	15.79351391650761

H	12.94193241214411	7.55320480914861	15.09490509331620
C	6.71443347828703	8.42694715633321	12.57768584477389
H	6.62932580183578	9.18883018485145	13.35296677844033
C	13.82431669075716	9.90587746568464	18.27625349697477
H	13.77782593740847	9.46239528547137	19.26761563098849
C	12.72907529291954	9.80573062823197	17.42500775905895
H	11.83877735609695	9.26990690276313	17.74002492372864
C	9.50354264381095	6.49297458424148	11.29384132076349
C	9.93388991188976	5.51793389236329	10.35862204993868
C	11.70367969806735	6.62675486205846	12.13399851559991
C	8.20564179247726	6.11031948653568	18.04415047773444
H	8.50539743918843	5.17995928327725	18.51655100646599
C	13.93995794896905	10.99709261861734	15.72322222878494
H	13.98103795663229	11.43399649600724	14.72864839487798
O	9.47970195529803	3.44581898383921	14.62963620447055
C	13.13688348981725	10.92158491772355	11.35434791621138
H	13.51491006995113	11.44076824350281	12.23150272004160
C	11.10485295458047	5.28443694867306	17.56531394341924
H	10.55802114201830	4.66545101123953	18.26956358052077
C	10.31391964927057	10.82436334389782	15.63112639079975
C	14.98291960574251	10.55731903372018	17.85624802723187
H	15.83984446950165	10.63409461139816	18.51987702200447
C	5.80933655986261	7.03718896550623	10.84762552619724
H	4.97178172230757	6.69089105023131	10.24850803151426
C	6.55630573638958	7.78551753842325	17.55332167836344
H	5.55695659246158	8.19719696078097	17.65165624486903
C	13.09704206165340	5.81330526760543	16.33828983368916
H	14.13044452350335	5.62122809863357	16.06754334694735
C	6.92094404981205	6.57845915033678	18.19700076007157
H	6.20059154632161	6.02841132657427	18.79427267398279
C	12.16845544254566	5.66969076974496	11.25538698685787
H	13.21108310093869	5.37229796356631	11.26957248948793
C	11.42995943578644	9.60248601768767	10.29186790471714
H	10.49451138174560	9.05389722186479	10.34645986364925
C	10.06071683646858	13.05071740666443	10.65459087561150
H	10.48109216088502	13.69775183304774	11.43335893185728
H	9.50282425938363	13.68313646801817	9.95254089734975
H	10.89304778246320	12.59118379994383	10.11081960028034
C	7.06739564152403	6.53144754202243	10.62658531681214
H	7.22094389774407	5.78539558047514	9.85338788403055
C	13.37669545760416	10.28505270115181	9.03743526832995
H	13.94575754594318	10.29388234256148	8.11186665986795
C	13.86496349874559	10.93746850597463	10.16854969541446
H	14.81520299812512	11.46330662212680	10.12595483291719
C	5.61081585687415	8.00519229379271	11.86325019013782
H	4.63090633217844	8.42052559683146	12.07133004257664
C	15.03755953555014	11.09834540916676	16.57293793555755
H	15.93712126459179	11.60521058517928	16.23346356446112
C	11.24567334704570	5.11094718497229	10.33681283022045
H	11.57127405874327	4.36632351918777	9.61575394491106
C	11.32726244838494	13.13387502094881	17.45074335494952
H	12.27001859422772	12.65629829576535	17.73693887102504
H	11.03309181951111	13.82096069620037	18.25405518937042
H	11.50792981336039	13.72723216548874	16.54669624325570
C	12.15767263592451	9.61328008833374	9.10611633434115
H	11.77562904487506	9.08585321323511	8.23578378470359

C	12.40781409493122	4.97776046926177	17.24717571312313
H	12.89666139332329	4.11539704275707	17.68951827580724
C	8.21027545632994	10.70920137472090	9.98255069469312
H	8.98120839520518	10.40839111202375	9.26691348538512
H	7.46519240855354	11.30633108813973	9.44130869340719
H	7.71282849708460	9.80580580870071	10.35233360725567
C	7.43691400432807	12.65655316477365	12.15012415409842
H	6.69441121682535	11.96044216889454	12.55615637509579
H	6.94971592090063	13.25657149794965	11.37099460415003
H	7.74203505059526	13.32672157192240	12.96122813487355
C	9.71233670169940	10.88208113687735	18.76250745457428
H	9.07214289742537	10.00817315008685	18.59753803212057
H	9.22557597826183	11.52478178200372	19.50703800255566
H	10.65965167943127	10.53625328057256	19.18687194772356
C	8.35405078010977	12.82166005895869	16.89668949146129
H	8.39863971461204	13.44390980806191	15.99613767536475
H	8.17824610599359	13.47566959066057	17.76031739830659
H	7.49196763211639	12.15295454438566	16.79589155923616
C	5.78915053581171	3.89538745744862	15.65207375846739
H	5.31631030520531	4.53560156484669	16.41050912986647
H	6.74549301582354	3.52885730191170	16.04539964046873
C	10.87326722063693	3.46996021539831	14.20950603922446
H	11.50853229994881	3.18991599417296	15.05752898718866
H	11.12082565386220	4.50182613062959	13.92091669659778
C	8.78644436394198	2.43030102045259	13.87174639422876
H	8.82452484395282	1.47008929001508	14.40989904017576
H	7.74233334450806	2.74658815398284	13.77535473046591
C	5.10212266220586	4.35413491145587	13.43134232674306
H	5.62395280598933	3.79575384315527	12.63984344774267
H	4.71346610915138	5.28588152513079	13.00738225318163
C	4.85052937097067	2.78612755532708	15.19624969660778
H	5.42088015549535	1.95427364141926	14.76575180581855
H	4.23518594064990	2.40159656818147	16.01423217780271
C	10.99176802815818	2.50059822159740	13.02751727628066
H	11.37962327721220	1.53262264344818	13.36279024078688
H	11.65379696244519	2.89030992936969	12.24958701973186
C	4.03866054592945	3.49756654721625	14.10891497535323
H	3.55461392292257	2.80941458707771	13.41053098532144
H	3.26926162882502	4.13218836898020	14.56393871348070
C	9.54077687154521	2.35280262546909	12.55464994948202
H	9.25932359776061	3.19353550266162	11.90810371193813
H	9.35844236436274	1.41895837323344	12.01519078631007
H	12.79550207515901	9.40229426148578	13.70785432262728
H	9.22608192442593	5.09527299633337	9.65263802023017
H	12.37300690841097	7.10842653169712	12.84431302876710

References

- [1] G. Märkl, *Angew. Chem. Int. Ed. Engl.* **1966**, *5*, 846–847.
- [2] a) K. K. Baldrige, M. S. Gordon, *J. Am. Chem. Soc.* **1988**, *110*, 4204–4208; b) L. Nyulaszi, T. Veszpremi, J. Reffy, B. Burkhardt, M. Regitz, *J. Am. Chem. Soc.* **1992**, *114*, 9080–9084; c) L. Nyulászi, *Chem. Rev.* **2001**, *101*, 1229–1246.
- [3] a) N. Mézailles, P. Floch, *Curr. Org. Chem.* **2006**, *10*, 3–25; b) C. Müller, D. Vogt, *Dalton Trans.* **2007**, 5505–5523; c) C. Müller, L. E. E. Broeckx, I. de Krom, J. J. M. Weemers, *Eur. J. Inorg. Chem.* **2013**, *2013*, 187–202; d) N. T. Coles, A. Sofie Abels, J. Leitl, R. Wolf, H. Grützmacher, C. Müller, *Coord. Chem. Rev.* **2021**, *433*, 213729.
- [4] P. Le Floch, F. Mathey, *Coord. Chem. Rev.* **1998**, *178-180*, 771–791.
- [5] J. Deberitz, H. Nöth, *J. Organomet. Chem.* **1973**, *49*, 453–468.
- [6] a) K. C. Dash, J. Eberlein, H. Schmidbaur, *Synth. React. Inorg. Met-Org. Chem.* **1973**, *3*, 375–380; b) M. Fraser, D. G. Holah, A. N. Hughes, B. C. Hui, *J. Heterocycl. Chem.* **1972**, *9*, 1457–1459.
- [7] C. Elschenbroich, M. Nowotny, A. Behrendt, W. Massa, S. Wocadlo, *Angew. Chem. Int. Ed. Engl.* **1992**, *31*, 1343–1345.
- [8] C. Elschenbroich, M. Nowotny, A. Behrendt, K. Harms, S. Wocadlo, J. Pebler, *J. Am. Chem. Soc.* **1994**, *116*, 6217–6219.
- [9] C. Elschenbroich, M. Nowotny, J. Kroker, A. Behrendt, W. Massa, S. Wocadlo, *J. Organomet. Chem.* **1993**, *459*, 157–167.
- [10] C. Elschenbroich, M. Nowotny, B. Metz, W. Massa, J. Graulich, K. Biehler, W. Sauer, *Angew. Chem. Int. Ed. Engl.* **1991**, *30*, 547–550.
- [11] P. L. Arnold, F. G. N. Cloke, K. Khan, P. Scott, *J. Organomet. Chem.* **1997**, *528*, 77–81.
- [12] N. Mézailles, L. Ricard, F. Mathey, P. Le Floch, *Organometallics* **2001**, *20*, 3304–3307.
- [13] M. Doux, L. Ricard, F. Mathey, P. L. Floch, N. Mézailles, *Eur. J. Inorg. Chem.* **2003**, *2003*, 687–698.
- [14] A. Moores, N. Mézailles, L. Ricard, Y. Jean, P. Le Floch, *Organometallics* **2004**, *23*, 2870–2875.
- [15] B. Rezaei Rad, U. Chakraborty, B. Mühlendorf, J. A. W. Sklorz, M. Bodensteiner, C. Müller, R. Wolf, *Organometallics* **2015**, *34*, 622–635.
- [16] C. M. Hoidn, R. Wolf, *Dalton Trans.* **2016**, *45*, 8875–8884.
- [17] C. M. Hoidn, J. Leitl, C. G. P. Ziegler, I. G. Shenderovich, R. Wolf, *Eur. J. Inorg. Chem.* **2019**, *2019*, 1567–1574.
- [18] F. Nief, J. Fischer, *Organometallics* **1986**, *5*, 877–883.
- [19] K. C. Nainan, C. T. Sears, *J. Organomet. Chem.* **1978**, *148*, C31–C34.
- [20] B. Schmid, L. M. Venanzi, T. Gerfin, V. Gramlich, F. Mathey, *Inorg. Chem.* **1992**, *31*, 5117–5122.
- [21] P. A. Cleaves, S. M. Mansell, *Organometallics* **2019**, *38*, 1595–1605.
- [22] a) A. Breque, C. C. Santini, F. Mathey, J. Fischer, A. Mitschler, *Inorg. Chem.* **1984**, *23*, 3463–3467; b) A. Campos-Carrasco, L. E. E. Broeckx, J. J. M. Weemers, E. A. Pidko, M. Lutz, A. M. Masdeu-Bultó, D. Vogt, C. Müller, *Chemistry* **2011**, *17*, 2510–2517; c) I. de Krom, E. A. Pidko, M. Lutz, C. Müller, *Chemistry* **2013**, *19*, 7523–7531.
- [23] J. Leitl, P. Coburger, D. J. Scott, C. G. P. Ziegler, G. Hierlmeier, R. Wolf, N. P. van Leest, B. de Bruin, G. Hörner, C. Müller, *Inorg. Chem.* **2020**, *59*, 9951–9961.
- [24] J. Leitl, M. Marquardt, P. Coburger, D. J. Scott, V. Streitferdt, R. M. Gschwind, C. Müller, R. Wolf, *Angew. Chem. Int. Ed. Engl.* **2019**, *58*, 15407–15411.
- [25] K. Eggers, F. W. Heinemann, M. Hennemann, T. Clark, P. Binger, U. Zenneck, *C. R. Chim.* **2010**, *13*, 1203–1212.
- [26] N. Mézailles, P. Rosa, L. Ricard, F. Mathey, P. Le Floch, *Organometallics* **2000**, *19*, 2941–2943.
- [27] W. W. Brennessel, J. E. Ellis, *Inorg. Chem.* **2012**, *51*, 9076–9094.
- [28] D.-H. Ha, L. M. Moreau, C. R. Bealing, H. Zhang, R. G. Hennig, R. D. Robinson, *J. Mater. Chem.* **2011**, *21*, 11498.
- [29] W. W. Brennessel, J. E. Ellis, *Acta Crystallogr. E: Crystallogr. Commun.* **2014**, *70*, m180.
- [30] a) C. G. Kreiter, A. Georg, G. J. Reiß, *Chem. Ber.* **1997**, *130*, 1197–1200; b) Y.-Y. Zhou, D. R. Hartline, T. J. Steiman, P. E. Fanwick, C. Uyeda, *Inorg. Chem.* **2014**, *53*, 11770–11777; c) K. Jonas, G. Koepe, L. Schieferstein, R. Mynott, C. Krger, Y.-H. Tsay, *Angew. Chem. Int. Ed. Engl.* **1983**, *22*, 920–928; d) K. Jonas, V. Wiskamp, Y. H. Tsay, C. Krueger, *J. Am. Chem. Soc.* **1983**, *105*, 5480–5481.
- [31] L. Pauling, *Proc. Natl. Acad. Sci. U.S.A.* **1976**, *73*, 4290–4293.
- [32] a) J. Y. Liu, B. Yuan, L. J. Zhang, Y. Wang, B. Ding, X. J. Zhao, *Inorg. Chim. Acta* **2013**, *407*, 126–130; b) G. Lyubartseva, S. Parkin, *Acta Crystallogr. E: Crystallogr. Commun.* **2010**, *66*, m475–6; c) N. Singh, K. Diwan, M. G.B. Drew, *Polyhedron* **2010**, *29*, 3192–3197.
- [33] E. Gore-Randall, M. Irwin, M. S. Denning, J. M. Goicoechea, *Inorg. Chem.* **2009**, *48*, 8304–8316.
- [34] a) M. Irwin, R. K. Jenkins, M. S. Denning, T. Krämer, F. Grandjean, G. J. Long, R. Herchel, J. E. McGrady, J. M. Goicoechea, *Inorg. Chem.* **2010**, *49*, 6160–6171; b) B. N. Williams, W. Huang, K. L. Miller, P. L. Diaconescu, *Inorg. Chem.* **2010**, *49*, 11493–11498.
- [35] D. F. Evans, *J. Chem. Soc.* **1959**, 2003.
- [36] S. Grimme, A. Hansen, S. Ehlert, J.-M. Mewes, *J. Chem. Phys.* **2021**, *154*, 64103.
- [37] C. Adamo, V. Barone, *J. Chem. Phys.* **1999**, *110*, 6158–6170.
- [38] F. Weigend, R. Ahlrichs, *Phys. Chem. Chem. Phys.* **2005**, *7*, 3297–3305.
- [39] K. Jonas, US patent 4169845, **1977**.

- [40] a) SCALE3ABS, CrysAlisPro, Agilent Technologies Inc., Oxford, GB, **2012**; b) G. M. Sheldrick, SADABS, Bruker AXS, Madison, USA, **2007**.
- [41] R. C. Clark, J. S. Reid, *Acta Cryst. A* **1995**, *51*, 887–897.
- [42] G. M. Sheldrick, *Acta Cryst. A* **2015**, *71*, 3–8.
- [43] O. V. Dolomanov, L. J. Bourhis, R. J. Gildea, J. A. K. Howard, H. Puschmann, *J. Appl. Crystallogr.* **2009**, *42*, 339–341.
- [44] G. M. Sheldrick, *Acta Cryst. A* **2008**, *64*, 112–122.
- [45] G. M. Sheldrick, *Acta Cryst. C* **2015**, *71*, 3–8.
- [46] M. H. Chisholm, J. C. Huffman, I. P. Rothwell, P. G. Bradley, N. Kress, W. H. Woodruff, *J. Am. Chem. Soc.* **1981**, *103*, 4945–4947.



6 Summary and Outlook

This thesis highlights both the challenges and opportunities in 3d transition metal and main group metal catalysed (asymmetric) hydrofunctionalisation. After an introduction which provides a review of the historical and contemporary development of enantioselective hydrofunctionalisations (*Chapter 1*), the following chapter showcases the effectiveness of simple, commercially available bases as catalysts in hydroboration reactions (*Chapter 2*). Subsequently, different methods for using chiral ligands together with magnesium (*Chapter 3*) and 3d transition metal catalysts (*Chapter 4*) are investigated for their activity and enantiodiscrimination in hydrofunctionalisation reactions. The final chapter of this thesis describes a separate project focused on the coordination chemistry of phosphinines towards metalates. Phosphinine cobaltate complexes are reported which feature the phosphinine in unusual (η^4) or novel ($\mu, \eta^4: \eta^4$) coordination modes (*Chapter 5*).

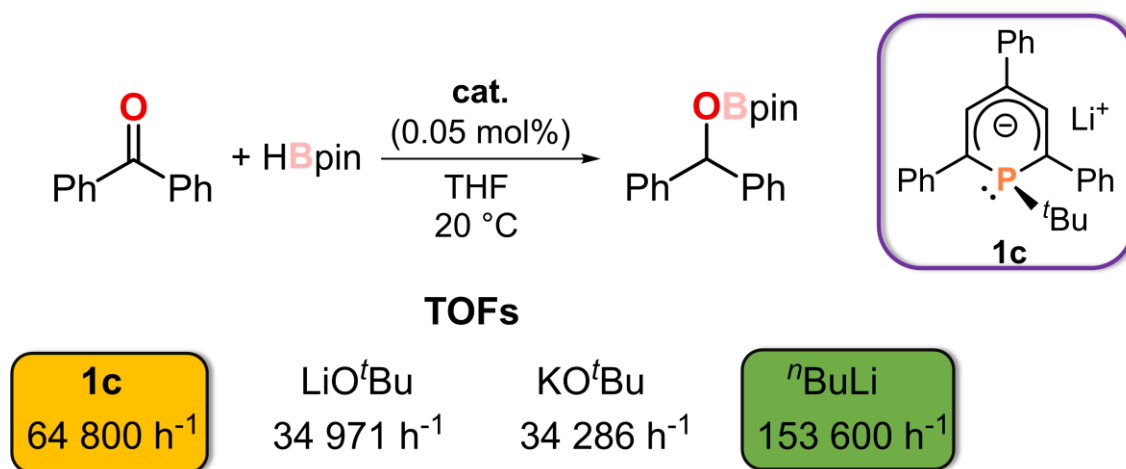
Chapter 1. Enantioselective Hydrofunctionalisation Reactions with Early Transition and Main Group Metals

This introductory chapter gives an overview of enantioselective hydrofunctionalisation reactions catalysed by early transition and main group metals. After a brief discussion of the general importance of chirality, this chapter is divided into three sections covering asymmetric hydrogenation, hydroboration and hydrosilylation. The first highly enantioselective hydrofunctionalisation reactions were performed in the 1970s by *Knowles* using chiral diphosphine ligands together with a rhodium catalyst in the hydrogenation of olefins. Since then, a plethora of catalysts with 4d and 5d transition metals and various chiral ligands have been developed, covering various enantioselective hydrofunctionalisation reactions. To improve sustainability contemporary research shifted its focus from using precious metals to 3d transition or main group metals. A number of catalysts using cheap and readily available metals have been developed that efficiently catalyse hydrofunctionalisation reactions in an asymmetric fashion. However, catalysts rivalling 4d or 5d transition metal compounds in their activity and selectivity remain scarce. The development of new competitive catalysts therefore remains an important challenge for contemporary research.

Chapter 2. Expedient Hydrofunctionalisation of Carbonyls and Imines initiated by Phosphacyclohexadienyl Anions

Hydrofunctionalisation reactions, especially hydroboration and hydrosilylation, play an important role in many industrial processes. Recent years have seen an influx of main group catalysed hydroboration reactions, sometimes rivalling even transition metal catalysed processes. In *Chapter 2*, phosphacyclohexadienyl anions $[\text{Li}(1\text{-R-PC}_5\text{Ph}_3\text{H}_2)]$ [R = Me (**1a**), *n*Bu (**1b**), *t*Bu (**1c**), Ph (**1d**) and CH_2SiMe_3 (**1e**)] were investigated in their catalytic capabilities in

hydrofunctionalisation reactions and compared to commercially available compounds such as alkali metal alkoxides and organolithium reagents. Compound **1c** was shown to efficiently catalyse the hydroboration of various substrates including ketones, imines, esters and even carbon dioxide. Acetophenone was fully converted to the corresponding alcohol with a catalyst loading as low as 0.01 mol% in less than 8 minutes resulting in a turnover frequency (TOF) of over 75 000 h⁻¹, rivalling the most rapid hydroborations employing HBpin in the literature. Previous reports using commercially available bases such as LiO^tBu, KO^tBu and ⁿBuLi suggest these bases to be drastically slower than **1c**. However, in the direct comparison of **1c** with these bases, it was found that the alkoxides and especially ⁿBuLi are remarkably effective catalysts with TOFs of over 150 000 h⁻¹ in the hydroboration of benzophenone (**Scheme 1**).

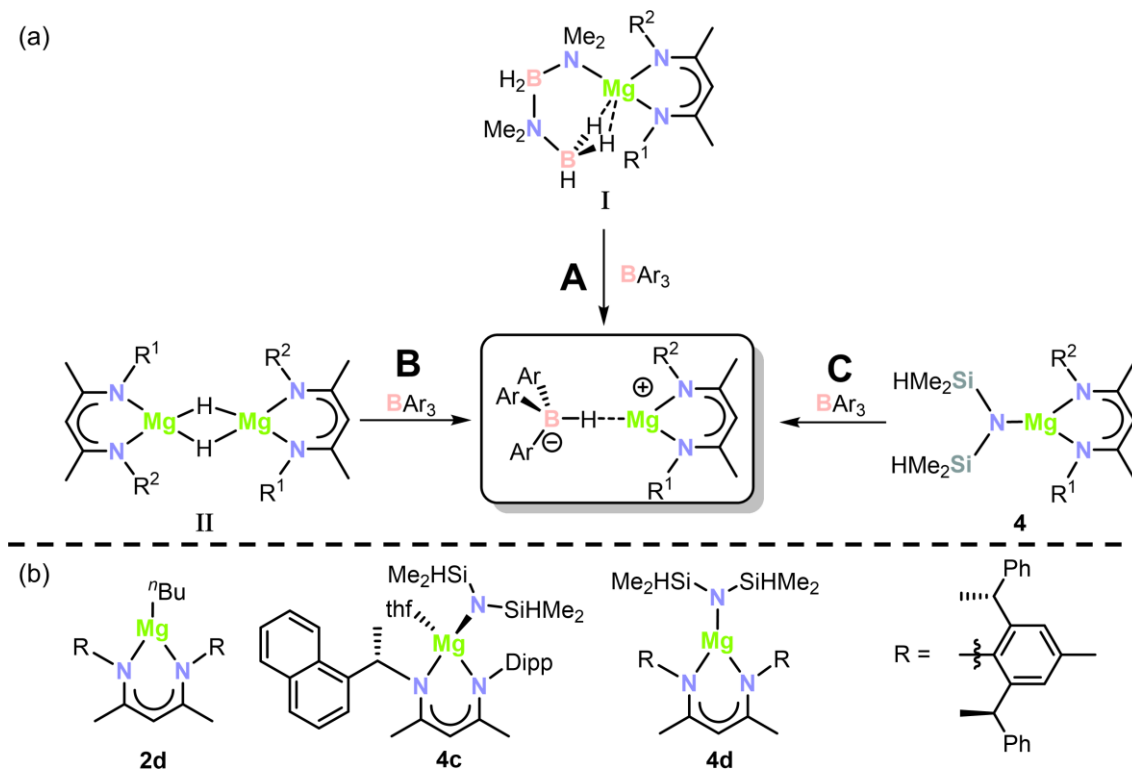


Scheme 1. Comparison of the turnover frequencies (TOFs) of **1c**, LiO^tBu, KO^tBu and ⁿBuLi in the hydroboration of benzophenone.

This high activity was also observed in the hydroboration of various challenging substrates, including imines and esters. In the hydroboration of CO₂ only **1c** was able to selectively catalyse the reduction MeOBpin. In order to improve our understanding of the reaction mechanism, ReactIR kinetic measurements were conducted suggesting a zero-order dependency on ketone concentration and a first order dependency on **1c** and HBpin. Experiments including different stoichiometries of **1c**, HBpin and 2'-methylacetophenone suggest the catalytic pathway commences *via* the formation of an adduct (**2**), which can then further react with HBpin to form the desired borolane, whilst also regenerating **1c**. Altogether, this chapter showcases the high catalytic activity and substrate scope of phosphacyclohexadienyl salts **1a-e** in hydrofunctionalisation reactions. Furthermore, the surprisingly good catalytic activities of commercially available alkoxides and organolithium reagents emphasise the underestimated potential of such simple reagents.

Chapter 3. Asymmetric Hydrofunctionalisation Reactions Catalysed by Chiral β -Diketiminato Magnesium Complexes

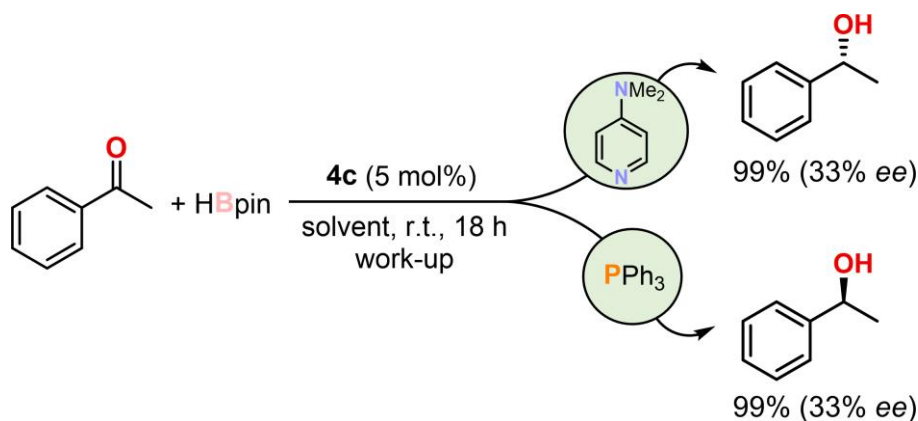
The goal of *Chapter 3* was the synthesis of a chiral β -diketiminato (NacNac) magnesium borohydride and the investigation of its catalytic activity in asymmetric hydrofunctionalisation reactions. The synthesis of the desired borohydride complex was attempted *via* the addition of a triarylborane to a magnesium complex bearing an amidoborane derivative (**route A**, **Scheme 2a**), a molecular magnesium hydride (**route B**) and a closely-related tetramethyldisilazide (**route C**).



Scheme 2. Different synthetic strategies towards the desired magnesium hydridoborate (a) and the synthesised magnesium complexes (b).

The desired starting materials for **routes A** and **B** (**I** and **II**, respectively) were only obtained in modest yields and could not be isolated cleanly. For **route C**, chiral NacNac magnesium complexes **2d**, **4c** and **4d** were synthesized as starting materials and structurally characterized (**Scheme 2b**). As almost no reaction occurred between **4c** and BPh_3 , the more Lewis acidic borane, $\text{B}(\text{C}_6\text{F}_5)_3$, was used in order to promote the desired β -SiH abstraction. In THF, the reaction of **4c** with $\text{B}(\text{C}_6\text{F}_5)_3$ instead yielded the known NacNac-free magnesium complex $[\text{Mg}(\text{thf})_6][\text{HB}(\text{C}_6\text{F}_5)_3]_2$. Performing the abstraction in toluene yielded a complex mixture of different species, as observed in the ^1H NMR spectrum. Attempts to isolate any of the formed species have so far been unsuccessful. Thus, none of the attempted approaches (**routes A-C**) yielded the desired chiral NacNac-magnesium borohydride salt. Complexes **2d**, **4c** and **4d** were investigated as precatalysts in the hydroboration of acetophenone. High conversions, but low enantiomeric excesses (up to 19%) were obtained with all catalysts. Upon investigating the effect

of different additives, in particular Lewis bases, it was found that the enantioselectivity can be switched from the (*R*)- to the (*S*)-enantiomer depending on the additive and the solvent (**Scheme 3**). The molecular structure of the proposed (pre)catalyst generated by the addition of DMAP to **4c** was determined by single crystal X-ray diffraction analysis. The results of these studies suggest that the widely-used NacNac ligand may have potential in asymmetric main-group metal catalysed transformations, even though only moderate enantioselectivities were observed in the specific reactions investigated in this chapter.

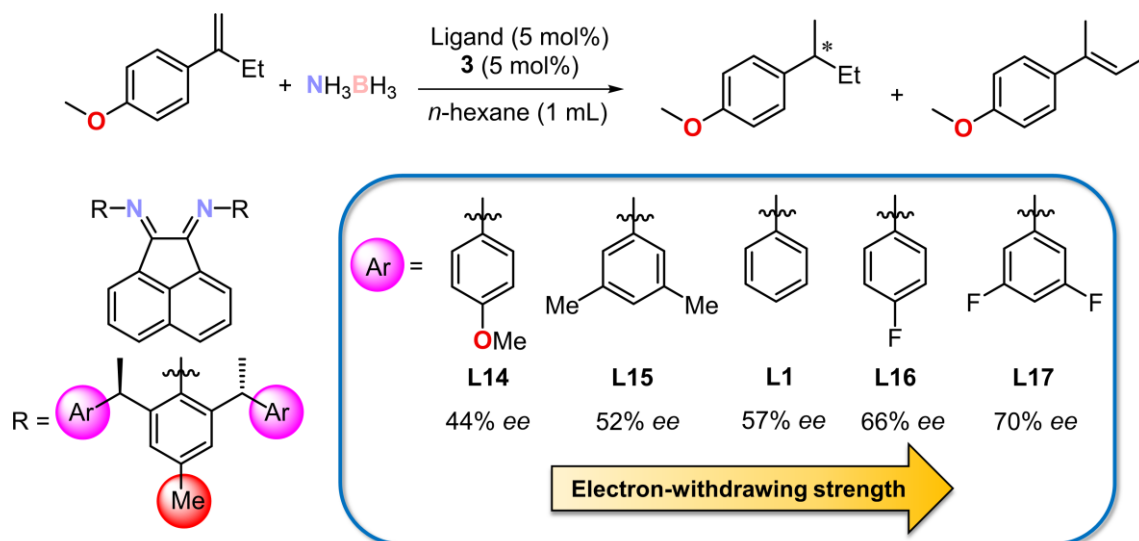


Scheme 3. Tuning of the enantioselectivity observed in the hydroboration of acetophenone catalysed by **4c** via the addition of different bases.

Chapter 4. Asymmetric Transfer Hydrogenation Reactions Catalysed by an α -Diimine Stabilised Cobaltate Complex

Chapter 4 presents the synthesis of bis(aryl)acenaphthenequinonediimine (BIAN) cobalt and iron complexes and their catalytic properties in asymmetric hydrofunctionalisation reactions. Dibromide cobalt(II) and iron(II) complexes **1** and **2** were synthesized. These complexes efficiently promote the hydroboration, hydrosilylation and (transfer) hydrogenation of ketones, imines and olefins after *in-situ* activation with LiBEt₃H. Unfortunately, the products were mostly obtained in low optical purities. The ligand exchange reaction of K[Co(cod)₂] (**3**) with **L1** yielded [K(thf)_x][(L1)Co(cod)] (**4**), which catalyses the transfer hydrogenation (TH) of olefins with ammonia borane. The enantioselectivity was highly solvent dependent, yielding racemic mixtures in THF and moderate enantiomeric excesses in *n*-hexane (up to 57% *ee*). An extensive study using different backbones in the α -diimine ligand revealed the BIAN moiety to be crucial for the selectivity. In order to improve the yields and the selectivity, BIAN ligands **L10-L17** were synthesised and tested as ligands in the TH of 1-(but-1-en-2-yl)-4-methoxybenzene (**S1**) with ammonia borane and precatalyst **3**. The electronic properties of the ligand were observed to effect the enantioselectivity. Electron-donating groups resulted in products with decreased optical purities, while electron-withdrawing groups led to higher enantiomeric excesses (up to 70% *ee*).

Unfortunately, the conversion decreased for all ligands **L10-L17**, when compared to **L1**, which thereby remained the most optimal ligand.

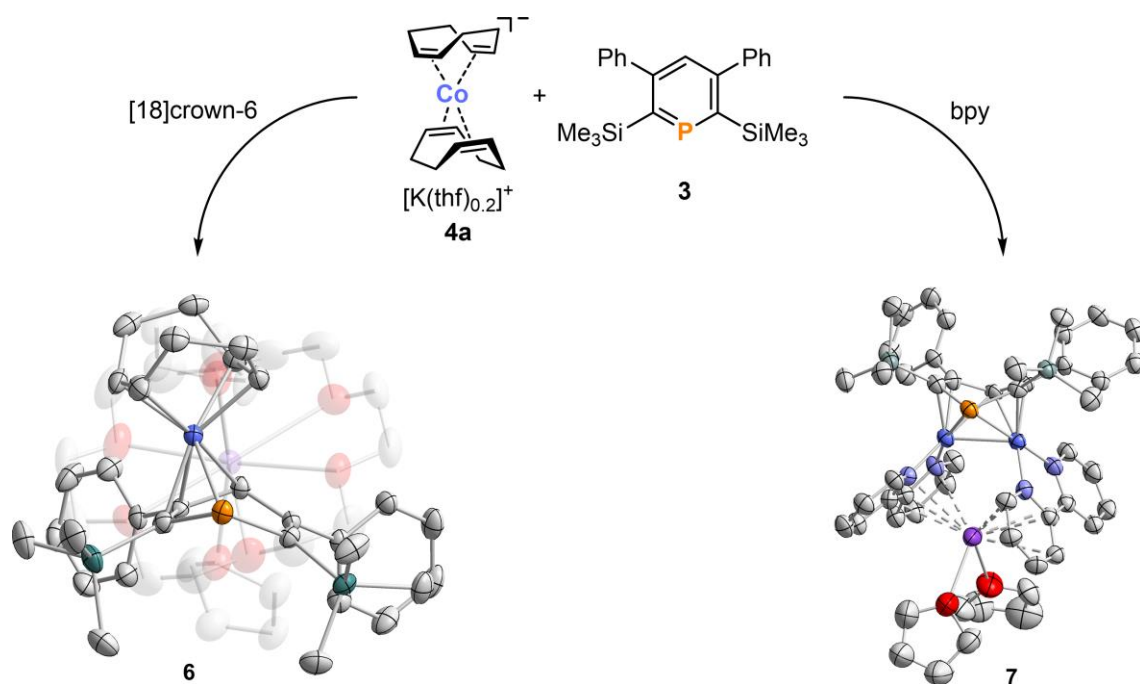


Scheme 4. Influence of the electron-withdrawing strength of the BIAN ligand in the TH of **S1**.

In order to improve the yields of the TH reaction, the reaction was performed in an H_2 atmosphere. This approach furnished the desired product in good yields but low optical purities. Upon investigating the influence of the amine borane, substituted amine boranes (NR_2HBH_3) were tested but were ineffective as H_2 -donors. Increasing the equivalents of ammonia borane resulted in improved yields and enantioselectivities (28% yield, 84% *ee*). No improvements in the optical purity were observed upon testing different additives, such as i -PrOH, menthol, K_2CO_3 , [18]crown-6 and [12]crown-4. Poisoning experiments with mercury, $\text{P}(\text{OMe})_3$ and dibenzo[*a,e*]cyclooctatetraene strongly suggested that the catalytically active species is homogeneous in nature. Altogether, this system displays good enantioinduction, but only gives poor to moderate activity in the TH of olefins. Nonetheless, this work can be seen as a first step into the underexplored area of base metal catalysed transfer hydrogenation reactions using NH_3BH_3 as the hydrogen transfer reagent.

Chapter 5. Synthesis and Characterisation of Low-Valent Phosphine Cobalt Complexes

Finally, *Chapter 5* of this thesis covers the synthesis of novel phosphine cobaltate complexes. Initially, the reactivity of 2-pyrid-2-yl-4,6-diphenylphosphine (**1**), 3,5-dimethyl- (**2**) and 3,5-diphenyl-2,6-bis(trimethylsilyl)phosphine (**3**) towards highly reduced metal complexes was investigated. No products were isolable from the reactions of **1** with $[\text{K}(\text{thf})][\text{Co}(\text{cod})_2]$ (**4a**), $[\text{Li}_2(\text{dme})_2][\text{Fe}(\text{cod})_2]$ (**4b**) or $[\text{K}([\text{18}]\text{crown-6})][\text{Fe}(\text{C}_{14}\text{H}_{10})_2]$. The reaction of **2** with **4a** was unselective, resulting in the formation of several species as observed in the $^{31}\text{P}\{^1\text{H}\}$ NMR spectrum. Reaction of **3** with **4a** selectively yielded compound **6** (**Scheme 5**), in which the phosphine binds to the cobalt centre in the rare η^4 -coordination mode.



Scheme 5. Synthesis of phosphinine cobalt complexes **6** and **7**.

Reactions of small molecules (P_4 , $t\text{BuCP}$ and CO_2) towards cobaltate salt **6** yielded intractable product mixtures. However, reaction of **3** with **4a** in the presence of 2,2'-bipyridine (bpy) in a 1:2:4 stoichiometry, X-ray structure determination on single crystals obtained from this reaction mixture showed the formation of the dinuclear complex **7**, which features the phosphinine in an unprecedented $\mu, \eta^4: \eta^4$ -coordination mode. The magnetic moment of paramagnetic **7** ($\mu_{\text{eff}} = 3.42 \mu_{\text{B}}$, Evans method) lies between the spin-only values of two and three unpaired electrons. The EPR spectrum displayed a broad rhombic signal besides small amounts of an impurity. Applying the $r^2\text{SCAN-3c}$ method, DFT calculations were performed to further investigate the electronic properties. Analysis of the total energy of the optimised geometries for three different ground-state multiplicities ($S = 1/2, 3/2, 5/2$) revealed the quartet and the doublet spin state to be energetically similar, whilst the sextet state is the energetically least favourable ($\Delta E = 9.9 \text{ kcal}\cdot\text{mol}^{-1}$). Analysis of the SOMOs of **7** for either the doublet or quartet state ($S = 1/2, 3/2$) showed that the orbitals exhibit strong ligand character in both cases. The accumulated data is consistent with **7** being in the quartet spin state ($S = 3/2$) with both bpy ligands present as radical anions ($\text{bpy}^{\cdot -}$). However, the isolation of pure **7** remains challenging and is a goal for future research.

Outlook

This thesis investigated the capabilities of 3d transition metal and main group element-based complexes as catalysts in asymmetric hydrofunctionalisation reactions. The catalysts tested showed either a good catalytic activity with poor to moderate enantiodiscrimination or, *vice versa*, poor to moderate catalytic activity combined with moderate to good enantioselectivity. Although the results did not meet a competitive level of enantioselectivity this thesis records developments in the ongoing pursuit of sustainable systems for asymmetric hydrofunctionalisation reactions by highlighting the strengths and weaknesses of the investigated systems.

The combination of NacNac-supported alkaline earth metal cations with metalates has been shown in the literature to form either a contact ion pair or a solvent separated ion pair depending on the solvent. As 3d transition metalates have already been shown to be versatile catalysts, introducing optically active NacNac ligands might give access to new catalysts active in asymmetric hydrofunctionalisation reactions.

Computational approaches, data-driven mathematical modeling and machine learning have advanced rapidly and are increasing traction in almost all domains of science and technology. The accuracy of such methods is highly dependent on the number of available data sets. Therefore, all data sets, no matter whether the catalysts yielded highly enantioselective or racemic mixtures, are important in advancing such approaches. Upon employing large data sets, machine learning has allowed the prediction of reaction outcomes with increasing rates of success. Employing such methods can improve selectivity prediction, reaction optimisation and catalyst design, possibly enabling unprecedented precision and efficiency in this pivotal field of research.

These methods have already been investigated in asymmetric hydrofunctionalisations catalysed by 4d and 5d transition metal complexes, but the amount of available data sets for such reactions catalysed by 3d transition metal and main group element-based complexes does not allow for precise predictions. Especially research using similar systems with varying degrees of success (compare the investigation of the influence of the ligand in *Chapter 4*) will help to increase the accuracy and therefore, the success of these methods. Upon exploring the synergies between chemistry and artificial intelligence, the potential to unlock novel, sustainable pathways for asymmetric hydrofunctionalisation reactions has never been greater.

7 Acknowledgements

Diese Arbeit wurde nur durch die Unterstützung zahlreicher Personen möglich. Im Folgenden möchte ich mich für deren Einsatz und Förderung bedanken.

Zuerst und ganz besonders möchte ich mich bei Prof. Dr. Robert Wolf für die Betreuung in den letzten Jahren bedanken. Danke für deine Unterstützung bei sämtlichen Belangen und für die Freiheit in meiner Forschung.

Prof. Dr. Manfred Scheer und Prof. Dr. Hendrik Zipse möchte ich für die Begutachtung meiner Arbeit danken. Prof. Dr. Patrick Nürnberger danke ich für die Bereitschaft, den Vorsitz zu übernehmen.

Den Mitarbeitern der zentralen Analytik und Werkstätten möchte ich ebenfalls Danke sagen, insbesondere Sabine Stempfhuber, Birgit Hischa und Florian Meurer (Röntgenstrukturanalyse), Georgine Stühler, Fritz Kastner, Veronika Scheidler, Annette Schramm, Tuan Anh Ngyuen und Dr. Ilya Shenderovich (NMR-Abteilung), Barbara Baumann und Helmut Schüller (Elementaranalyse), Markus Lindner (Glasbläserei) und Peter Fuchs (Elektronikwerkstatt).

Auch Kooperationspartner haben einen wichtigen Beitrag zu dieser Arbeit geleistet. Großer Dank gelten Prof. Dr. Nicolai Cramer (École Polytechnique Fédérale de Lausanne), Prof. Dr. Christian Müller (Freie Universität Berlin) und Prof. Dr. Hendrik Zipse (Ludwig-Maximilians-Universität München) für ihre wertvollen Beiträge, ihr hohes Engagement und die interessanten Diskussionen.

Für Unterstützung im Labor bedanke ich mich bei den Bacheloranden und Forschungspraktikanten Benjamin Falge, Phillip Bomke, Sonja Deschl, Johannes Luibl und Jonas Düker für ihre Mitwirkung an den Projekten.

Des Weiteren bedanke ich mich bei den aktuellen und früheren Arbeitskreismitgliedern für die gute Stimmung im Arbeitskreis. Vielen Dank auch an alle (ehemaligen) Laborkollegen (Matthew Margeson, Julia Leitl, Martin Gawron, John Kelly, Franziska Gilch, Maria Uttendorfer, Riccardo Grande) für die entspannte Labor-Atmosphäre.

Special thanks to Martin and Jose, I am very grateful for our friendship and sorry for being such a terrible friend.

Thanks to Dr. Thomas Horsley Downie and Dr. Gábor Balázs for going through almost every page of this thesis.

Danke auch an alle „Ducks“. Jede Woche ist etwas leichter, wenn man weiß, dass man noch mit euch musizieren kann.

All meinen Freunden sowie meinem Bruder Till und meinen Eltern Mathias und Maria gilt ganz besonderer Dank für ihr großes Verständnis und die Unterstützung in vielerlei Hinsicht.

8 Curriculum Vitae

Education

- November 2019 to present: Ph.D. in the group of Prof. Dr. Robert Wolf, University of Regensburg, Institute of Inorganic Chemistry
- Jan 2022 – April 2022: Research visit during Ph.D. in the group of Prof. Dr. Nicolai Cramer, Lausanne, Switzerland
- Oct 2017 – Sept 2019: Master of Science in Chemistry, University of Regensburg

Master's thesis in the group of Prof. Dr. Robert Wolf (Institute of Inorganic Chemistry): "*Phosphacyclohexadienyl Salts as Catalysts in Asymmetric Hydrofunctionalisation Reactions*"
- Aug 2018 – Sept 2018: Research Internship in the group of Prof. Dr. Michael Whittlesey, University of Bath, England
- Oct 2014 – Sept 2017: Bachelor of Science in Chemistry at the University of Regensburg
- Sept 2006 – July 2014: Allgemeine Hochschulreife (A-levels), Maximilian-von-Montgelas Gymnasium Vilsbiburg

Conference Contributions

- Aug 2022 Talk – Wissenschaftliches Kolloquium von Arbeitsgruppen für Anorganische Chemie 2022, Hirschegg, Austria
- July 2022 Poster – 29th International Conference on Organometallic Chemistry, Prague, Czech Republic
- Feb 2020 Poster – 17th European Workshop in Phosphorus Chemistry, Rennes, France

9 List of Publications

- 3) B. N. Baumann, H. Lange, F. Seeberger, P. Büschelberger, R. Wolf, M. Hapke, “Cobalt and Iron Metallates as Catalysts for Cycization Reactions of Triynes: [2+2+2] Cycloaddition vs. Garret-Braverman Reaction”, *Mol. Catal.* **2023**, 550, 113482.
- 2) M. J. Margeson, F. Seeberger, J. A. Kelly, Julia Leitl, P. Coburger, R. Szlosek, C. Müller, R. Wolf, “Expedient Hydrofunctionalisation of Carbonyls and Imines Initiated by Phosphacyclohexadienyl Anions”, *ChemCatChem* **2021**, 13, 3761-3764.
- 1) J. W. Hall, F. Seeberger, M. F. Mahoon, M. K. Whittlesey, “(carbene)CuF Complexes Featuring Bulky Arduengo-Type, Ring-Expanded, and Cyclic (Alkyl)(amino)carbenes: Applications in Catalytic Aldehyde Allylation”, *Organometallics* **2020**, 39, 227-233.

Supporting Information

The Supporting Information of this thesis contains the supporting information of all published material (chapter 2). It contains analytical data (NMR spectra, UV/Vis spectra, IR spectra, EPR spectra, X-ray crystallography and cyclic voltammograms) as well as details on quantum chemical calculations. The pdf file is stored on an external CD-ROM, which is supplied with this thesis.

Eidesstattliche Erklärung

Ich erkläre hiermit an Eides statt, dass ich die vorliegende Arbeit ohne unzulässige Hilfe Dritter und ohne Benutzung anderer als der angegebenen Hilfsmittel angefertigt habe; die aus anderen Quellen direkt oder indirekt übernommenen Daten und Konzepte sind unter Angabe des Literaturzitats gekennzeichnet. Die Arbeit wurde bisher weder im In- noch im Ausland in gleicher oder ähnlicher Form einer anderen Prüfungsbehörde vorgelegt.

Felix Seeberger